l. 141, September 1, 1982
mplete in one issue

ISSN 0003-2670

ANALYTICA CHIMICA ACTA

International journal devoted to all branches of analytical chemistry

ELSEVIER SCIENTIFIC PUBLISHING COMPANY

ANALYTICA CHIMICA ACTA

International journal devoted to all branches of analytical chemistry
Revue internationale consacrée à tous les domaines de la chimie analytique
Internationale Zeitschrift für alle Gebiete der analytischen Chemie

PUBLICATION SCHEDULE FOR 1982

	J	F	M	A	M	J	J	A	S	O	N	D
Analytica Chimica Acta	134	135/1	135/2	136	137	138	139	140/1 140/2	141	142	143	144

Scope. *Analytica Chimica Acta* publishes original papers, short communications, and reviews dealing with ev aspect of modern chemical analysis, both fundamental and applied.

Submission of Papers. Manuscripts (three copies) should be submitted as designated below for rapid and effici handling:

Papers from the Americas to: Professor Harry L. Pardue, Department of Chemistry, Purdue University, West Lafaye IN 47907, U.S.A.

Papers from all other countries to: Dr. A. M. G. Macdonald, Department of Chemistry, The University, P.O. Box 3 Birmingham B15 2TT, England. Papers dealing particularly with computer techniques to: Professor J. T. Cl Universität Bern, Pharmazeutisches Institut, Sahlistrasse 10, CH-3012 Bern, Switzerland.

Submission of an article is understood to imply that the article is original and unpublished and is not being consider for publication elsewhere. Upon acceptance of an article by the journal, authors resident in the U.S.A. will be asked transfer the copyright of the article to the publisher. This transfer will ensure the widest dissemination of informati under the U.S. Copyright Law.

Information for Authors. Papers in English, French and German are published. There are no page charg Manuscripts should conform in layout and style to the papers published in this Volume. Authors should cons Vol. 132, p. 239 for detailed information. Reprints of this information are available from the Editors or from: Elsev Editorial Services Ltd., Mayfield House, 256 Banbury Road, Oxford OX2 7DH (Great Britain).

Reprints. Fifty reprints will be supplied free of charge. Additional reprints (minimum 100) can be ordered. An or form containing price quotations will be sent to the authors together with the proofs of their article.

Advertisements. Advertisement rates are available from the publisher.

Subscriptions. Subscriptions should be sent to: Elsevier Scientific Publishing Company, P.O. Box 211, 1000 Amsterdam, The Netherlands.

Publication. *Analytica Chimica Acta* appears in 11 volumes in 1982. The subscription for 1982 (Vols. 134–144) Dfl. 1815.00 plus Dfl. 220.00 (postage) (total approx. U.S. $814.00). Journals are sent automatically by airmail to t U.S.A. and Canada at no extra cost and to Japan, Australia and New Zealand for a small additional postal charge. earlier volumes (Vols. 1–133) except Vols. 23 and 28 are available at Dfl. 182.00 (U.S. $72.80), plus Dfl. 14.00 (U $5.60) postage and handling, per volume.

Claims for issues not received should be made within three months of publication of the issue, otherwise they can be honoured free of charge.

Customers in the U.S.A. and Canada who wish to obtain additional bibliographic information on this and otl Elsevier journals should contact Elsevier Science Publishing Company Inc., Journal Information Center, 52 Vanderl Avenue, New York, NY 10017. Tel: (212) 867-9040.

Concentrates and ready made-up solutions for volumetric analysis

Reagents

MERCK

An all-purpose assortment of concentrated and volumetric solutions, part of our extensive reagents range:

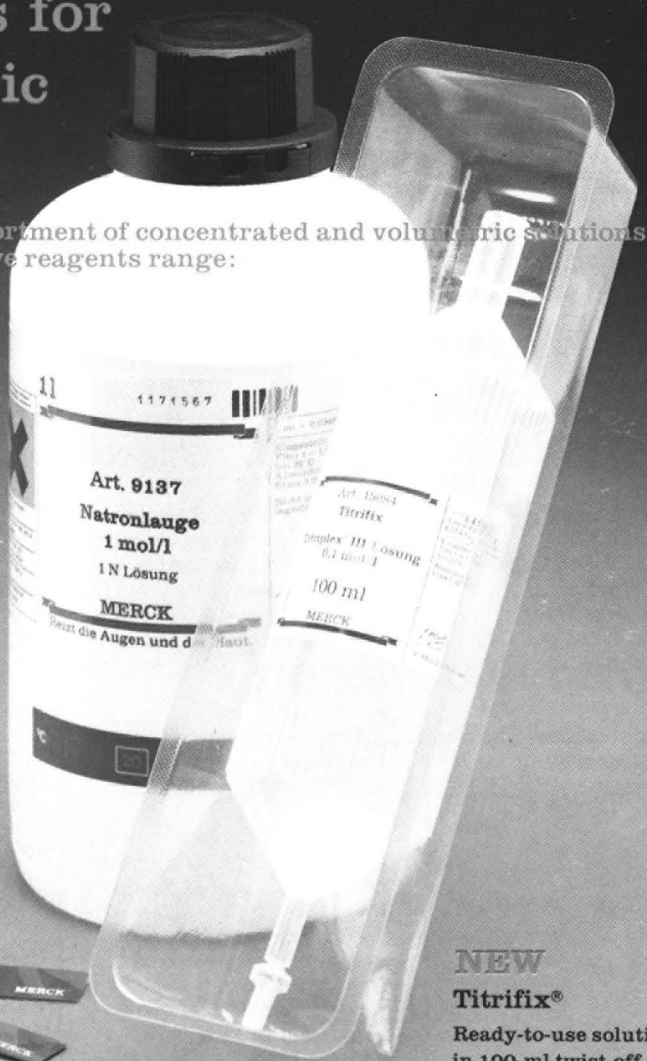

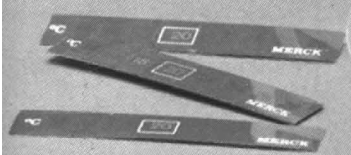

NEW

Titrifix®

Ready-to-use solutions in 100-ml twist-off ampoules

Titrisol®

Concentrated solutions in tapered ampoules for easy preparation of volumetric solutions

Combi-Titrisol®

The precise volume (1.000 litre) and titre (t = 1.000) of the solution supplied permit its use as a Titrisol® or as a volumetric solution

Volumetric solutions

Ready-to-use solutions. In handy 1-litre bottles and economical 25-litre containers

Temperature checks are easily performed with the aid of the temperature measurement strips supplied with the solutions.

●

The titre of all concentrated and ready made-up solutions is adjusted to t = 1.000 at 20 °C.

●

Long-term titre stability guaranteed (over a period of years).

●

Please send for our special brochure.

E. Merck, Darmstadt, Federal Republic of Germany

JOURNAL OF ANALYTICAL AND APPLIED PYROLYSIS

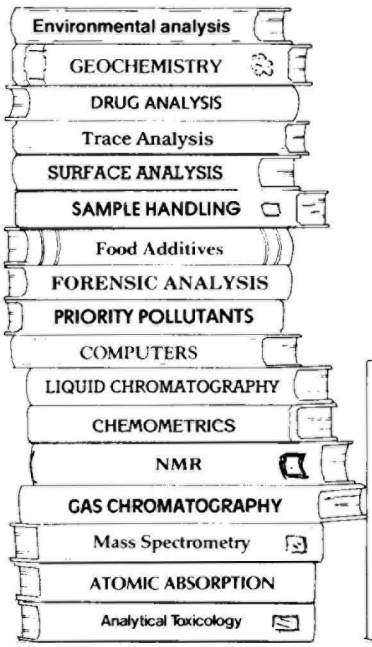

Let TrAC cover the whole of analytical chemistry for you!

A SAMPLE COPY IS NOW AVAILABLE IN YOUR LIBRARY

TrAC trends in analytical chemistry

TrAC - Trends in Analytical Chemistry is a topical monthly which provides you with an easy-to-read interdisciplinary digest of current developments and new ideas in the analytical sciences.

TrAC's authors are leading scientists, its articles practically oriented, its coverage international.

TrAC covers the broader issues which affect those who develop and use analytical methods, such as the impact of computers on the analytical laboratory and the implications of new governmental regulations.

TrAC comes from the publishers of the **Journal of Chromatography** and **Analytica Chimica Acta.**

Subscription Information
Personal edition: 12 issues -
U.K. £20.00, USA and Canada US$42.50,
Europe 91.50 Dutch guilders, Rest of World 95.50 Dutch guilders.

Library edition: Vol. 1 (16 issues) -
US$ 133.25 or 260 Dutch guilders.

Prices include air delivery worldwide.

Send now for a free sample copy to

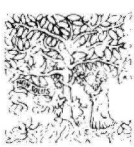

Elsevier Scientific Publishing Company

P.O. Box 330
1000 AH Amsterdam
The Netherlands

52 Vanderbilt Avenue
New York, NY 10017
U.S.A.

Elite-Inn Yushima IF
3-28-1 Yushima, Bunkyo-ku,
Tokyo 113, Japan

7242A

DRUGS OF ABUSE

by LAWRENCE FISHBEIN, *National Center for Toxicological Research, Jefferson, AR, and University of Arkansas for Medical Sciences, Little Rock, AR, U.S.A.*

CHROMATOGRAPHY OF ENVIRONMENTAL HAZARDS – VOLUME IV

The main objective of this volume is to provide the analytical and clinical chemist, as well as the forensic toxicologist, with a practical text which is also a literature reference source, of selected descriptive chromatographic procedures that stress the separation, detection and quantification of a spectrum of drugs of abuse, e.g. depressants, narcotics and analgesics, stimulants and hallucinogens, from biological, licit and illicit samples. The principal methods are thin-layer chromatography, gas-liquid chromatography, gas-liquid chromatography-mass spectrometry and high performance liquid chromatography. The procedures described are those which are primarily useful in therapeutic monitoring and pharmacokinetic studies, emergency, clinical, forensic and toxicological analyses and in monitoring in drug abuse screening programs.

Relevant information has been included, where available, regarding the synthesis or isolation from natural sources, the salient chemical, biological and physical properties, as well as the pharmacology, metabolism, pharmacokinetics, disposition and toxicity of the abused drugs. This information is important to investigators in diverse disciplines including biochemistry, clinical chemistry and medicine, pharmacology, toxicology, public health, and others such as clinicians and drug counselors who are all equally concerned with detecting, ameliorating, managing or eliminating the effects of this social and environmental hazard.

CONTENTS: Chapters 1. Introduction. **Part 1. Depressants (including Sedatives, Tranquillizers and Hypnotics).** 2. Alcohol. 3. Barbiturates. 4. Benzodiazepine Antianxiety Agents. 5. Phenothiazines. 6. Ethchlorvynol. 7. Carbamates and Ureides. 8. Antihistaminics. 9. Methaqualone. **Part 2. Narcotics and Analgesics.** 10. Opium Alkaloids - Morphine and Codeine. 11. Heroin. 12. Methadone and alpha-Acetylmethadol. 13. Salicylates. 14. Phenacetin and Acetaminophen. 15. Propoxyphene. 16. Meperidine. **Part 3. Stimulants.** 17. Amphetamine and Methamphetamine. 18. Cocaine. 19. Tricyclic Antidepressants. 20. Methylphenidate and Phenmetrazine. **Part 4. Hallucinogenic Agents (including Psychotogenic, Psychotomimetic and Psychedelic Drugs).** 21. Marihuana, Cannabis Constituents and Hashish. 22. Psilocin, Psilocybin, Peyote and Mescaline. 23. LSD. 24. Mono- and Dimethoxyamphetamines and 3,4-Methylenedioxyamphetamine. 25. Phencyclidine. 26. Ketamine. **Subject Index.**

All chapters are followed by copious references.

1982 x + 490 p.
Price: US $104.75/Dfl. 225.00
ISBN 0-444-42024-X

Chromatography of Environmental Hazards

Vol. 3
Pesticides

1975 xvi + 820 p.
US $135.00/Dfl. 290.00
ISBN 0-444-41158-5

"...very useful and the sheer amount of information between these covers is a monument to the energy and enthusiasm of the author."
Pans

Vol. 2
Metals, Gaseous and Industrial Pollutants

1973 xii + 637 p.
US $107.00/Dfl. 230.00
ISBN 0-444-41059-7

"The author has accomplished a monumental task in compiling so much data within a 600-page volume ... the book is a worthy addition to the library of the researcher actively involved in this very complex area of chemical analysis."
Journal of Chromatography

ELSEVIER

P.O. Box 211,
1000 AE Amsterdam,
The Netherlands.

52 Vanderbilt Ave.,
New York. N.Y. 10017.

The Dutch guilder price is definitive. US $ prices are subject to exchange rate fluctuations.

Biomolecular Information Theory

by SERAFIN FRAGA, K.M.S. SAXENA, *and* MANUEL TORRES, *Department of Chemistry, University of Alberta.*

Studies in Physical and Theoretical Chemistry 4

Advances in computer technology have led to unforeseeable possibilities in the theoretical study of biological processes. The purpose of the present work is to review, update and summarize the applicability of molecular recognition theory in quantum biology and quantum biochemistry. The book will be particularly valuable because of its comprehensive summary (in tabular form and in figures) of all the practical information required for the theoretical construction of biopolymers and the evaluation of their interactions.

ABBREVIATED CONTENTS: **I. Introduction. II. Biomolecular Information.** Chapters: 1. The Code and its Origins. **III. Molecular Information Theory.** 2. Recognition Processes. 3. Interaction Energies. 4. Computational Simulations. **IV. Appendices:** Coordinates. Transformation of Coordinates. Determination of Cartesian Coordinates. Spherical Harmonics. Basic Statistical-Thermodynamical Formulas. Electric Fields and Moments. Density Distributions: Population Analysis and Properties. Bond-Energy Analysis. **V. References. VI. Author Index. VII. Subject Index.**

1978 x + 272 pages US $61.00 / Dfl. 125.00 ISBN 0-444-41736-2

Tritium in Organic Chemistry

Isotopes in Organic Chemistry, Volume 4

edited by E. BUNCEL, *Queen's University, Kingston, Ontario, Canada, and* C.C. LEE, *University of Saskatchewan, Saskatoon, Saskatchewan, Canada.*

with a foreword by Lars Melander.

This series is rapidly gaining recognition as an indispensible work, of value to lecturers, students, and research workers alike.

ABBREVIATED CONTENTS: Chapters: 1. Tritium Nuclear Magnetic Resonance Spectroscopy *(J.A. Elvidge, J.R. Jones, V.M.A. Chambers and E.A. Evans).* 2. The Use of Tritium and Deuterium in Photochemical Electrophilic Aromatic Substitution *(W.J. Spillane).*3. Reactions of Energetic Tritium Atoms with Organic Compounds *(Y.-N Tang).*4. Stereospecific Synthesis of Tritium Labelled Organic Compounds Using Chemical and Biological Methods *(D.W. Young).* Subject Index.

1978 xvi + 300 pages US $73.25 / Dfl. 150.00 ISBN 0-444-41741-9

ELSEVIER

The Dutch guilder price is definitive. US $ prices are subject to exchange rate fluctuations.

P.O. Box 211,
1000 AE Amsterdam
The Netherlands

52 Vanderbilt Ave
New York, N.Y. 10017

7106A

ANALYTICA CHIMICA ACTA
VOL. 141 (1982)

ANALYTICA CHIMICA ACTA

International journal devoted to all branches of analytical chemistry

ELSEVIER SCIENTIFIC PUBLISHING COMPANY

Anal. Chim. Acta, Vol. 141 (1982)

Analytica Chimica Acta, 141 (1982) 1—13
Elsevier Scientific Publishing Company, Amsterdam — Printed in The Netherlands

INDUCED BACTERIAL ELECTRODE FOR THE POTENTIOMETRIC MEASUREMENT OF TYROSINE

C. L. DI PAOLANTONIO and G. A. RECHNITZ*
Department of Chemistry, University of Delaware, Newark, DE 19711 (U.S.A.)
(Received 22nd February 1982)

SUMMARY

A bacterial tyrosine-selective potentiometric electrode is proposed in which the desired biocatalytic activity is biochemically induced during growth of the bacterial cells. As the result of this induction, a normally ineffective biocatalyst, *Aeromonas phenologenes* ATCC 29063 can be coupled with an ammonia gas-sensing electrode in order to produce a useful tyrosine-selective electrode. The sensor shows excellent response characteristics, having a slope of 50—58 mV/decade, a range of logarithmic response from 8.3×10^{-5} M to 1.0×10^{-3} M tyrosine, a lower limit of detection of 3.3×10^{-5} M tyrosine, response times of 4—6 min, and a useful lifetime in excess of one week. Specific enzyme inhibitors are employed to enhance the selectivity of the electrode while maintaining high biocatalytic activity with respect to tyrosine.

The development of new bioselective membrane electrodes utilizing bacterial cells with potentiometric sensors has resulted [1] in novel probes for numerous substrates of biological interest and is of special importance for cases where isolated enzymes are not available, are unstable, or have insufficient biocatalytic activity. This paper proposes a new type of bacterial sensor where cells, which do not have a suitable level of biocatalytic activity in their normal state, are altered during their growth phase to induce the desired biochemical pathway. It will be shown that such biochemical induction can result in a sharp increase of biocatalytic activity without loss of selectivity. While this new approach to the development of bioselective membrane electrodes is illustrated here specifically for a tyrosine-selective electrode, the induction concept involved may have fundamental utility for the future design of cell-based potentiometric electrodes in general.

L-Tyrosine is an essential mammalian amino acid which is present in physiological fluids as a result of protein degradation or as a L-phenylalanine metabolite. Several methods have recently been developed for the measurement of tyrosine in aqueous and biological samples, including high-performance liquid chromatography [2], gas chromatography [3], spectrophotometry [4, 5], mass spectrometry [6, 7], and enzyme-coupled amperometry [8] and potentiometry [9—11]. Many of the chromatographic and colorimetric techniques require derivatization steps, while the electro-

0003-2670/82/0000-0000/$02.75

chemical methods either require fresh aliquots of enzyme for each measurement or exhibit poor probe stability and short useful lifetimes.

Tyrosine is known to undergo a variety of biochemical conversions in both prokaryotic and eukaryotic cells, one of which is a deaminating hydrolysis reaction [12, 13]

$$\text{L-tyrosine} + H_2O \xrightarrow[\text{pyridoxal-5-phosphate}]{\text{tyrosine phenol lyase (E.C. 4.1.99.2)}} \text{pyruvate} + \text{phenol} + NH_3 \qquad (1)$$

The enzyme involved is not available commercially, although an aerobic strain of bacteria containing high tyrosine phenol lyase activity has been isolated from refrigerated stored haddock [14]. Phenol accumulation in the fish led to the isolation and characterization of *Aeromonas phenologenes* (also called *Citrobacter freundii*) ATCC 29063. It was found that growth of this bacterium in media containing L-tyrosine produces a six-fold increase over normal concentrations of tyrosine phenol lyase [14]. Thus, this enzyme has been demonstrated to be inducible in this bacterial strain via the formation of the specific enzyme or group of enzymes in response to the introduction of the substrate into the growth medium. This enhancement results in bacterial cells with sufficient deaminating activity for use as biocatalysts in conjunction with an ammonia gas-sensing electrode. The resulting bacterial probe combines the simplicity and low cost of a potentiometric detector with the stability and reusability inherent to immobilized whole cell biocatalysts.

EXPERIMENTAL

Apparatus and reagents

All potentiometric measurements were made with a Corning model 12 pH/mV meter in conjunction with a Heath-Schlumberger model SR-240 potentiometric recorder. Measurements were made in thermostatted cells controlled at 30 ± 0.1°C with a Haake model FS water bath. The ammonia gas sensor used for all work was the Orion model 95-10 electrode. An IEC model HT centrifuge was modified for refrigerated use. The bacteria were grown in a New Brunswick Scientific model G76 gyrotary water-bath shaker adjusted to 30°C.

All solutions were prepared with distilled—deionized water. Analytical-grade reagents were used except where otherwise noted. L-Tyrosine and all other amino acids, creatinine, pyridoxal-5-phosphate, isonicotinic acid hydrazide, 6-diazo-5-oxo-L-norleucine, and iodoacetamide were purchased from Sigma Chemical Co., St. Louis, MO. The fumaric acid was from J. T. Baker, Phillipsburg, NJ, and the urea from Schwarz/Mann, Orangeburg, NY. Nutrient broth media were obtained from Difco Laboratories, Detroit, MI. The bacterium *Aeromonas phenologenes* ATCC 29063 was purchased from the American Type Culture Collection, Rockville, MD.

Procedures

Growth and preparation of the bacterial biocatalyst. Aeromonas phenologenes was grown in a distilled water medium containing either nutrient broth or 0.1% tyrosine in nutrient broth; the latter is the induction medium. The solution was heated with stirring to approximately 90°C for 10 min until the components completely dissolved. The growth medium was divided among 125-ml culture flasks and autoclaved at 15 psi for 20 min. The flasks were cooled to room temperature before culturing aseptically with bacteria. Any media not used immediately were refrigerated until needed and induction media were reheated to dissolve the tyrosine before innoculation occurred.

The innoculated flasks were placed in a shaker bath, rotating at approximately one-third of the maximum rate. Growth proceeded for 12 h, at which time marked turbidity was noted. Bacteria were initially grown on nutrient broth media; from this stock innocula were taken each time for subsequent induction broth growth. Cells grown on induction media were centrifuged and washed twice in a pH 7.0, 0.02 M potassium phosphate buffer. The washed cells were collected by centrifugation as a slurry, and 7—10 μl were applied to the gas-permeable membrane of an ammonia electrode. The cells were supported at the gas-permeable membrane with a circular dialysis membrane, as previously described [15].

The probe was conditioned first for 1 h in a working buffer consisting of 0.2 M boric acid, 3×10^{-2} M KCl, 1×10^{-3} M $MgCl_2 \cdot 7H_2O$, adjusted to pH 8.75 with sodium hydroxide and made 1×10^{-4} M in pyridoxal-5-phosphate immediately before use. Stock solutions of pyridoxal-5-phosphate were made daily in the above buffer and kept cold and in the dark between use. The probe was then conditioned in 1×10^{-3} M 6-diazo-5-oxo-L-norleucine (DON)—working buffer for three hours, and finally conditioned in 1×10^{-3} M iodoacetamide—working buffer prior to use. The probe, stored and used in working buffer at 30°C, was reconditioned in DON—working buffer every three days during its useful lifetime.

Optimization of deaminating activity. The relative tyrosine deaminating activity of the bacterial electrode was measured by the previously described initial rate method [16]. The pH values of the working buffer, potassium and magnesium concentrations were varied independently in 2.1 ml of 0.2 M borate—sodium hydroxide or sodium phosphate buffers containing 4.5×10^{-4} M tyrosine. The initial rate of production of ammonia was obtained from a potential vs. time curve as previously described [17]. Measurements of this type yield information regarding the efficiency of both the biocatalyst and the ammonia gas-sensing electrode, allowing simultaneous optimization of experimental conditions with respect to each.

Estimation of effective biocatalytic activity units. The effective number of biocatalytic activity units was estimated for the bacterial cells by monitoring the rate of production of ammonia from tyrosine using the ammonia gas-selective electrode. Various aliquots of the bacterial cell slurry were added to a 30°C cell containing 10.1 ml of working buffer and 5.6×10^{-4} M tyrosine.

The moles of ammonia produced were calculated from an ammonia calibration curve at various time intervals. The slope of a plot of micromoles of ammonia produced vs. time was taken as the number of effective biocatalytic activity units (μmol NH_3 min^{-1}) for the bacterial aliquot added.

RESULTS AND DISCUSSION

Effect of induction on electrode response

Cells of the strain *Aeromonas phenologenes* were grown simultaneously in conventional growth media containing no tyrosine, and in induction media supplemented with 0.1% tyrosine. The bacteria were treated identically but separately and the same volume of packed cells was immobilized on two ammonia electrodes. Tyrosine calibration curves, shown in Fig. 1, demonstrate the dramatic effect of tyrosine phenol lyase induction during bacterial growth. While induced cells resulted in a sensor with a slope of 53 mV/decade and a lifetime exceeding one week, the non-induced cells produced a probe having a slope of only 19 mV/decade which lost all deaminating activity within four days.

It was critical that the tyrosine present in the induction media be completely dissolved; cells propagated in induction media containing precipitated tyrosine resulted in bacterial probes displaying slopes of only 39—43 mV/decade change in tyrosine concentration. Similarly, successive cycles of bacterial growth in induction media ultimately produced decreased sensor slope, possibly owing to the long-term development of alternative metabolic tyrosine degradation pathways. A non-induced pool of cells was retained under refrigeration for periods of up to one week as a source for all innoculations of induction media.

Bacterial probe characteristics

A typical calibration curve showing the bacterial probe response to tyrosine in a working buffer is shown in Fig. 2. The slope of a freshly prepared sensor ranged from 50 to 58 mV/decade change in tyrosine concentration, with the lower limits of detection averaging 3.3×10^{-5} M tyrosine. The useful logarithmic range of response was between 8.3×10^{-5} and 1.0×10^{-3} M; above this concentration range there is a potential change corresponding to an increase in the pH of the solution. This results from the fact that tyrosine stock solutions must be made more alkaline than the working buffer if precipitation is to be avoided; at millimolar tyrosine concentrations the buffering capacity of the system is surpassed, as shown in Fig. 2 by the response of the ammonia electrode alone to tyrosine. The logarithmic range is narrower than with some bioselective membrane electrodes although it occurs at a sufficiently low concentration range to allow samples to be diluted, thus rendering it useful. Electrode response times were between 4 and 6 min, while the recovery time between tyrosine determinations was 15—20 min. The responses of six separate tyrosine electrodes are summarized in Table 1.

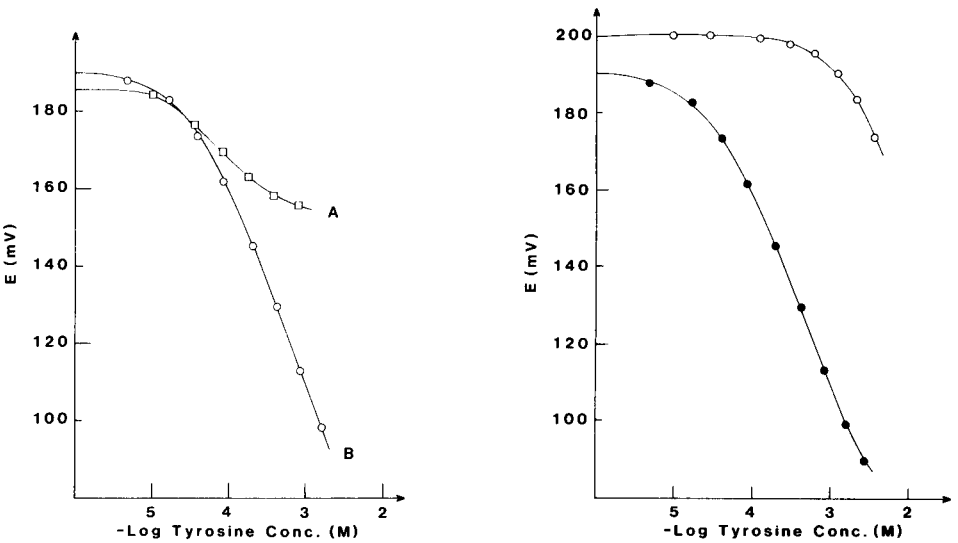

Fig. 1. Effect of bacterial induction on the response of the tyrosine sensor: (A) no tyrosine present during growth; (B) 0.1% tyrosine present during growth.

Fig. 2. Response to tyrosine of an ammonia electrode: (•) with immobilized bacteria; (○) without bacteria.

TABLE 1

Tyrosine bacterial electrode response characteristics[a]

Electrode	Number of points	Slope ± s.d.	Standard error of estimate (mV/log conc., M)	Lower limit of logarithmic range[b] (M)	Lower limit of detection (M)
1	5	54.0 ± 0.5	1.2	7.1×10^{-5}	3.3×10^{-5}
2	4	53.0 ± 0.2	0.5	7.9×10^{-5}	2.9×10^{-5}
3	3	51.4 ± 0.2	1.0	1.0×10^{-4}	3.8×10^{-5}
4	4	57.5 ± 0.7	2.6	6.3×10^{-5}	3.3×10^{-5}
5	4	52.7 ± 0.1	0.4	8.9×10^{-5}	1.6×10^{-5}
6	3	49.9 ± 0.4	1.5	1.0×10^{-4}	4.6×10^{-5}
Av. ± s.d.		53.1 ± 2.6		$(8.3 \pm 1.5) \times 10^{-5}$	$(3.3 \pm 1.0) \times 10^{-5}$

[a]Tyrosine response was tested in a pH 8.75 borate buffer containing 3.5×10^{-2} M K^+, 1×10^{-3} M Mg^{2+}, and 1×10^{-4} M pyridoxal-5-phosphate at 30.0°C. [b]Upper limit of logarithmic range extended above 1×10^{-3} M tyrosine in all cases.

Effective units of biocatalytic activity

The effects of induction upon the production of tyrosine phenol lyase in the bacterial cells was measured homogeneously, as shown in Fig. 3. Approximately 6.9 × 10^{-3} units of effective biocatalytic activity were found per microliter of packed induced bacterial cells, while non-induced cells showed no significant correlation between enzyme activity and cell volume. As 7—10 μl of packed cells were used in the preparation of each bacterial electrode, a 5—8-fold increase in enzymatic activity was achieved through the induction technique.

Optimization of working buffer conditions

Working buffer conditions were adjusted in order to obtain optimal electrode response characteristics. The pH profile for the bacterial probe is shown in Fig. 4, with maximal initial rates of tyrosine deamination occurring at pH 8.75. This pH represents a compromise between that favored by the ammonia gas sensor and the pH at which the biocatalyst shows highest activity, as has been noted with other biocatalytic electrodes [18]. Several different buffers were tested over the pH range 7.5—10.0, with maximal initial rates of deamination occurring in a borate—sodium hydroxide buffer at 8.75. Interestingly, the initial rate of deamination obtained when Tris—HCl buffers were used decreased as the probe dialysis time increased. This effect, coupled with a change in the color of the working buffer from clear to bright yellow, suggested that the Tris buffer may have been complexing the pyridoxal-5-phosphate prosthetic group, making it unavailable to the tyrosine phenol lyase apoenzyme.

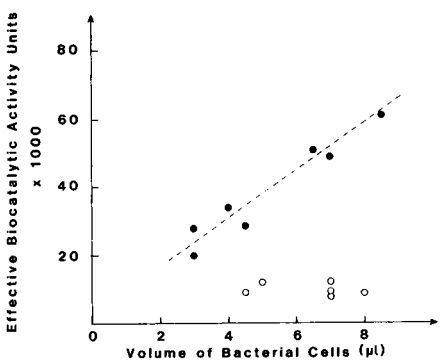

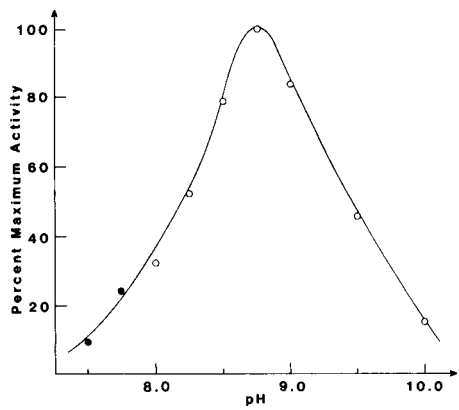

Fig. 3. Effective biocatalytic activity units as a function of bacterial volume in induced (•) and non-induced (○) *Aeromonas phenologenes*.

Fig. 4. Effect of pH on the response of the bacterial electrode with different buffers: (•) 0.2 M sodium phosphate; (○) 0.2 M borate—sodium hydroxide. Experimental conditions: [K^+] = 1 × 10^{-3} M; [Mg^{2+}] = 1 × 10^{-3} M; [pyridoxal-5-phosphate] = 1 × 10^{-4} M; [tyrosine] = 4.6 × 10^{-4} M.

Various mono- and divalent ions have been correlated with increased stability and/or activity of isolated bacterial tyrosine phenol lyase enzyme. Since K^+, NH_4^+, and Rb^+ were reported to be essential for firm binding of the apoenzyme to its prosthetic group [19], the monovalent ion effect was studied with respect to the bacterial probe. To avoid interference with the ammonia detector, potassium ion concentrations were varied and the initial rate of tyrosine deamination was measured, as shown in Fig. 5A. Optimal potassium ion concentrations were approximately 3.5×10^{-2} M, and this concentration level was incorporated into all working and storage buffers. Similarly, divalent ions have been reported to activate tyrosine phenol lyase obtained from certain bacterial sources [20], although no essential requirement was noted by workers who isolated this enzyme from *Aeromonas phenologenes*. Nonetheless, a small activation was noted when the bacterial probe was dialyzed in the presence of millimolar concentrations of magnesium (Fig. 5B).

Selectivity

One of the major difficulties facing developers of bacterial membrane electrodes is that of achieving adequate selectivity toward the substrate of interest [21]. Glutamine is often the compound through which excess of ammonia in microbial systems is shunted, leading to eventual excretion; hence many strains contain glutaminase enzymes. *Aeromonas phenologenes* apparently includes some glutaminase activity, for glutamine poses significant interference if present in the aqueous sample (Fig. 6A). Incubation of the bacterial probe in a 1×10^{-3} M solution of 6-diazo-5-oxo-L-norleucine (DON)—working buffer for three hours, effectively mitigates this effect without reducing the tyrosine deaminating response, as shown in Fig. 6B. DON, a glutamine agonist, is known to be an effective irreversible competitive inhibitor for both prokaryotic and eukaryotic glutaminases [22—25].

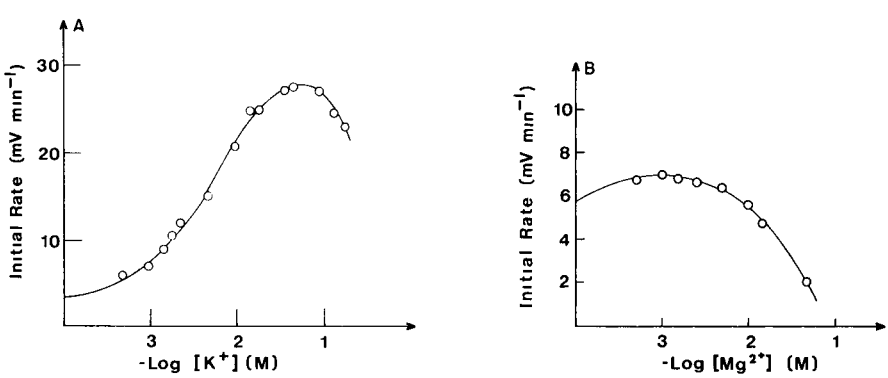

Fig. 5. Effects of (A) potassium ion concentration, and (B) magnesium ion concentration, on the response of the bacterial sensor.

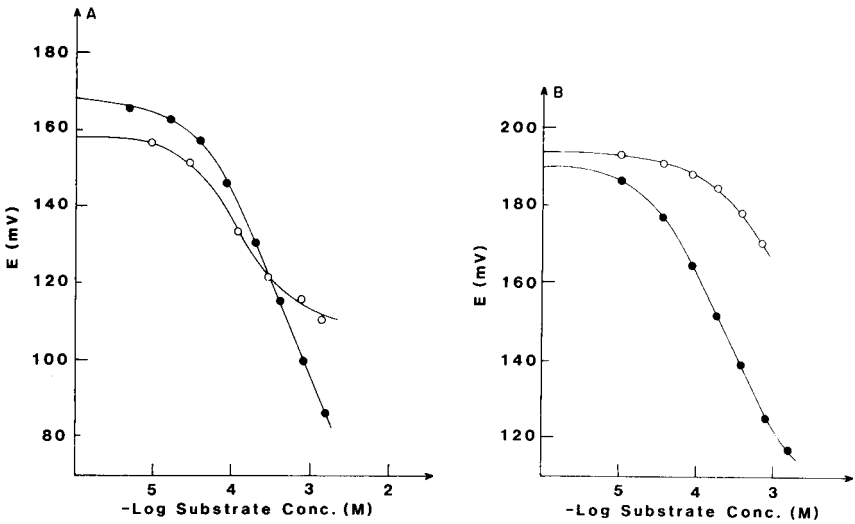

Fig. 6. Response of the tyrosine electrode to (•) tyrosine, and (○) glutamine: (A) before DON treatment; (B) after 3 h dialysis in 1×10^{-3} M DON—working buffer.

Treatment with DON must be repeated every three days, however, probably because not all of the cellular glutaminase is accessible to the inhibitor during a single dialysis. Neither increasing the DON concentration tenfold nor allowing the probe to dialyze for a longer period of time prevented eventual interference by glutamine, supporting this hypothesis. It is doubtful that much enzyme synthesis occurs in the cells during the period of immobilization, as starvation conditions prevail. DON is also known to inhibit *Escherichia coli* glutaminase B by 80% and borate anions are reported to be the most effective stabilizers of this enzyme under certain conditions [26]; this may explain why glutamine interference of the *Aeromonas phenologenes* probe can be lessened but not entirely prevented.

Further interference was posed by the amino acids glycine, serine, and threonine, as shown in Fig. 7A. A single 3-h dialysis in 1×10^{-3} M iodoacetamide—working buffer effectively curtailed response from these interferents, as shown in Fig. 7B. Figures 6B and 7B effectively indicate the high retention of tyrosine phenol lyase activity following treatment with inhibitors; this factor is essential in choosing appropriate selectivity enhancement methods.

Competitive inhibition of isolated tyrosine phenol lyase has been reported [13, 27] by alanine, phenylalanine and the end product of the tyrosine degradation, phenol. The Michaelis-Menten inhibition constants for these compounds, reported to be in the range 5×10^{-3} M—5×10^{-2} M, represent the concentration of inhibitor which causes the initial rate of deamination to be half-maximal. Tyrosine calibration curves constructed in the presence of 0.01 M inhibitor showed no significant changes in electrode response

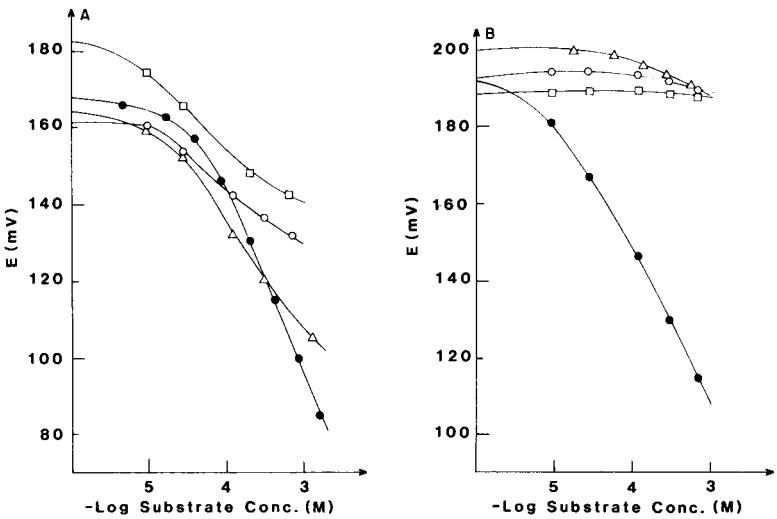

Fig. 7. Response of the tyrosine electrode to (□) glycine, (○) threonine, (△) serine, and (●) tyrosine. (A) Before exposure to iodoacetamide; (B) after 3 h dialysis in 1 × 10^{-3} M iodoacetamide—working buffer.

characteristics, and the electrode failed to respond to inhibitor alone. This suggests that the tyrosine phenol lyase enzyme is present in such high activity that, despite considerable inhibition, sufficient enzyme is present to effect the desired deamination or that the cellular enzyme is not inhibited to the same extent as the isolated enzyme.

Other compounds tested for possible interference using three separate tyrosine probes are summarized in Table 2. Response times for the interferents were generally 30—50% longer than those for tyrosine. Very good selectivity was demonstrated toward tyrosine over all compounds tested except glutamine, histidine, and asparagine. Suppression of glutamine interference has been discussed in detail; similar strategies may yet prove to be feasible for the suppression of asparagine and histidine deaminating enzymes while retaining good tyrosine phenol lyase activity.

Electrode lifetime

The bacterial electrode showed good response characteristics for at least eight days, as shown in Fig. 8. The slope decreased slightly, from approximately 54 mV/decade to 50 mV/decade, and the logarithmic range of response narrowed to approximately millimolar tyrosine concentrations, though this was effectively the upper limit of detection owing to the tyrosine blank, as was shown in Fig. 1.

In addition to steady-state measurement, kinetic studies were also conducted at various stages during the lifetime of the electrode. The initial rate of deamination was measured as a function of tyrosine concentration, and Fig. 9

TABLE 2

Response of bacterial electrode toward possible interfering compounds[a]

Compound	ΔE^b (mV)	Compound	ΔE^b (mV)	Compound	ΔE^b (mV)
Tyrosine	54.6	Lysine	0.3	Leucine	3.5
Urea	2.2	Tryptophan	0.2	Isoleucine	4.1
Glutamine	13.5	Histidine	11.9	Alanine	2.4
Creatinine	4.2	Glycine	0	Cysteine	4.0
Phenylalanine	0	Valine	2.2	Proline	1.5
Serine	5.2	Glutamic acid	3.0	Ornithine	1.2
Threonine	0.9	Fumaric acid	1.8	Adenosine-5'-monophosphate	2.4
Asparagine	63.0				

[a]Interferents were tested using DON- and iodoacetamide-treated probes in a pH 8.75 borate buffer containing 3.5×10^{-2} M K^+, 1×10^{-3} Mg^{2+}, and 1×10^{-4} M pyridoxal-5-phosphate at 30.0°C. [b]Change in potential corresponding to 3×10^{-4} M interferent.

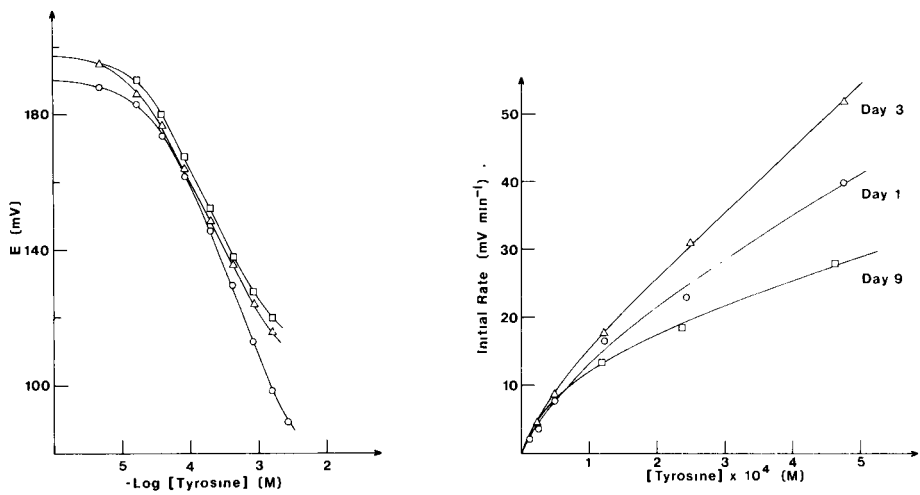

Fig. 8. Response of the bacteria-based tyrosine electrode to tyrosine at various electrode ages: (○) day 2; (△) day 7; (□) day 8.

Fig. 9. Kinetic response of the tyrosine-selective electrode at various ages.

illustrates the kinetic response of the tyrosine bacterial electrode on days 1, 3, and 9. As with previous bacterial systems [28, 29], an initial enhancement in response profile occurred between days 1 and 3, with subsequent decrease in the initial rates of reaction until the end of the lifetime of the probe. The decrease in initial rate of reaction affected neither the steady-state response time nor the electrode recovery time, however.

With aging of the *Aeromonas phenologenes*-based electrodes, the electrode

baseline potentials tended to increase, as has been noted with previous bacterial probes [30]. Other workers [28, 31] have circumvented this problem by adding isonicotinic acid hydrazide (INH) to all working and storage buffers; this is known to inhibit bacterial ammonia assimilation [32]. Unfortunately, INH has been reported to inhibit the activity of tyrosinase (E.C. 1.14.18.1) [33], bind to mammalian brain pyridoxal-5-phosphate [34], and impair nicotinic acid uptake in certain bacterial strains, resulting in general bactericidal properties [35, 36]. Tyrosine phenol lyase within the *Aeromonas phenologenes* strain tends to be similarly INH-sensitive, as working buffers containing INH turned from clear to bright yellow, as when Tris was present, and electrode response degraded significantly over time, as shown in Fig. 10. The electrode was thus never exposed to INH, and tyrosine calibration curves were repeated on a daily basis to compensate for the increasing starting potentials.

Recovery studies

Percentage recovery studies, shown in Table 3, were conducted on 2.1-ml aqueous samples whose tyrosine concentrations ranged from 4.7×10^{-5} M to 4.9×10^{-4} M. Average recoveries were between 94% and 101%, with an average standard deviation of 4%, even at concentrations which were below the linear range of response of the probe.

The tyrosine-sensitive bacterial electrode described in this paper thus shows

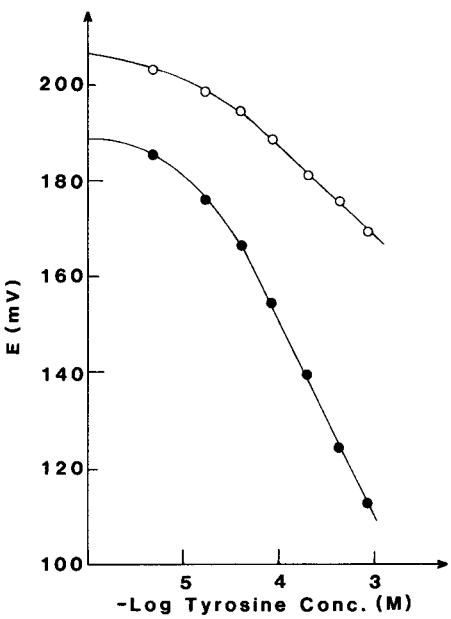

Fig. 10. Response of the bacterial electrode to tyrosine before (•) and after (○) 48-h dialysis in 1×10^{-4} M INH—working buffer.

TABLE 3

Recovery studies using standard addition technique[a]

L-Tyrosine conc. ($\times 10^5$ M)		Average recovery ± s.d. (%)
Added	Found ± s.d.	
4.7	4.5 ± 0.3	96 ± 6
16	17 ± 0.6	101 ± 5
28	27 ± 1.0	98 ± 3
49	46 ± 1.2	94 ± 2

[a]Percentage recovery was tested using 2.1 ml of a pH 8.75 borate buffer containing 3.5×10^{-3} M Mg^{2+}, and 1×10^{-4} M pyridoxal-5-phosphate at 30°C.

excellent response characteristics, including good slope, low limits of detection, useful range of linear response, fast response times, and a lifetime in excess of one week. The selectivity of the probe can be greatly enhanced through exposure to a variety of deaminating enzyme inhibitors, while maintaining good response toward the substrate of interest. Most importantly, appropriate biochemical induction alters the bacterial metabolism in such a manner as to render a nominally useless strain into a highly effective and selective biocatalyst. This combination of cellular induction and interference pathway manipulation may serve greatly to extend the range of possible bacterial electrodes with analytical feasibilities.

The authors acknowledge the support of the National Institutes of Health Grant GM-25312.

REFERENCES

1 G. A. Rechnitz, Science, 214 (1981) 287.
2 W. S. Hancock, C. A. Bishop and M. T. W. Hearn, Anal. Biochem., 92 (1979) 170.
3 S. L. MacKenzie and D. Tenaschuk, J. Chromatogr., 2 (1979) 195.
4 J. Ellis, A. M. Holland and R. A. Holland, Anal. Chim. Acta, 93 (1977) 349.
5 S. Takahashi, J. Biochem. (Tokyo), 83 (1978) 57.
6 B. Sjoequist, Biomed. Mass Spectrom., 6 (1979) 392.
7 J. M. L. Mee, J. Korth, B. Halpern and L. B. James, Biomed. Mass Spectrom., 4 (1977) 178.
8 A. Kumar and G. D. Christian, Clin. Chem., 21 (1975) 325.
9 G. G. Guilbault and F. R. Shu, Anal. Chem., 44 (1972) 2161.
10 A. M. Berjonneau, D. Thomas and G. Broun, Pathol.-Biol. (Fr.), 22 (1974) 497.
11 C. Calvot, A. M. Berjonneau, G. Gellf and D. Thomas, FEBS Lett., 59 (1975) 258.
12 H. Kumagai, H. Yamada, H. Matsui, H. Ohkishi and K. Ogata, J. Biol. Chem., 245 (1970) 1767.
13 H. Kumagai, H. Yamada, H. Matsui, H. Ohkishi and K. Ogata, J. Biol. Chem., 245 (1970) 1773.
14 G. M. Carman and R. E. Levin, Appl. Environ. Microbiol., 33 (1977) 192.
15 D. S. Papastathopoulos and G. A. Rechnitz, Anal. Chim. Acta, 79 (1975) 17.
16 M. A. Arnold and G. A. Rechnitz, Anal. Chem., 53 (1981) 515.

17 P. D'Orazio, M. E. Meyerhoff and G. A. Rechnitz, Anal. Chem., 50 (1978) 1531.
18 P. W. Carr and L. D. Bowers, Immobilized Enzymes in Analytical and Clinical Chemistry, Wiley, New York, 1980, p. 245.
19 T. Toraya, T. Nihara and S. Fukui, Eur. J. Biochem., 69 (1976) 411.
20 N. Brot and H. Weissbach, in H. Tabor and C. W. Tabor (Eds.), Methods of Enzymology, Vol. 17A, Academic Press, New York, 1970, p. 642.
21 R. K. Kobos, in H. Freiser (Ed.), Ion-Selective Electrodes in Analytical Chemistry, Plenum, New York, 1980, p. 72.
22 S. Prusiner and E. R. Stadtman, Biochem. Biophys. Res. Commun., 45 (1971) 1474.
23 S. Prusiner and E. R. Stadtman, J. Biol. Chem., 251 (1976) 3457.
24 L. M. Pinkus and H. G. Windmueller, Arch. Biochem. Biophys., 182 (1977) 506.
25 R. A. Shapiro, V. M. Clark and N. P. Curthoys, J. Biol. Chem., 254 (1979) 2835.
26 S. Prusiner, J. N. Davis and E. R. Stadtman, J. Biol. Chem., 254 (1976) 3447.
27 G. M. Carman and R. E. Levin, J. Food Biochem., 1 (1977) 285.
28 C. L. Di Paolantonio, M. A. Arnold and G. A. Rechnitz, Anal. Chim. Acta, 128 (1981) 121.
29 P. W. Carr and L. D. Bowers, Immobilized Enzymes in Analytical and Clinical Chemistry, Wiley, New York, 1980, p. 238.
30 R. K. Kobos and G. A. Rechnitz, Anal. Lett., 10 (1977) 751.
31 R. K. Kobos, D. J. Rice and D. S. Flournoy, Anal. Chem., 51 (1979) 1122.
32 S. Taniguchi, R. Sato and F. Egani, in W. D. McElroy and B. Glass (Eds.), Inorganic Nitrate Metabolism, Johns Hopkins Press, Baltimore, MD, 1956, p. 98.
33 J. Fourche, C. R. Acad. Sci., Ser. D., 287 (1978) 365.
34 S. Saraswathi and B. K. Bachhawat, Bull. Natl. Inst. Sci. India, No. 25 (1964) 31.
35 K. Takayama and L. A. Davidson, Antibiot. (N.Y.), 5 (1979) 98.
36 H. J. Nestler, Arzneim.-Forsch., 16 (1966) 1442.

Analytica Chimica Acta, 141 (1982) 15—21
Elsevier Scientific Publishing Company, Amsterdam — Printed in The Netherlands

MICROSOMAL ELECTRODES FOR REDUCED NICOTINAMIDE ADENINE DINUCLEOTIDE AND ITS PHOSPHATE, GLUCOSE-6-PHOSPHATE AND ASCORBATE

F. SCHUBERT*, F. SCHELLER and D. KIRSTEIN

Central Institute of Molecular Biology, Academy of Sciences of the GDR, Department of Applied Enzymology, 1115 Berlin-Buch (E. Germany)

(Received 4th March 1982)

SUMMARY

Rat liver microsomes have been immobilized in a membrane by gelatin entrapment. The resulting membranes can be attached to an oxygen electrode to provide a sensor for several compounds. NADPH and NADH are determined by utilizing the liver microsomal NADPH oxidase activity, which is, at least in part, due to the cytochrome P-450 system. The calibration graph for NADPH is linear up to 1 mM. A multi-enzyme system localized in liver microsomes allows the determination of 20—800 μM glucose-6-phosphate. The non-enzymatic lipid peroxidation in liver microsomes, which is induced by ascorbate, allows 0.5—2.5 mM ascorbate to be determined.

Electrodes for the determination of numerous biochemically important substances have been developed in the last decade [1, 2]. In most cases the sensors have consisted of an appropriate membrane electrode coupled with one or more immobilized enzymes, in a relatively pure form. Recently, isolated enzymes in such electrodes have been replaced by higher, integrated systems. This method eliminates the need for laborious enzyme extraction and purification procedures and usually offers the advantage of increased biocatalyst stability. However, it may suffer from a poorer selectivity.

Recent work in this direction has resulted in the development of several microbial electrodes [3—6], and, as one of the latest approaches, of sensors utilizing subcellular organelles as the biologically-active phase [7—10]. In these electrodes (organelle sensors [8]), mitochondrial fractions from different cell species were employed for the measurement of NADH and succinate [7, 8] and glutamine [9]. The immobilized microsomal fraction of liver has been used in combination with a rotating graphite electrode to determine aniline, a frequently used substrate for the microsomal cytochrome P-450 system [10]. Once the applicability of liver microsomes in bioelectrochemical sensors had been demonstrated, further studies were undertaken with regard to analytical application of other biochemical reactions taking place in this complex organelle. The results of these investigations are described in this paper.

Liver microsomes catalyze the oxidation of NADPH not only through cytochrome P-450-mediated substrate hydroxylation, but also by NADPH oxidase activity in the absence of added substrate

$$NADPH + H^+ + O_2 \rightarrow NADP^+ + H_2O_2$$

This activity was first described in 1957 [11] and has since been the subject of much speculation. It is currently viewed as going only in part through the microsomal cytochrome P-450 system [12, 13]. In microsomes, a number of other oxidative pathways (e.g., lipid peroxidation, fatty acyl CoA desaturase) exist, some of which should account for a considerable portion of NADPH oxidation. In this paper, these combined activities are used for NADPH determination by employing immobilized liver microsomes coupled with a Clark-type oxygen electrode.

In principle, such an electrode for measuring NADPH should be applicable to all processes where the pyridine nucleotide is involved. A reaction sequence causing reduction of $NADP^+$ accompanied by dehydrogenation of glucose-6-phosphate is also present in liver microsomes. By utilizing these reactions the microsomal electrode concept was extended to glucose-6-phosphate determination. Thus, the organelle was employed as a multi-step catalyst in the sensor.

As a further use of liver microsomes, lipid peroxidation induced by ascorbate was utilized to measure ascorbate with the organelle electrode.

EXPERIMENTAL

Materials and preparation of membranes

Liver microsomes from phenobarbital-treated rats were prepared by established methods [14, 15]. Protein was determined by using the Folin-phenol reagent [16]. Reduced and oxidized pyridine nucleotides were obtained from AWD Dresden (E. Germany), glucose-6-phosphate was purchased from Boehringer Mannheim (W. Germany) and L-ascorbic acid was from Reanal (Budapest, Hungary). Gelatin for organelle immobilization was obtained from VEB Gelatinewerk, Calbe (E. Germany). All other reagents were of reagent grade and were used as received.

The liver microsomes were immobilized by entrapment in gelatin as previously described [10]. A 5% gelatin solution at 37°C was mixed with the microsomal suspension and the mixture was cast to yield 2.7 mg of microsomal protein per cm^2 of membrane. Membranes were dried and stored under refrigeration until used.

Apparatus and procedures

An approximately 4 × 4-mm piece of gelatin membrane containing microsomes was attached to the polyethylene membrane of an oxygen electrode (Meinsberg, E. Germany) by covering it with a kidney dialysis membrane and fixing them with an O-ring. The electrode, consisting of a platinum cathode

(3 mm diameter) and a silver/silver chloride anode, was polarized to —600 mV and the current corresponding to the oxygen concentration was measured with a GWP-polarograph (ZWG Berlin, E. Germany) connected to a chart recorder.

The measurements were made at 20° C in a thermostated cell containing 3 ml of 0.05 M Tris—HCl buffer, pH 7.4. When the current output reached a constant value, the sample was added to the measuring cell and the total current charge was monitored. NAD(P)H oxidation experiments with microsomal suspensions were done in the same manner in a closed measuring cell.

RESULTS AND DISCUSSION

NADPH measurement

A typical response curve of the sensor to NADPH is shown in Fig. 1. Upon addition of NADPH, the NADPH oxidase consumes part of the dissolved oxygen in the immobilized microsomal layer. This consumption causes a decrease in the current output of the electrode which is proportional to the NADPH concentration. A new constant current is reached after about 2.5 min. The current decrease depends linearly on the NADPH concentration up to 1 mM in the measuring cell (Fig. 2).

The responses of the sensor to NADH and NADPH were compared. The results are given in Table 1. They show that whereas the free microsomal suspension was only 25% as effective in oxidizing NADH as NADPH, the organelle sensor was more sensitive to NADH than to NADPH. This suggests

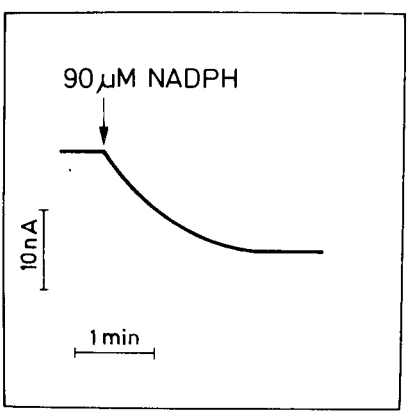

Fig. 1. Response curve of the rat liver microsomal electrode to NADPH.

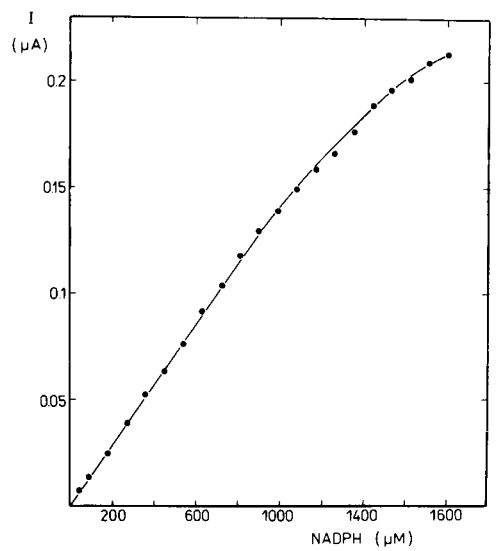

Fig. 2. Relationship between the current decrease of the microsomal electrode and NADPH concentration in the measuring cell.

TABLE 1

Rat liver microsomal oxidizing activities for NADPH and NADH

	NADPH[a]	NADH[a]
Microsomal suspension[b] (nA min^{-1} mg^{-1} protein)	19.3 ± 2.1	4.7 ± 0.7
Organelle electrode (nA μM^{-1})	0.102 ± 0.005	0.166 ± 0.006

[a]Mean ± standard deviation, for 3 measurements. [b]Determined polarographically with 1 microsomal protein (1.29 mg ml^{-1}) in a closed measuring cell equipped with an oxygen electrode.

that the accessibility of NADH to its oxidation site is enhanced, possibly as a result of structural changes in the microsomal membrane during or after immobilization. Furthermore, the ratio of NADPH to NADH oxidizing activities may have been changed during immobilization owing to partial inactivation of NADPH oxidase.

Multi-step reaction for glucose-6-phosphate measurement

Rat liver microsomes contain a hexose-6-phosphate dehydrogenase (EC 1.1.1.47) [17] which is selective for glucose-6-phosphate, galactose-6-phosphate and glucose when either NAD^+ or $NADP^+$ is used as electron acceptor [18]. This enzyme is probably related to the microsomal electron transport system, functioning in vivo as an NADPH generator [19]. This interrelationship was utilized in the organelle sensor to determine glucose-6-phosphate. Figure 3 shows the current—concentration dependence for this sensor. Excess of $NADP^+$ had to be added to the measuring solution. When NADPH and glucose-6-phosphate were determined with the same electrode preparation under identical experimental conditions, double the sensitivity

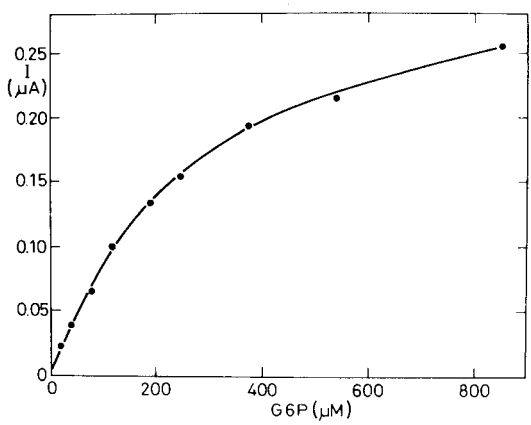

Fig. 3. Relationship between current decrease of the microsomal electrode and glucose-6-phosphate (G6P) concentration. The measuring solution contained 2 mM $NADP^+$.

towards glucose-6-phosphate was observed. Results of a typical experiment with 2 mM $NADP^+$ in the measuring solution were 0.128 ± 0.008 nA μM^{-1} for NADPH and 0.233 ± 0.011 nA μM^{-1} for glucose-6-phosphate. Besides the better permeability of the membrane to the smaller glucose-6-phosphate molecules, the reaction of microsomal 6-phosphogluconate dehydrogenase (EC 1.1.1.44) [20] seems to be responsible for this increased sensitivity. This enzyme would dehydrogenate 6-phosphogluconate produced from glucose-6-phosphate and thus reduce a second molecule of $NADP^+$ for each glucose-6-phosphate:

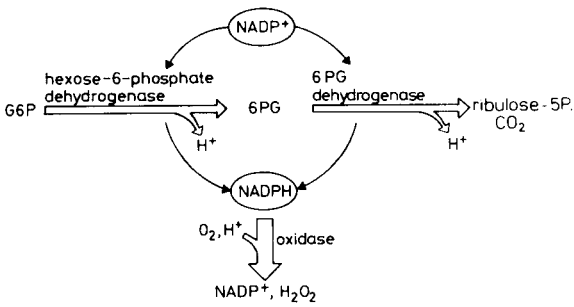

Obviously, this complicated reaction chain readily proceeds in the immobilized organelle layer. Remarkably, the immobilized microsomes retained about 80% of their glucose-6-phosphate activity after 8 months of storage at 4° C. Hence, it can be concluded that the multi-enzyme system involved is very stable when immobilized in the manner described.

Ascorbate measurement

Ascorbate is a potent inducer of liver microsomal lipid peroxidation [21, 22]. This non-enzymatic process is accompanied by oxygen consumption and the disappearance of some polyunsaturated fatty acids from the phospholipids.

When in contact with ascorbate, the microsomal electrode exhibited a current decrease corresponding to the oxygen consumption in the immobilized organelle membrane. This behaviour indicates that the immobilized microsomes retained their lipid peroxidation function. The current—concentration curve is linear up to 2.5 mM ascorbate (Fig. 4). However, the sensitivity of the sensor towards ascorbate was low and decreased further after some days of operation. It is very likely that this low stability is due to exhaustion of the polyunsaturated fatty acids within the microsomal membrane.

Conclusions

In the work presented here, the microsomal electrode has been extended from aniline measurement [10] to determination of NAD(P)H, glucose-6-phosphate and ascorbate. Particularly the measurement of NAD(P)H is felt to be of great potential because enzyme reactions which involve these co-

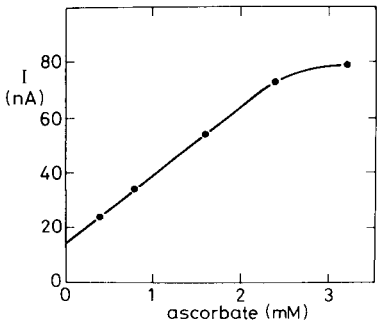

Fig. 4. Calibration curve of the microsomal electrode for ascorbate.

factors can be coupled to oxidase reactions. This has been demonstrated by glucose-6-phosphate determination with the microsomal electrode. Moreover, there is a great number of dehydrogenases which could be co-immobilized with the liver microsomes or added to the measuring solution to determine substances of analytical importance, such as isocitrate, ethanol or lactate.

Contrary to other proposed methods for pyridine nucleotide measurement, the microsomal electrode can be applied to crude solutions of any turbidity. Furthermore, protected by the oxygen-selective polyethylene membrane, the platinum sensor is insensitive to contamination by the sample. In this respect, it may well compete with the recently reported mitochondrial electrode [7, 8] which, however, responds only to NADH and not to NADPH.

Immobilized liver microsomes are shown to mediate complex reaction sequences at an oxygen electrode. This ability was utilized to measure glucose-6-phosphate without additional enzymes. Such multi-step reactions in bioelectrodes can be performed by two or more immobilized enzymes, too. However, when this latter approach is used, immobilization and operation conditions must be chosen carefully because of differences in the behaviour of the enzymes used. These problems can be overcome by the use of a single biocatalyst phase mediating the desired sequence, as was accomplished with microbial cells [23] and, as demonstrated here, with the liver microsomal fraction.

REFERENCES

1 G. G. Guilbault, Enzyme Microb. Technol., 2 (1980) 258.
2 F. Scheller and D. Pfeiffer, Z. Chem., 18 (1978) 50.
3 S. Suzuki and I. Karube, in Annals of the New York Academy of Sciences, Biochemical Engineering, Vol. 326, The New York Academy of Sciences, New York, 1979, p. 255.
4 G. A. Rechnitz, T. L. Riechel, R. K. Kobos and M. E. Meyerhoff, Science, 199 (1978) 440.
5 J. J. Kulys, Anal. Lett., 14 (1981) 377.
6 U. Wollenberger, F. Scheller and P. Atrat, Anal. Lett., 13 (1980) 825.
7 G. G. Guilbault, Lecture at Joint Meeting U.S.S.R.—U.S.A. on Applied Microbiology, Tallinn, U.S.S.R., 1977.

8 M. Aizawa, M. Wada, S. Kato and S. Suzuki, Biotechnol. Bioeng., 22 (1980) 1769.
9 M. A. Arnold and G. A. Rechnitz, Anal. Chem., 52 (1980) 1170.
10 F. Schubert, D. Kirstein, F. Scheller and P. Mohr, Anal. Lett., 13 (1980) 1167.
11 J. R. Gillette, B. B. Brodie and B. N. LaDu, J. Pharmacol. Exp. Ther., 119 (1957) 532.
12 G. Powis and I. Jansson, Pharmacol. Ther., 7 (1979) 297.
13 J. L. Holtzman, Pharmacol. Ther., 4 (1979) 601.
14 Y. Imai and R. Sato, J. Biochem. (Tokyo), 75 (1974) 689.
15 D. Baess, G.-R. Jänig and K. Ruckpaul, Acta Biol. Med. Ger., 34 (1975) 1745.
16 O. H. Lowry, N. J. Rosebrough, A. L. Farr and R. J. Randall, J. Biol. Chem., 193 (1951) 265.
17 E. Beutler and M. Morrison, J. Biol. Chem., 242 (1967) 5289.
18 Y. Hino and S. Minakami, Biochem. Biophys. Res. Commun., 98 (1981) 1016.
19 K. Kimura, H. Endou, J. Sudo and F. Sakai, J. Biochem. (Tokyo), 85 (1979) 319.
20 C. Bublitz, Biochem. Biophys. Res. Commun., 98 (1981) 588.
21 L. Ernster and K. Nordenbrand, in R. W. Estabrook and M. E. Pullman (Eds.), Methods in Enzymology, Vol. 10, Academic Press, New York, 1967, p. 574.
22 E. D. Willis, Biochem. J., 113 (1969) 315.
23 R. K. Kobos and H. Y. Pyon, Biotechnol. Bioeng., 23 (1981) 627.

Analytica Chimica Acta, 141 (1982) 23—32
Elsevier Scientific Publishing Company, Amsterdam — Printed in The Netherlands

DIRECT ELECTRON TRANSFER IN IMMOBILIZED FLAVOENZYME CHEMICALLY MODIFIED GRAPHITE ELECTRODES

ROBERT M. IANNIELLO, THOMAS J. LINDSAY and ALEXANDER M. YACYNYCH*
Department of Chemistry, Rutgers — The State University of New Jersey, New Brunswick, NJ 08903 (U.S.A.)

(Received 20th January 1982)

SUMMARY

Direct electron transfer between covalently immobilized flavoenzymes and a cyanuric chloride-modified graphite electrode is observed via differential pulse voltammetry. L-Amino acid oxidase and xanthine oxidase display peaks arising from the reduction of flavin adenine dinucleotide. Peak current enhancements are observed for both covalently attached enzymes compared to their free and adsorbed state voltammograms. Studies concerning flavin removal and reconstitution indicate that xanthine oxidase contains multiple flavin chromophores which are nonequivalent.

The development of chemically modified electrodes as selective chemical sensors is a relatively new application of these devices. It has been shown [1—5] that the intimate contact between the bonded active species and the electrode surface may result in a species-selective detector possessing superior response characteristics when compared to conventional methods. Most recently, various enzymes have been covalently attached to chemically modified carbonaceous electrode surfaces to yield amperometric [6—8] and potentiometric [9, 10] sensors. In some cases, covalent immobilization of the enzyme molecule may result in a unique conformational fixation of the enzyme on the electrode surface.

Fixation of enzyme conformation can lead to direct electron transfer between the enzyme active center and the electrode (i.e., oxidation or reduction of a metal ion or prosthetic group) if the electroactive species is accessible to the electrode surface. Direct electron transfer has been demonstrated for flavoenzymes [11, 12] and hemoproteins [13] adsorbed on a mercury electrode by using differential pulse polarography and cyclic voltammetry. For these systems, Hg—disulfide interaction apparently results in optimum orientation of the electroactive enzymatic centers towards the electrode surface.

Covalent attachment of an enzyme on a chemically modified graphite electrode can facilitate direct electron transfer without the drawbacks that occur with adsorption on a mercury electrode. While the molecule is secured in a fixed conformation on the electrode surface, protein flattening (common

0003-2670/82/0000-0000/$02.75

for enzymes adsorbed on mercury) is avoided because of the spacing provided by the linking agent. The direct electron transfer between covalently immobilized glucose oxidase and a graphite electrode has been recently reported [14]. Differential pulse voltammetry (d.p.v.) is used in this study because of its low detection limits, and in order to minimize the effects of charging current (which is substantial for carbonaceous electrodes). The possible advantages of direct electron-transfer enzyme electrodes as analytical sensors in a variety of applications has warranted a more detailed investigation of this phenomenon for other enzymes.

The purpose of this work is to report on the direct electron transfer between covalently attached enzymes and a cyanuric chloride-modified graphite electrode. As general examples, L-amino acid oxidase and xanthine oxidase, bound to modified electrodes, are examined by using differential pulse voltammetry. These enzymes contain flavin adenine dinucleotide (FAD) as the prosthetic group, which is reducible at the graphite electrode. Both covalently attached enzymes display fairly intense peaks between −0.51 and −0.54 V vs. Ag/AgCl reference electrode, which are of greater magnitude than those obtained for either the free or adsorbed species. Flavin adenine dinucleotide can be completely removed from the bound L-amino acid oxidase by treatment with 3 M KCl. This treatment, however, is effective in removing only 41% of FAD from the bound xanthine oxidase. A plausible explanation, based on the relative FAD compositions of the two enzymes, is presented.

EXPERIMENTAL

Apparatus and materials

Differential pulse voltammograms were recorded on a Model 364 polarographic analyzer and Model RE0073 X—Y recorder (Princeton Applied Research, Princeton, NJ). Voltammograms were recorded with experimental settings of 2 mV s^{-1} scan rate, 50-mV pulse amplitude, and +0.1 V (vs. Ag/AgCl) as the initial potential. For bulk electrolysis of the supporting electrolyte, a high-current potentiostat (ECO Inc., Cambridge, MA) was used in a three-electrode configuration. Spectroscopic-grade graphite, platinum wire (1-mm diameter), and Ag/AgCl (saturated KCl) were employed as the working electrode, auxiliary electrode, and reference electrode, respectively.

Xanthine oxidase (Type IX from buttermilk, 50 IU mg^{-1}) and L-amino acid oxidase (Type VI from *Crotalus atrox* venom, 0.33 IU mg^{-1}) were obtained from Sigma Chemical Co. These materials were stored in the dark at 0°C until used. Tris(hydroxymethyl)aminomethane (purified, Fisher Scientific Co.) was used for all buffer solutions. The supporting electrolyte (0.1 M Tris, pH 8.0) was electrolyzed at a mercury pool (−1.2 V vs. SCE) for 24 h before use. Cyanuric chloride (analytical grade) and lithium aluminum hydride (95+%; Aldrich Chemical Co.) were used as received.

High-purity nitrogen (>99.998%) was used. Graphite electrodes (spectroscopic grade, type AGKSP with conical ends, National Carbon Co.) were extracted with anhydrous methanol, dried at 120°C, and stored in vacuo at 2°C before chemical modification. Stock enzyme solutions were prepared from deoxygenated buffer and stored in the dark at 2°C. Distilled—deionized water was used for the preparation of all aqueous solutions. All other chemicals were of reagent grade.

Procedure

Graphite electrodes were subjected to chemical modification according to the scheme described previously [14]. The enzymes were covalently immobilized on cyanuric chloride-modified electrodes by reaction of the electrodes with concentrated enzyme solutions (see figure legends) for 0.5 h (L-amino acid oxidase) or 2 h (xanthine oxidase). It was found that these reaction times resulted in maximum peak heights. The electrodes were then washed three times each with cold distilled water, 1 M NaCl, and Tris buffer. Enzymes were adsorbed on graphite electrodes using the procedure described above. All procedures involving FAD incubation or enzyme immobilization were conducted in the dark to avoid FAD photodecomposition [15]. When necessary, the immobilized enzyme electrodes were stored in 0.1 M pH 8.0 Tris buffer at 2°C between trials.

Differential pulse voltammograms of both the enzyme solutions and immobilized enzyme electrodes were recorded by using the following procedure. Electrolyzed buffer solutions (2.0 ml) were pipetted into a 5.0-ml cell which was covered with a four-hole Lucite plate. Purified nitrogen (water saturated) was bubbled through the solutions for 15—30 min. During this time, the graphite electrodes were impregnated with mineral oil (Nujol). The appropriate stock solutions were then added to the cell. Because of the current limitations of the polarographic system employed in this study, the tip of the graphite electrode was immersed only 1 mm in the solution during voltammetric measurements. In the case of the enzyme electrodes, voltammograms were obtained in enzyme-free and FAD-free buffer solutions. All differential pulse voltammograms were recorded in the potential range +0.1 to —0.7 V vs. Ag/AgCl. Solutions were blanketed with water-saturated nitrogen during measurements.

RESULTS AND DISCUSSION

The enzymes used in this study can be considered to be "extremes" of the flavin-containing oxidase family of enzymes. L-Amino acid oxidase is a so-called "simple" flavoenzyme. It contains one FAD moiety per enzyme molecule which is solely responsible for its enzymatic activity [16]. The prosthetic group is loosely held and can be removed by simple incubation with salt solutions [17]. In contrast, xanthine oxidase is one of the most complex of the flavoproteins. It has been established [18—20] that the

enzymatic activity of the enzyme is due to a complex interaction of FAD, molybdenum, iron, and labile sulfur moieties at or near the active site. These species are present in the molar ratio 1:1:4:4, respectively. The enzyme contains two FAD moieties per enzyme molecule, which are independent (i.e., non-equivalent) redox centers [21]. Previous work has shown [20, 21] that xanthine oxidase resists complete removal of its flavin chromophores while in the native (oxidized) state.

The electrochemical behavior of L-amino acid oxidase does not seem to have been reported. In preliminary experiments, the electrochemical behavior of L-amino acid oxidase was investigated using differential pulse polarography (Hg working electrode). Peaks attributable to FAD and cysteinyl reduction were observed at —0.35 V and —0.68 V (vs. Ag/AgCl), respectively. This is quite similar to the behavior of D-amino acid oxidase [12].

The differential pulse voltammetric behavior of L-amino acid oxidase in solution at the graphite electrode is shown in Fig. 1. The peak observed at —0.51 V vs. Ag/AgCl can be attributed to the reduction of enzymatically bound FAD. This peak potential is about 50 mV more cathodic than that observed for reduction of free FAD [14]. The extent of adsorption of L-amino acid oxidase on graphite was investigated and yielded the voltammogram shown in Fig. 2. In this experiment, the electrode was washed only with Tris buffer prior to the measurement step in order to minimize removal of enzyme from the electrode surface. Adsorbed L-amino acid oxidase yields

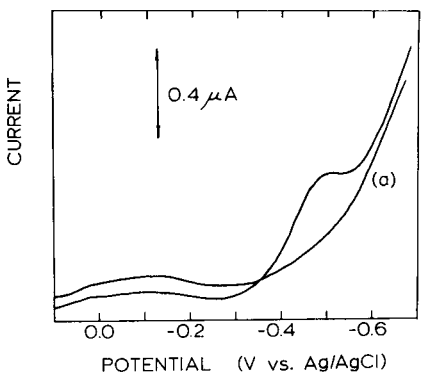

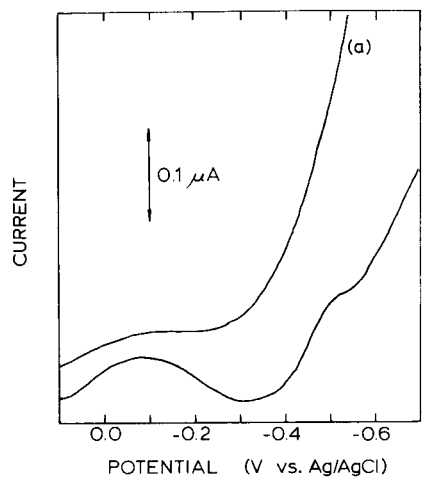

Fig. 1. Differential pulse voltammogram of 100 μM L-amino acid oxidase in 0.1 M pH 8.0 Tris buffer. (a) Background scan.

Fig. 2. Differential pulse voltammogram of L-amino acid oxidase adsorbed on graphite. Electrode was immersed in 1.9 mM enzyme solution (pH 8.0 Tris buffer) for 30 min and rinsed with Tris buffer prior to voltammetric measurement. (a) Response of same electrode after exposure to flowing stream (1.5 ml h^{-1}) of 3 M KCl for 15 h.

one reduction peak of identical peak potential but of significantly decreased current magnitude (ca. 15%), as compared with the free enzyme. One possible explanation of the phenomenon is that the orientation of the enzyme-bound FAD when L-amino acid oxidase is adsorbed is not favorable for prosthetic group reduction. Another explanation is that the adsorption process itself is not favorable, which results in low enzyme coverage on the electrode. Behavior of the former type has been observed for glucose oxidase [14]. Figure 2 also illustrates the effect of treating the adsorbed enzyme with 3 M KCl. As shown, this treatment is effective in removing the FAD reduction peak. In this instance, the result can be interpreted in two possible ways. One explanation is that the salt treatment removes the adsorbed enzyme molecule from the electrode surface. However, previous work has indicated that graphite electrodes retain (slightly) adsorbed flavoenzymes despite treatment with salt solutions [6]. The second explanation is that the enzyme-bound FAD is removed from the adsorbed L-amino acid oxidase molecule. This would be consistent with the behavior of a simple flavoenzyme [17].

The differential pulse voltammetric response of covalently attached L-amino acid oxidase is shown in Fig. 3. The FAD reduction peak, centered at −0.51 V, is of greater magnitude than both the free (1.5×) and adsorbed (9.8×) species. Considering that the solution concentrations and contact times were identical for all cases, the result for the covalently bonded enzyme may be interpreted as being due to a favorable conformational fixation of the molecule which efficiently exposes the prosthetic group to the electrode surface. Previous work with various enzymes adsorbed and covalently attached on carbonaceous materials has shown that, in spite of similar enzyme loadings in both cases, covalently bonded enzymes have higher specific activities [22]. This would lend credence to the explanation

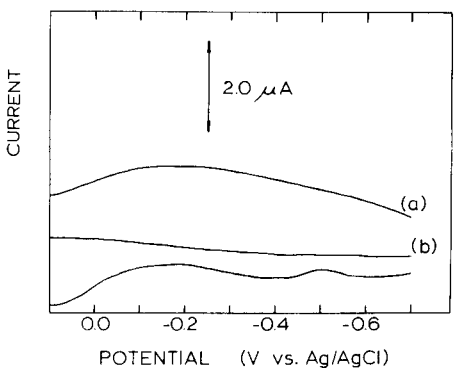

Fig. 3. Differential pulse voltammogram of covalently attached L-amino acid oxidase. Cyanuric chloride-modified electrode was immersed in 1.9 mM enzyme solution for 30 min and rinsed with distilled water, 1 M NaCl, and pH 8.0 Tris buffer. (a) Response of same electrode after exposure to 3 M KCl (see Fig. 2); (b) background scan.

of the results obtained for covalently attached enzymes in this study. Similar behavior has been observed for covalently attached glucose oxidase [14]. It should be noted that low instrumental sensitivity was used for the voltammogram of immobilized L-amino acid oxidase because of the unusually high background current observed; attempts to increase sensitivity resulted in instrumental current overload.

The differential pulse voltammetry of xanthine oxidase in solution is depicted in Fig. 4. A broad peak centered at —0.42 V is obtained, which can be attributed to FAD reduction. No specific peaks from molybdenum or iron sulfide complex reductions are observed. This is in contrast to the polarographic response of the enzyme, which is characterized by three waves arising from FAD, FeS, and sulfhydryl reductions [12]. Flavin reduction in free xanthine oxidase is about 40 mV more anodic than free FAD and 90 mV more anodic than free L-amino acid oxidase. This would indicate that the prosthetic group in xanthine oxidase is in an altered environment (compared to L-amino acid oxidase and adsorbed FAD) which results in its changed reduction potential. This situation (regarding reduction potentials) is completely reversed for xanthine oxidase and L-amino acid oxidase at the mercury electrode [12]. The extent of adsorption of xanthine oxidase at the graphite electrode was investigated and is shown in Fig. 5. The adsorbed enzyme is characterized by one peak (E_p = —0.52 V) which is due to FAD reduction. A significant cathodic shift of peak potential occurs for the adsorbed enzyme which may be the result of a somewhat unfavorable orientation of FAD, compared to free xanthine oxidase. It is interesting to note that after treatment with 3 M KCl, the reduction peak is not completely removed. One

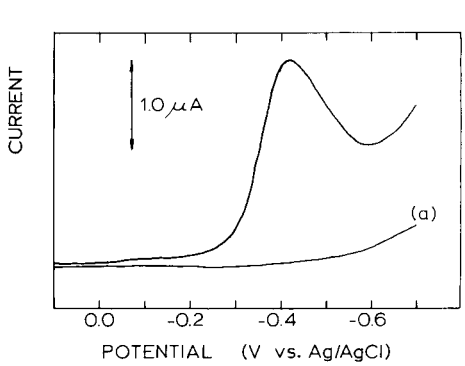

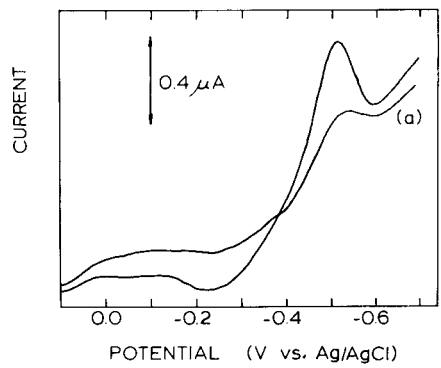

Fig. 4. Differential pulse voltammogram of 38 μM xanthine oxidase in pH 8.0 Tris buffer. (a) Background scan.

Fig. 5. Differential pulse voltammogram of xanthine oxidase adsorbed on graphite. Electrode was immersed in 38 μM enzyme solution (pH 8.0 Tris buffer) for 2 h and rinsed with Tris buffer prior to voltammetric measurements. (a) Response of same electrode after exposure to 3 M KCl (see Fig. 2).

obvious interpretation from this result is that the KCl treatment is not effective in removing all adsorbed enzyme. It is also apparent that the FAD which is removed is associated with the adsorbed xanthine oxidase molecule and not simply adsorbed (as free FAD) on the electrode surface. In addition, while the peak is significantly decreased compared to the untreated adsorbed enzyme (ca. 67% decrease), the peak which results is cathodically shifted by 20 mV. This result would indicate that the flavin chromophores in xanthine oxidase are non-equivalent. Previous work with this enzyme immobilized on cellulose has indicated the nonequivalence of the flavin moieties using kinetic methods [21].

Covalently attached xanthine oxidase yields the differential pulse voltammogram given in Fig. 6. An intense peak at −0.52 V is obtained which is of greater magnitude than those obtained for free (3.6X) and adsorbed (10.9X) xanthine oxidase. This trend is similar to that observed for covalently attached L-amino acid oxidase. Again, it can be envisioned that covalent attachment of the enzyme results in an improved orientation of the prosthetic group towards the electrode surface. At this point, it is of interest to note the differences in peak size between the two covalently attached enzymes. The much greater peak obtained for xanthine oxidase may be due to a combination of factors. First, this enzyme contains twice as much FAD per molecule as does L-amino acid oxidase. Second, the xanthine oxidase preparation employed is of much greater specific activity (higher purity) than L-amino acid oxidase. Hence, in the case of L-amino acid oxidase, it is possible that much of the bound protein is in an inert (FAD-free) form. Finally, the bonding which occurs for the two enzymes may involve different amino acid residues, resulting in an improved orientation of the FAD moiety for immobilized xanthine oxidase.

Of particular interest in this study was the behavior of the bound enzymes toward concentrated potassium chloride solutions. As mentioned previously,

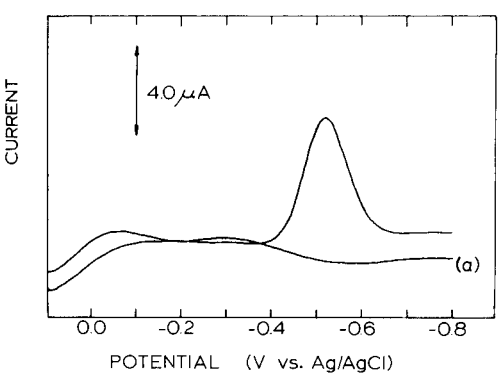

Fig. 6. Differential pulse voltammogram of covalently attached xanthine oxidase. Cyanuric chloride-modified electrode was immersed in 38 μM enzyme solution (pH 8.0 Tris buffer) for 2 h and rinsed with distilled water, 1 M NaCl, and Tris buffer. (a) Background scan.

the simple flavoenzymes will become devoid of enzymatic activity after exposure to salt solutions. This is due to dissociation of FAD from the enzyme molecule. On the other hand, flavoenzymes containing multiple, non-equivalent flavin moieties will resist complete flavin removal. In particular, it has been shown that milk xanthine oxidase can only be completely stripped of its FAD content after pre-reduction with xanthine [21] or treatment with calcium chloride [19]. Both types of enzyme can be reactivated, after FAD stripping, by incubating the apoenzyme with FAD. This type of behavior is demonstrated by the results presented in Table 1. Covalently attached L-amino acid oxidase and xanthine oxidase were subjected to salt treatment (to remove FAD), FAD incubation (to restore FAD), and further salt treatment (to again remove FAD). L-Amino acid oxidase became devoid of FAD content after the first solution exposure, in agreement with the properties of a simple flavoenzyme. Incubation with FAD resulted in a single peak (E_p = —0.51 V) of greatly increased magnitude compared with the immobilized enzyme. The reasons for this peak current enhancement are not understood. It is believed that free FAD adsorption, coupled with association of FAD with inert attached protein [12], is the primary contributors to the current response. Exposure of the reconstituted L-amino acid oxidase to 3 M KCl yields a reduced reduction peak, centered at —0.52 V. The fact that the resulting peak is of greater magnitude than that obtained for the covalently attached L-amino acid oxidase would be expected if adsorbed FAD were present. It is also believed that the enzyme active site may be slightly altered by salt treatment [23], resulting in the small cathodic shift of the reconstituted L-amino acid oxidase.

Covalently attached xanthine oxidase subjected to 3 M KCl results in a slightly shifted peak of reduced magnitude (ca. 41% reduction). Incubation of the salt-treated enzyme results in regeneration of 90% of the original FAD content of the enzyme. Further salt solution exposure results in a substantial cathodic shift of the FAD reduction peak. In addition, the peak magnitude is less than that obtained for the immobilized-stripped enzyme. The behavior

TABLE 1

Differential pulse voltammetric response of covalently immobilized enzyme electrodes

Enzyme	E_p (mV)	i_p (μA)	Enzyme	E_p (mV)	i_p (μA)
L-Amino acid oxidase			*Xanthine oxidase*		
Immobilized	—0.51	0.1	Immobilized	—0.52	5.5
Immob.-strip	no peak	0	Immob.-strip	—0.53	3.2
Incubated[a]	—0.51	6.9	Incubated[b]	—0.52	4.9
Inc.-strip	—0.52	1.9	Inc.-strip	—0.54	1.8

[a] C°_{FAD} = 100 μM in pH 8.0 Tris buffer; reacted for 0.5 h.
[b] C°_{FAD} = 100 μM in pH 8.0 Tris buffer; reacted for 2 h.

of bound xanthine oxidase may be interpreted in the following manner. It has been reported [19] that exposure of xanthine oxidase to certain salt solutions can result in partial denaturization of its nonflavin chromophores. If this is indeed the case, the salt solution treatment may modify the FAD and/or the active site. This is evidenced by the slight cathodic shift of peak potential after salt treatment. Incubation with FAD restores most of the original flavin content of the enzyme. It is conceivable that the salt treatment which follows removes both the added FAD and "modified" flavin (the form of this flavin is unknown). This study would add support to the belief in the presence of two independent redox centers (non-equivalent flavins) in milk xanthine oxidase.

Conclusions

Direct electron transfer between the enzyme active centers in L-amino acid oxidase and xanthine oxidase and a modified electrode surface has been demonstrated. Differential pulse voltammetry is shown to be a sensitive probe in this situation. The electrochemical results are in agreement with classical enzyme activity measurements in measuring the relative FAD content of the two enzymes. In addition, the non-equivalence of flavin moieties in xanthine oxidase is shown.

By the demonstration of direct electron transfer between covalently attached enzymes and the electrode surface, the construction of analytical probes which function by direct measurement becomes feasible. With direct electron transfer, current flow in the electrode would be directly linked to the enzyme-substrate interaction, and would not depend on monitoring reactants or products. Possible applications of this phenomenon are currently being investigated and will be reported later.

A. M. Y. thanks Biomedical Research Support Grants, the National Science Foundation (grant number CHE 8022237), the National Institutes of Health (grant number GM 28125-01) for research support, and Rutgers University for a Junior Faculty Fellowship. R. M. I. is thankful for the support of the American Chemical Society (Division of Analytical Chemistry) and the Procter and Gamble Company for the award of a Full Year Fellowship.

REFERENCES

1 G. T. Cheek and R. F. Nelson, Anal. Lett., 11 (1978) 393.
2 N. Oyama and F. C. Anson, J. Am. Chem. Soc., 101 (1979) 3450.
3 J. W. Siria and R. P. Baldwin, Anal. Lett., 13 (1980) 577.
4 J. F. Price and R. P. Baldwin, Anal. Chem., 52 (1980) 1940.
5 W. R. Heineman, H. J. Wieck and A. M. Yacynych, Anal. Chem., 52 (1980) 345.
6 R. M. Ianniello and A. M. Yacynych, Anal. Chem., 53 (1981) 2090.
7 C. Bourdillon, J. P. Bourgeois and D. Thomas, J. Am. Chem. Soc., 102 (1980) 4231.
8 R. Kamin and G. S. Wilson, Anal. Chem., 52 (1980) 1198.

9 R. M. Ianniello and A. M. Yacynych, Anal. Chim. Acta, 131 (1981) 123.
10 N. Yamamoto, Y. Nagasawa, M. Sawai, T. Sudo and H. Tsubomura, J. Immunol. Methods, 22 (1978) 309.
11 F. Sheller, G. Strand, B. Neumann, M. Kuhn and W. Ostrowski, Bioelectrochem. Bioenerg., 6 (1979) 117.
12 B. Kuznetsov, N. Mestechkina and G. Shumakovich, Bioelectrochem. Bioenerg., 4 (1977) 1.
13 F. Scheller, M. Janchen, J. Lampe, H.-J. Prumke, J. Blanck and E. Palecek, Biochim. Biophys. Acta, 412 (1975) 157.
14 R. M. Ianniello, T. J. Lindsay and A. M. Yacynych, Anal. Chem., 54 (1982) 1098.
15 B. Janik and P. J. Elving, Chem. Rev., 68 (1968) 312.
16 T. P. Singer and E. B. Kearney, Arch. Biochem., 29 (1950) 190.
17 V. Massey and B. Curti, J. Biol. Chem., 241 (1966) 3417.
18 V. Massey, P. E. Brumby, H. Komai and G. Palmer, J. Biol. Chem., 244 (1969) 1682.
19 H. Komai, V. Massey and G. Palmer, J. Biol. Chem., 244 (1969) 1692.
20 M. Kanda, F. O. Brady, K. V. Rajagopalan and P. Handler, J. Biol. Chem., 247 (1972) 765.
21 M. P. Coughlan and D. B. Johnson, Biochim. Biophys. Acta, 302 (1973) 200.
22 J. A. Osborn, R. M. Ianniello, H. J. Wieck, T. Decker, S. Gordon and A. M. Yacynych, Biotechnol. Bioeng., 24 (1982) in press.
23 D. B. Morrell, Biochem. J., 51 (1952) 657.

Analytica Chimica Acta, 141 (1982) 33—47
Elsevier Scientific Publishing Company, Amsterdam — Printed in The Netherlands

THE ELECTROANALYTICAL RESPONSE OF THE BILAYER LIPID MEMBRANE TO VALINOMYCIN: MEMBRANE CHOLESTEROL CONTENT

MICHAEL THOMPSON* and U. J. KRULL

Department of Chemistry, University of Toronto, 80 St. George Street, Toronto, Ont. M5S 1A1 (Canada)

(Received 20th April 1982)

SUMMARY

Under certain conditions the current—time response of the phosphatidyl choline bilayer membrane to valinomycin is biphasic. Residual, final, and first and second maximum currents have been measured for a series of membranes of different overall concentrations of cholesterol and its derivatives generated by oxidation. The factors contributing to the variation of results for particular membrane compositions are discussed. The first short-time maximum is not related to local concentration effects, but is likely associated with a perturbation of the membrane surface structure where transport parameters are changing with time. Thermal properties of membrane electrochemistry are also discussed.

The bilayer lipid membrane (BLM) exhibits properties which can allow sensitive [1—3] and potentially selective electrochemical measurements [4—16]. Previous work has shown that the prototype perturbant, valinomycin, which replaces the hydration component of complexed ions with a hydrophobic coat, results in a biphasic current—time course on its interaction with BLM [2, 3]. In order to rationalize this system, it is necessary to review the influence of membrane physical chemistry on the generation of the electrochemical signal. In this area an extensive body of both theoretical and experimental work has been concerned with the effects on particular membrane parameters by two distinct categories of probes, i.e., the hydrophobic organic ion and the ion-carrying organic complex. Interaction of probe characteristics such as net charge, physical size and hydrophobicity with membrane dipolar potential, fluidity, dielectric barrier shape, surface charge, thickness, and location of the probe adsorption plane are known to be important in determining the incorporation and kinetics in BLM [17—19].

The most striking examples of evidence for the existence of the dipolar potential involve studies using charged hydrophobic species to probe planar BLM of varying cholesterol content. Mono-olein membranes with increased cholesterol content exhibit significantly diminished conductance to positive ions [17, 18, 20], whereas increased condunctance is observed for negative species [17, 21, 22]. These results have been discussed in terms of the rela-

0003-2670/82/0000-0000/$02.75

tively large positive potential at the surface of the planar membrane which arises from layers of oriented molecular dipoles [23]. The surface potential is a function of the net perpendicular lipid headgroup dipole moment, which has its origin in the ester carbonyls for lipids such as phosphatidyl choline and headgroup-bound oriented water molecules [24—26]. N.m.r. studies have also indicated that a significant dipole vector caused by the zwitterionic headgroup nature can under certain conditions contribute to the perpendicular dipole moment [27—29]. Work involving infrared dichroism has indicated that a substantial contribution from the P—N vector may develop upon cholesterol incorporation into a lecithin membrane [30, 31]. Monolayers of mono-olein and lecithin have been found to possess potentials of +320 mV and +440 mV, respectively [32]. As the corresponding value for a cholesterol monolayer is +390 mV [33], it has been proposed that the surface potential will become increasingly positive for a mono-olein BLM of increased cholesterol content [19]. Conversely, the lecithin potential might be expected to decrease. However, the validity of this concept is questionable in view of the fact that the latter result has not been observed [32]. A direct correlation between surface potential and lipid/cholesterol content of a membrane should not be expected, for such a concept is based on the assumption that no lipid—cholesterol interaction occurs. It has been demonstrated that a complicated dipolar re-orientation arising from intermolecular interactions may occur, because the hydroxyl function of cholesterol appears to undergo hydrogen bonding to ester carbonyls [34, 35] and possibly also to the phosphate group of lecithins [30, 36]. These effects distort the net perpendicular dipolar vectors and directly affect the surface potential. A further important consideration with respect to dipolar potential is the nature of adsorption of the probe to the membrane. It appears that hydrophobic ions adsorb at the membrane/solution interface, whereas protein-like carrier molecules adsorb inside the dipolar layer at the hydrocarbon interface [17—19].

Fluidity of the membrane is associated with the internal motions and total viscosity of particular areas such as the hydrocarbon phase. Cholesterol serves to increase the viscosity of this phase in the same manner as an internal protein [22, 37]. Furthermore, addition of cholesterol in the case of lipid monolayers and vesicles has been found to result in a condensation effect [38—42], which serves to reduce fluidity with a general decrease in permeability [43]. Inherent lipid properties such as the number of double bonds in the hydrocarbon chain will also affect fluidity. For example, this parameter increases with greater chain unsaturation [18, 22]. Fluidity is also extremely sensitive to temperature. For pure lipid membranes, a transition temperature exists which is related to a change from a crystalline state to a liquid crystalline state (with a concomitant increase of fluidity) [44]. Such phase transitions alter greatly with increased cholesterol content [45, 46]. Temperature elevation of a membrane in the liquid crystalline state produces a general increase of fluidity [44].

Dielectric barrier height and shape is a function of the composition of the membrane with respect to cholesterol content and lipid/solvent characteristics. For example, increase of chain unsaturation results in a decrease of the height of the dielectric barrier [18]. This effect could possibly be due to a decrease in membrane thickness. The width of the BLM is partially determined by its solvent content. The formation of most membranes involves use of solvents ranging from *n*-octane to *n*-hexadecane; this eliminates mixed solvent problems that are encountered in methanol/chloroform systems [47]. An increase in thickness is generally observed for membranes formed from solvents [48, 49] and lipids (with identical headgroup structure) [50, 51] of shorter hydrocarbon chain length. In this respect, it is important to note that similar polar headgroup densities and, therefore, surface potentials and interactions, are found whether the membrane contains hydrocarbons or is solvent-free [32].

The net surface charge of membranes formed from charged lipids will be reflected as a contribution to the potential course over the membrane and can greatly affect a surface interaction with charged probes [52—55]. These processes can be predicted through the use of surface potential models such as the classical Gouy—Chapman theory [56].

The influence of the various parameters outlined above on the incorporation and kinetics of the two categories of membrane probe is summarized in Tables 1—3. These results indicate that hydrophobic ion kinetics are significantly affected by dipolar potential and membrane thickness while carrier kinetics are affected by dipolar potential and fluidity. In the present work, the possible effects of a number of these factors on the conductance of the BLM on interaction with valinomycin over specific time spans are evaluated through a study of current measurement with variation of membrane cholesterol content.

TABLE 1

Summary of membrane and transport parameters involved in regulating BLM electrochemistry

Subject	Variable	Definition
Membrane	d	Dielectric thickness
[19]	V_D	Dipolar potential
	C_m	Specific membrane capacity
Hydrophobic ion	K_i	Translocation rate constant
[19]	β	Partition coefficient, provides membrane surface concentration relative to that in solution
Carrier complex	K_{MS}	Translocation rate of complex
[19, 53, 57, 58]	K_S	Translocation rate of free carrier
	K_D	Rate constant of dissociation
	K_R	Rate constant of association
	γ_S	Partition coefficient
	K_H	Complex stability = K_R/K_D

TABLE 2

Summary of relationships between membrane and hydrophobic ion parameters

Ion[a]	Observation	Explanation	Ref.
TFB^- $CCCP^-$	Conductance increased with increasing cholesterol content of a mono-olein BLM	Increasing positive V_D with cholesterol content increases/decreases the negative/positive ion conductance, respectively. The ion charge and not the size or chemical properties determine conductance changes. The most important effect is a potential change and not that due to fluidity decrease.	20
TFP^+ CC_5^+	Conductance decreased		
DPA^-	Large K_i increases as change in solvent from *n*-octane to *n*-hexadecane	Decrease thickness *d*	18
DPA^-	β decreases as number of double bonds increases		18
DPA^-	β insensitive to cholesterol content for dioleoyllecithin BLM, but K_i increases	Dipolar layers affect β and K_i, but this depends on the position of the adsorption plane. If the adsorption plane is at the membrane/aqueous interface, then V_D acts only on K_i.	18
DPA^-	K_i increases as cholesterol content of mono-olein membrane increases	V_D increases and thickness *d* decreases	19
DPA^-	Increased K_i for dioleoyllecithin membranes + *n*-decane as cholesterol content increases	Decrease in *d*	18, 19
TFB^-	Increased K_i for mono-olein membranes + *n*-decane as cholesterol content increases	V_D increase, decrease in *d*	17, 19
DPA^-	K_i increases for mono-olein membrane + *n*-hexadecane as cholesterol content increases	V_D increase, no substantial change in *d*	19
DPA^-	β increases, K_i decreases in lecithin membranes compared to phosphatidyl ethanolamine membranes	Stronger interaction of ion with lecithin headgroup	18

[a]TFB^- tetraphenylborate; CC_5^+ 3,3'-dipropyloxadicarbocyanine iodide; $CCCP^-$ carbonylcyanide *m*-chlorophenylhydrazone; DPA^- dipicrylamine; TFP^+ tetraphenylphosphonium.

EXPERIMENTAL

Reagents and equipment

The lipid used exclusively for BLM formation was lyophilized egg phosphatidyl choline (Avanti Biochemicals, Birmingham, AL). The membrane

TABLE 3

Summary of relationships between membrane and valinomycin (carrier) parameters

Ion	Observation	Explanation	Ref.
Rb^+	K_{MS} almost insensitive to variation in d of mono-olein membranes as caused by hydrocarbon solvents	The large size of the complex implies considerable sensitivity to fluidity and a possible compensation effect occurs between fluidity and the dielectric barrier	18
Rb^+	K_H, K_R, K_S, K_{MS} reduce for mono-olein membrane + *n*-hexadecane as cholesterol content increases	K_S, K_{MS} reduction due to reduced fluidity. K_R reduced due to increased surface potential which reduces K_H. As V_D increases greater barrier to Rb^+ transfer from solution so that K_R decreases	19
Rb^+	γ_s increases with increasing cholesterol content for a glycerol mono-oleate membrane + *n*-decane		22
K^+	Negative temperature coefficient of γ_s		30
Rb^+	Only a small effect on transport is observed as cholesterol content increases in dioleoyllecithin membranes		18

probe utilized in this work was valinomycin (Sigma Chemical Co., St. Louis, MO). The cholesterol used to form membranes was partially oxidized and consisted of an initial ratio of 65% cholesterol/35% oxidation products. All other chemicals were of reagent grade.

The membrane support consisted of a teflon sheet (0.1 mm thick) with a circular orifice (1 mm diameter) separating two identical aqueous compartments of 6-ml volume in a perspex cell. Transmembrane current was monitored using single-junction silver—silver chloride electrodes (Orion Research, Cambridge, MA) in conjunction with a microprocessor-controlled digital electrometer (Keithley, Cleveland, OH) as previously described [3]. An in-house temperature controller utilizing a heating tape, hot plate and thermistor control was used to attain elevated temperatures.

Procedures

The BLM were formed by a brusn technique from *n*-decane solutions containing lipid/cholesterol in 2%/0.25% to 2%/4% (w/v) ratio ranges as previously described [1, 3]. The teflon support was pretreated by applying a thin coat of the membrane-forming solution on the polymer surface around the aperture, allowing the film to air-dry. Teflon was first cleaned by strong base and chromic acid treatments. Lipid-forming solutions were monitored by

thin-layer chromatography and the purity of lipid and cholesterol was determined on a continual basis.

Membranes were formed under an applied potential (+10 mV) and the probe was introduced to the stirred 0.1 M KCl electrolyte in one aqueous compartment by variable-volume pipette. To avoid problems associated with the presence of excess of membrane-forming solution arising from the brush technique, as performed in one solution compartment, probe additions were performed in the other compartment. Numerous variations with respect to stir modes, probe solutions and probe addition techniques were examined to determine effects on the current—time profile. Experiments requiring elevated temperatures were initiated as described at room temperature and consisted of preparing a stable membrane. After a ramping of ca. 10°C/5 min, the system was allowed to reach equilibrium and a delay period of 10 min elapsed before probe addition.

RESULTS AND DISCUSSION

Response variation

Figure 1 shows typical biphasic current—time profiles obtained on addition of valinomycin to a lecithin membrane [3]. The current level before addition of antibiotic will be termed the "residual current". The two peaks are identified as the "first maximum" and "second maximum" with respect

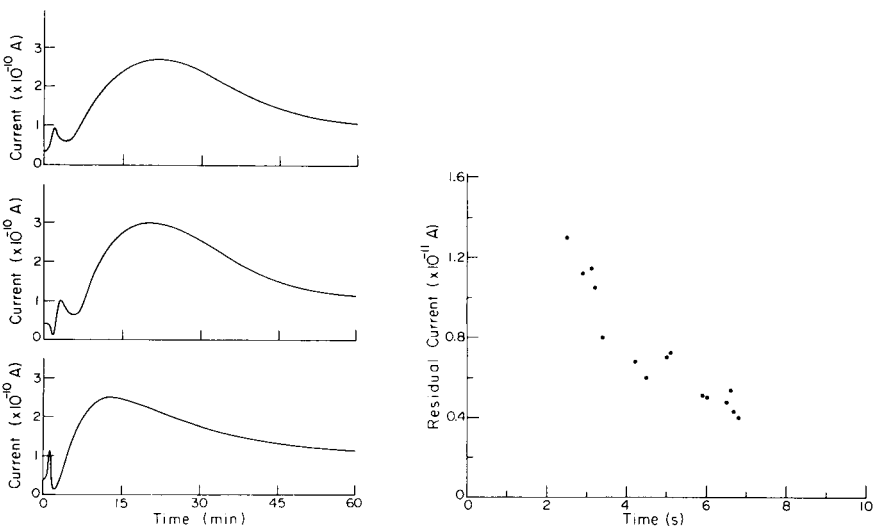

Fig. 1. Current—time profiles generated by BLM response to valinomycin, illustrating three common trends observed when first maximum evolution exists.

Fig. 2. Variation of BLM residual current as a function of membrane charging time, indicating substantial differences in the physical properties of a sequence of membranes formed from one lipid/solvent solution.

to time. After a period of 60—90 min, the signal generally decays to an approximately constant value, which will be referred to as the "final current". It should be noted that if a period of hours elapses, the final current may increase significantly because of equilibration of partitioning of valinomycin and possibly further membrane thinning caused by the slow extrusion of *n*-decane [44]. The magnitude of these signals has been measured for membranes with variation of overall content of cholesterol. The incorporation of the sterol offers alteration of the intra-membrane physical chemistry outlined above in addition to the usual increase in planar membrane strength and stability. In attempts to rationalize the results of the study, it is important to recognize the factors that contribute to experimental reproducibility in this area of electrochemistry.

Incorporation of the sterol in an unmodified form alone does not significantly affect membrane durability. The material must first undergo an oxidative transformation to an entity with increased polarity. This is easily achieved by refluxing the parent compound in an oxygen atmosphere [59], and also, as was shown in the present work, by storage in hydrocarbon solutions at ambient conditions. At least fifty derivatives are involved in the autooxidation of cholesterol [60]; we have shown that only approximately fifteen are produced in sufficient quantities to be deemed important. The complex mixture may contain substances of both membrane stabilizing and destabilizing influence though the former seems predominant. Analysis indicates that conversion of the cholesterol hydroxyl group and B-ring unsaturation to more polar moieties assists membrane stabilization. Formation and rearrangements with respect to ring position of carbonyl, peroxide and hydroxyl residues at the A and B ring positions are common [60]. Similarly, peroxides and other polar residues can form at the hydrocarbon chain position [61] which would cause inherent membrane destabilization.

The variability in the concentration of cholesterol and its array of derivatives in membranes produced from an identical solution is clearly one factor which will result in adverse effects on reproducibility. The ratio of derivative concentrations continually varies with time as more stable compounds are produced. This process can readily be observed as a reduction of cholesterol in the membrane-forming mixture. In this work, the initial cholesterol content accounted for about 65% of the total partially-oxidized cholesterol sample used to prepare membranes. After storage for a period of one to two weeks (daily 8 h at ambient room conditions, 16 h in darkness below 0°C), the cholesterol content decreased to approximately 40% on a molar basis. (Most results quoted were obtained for 55—45% cholesterol mixtures.) It is important to note that lipid oxidation at unsaturated double bonds in the hydrocarbon chains also occurs, resulting in the introduction of a polar residue into the BLM hydrocarbon zone. It was found that extensive lipid oxidation results in membrane destabilization and occurs rapidly as the cholesterol content of the BLM-forming solutions decreases because cholesterol can act as an antioxidant. In addition to the question of membrane

oxidative chemistry, it has been shown that a solution prepared from known quantities of lipid and cholesterol may not produce membranes composed of an identical ratio of these two compounds [62].

A further problem which may cause significant variation in the physical nature of the planar membrane and, therefore, in the observed electrical characteristics, lies in the method of lipid introduction to the support aperture by the brush technique. Charging time experiments have been interpreted in terms of variation of membrane thickness and torus volume [59]. These factors are undoubtedly responsible for the electrical diversity depicted in Fig. 2.

The specific current measurements vs. overall cholesterol level in the membrane are given in Figs. 3—6 and are accompanied by representation of the 80% confidence level about a mean value. The large deviation about the mean certainly reflects an accumulation of variation from the sources discussed above. Unfortunately, more extensive sampling will not readily reduce this spread in view of the present experimental method.

Residual and final current

This work provides no direct experimental evidence as to the identity of the membrane-permeable ion, but because of the large positive dipolar potential of bilayer lipid membranes formed from lecithins [32], an applied potential across the membrane is expected to produce net movement of anion between solution compartments [32, 63]. For the potassium chloride electrolyte solution used in this work, the quantity of chloride crossing the membrane may be up to two to three orders of magnitude greater than potassium ion [63]. The silver—silver chloride electrodes, being sensitive to chloride ion activity, can be used to observe the minute current flux.

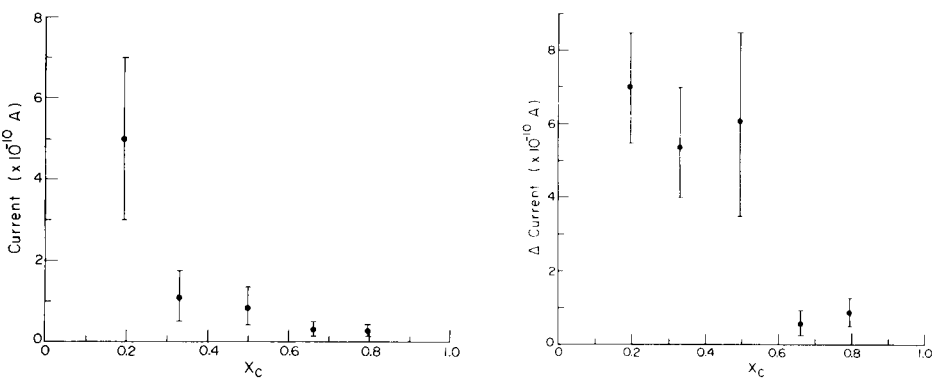

Fig. 3. BLM residual current as a function of total mole fraction of cholesterol and its oxidation-derived products. (Error bars represent 4—6 determinations at each mole fraction cholesterol content at around the 80% confidence level of the mean value for Figs. 3—6.)

Fig. 4. The final carrier-mediated current for valinomycin as measured from the initial residual BLM current indicating a strong dependence on cholesterol concentration.

The relationship of residual current to the cholesterol content of the membrane, the latter expressed as the mole fraction (X_C) of total lipid/cholesterol, is illustrated in Fig. 3. The most significant feature is the initial rapid decrease in current in the range of 0.2—0.35 mole fraction of cholesterol. For such lecithin membranes containing *n*-decane solvent, the incorporation of cholesterol may produce the following important effects: a reduction of membrane width [19], a decrease in internal membrane fluidity [22, 37], and a possible decrease in dipolar potential [19]. A reduction of the width of the hydrophobic barrier should cause an increase in the observed background current. Because this reduction is significant for membranes containing *n*-decane as the cholesterol content increases, it must be assumed that the dominant process is both in opposition to, and much greater in effect than width reduction. Whether fluidity effects will prevail in this case is questionable because they appear to have little effect on small hydrophobic ions in comparison with dipolar potential [19]. Furthermore, a reduction of the positive dipolar potential may not occur to a significant extent [32]. However, it is plausible that both the effects act in concert to yield the diminishing current with respect to cholesterol content depicted in Fig. 3. It is interesting to note that intermolecular electrostatic interactions between phosphatidyl choline headgroups diminishes to insignificance at mole fraction cholesterol contents of ca. 0.3 [27, 64, 65].

The final (carrier-mediated) current measured from the residual current shows a rapid reduction at a mole fraction of membrane cholesterol content of about 0.5 (Fig. 4). The current is governed by the kinetics and membrane partitioning of valinomycin. The rate constants, K_{MS} and K_S, would be expected to decrease as fluidity diminishes [19]. Concomitantly, a competitive increase in the two constants may occur as membrane thickness decreases, which appears to become significant at high cholesterol contents. This has been shown in some instances completely to negate effects associated with fluidity [18]. Because the valinomycin adsorption plane is probably located between the hydrocarbon phase and dipolar headgroups, the partition coefficient may also be affected [18]. In addition, the net decrease in positive dipolar potential caused by increasing cholesterol content would reduce the permeation barrier for potassium ions from the aqueous solution to the valinomycin adsorption plane (and increase K_R and K_H).

Although a compromise between the above factors clearly determines the final current, it appears that fluidity reduction is largely responsible for the current decrease at $X_C \approx 0.5$. At high cholesterol content, the variation of fluidity may be minimal so that decreasing membrane thickness, which becomes significant at mole fraction cholesterol contents above 0.6 [18], and dipole potential could result in a reversal of the afore-mentioned trend. It should be emphasized that there is some doubt associated with the assumption of homogeneity of membranes of very high cholesterol content, although the procedures used to prepare membranes in this work should still produce homogeneous membranes at cholesterol mole fractions of 0.6—0.7 [66].

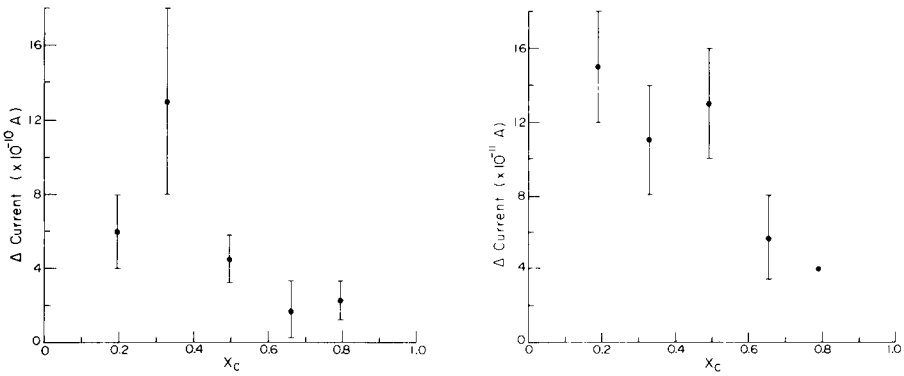

Fig. 5. The effect of cholesterol concentration on the valinomycin-induced second current maximum, the change in current being measured relative to the initial BLM residual current.

Fig. 6. The magnitude of current increase for the valinomycin-induced first current maximum as a function of mole fraction cholesterol content.

Dealing with the second maximum first, we note that there is a significant reduction in the carrier-mediated current, measured from the residual value, between $X_C = 0.4$ and 0.5 (Fig. 5). These results are similar to those expressed for the final current above, and are likely due to fluidity and dipolar potential changes. However, the current—cholesterol content curve shows peak behaviour at around $X_C = 0.3$. This is in complete contrast to the substantial residual current decrease observed over the same range and is attributed, therefore, to a dipolar potential decrease and/or an increase in the partition coefficient for valinomycin (because a large probe concentration exists at the membrane/solution interface).

Turning to the first current maximum, possible explanations for the effect lie in a current "surge" caused by a concentration gradient, where no changes in transport parameters are involved, or genuine membrane permeability associated with increased carrier and/or free ion transport. With respect to the former various experiments were conducted which involved very rapid mixing in the aqueous compartment, introduction of excess of lipid/solvent to act as an extraction medium, probe additions on either side of the membrane and probe additions in close proximity to, and far away from, the membrane surface (including concentration studies). There was no correlation with the appearance of the first current maximum. Recent work involving flowing streams, analogous to a flow injection system, has shown that the two maxima are still evident and, therefore, are not caused by a concentrated transient plug of electroactive material [67]. In this system, membrane saturation with valinomycin produced a first signal substantially larger than the second, indicating that a membrane perturbation effect is present. This is further substantiated by recently published experiments involving the surface perturbation of membranes which already contained

valinomycin [68, 69]. The result was a transient increase in current flux which was directly related to surface perturbation. Experiments involving the use of materials known to interact with membrane surfaces and which can potentially cause dipolar perturbation have also produced transient current fluxes upon membrane interaction [70].

The current profile observed for the first maximum measured from the residual current with respect to cholesterol content (Fig. 6) is similar to that observed for the final current. This may indicate that the same membrane parameters control both processes and, therefore, the first current maximum relates to permeation of the potassium-valinomycin complex.

It has been noted that the incorporation of hydrophobic ions into a membrane should result in membrane perturbation because these species are of significant size [18]. This effect should be even more evident for the valinomycin complex because it is much larger than most hydrophobic ion probes. Furthermore, its adsorption plane lies under the dipolar layer. Such a perturbation should result in the disorientation of the lipid and cholesterol dipoles, effectively causing a net reduction of the positive dipolar potential. This would immediately have an impact on the residual current, which should significantly decrease, and on the carrier-mediated current which will greatly increase because of K_R and K_H. The effect should be somewhat synergic in action in that as more valinomycin enters the membrane, the dipolar potential will further decrease, amplifying and assisting the carrier-mediated process. Valinomycin, in contrast to cholesterol, is known to increase membrane fluidity [71]. This will also enhance the carrier-ion current. It is apparent that the nature of the current—time signal associated with the surface dipole perturbation will be dependent on the concentration of the antiobiotic at the membrane surface and membrane fluidity. Finally, the possible influence of the expected membrane-induced conformational change of valinomycin cannot be ruled out. Although the current increase will not be generated by the sweeping out of conformational volumes, such a structural change may be partially responsible for disturbing the dipole matrix.

Thermal properties

It is generally the case that raising the temperature of a specific membrane results in an increase of fluidity [44]. The increase of residual current with temperature shown in Fig. 7 confirms that fluidity effects are important in controlling the ion flux involved in Fig. 3. Yet, increase of internal motion in the membrane may lead to a reduction of the net positive dipolar potential. For valinomycin, this implies that an increase of carrier current may occur, because K_S and K_{MS} are fluidity-related and K_R may also be increased by a reduced potential barrier. It appears that only the partition coefficient decreases with increase in temperature [44].

The time required to reach the second current maximum decreases with increasing temperature, but is greater for membranes of lower cholesterol content in the small range investigated (Fig. 8). Moreover, it is clear that

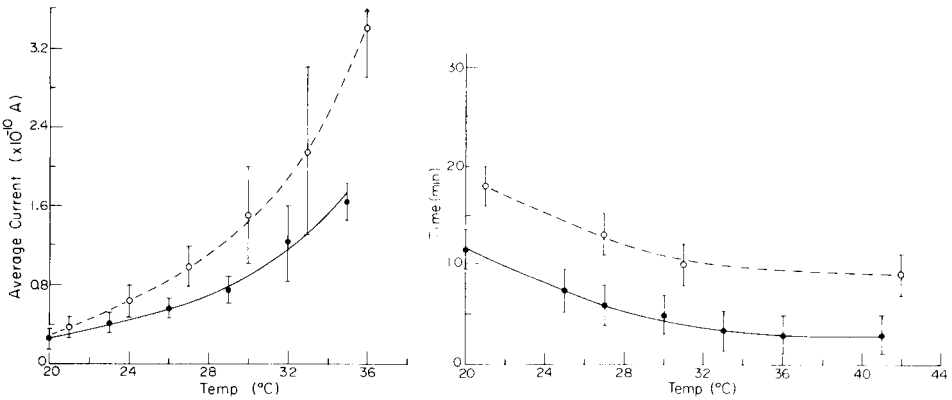

Fig. 7. The influence of temperature on the residual current of BLM compared from lipid solutions containing two different cholesterol contents: (○) $X_C = 0.66$; (●) $X_C = 0.80$.

Fig. 8. Time required for evolution of the second current maximum for valinomycin response as a function of temperature: (○) $X_C = 0.66$; (●) $X_C = 0.80$.

there is a substantial difference in the current for the second maximum (measured relative to residual current) with respect to the sterol/lipid ratio (Fig. 9).

A comparison of these curves suggests that when two particular systems require approximately the same period of time to reach the second current maximum, the relative change in currents are similar. The results also indicate that greater relative current changes can be attained if the maximum can be forced to appear in a shorter time.

The results of these experiments indicate that the relative effects of changes in fluidity, dipolar potential and partitioning are more significant for membranes of higher cholesterol content in this content range. However,

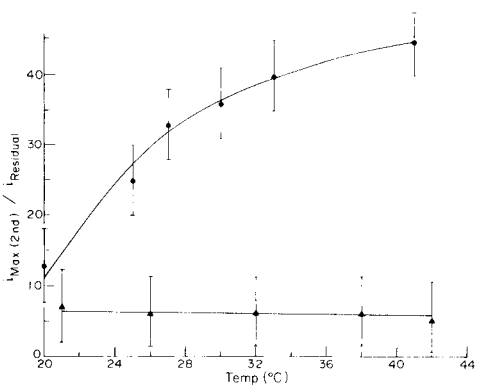

Fig. 9. The valinomycin-generated relative current increase at the second current maximum as a function of temperature: (▲) $X_C = 0.80$; (●) $X_C = 0.66$.

any attempt to explain differences in this range must be tempered with the knowledge that membranes of mole fraction cholesterol content above 0.8 may not be homogeneous. Limitations in signals derived from membrane probes occur and indicate a solubility saturation of the probe in the membrane [72] as observed for current—time profiles which do not reach a point of second current maximum but instead show a maximum plateau region. Such current saturation effects will undoubtedly be observed for selective surface interactions also. Perhaps one of the most interesting results from the temperature experiments is the indications of criteria necessary for the development of curves as in Fig. 1. Membranes of high cholesterol content most often develop current—time profiles which in contrast to first maximum generation, have a barely resolved first maximum merged into the second maximum. An elevation of temperature for identical membranes and subsequent probe addition can eventually resolve the two maxima clearly, suggesting that membrane fluidity may play an important role, as expected.

We are indebted to the Natural Sciences and Engineering Research Council of Canada for support of this work and for the award of a Fellowship to U. J. K. Also, we are particularly appreciative of funds for equipment provision from the Atkinson Foundation, Toronto.

REFERENCES

1 M. Thompson, P. J. Worsfold, J. Holuk and E. A. Stubley, Anal. Chim. Acta, 104 (1979) 195.
2 P. J. Worsfold, Ph. D. Thesis, University of Toronto, 1980.
3 M. Thompson, U. J. Krull and P. J. Worsfold, Anal. Chim. Acta, 177 (1980) 121.
4 E. Toro-Goyco, A. Rodriguez and J. del Castillo, Biochem. Biophys. Res. Commun., 23 (1966) 341.
5 J. del Castillo, A. Rodriguez, C. A. Romero and V. Sanchez, Science, 153 (1966) 185.
6 J. del Castillo, A. Rodriguez and C. A. Romero, N. Y. Acad. Sci. Ann., 144 (1967) 803.
7 M. H. Jain, L. E. Mehl and E. H. Cordes, Biochem. Biophys. Res. Commun., 51 (1973) 192.
8 W. Leuzinger and M. Schneider, Experientia, 28 (1972) 256.
9 K. Kaufman and I. Silman, Naturwissenschaften, 67 (1980) 608.
10 O. V. Kolomytkin and L. N. Yermishkin, Biophysics, 21 (1976) 1031.
11 M. T. Tosteson, F. Lau and D. C. Tosteson, Nat. Biol., 243 (1973) 112.
12 J. D. Mountz and H. Ti Tien, in A. N. Martinosi (Ed.), The Enzymes of Biological Membranes, Vol. 1, Plenum, New York, 1976.
13 M. Parisi, T. A. Reader and E. de Robertis, J. Gen. Physiol., 60 (1972) 454.
14 G. Kemp, J. O. Dolly, E. A. Barnard and C. E. Werner, Biochem. Biophys. Res. Commun., 54 (1973) 607.
15 H. Schindler and U. Quast, Proc. Natl. Acad. Sci., U.S.A., 77 (1980) 3052.
16 E. Fesenko and G. Ya. Pervukhin, Stud. Biophys., 58 (1976) 215.
17 G. Szabo, in M. R. Heinrich (Ed.), Extreme Environment; Mechanism of Microbial Adaptation, Academic Press, New York, 1976.
18 R. Benz and P. Läuger, Biochim. Biophys. Acta, 468 (1977) 245.
19 R. Benz and D. Cros, Biochim. Biophys. Acta, 506 (1978) 265.

20 G. Szabo, Nature, 252 (1974) 47.
21 G. Szabo, G. Eisenman and S. Ciani, J. Membr. Biol., 1 (1969) 346.
22 R. Benz, O. Frölich and P. Läuger, Biochim. Biophys. Acta, 464 (1977) 465.
23 S. B. Hladky and D. A. Haydon, Biochim. Biophys. Acta, 318 (1973) 464.
24 F. Paltauf, H. Hauser and M. C. Philips, Biochim. Biophys. Acta, 249 (1971) 539.
25 M. M. Standish and B. A. Pethica, Trans. Faraday Soc., 64 (1968) 1113.
26 K. C. Sehgal, W. F. Pickard and C. M. Jackson, Biochim. Biophys. Acta, 552 (1979) 11.
27 M. F. Brown and J. Seelig, Biochemistry, 17 (1978) 381.
28 M. F. Brown and J. Seelig, Nature, 269 (1977) 721.
29 H. Hauser, W. Guyer, B. Levine, P. Skrabal and R. J. P. Williams, Biochim. Biophys. Acta, 508 (1978) 450.
30 S. P. Verma and D. F. H. Wallach, Biochim. Biophys. Acta, 330 (1973) 122.
31 S. P. Verma, D. F. H. Wallach and I. C. P. Smith, Biochim. Biophys. Acta, 345 (1974) 129.
32 D. A. Haydon, N. Y. Acad. Sci. Ann., 264 (1975) 2.
33 N. K. Adam, The Physics and Chemistry of Surfaces, Dover, New York, 1968.
34 N. P. Franks, J. Mol. Biol., 100 (1976) 345.
35 D. L. Worcester and N. P. Franks, J. Mol. Biol., 100 (1976) 359.
36 A. Darke, E. G. Finer, A. G. Flook and M. C. Philips, J. Mol. Biol., 63 (1972) 265.
37 U. Cogan, M. Shinitzky, G. Weber and T. Nishida, Biochemistry, 12 (1973) 521.
38 B. A. Pethica, Trans. Faraday Soc., 50 (1955) 1402.
39 R. A. Demel and B. de Kruyff, Biochim. Biophys. Acta, 457 (1976) 109.
40 E. Oldfield, D. Chapman and W. Derbyshire, FEBS Lett., 16 (1971) 102.
41 J. L. Lippert and W. L. Peticolas, Proc. Natl. Acad. Sci. U.S.A., 68 (1971) 1572.
42 G. W. Stockton and I. C. P. Smith, Chem. Phys. Lipids, 17 (1976) 251.
43 J. de Gier, J. G. Mandersloot and L. L. M. van Deenen, Biochim. Biophys. Acta, 150 (1969) 666.
44 G. Stark, R. Benz, G. W. Pohl and K. Janko, Biochim. Biophys. Acta, 266 (1972) 603.
45 B. D. Ladbrooke, R. M. Williams and D. Chapman, Biochim. Biophys. Acta, 50 (1968) 333.
46 P. R. Cullis, B. de Kruyff and R. E. Richards, Biochim. Biophys. Acta, 426 (1976) 433.
47 R. Fettiplace, L. G. M. Gordon, S. B. Hladky, J. Requena, H. P. Zingsheim and D. A. Haydon, Methods in Membrane Biology, 4 (1975) 1.
48 R. Fettiplace, D. M. Andrews and D. A. Haydon, J. Membr. Biol., 5 (1971) 277.
49 S. H. White, Biophys. J., 15 (1975) 95.
50 R. Benz, O. Fröhlich, P. Läuger and M. Montal, Biochim. Biophys. Acta, 394 (1975) 323.
51 J. Requena and D. A. Haydon, Proc. R. Soc. London, Ser. A, 347 (1975) 161.
52 R. C. MacDonald and A. D. Bangham, J. Membr. Biol., 7 (1972) 29.
53 G. Stark and R. Benz, J. Membr. Biol., 5 (1971) 133.
54 S. G. A. McLaughlin and H. Harary, Biochemistry, 15 (1976) 1941.
55 S. G. A. McLaughlin, G. Szabo, G. Eisenman and S. M. Ciani, Proc. Natl. Acad. Sci. U.S.A., 67 (1970) 1268.
56 R. C. MacDonald and A. D. Bangham, J. Membr. Biol., 7 (1972) 29.
57 P. Läuger and G. Stark, Biochim. Biophys. Acta, 211 (1970) 458.
58 G. Stark, B. Ketterer, R. Benz and P. Läuger, Biophys. J., 11 (1971) 981.
59 H. Ti Tien, Bilayer Lipid Membranes, Dekker, New York, 1974.
60 G. A. S. Ansari and L. L. Smith, J. Chromatogr., 175 (1979) 307.
61 L. L. Smith, W. S. Matthews, J. C. Price, R. C. Bachmann and B. Reynolds, J. Chromatogr., 27 (1967) 187.
62 R. E. Pagano, J. M. Ruysschaert and J. R. Miller, J. Membr. Biol., 10 (1972) 11.
63 M. K. Jain, The Bimolecular Lipid Membranes, Van Nostrand Reinhold, New York, 1972.
64 P. L. Yeagle, W. C. Hutton, C. Huang and R. B. Martin, Biochemistry, 16 (1977) 4344.
65 R. A. Haberkorn, R. G. Griffin, M. D. Meadows and E. Oldfield, J. Am. Chem. Soc., 99 (1977) 7353.

66 R. A. Demel and B. de Kruyff, Biochim. Biophys. Acta, 457 (1976) 109.
67 M. Thompson and U. J. Krull, Anal. Chim. Acta, 141 (1982) 49.
68 P. Smejtek, M. Paulis-Illangasekare and K. Hsu, Biophys. J., 25 (1979) 180a.
69 N. R. Clement and J. M. Gould, Biochemistry, 20 (1981) 1539.
70 H. P. Ting-Beall, D. J. Benos, J. E. Hall and D. C. Tosteson, Biophys. J., 15 (1975) 308a.
71 H. Susi, J. Sampugna, J. W. Hampson and J. S. Ard, Biochemistry, 18 (1979) 297.
72 E. A. Liberman and V. P. Topaly, Biochim. Biophys. Acta, 163 (1968) 125.

Analytica Chimica Acta, 141 (1982) 49—56
Elsevier Scientific Publishing Company, Amsterdam — Printed in The Netherlands

THE ELECTROANALYTICAL RESPONSE OF THE BILAYER LIPID MEMBRANE TO VALINOMYCIN: AN EMPIRICAL TREATMENT

MICHAEL THOMPSON* and U. J. KRULL

Department of Chemistry, University of Toronto, 80 St. George Street, Toronto, Ont. M5S 1A1 (Canada)

(Received 20th April 1982)

SUMMARY

A previous kinetic and partitioning model for the interaction of valinomycin with the phosphatidyl choline bilayer membrane is adapted to account for unilateral addition and antibiotic loss via the torus and excess lipid/solvent sinks. A model for the biphasic current response is discussed.

The current—time response of the bilayer lipid membrane (BLM) to the ion carrier valinomycin has been shown to be biphasic [1]. In the preceding paper [2], the possible roles of membrane dipolar potential, fluidity, dielectric barrier shape, surface charge and thickness on the conductance of the BLM on interaction with valinomycin were discussed in terms of a study of current measurement over specific time spans with variation of membrane cholesterol content. Analysis of residual, first and second maximum currents implies that the short-time signal is caused by perturbation of the intramembrane surface dipole potential. In the present work, a previous quantitative model [3—7] that includes kinetic and partitioning parameters for addition of the antibiotic to both sides of the BLM is used to derive an empirical description of the biphasic current behaviour of unilateral addition. The model has been structured to account for valinomycin loss to the Plateau-Gibbs border and the excess lipid/solvent sink associated with membrane preparation.

EXPERIMENTAL

The reagents, apparatus and procedures used have been completely described [2]. In summary, lyophilized egg phosphatidyl choline—cholesterol membranes were prepared using a brush technique on teflon supports with a 1-mm diameter orifice. Aqueous valinomycin solution was added to one solution compartment, the current being monitored via silver—silver chloride electrodes and a digital electrometer system.

RESULTS AND DISCUSSION

Empirical model

A semi-quantitative description of the interaction of valinomycin with a BLM on unilateral addition is shown in Fig. 1 and is based on the model proposed by Benz et al. [5]. The parameters specified in this diagram and in subsequent equations are defined in Table 1. From an initial concentration, C_S, the free antibiotic is drawn into a membrane plane located between the hydrocarbon interior and dipolar layers where preferential complexation occurs assisted by the interfacial potential. In the opposing aqueous phase, free carrier is scavenged by excess lipid/solvent, and generally by the Plateau-Gibbs border.

The rate of partitioning of valinomycin into the membrane is governed by γ_S and K^{ma} where the latter reflects slow diffusion across unstirred layers and a slow interfacial process. In these experiments, the current, which must be proportional to the total population of carrier molecules in the membrane, is measured in time spans at least six orders of magnitude greater than those involved in the kinetic behaviour of intramembrane antibiotic. Thus, an expression for the current can be defined in terms of rate of carrier partitioning [3, 6]

$$J = FN_o \{K_R C_M K_{MS}/[K_R C_M + K_D]\} \{\sinh(\mu/2)/[1 + A\cosh(\mu/2)]\} \quad (1)$$

where

$$A = [(2K_{MS})(K_R C_M + 2K_S + K_S^{ma})]/[(K_D + K_{MS}^{ma})(K_R C_M + 2K_S + K_S^{ma}) - (K_R C_M K_D)] \quad (2)$$

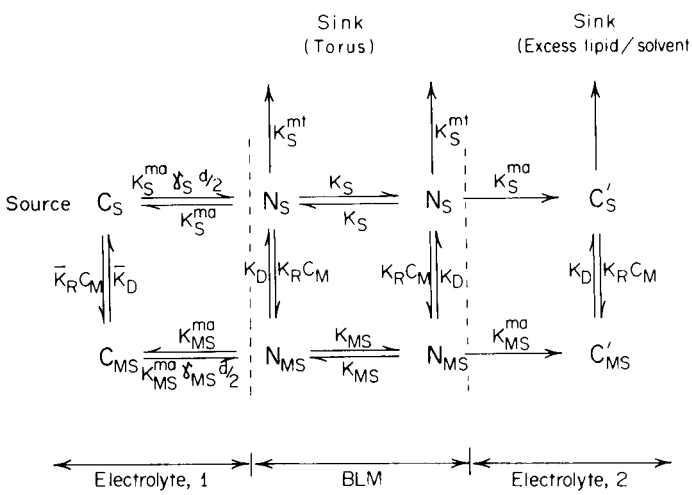

Fig. 1. Schematic representation of valinomycin distribution and action on unilateral addition to BLM (based on Benz et al. [5]).

TABLE 1

Definitions of kinetic and other parameters used in the semi-quantitative model for interaction of unilateral addition of valinomycin to the BLM

Symbol	Variable	Unit
C_S	Aqueous free carrier concentration	(M cm^{-3})
C_{MS}	Aqueous complex concentration	(M cm^{-3})
$\bar{K}_R$	Aqueous complex association rate	(M^{-1} s^{-1})
$\bar{K}_D$	Aqueous complex dissociation rate	(s^{-1})
K_{MS}^{ma}	Rate of membrane/solution complex transfer	(s^{-1})
K_S^{ma}	Rate of membrane/solution free carrier transfer	(s^{-1})
γ_S	Partition coefficient of free carrier for membrane	
γ_{MS}	Partition coefficient of complex for membrane	
d	Width of bilayer	(cm)
N_S	Interfacial concentration of free carrier	(M cm^{-2})
N_{MS}	Interfacial concentration of complex	(M cm^{-2})
K_D	Rate of complex dissociation	(s^{-1})
K_R	Rate of complex association	(M^{-1} s^{-1})
K_S	Rate of translocation of free carrier	(s^{-1})
K_{MS}	Rate of translocation of complex	(s^{-1})
K_S^{mt}	Rate of loss of free carrier to torus	(s^{-1})
C_M	Aqueous concentration of metal ion	(M)
J	Current density	(A cm^{-2})
N_o	Total interfacial concentration of carrier	(M cm^{-2})
μ	Reduced potential FU/RT	(V)
U	Applied potential	(V)

It can be assumed that the exchange rates are slow [3], that $K_S^{ma} \ll K_R C_M + 2K_S$ and that $K_{MS}^{ma} \ll K_D$, thus

$$A = (2K_{MS}/K_D) + (K_{MS}K_R C_M/K_S K_D) \quad (3)$$

Accordingly, the rate of change of intramembrane carrier concentration is

$$dN_o/dt = C_S K_S^{ma} \gamma_S \frac{d}{2} + C_{MS} K_{MS}^{ma} \gamma_{MS} \frac{d}{2} - 2(K_S^{ma} N_S + K_{MS}^{ma} N_{MS} + K_S^{mt} N_S) \quad (4)$$

Thus where [5]

$$N_S = N_o K_D/2(K_R C_M + K_D); \quad N_{MS} = N_o K_R C_M/2(K_R C_M + K_D)$$

and $C_{MS} = KC_M C_S$

$$dN_o/dt = C_S\, d/2(K_S^{ma} \gamma_S + KC_M K_{MS}^{ma} \gamma_{MS})$$
$$-2N_o[(K_S^{ma} K_D + K_{MS}^{ma} K_R C_M + K_S^{mt} K_D)/(K_R C_M + K_D)] \quad (5)$$

The integral of Eqn. (5) can be represented in a simple empirical form as previously observed [5]

$$N_o = \frac{b}{a}\,[1 - \exp(-at)] \tag{6}$$

This type of approximation is useful in the analysis of trends in transmembrane current behaviour and is applied in this case to emphasize that the model defined above is consistent with the previous qualitative discussion of the effects of membrane parameters [2].

Membrane parameters and ion flux

On the assumption that decreased fluidity is the major factor responsible for diminished current at elevated membrane cholesterol content for phosphatidyl choline membranes [8, 9], an attempt can be made to correlate the experimentally observed residual current caused by anion/cation flux to trends in calculated values. The validity of comparing results for the permion to the valinomycin carrier ion case may be questioned because no complexation kinetics are involved and facilitated transport is not present. However, elimination of complexation parameters produces a three-step kinetic process applicable to both ions [10]. Any ion transport across a BLM interior is ultimately regulated by transmembrane potential and fluidity. Because both the carrier-ion and electrolyte ions have unit charge, and assuming that the transmembrane dipolar potential and membrane thickness remain relatively constant for mole fraction cholesterol contents below 0.6 (at least for lecithin membranes containing *n*-decane) [9], only changes in membrane fluidity are expected to occur and will affect both ion currents similarly. Considering these conditions, it is interesting to note that by the adjustment of K_S and K_{MS}, the two rate constants governed by fluidity, a simple mathematical relationship can be derived which conforms extremely well to the BLM residual current/cholesterol content relationship observed experimentally. This work is summarized in Tables 2 and 3, and indicates that a decrease in K_S and K_{MS} results in a proportional decrease in current. Such a trend is not observed experimentally, but instead, for every 0.2 mole fraction cholesterol increase, the rate constant, and therefore the relative currents, decrease by a factor of two (Table 3). (Values for the variables involved in the solution of the equations were obtained from the literature [3—5].) It should be noted that discrepancy between calculated and experimental relative current values occurs in cases where potential and membrane thickness effects may become competitive.

TABLE 2

Predicted sensitivity of valinomycin-induced current to membrane fluidity as represented by K_{MS} and K_S

% of K_{MS}, K_S	100	80	60	40	20
Calc. relative current for valinomycin	1.00	0.82	0.65	0.45	0.24

TABLE 3

Observed current for membranes with variation of membrane cholesterol content (X_C)

X_C	% of K_{MS}, K_S	Calc. relative current for valinomycin	Exp. relative current for ion flux
0	100.0	1.00	1.00
0.2	50.0	0.55	0.50
0.4	25.0	0.29	0.28
0.6	12.5	0.15	0.13
0.8	6.3	0.08	0.04

Membrane perturbation

The BLM has a large, positive dipolar potential associated with the orientation of hydrated lipid headgroups [11—14]. Introduction of valinomycin into the membrane should cause a significant transient perturbation of this zone. Evidence for direct dipolar interaction has been observed for surface-active compounds such as phloretin [15], but data indicating transient dipolar change by physical perturbation are scarce. Clearly, the net quantity and rate of change of membrane concentration of valinomycin will determine the extent of the perturbation. Both these factors can be estimated in relative terms through Eqns. (5) and (6). Previous work has shown that for membranes of similar area to those employed in this study, the time necessary to reach equilibrium (i.e., $dN_o/dt \approx 0$) is approximately 10 min [3—5]. (True equilibrium in all cases is not established because loss to the torus is a major factor, but the net change of N_o with time may be negligible.) Similarly, the minimum time necessary to reach equilibrium with a diffusion-limited transfer process is about 15 min [4]. Choice of the appropriate time constant can be used to evaluate the exponential of Eqn. (6); this parameter represents a relative weighting of N_o at equilibrium. Assuming that $b/a \approx 1$ (for simplicity), the value of dN_o/dt can be determined as a similar relative factor. These parameters will vary with the value of K_R which is calculated by the perturbation of the dipolar potential. The product of the two factors (net quantity and rate of concentration change) produces a value which can be applied to K_R to determine the relative effect of perturbation on the current. An example of such a calculation is shown in Table 4. Note that the relative effect of $N_o \times dN_o/dt$ has been adjusted to enlarge the value of K_R. The manner in which such adjustment is accomplished is arbitrary and therefore illustrates only a trend. The results are further depicted in Fig. 2, where the development of a rapid current maximum occurs within one to four minutes after valinomycin addition.

It has been reported that valinomycin acts to increase membrane fluidity [16]. This effect would become important at high values of N_o, the time dependence of which is given by Eqn. (6). An increase of fluidity results in an increase of the rate constants K_{MS} and K_S. If N_o is used as a weighting factor, the relative variation of current with time and fluidity can be

TABLE 4

Effect of K_R on calculated current (for $t_{equil.} \approx 10$ min)

Time (s)	$1-\exp(-at)$	dN_o/dt ($\times 10^{-3}$ M cm^{-2}s^{-1})	Relative increase of K_R	Relative carrier current
0	0.000	8.00	1.00	1.00
10	0.077	7.38	1.57	1.49
50	0.330	5.36	2.77	2.40
100	0.551	3.59	2.98	2.54
200	0.798	1.62	2.29	2.06
400	0.959	0.33	1.32	1.27
600	0.992	0.06	1.06	1.05

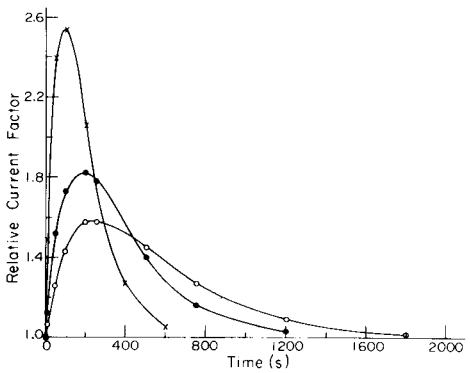

Fig. 2. The development of a carrier-ion current maximum based on a dynamic variation of the kinetic factor K_R caused by membrane perturbation: (X) for $t_{equil.}$ = 600 s; (•) for $t_{equil.}$ = 1200 s; (○) for $t_{equil.}$ = 1800 s. (The value of $t_{equil.}$ represents the time constant in Eqn. 6).

calculated assuming N_o in Eqn. (1) to be constant. Sample values are listed in Table 5 and contrasted in Fig. 3 over the time range of interest. The assumption of a linear effect of valinomycin content on fluidity may be erroneous, as demonstrated by the effect of cholesterol. From the trends indicated in Figs. 2 and 3, current—time profiles similar to those commonly observed experimentally can be constructed. It is important to note that the direct application of the relative current factors to the expected variation of N_o with time in Eqn. (1) does not produce a current—time profile with a first maximum. A profile containing a shoulder in place of the first maximum is generated and such profiles are also experimentally observed. However, it should be noted that the model is not only empirical but also that the assumption of constant or exponentially changing N_o with time is probably incorrect; the change will generally follow a more complicated trend. For example, an increased rate of incorporation as perturbation occurs may be possible because transient increases of K_S^{ma} and K_{MS}^{ma} with time will cause a

TABLE 5

Effect of K_{MS} and K_S on calculated current

Time (s)	Fraction of final N_o	Relative increase of K_{MS}, K_S	Relative carrier current
0	0.000	1.000	1.00
10	0.077	1.077	1.06
50	0.330	1.330	1.24
100	0.551	1.551	1.39
200	0.798	1.798	1.54
400	0.959	1.959	1.63
600	0.992	1.992	1.65

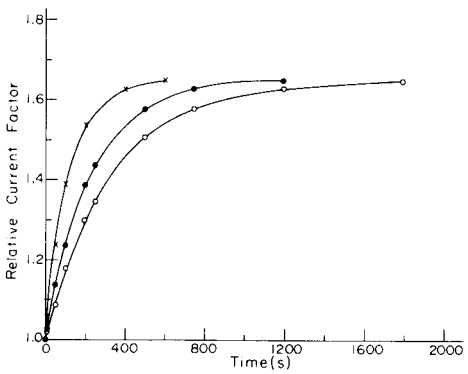

Fig. 3. The increase of carrier-mediated current as induced by the fluidity-sensitive kinetic factors K_{MS} and K_S on the increase in BLM fluidity caused by entry of valinomycin to the membrane. The representations for different time constants applied in Eqn. (6) are identical to the scheme used in Fig. 2.

similar transient increase of N_o, even though the final value of the latter at $t = \infty$ does not change. It would seem to be inherently impossible to determine the magnitudes of the relative weighting factors which should be applied to generate simulated profiles when such a simplistic model is used.

When valinomycin is added into only one solution compartment, a second maximum is observed [1, 2, 4], which is not apparent when simultaneous addition in both compartments is attempted. The final value of the current is determined by the relative magnitudes of the flux of valinomycin into the membrane and the loss to the two defined sinks. It would seem that a maximum in valinomycin concentration occurs in the membrane to generate the second peak. As the concentration decreases, the current becomes smaller because less carrier is present, but this would necessarily affect factors K_R, K_{MS} and K_S which would enhance the current reduction. According to the explanation presented in this work, the first maximum should be observable for any type of aqueous addition of valinomycin but apparently has not

been commonly observed. Careful analysis of membrane composition indicates that the evolution of the first peak is intimately related to the degree of membrane cholesterol content, the content of the autooxidation products of cholesterol, and perhaps also to lipid oxidation product content [2, 17]. Of these factors, the content of oxidized cholesterol should be the most influential property, changing dipolar potentials and/or orientation.

We are indebted to the Natural Sciences and Engineering Research Council of Canada for support for this work and for provision of a Fellowship to U. J. K. Also, we are particularly appreciative of funds for equipment provision from the Atkinson Foundation, Toronto, Ontario.

REFERENCES

1 M. Thompson, U. J. Krull and P. J. Worsfold, Anal. Chim. Acta, 117 (1980) 121.
2 M. Thompson and U. J. Krull, Anal. Chim. Acta, 141 (1982) 33.
3. G. Stark and R. Benz, J. Membr. Biol., 5 (1971) 133.
4 S. B. Hladky, Biochim. Biophys. Acta, 307 (1973) 261.
5 R. Benz, G. Stark, K. Janko and P. Läuger, J. Membr. Biol., 14 (1973) 339.
6 G. Stark, R. Benz, G. W. Pohl and K. Janko, Biochim. Biophys. Acta, 266 (1972) 603.
7 P. Läuger, J. Membr. Biol., 57 (1980) 163.
8 R. Benz and D. Cros, Biochim. Biophys. Acta, 506 (1978) 265.
9 R. Benz and P. Läuger, Biochim. Biophys. Acta, 468 (1977) 245.
10 H. D. Price and T. E. Thompson, J. Mol. Biol., 41 (1969) 443.
11 H. Hauser, I. Pascher, R. H. Pearson and S. Sundell, Biochim. Biophys. Acta, 650 (1981) 21.
12 G. Büldt and R. Wohlgemuth, J. Membr. Biol., 58 (1981) 81.
13 K. C. Sehgal, W. F. Pickard and C. M. Jackson, Biochim. Biophys. Acta, 552 (1979) 11.
14 D. A. Haydon, N.Y. Acad. Sci. Ann., 264 (1975) 2.
15 O. S. Andersen, A. Finkelstein, I. Katz and A. Cass, J. Gen. Physiol., 67 (1976) 748.
16 H. Susi, J. Sampugna, J. W. Hampson and J. S. Ard, Biochemistry, 18 (1979) 297.
17 G. A. S. Ansari and L. L. Smith, J. Chromatogr., 175 (1979) 307.

Analytica Chimica Acta, 141 (1982) 57—64
Elsevier Scientific Publishing Company, Amsterdam — Printed in The Netherlands

RESPONSE PROPERTIES, APPLICATIONS AND LIMITATIONS OF CARBONATE-SELECTIVE POLYMER MEMBRANE ELECTRODES

JULIE A. GREENBERG and M. E. MEYERHOFF*
Department of Chemistry, The University of Michigan, Ann Arbor, MI 48109 (U.S.A.)
(Received 23rd March 1982)

SUMMARY

The preparation and response characteristics of a carbonate-selective polymer membrane electrode are reported. The electrode is prepared by incorporating Aliquat 336, trifluoroacetyl-*p*-butylbenzene and di-2-ethylhexyl sebacate or dioctyl phthalate in a poly(vinylchloride) membrane matrix. The effect of membrane composition and electrode response in various buffer systems are examined. Under buffer conditions appropriate for practical measurements, potentiometric data yield the following selectivity pattern: ClO_4^- = salicylate > total carbon dioxide species > I^- > NO_3^- > acetate > Cl^- > Br^-. The electrode can be readily fabricated in tubular form and utilized within a very simple flow-injection arrangement to determine total carbon dioxide species. The possible applications of the electrode to serum CO_2 measurements as well as within newly devised gas-sensing arrangements for dissolved CO_2 are also examined.

The accurate and rapid determination of total carbon dioxide species (e.g., CO_2, hydrogencarbonate, and carbonate) in physiological, industrial, and environmental samples presents a formidable challenge. At present, total CO_2 is most often determined with a Severinghaus-type potentiometric gas sensor [1] after the sample has been acidified to pH < 5.5. In such systems, measurements are based on the diffusion of CO_2 through a silicone rubber membrane into a thin film of hydrogencarbonate solution in contact with a glass pH electrode. A change in pH results within the aqueous film as complete equilibration of the gas across the membrane is achieved. While widely employed, the Severinghaus design suffers from limitations because of its slow response times, the fragile and costly nature of the required flat-bottom pH glass electrode, and the large response of the sensor to volatile as well as some less volatile organic acids [2].

In view of these limitations, there have been numerous attempts to prepare alternative potentiometric devices capable of detecting total CO_2 species in solution. These devices include membranes based on solid ion-exchange resins sensitive to hydrogencarbonate [3] and pseudo "bicarbonate"-responsive electrodes based on dual pH sensitive/CO_2 permeable polymer membranes [4, 5]. The former lacked selectivity while the latter were really gas-sensing electrodes in which response to hydrogencarbonate occurred as equilibrium levels of CO_2 (in the hydrogencarbonate solutions) permeated a polymeric

pH-responsive membrane, altering the internal membrane potential of the sensor (i.e., changed pH at the internal surface of the membrane). Another "bicarbonate" electrode, based on a liquid membrane with a fluorinated ketone anion-exchanger was patented by Corning [6]. It was subsequently demonstrated by Herman and Rechnitz [7, 8] that this electrode (utilizing Aliquat 336 in trifluoroacetyl-*p*-butylbenzene as the active membrane phase) was really selective for carbonate, not hydrogencarbonate. Indeed, these workers were able to use this liquid membrane probe to determine total CO_2 in blood by measuring equilibrium amounts of carbonate at pH 8.4 [9]. Kodak Corporation now utilizes a polymer form of this membrane to measure serum CO_2 within their new Ektachem clinical analyzer [10], but no literature report has appeared describing the preparation and properties of such a membrane.

The purpose of this paper is to report our findings on the preparation, optimization, and response characteristics of a carbonate-selective polymeric membrane electrode. In addition, a novel tubular form of the electrode is described and utilized in a simple flow-injection arrangement for the determination of total CO_2. Limitations on the use of this membrane electrode system for direct blood CO_2 measurements are discussed. Finally, the concept of incorporating this polymer membrane electrode within a newly devised gas-sensing arrangement, highly selective for CO_2, is also examined.

EXPERIMENTAL

Apparatus

All static and flow-injection potentiometric measurements were made with a Corning Model 12 pH/mV meter used in conjunction with a Heath-Schlumberger Model 204 strip-chart recorder. All measurements were made vs. a saturated calomel reference electrode at room temperature. An Orion Model 92-00 liquid-membrane electrode body was used to evaluate the static response of carbonate-selective polymer membranes.

A schematic diagram of the carbonate electrode-based flow-injection system is shown in Fig. 1. The system consists of a Rainin-Rabbit peristaltic pump, a Rheodyne 4-way rotary injection valve (with 100-μl sample loop), 50 cm of 1.14-mm i.d. polyethylene tubing coiled in 1-inch loops, and a tubular carbonate polymer membrane electrode.

Reagents

All chemicals were of the purest grade available. Standard solutions and reagent buffers were prepared with distilled—deionized water. Most experiments were carried out with either a 0.05 M or 0.10 M tris-(hydroxymethyl)-aminomethane—hydrogen sulfate (Tris—SO_4) buffer, pH 8.75, as the sample or diluent reagent.

Trifluoroacetyl-*p*-butylbenzene (TFBB) was synthesized as described previously [8]. Aliquat 336 (tricaprylylmethylammonium chloride) was

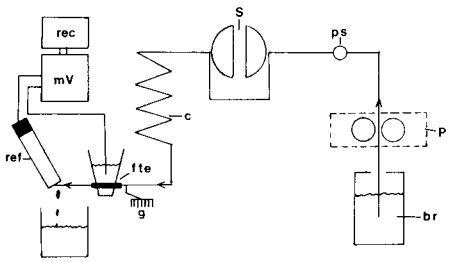

Fig. 1. Schematic diagram of the polymer carbonate electrode-based flow-injection system: (fte) tubular flow-through carbonate electrode; (g) electrical ground; (c) coiled polyethylene tubing; (s) sample injection valve; (ps) pulse suppressor; (p) peristaltic pump; (br) buffer reservoir.

obtained from Aldrich Chemical Co. Dioctyl phthalate and dioctyl sebacate were Kodak products, while di-2-ethylhexyl sebacate was obtained from ICN Pharmaceuticals.

Preparation and evaluation of membrane electrodes and gas sensor

For static electrode studies, the carbonate-selective membrane was prepared as follows. Poly(vinylchloride) (55 mg), plasticizer (50 μl), TFBB (50 μl) and THF (1 ml) were mixed thoroughly and the resulting solution was poured into a glass ring (1-inch diameter) placed on top of a glass slide. After the solvent had evaporated, the membrane was peeled from the slide and smaller round discs were cut out (3-mm diameter). Such a piece was placed in the end of an Orion liquid electrode body and secured in place by tightening the outer cap. The electrode was filled with an internal solution of 0.01 M $NaHCO_3$—0.01 M NaCl before testing.

For evaluation within the gas sensor arrangement, a small piece of the above membrane was affixed to the end of a plastic pipet—tygon tubing assembly as described previously for an ammonium-selective membrane [11, 12]. The rest of the gas sensor was also assembled in an analogous manner to the earlier ammonia probe [12] except that a silicone rubber membrane was used as the outer gas-permeable material.

A tubular flow-through carbonate electrode was prepared with a slightly different membrane composition. Instead of 55 mg of PVC, 25 mg was used in the casting solution. The electrode was made in a 0.89-mm i.d. piece of tygon tubing by methods recently described for tubular ammonium electrodes [13]. The electrode was encased in an appropriate housing into which the internal reference solution (0.01 M $NaHCO_3$—0.01 M NaCl) and a Ag/AgCl reference wire were placed.

The static electrode potentiometric response and selectivity characteristics were evaluated by making standard additions of 0.1 M $NaHCO_3$, or interferents, to 25 ml of well stirred Tris–SO_4 buffer. The pH of the buffer was simultaneously monitored with a glass electrode to determine whether

responses observed were a result of pH changes caused by the addition of test reagents (a pH change shifts the CO_3^{2-}/HCO_3^- equilibrium and the electrode responds to OH^-). For evaluation of the gas sensor, CO_2 was formed by standard addition of $NaHCO_3$ to a 0.2 M citrate buffer, pH 4.50.

RESULTS AND DISCUSSION

In preliminary efforts to utilize the liquid-membrane components described by Herman and Rechnitz [7] within a polymer matrix, it was found that TFBB was not a suitable plasticizer for PVC type membranes. Consequently, a mixture of that solvent along with more traditional plasticizers must be used in order to make functioning electrodes. Several plasticizers were tested and the response properties of the electrode were found to vary somewhat, depending on the plasticizer utilized. In general, these effects were not dramatic; however, optimal response with regard to slope was obtained with di-2-ethylhexyl sebacate and dioctyl phthalate. The ratio of plasticizer to solvent-exchanger, and the amount of PVC within the membrane were also studied. Again, no significant trend was observed, although a membrane composed of 23% plasticizer, 23%—4% Aliquat 336 in TFBB and 54% PVC consistently yielded optimal response.

Characteristics of the electrode

A considerable effort was made to determine the best buffer composition to use for practical evaluation of the electrode. Herman and Rechnitz [9] reported the use of a Tris—HCl buffer, pH 8.40, for automated serum CO_2 measurements using a liquid-membrane carbonate electrode. For the polymer membrane electrode, several buffer systems (e.g., Tris, 2-amino-2-methyl-1,3-propane-diol, 2-amino-2-methyl-1-propanol) were studied to find the one which yielded optimal response to total CO_2 species. In addition, the counter-ion was varied within the buffers. For example, Fig. 2 shows the response of the static carbonate polymer electrode to total carbonate—hydrogencarbonate species in a series of 0.05 M Tris—X buffers, all at pH 9.0. It can be seen that Tris—SO_4 offers the widest dynamic range and the best slope (typically 25—27 mV/decade). Clearly, the data from this study reflect the innate selectivity of the membrane with respect to various buffer anions. After it had been shown that Tris—SO_4 was the most useful working buffer for quantitative purposes, a more complete selectivity study was done with this buffer solution as a constant background. Figure 3 shows the response of the carbonate electrode to total CO_2 species (i.e., carbonate and hydrogencarbonate) and to other anions in 0.1 M Tris—SO_4, pH 8.75. It can be seen that the electrode responds logarithmically to total CO_2 species between 7×10^{-4} and 1×10^{-2} M, although useful response is observed to 10^{-4} M. It should be realized that at pH 8.75, only 2.4% of the total CO_2 species is carbonate and thus the membrane is far more selective for carbonate than it appears from Fig. 3. However, because the electrode also has a large Nernstian

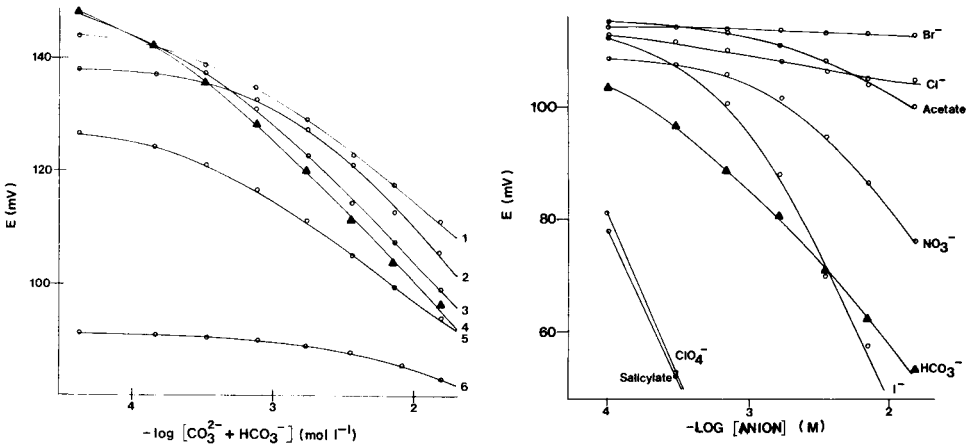

Fig. 2. Response of static carbonate polymer-membrane electrode to total CO_2 (predominately carbonate and hydrogencarbonate) in various 0.05 M Tris—X buffers, pH 9.0: (1) Tris—HCl; (2) Tris—citric acid; (3) Tris—HBr; (4) Tris—H_2SO_4; (5) Tris—HF; (6) Tris—HI.

Fig. 3. Potentiometric response of polymer carbonate electrode to various anions in a background of 0.1 M Tris—SO_4, pH 8.75.

response to hydroxide ion, increasing the working pH would result in poorer detection limits toward total CO_2 species. Indeed, pH 8.75 was found to be a good compromise for practical measurement purposes and, therefore, Fig. 3 reflects the practical selectivity relative to total CO_2 measurements (not relative only to carbonate). Figure 3 indicates that perchlorate and salicylate are the major interferences and that the selectivity order of the electrode is as follows: salicylate = perchlorate > total CO_2 species $\geq I^-$ > NO_3^- > acetate > Cl^- > Br^-.

For the data shown in Figs. 2 and 3, a 0.01 M $NaHCO_3$—0.01 M NaCl solution was used as the internal reference solution. Response times were typically 20 s—1 min for complete equilibration. The effect of using buffered internal reference solutions was examined with the aim of avoiding any effect that CO_2 diffusion through the PVC membrane [4, 5] might have on the equilibration time and slope of the electrode (e.g., CO_2 diffusion could alter the pH of the internal solution and continuously change the E° of the electrode). The following buffers, all containing 10^{-2} M NaCl, were evaluated: 0.1 M Tris—SO_4, pH 8.75; 0.1 M phosphate, pH 7.00; 0.1 M citrate, pH 5.50. Although shifts in the initial potentials were observed, the electrode performance for all of these internal buffers was essentially the same as when the unbuffered internal solution was used. This suggests that free CO_2 gas levels are so low when the sample solution is at pH 8.75 (0.4% of total CO_2 species), that no concern need be given to the CO_2 diffusion problem, at least in the 10^{-4}—10^{-2} M total CO_2 working range.

Flow-injection system

In an effort to utilize the electrode for rapid and accurate total CO_2 determinations, it was judged desirable to incorporate the polymer membrane electrode into a flow-injection system. When a novel tubular electrode assembly [14] was used with a flow-injection system (Fig. 1) and a 0.1 M Tris—SO_4 (pH 8.75) diluent stream, the potentiometric recording shown in Fig. 4 was obtained. These data were recorded by injecting $NaHCO_3$ standards from the 100-μl injection value. Typically, 40—50 samples per hour can be handled with good reproducibility ($\leqslant \pm 0.8$ mV). In this flowing system, the electrode had a slightly lower slope, typically 23—25 mV/decade between 5×10^{-3} and 1×10^{-1} M total CO_2 species. The shift in calibration plots when compared to Figs. 2 and 3 reflects the internal dilution factor within the flow-injection system. In this regard, because exact pH adjustment of the sample is critical for accurate total CO_2 measurements, greater dilution within the system is required (achieved by using tubing of wider diameter and greater length).

In attempts to utilize the above flow-injection system for serum CO_2 measurements, it was found that large positive errors resulted (using preassayed commercial control serum). This was apparently due to the presence of salicylate anions in the control serum (at 3.65×10^{-4} M [15]). Normal salicylate levels in blood are typically less than 1.0×10^{-4} M [16], but therapeutic levels for aspirin users are approximately 1.5×10^{-3} M [16]. It is clear from Fig. 3 that any salicylate greater than normal levels will cause substantial positive errors in total CO_2 measurements via the polymer carbonate electrode-based methods. The carbonate-responsive polymer membrane utilized by Kodak Corporation in their new instrument must also suffer salicylate response, because a recent patent [17] describes a buffer overcoat layer which is supposed to eliminate organic anion interferences.

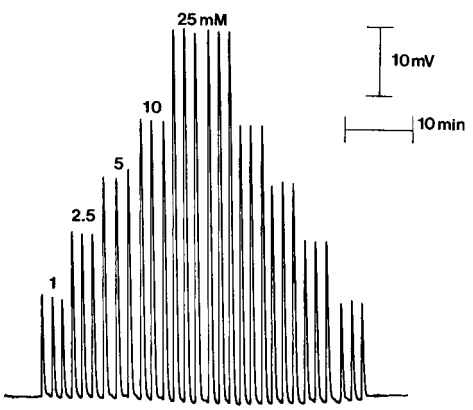

Fig. 4. Typical strip-chart recording and reproducibility obtained with carbonate electrode-based flow-injection system. Carrier flow rate, 2.0 ml min^{-1}; 100-μl injections.

Because the Kodak system involves a single use, disposable, static membrane electrode arrangement, such a solution to this problem is feasible. However, such an approach could not be utilized in a flowing arrangement in which the membrane electrode is continuously being reused.

To improve the selectivity of the static carbonate polymer membrane, the feasibility of utilizing the electrode as an internal sensing element in a conventional total CO_2 gas sensing arrangement was examined. The concept of using polymer electrodes as inner sensing elements was recently introduced via a new ammonia sensor [11]. Figure 5 illustrates the device used in this study. When a 0.1 M Tris—SO_4 buffer, pH 8.75, served as the internal electrolyte, very small potentiometric responses were obtained as standard $NaHCO_3$ was added to a sample solution of pH 4.50. Indeed, for such an experiment, the predominant response was in the positive potential direction. This was because CO_2 diffusion across the outer gas-permeable membrane caused a pH change within the thin film of buffer at the sensor tip. Such an effect is enhanced by the relatively large pH difference between the sample solution and the internal buffer solution (i.e., large buffer trap effect). When the internal buffer solution was replaced with stronger buffer solution, e.g., 0.5 M Tris—SO_4, pH 8.75, the calibration plot shown in Fig. 6 was obtained. Response times were typically 2 min; however, the slope was lower than expected (20 mV/decade) and the logarithmic range was quite narrow. Again, at total CO_2 levels greater than 10^{-3} M, the potentiometric response reverses because of a lowering of the pH in the buffer film (reduced carbonate ion levels in film). To overcome this problem, it would be desirable

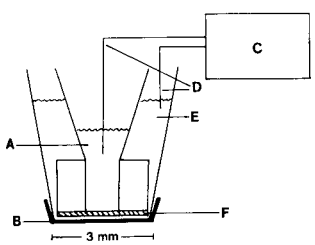

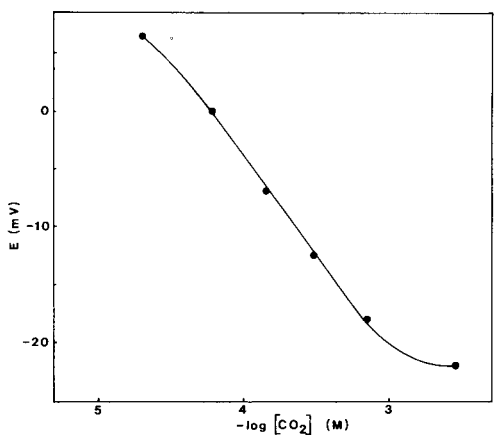

Fig. 5. Schematic diagram of polymer electrode-based carbon dioxide-responsive gas sensor: (A) 0.01 M $NaHCO_3$—0.01 NaCl solution; (B) silicone rubber membrane; (C) pH/mV meter; (D) Ag/AgCl electrodes; (E) Tris—SO_4 buffer; (F) poly(vinylchloride) carbonate-selective membrane.

Fig. 6. Calibration curve for carbonate electrode-based potentiometric CO_2 gas sensor.

to utilize a hydrogencarbonate-responsive internal sensing element. This would allow the use of a lower pH internal buffer and thus would reduce the pH changes caused by the buffer trap effect. Work on this concept is currently underway.

The authors acknowledge the laboratory work of Mr. Jeff Rosen and Mr. Leonidas Bachas in doing some of the experiments cited. This work was supported by the National Institutes of Health (Grant GM 28882-01).

REFERENCES

1 J. W. Severinghaus and A. F. Bradley, J. Appl. Phys., 13 (1958) 575.
2 R. K. Kobos, S. J. Parks and M. E. Meyerhoff, Anal. Chem., in press.
3 A. L. Grekovich, E. A. Materova and N. V. Garbuzova, Zh. Anal. Khim., 28 (1973) 1206.
4 L. W. Niedrach, U.S. Patent No. 3,898,147, August 5, 1975.
5 R. J. J. Funck, W. E. Morf, P. Schulthess, D. Ammann and W. Simon, Anal. Chem., 54 (1982) 423.
6 W. M. Wise, U.S. Patent No. 3,723,281, March 27, 1973.
7 H. B. Herman and G. A. Rechnitz, Science, 184 (1974) 1074.
8 H. B. Herman and G. A. Rechnitz, Anal. Chim. Acta, 76 (1975) 155.
9 H. B. Herman and G. A. Rechnitz, Anal. Lett., 8 (1975) 147.
10 S. H. Kim, B. E. Babb, M. J. Bogdanowicz, J. C. Chang, D. S. Dancel, T. R. Kissel, M. W. Pipal, J. R. Sandifer, P. N. Schipelsky, R. Searle, R. W. Spayd and T. J. Steele, Clin. Chem., 26 (1980) 991.
11 M. E. Meyerhoff, Anal. Chem., 52 (1980) 1532.
12 M. E. Meyerhoff and R. H. Robins, Anal. Chem., 52 (1980) 2383.
13 Y. M. Fraticelli and M. E. Meyerhoff, Anal. Chem., 53 (1981) 992.
14 M. E. Meyerhoff and Y. M. Fraticelli, Anal. Lett., 14 (1981) 415.
15 Data Sheet for Fisher Sera-Chem Control Serum, Lot no. 306-010, Fisher Scientific, Pittsburgh, PA, 1980.
16 R. B. Banke, in N. W. Tietz (Ed.), Fundamentals of Clinical Chemistry, W. B. Saunders, Philadelphia, 1976, Ch. 21.
17 S. A. Kim and H. J. Chang, U.S. Patent No. 4,272,328, June 9, 1981.

Analytica Chimica Acta, 141 (1982) 65—72
Elsevier Scientific Publishing Company, Amsterdam — Printed in The Netherlands

ELECTROLYSIS AT THE INTERFACE BETWEEN TWO IMMISCIBLE ELECTROLYTE SOLUTIONS BY MEANS OF A HANGING ELECTROLYTE DROP ELECTRODE

VLADIMÍR MAREČEK* and ZDENĚK SAMEC

J. Heyrovský Institute of Physical Chemistry and Electrochemistry, Czechoslovak Academy of Sciences, Utováren 254, 102 00 Prague 10-Hostivař (Czechoslovakia)

(Received 2nd March 1982)

SUMMARY

A three-electrode system with a hanging electrolyte drop electrode is described. The system facilitates analytical exploitation of electrolysis at the interface between two immiscible electrolyte solutions. Its use is demonstrated for the determination of micromolar concentrations of tetraethylammonium cation by differential pulse stripping voltammetry, based on transfer of the cation from water to nitrobenzene.

The exploitation of the polarization phenomena at the interface between two immiscible electrolyte solutions for electroanalytical purposes has been envisaged [1, 2]. In fact, striking analogies between these phenomena and those at a metal/electrolyte solution interface [3—6] have indicated that the methods of conventional electroanalysis may well be applicable for the determination of the species participating in a charge-transfer reaction at interfaces between immiscible electrolytes.

Ions or electrons can be transferred across the interface of the phases α and β according to the overall reaction [4, 7]

$$M^{z+}(\alpha) \rightleftharpoons M^{z+}(\beta) \text{ or } O1(\alpha) + R2(\beta) \rightleftharpoons R1(\alpha) + O2(\beta)$$

respectively, where M^{z+} is an ion with charge number z, O1/R1 is the redox couple in the phase α, and O2/R2 is the redox couple in the phase β. Moreover, the transfer of an ion M can be facilitated by the presence of a substance L which forms the complex ML at the interface and acts as an ion-carrier [1, 2]: $M(\alpha) + L(\beta) \rightleftharpoons ML(\beta)$. The effects of several synthetic or naturally-occurring ion-carriers on the transfer of alkali or alkaline earth metal cations across a water/nitrobenzene interface have been reported [1, 2, 8, 9].

Until recently, it was assumed [1, 2, 4, 6] that the four-electrode system is required for accurate polarization measurements at interfaces between immiscible electrolytes. However, this rather complicated experimental set-up and the large area of the water/nitrobenzene interface (about 100 mm^2

0003-2670/82/0000-0000/$02.75

[6, 10]) made it impossible to employ fast pulse techniques because of the high time constant of the circuit. Therefore, a simpler three-electrode system has been developed with a hanging electrolyte drop electrode (HEDE). The preliminary results were encouraging [11]; the system is described in detail in this paper. It can be used for the determination of the tetraethylammonium cation by differential pulse stripping voltammetry (d.p.s.v.) based on the reversible transfer of TEA^+ from water to nitrobenzene.

EXPERIMENTAL

Apparatus

The assembly for the HEDE is shown in Fig. 1. A small drop of the nitrobenzene solution (a) is formed at the capillary tip (b) of a glass tube which is immersed in the aqueous test solution (c). The base electrolytes for the nitrobenzene or aqueous phase were tetrabutylammonium tetraphenylborate or lithium chloride, respectively. The capillary tip of about 1-mm i.d. is drawn from branched Simax glass tube (4-mm i.d.). The volume of the nitrobenzene drop is controlled by a calibrated microsyringe which is connected to one branch (d) of the glass tube. The metal wire counter electrode CE 2 and the Ag/AgCl reference electrode RE 2 are fixed in the other two branches (e, f). The latter reference electrode is dipped into an aqueous solution of tetrabutylammonium chloride (g). The counter electrode CE 2 is a platinum or copper wire (h) isolated by teflon (i) so that only a metal disc with an area of 0.126 mm^2 is exposed to the nitrobenzene solution (a). A motor-driven glass stirrer (j) and the Ag/AgCl reference electrode RE 1 are dipped in the aqueous test solution (c).

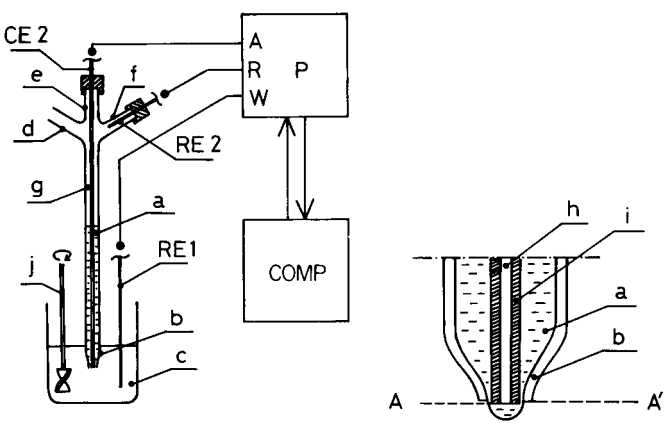

Fig. 1. Assembly for the hanging electrolyte drop electrode. RE 1 and RE 2 are Ag/AgCl reference electrodes, CE 2 is the counter electrode, P is a conventional three-electrode potentiostat with outputs for the working (W), auxiliary (A), and reference (R) electrode. COMP is a microcomputer. The right-hand diagram shows the capillary tip of the HEDE in greater detail (see text).

The geometric area, 2.9 mm^2, of the water/nitrobenzene interface at the surface of the nitrobenzene drop was calculated from the peak current on a cyclic voltammogram of cesium ion, using the diffusion coefficient reported previously [6]. The interface is polarized from a 12-bit pulse generator (DAC 12 QZ, Analog Devices, operated by an Intel 8080 microprocessor) through the three-electrode circuit. The counter electrode CE 2, the Ag/AgCl reference electrode RE 2, and the Ag/AgCl reference electrode RE 1, are connected to the outputs for the auxiliary reference and working electrodes of the conventional three-electrode potentiostat. In this way, the metal connection to the silver of reference electrode RE 1 is held virtually at ground while the potential E (vs. ground) at the metal connection to the silver of reference electrode RE 2 can be varied according to the chosen program. The current is supplied from the output for the auxiliary electrode by means of counter electrode CE 2, then passes through the water/nitrobenzene interface at the surface of the drop, and finally is picked up by reference electrode RE 1, which thus comprises the function of the counter electrode CE 1 of the four-electrode system [6].

The potential E decomposes into the following components

$$E = \varphi_{RE1}(Ag) - \varphi_{RE2}(Ag) = \Delta_n^w \varphi - \Delta_n^w \varphi_{RE2} + \Delta_w^{Ag} \varphi_{RE1} - \Delta_w^{Ag} \varphi_{RE2} + I(R_w + R_n) \quad (1)$$

where $\Delta_n^w \varphi = \varphi(w) - \varphi(n)$ is the Galvani potential difference between the aqueous test solution (c) and the nitrobenzene solution (a), and $\Delta_n^w \varphi_{RE2}$ is the potential difference inside the glass tube between the aqueous solution of tetrabutylammonium chloride (g) and the nitrobenzene solution (a). The latter potential difference is controlled by the distribution of the shared ion, i.e. tetrabutylammonium (TBA^+)

$$\Delta_n^w \varphi_{RE2} = \Delta_n^w \varphi^{\ominus}_{TBA^+} + (RT/F)\ln [c^0_{TBA^+}(n)/c^0_{TBA^+}(w)] \quad (2)$$

where $\Delta_n^w \varphi^{\ominus}_{TBA^+}$ is the formal potential difference for the tetrabutylammonium ion, and $c^0_{TBA^+}$ (n) and $c^{\ominus}_{TBA^+}$ (w) are the bulk concentrations of tetrabutylammonium ion in the nitrobenzene (a) and aqueous (g) phases, respectively. The value $\Delta_n^w \varphi^{\ominus}_{TBA^+} = -0.248$ V was calculated [4] from extraction data [12]. Other terms in Eqn. (1) are the Galvani potential differences, $\Delta_w^{Ag} \varphi_{RE1}$ and $\Delta_w^{Ag} \varphi_{RE2}$, between the silver phase and the aqueous phase of reference electrodes RE 1 and RE 2, respectively. Polarization of the former reference electrode by the current flowing through the system is practically avoided by using a large-area Ag/AgCl electrode. The last term in Eqn. (1) is the sum of the ohmic potential differences in the aqueous (c) and the nitrobenzene (a) solutions, i.e., the ohmic potential difference between the reference electrode RE 1 in the aqueous phase (c) and the surface of the nitrobenzene drop, and the ohmic potential difference between the surface of the nitrobenzene drop and the equipotential surface in the nitrobenzene phase (a) at which the potential is controlled in the defined manner. The location of the latter equipotential surface depends on the position of the

metal disc of the counter electrode CE 2 (plane A in Fig. 1) with respect to the capillary tip (plane A′ in Fig. 1). When the metal disc is positioned just at the plane A′ of the tip or beyond it, i.e., inside the nitrobenzene drop, the capillary tip serves as the Luggin capillary of the reference electrode RE 2. In contrast, when the metal disc of CE 2 is located inside the tube, the equipotential surface at which the potential is controlled is the plane A, and the resistance R_n includes the electrolyte resistance between planes A and A′ In this latter case, there is a large ohmic potential drop to be compensated, but when the metal disc of CE 2 is located inside the nitrobenzene drop, the system tends to oscillate. The best configuration found here was a hemispherical nitrobenzene drop with the metal disc of CE 2 located exactly in plane A′ of the capillary tip.

The concentrations of all the electrolytes in the system (lithium chloride, tetrabutylammonium tetraphenylborate and tetrabutylammonium chloride) were always the same. Under these conditions Eqn. (1) reduces to

$$E = \Delta_n^w \varphi - \Delta_n^w \varphi_{TBA^+}^{\circ} + I(R_w + R_n) \quad (3)$$

Automatic compensation of the ohmic potential drop $I(R_w + R_n)$ is accomplished by a positive feedback which is adjusted to a value as close as possible to the value that makes the potentiostat oscillate.

Reagents

Analytical reagent-grade chemicals were used throughout except for tetrabutylammonium tetraphenylborate which was prepared by precipitation of tetrabutylammonium iodide (Schuchardt) with sodium tetraphenylborate (Fluka, puriss. p.a.) in ethanol; the salt was recrystallized twice from acetone. Nitrobenzene and double-distilled water were used for preparation of the electrolyte solutions of tetrabutylammonium tetraphenylborate and lithium chloride or tetrabutylammonium chloride, respectively. Aqueous test solutions of tetraethylammonium bromide (Merck) were freshly prepared just before use. Experiments were done with the air-saturated solutions at room temperature (22 ± 2° C).

Procedure

The potential waveform for d.p.s.v. is shown in Fig. 2. The staircase voltage pulse (1 mV/20 ms) is applied to the HEDE starting at the initial potential E_i = 0.110 V towards the potential of pre-electrolysis E_e = 0.430 V. During the time of pre-electrolysis, t_e = 60 s, the test aqueous solution is stirred (1000 rpm). The stripping of the tetraethylammonium ion which has been concentrated into the nitrobenzene drop, is accomplished by application of a series of ΔE = 40 mV high potential pulses, each beginning at a different potential. The pulse duration (t_1) and the time interval between two pulses ($t_1 + t_2$) are 100 and 200 ms, respectively. By means of the data acquisition system (SDM 853, Burr-Brown, operated by an Intel 8080 microprocessor), the current is sampled twice: once during the last 20 ms

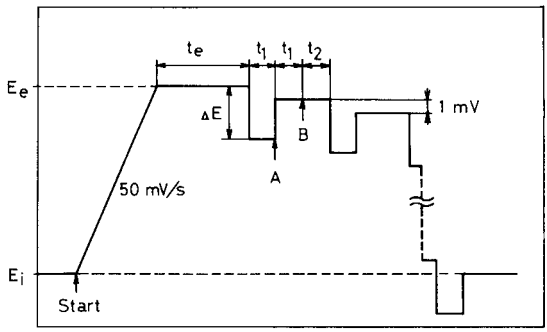

Fig. 2. Potential waveform for differential pulse stripping voltammetry. ΔE = 40 mV; duration of pre-electrolysis t_e = 60 s; pulse duration t_1 = 100 ms; time interval between two pulses $t_1 + t_2$ (variable) = 200 ms; sampling time intervals A and B, 20 ms.

of the pulse duration (A) and then again during 20 ms just before half the time interval between two pulses (B). The difference of the sample currents is stored in the memory (RAM, Intel 2114) as a 12-bit value.

RESULTS AND DISCUSSION

Figure 3 shows the voltammogram of the base electrolyte. In the potential region from 0.150 V to 0.450 V, the current is controlled mainly by charging the interface (the double-layer region), whereas at more positive or more negative potentials the predominant control is the transfer of ions of the base electrolyte from the aqueous phase to the nitrobenzene or back. With respect to the standard Gibbs energies of transfer of the individual ions present in the system [4, 12], the current at potentials more negative than 0.150 V should correspond to the transfer of tetrabutylammonium cations,

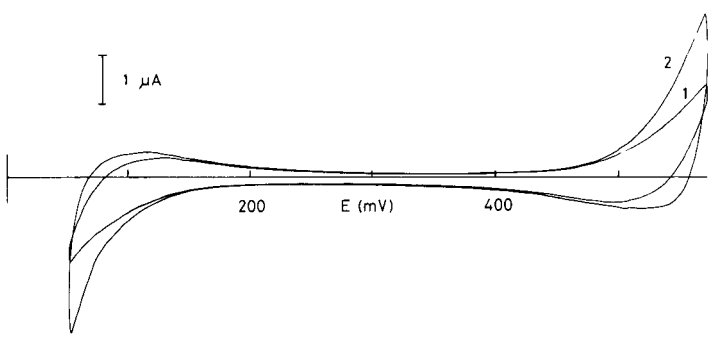

Fig. 3. Cyclic voltammogram of the base electrolytes, 0.005 M LiCl in water and 0.005 M tetrabutylammonium tetraphenylborate in nitrobenzene at the HEDE (geometric area 2.9 mm^2): without (1) and with (2) the ohmic potential drop compensation, R = 11 kΩ. Polarization rate 25 mV s^{-1}.

whereas the current at potentials more positive than 0.450 V is due to the transfer of tetraphenylborate anions. By definition [4, 6], the current is considered as positive when positive charge is transferred in the direction from water to nitrobenzene.

The single potential-step method was used in testing the dynamic properties of the system in the double-layer region. Figure 4 shows the response of the system to a 20-mV high potential pulse for the cases with and without the *IR* drop compensation. It can be seen that the charging of the interface is completed within about 2 ms. The introduction of *IR* drop compensation becomes essential for current signals higher than about 0.1 μA (cf. Fig. 3) which corresponds to an error of 1 mV at a solution resistance of 10 kΩ.

For a reversible system, the shape of the current—potential curve in differential pulse polarography corresponds approximately to the first derivative of the normal polarographic wave (see, e.g., [13, 14]). It may be assumed that this is also true in d.p.s.v., thus

$$I \simeq (\partial \langle I \rangle / \partial E)\,\Delta E = (nF\,\Delta E\,\langle I_{lim} \rangle / RT) P(1+P)^{-2} = 4 I_p P (1+P)^{-2} \qquad (4)$$

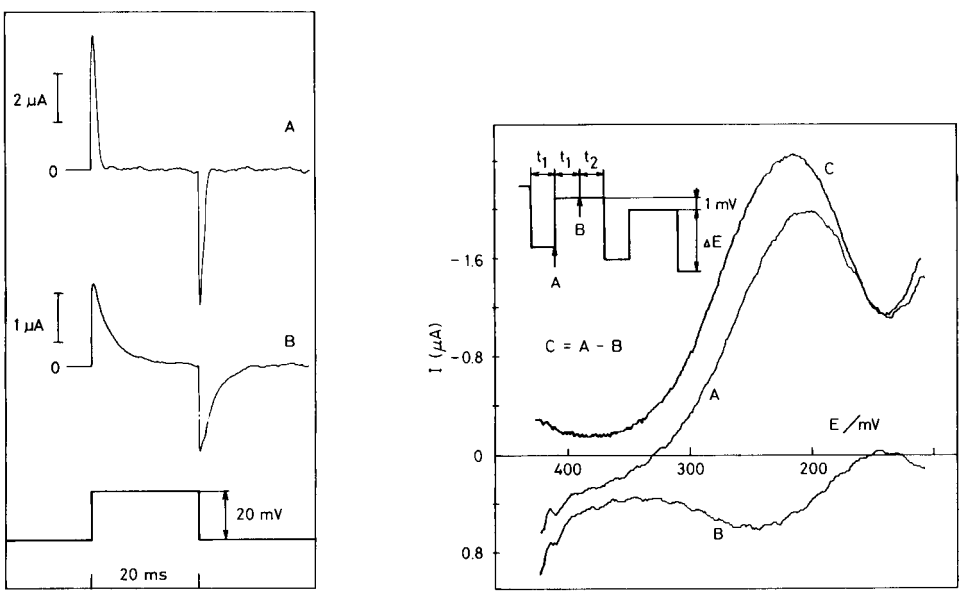

Fig. 4. Potential-step experiment at the HEDE with (A) and without (B) the ohmic potential drop compensation, R = 9 kΩ; E_i = 0.290 V and E_p = 0.310 V. The base electrolytes were 0.005 M LiCl in water and 0.005 M tetrabutylammonium tetraphenylborate in nitrobenzene.

Fig. 5. Differential pulse stripping voltammogram of tetraethylammonium (for 10 ppm tetraethylammonium bromide in water) without the ohmic potential drop compensation, R = 4.75 kΩ. The base electrolytes were 0.01 M LiCl in water and 0.01 M tetrabutylammonium tetraphenylborate in nitrobenzene.

where $\langle I \rangle$ or $\langle I_{lim} \rangle$ is the mean polarographic current or the mean limiting diffusion current, respectively; I_p is the peak current of the d.p.s.v. curve; and $P = \exp [zF(E - E_{1/2})/RT]$, where $E_{1/2}$ is the half-wave potential of the polarographic wave for reversible charge-transfer, i.e., $M^{z+}(\alpha) \rightleftharpoons M^{z+}(\beta)$. The half-wave potential can be expressed [6] by

$$E_{1/2} = E^{\ominus} + (RT/zF) \ln [D(w)/D(n)]^{1/2} \quad (5)$$

where $E^{\ominus}$ is the formal potential for the charge-transfer reaction, and $D(w)$ or $D(n)$ are the diffusion coefficients of the transferred ion in the aqueous or nitrobenzene phase, respectively. From extraction data [12], the value $\Delta_n^w \varphi^{\ominus}_{TEA^+} = -0.059$ V was calculated [4], which yields $E^{\ominus} = 0.189$ V when referred to the formal potential for the tetrabutylammonium cation. On the basis of the ratio of the viscosity coefficient of nitrobenzene to that of water (1.95), it is assumed that $D(w)/D(n) = 1.95$, and consequently, $E_{1/2} = 0.198$ V for the tetraethylammonium cation.

Figure 5 shows the d.p.s.v. curve of tetraethylammonium ions obtained without *IR* drop compensation (curve C); the curve C is the difference between the current $A = I(t_1)$ and $B = I(2t_1)$. The pulse amplitude is lowered by the ohmic potential drop $\delta\Delta E = (R_w + R_n)[I(t_1) - I(o)]$, where $I(o)$ is the current at the end of the time interval between two pulses, which can be estimated as $I(o) \simeq I(2t_1)[t_1/(t_1 + t_2)]^{1/2} = I(2t_1)/\sqrt{2}$ for a diffusion-controlled process. Because the peak current I_p is proportional to ΔE, it is possible to estimate the relative decrease in the peak current $\delta I_p/I_p$ arising from the uncompensated ohmic potential drop as $\delta I_p/I_p = \delta\Delta E/\Delta E$. In the

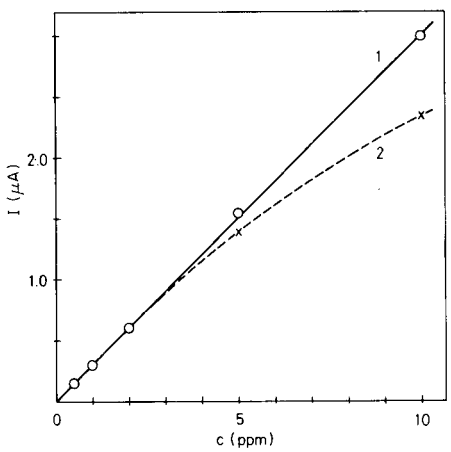

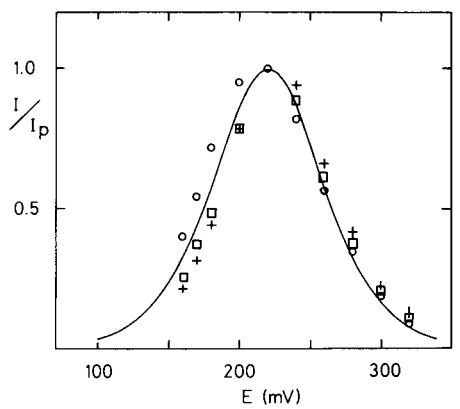

Fig. 6. Plot of the peak height of tetraethylammonium vs. concentration of tetraethylammonium bromide in water, with (1) or without (2) the ohmic potential drop compensation, $R = 4.75$ kΩ.

Fig. 7. Shape of the differential pulse stripping voltammogram of tetraethylammonium. Concentration of tetraethylammonium bromide in water (ppm): (+) 1.0; (□) 2.0; (○) 5.0. Full line was calculated according to Eqn. (4).

example which is illustrated in Fig. 5, the value $\delta I_p/I_p = 0.25$ is obtained for the solution resistance 4.75 kΩ (cf. below).

In Fig. 6, peak heights are plotted vs. concentration of tetraethylammonium bromide; 1 ppm corresponds to a 4.8 μM concentration of the compound. If the potential drop caused by the solution resistance 4.75 kΩ is compensated, the linearity is good for concentrations of tetraethylammonium bromide in water between 0.5 and 10 ppm (Fig. 6). Without the ohmic drop compensation there is some decline from linear response at concentrations higher than 5 ppm; this makes $\delta I_p/I_p = 0.2$ at 10 ppm, in good agreement with the estimate above.

Finally, Fig. 7 illustrates that the d.p.s.v. curves of the tetraethylammonium ion conform closely with the curve described by Eqn. (4). According to Eqn. (4), the peak potential E_p coincides with the half-wave potential $E_{1/2}$, i.e., in the present case $E_{1/2} = 0.220$ V. This value agrees well with that derived from the extraction data.

REFERENCES

1 J. Koryta, Electrochim. Acta, 24 (1979) 293.
2 D. Homolka, Le Q. Hung, A. Hofmanová, M. W. Khalil, J. Koryta, V. Mareček, Z. Samec, S. K. Sen, P. Vaňýsek, J. Weber and M. Březina, Anal. Chem., 52 (1980) 1606.
3 C. Gavach and F. Henry, J. Electroanal. Chem., 54 (1974) 361.
4 J. Koryta, P. Vaňýsek and M. Březina, J. Electroanal. Chem., 75 (1977) 211.
5 Z. Samec, V. Mareček, J. Weber and D. Homolka, J. Electroanal. Chem., 99 (1979) 385.
6 Z. Samec, V. Mareček and J. Weber, J. Electroanal. Chem., 100 (1979) 841.
7 Z. Samec, J. Electroanal. Chem., 99 (1979) 197.
8 D. Homolka, V. Mareček, Z. Samec, O. Ryba and J. Petránek, J. Electroanal. Chem., 125 (1981) 243.
9 A. Hofmanová and Le Q. Hung, Proceedings of J. Heyrovský Memorial Congress on Polarography, Prague, August 25—29, 1980, p. 66.
10 D. Homolka and V. Mareček, J. Electroanal. Chem., 112 (1980) 91.
11 V. Mareček and Z. Samec, Anal. Lett., 14 (1981) 1241.
12 J. Rais, Collect. Czech. Chem. Commun., 36 (1971) 3253.
13 J. Heyrovský and J. Kůta, Principles of Polarography, Academic Press, New York, 1965, p. 490.
14 E. P. Parry and R. Osteryoung, Anal. Chem., 37 (1965) 1634.

Analytica Chimica Acta, 141 (1982) 73—94
Elsevier Scientific Publishing Company, Amsterdam — Printed in The Netherlands

DEVELOPMENT OF PHYSICO-CHEMICAL SPECIATION PROCEDURES TO INVESTIGATE THE TOXICITY OF COPPER, LEAD, CADMIUM AND ZINC TOWARDS AQUATIC BIOTA

T. M. FLORENCE

Analytical Chemistry Section, CSIRO Division of Energy Chemistry, Private Mail Bag 7, Sutherland, N.S.W. 2232 (Australia)

(Received 10th May 1982)

SUMMARY

A range of model compounds was studied to test the effect of complexing agents on the adsorption of copper, lead, cadmium and zinc by Chelex-100 resin, oxine porous glass, thiol porous glass and thiol resin, from seawater and distilled water. The thiol materials, while showing behaviour similar to Chelex-100 resin and oxine porous glass for zinc, cadmium and lead, retained copper much more strongly. Methods for measuring lipid-soluble metal complexes in waters were also studied. Bio-Rad SM2 resin was the most suitable extractant, although a citrate buffer of pH 5.7 was needed to prevent the co-adsorption of free metal ions. Seawater and various fresh waters were analyzed for trace metal speciation by using Chelex-100 resin, thiol resin and anodic stripping voltammetry to determine labile metal. Bio-Rad SM2 resin and hexane—butanol extraction were used for the estimation of lipid-soluble metal. The polluted water samples had higher fractions of labile and organic-soluble metal, but it was concluded that some of the waters contained unidentified ligands which caused speciation behaviour different from that of the synthetic solutions with model ligands. The factors involved in the choice of speciation procedures for the measurement of the toxic fraction of a metal in a water sample are discussed in detail.

In recent years, increasing efforts have been made to identify the ligands which dominate heavy metal speciation in natural waters, and to develop a speciation scheme for measuring the fraction of the trace metal concentration which is toxic to aquatic biota. Direct measurement of the toxicity of a water can be made by using bioassays with algae, fish, or other plants or animals. However, bioassays are slow, have poor precision, and demonstrate only gross effects. Chemical speciation schemes are more amenable to standardisation, and can yield information on the concentrations of the different chemical species in the water. For a speciation scheme to be useful, however, it must reliably detect all the important toxic forms of the metals present. Also, information must be available about the relative toxicities of the various forms measured by the scheme. It is unlikely that any type of physico-chemical speciation measurement will replace bioassays for the definitive assessment of the toxicity of a water, but a simple and rapid chemical procedure would be invaluable for the preliminary screening of natural and waste waters, and for the identification of the toxic metal species.

Most trace metal speciation procedures developed to date use anodic stripping voltammetry, ion exchange with Chelex-100 resin (an iminodiacetate resin), ultrafiltration or dialysis, or various combinations of these techniques [1, 2]. Anodic stripping voltammetry (a.s.v.) is the simplest method [3], and involves the measurement of a.s.v.-labile metal in a water sample, i.e., the fraction of the metal concentration that is electroactive under well-defined conditions of stirring, temperature, deposition potential, pulse duration, electrolyte composition, etc. [4, 5]. The a.s.v. measurement will include free metal ion and metal dissociated from complexes in the diffusion layer. Metal complexes which contribute to the a.s.v. signal need not be thermodynamically weak; even the Cu—EDTA complex, because it is kinetically labile, will dissociate completely at a mercury electrode [6]. Deposition potentials sufficiently negative of the peak potential of the free metal ion may also lead to the direct reduction of some metal complexes [5—7]. No information is available about the relative toxicity of these directly-reducible complexes but, unless they are lipid-soluble, it is unlikely that they would be as toxic as free metal ion. Metal adsorbed on colloidal particles might not be expected to contribute significantly to the a.s.v.-labile current, because the diffusion coefficients of colloids are so small. However, it is possible that metal ion may dissociate from a colloid at the diffusion layer boundary because of the concentration gradient, as has been observed for metalloenzymes and protein persulphides [8].

Several studies have found a correlation between a.s.v.-labile metal and toxicity to aquatic biota, although the a.s.v. conditions used have varied considerably [2, 9, 10]. Much more data are required before a.s.v. measurements can be confidently used to evaluate aquatic toxicity. A serious problem in the application of a.s.v. to natural waters is that organic matter in the waters can adsorb on the electrode and give rise to unpredictable effects on the peak current [1, 2].

Chelex-100 resin was first used for speciation studies by Florence and Batley [11, 12]. The resin has a pore diameter of about 2 nm [13]; colloidal particles are therefore excluded from the resin matrix, providing a simple and contamination-free method for separating ionic and colloidally-associated metal. As in the case of a.s.v., however, it is possible that some metal will dissociate from colloidal particles during passage through a Chelex-100 column. Metal pseudocolloids, i.e., metal ion adsorbed on colloidal particles, are an important component of the dissolved fraction of a water sample. In fact, organically-coated colloidal particles, e.g., humic acid-coated iron oxide, probably dominate heavy metal speciation in both freshwater and seawater [2, 14—17]. Batley and Florence [18] combined Chelex-100 separation with a.s.v. and u.v. irradiation to develop a speciation scheme which divided dissolved metal in a water sample into seven different behavioural groups. Figura and McDuffie [19] used both column and batch techniques to vary the contact time of the water sample with Chelex-100 resin. In this way they were able to classify the metal into groups based on

their lability to Chelex-100. Laxen and Harrison [20] combined ultrafiltration with a.s.v. and Chelex-100 measurements to develop a detailed scheme based principally on size fractionation of the metal species. Ultrafiltration is a powerful technique for measuring the size distribution of metal species, but suffers from adsorptive losses of metals and contamination [1, 2]. Florence [2] pointed out that many studies of adsorptive losses of trace metals to filtration membranes and storage containers are misleading, because metal ions added to a natural water are adsorbed much more strongly than the metal species naturally present in the water. Contamination from ultrafiltration membranes and cells is, however, a more serious problem because the filtered volume is small and the surface/volume ratio is very large.

The toxicity of a dissolved metal species towards aquatic organisms is basically related to the ability of the metal species to react with a biological membrane [21]. Acute toxicity of metals towards fish often results from the reaction of the metal with the gill epithelium to produce morphological changes which hinder the transport of oxygen and affect the ionic balance [22]. Transport of metals across the gill membrane occurs principally by carrier-mediated transport of ions [23], or by direct lipid solubility of a metal complex. There is a growing body of evidence that the toxicity of heavy metal ions towards aquatic biota is correlated with the ability of the metal to react with sulfhydryl compounds [24, 25]. The membrane carrier proteins may be similar to metallothioneins, which react with metals via sulfhydryl groups [26]. Once inside the cell, the metal could be bound by glutathione or similar cytoplasmic sulfhydryl compounds. A thiol resin [27—30] could therefore be more suitable for determining reactive metal in a water sample than Chelex-100, which uses oxygen and nitrogen donors for metal binding [2, 31].

Few trace metal speciation schemes include a step for the measurement of metal complexes which are directly lipid-soluble, even though some such species are known to be highly toxic [2, 21]. Lipid-soluble metal complexes may not be a.s.v.-labile, and may not be dissociated by a chelating resin, so that other techniques are needed for their detection.

A biological membrane is a highly complex structure, and the mechanism of membrane transport is still poorly understood, although diffusion rates are known to be critically dependent on the composition of the lipid bilayer [2, 32]. Use of artificial membrane mixtures to measure lipid solubility is not suitable for routine trace metal speciation determinations [2]; a simpler chemical model is more useful. Organic solvents such as chloroform and hexane—butanol, which have dielectric constants similar to that of membrane lipid mixtures, have been used [33]. An even more convenient material for a lipid model is Bio-Rad SM2 resin, which is a neutral, non-polar, macroporous, styrene—divinylbenzene copolymer with a high affinity for molecules containing both hydrophilic and hydrophobic moieties. It has a molecular weight exclusion limit of 14 000, and contains little leachable metal impurity. Sugimura et al. [34, 35] used Amberlite XAD-2 resin, similar to

Bio-Rad SM2, to separate organically-bound iron and other metals from seawater. The adsorbed metals were then determined after elution with methanol. Florence [2] pointed out that these resins also strongly adsorb free metal ion, although the adsorbed inorganic forms may not be eluted by methanol [36].

In the present paper, Chelex-100 resin, an oxine porous glass [37], and various thiol ion-exchange materials were used to determine reactive copper, lead, cadmium and zinc in some natural and polluted waters, and in synthetic solutions containing model compounds. Labile metal was also measured by a.s.v., and the metal fractions soluble in Bio-Rad SM2 resin and hexane—butanol were determined.

EXPERIMENTAL

Apparatus

Voltammeter. An E.G. and G. Princeton Applied Research Model 384 polarographic analyzer with a hanging mercury drop electrode was used in the differential pulse mode for all a.s.v. measurements. The following instrumental parameters were used throughout: stirrer speed, fast; drop size, small; initial potential, —1.3 V; deposition time, 900 s; pulse amplitude, 25 mV; scan rate, 2 mV s^{-1}. All electrode potentials refer to the silver—silver chloride reference.

U.v. lamp. A fan-cooled 550-W mercury arc lamp with a silica sheath was mounted in the centre of an aluminium stand [38, 39]. Six sample tubes could be irradiated simultaneously.

Ion-exchange columns. Bio-Rad Econo columns, 10 cm × 0.7 cm diameter, were used throughout, with a flow rate of 1.5 ml min^{-1}. They were filled to a height of 4 cm with the ion exchangers, and 8 cm with SM2 resin. A perspex rack was designed to hold six columns. An average contact time (void volume/flow rate) of 19 s was calculated for the chelating resin columns [6].

Working area. All water filtration, separation and determination procedures were carried out in a class-100 clean room controlled at a temperature of 25.0 ± 0.5°C. The ion-exchange separations were done in a laminar flow cupboard in the clean room.

Reagents

Resins and ion-exchange materials. Chelex-100 resin (sodium form, 100—200 mesh, 2 nm pore diameter) and Bio-Beads SM2 resin were obtained from Bio-Rad Laboratories, CA. Thiol, dihydrolipoamide, and oxine-coated porous glass beads, 80—120 mesh, with a nominal pore diameter of 55 nm, were from Pierce Chemical Company, IL. A sample of Spheron 300 thiol resin, 100—200 mesh, was a gift from Lachema, Brno, Czechoslovakia. Another thiol resin was synthesized from Amberlite XAD-4 macroreticular resin (5 nm pore diameter) and thioglycolic acid [27]. A 100—200 mesh fraction was used in all experiments.

The resins and ion-exchange materials were suspended in water, decanted to remove fines, and then slurried into the ion-exchange columns. They were washed with distilled demineralised (d.d.) water or seawater until the pH of the effluent was constant. The porous glass materials were first evacuated under water to displace air. The thiol resins, and lipoamide and thiol porous glasses, were treated on the column with 20 ml of aqueous 5% mercaptoethanol (pH 8.0) to reduce disulphide groups, then washed. Between experiments, the columns were tightly stoppered to exclude air. The SM2 resin was kept as a slurry in 0.2 M nitric acid, and a new resin column prepared for each experiment. The Chelex-100 resin was replaced, and the thiol columns regenerated, after testing each model compound. However, when used for routine water analysis, both the Chelex and thiol resins could be used for 10—20 samples before regeneration, depending on the nature of the sample.

Waters Associates C_{18} Sep-Pak cartridges were attached directly to the luer fitting of the Bio-Rad ion-exchange columns, which were used as a solution reservoir. The cartridges were made hydrophilic by passing a little methanol, and then were washed with dilute nitric acid and water.

Chemicals. Sodium acetate and nitric acid were Merck Suprapur. Nitrilotriacetic acid was Aldrich gold label, and all other chemicals, unless otherwise specified, were Merck G.R.

Fulvic acid was prepared from loam by 0.5 M NaOH extraction and XAD-4 resin separation [40, 41]. Analysis of the vacuum-dried fulvic acid gave, in $\mu g\ g^{-1}$: Cu, 15; Pb, 2.1; Cd, 3.6; Zn, 16.

Colloidal solutions of iron(III), humic acid (Aldrich), and a humic acid—iron(III) mixture were prepared as follows. Iron(III) nitrate hexahydrate (12 g) was dissolved in 50 ml of d.d. water, and then 5 g of sodium hydrogencarbonate was added slowly with stirring over 30 min. After standing overnight, the solution was filtered through a 0.2-μm membrane filter. A 1-ml aliquot of the filtrate was diluted with water to 500 ml to give a stock solution which was found to have an iron concentration of 62 mg l^{-1} and a pH of 5.7.

Humic acid (0.2 g) was suspended in 100 ml of 2.5×10^{-4} M sodium carbonate and stirred for 60 min. The solution was then filtered through a 0.2-μm membrane filter. Spectrophotometric analysis showed that the solution contained 1.59 g l^{-1} humic acid.

A humic acid—iron(III) colloidal solution was prepared by mixing 25 ml of the iron stock solution with either 5 ml (solution 1) or 25 ml (solution 2) of the humic acid stock solution, and then adjusting the pH to 6.5 by dropwise addition of 4 M nitric acid. Solution 1 contained 52 mg Fe l^{-1} and 265 mg humic acid l^{-1}, while solution 2 contained 31 mg Fe l^{-1} and 795 mg humic acid l^{-1}. These colloidal solutions showed no precipitation for at least one year.

Collection and preparation of samples

Water samples were collected in polyethylene bottles which had been soaked in 1.5 M nitric acid for a week, then rinsed with d.d. water. Surface seawater samples were taken over the bow of a fibreglass boat [2]. One

sample (1 km seawater) was collected in the Pacific Ocean 1 km east of Port Hacking, N.S.W. This coastal sample would probably be affected to some extent by Sydney's ocean sewage outfalls [42]. A second seawater sample (marina seawater) was taken in a marina in Dolans Bay, Port Hacking. Two riverwater samples were taken from South Creek, St. Marys, Sydney, sample 1 before, and sample 2 after, a sewage treatment works situated on the creek. In addition, samples of Lucas Heights sludge-blanket treated septic water were taken before and after chlorination, as well as a sample of the laboratory cold tap water supply. The water samples were filtered on the day of collection through an acid-washed 0.45-μm membrane filter, and the filtrates were stored at 4°C in polyethylene bottles. Analytical results for these samples are shown in Table 1. Fulvic acid concentrations were estimated by the u.v. spectrophotometric method of Lawrence [43].

Recommended procedures

Determination of total metal. Place 25 ml of filtered water sample in a silica u.v. irradiation tube (22 cm × 1.5 cm diameter) with 0.5 ml of 4 M nitric acid and 0.05 ml of 30% hydrogen peroxide. Irradiate for 12 h, add 1.0 ml of 2% hydroxylammonium sulphate and 1.0 ml of 4 M sodium acetate, and place the tube in a boiling water bath for 15 min. Cool, and determine Zn, Cd, Pb and Cu by a.s.v.

Determination of chelating resin-labile metal. Pass 25 ml of water sample through the chelating resin column at a rate of 1.5 ml min^{-1}. Determine the total metal in, the column effluent as described above. Calculate the resin-labile metal as the difference between the total and effluent metal concentrations.

Determination of SM2-soluble metal. To 25 ml of water sample, add 0.25 ml of citrate buffer pH 5.7 (20 ml of 1 M trisodium citrate and 2.5 ml of 4 M nitric acid). Pass the mixture through a column of Bio-Beads SM2 resin at a rate of 1.5 ml min^{-1}. Determine the total metal in the column effluent as described above, and calculate the SM2-soluble metal by difference.

Determination of hexane—butanol-soluble metal. Place 25 ml of water sample in a 50-ml siliconized separating funnel. For freshwater samples only, add 0.2 ml of 4 M acetate buffer pH 5.7 (20 ml of 4 M sodium acetate and

TABLE 1

Some characteristics of the filtered freshwater samples analyzed

Sample	pH	Conductivity (μS cm^{-1})	Alkalinity (mg $CaCO_3$ l^{-1})	Iron (mg l^{-1})	DOC (mg l^{-1})	Fulvic acid (mg l^{-1})
Tapwater	7.65	120	15	0.015	4.1	1.7
Septic before Cl_2	6.65	440	70	0.010	4.2	—
Septic after Cl_2	7.56	580	70	0.010	5.9	—
South Cr. 1	7.32	500	75	1.84	13.9	11
South Cr. 2	7.43	410	60	0.40	8.0	7.0

1.8 ml of 4 M nitric acid). Add 5 ml of *n*-hexane—10% *n*-butanol and shake for 3 min. Allow the phases to separate, and run the aqueous (lower) phase into a 50-ml silica evaporating dish. Evaporate in a clean air fume cupboard just to dryness on a low-temperature hot plate. Add 0.5 ml of 4 M nitric acid and 4.5 ml of d.d. water to the dish and warm to dissolve the residue. Transfer the solution to a u.v. irradiation tube, using 20.0 ml of d.d. water. Determine the total metal as described above, and calculate the hexane—butanol-soluble metal by difference.

Determination of a.s.v.-labile metal. To 25 ml of water sample add 0.5 ml of 2.7 M acetate buffer pH 4.7 (20 ml of 4 M sodium acetate and 10 ml of 4 M nitric acid). Analyze immediately by a.s.v. using an appropriate deposition potential (—1.3 V unless otherwise stated). If the measurement is to be made at the natural pH, omit the buffer.

Procedural blanks. Total procedural blank values, in $\mu g\ l^{-1}$ in the original sample, and shown in the order, Zn, Cd, Pb, Cu, were as follows: total metal procedure, 0.28, 0.01, 0.07, 0.06; a.s.v.-labile metal procedure, 0.07, <0.01, 0.02, 0.02; SM2-soluble metal procedure, 0.32, 0.02, 0.07, 0.08; hexane—butanol-soluble metal procedure, 0.77, 0.04, 0.12, 0.15.

RESULTS AND DISCUSSION

U.v. irradiation

Difficulty was initially experienced in measuring the stripping peak of zinc in u.v.-irradiated acidified solutions because of a high current negative of the zinc wave. The magnitude of this current was independent of deposition time, was higher in seawater than in freshwater, and only appeared when solutions were irradiated in the presence of acid. The problem was overcome by treating the irradiated solutions with hydroxylammonium sulphate (Table 2).

In the speciation scheme used by Florence [13] and Batley and Florence [18], u.v. irradiation of the sample at natural pH was used to determine organically-associated metal. It has been pointed out [20, 31, 44] that in some freshwater samples this procedure leads to the precipitation of a brown deposit, probably hydrated iron(III) oxide. Both South Creek samples produced a brown deposit when irradiated at natural pH. Sample 1, which had the higher iron concentration (Table 1), gave a greater volume of precipitate. Low results were obtained for lead, and to a lesser extent, copper, probably as a result of coprecipitation in the iron oxide deposit. Precipitation is believed [2, 17] to occur when the humic acid coating, which stabilizes the colloidal iron oxide particle, is destroyed by u.v. irradiation. Tests with humic acid—iron colloidal solutions showed that visible flocculation occurred during irradiation, with losses of lead and copper, if the iron concentration exceeded about 100 $\mu g\ l^{-1}$. The use of u.v. irradiation at natural pH to determine organically-associated metal may therefore be valid only for seawater and freshwater of low iron concentration [13]; but for such waters it is the most convenient method.

TABLE 2

Effect of u.v. irradiation (12 h) on current at −1.3 V vs. Ag/AgCl

Sample	Acid added before irradiation (per 25-ml sample)	Current at −1.3 V[a] (nA)
Seawater[b]	None	53
	0.5 ml 4 M HNO_3	600
	0.5 ml 4 M HCl	700
	0.5 ml 4 M HNO_3[c]	95
Distilled demineralised water	None	38
	0.5 ml 4 M HNO_3	270
	0.5 ml 4 M HNO_3[c]	25

[a]Acetate buffer pH 4.7. The unirradiated waters gave currents of 60 nA for seawater and 25 nA for d.d. water. [b]Charcoal filtered to remove organics. [c]Irradiated sample plus 1.0 ml of 4 M sodium acetate and 1.0 ml of 2% hydroxylammonium sulphate heated to boiling for 15 min.

An anomalous copper stripping wave was sometimes observed when freshwater samples containing acetate or citrate buffers were u.v.-irradiated for a period insufficient to destroy all organic matter. This wave appeared at +0.025 V in acetate buffer pH 4.7 and had a peak width at half-wave height which corresponded to $\bar{n} = 3$, whereas the normal copper wave occurred at −0.11 V and had $\bar{n} = 2$, although the areas of the two waves were almost identical for the same copper concentration. A similar anomalous copper wave was observed for unirradiated solutions containing glutathione. These unusual stripping waves doubtlessly involve adsorption processes, but no detailed study of the mechanism was attempted.

Effect of model compounds on a.s.v.-labile metal

The effect of some model compounds on the height of the a.s.v. stripping peak in d.d. water plus acetate buffer was studied (Table 3) to assist in the interpretation of a.s.v.-labile metal results on the water samples analyzed. The largest effects on peak current were caused by fulvic acid, tannic acid and ammonium pyrrolidinedithiocarbamate (APDC). The copper wave was eliminated by APDC, which however, had no effect on the zinc peak. Tannic acid strongly depressed the zinc wave, while fulvic acid had most effect on zinc and copper. The humic acid and iron-humate colloids mainly affected the copper wave, as did the thiol compounds cysteine and glutathione.

A similar study was made in seawater (Table 3). In general, the ligands had less effect in seawater than in d.d. water, although APDC was an exception. The lower complexing ability of compounds such as nitrilotriacetic acid and fulvic and tannic acids in seawater is probably attributable to partial masking of the ligands by magnesium and calcium.

TABLE 3

Effect of ligands on a.s.v.-labile metal in distilled demineralised water and in seawater (2×10^{-7} M metal and 4×10^{-6} M ligand in 0.05 M acetate buffer pH 4.7. Deposition potential −1.3 V vs. Ag/AgCl)

Ligand	A.s.v.-labile metal (% of total)			
	Zn	Cd	Pb	Cu
Distilled demineralised water				
Glycine	100	100	100	100
Histidine	100	100	100	100
Phenylalanine	100	94	91	90
Cysteine	100	100	100	63
Glutathione (SH)	100	100	100	70
Nitrilotriacetic acid	53	100	83	58
APDC[a]	100	23	39	0
Tannic acid	12	36	88	50
Fulvic acid[b]	27	71	65	31
Iron sol[c]	90	79	81	82
Humic acid sol[d]	77	93	89	53
Iron–humic sol 1[e]	81	87	85	69
Seawater				
Nitrilotriacetic acid	100	100	88	92
APDC[a]	100	0	0	0
Tannic acid	100	77	100	68
Tannic acid[f]	3.4	75	15.5	0
Fulvic acid[b]	100	100	86	83
Fulvic acid[b,f]	50	75	53	48
Iron sol[c]	100	97	92	100
Humic acid sol[d]	100	100	100	73
Iron–humic sol[e]	68	76	76	58
Iron–humic sol[e,f]	100	100	100	85
Algal exudate[g]	100	100	100	100

[a]Ammonium pyrrolidine dithiocarbamate. [b]20 mg l^{-1}. [c]0.62 mg Fe l^{-1}. [d]8.0 mg l^{-1}. [e]1.04 mg Fe l^{-1} and 5.3 mg humic acid l^{-1}. [f]Natural pH (pH 8.2). [g]*Nitzschia sp.*, 1.3×10^6 cells ml^{-1}.

Tannic and fulvic acids had a much greater effect at the natural pH of seawater (pH 8.2) than in acetate buffer. There has been considerable dispute as to whether a.s.v.-labile measurements should be made at the natural pH of the test water, or after addition of a buffer, such as acetate [2, 20, 31]. If a.s.v.-labile measurements are made to determine the toxic fraction of a metal, the ideal pH for a.s.v. can be determined only by comparison with bioassays, but it would be purely coincidental if it were equal to the natural pH.

TABLE 4

Effect of model compounds on the removal of zinc from waters by chelating adsorbents (2×10^{-6} M zinc, 2×10^{-5} M ligand. Seawater, pH 8.2; distilled demineralised (d.d.) water, pH 6.5)

Ligand	Zinc in column effluent (% of total)					
	Chelex-100		Oxine		Thiol	
	d.d.	sea	d.d.	sea	d.d.	sea
None	0.07	0.02	0.05	0.04	0.05	0.02
Histidine	—	0.01	—	0.01	—	0.48
Cysteine	1.28	0.20	0.75	0.49	0.36	0.54
Glutathione (SH)	0.91	0.28	0.85	0.14	1.44	0.61
Nitrilotriacetic acid[a]	7.1	0.47	—	—	1.66	0.33
Tannic acid	0.66	0.49	0.75	0.14	1.30	<0.01
Fulvic acid[b]	2.37	1.04	0.96	0.15	1.46	0.18
Humic acid sol[c]	4.07	—	—	—	3.5	—
Iron–humic sol 1[d]	13.7	0.71	6.1	1.08	11.4	4.0
Iron–humic sol 2[e]	57	—	—	—	20.2	—
Urease[f]	—	1.25	—	0.23	2.13	1.25
Algal exudate[g]	—	0.02	—	0.03	—	0.02

[a] 1×10^{-5} M. [b] 45 mg l^{-1}. [c] 32 mg l^{-1}. [d] 1.04 mg Fe l^{-1} and 5.3 mg humic acid l^{-1}. [e] 6.2 mg Fe l^{-1} and 159 mg humic acid l^{-1}. [f] 100 mg l^{-1}. [g] *Nitzschia sp.* 1.3×10^{6} cells ml^{-1}.

TABLE 5

Effect of model compounds on the removal of cadmium from waters by chelating adsorbents
(2×10^{-6} M cadmium, 2×10^{-5} M ligand. Seawater, pH 8.2; distilled demineralised (d.d.) water, pH 6.5)

Ligand	Cadmium in column effluent (% of total)					
	Chelex-100		Oxine		Thiol	
	d.d.	sea	d.d.	sea	d.d.	sea
None	0.09	0.04	0.02	<0.01	0.01	<0.01
Histidine	—	0.05	—	0.05	—	0.26
Cysteine	0.29	0.04	0.23	0.03	0.20	0.08
Glutathione (SH)	0.16	0.06	0.37	0.03	0.20	0.08
Nitrilotriacetic acid[a]	5.6	0.02	—	—	1.54	0.24
Tannic acid	0.12	0.02	0.08	<0.01	0.30	<0.01
Fulvic acid[b]	0.14	0.02	0.09	<0.01	1.51	0.15
Humic acid sol[c]	7.0	—	—	—	4.1	—
Iron–humic sol 1[d]	2.5	0.08	1.16	0.08	1.57	0.26
Iron–humic sol 2[e]	29	—	—	—	16.4	—
Urease[f]	—	3.7	—	3.2	0.55	0.55
Algal exudate[g]	—	0.03	—	0.01	—	0.02

[a]–[g] See Table 4.

TABLE 6

Effect of model compounds on the removal of lead from waters by chelating adsorbents (2×10^{-6} M lead, 2×10^{-5} M ligand. Seawater, pH 8.2; distilled demineralised (d.d.) water, pH 6.5)

Ligand	Lead in column effluent (% of total)					
	Chelex-100		Oxine		Thiol	
	d.d.	sea	d.d.	sea	d.d.	sea
None	0.17	0.07	0.04	<0.01	0.02	<0.01
Histidine	—	0.17	—	0.02	—	0.41
Cysteine	4.4	0.02	0.39	0.08	0.13	0.04
Glutathione (SH)	1.15	0.91	0.29	0.08	0.53	0.03
Nitrilotriacetic acid[a]	5.9	1.25	—	—	0.64	0.41
Tannic acid	7.5	0.12	0.32	0.05	0.09	0.29
Fulvic acid[b]	1.93	3.1	0.27	0.45	0.56	0.33
Humic acid sol[c]	4.2	—	—	—	1.22	—
Iron—humic sol 1[d]	18.1	0.23	15.4	0.23	5.5	0.08
Iron—humic sol 2[e]	78	—	—	—	29	—
Urease[f]	—	3.8	—	3.9	4.3	4.1
Algal exudate[g]	—	0.09	—	0.02	—	0.02

[a—g]See Table 4.

TABLE 7

Effect of model compounds on the removal of copper from waters by chelating adsorbents (2×10^{-6} M copper, 2×10^{-5} M ligand. Seawater, pH 8.2; distilled demineralised (d.d.) water, pH 6.5)

Ligand	Copper in column effluent (% of total)					
	Chelex-100		Oxine		Thiol	
	d.d.	sea	d.d.	sea	d.d.	sea
None	0.04	0.21	<0.01	<0.01	<0.01	<0.01
Histidine	—	0.12	—	<0.01	—	<0.01
Cysteine	22.9	<0.01	1.50	0.38	0.05	0.39
Glutathione (SH)	55	1.01	0.83	0.20	0.07	0.70
Nitrilotriacetic acid[a]	4.3	0.27	—	—	0.25	0.24
Tannic acid	14.5	0.14	0.54	<0.01	<0.01	0.02
Fulvic acid[b]	15.6	7.4	0.50	0.35	0.81	0.41
Humic acid sol[c]	28	—	—	—	2.11	—
Iron—humic sol 1[d]	34	2.30	19.7	1.39	3.0	1.28
Iron—humic sol 2[e]	89	—	—	—	11.3	—
Urease[f]	—	17.5	—	1.86	3.6	3.5
Algal exudate[g]	—	0.16	—	0.03	—	0.02

[a—g]See Table 4.

Effect of model compounds on removal of metals from waters by chelating adsorbents

Mixtures of zinc, cadmium, lead or copper with various ligands in seawater and d.d. water were passed through the chelating columns, and the effluents were analyzed for total metal by a.s.v. The results are shown in Tables 4—7. Since the percentage removals of metals by the two thiol resins and the thiol and lipoamide porous glass were similar, only the results for the XAD-4 thiol resin [27] are shown. The thiol porous glass was easily oxidized, and required frequent regeneration with mercaptoethanol. The XAD-4 thiol resin was used in all subsequent work.

The following conclusions can be drawn from Tables 4—7. First, in the absence of ligands, removal of zinc, cadmium and lead was more efficient from seawater than from d.d. water. This may be due to the formation, in pure d.d. water, of some metal pseudocolloids which evade ion exchange [45]. Chloride and carbonate complexing in seawater would inhibit the formation of pseudocolloids. Second, the thiol resin and oxine porous glass were generally more efficient than Chelex-100 resin for removal of metals. Third, the thiol compounds cysteine and glutathione, and the SH-containing protein urease caused, in d.d. water, a much greater leakage from Chelex-100 of copper than of the other metals. Fourth, it is evident that adsorption of the metal ions onto the iron-humate colloid is weaker in seawater than in d.d. water [46]. Fifth, the model compounds generally caused losses of less than 5% from the thiol resin. Only the iron-humate colloid caused significant leakage, and then only when its concentration was considerably higher than is found in most natural waters [43]. Sixth, the greatest differences in behaviour between the Chelex-100 and the thiol resins occurred with copper in d.d. water (Table 7). The thiol resin probably reduces copper(II) to copper(I), which is a soft acid that forms highly stable complexes with soft bases, such as some sulphur ligands [42]. Many of the ligands caused relatively large leakages of copper from Chelex-100, but little from the thiol resin. This result could have important implications in toxicity measurements, because use of a thiol resin for speciation determination may often detect a higher fraction of labile copper [2]. Seventh, the ligands had considerably more effect on a.s.v.-labile than on resin-labile metal (Table 3). Tannic acid, for example, which almost eliminated the a.s.v. waves of zinc and copper in seawater at natural pH, had a negligible effect on thiol resin-labile metal. Eighth, algal exudate caused no loss of metals from the columns. Studies with the marine diatom *Nitzschia closterium* (Lumsden and Florence, unpublished results) showed that the amount of copper complexing agent excreted by the algae was proportional to the concentration of copper in solution. No free complexing agent appeared in solution. This is reasonable, because the unprovoked production of protective agents would be wasteful of energy.

Extraction of metal complexes

Determination of the percentage extraction of metal organocomplexes by SM2 resin or hexane—butanol is complicated by the adsorption of free metal ion onto the resin or glass [2] (Fig. 1). No losses were observed from seawater for ionic zinc, cadmium, lead or copper (2×10^{-7} M) onto a siliconized pyrex glass separating funnel, but in d.d. water, pH 6.5, the losses were: 47% Zn, 45% Cd, 74% Pb, 92% Cu. Tannic acid and iron—humate sol had little effect on the percentage of metal adsorbed by SM2 resin from d.d. water, whereas fulvic acid, humic acid, and urease significantly decreased the adsorption of lead and copper. The adsorption behaviour of C_{18} Sep-Pak was similar to that of SM2 resin.

Although most natural waters contain little zinc, cadmium, lead or copper present as the free hydrated metal ion, it is undesirable that a speciation step aimed at measuring lipid-soluble metal could also include some free ionic metal. Adsorption of free metal ion was prevented by lowering the pH of the sample to below pH 4.0 [2] or, preferably, by adding a complexing buffer. Acetate buffer, pH 5.7, was adequate to prevent adsorption of metals onto siliconized glass, but citrate, pH 5.7, was necessary to prevent adsorption, especially of copper, onto SM2 resin. Adjustment of water samples to pH 4.0 led to the retention on SM2 resin of a high percentage of the humic acid content of the sample, plus much of the copper and lead [2]. Although about 20% of the humic acid was still adsorbed by SM2 resin in a citrate buffer of pH 5.7, no adsorption of metals occurred.

Addition of citrate to a water sample may dissociate, or partially dissociate,

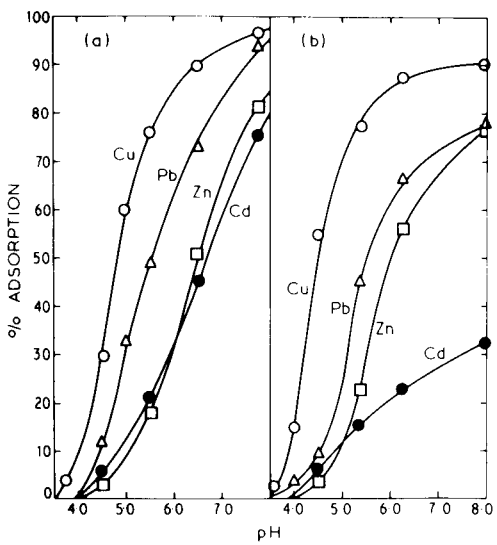

Fig. 1. Adsorption of ionic copper, lead, cadmium and zinc (2×10^{-7} M) onto Bio-Rad SM2 resin: (a) distilled demineralised water; (b) seawater.

some metal organocomplexes, but its use is unavoidable if organically-associated metal is to be determined in the column effluent. An alternative procedure may be elution of adsorbed organics with methanol [34]; Mills and Quinn [36] showed that adsorbed inorganic copper species are not eluted from C_{18} Sep-Pak by methanol. However, there is no information about the efficiency of elution of natural metal organocomplexes by methanol; but analysis of the column effluent would measure all adsorbed metal forms. The estimation of "lipid-soluble metal" with SM2 resin in citrate media is, like all other speciation methods, an operationally-defined measurement.

The APDC and oxine complexes of zinc, cadmium, lead and copper were extracted from 0.01 M citrate buffer pH 5.7 by SM2 resin, hexane—butanol, and C_{18} Sep-Pak to the extent of 70—90% for both seawater and d.d. water. No extraction of metals was found in the presence of citrate, triethanolamine, acetylacetone, histidine, methionine, glutathione, urease, algal exudate, tannic acid, fulvic acid, humic acid, or iron—humate colloid. However, several of the ligands (APDC, oxine, glutathione, and tannic, fulvic and humic acids) were themselves adsorbed to some extent by SM2 resin.

No further work was carried out with C_{18} Sep-Pak, because it was found that the cartridges were seriously contaminated with heavy metals, some of which entered the effluent, and could not be completely removed by prolonged washing with acid. In addition, the C_{18} hydrocarbon chain of Sep-Pak is not as suitable a model for lipid solubility as SM2.

Analysis of water samples

Total metal concentrations. These were determined after u.v. irradiation in acid solution, and the results are shown in Table 8. The higher concentrations of all four metals, but especially zinc and copper, in South Creek sample 2 reflects anthropogenic pollution from sewage, whereas the lower concentrations of iron and DOC (Table 1) indicate removal of iron and humic material in the sewage treatment plant. The higher DOC in the septic sample after chlorination probably results from partial breakdown of organic

TABLE 8

Total metal concentrations in filtered samples

Sample	Total metal ($\mu g\ l^{-1}$)			
	Zn	Cd	Pb	Cu
Tapwater	6.1	0.15	1.98	15.6
Septic before Cl_2	46.2	0.38	4.10	8.4
Septic after Cl_2	27.5	1.61	3.94	20.4
South Cr. 1	6.7	0.40	2.03	4.45
South Cr. 2	20.8	0.63	3.55	9.9
1-km seawater	2.16	0.28	0.50	1.40
Marina seawater	3.45	0.34	0.65	3.21

particulate matter by chlorine, and the production of more filterable organic carbon.

The marina seawater sample had a higher concentration of all four metals, probably originating from anti-fouling paints, sacrificial zinc anodes and leaded gasoline.

Speciation results. The results (means of three separate determinations) are shown in Tables 9—12. The precision of a.s.v. measurements at concentrations above 1×10^{-8} M was ±2—3%, and at the 1×10^{-9} M level was ±5—7%. Analyses involving resin columns were made on the column effluents, rather than by elution of the adsorbed metal. Percent adsorption was calculated from the difference between total and effluent metal concentrations. This procedure has the advantages that it is simpler, has lower blanks, involves much less opportunity for contamination, and eliminates doubt about efficiency of elution. The gain in sensitivity obtained by elution of the resin is negated to some extent by the increased blank, and relatively

TABLE 9

Speciation in tapwater

Technique	Labile metal (electroactive or extracted) (%)			
	Zn	Cd	Pb	Cu
A.s.v.[a]	56	100	100	79
U.v.—a.s.v.[a]	100	100	100	100
Chelex-100 resin	86	0	81	75
Thiol resin	84	0	59	76
SM2 resin	0	0	37	40
Hexane—butanol	0	21	4.0	4.5

[a]Acetate pH 4.7.

TABLE 10

Speciation in septic water

Technique	Labile metal (electroactive or extracted) (%)[a]							
	Zn		Cd		Pb		Cu	
	A	B	A	B	A	B	A	B
A.s.v.[b]	7.1	7.0	74	27	11.0	59	47	31
U.v.—a.s.v.[b]	100	90	100	75	57	70	81	76
Chelex-100 resin	17.1	31	10.5	0	3.2	0	6.4	52
Thiol resin	47	30	0	0	7.3	9.6	33	77
SM2 resin	14.3	0	0	0	41	0	40	0
Hexane—butanol	0	0	0	0	53	39	31	0

[a]A = before chlorination, B = after chlorination. [b]Acetate, pH 4.7.

TABLE 11

Speciation in South Creek water

Technique	Labile metal (electroactive or extracted) (%)[a]							
	Zn		Cd		Pb		Cu	
	A	B	A	B	A	B	A	B
A.s.v., acetate pH 4.7	10.9	9.6	100	95	27	53	4.5	24
A.s.v., natural pH	11.3	—	100	—	[b]	—	<0.5	—
Chelex-100 resin	55	83	0	90	3.4	55	0	48
Thiol resin	38	81	0	91	0	56	36	75
SM2 resin	17.1	16.3	0	0	0	0	5.8	57
Hexane—butanol	13.4	22	0	0	36	23	0	0

[a]A = South Cr. 1 (before sewage plant), B = South Cr. 2 (after sewage plant). [b]Not quantifiable.

TABLE 12

Speciation in seawater

Technique	Labile metal (electroactive or extracted) (%)[a]							
	Zn		Cd		Pb		Cu	
	A	B	A	B	A	B	A	B
A.s.v., acetate pH 4.7	75	65	100	100	100	100	19.3	26
A.s.v., natural pH	19	45	64	[b]	42	[b]	<1.5	16.2
U.v.—a.s.v.[c]	100	100	100	100	100	100	66	75
Chelex-100 resin	22	70	25	0	0	0	0	40
Thiol resin	22	60	29	0	0	0	7.9	24
SM2 resin	0	54	0	23	0	21	0	53
Hexane—butanol	67	57	0	0	0	40	0	22

[a]A = 1-km seawater, B = marina seawater. [b]Not quantifiable. [c]Acetate pH 4.7.

large volumes of sample must be used before a significant advantage is achieved. In cases where little adsorption occurs, however, analysis of the effluent has the disadvantage that percent adsorption is calculated as the difference between two large numbers.

A separate column of SM2 resin was used for each solution. The resin strongly adsorbs ligands such as fulvic and humic acids, which might affect subsequent samples. No memory effects were observed in the use of Chelex-100 or thiol resin columns on a succession of water samples. However, the columns were replaced or regenerated after 10—20 samples.

Batch techniques for resin equilibration were studied as an alternative to the use of columns. The water samples (25 ml) plus resin were shaken in 100-ml plastic bottles on a wrist-action shaker, and then the solution was separated from the resin by pouring it through a porous polypropylene

funnel. Equilibrium for ionic standards was attained after 30 min. However, removal of metals was less efficient than with a column, which has several theoretical separation plates. In addition, wet thiol resin was rapidly oxidised when not stored in a column.

A.s.v.-labile metal. All a.s.v.-labile measurements shown in Tables 9—12 were made with a deposition potential of —1.3 V, so that the four metals could be measured simultaneously. However, because very negative deposition potentials can lead to direct reduction of some metal complexes, measurements of labile copper were also made with deposition potentials of —0.4 V for freshwater and —0.6 V for seawater (Table 13). Both South Creek waters and the septic water showed higher a.s.v.-labile copper when deposited at —1.3 V, indicating the presence of reducible copper complexes. A pseudo-

TABLE 13

Effect of deposition potential on a.s.v.-labile copper in a 0.05 M acetate buffer, pH 4.7

Sample	A.s.v.-labile copper ($\mu g\ l^{-1}$)	
	—0.4 V[a]	—1.3 V[a]
Tapwater	12.4	12.3
Septic after Cl_2	0.27	6.3
South Cr. 1	<0.03	0.20
South Cr. 2	0.33	2.39
Marina seawater	0.78[b]	0.83

[a]Deposition potential (V vs. Ag/AgCl). Results at —0.4 V have been multiplied by 1.07 to account for the extra deposition which occurs while scanning in an unstirred solution from —1.3 V to —0.4 V. [b]Deposition potential, —0.6 V.

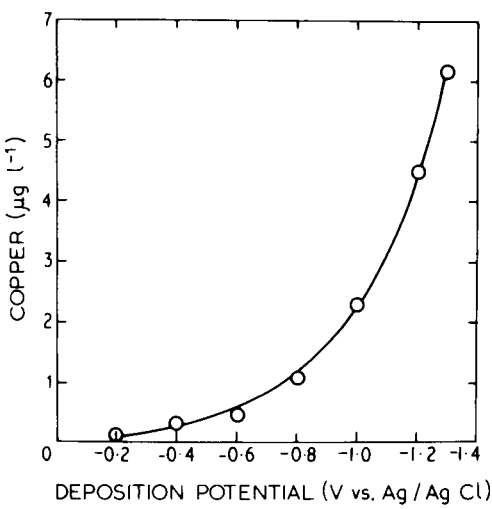

Fig. 2. Pseudopolarogram of septic water after chlorination.

polarogram (Fig. 2) of the septic water shows that a.s.v.-labile copper appears with deposition potentials above —0.8 V.

The a.s.v.-labile metal in seawater was considerably lower at natural pH than in acetate buffer (Table 12). However, the decrease in a.s.v.-labile metal, when the solution was changed from acetate buffer to natural pH, was much greater for the marina than the 1-km sample. This suggests that the metal pollution in the marina water exists as species which are relatively easily dissociated.

Bio-Rad SM2 resin extraction. The effect of citrate on the adsorption of metal ions from the water samples was determined (Table 14). Citrate generally lowered the percent extracted metal, especially in the case of zinc, but the results do not show whether the action of citrate is solely in preventing adsorption of free metal ion, or dissociating metal complexes, or both. It is interesting to note that in the cases of cadmium in tapwater, and lead and cadmium in 1-km seawater, where the metals are completely acetate-a.s.v.-labile, no adsorption took place on SM2 resin, even in the absence of citrate (Table 14). By contrast, the marina sample, in which the cadmium and lead were also entirely acetate-a.s.v.-labile, had significant SM2-soluble fractions of these metals. Lead alkyls are known to be a.s.v.-labile [47], and their presence in the marina seawater sample may provide the SM2-soluble lead.

Comparison of speciation results. The following observations can be made from Tables 9—12. First, for all samples except the marina seawater, thiol resin extracted more copper than Chelex-100. For the other metals, however, the two resins gave similar results. Second, there was no clear pattern in the relationship between a.s.v.-labile and resin-labile metal. In most of the samples, a.s.v.-labile cadmium and lead were higher than thiol resin-labile, but the reverse was true for zinc and copper. In the cases of cadmium and lead in seawater, and cadmium in tapwater, the metals were completely a.s.v.-labile, but showed zero adsorption on thiol and Chelex-100 resins. This behaviour of cadmium and lead in seawater was observed previously [18],

TABLE 14

Effect of citrate on extraction of metals by Bio-Rad SM2 resin

Sample	Metal extracted by SM2 (% of total)							
	No citrate				Citrate buffer[a]			
	Zn	Cd	Pb	Cu	Zn	Cd	Pb	Cu
Tapwater	47	0	50	92	0	0	37	40
South Cr. 2	59	0	0	67	16	0	0	57
1-km seawater	85	0	0	0	0	0	0	0
Marina seawater	95	50	35	50	54	23	21	53

[a]Citrate buffer, 0.01 M, pH 5.7.

and is quite different from their behaviour with model compounds (Tables 3—7), where thiol resin invariably removed a higher percentage of metal than was a.s.v.-labile. The water samples must have contained metal species of a nature quite different from those of the model compounds studied. Because the resin columns provide a reaction time of about 19 s, and the a.s.v. technique has an effective reaction time of less than 1 s [4], complexes with slow dissociation kinetics would be expected to yield more metal to the chelating resins. The contradictory behaviour observed in the water samples may have been caused by the presence of colloidal particles which cannot enter the resin network [1, 12], or to stable metal complexes which are directly a.s.v.-reducible. Third, ultra-violet irradiation of the seawater, tapwater, and septic water resulted in a significant increase in a.s.v.-labile metal, especially in the case of zinc. This implies that much of the metal which is not directly a.s.v.-labile is associated with organic matter. However, in the seawater and septic water samples, 20—30% of copper is still a.s.v.-inert, even after u.v. irradiation, and presumably is adsorbed on inorganic colloids [48]. Fourth, chlorination of the septic water increased the fraction of copper available to the chelating resins and decreased the percentage of zinc, lead and copper extractable by SM2 resin and hexane–butanol, despite the fact that filterable dissolved organic carbon increased after chlorination. Some metal-complexing organics were apparently destroyed or altered by chlorination. Fifth, the increase in a.s.v.-labile metal after u.v. irradiation gave no indication of the fraction of SM2 resin-soluble metal in a sample, showing that not all the metal—organic compounds are extractable. The sewage-affected creek water and the polluted marina seawater had relatively high concentrations of organic-soluble metal. Surprisingly, tapwater also contained some SM2-soluble cadmium, lead, and copper, and over half the zinc in coastal seawater was soluble in SM2 and hexane–butanol. Anthropogenic pollution appears to lead to an increase in organic-soluble metal, although it is difficult to suggest the types of compounds causing this behaviour. Experimentally, SM2 resin is more convenient to use than solvents such as hexane or chloroform, and the very small blanks associated with its use allows SM2-soluble metal to be measured confidently at low concentrations.

CONCLUSIONS

Studies with model compounds did not completely explain the speciation behaviour of trace metals in the water samples. It is likely that unidentified ligands are providing the a.s.v.-inert and thiol resin-inert metal compounds. McKnight and Morel [49] suggested that hydroxamate siderochromes, natural complexing agents excreted by algae, are important ligands. However, algal exudate, tested in this study, had no effect on a.s.v.-labile or resin-labile metal. Also, Tuschall and Brezonik [50] found that Desferal, a trihydroxamate siderochrome, formed cadmium and copper complexes that

were completely a.s.v.-labile, as were the complexes of histidine and the monomeric humic acid model compounds, pyrogallol, gallic acid and *p*-hydroxycinnamic acid, although bovine serum albumin produced a non-reducible copper complex. Hoffmann et al. [51] reported that trace heavy metals in the Mississippi and Minnesota rivers were mostly associated with compounds of 1000—10 000 molecular weight. They suggested that macrocyclic ligands, such as porphyrins and phthalocyanins, may play an important role in metal chelation in natural waters.

Fulvic and humic acids, and humate-coated inorganic particles have been suggested as the principal complexing agents in natural waters [2, 14—16]. Fulvic acid is usually the dominant compound [43], with typical concentrations of 0.05—1.3 mg l^{-1} in seawater (0.003—0.34 mg l^{-1} humic acid) [52], and 1.0—8.7 mg l^{-1} for river and lake waters [14, 43]. The complexing efficiency of humic acid decreases rapidly with increasing salinity [53]. However, in agreement with the conclusions of other workers [52, 53], complexation by fulvic and humic acids cannot explain the non-labile behaviour of the metals in the samples examined in this study. One area of doubt is whether laboratory-prepared fulvic and humic acids are representative of the natural compounds. Oxidation of the humic substances by iron(III) and oxygen in the strongly alkaline and acidic solutions used for separation may destroy chelating groups on the molecules [54].

The results of this study do not allow unequivocal recommendations to be made on trace metal speciation procedures for evaluation of aquatic toxicity. Such recommendations must await algal toxicity studies at present in progress. However, some preliminary statements can be made. First, a.s.v.-labile measurements, if used, should be made at a minimum of two different deposition potentials to detect labile and quasi-labile, or directly reducible complexes. Second, metal extractable by Bio-Rad SM2 resin is an important species and should be measured. Third, thiol resin, while yielding similar results to Chelex-100 resin for zinc, cadmium and lead, gives a much higher percentage of resin-labile copper. Whether or not this higher labile copper content correlates more closely with toxicity remains to be seen. Finally, ultra-violet irradiation of the sample, followed by a.s.v.-labile or resin-labile measurement of liberated metal, is a simple and contamination-free method of determining organically-associated metal. However, it cannot be used for freshwaters with iron concentrations greater than about 100 $\mu g\ l^{-1}$.

This work was supported by a grant from the Office of the Supervising Scientist. The assistance of Mr. B. R. Saunders with some of the experimental work is gratefully acknowledged.

REFERENCES

1 T. M. Florence and G. E. Batley, Crit. Rev. Anal. Chem., 9 (1980) 219.
2 T. M. Florence, Talanta, 29 (1982) 345.
3 Y. K. Chau and K. Lum-Shue-Chan, Water Res., 8 (1974) 383.
4 W. Davison, J. Electroanal. Chem., 87 (1978) 395.
5 H. P. Van Leeuwen, J. Electroanal. Chem., 99 (1979) 93.
6 P. Figura and B. McDuffie, Anal. Chem., 51 (1979) 120.
7 J. R. Tuschall and P. L. Brezonik, Anal. Chem., 53 (1981) 1986.
8 T. M. Florence, Biochem. J., 189 (1980) 507.
9 U. Borgmann, Can. J. Fish. Aquat. Sci., 38 (1981) 999.
10 C. E. Stephan, U.S. Environmental Protection Agency Report No. EPA-660/3-75-009, April 1975.
11 T. M. Florence and G. E. Batley, Talanta, 22 (1975) 201.
12 T. M. Florence and G. E. Batley, Talanta, 23 (1976) 179.
13 T. M. Florence, Water Res., 11 (1977) 681.
14 E. Tipping, Geochim. Cosmochim. Acta, 45 (1981) 191.
15 J. A. Davis and J. O. Leckie, Environ. Sci. Technol., 12 (1978) 1309.
16 L. Balistrieri, P. G. Brewer and J. W. Murray, Deep-Sea Res., 28A (1981) 101.
17 E. R. Sholkovitz, Earth Planet. Sci. Lett., 41 (1978) 77.
18 G. E. Batley and T. M. Florence, Mar. Chem., 4 (1976) 347.
19 P. Figura and B. McDuffie, Anal. Chem., 52 (1980) 1433.
20 D. P. Laxen and R. M. Harrison, Sci. Total Environ., 19 (1981) 59.
21 G. W. Bryan, in A. P. Lockwood (Ed.), Effects of Pollutants on Aquatic Organisms, Cambridge University Press, Cambridge, 1976, p. 7.
22 J. F. Skidmore, Q. Rev. Biol., 39 (1964) 227.
23 G. Giebisch, D. C. Tosteson and H. H. Ussing (Eds.), Membrane Transport in Biology, Vol. 1, Springer-Verlag, Berlin, 1978.
24 W. H. Shaw, Science, 120 (1954) 361.
25 N. S. Fisher and G. J. Jones, J. Phycol., 17 (1981) 108.
26 G. Roesijadi, Mar. Environ. Res., 4 (1980—81) 167.
27 R. J. Phillips and J. S. Fritz, Anal. Chem., 50 (1978) 1504.
28 Z. Slovák, M. Smrž, B. Dočekal and S. Slováková, Anal. Chim. Acta, 111 (1979) 243.
29 A. Deratani and B. Sebille, Anal. Chem., 53 (1981) 1742.
30 Chuen-Ying Liu and Peng-Joung Sun, Anal. Chim. Acta, 132 (1981) 187.
31 T. M. Florence and G. E. Batley, Anal. Chem., 52 (1980) 1962.
32 A. G. Lee, Nature, 294 (1981) 695.
33 D. Chapman (Ed.), Biological Membranes, Academic Press, London, 1968.
34 Y. Sugimura, Y. Suzuki and Y. Miyake, Proc. Third Nuclear Energy Agency Seminar on Marine Radioecology, Tokyo, October 1979, p. 131.
35 Y. Sugimura, Y. Suzuki and Y. Miyake, Deep-Sea Res., 25 (1978) 309.
36 G. L. Mills and J. G. Quinn, Mar. Chem., 10 (1981) 93.
37 F. Vernon and K. M. Nyo, Inorg. Nucl. Chem., 40 (1978) 887.
38 F. A. Armstrong and S. Tibbits, J. Mar. Biol. Assoc. U.K., 48 (1968) 143.
39 G. E. Batley and Y. J. Farrar, Anal. Chim. Acta, 99 (1978) 283.
40 S. M. Griffith and M. Schnitzer, Soil Sci., 39 (1975) 861.
41 G. R. Aiken, E. M. Thurman and R. L. Malcolm, Anal. Chem., 51 (1979) 1799.
42 J. O. Leckie and J. A. Davis, in J. O. Nriagu (Ed.), Copper in the Environment. Part 1. Ecological Cycling, Wiley-Interscience, New York, 1979, p. 89.
43 J. Lawrence, Water Res., 14 (1980) 373.
44 H. Blutstein and J. D. Smith, Water Res., 12 (1978) 119.
45 P. Beneš and V. Majer, Trace Chemistry of Aqueous Solutions, Elsevier, Amsterdam, 1980.

46 G. E. Millward, Environ. Tech. Lett., 1 (1980) 394.
47 S. E. Birnie and D. J. Hodges, Environ. Tech. Lett., 2 (1981) 433.
48 T. M. Florence and G. E. Batley, J. Electroanal. Chem., 75 (1977) 791.
49 D. M. McKnight and F. M. Morel, Limnol. Oceanogr., 24 (1979) 823.
50 M. R. Tuschall and P. L. Brezonik, Anal. Chem., 53 (1981) 1986.
51 M. R. Hoffmann, E. C. Yost, S. J. Eisenreich and W. J. Maier, Environ. Sci. Technol., 15 (1981) 655.
52 S. R. Piotrowicz, Anal. Chem., (1982) in press.
53 R. F. Mantoura, A. Dickson and J. P. Riley, Estuarine Coastal Mar. Sci., 6 (1978) 387.
54 E. M. Perdue, Geochim. Cosmochim. Acta, 42 (1978) 1351.

Analytica Chimica Acta, 141 (1982) 95—103
Elsevier Scientific Publishing Company, Amsterdam — Printed in The Netherlands

CADMIUM(II) BINDING BY SOIL-DERIVED FULVIC ACID MEASURED BY ANODIC STRIPPING VOLTAMMETRY

GAJANAN A. BHAT and JAMES H. WEBER*

University of New Hampshire, Chemistry Department, Parsons Hall, Durham, NH 03824 (U.S.A.)

(Received 3rd February 1982)

SUMMARY

Titrations of aqueous solutions of soil fulvic acid (30, 45, and 60 mg l^{-1}) with cadmium ion solutions at pH 6 and 7 reveal unusual shapes in the stripping current (i_s) vs. total cadmium ion ($C_{Cd^{2+}}$) curves. The expected inflections occur in the titration curves at 8—16 μM at pH 6 and 12—26 μM at pH 7. In addition, there is an initial rapid increase in i_s at very low $C_{Cd^{2+}}$. The initial rapid increase in current is attributed to labile cadmium—fulvic acid complexes that contribute to i_s by rapid dissociation. Subsequent addition of cadmium ion results in moderately labile complexes and i_s becomes partially kinetically controlled. The stripping current was corrected for kinetic current contributions from dissociation of complexes, and total ligand concentrations, conditional stability constants, and upper slopes were calculated from data well past the titration end-point. The use of upper slopes after kinetic current corrections as in situ calibration curves, allowed calculations of equilibrium cadmium concentrations. The data show that both kinetic current corrections and in situ calibration curves are necessary to avoid substantial errors in calculations of equilibrium cadmium concentrations from anodic stripping voltammetric experiments.

Humic acid and fulvic acid are very complex polyelectrolyte mixtures, and studies of their reactions with metal ions are very difficult. Previous work has emphasized binding of a variety of metal ions with isolated fulvic acid samples using ion-selective electrodes [1—5], fluorescence [5, 6], voltammetry [7], and dialysis [8, 9]. A major goal is to apply these techniques to metal ion speciation in natural water samples [10], a subject ably reviewed by Florence and Batley [11].

Cadmium complexes of fulvic acid have not been studied as extensively as complexes of several other metal ions. Recent cadmium studies include its complexation to components of sewage sludge [12] and sewage effluent [13], natural water samples [14], coal humic material [15] and isolated fulvic acid [2]. The studies generally show that cadmium binding to fulvic acid [2] varies with the $C_{Cd^{2+}}$/total fulvic acid ratio and increases as pH increases. Other papers [1, 16] describe similar behavior for binding with copper ions.

In a previous paper [7], the anodic stripping voltammetry (a.s.v.) technique of Shuman et al. [17, 18] was applied to a study of copper binding

0003-2670/82/0000-0000/$02.75

by soil fulvic acid. The major goal of the research was to determine total ligand concentrations (C_L) and equilibrium Cu^{2+} concentration ($[Cu^{2+}]$) from titrations with a.s.v. detection. This goal could not be achieved with uncorrected i_s data and calibration curves done in the absence of soil fulvic acid. Two major findings were that i_s should be corrected for kinetic current contributions, and that calibration curves should be done in the presence of soil fulvic acid to overcome the effects of its adsorption on the mercury electrode [19].

This paper extends the a.s.v. technique to cadmium—soil fulvic acid binding and shows evidence for initial formation of labile complexes and subsequently of moderately labile complexes. In this context, labile means that the rate of dissociation of the cadmium—soil fulvic acid complex is much faster than that of Cd^{2+} diffusion; moderately labile means that the dissociation rate is similar to the diffusion rate. In the earlier paper on copper [7] "moderately labile" but no "labile" behavior was observed. However, in that paper the term "labile" was used to describe the results.

EXPERIMENTAL

Apparatus and reagents

Details of the a.s.v. experimental conditions and apparatus can be found elsewhere [7]. A Perkin-Elmer model 204 spectrofluorimeter was used to obtain Rayleigh scattering data at 300 nm [6]. Stock cadmium nitrate solution was Fisher Scientific certified SO-C-118 1000 mg l^{-1} atomic absorption standard.

Procedures

Measurements by a.s.v. Differential pulse a.s.v. was used throughout. Solutions of soil fulvic acid were titrated with the cadmium solution at constant pH in duplicate experiments and stripping currents were measured in triplicate. The cadmium—fulvic acid diffusion coefficient (D) was chosen as 10^{-6} cm^2 s^{-1} [20] based on the lead(II)—humic acid value. The instrumental settings provided a 25 s plating time, a 5 mV s^{-1} scan rate, a 10 mV modulation amplitude, a −0.800 V (vs. Ag/AgCl) plating potential, and a 1.11×10^{-2} cm^2 surface area of the drop. The accumulation coefficient (γ) of 3.81 was determined for the above experimental conditions by measuring the plating current by d.c. voltammetry with stirring, measuring the a.s.v. current, and calculating the stripping current/plating current ratio.

Non-linear regression analysis. The data treatment was similar to that in the earlier paper [7], except that Eqn. (1) of that paper would not smooth the present titration data. The present application of the program NONREG is to fit the stripping current (i_s) and $C_{Cd^{2+}}$ data to the equation

$$i_s = (S_l C_M) + (S_i/2)\{C_M - C_L - K^{-1} + [(C_L - C_M + K^{-1})^2 + 4C_M K^{-1}]^{1/2}\} \quad (1)$$

The upper slope (S_u) is the slope well past the end-point, and the lower slope

(S_l) is the slope before the end-point. The fitted parameters are S_l, S_i (difference between S_u and S_l), and K (conditional stability constant). Total metal concentration is represented by C_M. The first term in Eqn. (1) accounts for labile species, and the second term is Shuman's equation [7, 17, 18] for a 1:1 complexation model and moderately labile complexes. Because of Rayleigh scattering (see below), data with $C_{Cd^{2+}}$ greater than 80 μM were not used.

Kinetic current corrections. Kinetic current corrections were generally made as previously described [7]. Two differences are that for cadmium, data before $C_{Cd^{2+}} \simeq 3$ μM were omitted and only first iteration values were used. The calculated rate constant (k_f) for dissociation of the cadmium—soil fulvic acid complexes is 7.5×10^2 s^{-1}. Constants K are calculated from data up to about $C_L/2$. Typical errors in the titration parameters for duplicate experiments are 10% with a maximum of 20%.

RESULTS

Data treatment prior to kinetic current correction

Figure 1 shows raw i_s vs. $C_{Cd^{2+}}$ data for titrations of soil fulvic acid (30, 45, and 60 mg l^{-1}) at pH 6 and 7. The i_s values rise as $C_{Cd^{2+}}$ increases; and all curves show inflections, which are more prominent at pH 7 than at pH 6. Values of C_L were estimated at each break by calculating the intersection of upper (S_u) and lower (S_l) curves by linear regression. The C_L values estimated are in the 8—16 μM range at pH 6 and the 12—26 μM range at pH 7. As expected, C_L increases as the fulvic acid concentration increases (Table 1). Table 1 also includes the upper slopes (S_u) of the i_s vs. $C_{Cd^{2+}}$ curves well past the end-points. As in analogous copper experiments [7], S_u decreases as soil fulvic acid concentration increases.

As a second step in the data treatment, the i_s vs. $C_{Cd^{2+}}$ data were fitted to

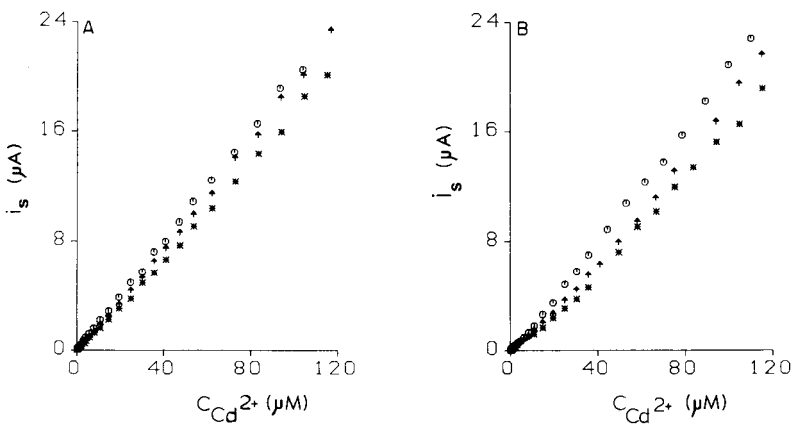

Fig. 1. Plots of stripping current vs. $C_{Cd^{2+}}$ in 0.1 M KNO_3 at (A) pH 6 and (B) pH 7. Soil fulvic acid concentration (mg l^{-1}): (○) 30; (♠) 45; (*) 60.

TABLE 1

Parameters obtained from titrations of soil fulvic acid (SFA) with cadmium ion solution

Status of data	[SFA] (mg l^{-1})	pH 7				
		C_L (μM)	S_l (μA μM^{-1})	S_i (μA μM^{-1})	S_u^a (μA μM^{-1})	10^{-5} K
Without fit	30	12	0.164	0.043	0.207	
	45	18	0.141	0.046	0.187	
	60	26	0.125	0.048	0.173	
NONREG fitted	30	11	0.149	0.067	0.216	20
	45	19	0.120	0.068	0.188	3
	60	27	0.111	0.073	0.184	30
Av.						20
Kinetic-current corrected	30	14			0.184	2
	45	19			0.141	1
	60	32			0.137	1
Av.						1
		pH 6				
Without fit	30	8	0.201	0.011	0.212	
	45	12	0.189	0.011	0.200	
	60	16	0.151	0.027	0.178	
NONREG fitted	30	27	0.190	0.006	0.196	40
	45	24	0.166	0.038	0.204	20
	60	28	0.146	0.037	0.183	8
Av.						20
Kinetic-current corrected	30	27			0.172	6
	45	32			0.128	7
	60	20			0.111	10
Av.						8

[a] S_u is 0.215 μA μM^{-1} in the absence of soil fulvic acid.

Eqn. (1) by the NONREG program. This step has relatively little effect on C_L. Values of S_l and S_i decrease and increase by about the same amounts, and S_u values are relatively unchanged. The NONREG treatment yields K of about 20×10^5 at pH 6 and 7.

Effect of kinetic current correction on titration parameters

Figure 1 effectively shows the moderately labile portion of the titration curve, but not the labile part. Expanded Fig. 2 for 30 mg l^{-1} soil fulvic acid at pH 7, emphasizes the early part of the titration curve where Cd^{2+} species are labile. This portion of the curve necessitates the first term of Eqn. (1) in order to fit the data. Figure 2 exemplifies the curve shape at low $C_{Cd^{2+}}$ that occurs with all titrations.

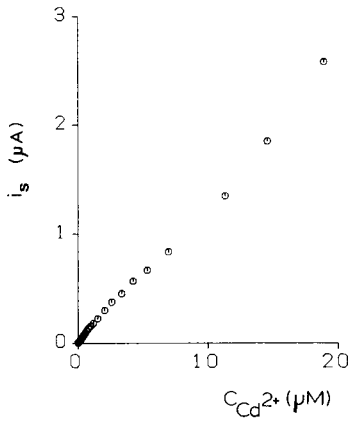

Fig. 2. Expanded scale plot of stripping current vs. $C_{Cd^{2+}}$ for soil fulvic acid (30 mg l^{-1}) at pH 7. Only initial data points are used to show the first titration curve break. Planting time is 30 s.

The kinetic current correction excludes data on labile complexes ($C_{Cd^{2+}} \leqslant 3\,\mu M$), and the treatment fits only the parameters C_L, S_u and K (Table 1). At pH 7, values of C_L increase by an average of 15% over the NONREG fitted values and S_u values decrease by an average of 22%. Both trends also occurred in the titrations with copper ions [7]. The average K value at pH 7 decreases from 20×10^5 for NONREG fitted data to 1×10^5 for kinetic current-corrected data.

DISCUSSION

Stripping current vs. concentration

The extent of complexation of cadmium by soil fulvic acid is small at pH 6, and the titration parameters have a larger error than at pH 7. This discussion focuses on the more reliable pH 7 data. The early part of the titration of 30 mg l^{-1} soil fulvic acid at pH 7 by cadmium ions (Fig. 2) shows an initial rapid rise in i_s suggestive of labile complexes. Addition of more Cd^{2+} causes a reproducible decrease in the slope because the bound cadmium dissociates more slowly. Finally, addition of more Cd^{2+} results in a gradual rise in i_s after the end-point. The different degrees of lability of bound cadmium require both terms of Eqn. (1), to smooth the data properly. Blank titrations demonstrated that the unusual curve shape did not occur in the absence of soil fulvic acid, and thus cannot be attributed to adsorption of cadmium ions on the titration vessel or on colloidal matter in the deionized–distilled water. Data from titrations of soil fulvic acid with copper ions [7] did not show this behavior and the second term of Eqn. (1) fitted the data.

The unusual shapes of titration curves requires close examination of the a.s.v. behavior of the cadmium–soil fulvic acid complexes. It is accepted now that fulvic acid is a mixture of ligands with a variety of molecular weights.

Consequently, the binding strengths of these ligands with metal ions vary during the titration. Initial addition of metal ion to soil fulvic acid results in preferentially stronger binding with some fractions of the fulvic acid, and binding would be weaker subsequently. Such a continuous change in the nature of binding over a considerable range of metal ion addition should result in decreasing average conditional stability constants. Ion-selective electrode titrations of fulvic acid by Weber and co-workers with Cd^{2+} [2], Pb^{2+} [3], and Cu^{2+} [1] as well as the results of Gamble et al. [16] with Cu^{2+}, confirm this expectation. Generally a large K value is indicative of a small dissociation rate constant (k_f) for metal complexes. Thus it is surprising that the strongest cadmium–soil fulvic acid complexes early in the titration have the greatest lability. We do not yet have an explanation for this result.

Several papers describe the lability of the cadmium complexes. Figura and McDuffie [14] showed with a.s.v. data that in sewage effluents and various natural water samples, most cadmium is either free or labile. The Florence and Batley review [11] lists similar results. Laxen and Harrison [13] noted that a.s.v. titrations yielded zero or nearly zero C_L values, demonstrating that added Cd^{2+} is either uncomplexed or bound to labile complexes. Some of the Cd^{2+} present in their samples is probably adsorbed on colloidal-sized particles. Truitt and Weber [10] by dialysis titrations demonstrated C_L values ranging from near zero to 9.7 μM for Cd^{2+} in fresh natural waters. Possibly the failure to detect binding capacity in a.s.v. experiments is due to lability of Cd^{2+} complexes rather than the absence of complexation.

Because fulvic acid is a mixture of ligands that forms a variety of complexes with Cd^{2+}, it is reasonable to expect the complexes to have a wide range of dissociation rates. Previous results discussed above indicate that the fraction of labile complexes will be quite large. The present titration curves, which are similar to earlier diagrams (fig. 11 in [13]), suggest that the initial added Cd^{2+} forms rapidly dissociating complexes and that most of the i_s value to the first break results from rapid dissociation of a cadmium–soil fulvic acid complex. When complexation to strongly binding ligands and formation of labile complexes is complete, subsequent Cd^{2+} additions result in i_s values that are partially kinetically controlled. Further addition of Cd^{2+} results in continued complexation and a distinct break in the titration curve.

Measurements of equilibrium concentrations of cadmium ($[Cd^{2+}]$) or other metal ions by a.s.v. in the presence of humic matter are usually done for metal ion speciation studies to distinguish free and complexed metal ions. Complex dissociation during the a.s.v. plating step can result in a large overestimation of free metal ion concentration because of measurement of free plus labile metal ion. The effect of such dissociation is evident in Fig. 3, which represents the plot of original and kinetically corrected $[Cd^{2+}]$ for different concentrations of soil fulvic acid. A similar plot for the copper complexes (fig. 3 in [7]) shows a much smaller effect from dissociation. The large difference for cadmium ions between corrected and uncorrected values

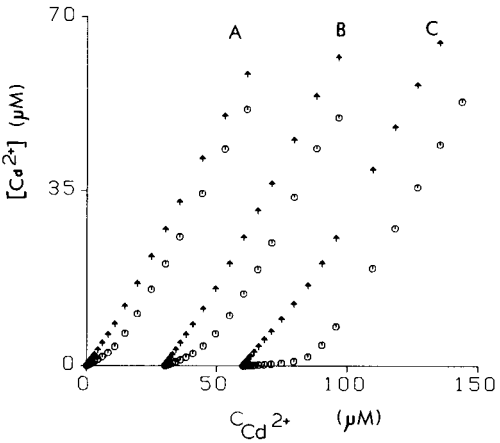

Fig. 3. Equilibrium vs. total Cd^{2+} concentration at pH 7 from NONREG fitted (+) and kinetic current-corrected (○) data for soil fulvic acid concentrations of: (A) 30 mg l^{-1}; (B) 45 mg l^{-1}; (C) 60 mg l^{-1}. Curves B (30 units) and C (60 units) are shifted to the right on the total $[Cd^{2+}]$ axis.

emphasizes the enhanced i_s value arising from dissociation of the complexes. This difference between corrected and uncorrected $[Cd^{2+}]$, which increases with increased soil fulvic acid concentration, is obviously due to increasing formation of labile complexes. A similar trend occurs at pH 6.

Table 1 gives the titration parameters at pH 6 and 7. The kinetic current-corrected C_L values are higher than the NONREG fitted values by an average of 15%. The 14 μM C_L value for 30 mg l^{-1} fulvic acid at pH 7 compares favorably with previous dialysis values of 16 μM [8] and 10 μM [9] for 10 mg l^{-1} soil fulvic acid solutions at the same pH. The K value of 1×10^5 at pH 7 is close to the value of 4×10^4 obtained for much more concentrated soil fulvic acid solutions [2]. Because K values for the cadmium complexes are higher at lower fulvic acid concentrations, the agreement is better than it first appears. In addition, the K value of 3×10^5 for the copper complexes by a.s.v. at pH 6 [7] is, as expected, higher than the value for Cd^{2+} at pH 7. The difference would be even greater if the value for the copper complexes at pH 7 were available.

Effect of adsorption on the stripping current

Adsorption of fulvic acid on the mercury electrode is another serious problem in a.s.v. [19]. Very strong adsorption might distort the wave and cause a non-linear relationship between i_s and the bulk metal ion concentration. Hence a great deal of caution should be exercised before adopting the a.s.v. technique for such titrations. The problem of fulvic acid adsorption has been discussed and methods to overcome this difficulty were devised [7].

The upper slopes (S_u) of titration curves (Fig. 1, Table 1) for the three soil fulvic acid concentrations are not the same even when cadmium ions are

in great excess. The decrease in S_u with increased soil fulvic acid concentration can be attributed to decreased i_s at constant $C_{Cd^{2+}}$. The adsorption of fulvic acid is one factor responsible for this effect [19]. Increased soil fulvic acid concentration results in increased coverage of the electrode and may decrease the rate of electron transfer. A second adsorption effect is caused by Cd^{2+} bound to adsorbed fulvic acid. When the adsorption/desorption process is slow compared to diffusion [19] and the rate of dissociation of any adsorbed cadmium complex is slow, some cadmium is unavailable for plating and the i_s value will be lower.

A non-adsorption phenomenon related to the effective diffusion coefficient (D) of the electroactive species also rationalizes lower S_u with increased soil fulvic acid concentration. A decrease in the effective D occurs when there are labile complexes. The stripping current has effective D contributions from both free Cd^{2+} and Cd^{2+} arising from the dissociation of labile complexes. Because the labile complexes are much larger than free cadmium ions, they will have smaller D values than that of Cd^{2+}, and so the effective D would be smaller than that of Cd^{2+} alone. Increased soil fulvic acid concentration results in higher concentrations of the cadmium complexes well past the end-point and consequently the effective D decreases. Because i_s is a function of D, the lower D value causes lower i_s and hence lower S_u.

Scattering experiments and aggregation

When $C_{Cd^{2+}}$ became greater than about 80 μM at pH 7, a fairly rapid and continuous pH increase occurred with each addition of cadmium ions. (A similar, but less pronounced effect occurs at pH 6.) Because metal ion addition normally decreases the pH because of H^+ dissociation from the soil fulvic acid, the pH increase was unexpected. This observation cannot be explained by Cd^{2+} hydrolysis which would decrease the pH. At the same region in the titration curve, Rayleigh scattering rapidly increases. The scattering is attributable to aggregation of soil fulvic acid by cadmium ions [3, 9]. Similar behavior occurs in the cadmium—humic acid system [15]. It is difficult to explain the simultaneous Cd^{2+}-induced fulvic acid aggregation and pH increase with present knowledge, and any mechanistic proposal would require further study.

Limitations of a.s.v. for cadmium—soil fulvic acid complexation studies

There are general difficulties in the measurement of free metal ion concentration by a.s.v. in the presence of fulvic acid. The first is the adsorption of fulvic acid on the mercury electrode. The magnitude of error associated with adsorption can be calculated by comparing the kinetic current-corrected S_u at pH 7 in Table 1 with the 0.215 μA μM^{-1} value in the absence of soil fulvic acid under the same conditions. For example, if one had used a calibration curve in the absence of fulvic acid to calculate $[Cd^{2+}]$ for 60 mg l^{-1} soil fulvic acid, the calculated values would be 57% too high. The error increases with increasing soil fulvic acid concentration.

Second, K values are usually 10^5—10^6, and early in the titration by metal ions, the free metal ion concentration is low. Consequently, the stripping current has the greatest error early in the titration where it is most important in calculating K. In contrast, low complexation, as in the pH 6 experiments, also leads to errors because of low concentrations of the cadmium—soil fulvic acid complexes. In addition, the computer program employed here for kinetic current corrections uses data only to $C_L/2$. Because average values of K decrease during titration of fulvic acid by metal ions, the K values might not be strictly comparable to those from, for example, fluorescence measurements which utilize all the experimental data [6].

Third, the correction of the stripping current for dissociation of the complex during the plating step is much larger for Cd^{2+} (Fig. 3) than for Cu^{2+} (fig. 3 in [7]). This difference is due to labile complexes which might be a significant fraction of the total complexes. The larger correction for Cd^{2+} results in a poorer estimation of $[Cd^{2+}]$ and K. The problem is exacerbated by the unusual shapes of the present titration curves which make data treatment difficult. After all data had been fitted to Eqn. (1), data for $C_{Cd^{2+}} \geqslant 3\,\mu M$ were used to calculate kinetic current corrections. The choice of data points was somewhat arbitrary because the regions of labile and moderately labile complexes overlap. Thus calculation of $[Cd^{2+}]$ after kinetic current corrections is difficult and the values are not as accurate as desired.

Partial support of this research was provided by grant OCE 79-10571 from the National Science Foundation.

REFERENCES

1 W. T. Bresnahan, C. L. Grant and J. H. Weber, Anal. Chem., 50 (1978) 1675.
2 R. A. Saar and J. H. Weber, Can. J. Chem., 57 (1979) 1263.
3 R. A. Saar and J. H. Weber, Environ. Sci. Technol., 14 (1980) 877.
4 R. A. Saar and J. H. Weber, Geochim. Cosmochim. Acta, 44 (1980) 1381.
5 R. A. Saar and J. H. Weber, Anal. Chem., 52 (1980) 2095.
6 D. K. Ryan and J. H. Weber, Anal. Chem., 54 (1982) 986.
7 G. A. Bhat, R. A. Saar, R. B. Smart and J. H. Weber, Anal. Chem., 53 (1981) 2275.
8 R. E. Truitt and J. H. Weber, Anal. Chem., 53 (1981) 337.
9 D. P. Rainville and J. H. Weber, Can. J. Chem., 60 (1982) 1.
10 R. E. Truitt and J. H. Weber, Environ. Sci. Technol., 15 (1981) 1204.
11 T. M. Florence and G. E. Batley, Crit. Rev. Anal. Chem., 9 (1980) 219.
12 G. Sposito, Environ. Sci. Technol., 15 (1981) 396.
13 D. P. H. Laxen and R. M. Harrison, Water Res., 15 (1981) 1053.
14 P. Figura and B. McDuffie, Anal. Chem., 52 (1980) 1433.
15 G. K. Pagenkopf and C. Whitworth, J. Inorg. Nucl. Chem., 43 (1981) 1219.
16 D. S. Gamble, A. W. Underdown and C. H. Langford, Anal. Chem., 52 (1980) 1901.
17 M. S. Shuman and G. P. Woodward, Jr., Anal. Chem., 45 (1973) 2032.
18 M. S. Shuman and J. L. Cromer, Environ. Sci. Technol., 13 (1979) 543.
19 J. Buffle and F.-L. Greter, J. Electroanal. Chem., 101 (1979) 231.
20 F.-L. Greter, J. Buffle and W. Haerdi, J. Electroanal. Chem., 101 (1979) 211.

Analytica Chimica Acta, 141 (1982) 105—114
Elsevier Scientific Publishing Company, Amsterdam — Printed in The Netherlands

ELECTROANALYTICAL CHEMISTRY OF CHLORINATED PHENOLS AT A GLASSY CARBON ELECTRODE

C. McCRORY-JOY

Analytical Chemistry Research Department, Bell Laboratories, Murray Hill, NJ 07974 (U.S.A.)

(Received 11th January 1982)

SUMMARY

The electroanalytical chemistry of chlorinated phenols at a glassy carbon electrode in various solvent—electrolyte media is described. Differential pulse voltammetry may be used to determine chlorinated phenols in a methanol—0.07 M sulfuric acid medium. The determination of pentachlorophenol in liquid formulations is described. Cyclic voltammetric studies are used to investigate the electrochemical reaction mechanisms of chlorinated phenols. The electrochemical oxidation products of these compounds are quite reactive, and follow-up chemical reactions result in electrode filming under the conditions studied.

Chlorinated phenols are used in many industrial applications, and their presence in the environment is currently a matter of concern because of their own toxicities as well as those of their possible reaction products [1–3]. Methods are needed for quantifying these compounds at all concentration levels as well as for the routine characterization of formulations containing them. A review of the earlier approaches to the determination of chlorinated phenols is available [4] and there are various other reports concerning determinations of these compounds [5—17], the impurities associated with them, and their possible reaction products. Most studies have been concerned with pentachlorophenol (PCP) and include techniques such as gas chromatography [5—9], mass spectrometry [10], colorimetry [11], neutron activation analysis [12], and scanning electron microscopy with energy-dispensive x-ray spectroscopy [13]. Information concerning the electroanalytical chemistry of these compounds is relatively scarce. One investigation involved classical d.c. polarography [14] and another a.c. polarography [15]. A recent paper by Hawkridge et al. [16] described differential pulse voltammetric (d.p.v.) procedures for the determination of pentachlorophenol based on the electroreduction of PCP at the carbon paste electrode and the dropping mercury electrode in phosphate buffers. The inconveniences associated with the carbon paste and dropping mercury electrodes and the necessity of purging sample solutions with nitrogen in the case of electrochemical reduction are possible disadvantages. The investigation reported here is concerned

with the differential pulse voltammetric determination of chlorinated phenols, with emphasis on PCP, based on electrochemical oxidation at a glassy carbon electrode in a methanol—sulfuric acid medium. The procedure described has been successfully applied in the analysis of a number of industrial formulations containing PCP. A recent study [17] involved liquid chromatography with electrochemical detection (l.c.e.c.) for which sub-picomole detection limits were reported for PCP. The procedure used allows significantly greater sensitivity for trace determinations than the d.p.v. procedure reported here, but for the type of PCP formulations described, d.p.v. is certainly adequate. Compared to the other techniques mentioned, d.p.v. has competitive capability for trace analysis, requires relatively inexpensive equipment, and is easy to operate. Some methods, e.g., scanning electron microscopy with energy-dispersive x-ray spectroscopy [13] may be used to quantify PCP in a solid matrix. The PCP present in certain materials is difficult to extract completely for accurate solution analysis [3, 13].

EXPERIMENTAL

Apparatus

A Princeton Applied Research Model 174 polarographic analyzer was used with a Houston Series 2000 X—Y recorder, and a PAR Model 173 potentiostat/galvanostat was used in conjunction with a Model 374 universal programmer with a Hewlett-Packard 7046A recorder. A glassy carbon electrode (GCE) (0.35 cm^2) served as the working electrode, with a saturated calomel reference electrode (SCE), and a platinum wire auxiliary electrode. A modulation amplitude of 5 mV and a sweep rate of 10 mV s^{-1} were used for d.p.v.

Reagents and liquid samples

The chlorinated phenols 2,3,4-, 2,3,5-, 2,3,6-, 2,4,5-, 2,4,6-, and 3,4,5-trichlorophenol (TCP), 2,3,4,5- and 2,3,5,6-tetrachlorophenols (TCP), and Gold Label pentachlorophenol (99+%) were obtained from Aldrich Chemical Company. The PCP material was further assayed by titration as the acid in acetonitrile—0.1 M $NaClO_4$ with tetramethylammonium hydroxide (TMAH) using amperometric detection at the GCE based on the measurement of the anodic current of the phenoxide ion produced. Acetonitrile (Omnisolv; Matheson, Coleman, and Bell), electronic-grade methanol (J. T. Baker), and distilled water further purified by passage through a Millipore purification system, were used in preparing solvent—electrolyte systems. Tetrabutylammonium perchlorate (TBAP; Eastman polarographic-grade), sulfuric acid, 20% (w/w) weight TMAH in methanol (Aldrich) and sodium perchlorate were used as supporting electrolytes. Solutions were purged with prepurified nitrogen to remove any oxygen present prior to experiments.

The liquid samples were designated as follows: (1) 4.47% PCP in petroleum, (2) 32.0% PCP in petroleum solvent plus emulsifier, (3) 7% PCP in petroleum

solvent, and (4) 6% (approximate) PCP in petroleum solvent plus emulsifier and deionized water. Appropriate dilutions were made prior to measurements in the methanolic medium.

Procedures

Differential pulse voltammetry was employed to obtain calibration plots and to analyze liquid samples containing PCP. Standards were prepared by dissolving a weighed quantity of PCP in the methanol—0.07 M H_2SO_4 medium and making appropriate dilutions. Cyclic voltammetry was used to investigate chlorinated phenols in methanol containing 0.07 M sulfuric acid and in some cases higher concentrations of sulfuric acid. Other solvent—electrolyte media investigated included: methanol—50% pH 4.5 buffer; acetonitrile—0.1 M TMAH or acetonitrile—0.1 M sodium perchlorate containing varied concentrations of TMAH; water containing 0.1 M TMAH; and various mixtures of water and methanol containing 0.1 M TMAH.

RESULTS AND DISCUSSION

Differential pulse voltammetry

All of the compounds investigated exhibit a single well-defined oxidation peak in methanol—0.07 M H_2SO_4. The peak potentials and calculated detection limits are given in Table 1, along with the slope and intercept of the least-squares lines and the standard error of estimate. Variations in substituents on the phenol ring produce shifts of the oxidation potential [18], as observed here. The peak potential for unsubstituted phenol under the same conditions is +1.12 V vs. SCE. Observations made during the preparation of d.p.v. calibration plots and cyclic voltammetric experiments indicated the formation of a passivating film on the electrode surface as a result of the electrochemical oxidation reaction, which is characteristic of the electro-

TABLE 1

Differential pulse voltammetric data for various chlorophenols

Chlorinated phenol	E_p (V vs. SCE)	Slope ± s.d. (μA/ppm)	Intercept ± s.d. (μA)	Standard error (μA)	Detection limit (ppm)
2,3,4-TCP	+1.21	0.45 ± 0.09	1.40 ± 0.02	0.18	2.9
2,3,5-TCP	+1.25	0.33 ± 0.01	1.10 ± 0.01	0.02	1.4
2,3,6-TCP	+1.12	0.35 ± 0.03	2.20 ± 0.02	0.09	2.9
2,4,5-TCP	+1.14	0.38 ± 0.06	0.31 ± 0.00	0.14	3.4
2,4,6-TCP	+1.10	0.31 ± 0.00	0.22 ± 0.00	0.00	0.5
3,4,5-TCP	+1.26	0.47 ± 0.01	1.33 ± 0.00	0.02	1.0
2,3,4,5-TCP	+1.21	0.41 ± 0.07	0.55 ± 0.00	0.16	3.4
2,3,5,6-TCP	+1.18	0.30 ± 0.06	1.73 ± 0.01	0.19	2.5
PCP	+1.13	0.52 ± 0.04	0.22 ± 0.00	0.08	1.1

chemical oxidation of phenols. Subsequent potential scans exhibited significantly reduced peak currents. The effects of filming may be removed in this case by polishing the electrode surface with a cloth wetted with methanol. When this procedure was used, the peak current measured for a given concentration was reproducible to within 1% for successive measurements.

Plots of peak current as a function of concentration for chlorinated phenols generally are linear over a range of 0—100 ppm. The data in Table 1 refer to the concentration range 0—50 ppm with ten data points obtained using the same concentrations for each compound, except for 3,4,5-TCP for which nine data points were taken over the range 0—45 ppm. The dependence of peak current on concentration of PCP is expressed by the regression equation

$$i_p\ (\text{uA}) = (0.52 \pm 0.04\ (\mu\text{A/ppm}))\ C\ (\text{ppm}) + (0.22 \pm 0.00)\ \mu\text{A}$$

Detection limits (d.l.) were calculated using the relationship $d.l. = st/k$ where s is the standard deviation, t is the appropriate constant at the 99% confidence level, and k is the slope of the least-squares line.

The differences in the samples supplied reflect an attempt to change the PCP formulation used from a petroleum to an aqueous medium. The results obtained by d.p.v. for diluted samples are summarized in Table 2; they compare favorably with the designated concentrations, with the exception of sample 4 for which an approximate concentration was given for the PCP content.

Chemical reactions of electrochemical oxidation products

Electrochemical oxidation of hindered alkylphenols [18—20] is generally characterized by rapid follow-up chemical reactions which result in the formation of passivating films on the electrode surface. The chemical behavior of oxidized intermediates of phenols is influenced by the substitution pattern of the phenol. Chlorinated phenols contain electron-withdrawing substituents which affect their chemical behavior and which are shown here to influence their electrochemical behavior. This investigation did not include a detailed identification of the chemical reaction products of chlorophenol intermediates produced by electrochemical oxidation, but did demonstrate the greater chemical reactivity of these intermediates relative to those derived

TABLE 2

Results obtained for liquid samples containing PCP

Sample	Description	PCP found (%)
1	4.47% PCP in petroleum	4.5
2	32.0% PCP in petroleum + emulsifier	32.1
3	7% PCP in petroleum	7.3
4	6% PCP (approx.) in petroleum + emulsifier + deionized water	10.7

from hindered alkylphenols [21, 22] and showed that the overall reaction mechanism depends on the specific chlorinated phenol investigated, and the solvent—electrolyte medium.

The chemical reactions of various chlorinated phenols have been investigated. A variety of reaction products, including certain undesirable ones, may be formed; e.g., thermal [23] and photolytic condensation [24] of chlorinated phenols result in the production of dioxins. The condensation of PCP to form octachlorodibenzodioxin proceeds readily in aqueous alkaline solution [25]. These reactions depend on the initial production of chlorophenoxy radicals, which may couple to form a variety of C—C and C—O coupled products. Conclusions concerning the electrochemical reaction mechanisms of chlorinated phenols are here based largely on comparison of their behavior to that of alkylphenols with emphasis on results from d.p.v. and cyclic voltammetry. Attempts to perform controlled-potential coulometry experiments produced inconclusive results, with fractional values of n probably reflecting the reaction of primary oxidation products during the time of the coulometric experiment [26]. A previous investigation using a mercury pool electrode for such coulometric experiments produced similarly inconclusive results [16].

Cyclic voltammetry

Methanolic media. The cyclic voltammogram for PCP in a methanol—0.07 M sulfuric acid medium is shown in Fig. 1. The peak current of the single oxidation peak obtained on the initial forward sweep decreased in magnitude with repeated scanning and after several sweeps the surface of the electrode was completely passivated. Similar behavior was observed for the trichloro- and tetrachloro-phenols. Increasing the concentration of sulfuric acid above 0.07 M had no significant effect on the peak potential or peak current, indicating that the undissociated phenol is indeed the only form present in the methanol—0.07 M H_2SO_4 medium.

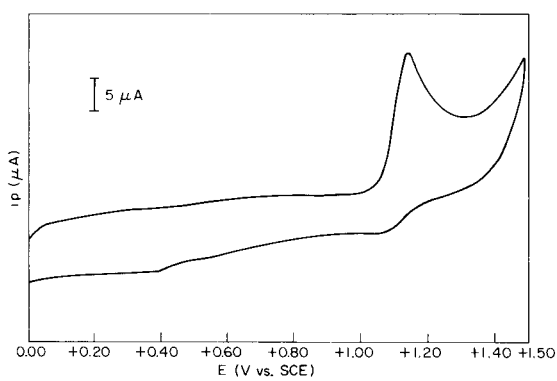

Fig. 1. Cyclic voltammogram of pentachlorophenol (3.8 mM) in methanol—0.07 M H_2SO_4 (50 mV s^{-1}).

The addition of TMAH produced markedly different cyclic voltammetric behavior compared to that for acidic conditions for 2,4,6-TCP. As the TMAH concentration is increased an oxidation peak grows in at less positive potential and the current magnitude of the original oxidation peak decreases steadily. This confirms the identification of the original peak as being caused by the undissociated phenol and the second as arising from the oxidation of the corresponding phenoxide ion. This is reminiscent of certain hindered alkylphenols for which the phenoxide ion undergoes reversible oxidation to the corresponding phenoxy radical in basic solution. No corresponding phenoxy radical reduction peak is observed for PCP on the reverse scan. However, most of the other chlorinated phenols do exhibit a reduction peak of small peak current magnitude with a wide potential separation of the oxidation and reduction peak, approximately 1.5 V in the case of 2,4,6-TCP, indicative of coupled chemical reactions [27].

Aqueous media. As the solvent composition is raised from 0% to 100% water and the TMAH concentration is maintained at 0.1 M, the oxidation peak potential of PCP does not change significantly but a new peak appears on the reverse sweep. The results of sweep-reversal experiments suggest a coupled chemical reaction involving water or facilitated by water, and the formation of electrochemically reducible products. Table 3 summarizes the dependence of the anodic peak and major cathodic peak potentials and the corresponding peak currents on the concentration of water for cyclic voltammetric studies at a scan rate of 50 mV s^{-1}. On the reverse scan, the cyclic voltammogram obtained for PCP in 50% water exhibits a sharp peak symmetrical about the peak potential, suggesting weak adsorption [28].

Scan rate studies for PCP in aqueous 0.1 M TMAH reveal a pronounced dependence of the catholic peak current on the sweep rate (Table 4). The symmetrical oxidation peak observed at slow sweep rates increases dramatically in current magnitude with increasing scan rate. Again a coupled chemical reaction is indicated, and the symmetrical appearance of the oxidation peak is a qualitative indication of reactant adsorption. The probable involvement of coupled chemical reactions makes any quantitative treatment of adsorption

TABLE 3

Dependence of pentachlorophenol peak potentials on water concentration by cyclic voltammetry

% H_2O	$E_{p,o}$ (V vs. SCE)	$E_{p,r}$ (V vs. SCE)	ΔE	i_a (mA)	i_c (mA)	i_c/i_a
0	+0.950	—	—	0.135	0	—
25	+0.948	−0.982	1.930	0.070	0.010	0.143
50	+0.820	−0.761	1.581	0.048	0.071	1.479
75	+0.748	−0.621	1.369	0.520	0.330	0.635
100	+0.715	−0.620	1.335	0.660	0.290	0.440

TABLE 4

Effect of scan rate on pentachlorophenol peak potentials and peak currents in aqueous 0.1 M TMAH by cyclic voltammetry

Scan rate ($mV\ s^{-1}$)	$E_{p,o}$ (V vs. SCE)	$E_{p,r}$ (V vs. SCE)	ΔE_p	i_a (mA)	i_c (mA)	i_c/i_a
10	+0.691	−0.441	1.132	0.022	0.002	0.091
20	+0.722	−0.500	1.222	0.034	0.006	0.176
50	+0.761	−0.618	1.379	0.060	0.014	0.233
100	+0.765	−0.721	1.516	0.089	0.054	0.606
200	+0.785	−0.760	1.545	0.125	0.105	0.840

inconclusive. A similar pattern is observed for 2,4,6-TCP as the water concentration is increased, with a complex sequence of reduction peaks observed on the reverse sweep (Fig. 2). Electrochemical experiments alone are not sufficient to determine the identity of the products and allow the proposal of detailed mechanisms. As coupling reactions are the most probable follow-up reactions in either case and 2,4,6-TCP has more unsubstituted positions available, coupling could proceed more readily to give a more complex assortment of products [21, 22], as suggested by the cyclic voltammetric results.

Acetonitrile media. Acetonitrile containing 0.1 M sodium perchlorate with varied concentrations of TMAH, and acetonitrile containing 0.1 M TMAH were used for further investigation. As the concentration of TMAH is raised, the cyclic voltammetric results at 50 $mV\ s^{-1}$ reveal a second oxidation peak corresponding to oxidation of the phenoxide ion (Fig. 3, Table 5) which grows as the magnitude of the original peak decreases. The appearance of this oxidation peak is accompanied by the appearance of a subsequent reduction peak having a small peak current magnitude. Increasing the scan

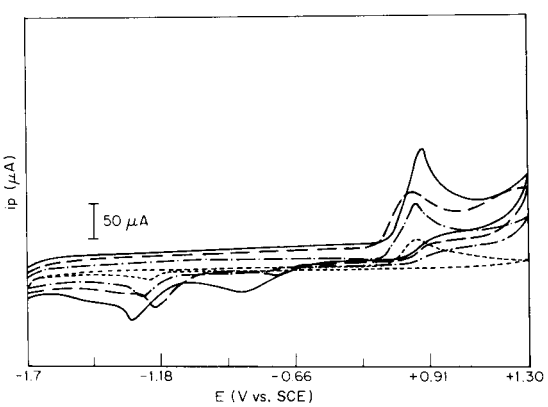

Fig. 2. Scan rate dependence of cyclic voltammogram for 2 mM 2,4,6-TCP in aqueous 0.1 M TMAH: (---) 10, (—·—) 50, (——) 100, (——) 200 $mV\ s^{-1}$.

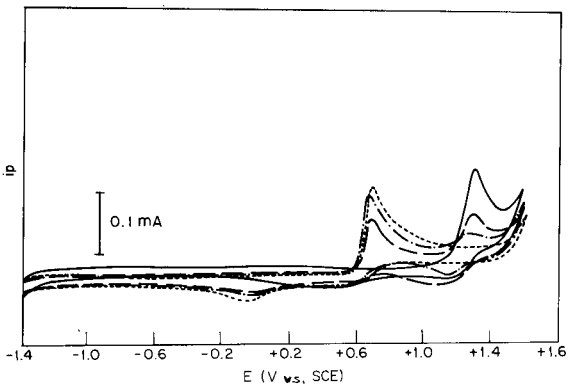

Fig. 3. Cyclic voltammogram of 2 mM PCP in acetonitrile—0.1 M $NaClO_4$, and the effect of added TMAH (50 mV s^{-1}). TMAH added: (——) 0 M, (— — —) 0.06 M, (—·—) 0.09 M, (---) 0.15 M.

TABLE 5

Cyclic voltammetric peak potentials for chlorophenols and chlorophenoxides in acetonitrile/0.1 M $NaClO_4$ with added TMAH

Compound	$E_{p,o}$ Phenol	$E_{p,o}$ Phenoxide	$\Delta E_{p,o}$	$E_{p,r}$	$E_{p,r}-E_{p,o}$ Phenoxide
PCP	+1.302	+0.695	0.607	—0.079	0.774
2,3,4,5	+1.421	+0.730	0.691	—0.106	0.836
2,3,5,6	+1.380	+0.682	0.698	ill-defined	—
2,3,4	+1.410	+0.678	0.732	—0.059	0.741
2,4,5	+1.421	+0.701	0.720	several	—
2,4,6	+1.300	+0.611	0.689	—0.062	0.673
3,4,5	+1.512	+0.782	0.730	ill-defined	—

rate results in an increase in the ratio of the cathodic to anodic peak currents, indicating a coupled chemical reaction. Chlorinated phenols in acetonitrile containing 0.1 M TBAP or 0.1 M $NaClO_4$ exhibit a single oxidation peak accompanied by two or more minor reduction peaks on the reverse sweep suggesting multiple chemical reaction products.

Conclusion

Differential pulse voltammetry at a glassy carbon electrode is useful for the determination of chlorinated phenols present as trace or major constituents. Pentachlorophenol has been determined in liquid samples.

Chlorinated phenols undergo electrochemical oxidation exhibiting a voltammetric response in a variety of solvent—electrolyte media. Well-defined oxidation peaks are observed in water, methanol, mixtures of water and methanol, and acetonitrile under neutral, acidic, or alkaline conditions. On the basis of similarities in electrochemical behavior, it is suggested that

analogous oxidations are observed for chlorinated and alkylated phenols, i.e., in acidic or neutral media, the chlorophenoxonium ion is produced and in alkaline solution, chlorophenoxide ions are oxidized to chlorophenoxy radicals. The phenoxonium ions in either case are highly reactive and electrode filming is observed under acidic or basic conditions. For certain 2,4,6-alkylphenols a reversible phenoxide ion/phenoxy radical couple is observed in alkaline media but chlorophenoxy radicals are highly reactive under the same conditions so that on the cyclic voltammetric time scale the radical is not detected. Electrode poisoning may be avoided in alkaline media for certain alkylphenols [18—20] but no conditions have been established at this point which eliminate the problem for chlorinated phenols. It has therefore been demonstrated that differential pulse voltammetry is a useful technique for the determination of chlorinated phenols in acidic media, but electrode poisoning limits the use of a glassy carbon electrode as an on-line detector under the various conditions described. Analytical capabilities are even more limited under conditions for which reactant adsorption is observed.

In alkaline media, the cyclic voltammetric trace obtained on the reverse sweep generally consists of several closely spaced cathodic peaks, pointing to a complex mixture of chemical reaction products which are electrochemically reducible. Several general resemblances of cyclic voltammetric results to the results of chemical oxidation studies of chlorinated phenols were observed. Chlorophenoxy radicals may undergo a variety of reactions producing a number of species including the products of coupling reactions. No two chlorinated phenols behave exactly alike under the same experimental conditions, and different mixtures of oxidation products are obtained depending on the extent and pattern of substitution. Chemical reaction product mixtures for PCP are less complex relative to less substituted chlorophenols. The ease of oxidation of chlorophenoxide ions relative to the undissociated phenol helps to explain the ease with which certain condensation products are formed via chlorophenoxy radicals in aqueous alkali [25].

REFERENCES

1 R. L. Rawls, Chem. Eng. News, 57 (1979) 23.
2 M. E. Zabik and M. J. Zabik, Bull. Environ. Contam. Toxicol., 24 (1980) 344.
3 L. L. Lamparskii, R. H. Stehl and R. L. Johnson, Environ. Sci. Technol., 14 (1980) 196.
4 A. Bevenue and H. Beckman, Residue Rev., 19 (1967) 83.
5 P. Svec and M. Zbirovsky, Sb. Vys. Sk. Chem.-Technol. Praze, Org. Chem. Technol., C21 (1974) 39.
6 H. Oka, I. Nagai and M. Tasaka, Shokuhin Eiseigaku Zasshi, 198 (1977) 419.
7 F. Dietz, Vom Wasser, 51 (1978) 235.
8 G. D. McGinnis, H. E. Ervin, B. C. Amlicke and L. L. Ingram, Jr., Proc.-Annu. Meet. Am. Wood-Preserv. Assoc., 75 (1979) 233.
9 C. R. Daniels and E. P. Swan, J. Chromatogr. Sci., 17 (1979) 628.
10 W. M. Shackelford and R. G. Webb, ASTM Spec. Tech. Publ., 686 (1979) 191.

11 Y. P. Misva, S. P. S. Dhakarey, R. K. Jaiswara and S. Gupta, J. Indian Chem. Soc., 52 (1975) 1167.
12 J. F. Siau and J. A. Meyer, Wood Sci., 6 (1973) 19.
13 J. B. Zicherman, Wood Fiber, 7 (1976) 110.
14 E. A. Zemkin, V. M. Gorokhovskii, N. A. Kalinovskaya, G. L. Logan and V. M. Cherepnev, Zh. Nauchn. Prikl. Fotogr. Kinematogr., 20 (1975) 44.
15 Y. Mizunoya, Bunseki Kagaku, 11 (1962) 393.
16 A. L. Wade, H. P. Williams and F. M. Hawkridge, Anal. Chim. Acta, 105 (1979) 91.
17 R. E. Shoup, LCEC Symposium. Environmental and Industrial Applications of LCEC and Voltammetry, No. 22, Indianapolis, IN, May 1981.
18 A. Ronlan, in A. J. Bard and H. Lund (Eds.), Encyclopedia of Electrochemistry of the Elements, Dekker, New York, 1978, Vol. XI, Ch. 2.
19 J. A. Richards, P. E. Whitson and D. H. Evans, Electroanal. Chem., 63 (1975) 311.
20 J. A. Richards and D. H. Evans, J. Electroanal. Chem., 81 (1977) 171.
21 M. L. Mihailovic and Z. Chekoviz, in S. Patai (Ed.), The Chemistry of the Hydroxyl Group, Part I, Interscience, New York, 1971, Ch. 10.
22 D. C. Nonhebel, J. M. Tedder and J. C. Walton, Radicals, Cambridge University Press, Cambridge, 1979, Ch. 13.
23 H. G. Langer, T. P. Brady, L. A. Dalton, T. W. Shannon and P. R. Briggs, Adv. Chem. Ser., 120 (1973) 26.
24 L. L. Lamparskii, R. H. Stehl and R. L. Johnson, Environ. Sci. Technol., 14 (1980) 196.
25 R. H. Stehl, R. R. Papenfuss, R. A. Bredeweg and R. W. Roberts, Adv. Chem. Ser., 120 (1973) 119.
26 A. J. Bard and K. S. V. Santhanam, in A. J. Bard (Ed.), Electroanalytical Chemistry, Dekker, New York, 1970, Vol. 4, pp. 216—311.
27 R. H. Wopschall and I. Shain, Anal. Chem., 39 (1967) 1514.
28 E. Jacobsen and T. Rojahn, Anal. Chim. Acta, 61 (1972) 320.

Analytica Chimica Acta, 141 (1982) 115—122
Elsevier Scientific Publishing Company, Amsterdam — Printed in The Netherlands

FAST-SCAN A.C. VOLTAMMETRY FOR BETTER RESOLUTION OF CHROMATOGRAPHICALLY OVERLAPPING PEAKS

ANTONÍN TROJÁNEK* and HANS G. DE JONG

Department of Analytical Chemistry, Free University, De Boelelaan 1083, 1081 HV Amsterdam (The Netherlands)

(Received 22nd January 1982)

SUMMARY

A fast-scan phase-sensitive a.c. voltammetric detector for high-performance liquid chromatography is described. The mercury drop electrode is periodically polarized over a certain potential range and only the maximum current value of each scan is plotted. The technique makes it possible to resolve chromatographically overlapping peaks provided that the voltammetric peak potentials of the corresponding compounds differ enough. Practical examples of application of the technique to nitro compounds are reported, and limitations are discussed.

Even with the most sophisticated chromatographic equipment, unresolved response peaks commonly occur in complex mixtures. Various methods for the resolution of such peaks into their various components have been developed and are applicable depending on the degree of overlap [1]. The use of voltammetric detectors in high-performance liquid chromatography (h.p.l.c.) may assist in recognizing the components of the mixtures if the electrochemical properties of the components are suitable. The selectivity of detection can be tuned by adjusting the value of the working potential, so that another dimension in separation is obtained in addition to the retention times. Modern voltammetric instrumentation simplifies the routine utilization of various a.c. and pulse techniques. When they are applied, improved selectivity [2—4] and reproducibility [3, 5] and decreased dependence of the signal on the flow rate [5, 6], are usually achieved. The relatively rare reports of increased sensitivity [4, 5, 7] are probably due to commonly used cell designs with a high time constant.

In general, techniques yielding peak responses (e.g., differential pulse, a.c., square-wave voltammetry) provide higher selectivity than simple d.c. voltammetry. By suitable adjustment of working potential, various components can often be detected selectively according to their peak potentials, whether the required component undergoes electrochemical reaction at

*Present address: The J. Heyrovský Institute of Physical Chemistry and Electrochemistry, Jilská 16, 11000 Praha 1, Czechoslovakia.

higher or lower potential than other peaks. There are obvious disadvantages in the approaches based on the use of a fixed potential. Thus it may be necessary to repeat the chromatographic procedure at various applied potentials in the detector, in order to detect all components of interest; this can be avoided by sequential application of different pre-selected potentials and separate recording of the corresponding current values [8]. Further, the sensitivity of the measured signal may depend on the precise adjustment of the working potential, which in practice can be affected by changes in the reference electrode and liquid junction potentials.

The optimal mode for the application of these techniques seems to be a fast potential scan, the potential of the working electrode being scanned periodically within a certain potential range. The selectivity of detection can be improved dramatically in this way, because continuous time resolution is combined with voltammetric resolution. Very little work has been published on applications of fast-scan h.p.l.c. detectors. Samuelsson et al. [9] reported on a computer-aided instrument that enabled a predetermined number of square-wave scans to be recorded and stored for each chromatogram; these data were then evaluated by a computer program which provided the peak position and the peak height for each component.

In this paper, a fast-scan voltammetric technique with simple electronic processing of the response signal is reported. The method helps to achieve better resolution of chromatographically overlapping peaks.

BASIS OF THE METHOD

The basis of the method may be explained by reference to Fig. 1. Compounds A and B are not well separated chromatographically, and when a universal detector (e.g., u.v. or d.c. amperometric detector at a constant high potential) is used, the corresponding recorded peaks a and b overlap badly (peak c) and are difficult to resolve and quantify. When a fast-scan technique is used with a voltammetric detector, components A and B give two well-separated voltammetric peaks at E_A and E_B within the time of each scan. The composition of the mixture entering the detector changes with time and the voltammetric response changes accordingly. At time t_1, practically only A is present, and at time t_6 only the voltammetric peak of B can be recorded. If the output current signal is processed in such a way that only the maximum current value from each scan is recorded, then the response for the emerging overlapped peaks a and b is shown by curve d. Provided that the voltammetric detector exhibits the same sensitivity of response as the universal detector, curve d is a clear representation of curves a and b, and the heights of the two peaks on curve d are related directly to components A and B without mutual interference. Up to time t_3, when the voltammetric peaks of A and B are equal in height, the detector signal does not include any contribution from B; after time t_3, component A does not contribute. At time t_3, the detector simply switches from detecting A to B.

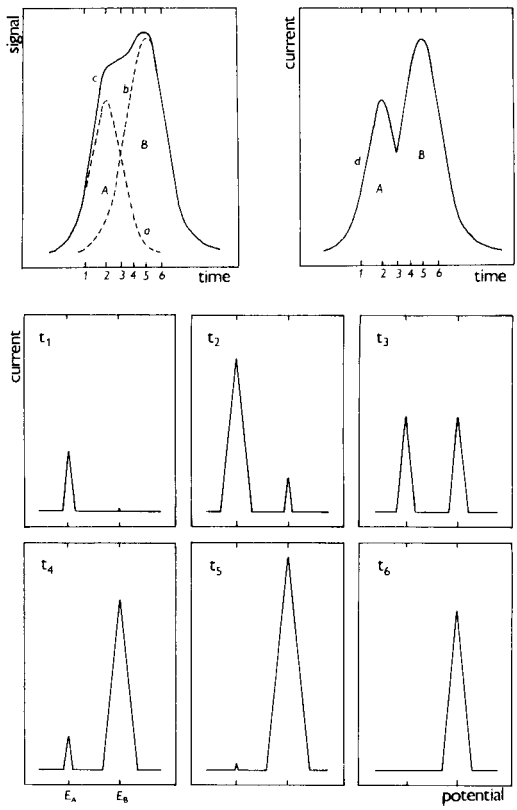

Fig. 1. Detector response and a diagrammatic representation of the corresponding voltammetric curves recorded at different times. For explanation, see text.

For practical verification of the proposed technique, phase-selective a.c. voltammetry was chosen. It is well known that this type of voltammetry gives generally good discrimination against the charging current which is to be expected when a fast potential scan is applied [10, 11]. In contrast to the results of Mooring and Kies [12], and in agreement with those of Hanekamp et al. [13], the phase-selective a.c. technique was found here to be applicable even at high scan rates, at least up to 0.5 V s^{-1}. Care is necessary in checking the time constants of the electronic circuitry, because if their values are inadequate, the shapes of the curves can be impaired considerably.

EXPERIMENTAL

Figure 2 is a schematic diagram of the experimental set-up for generation of the potential waveform and for current evaluation. The major parts were from E.G. & G. Princeton Applied Research. The static mercury drop electrode of the PAR 310 polarographic h.p.l.c. detector is polarized by the potential waveform (with a superimposed a.c. component of 60-mV ampli-

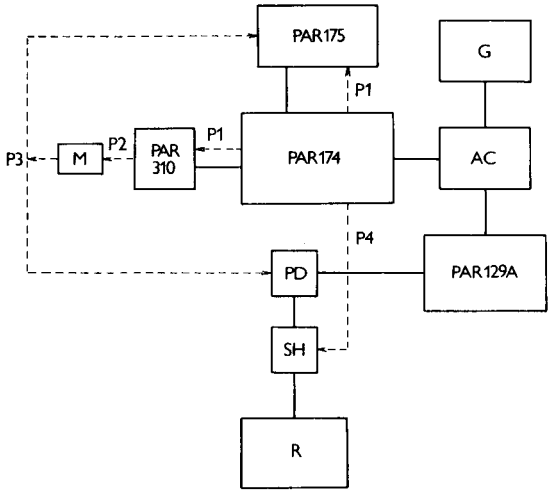

Fig. 2. Block diagram of the fast-scan a.c. polarograph with maximum current evaluation. For details, see text.

tude) indicated in Fig. 3. The d.c. component of the waveform is generated by a PAR 175 universal programmer, controlled by impulses P1 and P3. A home-made monostable circuit (M), triggered by impulse P2, introduces a quiescent period after a new mercury drop has been formed; the corresponding impulse P3 serves to reset a peak detector (PD) and to start the scan. The polarographic analyzer is complemented by a PAR 174/50 a.c. interface (AC), supplied with a sine wave of 50 Hz from the generator (G). The current

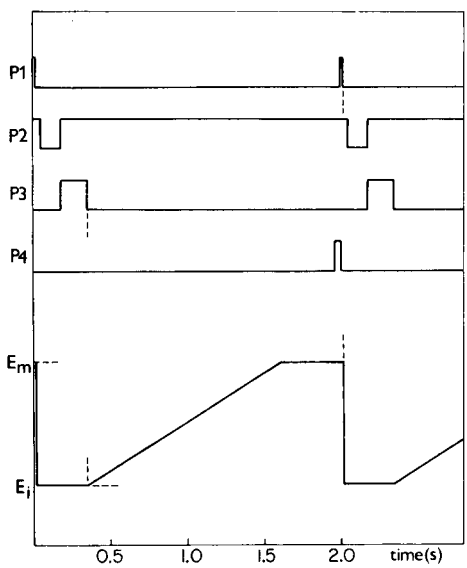

Fig. 3. The sequence of digital control impulses and the generated potential waveform for work with a 2-s drop-time cycle. P1, 18 ms; P2, 125 ms; P3, 170 ms; P4, 60 ms.

signal is processed by a PAR 129A two-phase/vector lock-in amplifier, which is provided with d.c. prefilters having selectable time constants of 100 ms and with output filters having time constants selectable in the range 1 s—100 ms. The time constant of the prefilter was permanently set to 100 ms, and the time constant of the filter was 10 ms or 100 ms. The output signal of the lock-in amplifier, corresponding to the zero degree component, is fed to the peak detector (PD), connected with a sample-and hold circuit (SH), both of which were constructed as described elsewhere [14].

In one measuring cycle, after a single point of the detector response has been obtained, the sequence of the steps is as follows (cf. Fig. 3): (1) at the pilot impulse P1 (drop-time impulse of the PAR 174), the mercury drop is dislodged and the potential is set to the initial value E_i; (2) during the P2 impulse (solenoid valve opening impulse of the PAR 310), a new drop is formed; (3) during the P3 impulse (monostable), the peak detector is reset and the trailing edge of P3 starts the potential scan; the potential is allowed to attain the maximum value E_m, preselected on the programmer 175, and then remains constant; (4) during the potential scan and the following period of constant potential application, the peak detector records the maximum current value within the selected potential range; (5) the output signal of the peak detector is transferred to the sample-and-hold current, controlled by the P4 pulse which is generated from the PAR 174 control pulses II and III, and displayed on the recorder.

The chromatographic system consisted of a Perkin-Elmer 601 pump, an electrochemical eluent scrubber [15] for removal of electrochemically active impurities, a 20-μl injection valve (Valco Instruments), and a 100 × 4.6-mm column packed with ODS Hypersil (5 μm). Current value was recorded by means of a Hewlett-Packard 7046A X—Y recorder and monitored by means of a Tektronix 5103N oscilloscope.

The nitro compounds chosen as samples and the components of the mobile phase (10^{-1} M KNO_3, 10^{-3} M HNO_3, 50% methanol, all analytical grade) were used as received.

RESULTS AND DISCUSSION

The efficiency of the fast-scan a.c. voltammetric detector was demonstrated for the chromatographic separation of a mixture of nitro compounds (4-nitroaniline, 4-nitrophenol, 4-nitrobenzoic acid) by comparison with ordinary sampled d.c. amperometry. In both modes, the detector system exhibited linear responses towards the detected compounds within the concentration range used, with regression coefficients close to one. In the amperometric d.c. mode, the detector behaved as a universal detector because the applied constant potential (—0.8 V vs. saturated Ag/AgCl) was high enough to ensure that all the components of the mixture were detected.

From the response of an amperometric detector (Fig. 4a), it is obvious that under the applied conditions only 4-nitroaniline was separated well,

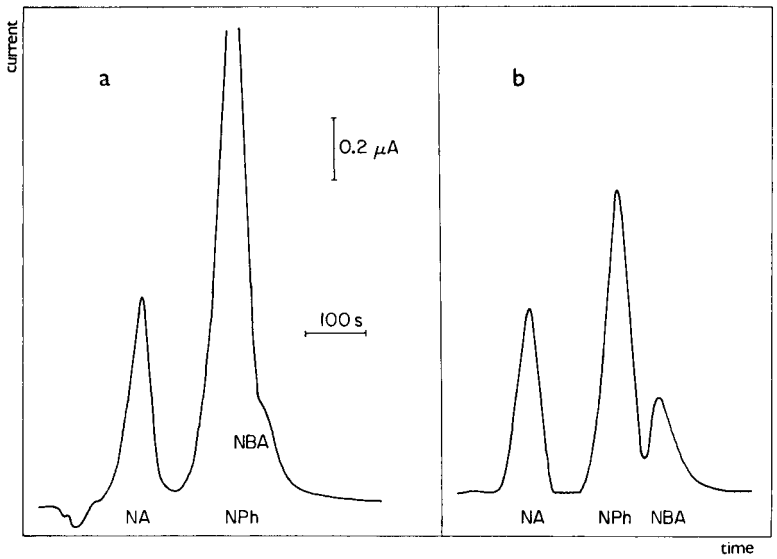

Fig. 4. Chromatograms of 4-nitroaniline (10^{-3} M, NA), 4-nitrophenol (4×10^{-3} M, NPh) and 4-nitrobenzoic acid (10^{-3} M, NBA). Flow rate 0.5 ml min^{-1}; injected volume 20 μl. (a) Sampled d.c. amperometry at −0.8 V; (b) the proposed fast-scan a.c. technique at a scan rate of 0.2 V s^{-1} in the potential range from −0.25 to −0.5 V (filter time constant 100 ms).

while 4-nitrophenol and 4-nitrobenzoic acid formed overlapping peaks. Voltammetric peaks of the latter two compounds were, however, readily distinguishable even at high scan rates (Fig. 5), which enabled the above-described technique to be applied. The response of the detector working in the fast-scan a.c. mode is presented in Fig. 4(b).

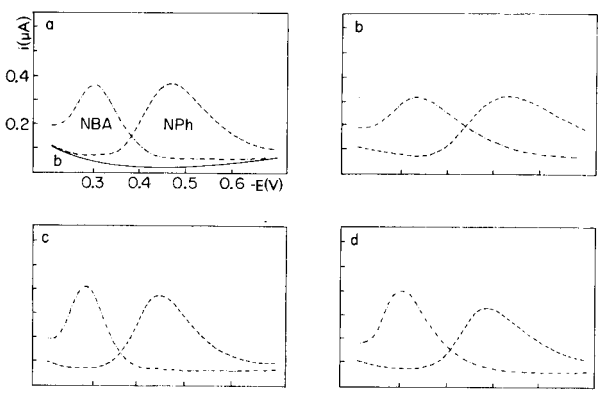

Fig. 5. Fast-scan phase-sensitive voltammograms of 4-nitrobenzoic acid and 4-nitrophenol in a flow system. Scan rates (mV s^{-1}) and time constants (ms) were: (a) 200, 100; (b) 500, 100; (c) 200, 10; (d) 500, 10. Curves were recorded separately after injection of 20 μl of stock 10^{-3} M solution with a 5-s drop-time cycle. The baseline in (a) was recorded in the pure mobile phase at a flow rate of 0.5 ml min^{-1}.

In order to verify the expected independence of the heights of the 4-nitrophenol and 4-nitrobenzoic acid peaks, mixtures containing these compounds in various ratios were injected. Figure 6(a) shows the dependence of the peak height for 4-nitrophenol on the concentration of 4-nitrobenzoic acid, and Fig. 6(b) shows the dependence of the peak height for 4-nitrobenzoic acid on the concentration of 4-nitrophenol. When a sampled d.c. technique was applied, the apparent peak heights were obviously dependent on each other, whereas excellent resolution was obtained with the fast-scan a.c. technique. When a 1-s drop cycle was used, so that a higher scan rate became necessary, the 4-nitrophenol peak height depended slightly on the concentration of 4-nitrobenzoic acid. This can be explained easily by the curves in Fig. 5(b); the overlap of the 4-nitrophenol peak by the tail of 4-nitrobenzoic acid peak is obvious.

Voltammetric detection by the proposed fast-scan a.c. technique supplemented by maximum current evaluation is useful in certain cases, as indicated above, but is obviously subject to certain limitations from the chromatographic as well as the electrochemical points of view. The method is applicable provided that at least a small valley exists between the two peaks a and b; in adverse cases only the higher peak would be recorded. Electrochemically, natural limitations arise from the differences in the peak potentials of the compounds which are to be distinguished. Insofar as theoretical studies regarding a.c. peak resolution are restricted to reversible processes [16], the decision on whether the method might be applied successfully or not must be taken on empirical evidence. Increase of the scan rate impairs the shape of the voltammetric peaks to an extent dependent on the time constants of the circuitry; that is why the slowest possible scan rate should

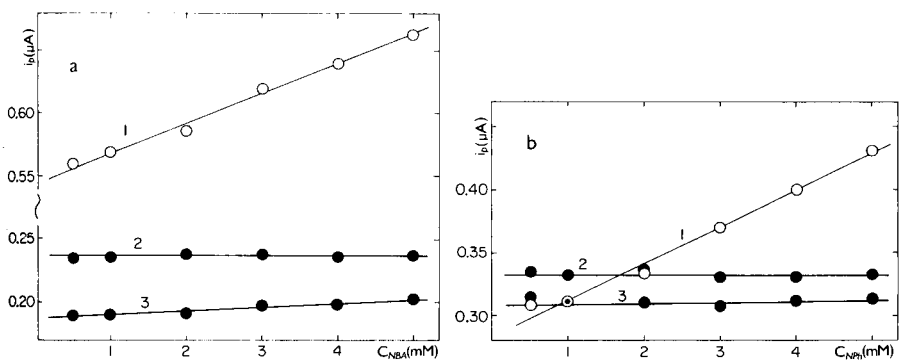

Fig. 6. Dependence of apparent peak heights on the concentration of the interfering compound. Flow rate 0.5 ml min^{-1}, injected volume 20 μl. (a) 10^{-3} M 4-nitrophenol with increasing concentrations of 4-nitrobenzoic acid; (b) 10^{-3} M 4-nitrobenzoic acid with increasing concentrations of 4-nitrophenol. The lines correspond to: (1) sampled d.c. at −0.8 V; (2) fast-scan a.c. with 2-s drop-time cycle, scan-rate 0.2 V s^{-1} from −0.25 to −0.5 V, filter time constant 100 ms; (3) fast-scan a.c. with 1-s drop-time cycle, scan rate 0.5 V s^{-1} from −0.3 to −0.6 V, filter time constant 100 ms.

always be used. Application of slower scan rates is facilitated by the fact that the proposed fast-scan a.c. technique does not require recording of the whole voltammetric curves; only the potential region including the required peak potentials need be covered.

Another electrochemical limitation would arise from a baseline which is not strictly horizontal. Because of the maximum current monitoring device, only peaks exceeding the height of the highest baseline level can be recorded. This threshold problem could be avoided by incorporating a baseline memory-subtraction device. In the above examples, this was not necessary, because the real baseline in the presence of the nitro compounds was almost horizontal and altogether different from the baseline recorded in the pure mobile phase (Fig. 5).

The technique described can be used advantageously even for the detection of components that are chromatographically well separated. In such cases, it is not necessary to adjust the working potential value precisely and different components can be detected at one injection.

A. T. thanks Dr. P. Bos and Dr. H. B. Hanekamp for their kind help and advice, and W. H. Voogt for technical assistance.

REFERENCES

1 J. T. Lundeen and R. S. Juvet, Jr., Anal. Chem., 53 (1981) 1369.
2 W. J. Mayer and M. S. Greenberg, J. Chromatogr. Sci., 17 (1979) 614.
3 W. A. MacCrehan, Anal. Chem., 53 (1981) 74.
4 H. B. Hanekamp, W. H. Voogt, R. W. Frei and P. Bos, Anal. Chem., 53 (1981) 1362.
5 A. MacDonald and P. D. Duke, J. Chromatogr., 83 (1973) 331.
6 D. G. Swartzfager, Anal. Chem., 48 (1976) 2189.
7 H. B.Hanekamp, W. H. Voogt and P. Bos, Anal. Chim. Acta, 118 (1980) 73.
8 E. B. Buchanan, Jr. and J. R. Bacon, Anal. Chem., 39 (1967) 615.
9 R. Samuelsson, J. ODea and J. Osteryoung, Anal. Chem., 52 (1980) 2215.
10 A. M. Bond, Anal. Chem., 44 (1972) 315.
11 A. M. Bond, Modern Polarographic Methods in Analytical Chemistry, Dekker, New York, 1980.
12 C. I. Mooring and H. L. Kies, Anal. Chim. Acta, 94 (1977) 135.
13 H. B. Hanekamp, P. Bos and O. Vittori, Anal. Chim. Acta, 131 (1981) 149.
14 A. Trojánek and I. Holub, Anal. Chim. Acta, 110 (1979) 161.
15 H. B. Hanekamp, W. H. Voogt, P. Bos and R. W. Frei, Anal. Chim. Acta, 118 (1980) 81.
16 A. M. Bond and J. H. Canterford, Anal. Chem., 44 (1972) 732.

Analytica Chimica Acta, 141 (1982) 123—129
Elsevier Scientific Publishing Company, Amsterdam — Printed in The Netherlands

ANALYTICAL APPLICATION OF SECOND-HARMONIC A.C. POLAROGRAPHY

NOBUAKI OGAWA*, IWAO WATANABE and SHIGERO IKEDA

Department of Chemistry, Faculty of Science, Osaka University, Toyonaka, Osaka 560 (Japan)

(Received 3rd March 1982)

SUMMARY

Phase-selective second-harmonic a.c. polarography can be used to distinguish two different species having similar reduction potentials. Because each species has a different phase angle depending on the electrode kinetics, a certain phase angle can be chosen to detect only one component in the mixture. In 1 M potassium chloride solution, indium(III) at the 4×10^{-6} M level can be determined in the presence of 50-fold amounts of cadmium(II), and zinc(II) at the 2×10^{-5} M level in the presence of 100-fold amounts of nickel(II).

Fundamental (1f) and second (2f) harmonic a.c. polarography [1, 2] has been investigated for many purposes, e.g., quantitative analysis [3—10], study of kinetics [11—13] and determination of reversible half-wave potentials for organic compounds [14—16]. In the present work, phase-selective second-harmonic a.c. polarography is used to determine one of two species having similar reduction potentials without any preliminary separation, selective complexation [17, 18], masking of certain electrode process [10], or computer technique [19—25]. The 2f mode is more advantageous than the 1f mode because the former has little contribution from the charging current over the whole range of the phase angle.

The present technique is different from the methods used by Devay et al. [6] and Fajioli et al. [7] in that it utilizes the difference in the dependence of phase angle on d.c. potential for two species, which results from the kinetics of two-electrode processes. As examples, two systems are chosen, i.e., in 1 M potassium chloride solution, indium(III) in the presence of excess of cadmium(II), and zinc(II) in the presence of excess of nickel(II).

EXPERIMENTAL

All chemicals were of analytical-reagent grade and were used as received. Deionized—distilled water was used for the preparation of all solutions. Solutions were thermostated at 25 ± 0.5° C and degassed with nitrogen gas for 15—20 min prior to recording of a.c. polarograms.

A.c. polarograms were obtained with a conventional three-electrode system [1]. The reference electrode was Ag/AgCl (saturated aqueous potassium chloride). The counter electrode was a platinum wire. The working electrode was a dropping mercury electrode; the capillary had a drop time of 3.96 s at −1.0 V vs. Ag/AgCl in 1 M potassium chloride solution and the mercury flow was 2.025 mg s^{-1} at a height of 70 cm.

The electrochemical instrumentation consisted of a home-made potentiostat, a home-made function generator and an X—Y recorder (Yokogawa Type 3086). The fundamental and second-harmonic alternating currents were measured by employing an oscillator (Kikusui Electronics Corp., RC Oscillator Model 4045) and a lock-in amplifier (NF Circuit Design Block Co., Model LI 507).

The phase angle of faradaic alternating current was determined by recording in-phase (0°) and quadrature (90°) components. The phase angle of the lock-in amplifier was calibrated by use of a dummy cell [26]. Applied a.c. voltage (ΔE) and frequency (f) were 5—10 mV (r.m.s.) and 15—200 Hz, respectively.

RESULTS AND DISCUSSION

For the simple electrode reaction, $O + ne \rightleftharpoons R$, where rate is controlled by diffusion and/or heterogeneous charge-transfer kinetics, the fundamental and second-harmonic alternating currents are given by the well-known equations [1, 27]

$$I(\omega t) = I(\omega t)_{rev} F_1\ (t)\ G_1\ (\omega) \sin\ (\omega t + \phi_1) \tag{1}$$

$$I(2\omega t) = I(2\omega t)_{rev} F_2\ (t)\ G_2\ (\omega)\ W_2\ (\omega) \sin\ (2\omega t + \phi_2) \tag{2}$$

where

$$I(\omega t)_{rev} = (nF)^2\ AC_o^*\ (\omega D_o)^{1/2}\ \Delta E\ [4RT \cosh^2\ (j/2)]^{-1} \tag{3}$$

$$I(2\omega t)_{rev} = (nF)^3\ AC_o^*\ (2\omega D_o)^{1/2}\ \Delta E^2 \sinh\ (j/2)\ [16R^2T^2 \cosh^3\ (j/2)]^{-1} \tag{4}$$

$$j = nF(RT)^{-1}\ (E_{dc} - E_{1/2}^r);\ \lambda = (k_s f_a/RT)\ (e^{-\alpha j} + e^{\beta j})$$

$$\phi_1 = \cot^{-1}\ [1 + (2\omega)^{1/2}/\lambda] \tag{5}$$

$$\phi_2 = \cot^{-1}\ \{[L(2\omega^{1/2}/\lambda + 1) + P]/[L - P(2\omega^{1/2}/\lambda + 1)]\} \tag{6}$$

The rest of the notations are the same as those used by Smith et al. [1, 27].

Equations (5) and (6) show that the fundamental and second-harmonic current phase angles (ϕ_1 and ϕ_2) change with d.c. potential. But for a process which displays a reversible wave in the a.c. or d.c. polarographic sense ($2\omega^{1/2}/\lambda \ll 1$ or $\lambda t^{1/2} \gg 50$), the ϕ_1 and ϕ_2 values are $\pi/4$ and $-\pi/4$, respectively, and these are independent of d.c. potential [1, 27]. These phase-angle relationships prove useful for separation of two species with similar redox potentials.

A mixed solution of cadmium(II) and indium(III) in 1 M potassium chloride (pH 3) was investigated as one such example. As the $Cd^{2+}/Cd(Hg)$ system in 1 M potassium chloride behaves as a reversible process (k_s = 2.5 ± 0.3 cm s^{-1}, α_c = 0.65 ± 0.03) [28], the phase angle of the system is 45° for 1f over the peak potential region and that for 2f is −45° at the more positive potential than the zero crossing potential and 135° at the more negative potential. In contrast, as the $In^{3+}/In(Hg)$ system in 1 M potassium chloride behaves as a quasi-reversible process (k_s = (6 ± 2) × 10^{-2} cm s^{-1}, α_a = 0.9 ± 0.1) [28], the phase angles of the system for both 1f and 2f are not constant but change with d.c. potential. Therefore, as expected from the above theoretical relation, when the phase angle of the lock-in amplifier is adjusted to 135° for 1f or to 45° for 2f, the alternating current only for indium(III) is detected without interference from cadmium(II).

Curves 1 and 2 in Fig. 1 were obtained individually for each of cadmium-(II) and indium(III) at 0.2 mM concentrations in 1 M potassium chloride acidified to pH 3 with hydrochloric acid. The peak potential difference between them for 1f was 45 mV. Curve 3 is for the mixed solution of 0.2 mM cadmium(II) and 0.2 mM indium(III). The polarograms of the mixture (curve 3) for the 0° component of 1f and for the 90° component of 2f show overlapping of the components. In contrast, the 135° component of 1f and the 45° component of 2f for the mixture display simple peaks corresponding

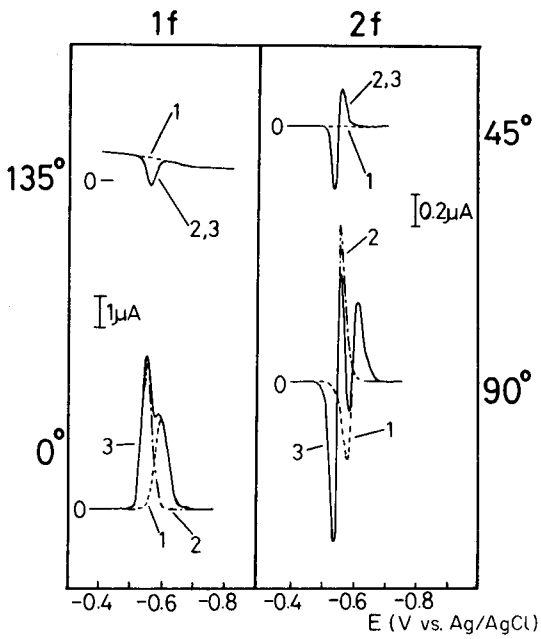

Fig. 1. Fundamental (1f) and second (2f) harmonic a.c. polarograms at various phase angles for cadmium(II), indium(III) and their mixture. (1) 0.2 mM Cd^{2+}; (2) 0.2 mM In^{3+}; (3) 0.2 mM Cd^{2+} + 0.2 mM In^{3+} in 1 M KCl (pH 3). ΔE = 10 mV (r.m.s.), f = 25 Hz.

to a single electrode reaction, and peaks for only indium(III) are detected; those for cadmium(II) are eliminated. As the contribution of the charging current is less in the 45° component of 2f than in the 135° component of 1f ($F/C < 50$ for 2f and $F/C \simeq 1$ for 1f, where F is the faradaic current and C is the charging current), the 2f mode is superior to the 1f mode in this case.

The calibration curves of indium(III) in the presence and in the absence of 0.2 mM cadmium(II) for 2f are given in Fig. 2. The upper curve is for the 45° component and the lower is for the 90° component in the absence of cadmium(II). Peak current (I_p) for the 90° component was measured at −0.538 V for indium(III), because the peak at −0.570 V for indium(III) overlaps with the peak at −0.572 V for cadmium(II) when the concentration of indium(III) is low. The I_p for the 45° component is the sum of positive and negative peak currents. The I_p value for the 90° component in the presence of cadmium(II) deviates from the calibration curve even at the concentration ratio of $C_{In^{3+}}/C_{Cd^{2+}} = 1/5$, but that for the 45° component in the presence of cadmium(II) lies on the calibration curve up to a ratio of 1/50 when $C_{In^{3+}}$ is 4×10^{-6} M.

A mixed solution of zinc(II) and nickel(II) in 1 M potassium chloride was also investigated. Figure 3A shows the dependence of the phase angle of the alternating current upon d.c. potential for zinc(II) in 1 M potassium chloride, and Fig. 3B shows that for nickel(II). As the $Zn^{2+}/Zn(Hg)$ system in chloride solution behaves as a quasi-reversible process in kinetics ($k_s = (5.05 \pm 0.05) \times 10^{-3}$ cm s^{-1}, $\alpha_c = 0.3 \pm 0.02$) [11, 13, 28], the phase angle changes with d.c. potential. In contrast, the phase angle for nickel(II) in 1f is zero ($k_s = 1.2 \times$

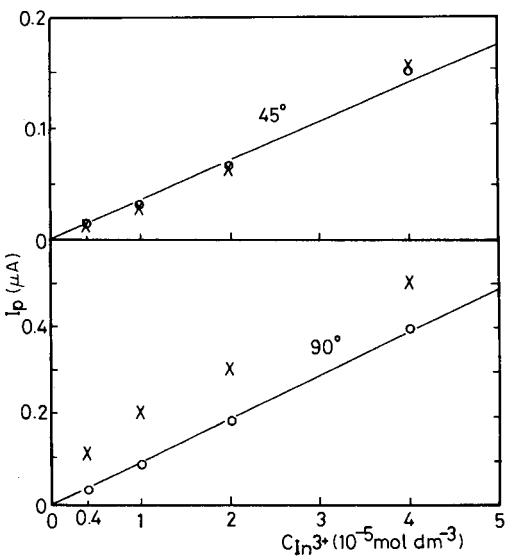

Fig. 2. Calibration curves for indium(III) in 1 M KCl (pH 3): (×) with 0.2 mM cadmium(II), and (○) without cadmium(II). The curves are for 45° (upper) and 90° (lower) components in the 2f mode. ΔE = 10 mV (r.m.s.), f = 25 Hz.

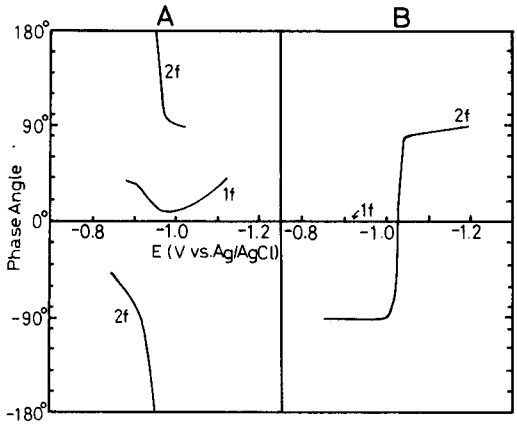

Fig. 3. The phase angle of fundamental (1f) and second (2f) harmonic currents for zinc(II) and nickel(II) in 1 M KCl. (A) 0.2 mM Zn^{2+}; (B) 0.8 mM Ni^{2+}. ΔE = 5 mV (r.m.s.), f = 15 Hz.

10^{-2} cm l mol^{-1} s^{-1}, $NiOH^{+} + 2e + Hg \rightleftharpoons Ni(Hg) + OH^{-}$ in 0.1 M KCl) [28]. The phase angle in 2f changes from —90° to +90° at the zero crossing potential. It has been suggested that the irreversibility of the Ni^{2+}/Ni(Hg) system in chloride solution is induced not by a very slow heterogeneous charge-transfer reaction but by other mechanisms [29—31]. The relationship between the kinetics and phase angle of nickel(II) will be discussed in detail elsewhere.

The phase angle—potential relationships indicate that the current of 1f for nickel(II) vanishes when the phase angle of the lock-in amplifier is adjusted to 90°, and that the current of 2f vanishes when the phase angle is adjusted to 0°, while the currents of both modes for zinc(II) should be detected at these phase angles. Figure 4 shows a.c. polarograms of the 0° and 90° components for 1f and 2f. Curves 1 and 2 were obtained individually for each of 2 mM nickel(II) and 0.1 mM zinc(II). The peak potential difference

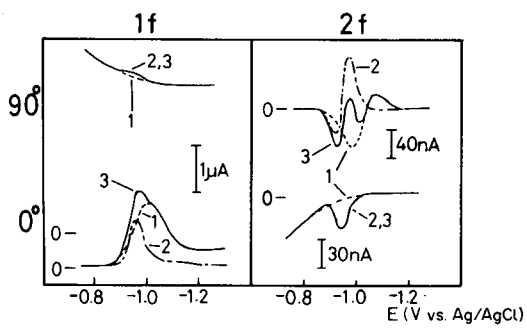

Fig. 4. Fundamental (1f) and second (2f) harmonic a.c. polarograms for zinc(II), nickel(II) and their mixture. (1) 2 mM Ni^{2+}; (2) 0.1 mM Zn^{2+}; (3) 2 mM Ni^{2+} + 0.1 mM Zn^{2+} in 1 M KCl. ΔE = 10 mV (r.m.s.), f = 100 Hz.

between them for 1f was 65 mV. Curve 3 is for a mixed solution of 2 mM nickel(II) and 0.1 mM zinc(II).

Practically, the polarograms of the mixture (curve 3) for the 0° component of 1f and the 90° component of 2f show overlapping of the components and one cannot separate them well from each other. The 90° component in 1f and the 0° component in 2f for the mixture are almost the same as those for zinc(II). The contribution of charging current to the whole current for the former is about 98% and that for the latter is about 10%. Therefore the 2f mode is superior to the 1f mode for quantitative work.

Figure 5 shows the calibration curves obtained by the use of the 2f mode for zinc(II) in the presence and in the absence of 2 mM nickel(II) in 1 M potassium chloride. The upper curve is for the 0° component and the lower is for the 90° component. The I_p is measured by the same method as in the case of indium(III) and cadmium(II). When the ratio of $C_{Zn^{2+}}/C_{Ni^{2+}}$ is less than 1/5, the I_p for the 90° component in the presence of nickel(II) deviates from the calibration curve obtained in the absence of nickel(II). Yet the I_p values for the 0° component in the presence and in the absence of nickel(II) are equal even when the $C_{Zn^{2+}}/C_{Ni^{2+}}$ ratio is 1/100 at $C_{Zn^{2+}} = 2 \times 10^{-5}$ M.

Conclusions

The phase-selective second-harmonic a.c. polarographic technique can be used to distinguish two species having similar peak potentials. The method presented, which utilizes phase-angle detection, can be used even when the peak potentials are the same, provided that each electrochemical system has a different phase angle depending on its behavior as reversible, quasi-rever-

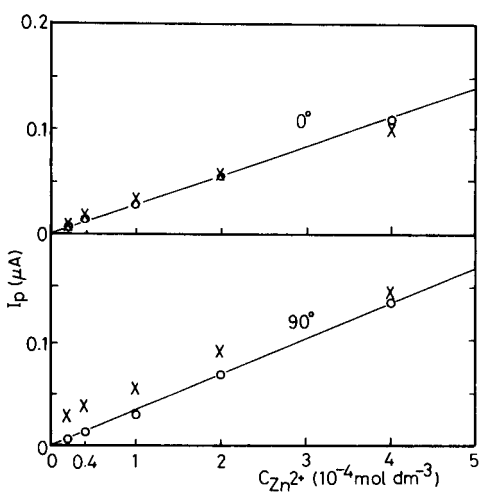

Fig. 5. Calibration curves for zinc(II) in 1 M KCl: (×) with 2 mM nickel(II), and (○) without nickel(II). The curves are for 0° (upper) and 90° (lower) components in the 2f mode. ΔE = 10 mV (r.m.s.), f = 100 Hz.

sible or irreversible. When a given species reacts with the electrode through two different electrode processes simultaneously, this method could be also applied to analyze the kinetics for each electrochemical reaction, provided that they give different phase angles.

REFERENCES

1 D. E. Smith, in A. J. Bard (Ed.), Electroanalytical Chemistry, Vol. 1, Dekker, New York, 1966, p. 1.
2 D. E. Smith, Crit. Rev. Anal. Chem., 2 (1971) 247.
3 R. Neeb, Fresenius Z. Anal. Chem., 186 (1962) 53; 188 (1962) 401.
4 D. Saur and R. Neeb, Fresenius Z. Anal. Chem., 290 (1978) 220.
5 H. H. Bauer, Aust. J. Chem., 17 (1964) 715.
6 J. Devay, T. Garai, L. Meszaros and B. Palagri-Fenyes, Hung. Sci. Instrum., 15 (1968) 1.
7 F. Fajioli, F. Dondi and C. Bighi, Ann. Chim. (Rome), 68 (1978) 111.
8 S. Fujiwara, M. Hirota, K. Sawatari, Y. Umezawa and H. Kojima, Bull. Chem. Soc. Jpn., 47 (1974) 499.
9 M. Kasagi and C. V. Banks, Anal. Chim. Acta, 30 (1964) 248.
10 E. Jacobsen and G. Tandberg, Anal. Chim. Acta, 47 (1969) 285.
11 T. G. McCord and D. E. Smith, Anal. Chem., 42 (1970) 126.
12 M. Hirota, Y. Umezawa, H. Kojima and S. Fujiwara, Bull. Chem. Soc. Jpn., 47 (1974) 2486.
13 M. Hirota, Y. Umezawa and S. Fujiwara, Bull. Chem. Soc. Jpn., 48 (1975) 1053.
14 R. Breslow and J. L. Grant, J. Am. Chem. Soc., 99 (1977) 7745.
15 E. Ahlberg and V. D. Parker, Acta Chem. Scand., B34 (1980) 91.
16 A. M. Bond and D. E. Smith, Anal. Chem., 46 (1974) 1946.
17 I. M. Kolthoff and J. J. Lingane, Polarography, Interscience, New York, 1952.
18 K. M. Suyan, S. K. Shah and C. M. Gupta, Analyst, 104 (1979) 883.
19 I. Ruzic and M. Branica, J. Electroanal. Chem., 22 (1969) 243, 422.
20 I. Ruzic, J. Electroanal. Chem., 25 (1970) 144; 29 (1971) 440.
21 B. S. Grabaric, R. J. O'Halloran and D. E. Smith, Anal. Chim. Acta, 133 (1981) 349.
22 W. F. Gutknecht and S. P. Perone, Anal. Chem., 42 (1970) 906.
23 P. A. Boudreau and S. P. Perone, Anal. Chem., 51 (1979) 811.
24 A. M. Bond and B. S. Grabaric, Anal. Chem., 48 (1976) 1624.
25 J. J. Toman and S. D. Brown, Anal. Chem., 53 (1981) 1497.
26 D. E. Glover and D. E. Smith, Anal. Chem., 43 (1971) 775.
27 T. G. McCord and D. E. Smith, Anal. Chem., 40 (1968) 289.
28 R. Tamamushi, Kinetic Parameters of Electrode Reactions, 1972 supplement to Electrochim. Acta, 9 (1964) 963.
29 D. E. Smith and T. G. McCord, Anal. Chem., 40 (1968) 474.
30 C. Nishihara and H. Matsuda, J. Electroanal. Chem., 28 (1970) 17.
31 R. de Levie and A. A. Husovsky, J. Electroanal. Chem., 20 (1969) 181.

Analytica Chimica Acta, 141 (1982) 131—146
Elsevier Scientific Publishing Company, Amsterdam — Printed in The Netherlands

THE DETERMINATION OF TRACES OF CADMIUM, LEAD AND THALLIUM IN FLY ASH BY POTENTIOMETRIC STRIPPING ANALYSIS

JOAN KAI CHRISTENSEN, LARS KRYGER* and NIELS PIND

Department of Chemistry, Aarhus University, Langelandsgade 140, DK-8000 Aarhus C (Denmark)

(Received 12th March 1982)

SUMMARY

The suitability of potentiometric stripping analysis for the determination of cadmium, lead and thallium in fly ash and in waters polluted by leaching of fly ash is assessed. By an appropriate choice of medium and of electrolysis potential and by employing a rotating working electrode, it is possible to eliminate interferences from electroactive species often found in fly ash in high concentrations. The accuracy obtained in a study of a certified coal fly ash (SRM 1633a) is satisfactory.

Because of the potential hazard involved in the deposition of fly ashes emitted from oil- or coal-fired power plants, numerous investigations have lately been directed towards understanding and predicting the effects of the interactions between this waste product and the environment. As a result of these efforts, several analytical methods have been proposed for the determination of the trace elemental distribution in fly ash and in waters polluted by leaching of fly ash [1—10]. While spectrometric methods and neutron activation analysis have frequently been employed in such studies, electroanalytical methods such as stripping analysis have seldom been used. This is probably because, despite their high sensitivity towards a number of electroactive species, electrochemical methods lack the selectivity often achieved with spectrometric methods and neutron activation analysis. The present paper reports the results of an investigation of the suitability of employing potentiometric stripping analysis (p.s.a.) [11, 12] for the determination of cadmium, lead and thallium in fly ash. Electrochemical stripping methods are particularly sensitive for species which undergo transport-controlled redox processes at a mercury electrode, and which, on reduction to the zero oxidation state, dissolve in the mercury. Elements such as cadmium, lead and thallium at nanomolar concentrations may, for example, be determined with only a few minutes of pre-electrolysis, provided that computerized monitoring of the transient stripping signals is exploited. Typically, the elements considered in this study are found at the 100 ppb—1000 ppm level in fly ash [1, 3, 10]. With suitable decomposition/dissolution procedures, aqueous samples for p.s.a. will be nano- to micro-molar with respect to the analytes.

Hence the sensitivity of p.s.a. is adequate for the analytical problem considered, and the elimination of interferences will therefore be of major concern in this paper.

In contrast to biological samples, fly ash often contains large amounts of elements which form electroactive species in solution: iron, titanium and vanadium, for example, are frequently found far above trace levels in fly ash. The soluble species of these elements and of a number of others (e.g., cobalt and chromium) are not reduced to the elemental state in stripping analysis, provided that the plating potential is not set cathodic of about —1000 mV vs. SCE; but their reduction to water-soluble species and subsequent accumulation at the working electrode during electrolysis in quiet or moderately stirred solutions may give rise to oxidation signals during the potentiometric stripping phase, thus distorting the stripping signals from the re-oxidation of amalgamated analytes. Such interferences may be eliminated by employing a rotating working electrode [13]. Species that are reduced to the elemental state may interfere, because their stripping signals appear in the same potential region as those of the analytes. Sometimes, by a careful choice of complexing medium and electrolysis potential, it is possible to eliminate this type of interference, partly because stripping potentials depend to some extent on the medium, and partly because the addition of a suitable complexing agent can be exploited to shift the reduction potential of some species cathodic of the plating potential, necessary to reduce the analytes.

A serious source of interference in electrochemical stripping analysis is the formation of stable, binary intermetallic compounds between plated analytes and other amalgamated metals. Mostly, such intermetallics, and so the fraction of the analyte bound in the intermetallic compound, are oxidized at potentials different from the stripping potentials of either of the two components, usually at some intermediate potential [14, 15]. Consequently, part or all of the analyte may escape detection, and precautions must be taken to avoid such inaccuracies. Sometimes accurate results may be obtained simply by choosing plating conditions such that one component of the intermetallic compound is not reduced. However, if the component reduced at the more cathodic potential happens to be the analyte, the possible interference from species that are reduced and amalgamated at more anodic potentials, must be investigated in detail.

EXPERIMENTAL

Instrumentation, electrochemical cell and electrodes

A general computerized instrument for electroanalytical work was employed [16, 17]. During the stripping phase of p.s.a., this device monitors the potential distribution, and the stripping of amalgamated metals is recorded as peaks. The background signal obtained with zero plating time was subtracted from all primary potentiograms. The instrument was operated at a data sampling frequency of 5 kHz.

The electrochemical cell comprised a Radiometer M12 rotating electrode assembly with a 50-ml polyethylene beaker. The rotating working electrode was made from a 3-mm thick piece of glassy carbon glued in glass tubing. The electrode was polished with diamond paste (down to 0.25 μm). The reference electrode was a Radiometer K401 saturated calomel electrode, while a glass-fitted platinum wire, 1 cm long and 0.5 mm thick, served as the counter electrode.

To plate the working electrode with a thin mercury film, the electrode assembly was placed in the sample solution (medium 1, see below), and the electrode potential was subsequently decreased from 0 to −400 mV vs. SCE over a period of 120 s.

Chemicals, samples and solutions

Triply-distilled water and analytical-grade chemicals were mostly used, but the mineral acids and the sodium acetate used for the preparation of buffers were of Suprapur grade (Merck). Fly ash samples were obtained from Cement-og Betonlaboratoriet, Aalborg Portland, Denmark, while the certified reference material 1633a (coal fly ash) was obtained from National Bureau of Standards (Washington, DC). For fusion of fly ash, a (66 + 34) mixture of dilithium tetraborate and lithium metaborate (Spectromelt A12, Merck) was used.

Stock solutions of the analytes and metals tested for interference were 10^{-2} M in 0.1 M hydrochloric acid, except for lead and silver (nitric acid) and gallium (HCl, HNO_3). The solutions prepared (with the starting material in parentheses) were: antimony (Sb_2O_3), arsenic (As_2O_3), bismuth ($Bi(NO_3)_3 \cdot 5H_2O$), cadmium ($CdCl_2$), chromium ($CrCl_3 \cdot 6H_2O$), cobalt ($CoCl_2 \cdot 6H_2O$), copper ($CuSO_4$), gallium (Ga), gold ($HAuCl_4 \cdot 4H_2O$), indium ($In_2(SO_4)_3$), lead ($Pb(NO_3)_2$), nickel ($NiSO_4 \cdot 7H_2O$), silver ($AgNO_3$), thallium (Tl_2SO_4), tin ($SnCl_2 \cdot 2H_2O$), and vanadium ($VOSO_4 \cdot 3H_2O$). Dilute metal solutions for standard addition were prepared daily and were kept in polyethylene vessels. When added to the sample solutions, some of the metal ions listed above are oxidized by the mercury(II) (added as the oxidizing agent for p.s.a.) to a higher oxidation state than that indicated, e.g., Sn(II) is converted to Sn(IV).

Prior to analysis, all solutions were deaerated with argon for 10 min.

Decomposition and dissolution of fly ash samples

Dry the fly ash samples in a desiccator over phosphorus pentoxide for 2 days. For decomposition and dissolution, fuse 1 g of fly ash with 2 g of Spectromelt A12 in a platinum crucible placed in a small electrically heated oven for 2 h at 900—1000°C. After cooling, dissolve all solid material by gentle heating with (1 + 3) hydrochloric acid, the total final volume being 100 ml. Filter off any precipitate (possibly siliceous material) formed during the subsequent cooling of the solution. Prepare samples for stripping analysis from 5 ml of the filtered solution, 0.5 ml of 2×10^{-2} M mercury(II) acetate

in 0.1 M hydrochloric acid and 1 ml of 0.25 M ethylenediamine. Adjust this mixture to pH 4.8 by adding 1 M sodium acetate, and dilute to 25 ml with triply-distilled water. In this ethylenediamine-containing medium (medium 1, 4×10^{-4} M in mercury(II) and 10^{-2} M in ethylenediamine), the stripping peak of cadmium is not overlapped by the stripping peak from traces of indium.

The medium referred to below as medium 2 was obtained by adding solid disodium EDTA to medium 1, so that the total EDTA concentration was 10^{-2} M. Reagent blanks were obtained by proceeding as above without fly ash.

Recommended procedure for p.s.a.

Carry out the electrolysis at —950 mV vs. SCE using a rotating mercury film electrode (plated in situ) for a period sufficiently long to produce stripping signals lasting for at least 100 ms (for the NBS SRM 1633a, a plating period of 8 min for cadmium and thallium and 1 min for lead was suitable). For the cadmium and lead determinations, add aliquots of the standard solutions until the stripping signals measured as peak heights on the background-corrected potentiograms are about doubled, and evaluate the concentrations from standard addition plots. For the thallium determination, add 10^{-2} M disodium EDTA to the sample and repeat the procedure. Correct for the effects of reagent blanks by similar experiments. Evaluate, by inspection of the potentiograms, whether any unusually high content of thallium or indium affects the height of the cadmium and lead peaks. If this is suspected, increase the plating potential such that the signals from thallium or indium are reduced relatively to the lead signal. If the thallium or indium signals are so high that they affect the peak height of the cadmium signal, no accurate determination of this element is obtained. However, at any rate, an upper limit for the lead and cadmium concentrations can be estimated. The determination of thallium in medium 2, of course, is not affected by cadmium, indium and lead.

RESULTS AND DISCUSSION

The large concentrations of electroactive species mostly found in decomposed, dissolved fly ash may affect the stripping signals from traces of cadmium, lead and thallium. By a careful choice of experimental conditions e.g., electrolysis potential, medium and by taking proper instrumental precautions, it is, however, possible to eliminate most of these effects.

Effects of high background concentrations of electroactive species acting as oxidizing agents

Decomposed, dissolved fly ash and aqueous samples contaminated by leaching of fly ash, mostly contain large background concentrations of oxidizing species, in particular iron(III). Such species cause rapid stripping of

amalgamated metals, even when only a little mercury(II) is added to the sample. However, when a standard addition technique is used for quantitative work, the added amounts of standards are similarly rapidly re-oxidized, and the effect is compensated. The concentrations of cadmium(II), lead(II), and thallium(III) in the solutions considered in this study range from nano- to micro-molar, and the duration of the stripping signals obtained after reasonably short plating times are mostly too short to be resolved instrumentally on a conventional x—t recorder. With computerized instrumentation, however, the duration of such transient time signals can be measured quantitatively [16—18]. Moreover, the instrument can be programmed so that at the end of the stripping phase potentiostatic control is resumed at a potential slightly cathodic of the mercury(II)/mercury equilibrium potential. This facility was exploited throughout this study, partly to prevent iron(III) from oxidizing the mercury film electrode, and partly to inhibit precipitation of mercury(I) chloride on the electrode through the reaction Hg(0) + Hg(II) → 2Hg(I) in the chloride-containing medium.

Interferences from electroactive substances forming water-soluble reduced species

Iron(III) is not reduced to elemental iron at a mercury electrode, unless electrolysis is done at potentials cathodic of about —1500 mV vs. SCE, hence no stripping signals from iron appear when plating is done at ca. —1000 mV vs. SCE. Furthermore, since oxidation of iron(II) in most media takes place at potentials anodic of the stripping signals of cadmium, lead and thallium, large background concentrations of iron(III) do not give rise to signals overlapping the required signals. The oxidized species of titanium, vanadium, chromium and cobalt are not reduced to the elements anodic of about —1000 mV vs. SCE, but their soluble reduced products formed by electrolysis accumulate at the working electrode in quiet or moderately stirred solutions. As these products may be re-oxidized at potentials similar to the stripping potentials of the amalgamated analytes, serious interferences may result [13]. To illustrate this type of interference, a quiet 10^{-2} M solution of vanadium(IV) in acetate buffer (pH 4.8) which was 2×10^{-4} M in mercury(II) was electrolysed for 10 s at —1150 mV vs. SCE, and the potential distribution was subsequently recorded (Fig. 1A). Clearly, the re-oxidation by mercury(II) of the reduced vanadium species accumulated at the working electrode, causes a signal in the potential region where stripping of lead can be expected. If, however, the experiment is repeated with a rotating working electrode, the accumulation of soluble reduced vanadium species and the depletion of mercury(II) at the working electrode are much less pronounced, and no oxidation signal is obtained (Fig. 1B). The stripping potentiograms obtained for traces of cadmium and lead in a quiet solution without (Fig. 1C) and with (Fig. 1D) addition of vanadium(IV) show the interference of the vanadium signal. The interference vanishes when the experiment is repeated with a rotating working electrode (Fig. 1E).

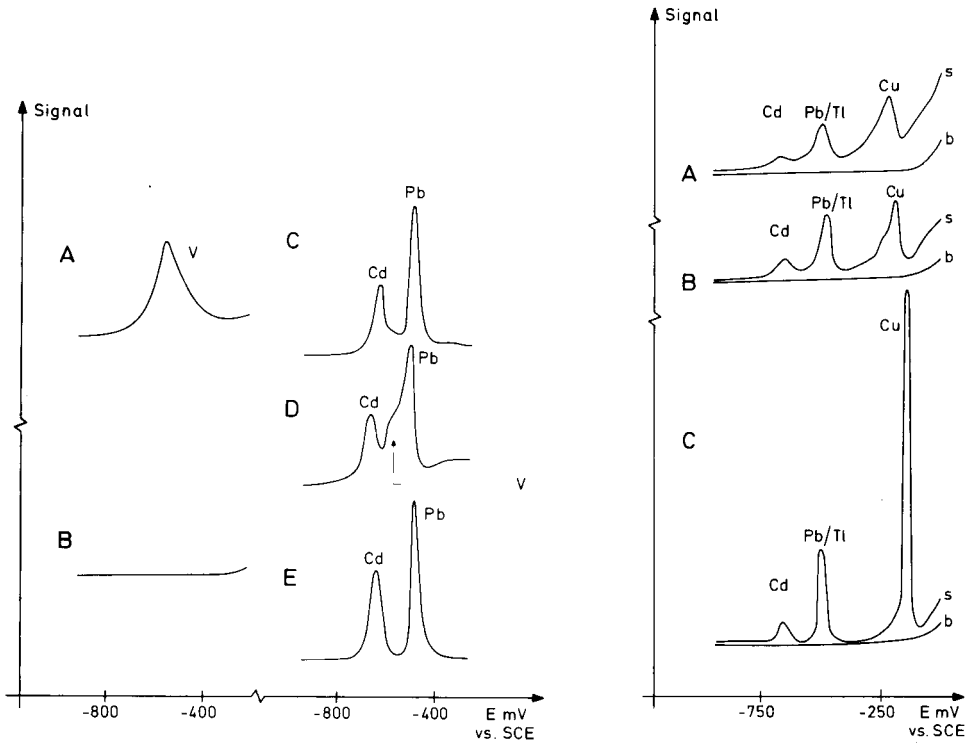

Fig. 1. Effect on stripping potentiogram of an electroactive substance forming a soluble reduced species. (A) 10^{-2} M vanadium(IV) in 1 M sodium acetate—0.5 M hydrochloric acid (pH 4.8) spiked with 2×10^{-4} M mercury(II); electrolysis at —1150 mV vs. SCE for 10 s, quiet solution. (B) As (A) but a rotating working electrode was employed (about 50 rps). (C) Stripping potentiogram of 5 μM cadmium(II) and lead(II), conditions as for (A). (D) As (C) after the addition of 10^{-2} M vanadium(IV). (E) As (D) but with the rotating electrode.

Fig. 2. Effect on stripping potentiogram of solution stirring and of exploiting a rotating electrode. Solution obtained by the leaching of a coal fly ash for 60 days in 0.1 M hydrochloric acid; pH adjusted to 4.8 with sodium acetate and solution made 2×10^{-4} M in mercury(II); plating at —950 mV vs. SCE for 60 s. (A) Quiet solution. (B) Stirring with 1-cm stirring bar, 3 cm below working electrode (about 10 rps). (C) With a rotating working electrode (about 50 rps). (s) Primary stripping signal; (b) background signal obtained with zero plating time.

The importance of inducing rapid transport rates by vigorous solution stirring or by employing a rotating working electrode in the potentiometric stripping analysis of multicomponent samples is further illustrated in Fig. 2. The sample studied was obtained by leaching of 1 g of a coal fly ash for 60 days in 1 l of 0.1 M hydrochloric acid. Obviously, this procedure resulted in dissolution of several electroactive species: after 60 s of electrolysis, peaks are visible on the potentiogram. However, if stripping is done from a quiet solution, the resolution of peaks on the primary signal (Fig. 2A, curve s) is

poor, and the signal does not at any point follow the background signal (Fig. 2A, curve b) obtained from a similar experiment with zero plating time. This effect, which is even more pronounced for dissolved, decomposed fly ash, where the concentrations of electroactive species are higher [13], can be attributed to interferences from elements such as titanium, vanadium, chromium and cobalt, which are not plated, but which during electrolysis form localized regions of high concentrations of reduced species around the working electrode. Figure 2B shows the result of a similar experiment where the solution was stirred slowly by a magnetic stirrer bar. The stirring clearly improves the resolution, but only with a rotating working electrode (Fig. 2C) is the resolution of peaks satisfactory for quantitative purposes. Throughout the remaining part of the study, a rotating working electrode (about 50 rps) was used.

In Table 1, elements frequently occurring in fly ash in significant concentrations are listed and classified according to their electrochemical behaviour. Some of these elements do not produce stripping signals in the region of interest (ca. −700 mV to −400 mV vs. SCE), either because reduction of soluble species to the elemental state requires potentials cathodic of −950 mV vs. SCE (class 4), or because stripping takes place anodic of −400 mV (class 2).

Choice of electrolysis potential

The feasibility of simultaneous multi-element analysis was investigated by subjecting samples of decomposed dissolved fly ashes to p.s.a. using varying plating potentials, the idea being that at very cathodic plating potentials, several metals are simultaneously plated. The results shown in Fig. 3 are characteristic of these experiments. Peaks from the stripping of cadmium and lead and a shoulder on the lead peak caused by thallium stripping were identified by standard additions. The peaks marked X and Y in Fig. 3B and C can be attributed to elements, which are reduced only at potentials cathodic of −1000 mV vs. SCE, but which require rather anodic overpotentials to produce a stripping signal. Similarly, the peak and shoulder in Fig. 3A, which overlap the lead signal, thus prohibiting quantitative lead measurements, can be attributed to large concentrations of elements such as nickel, chromium, cobalt, gallium, tin and manganese (class 4, Table 1).

Some of these elements are known to form binary intermetallic compounds with other elements co-deposited in the mercury film (the Cu—Zn and the Cu—Ga intermetallics, for example, are well known [14, 15, 19, 20]). Because the stripping of binary intermetallic compounds mostly takes place at an intermediate potential with respect to the stripping potentials of the two components, the large number of elements inevitably co-plated at very cathodic potentials may contribute to wide maxima such as those of Fig. 3A, B and C. A means of avoiding these interferences is, of course, to study simultaneously only those elements for which the necessary plating potential is only slightly cathodic of the stripping potential of the analyte.

TABLE 1

Survey of elements which form electroactive species in solution
(The elements selected are those which are most likely to interfere with the potentiometric stripping determination of cadmium, lead and thallium in fly ash)

Element	Class[a]	Amount added for interference tests (stated as mg g^{-1} ash equivalents)	Comment[b]
Antimony	2	0.6	
Arsenic	2	0.4	Reduction to As^{3-} is possible
Bismuth	2	1.0	
Cadmium	1		Reduction in medium 2 requires plating cathodic of −950 mV vs. SCE
Chromium	4	>3.0	(+)
Cobalt	4	0.3	(+)
Copper	2	0.3	
Gallium	4	0.3	
Germanium	2		Data from [14]
Gold	3		
Indium	1		
Iron	4		
Lead	1		Reduction in medium 2 requires plating cathodic of −950 mV vs. SCE
Manganese	4		Data from [14]
Nickel	2	0.3	
Silver	3	0.1	
Thallium	1		
Tin	4	0.6	(+)
Titanium	4		(+), data from [14]
Vanadium	4	>3.0	(+)
Zinc	4		

[a]Classification. (1) Potentially strong interference: reduced to elemental state anodic of −950 mV vs. SCE in medium 1; amalgamated species is oxidized by mercury(II) producing stripping signal cathodic of −400 mV vs. SCE. (2) Reduced to elemental state anodic of −950 mV vs. SCE, but re-oxidized by mercury(II) anodic of −400 mV. (3) Reduced to elemental state anodic of −950 mV vs. SCE in medium 1, but the amalgamated metal is not oxidized by mercury(II). (4) Reduction to elemental state requires electrolysis cathodic of −950 mV vs. SCE in both media. [b](+) Signals arising from redox conversions between soluble species in quiet or moderately stirred solutions, may interfere with signals from the stripping of amalgamated analytes.

This limits the number of elements that can be determined simultaneously, but the reward for refraining from attempts at multi-component analysis is an improved resolution of peaks (Fig. 3D).

A model experiment illustrated further the importance of narrowing the potential range studied: a solution containing traces of cadmium, gallium, lead and tin in (2 + 1) 1 M sodium acetate—1 M hydrochloric acid, with 2×10^{-4} mercury(II) was subjected to p.s.a. by using varying plating poten-

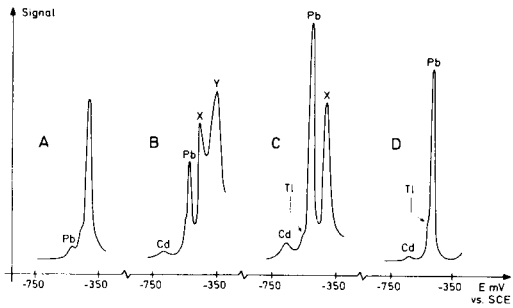

Fig. 3. Stripping potentiograms of decomposed, dissolved coal fly ash sample. Electrolysis for 8 min at (A) —1300 mV; (B) —1200 mV; (C) —1150 mV; and (D) —950 mV (all vs. SCE). Experimental amplitudes were multiplied by: (A) 1; (B) 5; (C) 20; and (D) 20, to produce the figure. For further explanation, see text.

tials. Gallium and tin were chosen as representatives of those elements for which a large cathodic overpotential is necessary for efficient reduction to proceed and/or for which a large anodic overpotential is necessary for the re-oxidation. Figure 4 shows that while the magnitude of the cadmium and lead signals is relatively independent of plating potential, efficient plating of gallium and tin occurs only when electrolysis is done at potentials cathodic

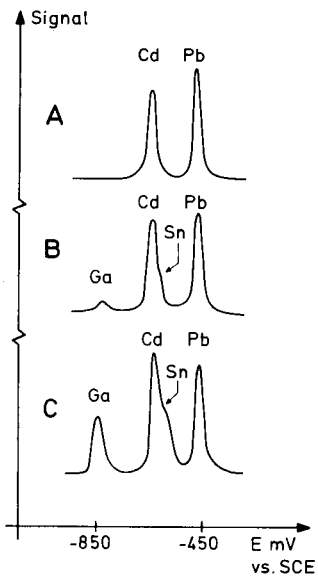

Fig. 4. Dependence on electrolysis potential of stripping potentiograms obtained with 10 s electrolysis of a solution containing 1 M sodium acetate—0.5 M hydrochloric acid and 5×10^{-4} M mercury(II), spiked with 10 μM cadmium(II), gallium(III), lead(II), tin(IV). Electrolysis potential: (A) —950 mV; (B) —1130 mV; and (C) —1350 mV (all vs. SCE).

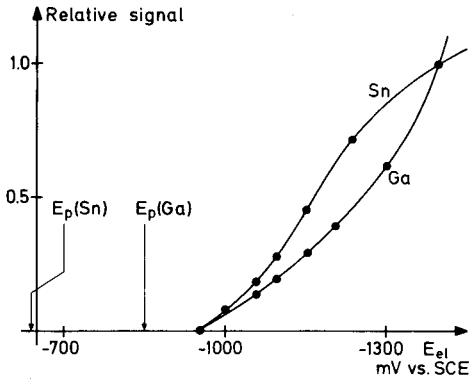

Fig. 5. Dependence on electrolysis potential (E_{el}) of the relative stripping signal for gallium and tin (10 μM). Electrolysis time 10 s; 1 M sodium acetate—0.5 M hydrochloric acid (pH 4.8) containing 5×10^{-4} M mercury(II). Stripping signals are relative to the signal obtained by electrolysis at —1400 mV vs. SCE. E_P(M) is the stripping potential for element M.

of about —1100 mV vs. SCE. Carrying out the pre-electrolysis at such potentials results in a severe interference between cadmium and tin. In Figure 5, the stripping signals of tin and gallium (relative to the signals obtained by plating at —1400 mV vs. SCE) are shown as a function of electrolysis potentials; the stripping potentials are also indicated. Because of the large differences between the stripping potentials and the plating potentials, anodic of which the stripping signals vanish, it is possible to discriminate against interferences from these elements, and against others with similar behaviour, by an appropriate choice of plating potential and by studying a limited potential range. In complexing media such as those employed in the study of fly ashes (medium 1 and medium 2), gallium(III) and tin(IV) are reduced to the metal only at potentials cathodic of —1000 mV vs. SCE. Based on the above observations, a plating potential of —950 mV vs. SCE was chosen for the determination of cadmium, lead and thallium.

Mutual overlap of stripping signals from cadmium, indium, lead and thallium

Choice of medium. If the pre-electrolysis is done at —950 mV vs. SCE using a mercury electrode in chloride-containing acetate buffer, the stripping signals appearing in the region —700 to —400 mV are due to the redissolution of amalgamated cadmium, indium, lead and thallium (class 1, Table 1). A literature survey [14, 21] indicated that only these four elements require sufficiently small cathodic and anodic overpotentials with respect to the equilibrium potential, determined by the dissolved/amalgamated species, to produce stripping signals within this potential range. The mutual overlap of the stripping signals from these elements was therefore subsequently studied. Figure 6A shows the results of an experiment similar to that of Fig. 5 with a solution containing traces of cadmium, lead and thallium: obviously, for

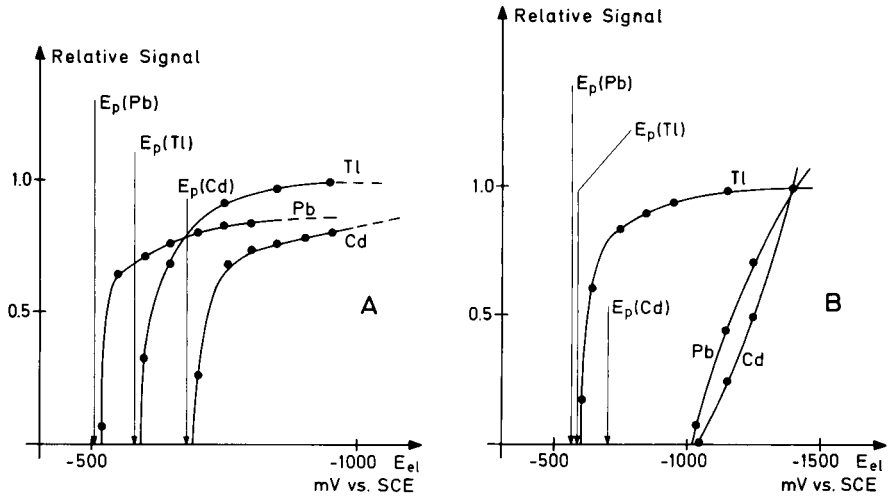

Fig. 6. Dependence on electrolysis potential of the relative stripping signals for cadmium, lead and thallium. Electrolysis time 10 s. Media: (A) 1 M sodium acetate—0.5 M hydrochloric acid (pH 4.8) with 5×10^{-4} M mercury(II) added; (B) as (A) after the addition of 10^{-2} M disodium EDTA. Stripping signals are relative to the signal obtained by electrolysis at —1400 mV vs. SCE. E_p (M) is the stripping potential for element M.

these elements, significant stripping signals can be obtained by conducting the electrolysis as little as 50 mV cathodic of the respective stripping signals. This means that lead can, in principle, be determined independently of thallium and thallium independently of cadmium. However, because the lead content in most fly ash samples is much larger than that of thallium, and because in the determination of thallium in medium 1, lead is inevitably co-plated, the cathodic tail of the lead peak overlaps a large proportion of the thallium peak (cf. Fig. 7A). The mutual interference of lead and thallium was studied by adding known amounts of the two metals to solutions of

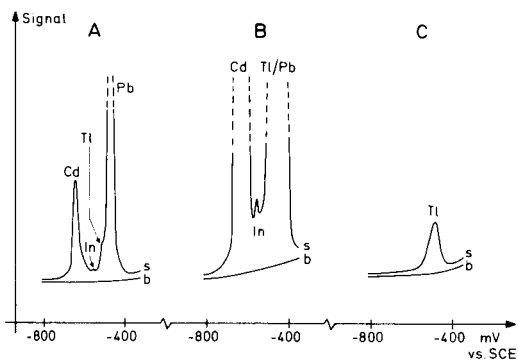

Fig. 7. Stripping potentiograms of a digested, dissolved coal fly ash. Electrolysis at —950 mV vs. SCE for 8 min. (A) Analysis in medium 1; (B) as in (A), figure enlarged 10 times; (C) as in (A) after the addition of 10^{-2} M disodium EDTA, figure enlarged 2 times.

decomposed coal fly ash (NBS SRM 1633a) in medium 1. It was found that with the decomposition/dissolution procedure described above, and with electrolysis as cathodic as —950 mV vs. SCE for 60 s, the peak height corresponding to 100 μg of lead per gram of ash was not affected by the peak corresponding to 100 μg of thallium per gram of ash. The mutual interference of cadmium and thallium was studied in a similar manner. The cadmium and thallium peaks are separated better than those of lead and thallium (cf. Fig. 7A), and 1 μg Cd g^{-1} ash can be determined in the presence of 40 μg Tl g^{-1} ash with no change in the cadmium peak height (8 min pre-electrolysis). When the thallium concentration in fly ash is small compared to that of lead, the thallium signal appears as a small shoulder on the lead signal in medium 1, and thallium cannot be determined accurately. However, as thallium(I) forms no stable complex with EDTA, it is possible to remove the lead (and cadmium) interferences by adding excess of EDTA, to the sample solution (medium 2). At pH 4.8, the conditional stability constants of the cadmium and lead complexes with EDTA are sufficiently large that no reduction takes place at potentials anodic of ca. —1000 mV vs. SCE (see Fig. 6B). The thallium peak shown in Fig. 7C was obtained after the addition of 5×10^{-2} M EDTA to the sample which produced the potentiogram of Fig. 7A. The minor peak appearing between the cadmium and the fused lead/thallium peaks can be attributed to a trace of indium(III) (identified by standard addition). In medium 1, which contains excess of ethylenediamine, the indium signal is reasonably well separated from the cadmium signal. This is not the case if ethylenediamine is omitted. The effect on the cadmium stripping signal of the addition of indium(III) to 1 M sodium acetate—0.5 M hydrochloric acid containing 10^{-3} M mercury(II), 4×10^{-5} M cadmium(II) and lead(II) without and with ethylenediamine is shown in Fig. 8A and B. Clearly, the cadmium and indium signals appear at similar potentials. Figure 8C shows the stripping potentiogram obtained after electrolysing a decomposed dissolved fly ash in the same medium for 8 min at —950 mV vs. SCE, while Fig. 8D (which is on a different scale) shows the result of the experiment repeated after the addition of 10^{-2} M ethylenediamine. The extra peak appearing on Fig. 8D was identified by standard addition as an indium peak; without ethylenediamine, this peak was completely overlapped by the cadmium peak. It was found that with 8-min plating, the peak height of the cadmium signal corresponding to 1 μg Cd g^{-1} ash and the peak height corresponding to 70 μg Pb g^{-1} ash were not affected by the addition of indium(III) corresponding to 50 μg In g^{-1} ash. Since thallium(I) is determined in the presence of EDTA, which forms a stable complex with indium-(III), the thallium determination is not affected by the presence of indium. Table 2 summarizes the results of the study of the mutual interferences between cadmium, indium, lead and thallium.

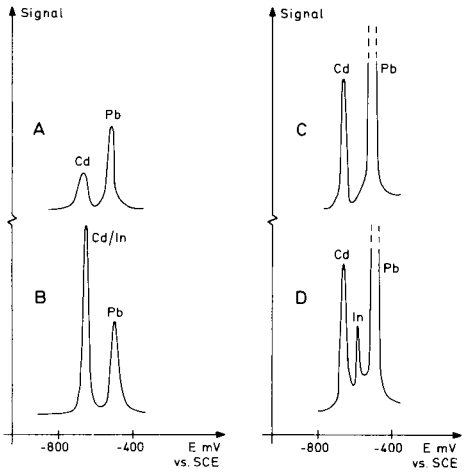

Fig. 8. Cadmium/indium interference. Stripping potentiograms: (A) 4×10^{-5} M cadmium(II), lead(II) in 1 M sodium acetate—0.5 M hydrochloric acid with 10^{-3} M mercury(II) after plating at —950 mV vs. SCE for 60 s; (B) as (A) after the addition of 4×10^{-5} M indium(III); (C) decomposed, dissolved fly ash in medium 1, without ethylenediamine after plating at —950 mV vs. SCE for 8 min; (D) as (C) after the addition of 10^{-2} M ethylenediamine.

TABLE 2

Mutual interferences between cadmium, indium, lead and thallium signals
(With the proposed decomposition/dissolution procedure and the plating times quoted, the stated amounts of thallium and indium do not affect the stripping peak heights of cadmium and lead)

Element	Amount in ash ($\mu g\ g^{-1}$)	Plating time (min)	Interfering element	Tolerable amount in ash[a] ($\mu g\ g^{-1}$)
Pb	100	1	Tl	100
Pb	70	1	In	50
Cd	1	8	Tl	40
Cd	1	8	In	50

[a]Amount not affecting the analyte signal.

Co-plated elements

Even though intermetallic formation between the analytes and elements such as manganese, nickel, zinc, gallium and tin can be avoided by choosing the electrolysis potential at —950 mV vs. SCE, traces of copper(II), antimony(III), bismuth(III) (class 2, Table 1) and silver(I) and gold(III) (class 3, Table 1) are inevitably reduced together with the analytes and dissolved in the mercury electrode. Hence the formation of intermetallic compounds between the analytes and these elements must be considered a potential source of interference. To study the effects of such co-plated

elements, tests were made on a decomposed dissolved coal fly ash (NBS SRM 1633a): stripping potentiograms were obtained before and after the addition of known amounts of the potentially interfering elements. Because interference from the formation of intermetallic compounds is likely to be more pronounced after long plating periods where amalgamated species are more concentrated, the maximum plating time employed during the entire study (8 min) was used. In Table 1 are shown the amounts of eleven elements (stated as mg g^{-1} ash equivalents) added to the fly ash solutions (both media). None of the amounts stated reduced the stripping signals of cadmium, lead and thallium when electrolysis was done at −950 mV vs. SCE.

Dissolved species of gold and silver are particular in the sense that while such species are mostly readily reduced at a mercury electrode, and while both gold and silver are soluble in mercury, no stripping takes place unless very strong oxidizing agents, which also oxidize the mercury film, are employed. This implies that when mercury(II) or dissolved oxygen is used as the oxidizing agent in p.s.a., traces of gold and silver will accumulate continuously over the lifetime of the working electrode. It was found that soluble species of gold may interfere strongly with the determination of cadmium: as a result of the steadily increasing gold concentration in the mercury film, an increasing proportion of amalgamated cadmium is converted to the cadmium—gold intermetallic, over successive plating/stripping cycles. The addition of an amount of gold(III) corresponding to 100 μg Au g^{-1} ash to a sample of decomposed dissolved fly ash (NBS SRM 1633a) resulted in a reduction of about 50% of the cadmium stripping signal after 8 min of electrolysis. The lead and thallium signals were not affected. When the experiment was repeated with a similar amount of silver(I), part of which exists as the soluble ethylenediamine complex in medium 1, no reduction of the stripping signals of any of the three analytes was observed.

Although the gold—cadmium interference can prevent in principle the determination of cadmium by p.s.a., its importance for accuracy in the analysis of a given fly ash sample is easily estimated: if the gold content of the ash is high (which is usually not the case), repeated plating/stripping cycles, where gold is gradually accumulated in the mercury film electrode, will result in systematically decreasing cadmium signals. In such cases, the application of a hanging mercury drop electrode, may reduce the effect. In the study of the NBS SRM 1633a coal fly ash, no indication of the interference was detected.

Determination of cadmium, lead and thallium in NBS SRM 1633a (coal fly ash)

Based on the previous experiments, the procedures described under Experimental were developed. In order to estimate the accuracy of the proposed method, several samples of NBS SRM 1633a (coal fly ash) were decomposed, and the contents of cadmium, lead and thallium in this reference material were determined by p.s.a. The results, shown in Table 3,

TABLE 3

Results of determinations of cadmium, lead and thallium in NBS SRM 1633a (coal fly ash) (Electrolysis at −950 mV vs. SCE for 8 min (cadmium and thallium) and for 1 min (lead))

Element	No. of detns.[a]	Metal found ($\mu g\ g^{-1}$)	No. of blanks[b]	Blank found ($\mu g\ g^{-1}$)	Average (blank corrected) ($\mu g\ g^{-1}$)	Certified value[c] ($\mu g\ g^{-1}$)
Cd	4	1.18	3	0.17	0.93	1.0 ± 0.15
		1.01		0.16		
		1.12		0.16		
		1.07				
Pb	6	76.7	5	5.7	68.8	72.4 ± 0.4
		73.6		7.0		
		72.5		4.2		
		72.5		3.5		
		78.7		7.4		
		72.0				
Tl	6	5.6	2	<0.1	5.3	5.7 ± 0.2
		5.3		<0.1		
		4.4				
		4.4				
		5.9				
		6.1				

[a]Number of independent decompositions and determinations. [b]Number of independent blank determinations. [c]Certified value with estimated uncertainty (NBS certificate).

indicate that no major source of interference has been overlooked. The number of independent determinations is too small for statistical analysis.

Apart from the determination of cadmium, lead and thallium in the NBS SRM 1633a coal fly ash, a small selection of different decomposed, dissolved coal and oil fly ash samples and aqueous samples contaminated by the leaching of fly ash were studied. No attempts were made to obtain quantitative results for these samples, but the stripping potentiograms acquired indicated that although the relative contents of cadmium, lead and thallium were quite variable, the thallium and indium contents were always sufficiently small that the heights of the cadmium and lead stripping peaks (in medium 1) were not affected. Mostly, no indium signal at all was seen when plating times sufficiently long for the cadmium determination were employed. The thallium signal typically appeared as a low shoulder on the cathodic slope of the lead peak. In none of the samples studied, was any sign of the gold—cadmium interference observed: the cadmium signal could be reproduced over several plating/stripping cycles. Because the concentration of other metallic species added in the interference tests were of the same order as, or larger than, the concentrations found in decomposed, dissolved fly ashes [1—10] and because these additions did not affect the stripping signals used for quantitative assessment, it seems likely that p.s.a. can

become a useful method for determinations of cadmium, lead and thallium in fly ash.

The authors thank D. Britz, J. Mortensen and S. E. Rasmussen for valuable discussions, and L. Hjort and S. Kjær Andersen, Aalborg Portland, for donation of the fly ash samples. A research fellowship (N.P.) from the Danish Technical Science Research Council (16-0193) and a grant (511-8032) from the Danish Natural Science Research Council for the computerized instrument are gratefully acknowledged.

REFERENCES

1 W. R. Roy, R. G. Thiery, R. M. Schuller and J. J. Suloway, Illinois State Geological Survey, Environmental Geology Notes 96, April, 1981.
2 L. D. Hulett, Jr., A. J. Weinberger, K. J. Northcutt and M. Ferguson, Science, 210 (1980) 1356.
3 W. M. Henry and K. T. Knapp, Environ. Sci. Technol., 14 (1980) 450.
4 R. A. Nadkarni, Anal. Chem., 52 (1980) 929.
5 A. W. Andren, D. H. Klein and Y. Talmi, Environ. Sci. Technol., 9 (1975) 856.
6 M. S. Germani, I. Gokmen, A. C. Sigleo, G. S. Kowalczyk, I. Olmez, A. M. Small, D. L. Anderson, M. P. Falley, M. C. Gulovali, C. E. Choquette, E. A. Lepel, G. E. Gordon and W. H. Zoller, Anal. Chem., 52 (1980) 240.
7 J. A. Campbell, J. C. Laul, K. K. Nielson and R. D. Smith, Anal. Chem., 50 (1978) 1032.
8 J. B. Green and S. E. Manahan, Anal. Chem., 50 (1978) 1975.
9 I. Obrusník, B. Stárková and J. Blažek, J. Radioanal. Chem., 31 (1976) 495.
10 E. S. Gladney, Anal. Chim. Acta, 118 (1980) 385.
11 D. Jagner and A. Graneli, Anal. Chim. Acta, 83 (1976) 19.
12 D. Jagner, Anal. Chem., 50 (1978) 1924.
13 J. K. Christensen, L. Kryger and N. Pind, Anal. Chim. Acta, 136 (1982) 39.
14 F. Vydra, K. Štulík and E. Juláková, Electrochemical Stripping Analysis, Horwood, Chichester, 1976.
15 T. R. Copeland, R. A. Osteryoung and R. K. Skogerboe, Anal. Chem., 46 (1974) 2093.
16 H. J. Skov and L. Kryger, Anal. Chim. Acta, 122 (1980) 179.
17 J. Mortensen, E. Ouziel, H. J. Skov and L. Kryger, Anal. Chim. Acta, 112 (1979) 297.
18 L. Kryger, Anal. Chim. Acta, 133 (1981) 591.
19 D. Jagner and L. Kryger, Anal. Chim. Acta, 80 (1975) 255.
20 L.-G. Danielsson, D. Jagner, M. Josefson and S. Westerlund, Anal. Chim. Acta, 127 (1981) 147.
21 L. Meites, Polarographic Techniques, 2nd edn., Wiley, New York, 1965.

Analytica Chimica Acta, 141 (1982) 147—156
Elsevier Scientific Publishing Company, Amsterdam — Printed in The Netherlands

FLOW POTENTIOMETRIC STRIPPING ANALYSIS FOR MERCURY(II)

DANIEL JAGNER*, MATS JOSEFSON and KERSTIN ÅRÉN

Department of Analytical and Marine Chemistry, Chalmers University of Technology and University of Göteborg, S-412 96 Göteborg (Sweden)

(Received 30th April 1982)

SUMMARY

The optimum experimental conditions, with respect to sample and stripping solution composition, in computerised flow potentiometric stripping analysis for mercury(II) with a gold working electrode are described. When pre-electrolysis was done in a sample to which ammonia and iodide had been added and stripping was done in an acidified bromide solution containing chromium(VI), a detection limit of 2 nM (0.4 $\mu g\ kg^{-1}$) was obtained after 90 s of pre-electrolysis, the dynamic range being almost three decades. Copper(II) interfered when present in a 1000-fold excess and silver(I) when present in a 5-fold excess over mercury(II).

Determination of mercury(II) by electroanalytical stripping techniques has recently been described by Sipos et al. [1], who used anodic stripping voltammetry and a gold working electrode, and by Jagner [2] who used potentiometric stripping analysis [3—5] and a glassy carbon working electrode. In the potentiometric stripping technique, elemental copper was co-deposited on the glassy carbon electrode during the potentiostatic deposition in order to make mercury adhere to the electrode surface. The co-deposition of copper caused problems in samples containing high concentrations of copper(II) and for this reason it was considered interesting to investigate the possibility of using a gold working electrode in potentiometric stripping analysis for mercury(II). More important, the potentiometric stripping flow mode recently described [6] makes it possible to perform the potentiostatic deposition and re-oxidation (stripping) in solutions of different composition, thus increasing both the selectivity and sensitivity.

The purpose of this paper is to outline the optimum experimental conditions, with respect to sample and stripping solution composition, for the potentiometric stripping analysis for mercury(II) with a gold working electrode in a flow system.

EXPERIMENTAL

Instrumentation and flow system

The Radiometer Ion Scanning System ISS820 [7] was supplemented with a laboratory-constructed microcomputer system [8]. The microcomputer

0003-2670/82/0000-0000/$02.75

system recorded the potentiometric stripping curve obtained after potentiostatic deposition and subsequently the background obtained after only two seconds of potentiostatic deposition. The background-corrected curve was then displayed on the strip-chart recorder of the ISS820 either as working electrode potential (E, mV) vs. stripping time (t, s) or as $dt(dE)^{-1}$ vs. t.

In the digital evaluation of the potentiometric stripping signal for Hg(Au) the microcomputer first added the number of potential measurements falling within the potential range, $E_1 - E_2$ (mV), specified by the operator as the potential range for the reaction Hg(Au) → Hg(II), and then subtracted the number of counts on the background curve in the same potential region [8]. Since the real-time sampling rate of the microcomputer was 30.3 kHz, one count was equal to a time duration of 33 μs. The time unit count is used throughout this paper, in order to emphasise the limited resolution in the measurement of potentiometric stripping times.

The flow system consisted of a six-channel inlet valve (Altex Model 204), an electrochemical flow cell and a pump [6]. The sample and the stripping and rinsing solutions were sucked through the valve and electrochemical cell into the pump. A non-pulsing flow was obtained by operating a modified syringe buret (Radiometer ABU80) in the reverse mode. The flow rate could be varied between 1.25 and 100 $cm^3\ min^{-1}$; a flow rate of 1.75 $cm^3\ min^{-1}$ was used in all experiments below.

The electrochemical cell was a modified Kissinger [9—11] thin-layer cell with a cell spacer thickness of 0.2 mm and a spacer channel width of 2 mm. The gold working electrode had a diameter of 1.5 mm. The glassy carbon counter electrode had a diameter of 2 mm and the center of the electrode was placed 3.0 mm downstream from the center of the gold electrode. The calomel reference electrode (Radiometer K4040) was placed after the electrochemical cell [9].

Chemicals

All chemicals used were of analytical grade except the mineral acids which were of Suprapur grade (Merck). Separate stock solutions were made 8 M in ammonium nitrate, 6 M in calcium bromide and 10 M in ammonia. A 2 $g\,l^{-1}$ stock solution of Au(III) was prepared by dissolving the metal in aqua regia and subsequent dilution to a hydrochloric and nitric acid concentration of ca. 2 M.

Pre-treatment of the gold working electrode

At intervals of about one week the gold electrode was polished with 3-μm diamond paste and then cleaned carefully with ethanol. After polishing, 2—3 pre-electrolysis/stripping cycles were conducted with a sample containing approximately 5×10^{-7} M mercury(II) until stable readings were obtained. The same procedure was used if the electrode had not been in use for some days. In such cases, the first pre-electrolysis/stripping cycle normally yielded a higher reading than the subsequent cycles. This was attributed to the spontaneous uptake of mercury(II) during storage of the gold electrode in, e.g., 0.1 M hydrochloric acid.

Procedure

The six-channel inlet valve was operated by the computer. After adjustment of the appropriate pre-electrolysis potential and time, the rotating valve was operated to a position where the stripping solution was allowed to flow through the cell. Five seconds later, the valve was operated to allow the sample solution to enter the cell and pre-electrolysis was started simultaneously. Thirty seconds before the end of the pre-electrolysis period, the stripping solution was again allowed to enter the cell. After recording of the stripping and background curves, a solution of 0.5 M hydrochloric acid in 50% (v/v) ethanol was passed through the cell for 10 s and finally the valve was operated to allow a 0.5 M sodium chloride solution to enter the cell.

The reason for starting the cycle in the stripping solution is that the gold working electrode may have reduced some mercury(II) from the rinsing solutions. This mercury is immediately stripped off when the stripping solution enters the cell. Passage of the acidified ethanol solution is in order to remove microbubbles of air which may have started to form inside the cell and the tubings.

RESULTS

Composition of the stripping solution

The main purpose of the stripping solution is to provide a medium where the reaction Hg(Au) → Hg(II) takes place at a considerably lower potential than the base level potential in the medium as defined by the Au/Au(III) or Au(I)/Au couples. Because of the very strong interaction between gold and mercury, the redox potential for Hg(Au) → Hg(II) is several hundred millivolts more positive than the redox potential for Hg → Hg(II) in the same medium. Consequently, the stripping solution must contain not only a strong oxidant but also species capable of strong complexation with mercury(II). Preferably the stability constant for the reaction $Hg(Au) + nX^{m-} \rightarrow HgX_n^{2-nm}$ should be greater than the stability constant for the reaction $Au + nX^{m-} \rightarrow AuX_n^{3-nm}$ in order to obtain optimum resolution. Furthermore, X^{m-} should be a monodentate ligand so that the full complexing capacity can be exploited during the rapid oxidation/complexation reaction [6].

Table 1 summarises the equilibrium constants for the most strongly complexing agents for mercury(II) and the corresponding data for gold(III). The stability constants for the gold(III) complexes were derived by assuming that the standard potential for the hypothetical $Au(H_2O)_4^{3+}/Au$ couple is equal to 1.52 V, as estimated by Skibsted and Bjerrum [12]. Figure 1 shows the stripping curves obtained after 90 s of pre-electrolysis in a sample containing 5×10^{-7} M mercury(II) and stripping in the four different stripping solutions specified in Table 2. Table 2 also gives the theoretical and experimental potential shifts obtained when 1 M chloride is used as reference.

The stability constants in Table 1 indicate that chloride ought to be the most suitable complexing agent because it has the smallest value for log

TABLE 1

Stability constants in the mercury(II) and gold(III) systems
(The gold(III) data have been taken from Skibsted and Bjerrum [12] and the mercury(II) data from Smith and Martell [13])

X	$\log \beta(HgX_4)$	$\log \beta(AuX_4)$	$\log \beta(AuX_4) - \log \beta(HgX_4)$
Cl^-	15.1	26	10.9
Br^-	21	34	13
I^-	29.8	49	19.2
SCN^-	20.9	45	24.1
CN^-	41.5	82	40.5
NH_3	19.4	60	40.6

$\beta(AuX_4) - \log \beta(HgX_4)$. In practice, however, its applicability is limited by the facts that chloride can only be used in combination with very strong oxidants (cf. Fig. 1d) and that stripping solutions containing strong oxidants will not be stable on storage. From this point of view, bromide is a much more suitable complexing agent. Table 2 also shows that the experimentally observed shifts in stripping peak potentials are of the same order of magnitude as those calculated theoretically from the $\log \beta(HgX_4)$ values. The discrepancies can probably be attributed to uncertainties in the stability constants at the

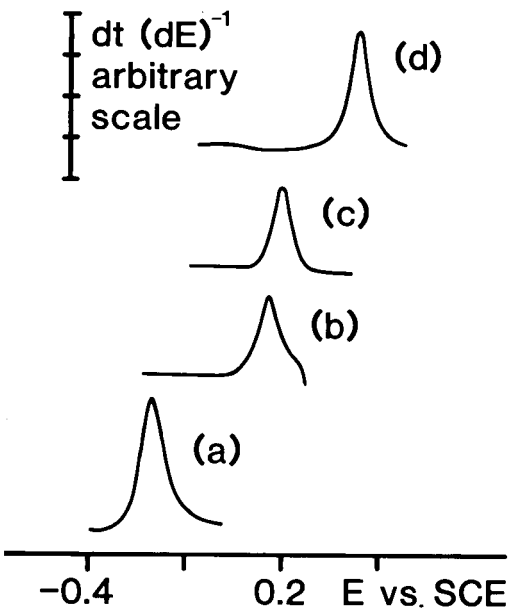

Fig. 1. Potentiometric stripping curves obtained after 90 s of pre-electrolysis in a sample containing 5 × 10^{-7} M mercury and subsequent stripping in different solutions: (a) 1 M iodide; (b) 1 M ammonia; (c) 1 M bromide; (d) 1 M chloride.

TABLE 2

Stripping potentials obtained in four different stripping solutions after 90 s of pre-electrolysis in a sample containing 2 M ammonia—2 M ammonium ion and 5×10^{-7} M mercury(II)
(The potential shifts were calculated with reference to 1 M chloride)

Pre-electrolysis potential E (V vs. SCE)	Stripping solution composition	Fig.	E_{peak} (V vs. SCE)	ΔE_{peak}(V)	
				Theoretical	Found
−0.4	1 M KI, 0.2 mM I_2, 75 μM Au(III)	1a	−0.18	0.43	0.57
−0.25	M NH_3—M NH_4^+, 0.4 mM I_2, 75 μM Au(III)	1b	0.19	0.12	0.20
−0.10	0.5 M $CaBr_2$, 0.1 M HCl, 3 mM Cr(VI), 75 μM Au(III)	1c	0.20	0.18	0.19
−0.10	0.45 M $CaCl_2$, 0.10 M HCl, 0.25 mM Au(III)	1d	0.39	0	0

relevant ionic strength and to lack of kinetic data for the complexation reactions. From Fig. 1 and Table 1 it can also be concluded that ammonia, in spite of its very strong mercury(II) complexes, is the least suitable of the four complexing agents investigated. This is, of course, due to the very high value for $\log \beta(AuX_4) - \log \beta(HgX_4)$ which makes it impossible to obtain a steady base level value for $dt(dE)^{-1}$ after the stripping peak. For the same reason, thiocyanate and cyanide are also unsuitable complexing agents.

The choice of oxidant when bromide is used as complexing agent in the stripping solution is not very critical. Solutions of chromium(VI) in dilute hydrochloric acid (Table 2) were found to be stable for several weeks although equilibrium data predict that bromide will be oxidised. The addition of small amounts of gold(III) (cf. Table 2) to the stripping solution simplified the attainment of a steady base level potential for the $AuBr_4^-/Au$ couple even though some of the gold(III) ions were oxidised by the bromide ions. In all experiments described below, the bromide-containing stripping solution had the composition specified in Table 2.

Composition of the matrix-modifying solution

In flow potentiometric stripping analysis, the stripping is done in stripping solutions with constant concentrations of oxidant. Accordingly, it is possible to quantify the concentrations of the trace metal analytes not only by means of standard addition but also by means of a calibration plot. When a calibration plot is used, it is, of course, necessary that the matrix of the sample be similar to the matrix used in the calibration solutions. For this reason it is normally necessary to add a matrix-modifying solution to the sample before measurements. The most important requirement with regard to the composition of the matrix-modifying solution is that it contains a strong complexing agent, X^{n-}, so that all mercury(II) species in the sample are converted to a well-defined mercury(II) complex, e.g. HgX_4^{2-4n}, irrespective of the sample composition. Preferably the matrix-modifying solution should also be capable of complexing interfering ions, thus preventing them from being deposited on the gold electrode during potentiostatic deposition. In the case of mercury(II) determination, masking of copper(II) is of

particular importance. Furthermore, it must be possible to prepare concentrated solutions of the matrix-modifying solution in order to avoid unnecessary dilution of the sample. Finally, it is important that the reagents in the matrix-modifying solution can be obtained commercially in pure form at a reasonable price.

The ligands specified in Table 1 fulfill some of the above requirements. In order to compare the relative merits of these ligands, solutions containing 2 M concentrations of ammonia, chloride, bromide and iodide and 0.1 μM of mercury(II) were pre-electrolyzed for 90 s at —0.25 V vs. SCE prior to stripping in the chromium(VI)/calcium bromide solution specified in Table 2. The results are summarised in Table 3. As can be seen from this table, the sensitivity, expressed as counts × (seconds of pre-electrolysis)$^{-1}$ [Hg(II)]$^{-1}$, depends on the chemical form of the mercury(II) species. It can also be concluded that the sensitivity is almost proportional to the square root of the relative molar weight, M_r, of the predominant mercury(II) species, i.e., the rate of mercury deposition on the gold electrode during pre-electrolysis is essentially diffusion-controlled and kinetic effects are of negligible importance. From Table 3, it can be concluded that ammonia is the most suitable reagent in the matrix-modifying solution. It can be obtained in high concentration and, by mixing freshly distilled ammonia with freshly distilled nitric acid, the matrix-modifying solution can be made very pure with a high buffering capacity and high ionic conductance. The equilibrium data in Table 1 show, however, that HgI_4^{2-} will be the predominant mercury(II) species if iodide ions are present in the sample, irrespective of the ammonia concentration, i.e., iodide ions in the sample will interfere if a calibration plot procedure is used for quantification. For this reason, a matrix-modifying solution consisting of, e.g., 6 M ammonium nitrate, 6 M ammonia and 0.1 M sodium iodide which is diluted three times in the sample seems suitable. The addition of iodide to the matrix-modifying solution decreases the sensitivity by a factor of ca. 3 (Table 2) but eliminates the possibility of iodide interference. It also eliminates the possibility of interference from high concentrations of strong complexing agents such as 1 M EDTA [14].

TABLE 3

Sensitivity of the mercury(II) determination in different complexing media (Pre-electrolysis for t = 90 s at —0.25 V vs. SCE in 2 M concentrations of the ligands)

[Hg(II)] (μM)	Ligand	Predominant Hg(II) species	M_r	Sensitivity (10^{-12} counts s^{-1} μM^{-1})	Sensitivity × $M_r^{1/2}$ (10^{-13} counts s^{-1} μM^{-1})
0.1	NH_3	$Hg(NH_3)_4^{2+}$	268.6	116	189
0.1	Cl^-	$HgCl_4^{2-}$	342.6	102	189
0.1	Br^-	$HgBr_4^{2-}$	520.2	75.6	173
0.1	I^-	HgI_4^-	708.2	70.1	186

Detection limit, precision and dynamic range

The detection limit in potentiometric stripping analysis is inversely proportional to the time of pre-electrolysis. In order to determine the detection limit, samples containing 2 M ammonium nitrate, 2 M ammonia and known concentrations of mercury(II) were pre-electrolyzed at −0.20 V vs. SCE for either 90 or 450 s. Five pre-electrolysis/stripping cycles were repeated at each mercury(II) concentration. The results are summarised in Table 4. As seen from this table the detection limit, on the one sigma level, is of the order of 2 nM (0.4 $\mu g\, l^{-1}$) at a pre-electrolysis time of 90 s. It can also be concluded from Table 4 that the potentiometric stripping signal is proportional to the pre-electrolysis time in the time interval investigated, 90—450 s.

The precision at different mercury(II) concentrations can be estimated from Table 4. Separate experiments showed that the relative standard deviation at mercury(II) concentrations above 0.2 μM was about 2%. Figure 2 shows the potentiometric stripping curves obtained after 450 s of pre-electrolysis at −0.20 V vs. SCE in 2 M ammonium/ammonia media containing 0, 10, 20 and 40 nM mercury(II).

The dynamic range was investigated by pre-electrolysis for either 90 s or 10 s of 2 M ammonia/ammonium samples containing 10^{-8}—$10^{-4.5}$ M mercury(II). The results given in Fig. 3 show that the dynamic range is close to three decades and that concentrations as high as 10^{-5} M mercury(II) can be determined without sample dilution provided that very short pre-electrolysis times are used. The reason for deviation from linearity at high mercury loading of the gold electrode is that the mercury stripping peak is split into a double peak. This may be due to saturation phenomena in the gold electrode but a more likely explanation is that the mercury(II) ions formed at the commencement of stripping react with Hg(Au) forming mercury(I) species.

Interferences

The determination of mercury(II) is subject to two kinds of interferences, namely, the presence of very strong complexing agents in the sample which

TABLE 4

Detection limits in potentiometric stripping analysis for mercury in a 2 M ammonium nitrate—2 M ammonia medium

[Hg(II)] (nM)	Pre-electrolysis time (s)	Signal counts[a]	Detection limit[b] (nM)
10	90	122 ± 7	0.6
20	90	225 ± 18	1.6
50	90	547 ± 23	2.1
90	90	945 ± 21	2.0
5	450	270 ± 23	0.4
10	450	520 ± 31	0.6

[a]Mean and standard deviation for $n = 5$. [b]1 σ.

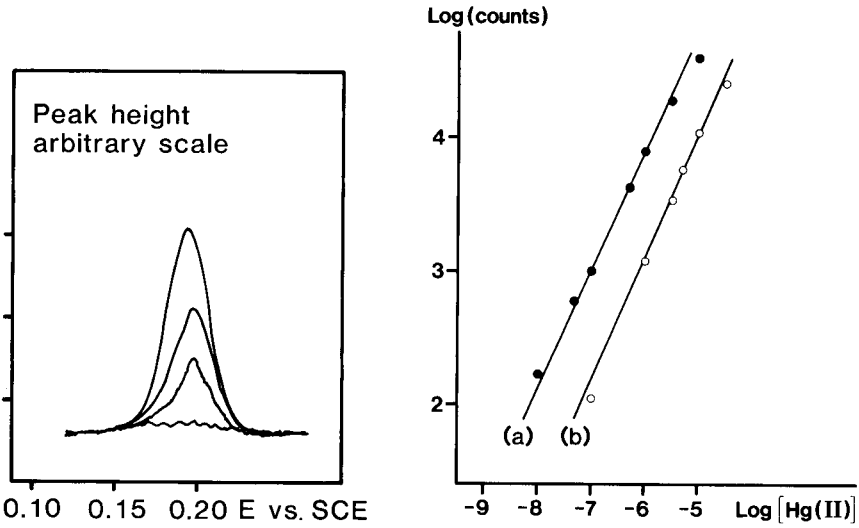

Fig. 2. Potentiometric stripping curves obtained after 450 s of pre-electrolysis in 2 M ammonia/ammonium medium containing 0, 10, 20 and 40 nM mercury(II).

Fig. 3. Dynamic range in the mercury(II) determination at pre-electrolysis times of 90 s (a) and 10 s (b).

are capable of removing mercury(II) from the HgI_4^{2-} complex, and the presence of metal ions in the sample which can be deposited on the gold electrode during pre-electrolysis and not properly resolved by the stripping solution. As mentioned above, only cyanide is capable of dissociating the HgI_4^{2-} complex and interference from cyanide can be overcome either by using a standard addition technique or by adding excess of cyanide to the calibration solutions. Alternatively, though not recommendable, cyanide could be removed by boiling the acidified sample prior to injection of the sample. Anaerobic samples containing sulphide must be oxidised before analysis.

Three metal ions can be deposited potentiostatically at the gold electrode during pre-electrolysis at —0.20 V vs. SCE in ammonia solutions, namely, copper(II), silver(I) and gold(III). Of these copper(II) is the most serious interfering ion because it is likely to be present in most samples. Other likely metal ion interferences such as bismuth(III) and antimony(III) are not reduced in basic solutions and platinum species are either not reduced or not reoxidised during stripping.

The interference from copper(II) on the mercury(II) determination is reduced by the complexing ability of the ammonia in the matrix-modifying solution [14] and by the resolving capability of the stripping solution. This is illustrated in Fig. 4 which shows the curves obtained when a solution containing 2 M ammonia, 2 M ammonium nitrate, 0.03 M sodium iodide and

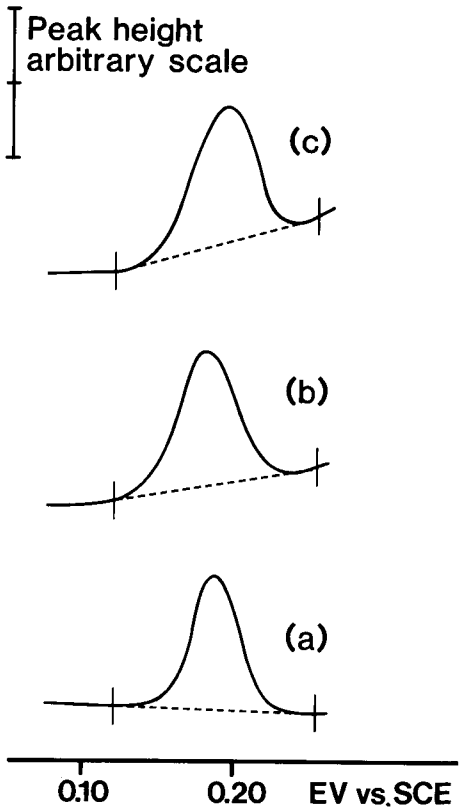

Fig. 4. Potentiometric stripping curves obtained after 90 s of pre-electrolysis at —0.20 V vs. SCE in 2 M ammonium nitrate, 2 M ammonia, 0.03 M sodium iodide and 5×10^{-7} M mercury(II): (a) without copper(II); (b) after addition of 0.5 mM copper(II); (c) after addition of 1.5 mM copper(II). The vertical bars indicate the potential regions used for the digital evaluation of the stripping signals. The area enclosed by the broken lines and the potentiometric stripping curves is taken as a measure of mercury(II) concentration.

5×10^{-7} M mercury was pre-electrolysed for 90 s at —0.20 V vs. SCE before and after the addition of 0.5 mM or 1.5 mM of copper(II). As can be concluded from Fig. 4, a 1000-fold molar excess of copper(II) does not cause any significant interference. This means that interference from copper(II) does not commence until the sample has a very distinct blue colour from the $Cu(NH_3)_4^{2+}$ complex. Increasing the free ammonia concentration from 2 M to 4 M makes it possible to determine mercury(II) in the presence of a 10 000-fold molar excess of copper(II).

The interference from silver(I) is more serious and experiments showed that only a five-fold excess of silver(I) can be tolerated. The interference from silver(I) can be eliminated by the addition of low iodide concentrations, of the order of 0.1 mM, and centrifugation of the silver iodide prior to the addition of the matrix-modifying solution. If high concentrations of silver(I)

are present in the sample, the addition of iodide must be continued until all silver has been precipitated.

The presence of gold(III) in the sample does not interfere with the mercury(II) determination, because the gold deposited during pre-electrolysis will behave as an integral part of the electrode material.

Applications of this flow potentiometric stripping system for mercury(II) in the analysis of clinical and biological samples will be reported in the near future.

REFERENCES

1 L. Sipos, J. Golimowski, P. Valenta and H.W. Nürnberg, Fresenius Z. Anal. Chem., 298 (1979) 1.
2 L. Jagner, Anal. Chim. Acta, 105 (1979) 33.
3 D. Jagner and K. Årén, Anal. Chim. Acta, 100 (1978) 375.
4 D. Jagner, Anal. Chem., 52 (1979) 1924.
5 D. Jagner, M. Josefson and S. Westerlund, Anal. Chim. Acta, 129 (1981) 153.
6 L. Anderson, D. Jagner and M. Josefson, Anal. Chem., 54 (1982) in press.
7 A. M. Graabaek and O. J. Jensen, J. Ind. Res. Dev., 21 (1979) 124.
8 A. Granéli, D. Jagner and M. Josefson, Anal. Chem., 52 (1980) 2220.
9 P. T. Kissinger, C. Refshauge, R. Dreiling and R. N. Adams, Anal. Lett., 6 (1973) 465.
10 G. C. Davis, P. T. Kissinger and R. E. Shoup, Anal. Chem., 53 (1981) 156.
11 D. A. Roston and P. T. Kissinger, Anal. Chem., 53 (1981) 1695.
12 L. H. Skibsted and J. Bjerrum, J. Indian Chem. Soc., 54 (1977) 102.
13 R. M. Smith and A. E. Martell, Critical Stability Constants, Vol. 4, Plenum, New York, 1976.
14 A. Ringbom, Complexation in Analytical Chemistry, Wiley, New York, 1963.

Analytica Chimica Acta, 141 (1982) 157—162
Elsevier Scientific Publishing Company, Amsterdam — Printed in The Netherlands

FLOW POTENTIOMETRIC STRIPPING ANALYSIS FOR MERCURY(II) IN URINE, SEDIMENT AND ACID DIGEST OF BIOLOGICAL MATERIAL

DANIEL JAGNER* and KERSTIN ÅRÉN

Department of Analytical and Marine Chemistry, Chalmers University of Technology and University of Göteborg, S-412 96 Göteborg (Sweden)

(Received 30th April 1982)

SUMMARY

In flow potentiometric stripping analysis for mercury in urine, the samples are acidified with concentrated nitric acid and heated to boiling for 10 min. After cooling, the samples are buffered by the addition of concentrated ammonia and then pre-electrolysed at a gold working electrode for 90 s at —0.25 V vs. SCE at a flow rate of 1.75 ml min^{-1}. The stripping solution is 1 M sodium bromide solution acidified with 0.1 M hydrochloric acid and containing chromium(VI). The detection limit at one sigma level is 0.05 μM. Orchard leaves, sediment and fish muscles are digested in nitric acid at 140°C for 30 min prior to buffering with ammonia and potentiometric stripping analysis for 200 s at —0.20 V vs. SCE at a flow rate of 1.75 ml min^{-1}.

The optimum experimental conditions for computerised flow potentiometric stripping analysis for mercury(II) have been described in a recent paper [1]. In the work described here, this procedure was applied to the determination of mercury(II) in samples of clinical and environmental interest.

EXPERIMENTAL

Instrumentation, flow-cell and chemicals

The computerised potentiometric stripping analyser has been described previously [1—3]. The flow system consisted of a six-channel rotating teflon valve and a modified Kissinger [4] thin-layer electrochemical cell. The gold working electrode had a diameter of 1.5 mm and the glassy carbon counter electrode had a diameter of 2.0 mm. By means of the computer-controlled inlet valve, the sample could be pre-electrolysed from a suitable solution, and then a solution of suitable composition could be allowed into the flow cell, thus making it possible to optimise the selectivity and sensitivity during potentiometric stripping.

All reagents were of analytical grade and were used as received. Care was exercised that the stock nitric acid and ammonia solutions were not exposed unnecessarily to the laboratory atmosphere.

Procedures

Urine. To 2 ml of urine sample, 1 ml of concentrated nitric acid was added and the mixture was heated to boiling for 10 min. After cooling to room temperature, the solution was treated with 2 ml of concentrated ammonia and 0.2 ml of 2.5 M sodium iodide. For potentiometric stripping analysis, a stripping solution consisting of 1 M sodium bromide, 0.1 M hydrochloric acid, 3 mM chromium(VI) and 75 μM gold(III) was first allowed into the cell for 5 s in order to oxidise Hg(Au) which might have formed spontaneously at the gold working electrode during previous cleaning of the electrodes [1]. The sample solution was then drawn into the cell and the pre-electrolysis voltage, —0.25 V vs. SCE, was started, the flow rate being 1.75 ml min^{-1} throughout the measurements. Pre-electrolysis was continued for 90 s, after which the stripping solution was again allowed into the cell. Thirty seconds later the stripping curve was recorded and five seconds later the background curve was recorded [1—3].

A rinsing solution consisting of 0.5 M hydrochloric acid in 50% (v/v) ethanol was then passed through the cell for 10 s in order to remove microbubbles which might have started forming in the cell and the tubings. Finally, the cell was rinsed with 0.5 M hydrochloric acid.

The mercury(II) concentration was evaluated either by a calibration plot procedure or by standard addition. The calibration solutions were prepared in the same way as the urine samples above, the urine being replaced by 0.01 M sodium chloride solution. The mercury(II) concentrations in the calibration solutions were in the range 0.1—1 μM. In the standard addition procedure, a urine subsample (2 ml) was treated first and this was followed by another subsample to which 0.5 μM mercury(II) had been added.

Sediments. To 1 g of dry sediment, 5 ml of concentrated nitric acid was added and the mixture was heated to 140°C for 30 min in a teflon autoclave (Perkin-Elmer Autoclave-3). After cooling, 15 ml of distilled water was added and 18 ml of the supernatant solution was decanted. To this solution, 10 ml of concentrated ammonia liquor containing 0.25 M citric acid was added, together with 1.5 ml of 2.5 M sodium iodide. Citric acid was added in order to prevent hydrated iron oxide from precipitating. The potentiometric stripping analysis was then done in the same way as for urine, except that the pre-electrolysis potential was —0.20 V vs. SCE and the pre-electrolysis time was 200 s. The calibration solutions were prepared in the same way as above, the sediment being replaced by known amounts of mercury(II) nitrate.

Two marine sediment reference samples, MESS-1 and BCSS-1, from the Marine Analytical Chemistry Standards Program, National Research Council, Canada, were analysed.

Orchard leaves. To 1 g (dry weight) of orchard leaves (Standard Reference Material 1571; National Bureau of Standards), 5 ml of concentrated nitric acid was added, and the mixture was heated to 140°C in the teflon autoclave for 30 min. The solution was then processed in the same way as the sediment samples above.

Fish muscle. To 2 g (wet weight) of muscle from pikes (Esox Lucius) caught in Swedish west coast lakes, 5 ml of concentrated nitric acid was added, and the mixture was heated to boiling point for 20 min and then allowed to cool. Alternatively, the same amount of fish muscle and nitric acid were heated in a teflon autoclave at 140°C for 10 min. The digests were processed in the same way as the urine samples above, except that 200 s of pre-electrolysis at −0.20 V vs. SCE was employed.

For comparison, the fish muscle digests were also examined with a Perkin-Elmer Mercury Analyzer, System Coleman 50.

RESULTS

Urine

Figure 1 shows the potentiometric stripping peaks obtained from nitric acid digests of urine samples to which 0, 0.25, 0.50 or 1.00 μM mercury(II) nitrate had been added prior to the acid treatment. The results are summarised in Table 1. As can be seen from the table, the agreement between the concentration of mercury(II) found by potentiometric stripping analysis and the concentration of mercury(II) added to the sample is satisfactory with both the standard addition and calibration plot procedures. That slightly higher values were obtained by the standard addition procedure was attributed to a reagent blank which was not corrected for in Table 1.

Accuracy. Mercury(II) concentrations in unexposed personnel is of the order of 0.01 μM, i.e., of the same order of magnitude as the reagent blank. Unfortunately, it was not possible to obtain urine samples from exposed persons, i.e., persons having mercury(II) concentrations above 0.25—0.50 μM. The analysis of such samples would indicate the accuracy of the technique.

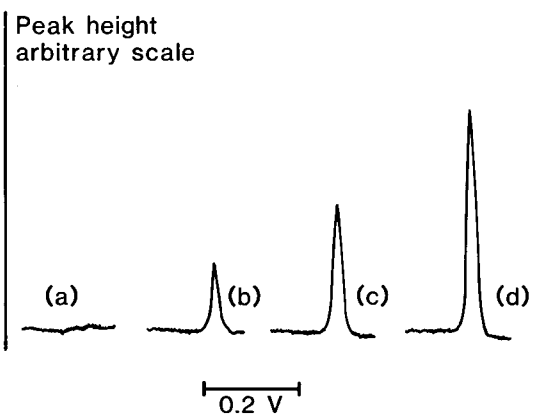

Fig. 1. Potentiometric stripping curves obtained after 90 s of pre-electrolysis at −0.25 V vs. SCE from acid-digested urine samples to which 0, 0.25, 0.50 and 1.00 μM mercury(II) had been added prior to acid treatment.

TABLE 1

Results from the potentiometric stripping analysis of urine samples

Mercury added (μM)	Chemical form	Mercury found (μM)[a]	
		Standard addition	Calibration plot
0	—	0.01 ± 0.02	−0.01 ± 0.02
0.25	$Hg(NO_3)_2$	0.27 ± 0.02	0.24 ± 0.04
0.50	$Hg(NO_3)_2$	0.54 ± 0.02	0.51 ± 0.04
0.50	CH_3HgCl	0.49 ± 0.04	0.57 ± 0.06
1.00	$Hg(NO_3)_2$	1.03 ± 0.06	0.97 ± 0.08

[a]Ten samples were taken; 5 were used for the standard addition procedure and 5 for the calibration plot procedure. The values given are the means and standard deviations.

Indirect evidence for accuracy was, however, obtained by adding mercury to urine samples from different persons. Further evidence for accuracy was obtained by adding mercury both in the form of mercury(II) nitrate and as methylmercury chloride (Table 1).

Possible loss of volatile mercury species during heating of the samples was investigated by allowing some of the acidified urine samples to evaporate to dryness. After such treatment, up to 80% of the mercury could be lost unless ca. 0.1 M sodium chloride was added to the acidified samples prior to evaporation. In such cases, no significant losses of mercury were observed when mercury was added as methylmercury chloride or as mercury(II) nitrate.

Precision. The precision of the procedure is shown in Table 1. The main contribution to the scatter originates from the acid treatment, the relative standard deviation in the potentiometric stripping analysis being approximately 3% at mercury concentrations equal to 0.5 μM.

Detection limit. From Table 1, the detection limit at the one sigma level after 90 s of pre-electrolysis can be estimated as 0.05 μM. Experiments showed that the detection limit was inversely proportional to the time of pre-electrolysis in the range 10—900 s, i.e., the detection limit could be decreased to 5 nM by increasing the time of pre-electrolysis to 15 min. In order to make such determinations meaningful the nitric acid and ammonia must, however, be purified further by means of distillation.

Interferences. The most serious interference in this potentiometric stripping method for mercury(II) is copper(II) [1]. However, the copper(II) concentration in urine samples is low, of the order of 0.7 μM or less, so that this element does not interfere even at pre-electrolysis potentials as low as −0.60 V vs. SCE.

Sediments and orchard leaves

The results from the analysis of sediments are summarised in Table 2; the reagent blank was subtracted from the values specified. As can be seen, the mercury values obtained by potentiometric stripping analysis are slightly

TABLE 2

Results from the potentiometric stripping analysis of reference samples

Reference sample	Certified range for mercury ($\mu g\ g^{-1}$)	Certified range for copper ($\mu g\ g^{-1}$)	Mercury found ($\mu g\ g^{-1}$)[a]	
			Standard addition ($n = 5$)	Calibration plot ($n = 3$)
Sediment Mess-1	0.157—0.185	21.3—28.9	0.23 ± 0.03	0.21 ± 0.04
Sediment BCSS-1	0.117—0.141	15.8—21.2	0.19 ± 0.02	0.16 ± 0.03
Orchard leaves	0.140—0.170	11—13	0.18 ± 0.04	0.16 ± 0.04

[a]Mean and standard deviation.

higher than those obtained by cold-vapour atomic absorption spectrometry and isotope-dilution solid-source mass spectrometry. This might be due to the more violent digestion of the sediments in the teflon autoclave which might have released more mercury from the mineral particles. Because the stripping curves showed no sign of a copper stripping peak, the possibility of copper(II) interference was ruled out. This was further demonstrated when the copper concentration in one sediment digest was increased by an order of magnitude, and the magnitude of the potentiometric stripping signal was found to be unchanged.

The results from the analysis of the orchard leaves are also summarised in Table 2. The scatter in the data tends to be slightly greater than those for the sediment samples. This was attributed to the presence of undigested cellulose residues in the sample, which affected the precision of the potentiometric stripping. The results, however, agree satisfactorily with the certified values.

Fish muscles

Muscle digests from three different pikes were analysed by the potentiometric stripping method and by cold-vapour atomic absorption spectrometry. Both procedures gave mercury(II) values in the range 0.2—0.3 $\mu g\ g^{-1}$ (wet weight). Five subsequent potentiometric stripping analyses of subsamples from one muscle sample yielded an average value of 0.28 $\mu g\ g^{-1}$ (wet weight) with a standard deviation of 0.02 $\mu g\ g^{-1}$, the corresponding cold-vapour value being 0.25 $\mu g\ g^{-1}$.

Conclusions

It has been shown that flow potentiometric stripping analysis for mercury(II) can be applied to a variety of samples. The optimum concentration range for potentiometric stripping work coincides with that of most interest in clinical and environmental samples. For example, mercury(II)

levels above 0.25 μM in urine are regarded as evidence for dangerous mercury exposure, and mercury(II) levels above 1.0 $\mu g\ g^{-1}$ in fish are regarded as unfit for regular human consumption.

The authors thank Dr. S. Westerlund for skilful assistance with the acid digestion of the biological samples.

REFERENCES

1 D. Jagner, M. Josefson and K. Årén, Anal. Chim. Acta, 141 (1982) 147.
2 L. Anderson, D. Jagner and M. Josefson, Anal. Chem., 54 (1982) in press.
3 D. Jagner, M. Josefson and S. Westerlund, Anal. Chim. Acta, 128 (1981) 155.
4 P. T. Kissinger, C. Refshauge, R. Dreiling and R. N. Adams, Anal. Lett., 6 (1973) 465.

Analytica Chimica Acta, 141 (1982) 163—171
Elsevier Scientific Publishing Company, Amsterdam — Printed in The Netherlands

ION-SELECTIVE ELECTRODES IN TITRATIONS INVOLVING AZO-COUPLING REACTIONS

K. VYTŘAS*, J. KALOUS and Z. KALÁBOVÁ[a]

Department of Analytical Chemistry, College of Chemical Technology, 532 10 Pardubice (Czechoslovakia)

M. REMEŠ

UNICHEM, General Directorate of Chemical Industry, 532 06 Pardubice (Czechoslovakia)

(Received 16th November 1981)

SUMMARY

An organic cation-selective indicator electrode based on a PVC membrane plasticized with 2-nitrophenyl 2-ethylhexyl ether can be used in potentiometric titrations of aromatic hydroxy compounds, amines, and compounds containing active methylene groups, with 4-methyl-, 4-bromo-, or 4-nitro-benzenediazonium chloride solutions as titrants. Useful results were obtained in determinations of 16 passive components, including 2-naphthol, some 2-naphthol sulfonic acids, 8-quinolinol and its 5-sulfonic acid, amino-1-naphthol-3-sulfonic acids, 1-naphthylamine sulfonic acids, resorcinol, 2,4-toluylenediamine, two acetanilide derivatives, and two substituted sulfophenyl pyrazolone derivatives. 4-Bromobenzenediazonium chloride proved to be the best titrant of the diazonium salts tested.

Titrimetric determinations of aromatic amines, phenols, and compounds containing active methylene groups with solutions of arenediazonium salts are important analytically, being widely used in the control of the dyestuff production. The topic has been reviewed [1]. Such titrations based on diazonium salts [2] are also called azo-coupling [3, 4] or diazometric [5, 6] titrations. An external spot test on filter paper is customarily used for end-point indication, although instrumental methods involving amperometric, thermometric, conductometric, and potentiometric indication have been described [1—6]. For the potentiometric titrations, platinum [4, 7] or copper [6] electrodes indicated the changes of redox potential.

Some years ago, applications of ion-selective electrodes in titrations of organic cations with sodium tetraphenylborate were reported [8, 9]. Arenediazonium salts were also examined [10]. Subsequently, further experiments were made in which these electrodes were applied to monitor titrations involving azo-coupling reactions. The first such titration curves were obtained by using a Crytur 19-15 electrode, pre-conditioned by titration of 4-chlorobenzenediazonium chloride with sodium tetraphenylborate, in titrations of

[a]Present address: Chemical Plants, n.c., 356 00 Sokolov, Czechoslovakia.

2-naphthol with this diazonium salt. The results obtained with newly developed electrodes for a much wider range of organic compounds are described below.

EXPERIMENTAL

Solutions

Solutions of 4-methyl-, 4-bromo-, and 4-nitro-benzenediazonium chlorides (0.1 M) for use as titrants were prepared from the respective amine solutions (0.2 M, dissolved with addition of hydrochloric acid) by titration with 1 M sodium nitrite under cooling with ice to 0° C. As the diazotization was monitored potentiometrically (with a cell consisting of platinum and saturated calomel electrodes), the concentration of the diazonium salt could be calculated from the consumption of the sodium nitrite solution. Accessible preparations of amines were used; 4-bromoaniline for quantitative studies was recrystallized twice from ethanol and its purity was checked by determination of nitrogen (theory 8.14%, found 8.16%). After diazotization, the amine solution (50 ml) was diluted to 100 ml with water to give the final concentration (0.1 M) of diazonium salt. This titrant solution was prepared daily and kept in an ice-box.

Solutions of passive compounds (0.1 M) were prepared. If necessary, sodium hydroxide solution was added to convert some of the aromatic hydroxy compounds and substituted pyrazolones to soluble forms. Acetoacetanilide was dissolved with addition of hydrochloric acid; 4-aminoacetanilide was dissolved in a mixture of water and ethanol (1 + 1).

Indicator electrodes

In a recent paper concerning titrations of arenediazonium salts with sodium tetraphenylborate [10], coated-wire electrodes with plasticized PVC membranes enabled readily reproducible results to be achieved. Unfortunately, the shapes of the titration curves for passive compounds with diazonium salts recorded with these electrodes changed for the worse, and the overall potential break decreased in each repeated titration. This could be explained by gradual washing-out of the ion-exchanger or by saturation of the organic phase (plasticizer) with the azo dyestuff formed. Whatever the explanation, these coated-wire electrodes could not be successfully applied in titrations with diazonium salts.

Ion-selective electrodes of more conventional type were therefore prepared, each type being equipped with an internal electrode (Ag/AgCl) and an internal electrolyte (0.01 M NaCl—0.01 M sodium tetraphenylborate). In one type, the membranes were prepared on a glass plate by casting and evaporating the solution of PVC (0.09 g; Slovinyl E621, Nováky) and plasticizer (0.2 ml) in tetrahydrofuran (3 ml). Then a membrane circle was cut out and attached to a Novodur tube (based on hard PVC; 10 mm o.d., 5 mm i.d.) with a PVC solution in tetrahydrofuran. In the second type, the membrane was formed

by coating a porous graphite rod sealed in a glass tube. The rod was dipped into a PVC/plasticizer solution and the solvent was allowed to evaporate. As before [10], no ion-exchanger was added to the PVC solution during membrane fabrication. Before the electrodes were used in titrations with diazonium salts, they were first pre-conditioned by repeated titrations of the appropriate arenediazonium salt with sodium tetraphenylborate. Thus the membrane plasticizer was gradually saturated with an ion-pair (arenediazonium tetraphenylborate) formed on the basis of solvent extraction principles. Different plasticizers [10, 11] were tested (2-nitrophenyl 2-ethylhexyl ether, dioctylphthalate, tricresylphosphate, *n*-butylbenzenesulfonamide, and 2-ethylhexyl-4-hydroxybenzoate) and compared in titrations of 2-naphthol and 2,4-toluylenediamine with 4-bromobenzenediazonium chloride. The electrode with a 2-nitrophenyl 2-ethylhexyl ether—PVC membrane had the best properties (Fig. 1). The type of electrode construction did not influence significantly the shape of potentiometric titration curves. Electrodes with this plasticizer were then used in further studies.

General procedure

Potentiometric measurements were done with an OP-204 pH meter (Radelkis, Budapest). The titration cell consisted of the respective ion-selective electrode and a saturated calomel electrode (SCE). The procedure was as follows: 5 ml of the solution of the substance to be titrated (0.1 M)

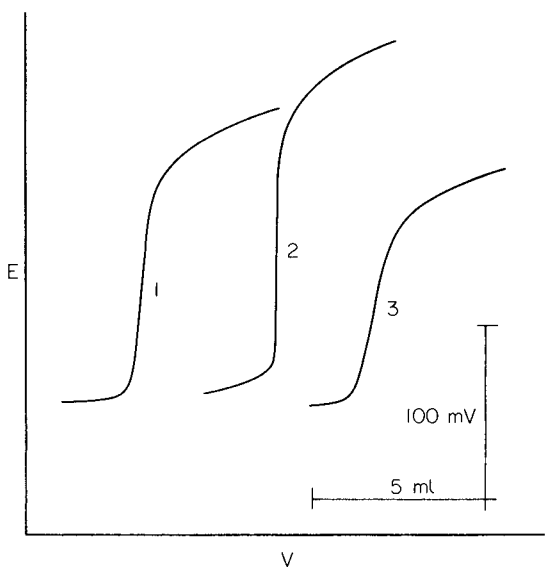

Fig. 1. Influence of plasticizer on the shape of potentiometric titration curves of 2-naphthol (0.01 M) titrated with 4-bromobenzenediazonium chloride (0.1 M) at pH 7 using an electrode with a membrane plasticized by (1) dioctylphthalate, (2) 2-nitrophenyl 2-ethylhexyl ether, and (3) tricresylphosphate.

and 45 ml of buffer solution were measured into a 150-ml beaker externally cooled with ice, and the arenediazonium salt titrant (0.1 M) was added from a 10-ml burette. Concentrated Britton-Robinson buffers (0.4 M H_3PO_4 + 0.4 M CH_3COOH + 0.4 M H_3BO_3 stock solution mixed with the desired amount of 2 M NaOH) were used, the pH value being checked potentiometrically with glass and saturated calomel electrodes.

RESULTS AND DISCUSSION

Reactivity of titrants and pH effects

Three arenediazonium salts were studied as titrants; the reactivity increased in the order: 4-methyl-, 4-bromo-, and 4-nitro-benzenediazonium chloride. This classification is based on so-called limiting oxidation potentials, which can be considered to reflect the electrophilic properties of arenediazonium ions [1]. The second important factor is the stability of the solutions of the aromatic diazo compound with regard to temperature and light, as has been discussed previously [10].

Among the possible side-reactions, a very important role is played by the protolytic equilibria of both the titrants and the passive components (phenols, amines, etc.). As shown by Conant and Peterson [12], the dependence of the rate of the azo-coupling reaction on the hydrogen ion concentration can be written in the form $\log k = \log k_o + \mathrm{pH}$, where k_o is the rate constant of azo-coupling at pH 0. Practically, this means that the rate of the reaction increases ten times per unit change of pH. However, the pH cannot be raised regardless of the hydrolytic equilibria of the arenediazonium salts in alkaline medium

$$\mathrm{Ar{-}N_2^+ + H_2O \overset{K_{a1}}{\rightleftharpoons} Ar{-}N_2{-}OH + H^+ \overset{K_{a2}}{\rightleftharpoons} Ar{-}N_2{-}O^- + 2\,H^+}$$

As the aryldiazohydroxide intermediate is not stable, only the product K_{a1} K_{a2} can be determined. Usually the $(pK_{a1} + pK_{a2})/2$ values are given in the literature [13, 14]; the values available are 9.2 for 4-nitrobenzenediazonium, 11.6 for 4-methylbenzenediazonium ions, and 10.9 for 4-chlorobenzenediazonium (which probably corresponds approximately to the value for 4-bromobenzenediazonium). These considerations indicate that specific conditions are required for each determination, taking into account the side-reactions of the participating compounds.

Titrations with 4-methylbenzenediazonium salt were slow. Although in the first stages of the titration, the equilibrium potential was fixed almost immediately after each addition of the titrant, it was necessary to wait for about 30 min for a potential value near the end-point. Thus such titrations took a long time, 50—70 min. As the 0.1 M 4-methylbenzenediazonium salt solution is not too stable and the burette was not cooled, the salt could partially decompose.

The solution of 4-nitrobenzenediazonium salt is much more stable and reactive. The time necessary for one titration with this salt was about 30 min;

the potential near the end-point could be read after 5 min. A disadvantage is that 4-nitrobenzenediazonium salt may not be used in more alkaline solutions because of the formation of diazotate ion.

Both these reagents were compared in titrations of 2-naphthol and 2-naphtholsulfonic acids (Table 1) in media buffered to pH 4—10. Azo-coupling at pH 4 and 6 was not quantitative and no useful titration curve was possible. The best results were obtained at pH 8, which is also the limiting value in titrations with 4-nitrobenzenediazonium chloride. It should be mentioned that 2-naphthol is not fully dissolved when the pH 8 buffer is added, but the titration curves are better than at pH 10.

The 4-bromobenzenediazonium salt seemed to be most satisfactory. Its solution is more stable than that of the 4-methylbenzenediazonium salt, and it can be used in a more alkaline medium than the 4-nitrobenzenediazonium chloride solution. Irrespective of titration time (some times are given in Table 1), the results were reproducible, with relative standard deviations less than 2.5%. As the titrant is the only ionic compound that changes concentration significantly during a titration, the shape of the potentiometric titration curve depends primarily on the sensitivity of the electrode to the particular arenediazonium cation. Of course, the titration time and curve are also influenced by the rate of azo-coupling reaction and by side-reactions of the components involved. For example, titrations of 1-naphthylaminesulfonic acids took longer times, while titrations of pyrazolones were among the shortest. Some examples of titration curves are given in Fig. 2. With regard to the pH value, pH 10 was found to be optimal for some passive components, namely, 8-quinolinol-5-sulfonic acid, 2-naphthol-6-sulfonic acid, and 1-naphthol-6-amino-3-sulfonic acid, 1-(4′-sulfophenyl)-3-methyl-5-pyrazolone, 2,4-

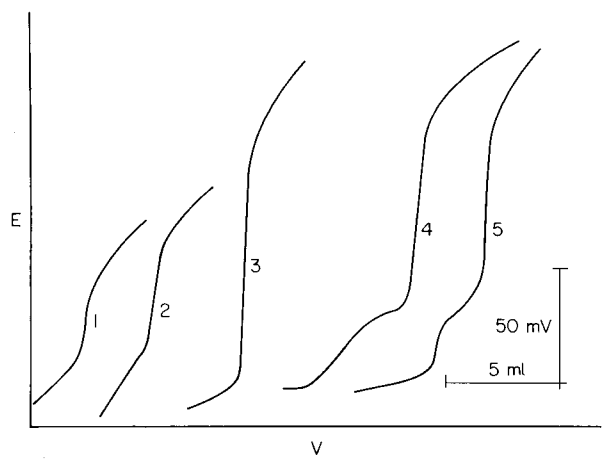

Fig. 2. Influence of pH on the shape of curves obtained in titrations with 4-bromobenzenediazonium chloride (0.1 M): (1—3) toluylenediamine and (4, 5) resorcinol (both 0.01 M). The titrated solutions were buffered to: (1, 4) pH 8; (2) pH 9; (3, 5) pH 10.

TABLE 1

Characterization of potentiometric titrations of some passive compounds (ca. 50 ml of 0.01 M solutions) with 0.1 M arenediazonium salts (2-nitrophenyl 2-ethylhexyl ether PVC membrane electrode and SCE)

Substance determined	pH	Titration curve[a]		Titra time (min
		Overall potential change (mV)	Steepness near end-point (mV/0.1 ml)	
With 4-methylbenzenediazonium chloride				
2-Naphthol	8	130—162	12—14	50
	10	103—117	6—8	50
2-Naphthol-7-sulfonic acid	8	190—197	17—18	60
	10	148—157	10—11	60
2-Naphthol-3,6-disulfonic acid	8	166—185	17—18	70
	10	202—219	13—14	60
With 4-nitrobenzenediazonium chloride				
2-Naphthol	8	162—194	9—15	30
	10	54—60	4—5	40
2-Naphthol-7-sulfonic acid	8	120—131	18—20	30
2-Naphthol-3,6-disulfonic acid	8	132—137	12—20	30
With 4-bromobenzenediazonium chloride				
2-Naphthol	7	220—232	45—70	60
	8	220—236	28—32	50
	10	160—194	12—13	50
2-Naphthol-6-sulfonic acid	8	144—150	14—15	40
	10	144—150	25—27	40
2-Naphthol-7-sulfonic acid	8	235—237	45—48	60
	10	88—90	6—8	60
2-Naphthol-3,6-disulfonic acid	8	217—230	11—17	50
	9	222—241	40—42	50
	10	86—100	11—12	50
8-Quinolinol	10	124—126	11—13	70
8-Quinolinol-5-sulfonic acid	8	37—50	3—4	60
	10	156—180	22—30	50
6-Amino-1-naphthol-3-sulfonic acid	6	195—208	31—34	60
	8	219—226	47—53	50
	10	176—186	53—60	90
7-Amino-1-naphthol-3-sulfonic acid	4	130—147	20—22	90
	6	100—110	26—28	80
	8	164—166	45—48	80
1-Naphthylamine-6-sulfonic acid	4	100—182	12—16	50
	6	206—220	32—34	45
	8	240—243	52—55	45
1-Naphthylamine-7-sulfonic acid	4	103—108	9—10	50
	6	147—150	35—39	50
	8	159—162	70—71	50
	10	150—163	32—34	60

TABLE 1 (continued)

Substance determined	pH	Titration curve[a]		Titration time (min)
		Overall potential change (mV)	Steepness near-end-point (mV/0.1 ml)	
Resorcinol	8	143—157	28—30	60
	10	140—158	25—30	50
2,4-Toluylenediamine	8	110—111	5—6	15
	9	121—123	7—8	15
	10	143—158	16—21	15
4-Aminoacetanilide	8	140—142	20—23	70
	10	116—129	10—12	90
Acetoacetanilide	8	92—110	10—13	15
	10	115—116	22—24	15
1-(4'-sulfophenyl)-3-methyl-5-pyrazolone	8	113—118	20—22	20
	9	116—170	20—22	15
	10	164—165	41—42	15
1-(2',5'-dichloro-4'-sulfophenyl)-3-carboxy-5-pyrazolone	8	240—242	94—95	25
	9	173—200	62—70	30
	10	124—130	20—25	30

[a]For comparison, in titrations of 2-naphthol with 4-chlorobenzenediazonium chloride at pH 8 using a Crytur 19-15 electrode, the overall potential change was 100—110 mV with a steepness of about 5 mV/0.1 ml near the inflexion point of the titration curve.

toluylenediamine, and acetoanilide. Others were titrated better at pH 8: 2-naphthol, 2-naphthol-7-, 1-naphthol-7-amino-3-, 1-naphthylamine-7-, and 2-naphthylamine-6-sulfonic acids, 4-aminoacetanilide, and 1-(2',5'-dichloro-4'-sulfophenyl)-3-carboxy-5-pyrazolone.

Reproducibility and accuracy

Reproducibility and accuracy of the results can also be influenced by choice of pH value. If an unsuitable buffer is used, the potential shifts are smaller and the end-points are less sharp. Other problems may occur when the arenediazonium cation is more reactive and can couple to more than one position. A mixture of monoazo and bisazo compounds is then formed in the solution titrated, but the formation of bisazo compound is not usually quantitative; for example, in titrations of 1-naphthylamine-7-sulfonic acid, the end-point reading increased with increasing pH value. Resorcinol reacted with the 4-bromobenzenediazonium salt to form a bisazo compound quantitatively, but the formation of the monoazo intermediate could also be observed on the titration curves (Fig. 2).

When the pH value of the titrated solutions is kept constant, the titration curves are readily reproducible in both shape and end-point reading. As shown by using a Lord's test in Table 2, statistically insignificant differences

TABLE 2

Statistical evaluation of potentiometric titrations of pure passive compounds with 4-bromobenzenediazonium chloride

Substance determined	pH	Taken (mg)	Found[a]				Lord's test	
			n	$\bar{x}$ (mg)	s (mg)	s_r (%)	u_o^{crit}	u_o
2,4-Toluylenediamine	8	48.88	3	51.14	0.28	0.55	1.3	4.8
	10	48.88	3	49.80	0.45	0.90	1.3	1.2
Resorcinol	8	33.03	4	32.94	0.57	1.7	0.72	0.08
	10	33.03	3	33.00	0.33	1.0	1.3	0.05
Acetoacetanilide	8	53.16	3	51.51	0.73	1.4	1.3	1.3
	10	53.16	3	52.10	0.62	1.2	1.3	1.0
1-(4'-Sulfophenyl)-3-methyl-5-pyrazolone	8	71.70	3	68.54	1.05	1.5	1.3	1.8
	9	71.70	4	70.85	3.33	4.7	0.72	0.12
	10	71.70	3	71.70	2.40	3.4	1.3	0.15

[a] n, number of determinations; $\bar{x}$, arithmetic mean; s, standard deviation calculated from the range R (summation of errors in standardization of titrant and in the titration was applied); s_r, relative standard deviation. The significance level $\alpha = 0.05$ (95% probability) was considered; the u_o values were calculated from the formula $u_o = (|\bar{x} - \mu|)/R$.

were obtained in determinations for which pure materials were used for preparation of both the titrant and the substance titrated. From the results in Table 2, it can be concluded that 2,4-toluylenediamine, resorcinol and substituted pyrazolones could be used for the standardization of solutions of 4-bromobenzenediazonium salts as titrants. Another possibility is the titration of the arenediazonium salt with standardized sodium tetraphenylborate solution [10].

An important factor influencing a measurement is the lifetime of the electrode membrane. The lifetime was rather short because some electrically neutral azo compounds formed in the titrations could extract into the membrane plasticizer. However, one electrode could usually serve for three or four weeks. When necessary, the concentration of electroactive substance in the membrane could be regenerated by repeated titrations of the arenediazonium salt with sodium tetraphenylborate. When the function of the electrode was restored in this way, the electrode could be used again for another 3—4 weeks in titrations with diazonium salts. Thus the titration of an arenediazonium salt with sodium tetraphenylborate can serve not only as a method of standardizing the titrant but also for refreshing the electrode.

Purposely, passive compounds used in the industrial production of azo dyestuffs were chosen for studying these determinations. However, most of the compounds were technical products and their purity was not seriously declared. This is why Table 2 contains a limited number of compounds; only compounds available in sufficiently pure quality are included. From

results of more than 300 titrations done here, it can be concluded that these PVC membrane electrodes are really suitable for titrations based on azo coupling reactions, and the method can be recommended for industrial analytical monitoring.

REFERENCES

1 M. Matrka and A. Spěvák, Chem. Listy, 61 (1967) 883.
2 M. R. F. Ashworth, Titrimetric Organic Analysis, Vol. 1, Direct Methods, Wiley, New York, 1964, p. 187.
3 R. P. Lastovskii and Yu. I. Vainshtein, Tekhnicheskii analiz v proizvodstve promezhutochnykh produktov i krasitelei, 3rd. edn., Goskhimizdat, Moscow, 1958, p. 191.
4 E. Bitterlin, Fresenius Z. Anal. Chem., 274 (1975) 363.
5 A. P. Terentev and I. S. Tubina, Zh. Anal. Khim., 18 (1963) 114.
6 M. Matrka, L. Držková, M. Remeš, Z. Ságner, J. Váňa and V. Zvěřina, Chem. Prum., 28 (1978) 79.
7 F. Müller, Z. Electrochem., 34 (1928) 63.
8 K. Vytřas and V. Říha, Cesk. Farm., 26 (1977) 9.
9 K. Vytřas, Collect. Czech. Chem. Commun., 42 (1977) 3168.
10 K. Vytřas, M. Remeš and H. Kubešová-Svobodová, Anal. Chim. Acta, 124 (1981) 91.
11 K. Vytřas, M. Dajková and M. Remeš, Cesk. Farm., 30 (1981) 61.
12 J. B. Conant and W. D. Peterson, J. Am. Chem. Soc., 52 (1930) 1220.
13 E. S. Lewis and H. Suhr, Chem. Ber., 91 (1958) 2350.
14 I. V. Grachev and N. A. Kirzner, Zh. Obshch. Khim., 18 (1948) 1525.

Analytica Chimica Acta, 141 (1982) 173—186
Elsevier Scientific Publishing Company, Amsterdam — Printed in The Netherlands

A NEW, DIRECTLY COMPUTER-CONTROLLED pH-STAT

RALPH E. LEMKE[a] and GARY M. HIEFTJE*
Department of Chemistry, Indiana University, Bloomington, IN 47405 (U.S.A.)
(Received 22nd February 1982)

SUMMARY

The design and implementation of a computer-controlled pH-stat is presented. The reagent delivery system used in the design of the pH-stat is based on a computer-controlled droplet generator able to add selectively reagent aliquots of 0.06 μl. Precise reagent control enables the stationary control of pH to within 0.0008 pH units. Algorithms for program operation are structured as autonomous concurrent tasks and are written entirely in FORTRAN. The pH-stat is operated by means of simple directives entered into a terminal. During an experiment, directives permit the graphic display of data and the alteration of experimental parameters. To evaluate the pH-stat, standard working curves were obtained from which the concentration of glucose in a sample of standard human blood serum was determined to within 3% of the value specified by the manufacturer. Two alternative measurement approaches, the fixed-time technique and the use of enzymatic induction times, were evaluated for the determination of glucose concentrations.

Currently, quantitative potentiometric reaction-rate methods find a wide range of applications and several such procedures and corresponding instrumentation have been described [1—5]. Innovations in reagent delivery systems and computer automation, in particular, have enabled rapid, accurate, automated reaction-rate determinations; of special interest is the development of a directly digital computer-controlled reagent delivery system capable of producing microliter aliquots [6].

In the present study, reaction-rate methods are investigated by an instrumental pH-stat [7, 8] placed under computer control. Real-time computer-controlled processing not only eliminates tedious calculations but also enables real-time parameter modification to be achieved according to experimental demands. Real-time control enhances the flexibility of such an experiment in two ways. First, feedback from the experiment permits accurate calculation of reagent rate, thus eliminating pH overshoot and undershoot by the pH-stat. Second, feedback from the experiment allows dynamic alteration of sampling frequency, thus permitting rapid response in a dynamic system. Real-time computer control and the precise nature of the direct digital computer-controlled reagent delivery system coupled with a

---

[a]Current address: Sylvania System Group, Western Division, GTE Products Corp., P.O. Box 205, Mountain View, CA 94042, U.S.A.

0003-2670/82/0000-0000/$02.75

highly sensitive electrometer, enable the pH to be controlled to within 0.0008 pH units in the present experiment.

To illustrate the performance of the pH-stat, the familiar glucose–glucose oxidase reaction was studied. The glucose–glucose oxidase reaction proceeds by a pseudo-first-order mechanism and has the following stoichiometry

$$\text{glucose} + O_2 \xrightarrow{\text{glucose oxidase}} \text{gluconic acid} + H_2O_2$$

Glucose concentrations are determined by potentiometrically measuring the rate at which gluconic acid is formed. In accordance with first-order reaction-rate kinetics, the initial rate of reaction is proportional to the initial substrate concentration [9, 10]. Because an enzyme-catalyzed reaction rate is pH-dependent, pH control is necessary [11]. To maintain a constant pH, the pH-stat adds alkaline reagent at a rate proportional to the formation of gluconic acid. Thus, the average reagent addition rate is proportional to the initial glucose concentration. A working curve is obtained, from which unknown sample concentrations can be determined. In this manner, determination of glucose concentrations as low as 10 μg ml^{-1} is possible.

EXPERIMENTAL

Instrumentation

The pH-stat (Fig. 1) is composed of four modular components, namely, (1) the microliter reagent addition system, (2) the pH detection system (a sensitive pH-meter), (3) a reaction vessel, and (4) a mini-computer with graphics display and disk storage. In operation, the pH-meter continuously monitors the pH of the reaction solution. At a selected frequency, the computer reads the output of the pH-meter, compares it with a stored reference potential, and determines whether a change in pH has occurred. If it has, the computer calculates the addition rate of reagent that is necessary to return the pH of the reaction solution to its command value. The reagent addition

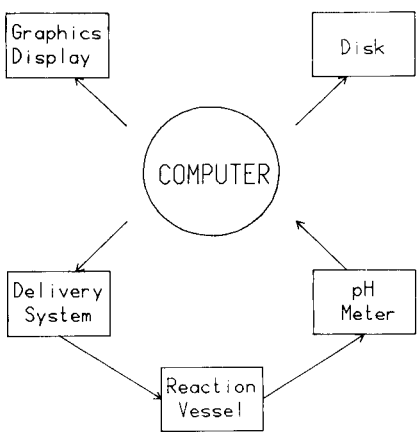

Fig. 1. Functional organization of a pH-stat.

rate is entered into the microliter droplet addition system and reagent is added to the reaction vessel at the specified rate. The average addition rate for several time intervals is directly proportional to the initial rate of reaction.

Microliter reagent addition system. Enabling the pH-stat to control the pH precisely is the microliter reagent addition system shown in Fig. 2. This system can, on command, add increments of reagent having a volume of approximately 0.06 μl. The design of the reagent delivery system is based not on a conventional syringe mechanism but rather on the generation and selection of charged droplets by an electric field. The reagent delivery system is designed with no moving parts, no burets that require refilling, and a fast response time to a request for the addition of reagent. An extensive description of the operation and design of this system has already been presented [6, 12, 13]. Only those features unique to the present device will be described here.

In the present apparatus, droplets are generated by a vibrating 27-gauge metal capillary. The capillary is mounted with epoxy cement perpendicular to one end of a piezoelectric ceramic bimorph (PZT-5H, Clevite Corp., Bedford, OH) through a 1/32-inch hole drilled into the bimorph. To drive the bimorph, an oscillator (Audio Oscillator, Model 202D, Hewlett-Packard, Palo Alto, CA) is used to generate a 1-kHz, 100-V P—P sine wave.

A charging electrode, placed immediately beyond (0.5 cm) the tip of the capillary, charges droplets when it is energized with an electrical pulse of appropriate amplitude and width. Separation of charged and uncharged droplets then occurs as the droplet stream passes through an electric field. In this system, two planar electrodes located 2 cm apart and 0.5 cm below the charging electrode are held at a differential potential of 1000 V by a high-

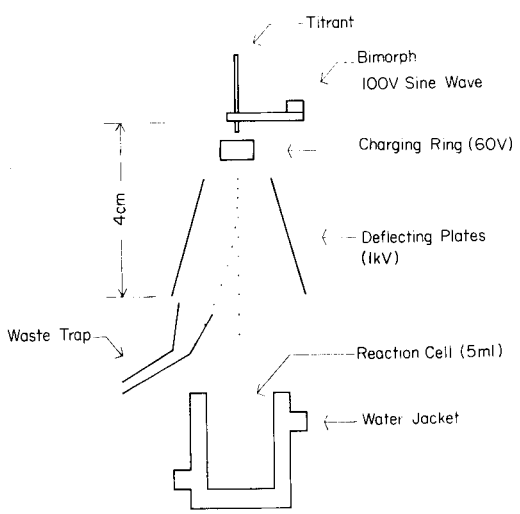

Fig. 2. Schematic diagram of the microliter reagent addition system.

voltage power supply (244 High-Voltage Power Supply, Keithley Instruments, Cleveland, OH).

Reagent is supplied to the microliter reagent addition system via a 1.0-l reservoir pressurized with air to 6 psi. Air pressure is controlled with a single-stage tank regulator (Model 02-2600, Air Products, Allentown, PA).

An evaluation was made of the precision with which the reagent can be delivered to the reaction vessel and also of the mean size of the droplets being dispensed. The droplet volumes are determined by instructing the addition system to deliver reagent at its maximum rate for a specific time period. The reagent is collected in a weighing bottle which is then immediately capped and weighed. The droplet volume can be calculated from the weight of collected reagent and the number of droplets added to the weighing bottle. With this technique, the average maximum reagent delivery rate is 0.056 ml s^{-1}, and the average droplet size is 0.056 μl; the relative standard deviation of delivering a 5.0-ml volume is 0.06%. These results are obtained using a 27-gauge capillary with a bimorph-driving frequency of 1 kHz.

Electrodes and reaction vessel. Changes in pH are measured potentiometrically with a combination Ag/AgCl ceramic junction electrode (No. 6023-03, 3.0-mm diameter, Ingold Electrodes, Lexington, MA), and electrometer (model 602 solid-state electrometer, Keithley Instruments, Cleveland, OH), the analog output of which (0—1 V) feeds the laboratory computer (PDP-11/34, Digital Equipment Corp., Maynard, MA). A sensitive electrometer is required because the total change in pH is less than 0.001 pH units over a typical observation period for a glucose concentration of 10 μg ml^{-1}.

During a determination and between determinations, the pH electrode was maintained in a solution of equal pH and ionic strength as the reaction solution in order to minimize any non-equilibrium drift [14]. The addition of enzyme to the reaction cell and the rinsing of electrodes after a determination are two procedural steps in which the pH and ionic strength of each solution must be carefully matched [11]. Also, because reaction products can change the ionic strength of the reaction solution, an electrolyte (0.01 M KCl) was added to mask any changes in ionic strength.

The 5.0-ml reaction cell is temperature-regulated at 30 ± 0.1°C by water circulated from a thermostated bath through a jacket surrounding the vessel. The reaction mixture is vigorously stirred by using a 1.0-cm teflon-covered magnetic bar driven by flowing water. To minimize electrode response time, the reagent entry point was placed as near as possible to the pH electrode in the reaction vessel. The proximity of reagent entry and electrode creates a region of high transient reagent concentration, giving the pH electrode an initial "kick".

Computer interface. The pH-stat is able to add reagent at computer-selectable rates, measured in terms of the number of droplets charged per second. The charging of droplets is accomplished by the computer interface shown in Fig. 3. The interface consists of three main units, namely, (1) a computer-controlled frequency divider, (2) pulse-delay and pulse-width adjustment circuitry, and (3) a high-voltage transistor switch.

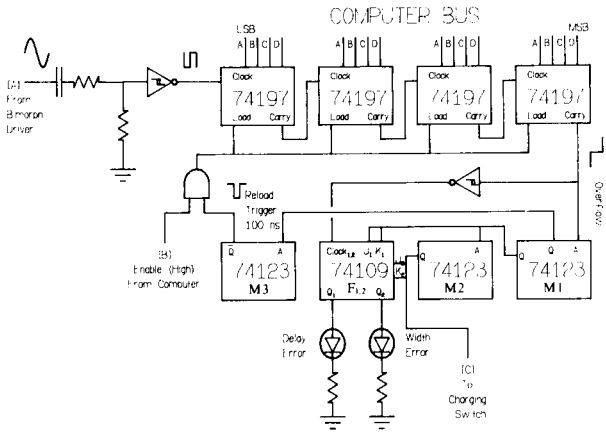

Fig. 3. Schematic logic circuit diagram of the reagent addition system—computer interface. This interface receives from the computer the reagent addition rate expressed as a binary number and produces a pulse train at an appropriate frequency and duty cycle. See text for discussion.

The rate at which droplets are to be charged and therefore deflected into the sample vessel is loaded by the computer onto its common instrument bus (designed in this laboratory). From this bus, the rate is latched into the frequency divider of Fig. 3 (74197 binary presettable counters/latches). The common instrument bus communicates with negative logic. Therefore, the rate which the frequency divider "sees" is the one's complement of the rate which the computer supplied. The bimorph driving signal, which is reduced to a TTL-compatible voltage with a voltage divider and shaped with a Schmitt trigger (7414 hex Schmitt-trigger inverters), clocks the frequency divider. When the frequency divider is enabled, the one's complement of the rate is latched into the counters which then count in a positive direction, toward zero. The transition of the counters from one to zero causes a negative transition in the sign bit, which triggers the pulse-generating circuitry and also triggers monostable M3 that generates a 100-ns pulse to reload the frequency divider.

The pulse-generating circuitry consists of two monostables (74123 dual retriggerable monostable multivibrators with clear), M1 and M2, respectively. When triggered by the frequency divider, M1 generates a positive pulse, termed the delay pulse. When triggered by the negative transition of the delay pulse, M2 generates a positive pulse, termed the charging pulse, which directly feeds the amplifier circuitry connected to the charging ring.

The width and temporal position of the charging pulse is crucial because it provides synchronization between droplet formation and droplet charging. Because the width and delay are empirically determined, an error checking circuit is provided in case the duration of either the pulse delay or width is too great. The error checking is accomplished with the use of two J-K flip-

flops (74109 dual J-K positive-edge-triggered flip-flops with preset and clear) in conjunction with the sign bit of the frequency divider and the outputs of M1 and M2. The outputs of M1 and M2 are connected to the J-K inputs of flip-flops F1 and F2, respectively; the sign bit is connected to the clock input of both flip-flops. The outputs of M1 and M2 should be low (pulses ended) at the transition of the sign bit; if not, the pulse delay or pulse width is too great. The flip-flops detect this condition because the negative triggering of the sign bit latches the J-K inputs to the Q outputs of the flip-flops. Thus a high at the Q output of the flip-flop indicates an error.

The charging pulse [C] is amplified by the simple high-voltage amplifier circuit shown in Fig. 4. The TTL charging pulse drives transistor T1 which fires the high-voltage transistor T2. The output of T2 feeds the charging ring of the droplet generator.

Computer program

The computer program that controls the pH-stat is written entirely in FORTRAN IV and operates under the PDP-11 RSX-11M V3.1 real-time operating system. This operating system supports many utility programs for the performance of concurrent tasks. Two important utilities in the present study are the resume—suspend constructs, and the event flags.

The resume—suspend constructs provide a means for tasks to gain partial control over task scheduling. A task can relinquish control of the processor by the "suspend" command. The processor, however, continues execution of other tasks. The suspended task cannot regain control of the processor until resumed by the "resume" command. Event flags are a means to accomplish task synchronization. Synchronization is accomplished when a task suspends execution until an event flag is activated. When the event flag is activated, execution is resumed.

Modularity in program design and efficient use of the CPU are achieved by

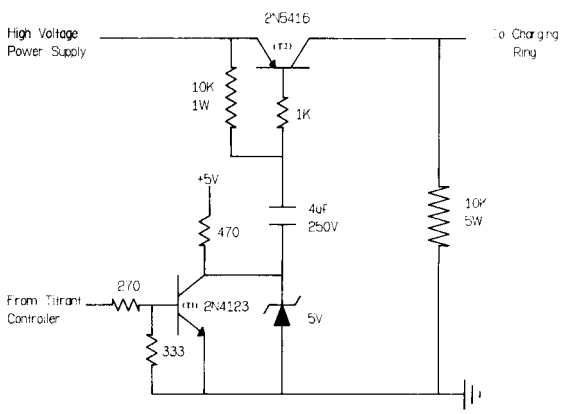

Fig. 4. Schematic circuit diagram of the high-voltage switch. This switch receives a TTL-compatible pulse as input and produces a high voltage pulse.

subdividing the program into individual concurrent tasks. Communication between tasks is accomplished using a shared data region; synchronization, when necessary, is accomplished with the use of event flags and suspend—resume constructs. All tasks are linked to a sharable, memory-resident FORTRAN library, thereby eliminating any unnecessary duplication of code.

There are eight concurrent tasks involved in controlling the pH-stat. They are (1) the monitor, (2) the data display, (3) the parameter change, (4) the data acquisition, (5) the decision maker, (6) the data store, (7) the calibrator, and (8) the results. The function of each of these tasks is discussed separately.

The monitor interfaces the operator to the pH-stat. It interprets the directives given by the operator and, depending on the directive, either sets an event flag, resumes a task, or aborts a task.

The display directive enables the operator to view parameters at any time throughout an experiment. The display is concurrent with data acquisition, permitting the operator to observe dynamic changes of the experimental parameters. Pertinent displayed parameters are: elapsed experimental time, average reagent addition rate, average change in reagent addition rate, sampling frequency and, if desired, all data points collected thus far.

The change directive enables the operator to alter program parameters from their default values. The change task is also concurrent with data acquisition, enabling parameter alteration as the determination progresses. The five parameters that can be altered are as follows.

(1) Sample type and concentration. The sample can be either a standard or an unknown; if the sample is a standard, its concentration must be declared.

(2) Minimum experiment duration. This is the minimum duration of the determination after which the pH-stat can terminate the run if the data are satisfactory.

(3) Maximum experiment duration. This is the maximum duration of a determination when the pH-stat has not automatically terminated the run.

(4) Initial sampling frequency. This is the frequency at which the acquisition task records data. This frequency can be dynamically modified to meet environmental conditions.

(5) Data base identification. All data are stored in a data base bearing this name.

The data acquisition directive initiates a determination by the simultaneous activation of the acquisition task and the decision maker. The combined efforts of these two programs accomplish the data acquisition, the determination of starting and ending times, and the sampling frequency.

A flow diagram of the acquisition program is shown in Fig. 5A. Upon inception, the task immediately suspends itself until resumed by the monitor after receipt of the data acquisition directive. Once the task has been resumed by the monitor, it records and saves the initial command pH. The following cycle is then initiated: the sampling frequency is loaded into the computer

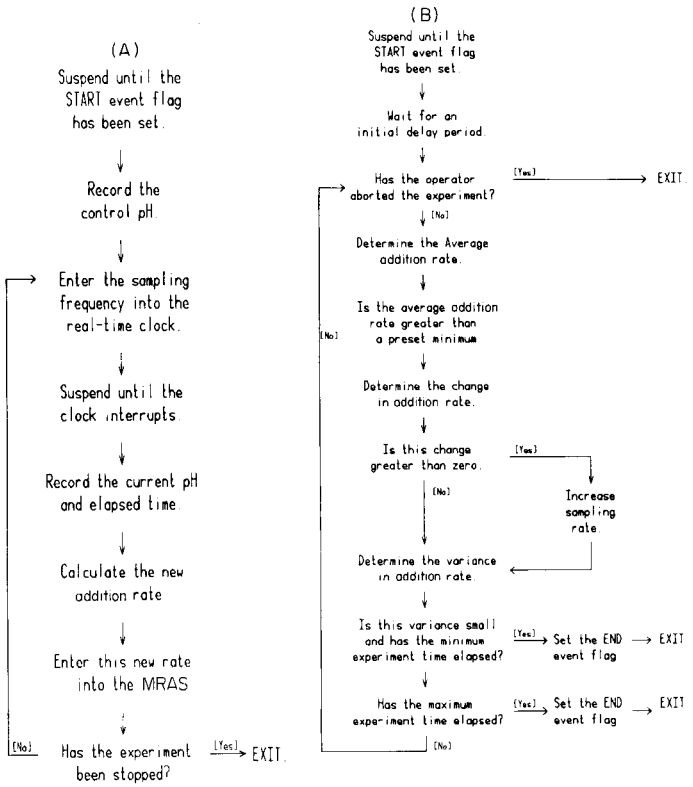

Fig. 5. Flow diagrams of (A) the acquisition task and (B) the decision maker. The acquisition system provides minimum control for the pH-stat; its objectives are to record the pH at a selected frequency and determine the corresponding change in reagent rate. The decision maker performs complex decisions in the control of the pH-stat; its objectives are to determine the start and end of the experiment and the sampling frequency.

and task execution is suspended until the clock interrupts; with the reactivation of the task by the clock interrupt, the pH and time are recorded, and a new reagent rate is calculated based on the difference between the current pH and its command value. This cycle continues until instructed to stop by either the decision maker on the determination of the end of a run, or by the monitor on a directive from the operator.

The algorithm for calculating a new reagent addition rate is critical in the new pH-stat. This algorithm does not calculate an absolute reagent addition rate from an observed change in pH, but rather determines the necessary incremental change from the current reagent addition rate. The algorithm considers two factors in the calculation of the change in reagent rate: the difference between the current pH and the control pH, and the difference between the pH at the last sampling and the current pH. The first factor insures that the reaction will be held at the control pH. The second factor

determines the direction and potential in which the pH is currently changing. This algorithm can be represented mathematically by

$$\text{Rate} = \text{Average}^{\circ}\text{Rate} - (f1(\text{pHcontrol} - \text{pH}) + f2(\text{pHlast} - \text{pH}))/(2f3) \quad (1)$$

where Rate is the new reagent rate, Average°Rate is the average rate, pHcontrol is the control pH, pH is the current pH, pHlast is the pH at the last sampling, f1 and f2 are weighting factors, and f3 is the conversion from change in pH to change in reagent rate.

The data collected by the acquisition system are viewed by the decision maker to determine the following conditions.

(1) The start of the determination. The determination is not considered to begin until after a significant rate has been noted. This delay encompasses any enzymatic induction period.

(2) The end of the determination. The operator sets a maximum measurement duration which the pH-stat does not exceed. Even if the data obtained prior to this duration limit have an average change in rate equal to zero (within selected tolerance limits) and have a low variance, the determination is ended.

(3) The sample frequency. Fast reactions have the potential of getting out of hand, and are sampled at a higher frequency than slow reactions. The sampling frequency varies in proportion to the reaction rate.

A flow diagram of the decision maker is shown in Fig. 5B. When activated, the decision maker pauses as the acquisition task collects the first few data points. This pause ensures that any unstable recordings caused by the initial mixing of enzyme and substrate solutions are ignored, after which the decision maker determines if the current reagent addition rate is significant by comparing its magnitude to a minimum rate value; if the rate is greater, the beginning of the determination is declared. Any changes to be made in sampling frequency are determined by comparing the change in reagent addition rate to zero; if the rate is changing (within tolerance limits), the sampling frequency is increased. The end of the determination is triggered by comparing the variation in reagent addition rate with a selected value; if they are equal and the minimum measurement duration has been exceeded, the procedure is ended. The procedure is also ended if the selected maximum measurement duration has been exceeded. After a run, the operator can elect to retain the data permanently by issuing a store directive. This directive enters all parameters and data including the current time and date into the data base.

The calibration directive determines a factor used by the acquisition task to convert the change in pH to the change in reagent rate. This factor is obtained by recording the change in pH when a constant rate of reagent is introduced into a blank reaction cell.

The results directive presents in tabular form both a summary of the standard substrate determinations used to obtain a working curve and the unknown sample data.

It should be noted that there are several advantages to the multi-tasking approach for the design of real-time systems. First, because the acquisition system and the decision maker operate concurrently, the computation time for the decision maker need not be limited to the sampling interval of the acquisition system, thus permitting the use of complex algorithms in a real-time environment. Secondly, other computer-controlled experiments and program development can be performed concurrently with a pH-stat determination. Thirdly, tasks such as the display, change, and store are loaded into memory only when they are requested, after which they are removed. This dynamic loading of tasks permits the overall program size to be very large while necessitating only a small portion of memory-resident code.

Reagents

To ensure that all solutions have nearly the same ionic strength and pH, they were made up in a 0.01 M KCl stock solution adjusted to pH 6.5 with sodium hydroxide. Because chloride ion (0.2 M) competitively inhibits the studied reaction [15, 16], the concentration of potassium chloride in the stock solution is kept low.

Glucose standards were prepared at concentrations encompassing the unknown concentration. Typical working curve ranges are 10—250 and 250—1000 $\mu g\ ml^{-1}$. A glucose oxidase solution was prepared by diluting 0.2 g of glucose oxidase (E.C. 1.1.3.4, No 6—6125, Sigma Chemical Company) to 250.0 ml and storing under refrigeration.

Standardized human blood serum (MONI-TROL I, Lot no. LTD-165, DADE Reagents, Miami, FL 33152) was deproteinized by the method described by Malmstadt and Pardue [17]. Because the blood sera are contained in 5-ml vials, the deproteinization procedure was slightly modified from that used for the 0.02-ml aliquots used in the previous work [17]. For deproteinization, a 5-ml aliquot of serum is mixed with 20 ml of a solution of 1.8% (w/v) barium hydroxide and 2.0% (w/v) zinc sulfate septihydrate. This mixture is filtered, and the filtrate is diluted to a total volume of 50 ml (1:10 dilution) and adjusted to pH 6.5 with dilute hydrochloric acid. For a single determination, a 2.0-ml aliquot of the deproteinized serum is used.

A solution of 0.0005 M NaOH served as the added reagent.

Procedure

A 2.0-ml glucose sample is introduced into the reaction vessel immediately followed by a 1.0-ml aliquot of the glucose oxidase reagent. The computer acquisition tasks are activated and the determination proceeds as outlined in the previous section. After the run, the reaction vessel is thoroughly rinsed with stock solution.

RESULTS AND DISCUSSION

Determination of attainable pH control

The required sensitivity of the pH detection system can be appreciated from the observed change in pH over a 60-s observation period for various glucose concentrations (Table 1). For example, a glucose concentration of 20 μg ml^{-1} produces a total change in pH of only 0.008 pH units or, equivalently, a change in electrode potential of 0.3 mV. The precision with which the pH-stat can maintain a constant pH was determined by measuring the noise at the output of the pH meter by means of a strip-chart recorder. With this technique, the noise was determined to be approximately 0.0008 pH units, or a change in electrode potential of 0.05 mV.

Glucose standards. To evaluate the performance of the pH-stat system, a series of standard glucose samples was examined. The concentration range of standards chosen was 10—1000 μg ml^{-1}. Typically, six measurements were recorded for each standard concentration in order to evaluate the precision of the system. The resulting linear plot followed the relation $y = (5.4 \pm 1) \times 10^{-3}\ x\text{-}(0.02 \pm 0.04)$ with a standard error of estimate (S_{yx}) = 0.087. The relative standard deviations at glucose concentrations of 10, 100, and 1000 μg ml^{-1} were 20%, 5%, and 2%, respectively.

Determination of glucose in human blood serum. To validate the performance of the pH-stat, the determination of glucose in a "real" sample (1:10 diluted human blood serum) was undertaken.

Glucose standards were prepared at concentrations of 50, 100 and 150 μg ml^{-1} and a linear working curve was obtained based on the measured reaction rate of each standard. From this working curve and the measurement of the sample reaction rate, the serum glucose concentration was directly printed out in terms of milligrams per deciliter.

The average measured concentration for six serum samples was 90 mg dl^{-1} with a relative standard deviation of 7%. This measured glucose concentration is in agreement with the value specified by the manufacturer (92 ± 3.6 mg dl^{-1} obtained by a Beckman glucose analyzer).

Glucose determinations by enzymatic induction times

The glucose—glucose oxidase reaction follows first-order kinetics only after an initial delay period, termed the induction time. The induction time can limit the utility of this reaction for time-critical procedures. However,

TABLE 1

Effect of glucose concentration on observed change in pH over 60-s period

Glucose conc. (μg ml^{-1})	1000	750	500	250	150	100	50	20
Average pH change	0.260	0.195	0.148	0.058	0.039	0.030	0.018	0.008

the induction period is known to be inversely proportional to substrate concentration [18]. Therefore, this time-to-concentration relationship provides an alternative method of determination.

To evaluate this alternative method, a series of standard glucose concentrations between 20 and 1000 $\mu g\ ml^{-1}$ was examined. All glucose standards were tested at two enzyme concentrations in order to determine the effect of enzyme activity on induction time. Ordinarily, six trials were performed at each standard concentration to verify precision. The induction time was determined from the first continuous deviation from a constant pH.

The relationship between reciprocal induction time (y) and glucose concentration (x) was found to be linear for enzyme concentrations of 0.28 g l^{-1} and 0.8 g l^{-1} with the corresponding least-squares equations being $y = (4.4 \pm 0.1) \times 10^{-5} x - (5.1 \pm 7) \times 10^{-4}$ and $y = (1.5 \pm 0.1) \times 10^{-4} x - (0.9 \pm 4) \times 10^{-4}$, respectively. The corresponding standard errors of estimate (S_{yx}) were 1.0×10^{-3} and 4.8×10^{-4}. The relative standard deviation for the induction time of each standard concentration was between 5 and 10%. The relative difference between the observed average induction time and the predicted value (by least squares fit) was 1—3%.

Understandably, the increase in enzyme concentration from 0.28 g l^{-1} to 0.8 g l^{-1} produced a corresponding decrease in induction time by a factor of approximately three. This dependency provides a convenient method for adjusting induction time so that determinations can be performed in a reasonable time period.

From these results, it is evident that induction times can be used for the precise determination of glucose concentrations. There are two apparent advantages to this method; first, instrumentation is simple and inexpensive, the only requirements being a sensitive pH-meter and a timer; second, pH effects are eliminated because the pH remains constant during the induction time. A pH-stat is obviously not needed for this method because the measured induction time occurs prior to reaction commencement.

Glucose determinations by fixed-time reaction-rate methods

Because pH affects the reaction rate, fixed-time techniques have not been widely utilized in potentiometric reaction-rate determinations [19]. However, if the measured change in pH is kept small (0.001—0.1 pH units), the effects of pH will not significantly affect the reaction-rate measurement. To evaluate the practical utility of fixed-time techniques in such a situation, the reaction rate of several glucose standards was measured by monitoring small changes in pH. In this experiment, the change in pH was recorded over the initial 30 seconds of the reaction.

In these studies, the relationship between fixed-time measured reaction rate and glucose concentration over the range 20—1000 $\mu g\ l^{-1}$ was found to be linear, with a slope of $4.3 \pm 0.1 \times 10^{-3}$ pH units per second per $\mu g\ ml^{-1}$ glucose and an intercept of $(0.05 \pm 0.07) \times 10^{-3}$ pH units per second. The standard error of estimate of the plot (S_{yx}) was 0.13.

CONCLUSION

The directly computer-controlled pH-stat has been shown to determine glucose concentrations accurately in human blood serum. The microliter reagent addition system was shown not to be the precision-limiting component of the pH-stat. This addition system has no moving parts, except for a vibrating bimorph, and is constructed from simple, inexpensive components [20].

The programs for controlling the pH-stat were structured as autonomous concurrent tasks, permitting the direct translation of simultaneous, real-time activities into structured tasks. Operator directives were accepted at any time throughout an experiment, permitting the real-time display of data and experimental parameters. Of course, many of these same individual tasks could be performed by an inexpensive microcomputer, many of which are currently available. However, the simultaneous processing of several tasks, found valuable in the present system, could be carried out only by a multitasking computer of the kind employed here, or by an array of microprocessors. In the future, one can expect that many such multi-microprocessor systems will be in use.

Under certain conditions, two alternative methods for the determination of glucose can be used. The fixed-time reaction-rate method can yield quantitative results when the measured change in pH is small. However, because the effects of pH are specific for each enzymatic reaction, the fixed-time technique must be evaluated for each reaction. The determination of glucose concentration by enzymatic induction time can also yield quantitative results. Again, however, induction times are specific for each reaction and this technique must therefore be evaluated for each reaction.

This work was supported in part by the National Science Foundation through grant CHE 80-25633 and by the Office of Naval Research. The paper is taken in part from the M.Sc. Thesis of R. E. Lemke.

REFERENCES

1 I. Rousseau and B. Atkinson, Analyst, 105 (1980) 432.
2 C. C. Cannella, B. Pensa and L. Pecci, Anal. Biochem., 68 (1975) 458.
3 H. K. Wart and W. C. Wilson, J. Am. Chem. Soc., 75 (1953) 6147.
4 H. B. Mark, Jr., Talanta, 19 (1972) 717.
5 M. Murijama, J. M. Conlon and G. C. Riggle, Anal. Chem., 33 (1961) 1454.
6 G. M. Hieftje and B. M. Mandarano, Anal. Chem., 44 (1972) 1616.
7 H. V. Malmstadt and E. H. Piepmeier, Anal. Chem., 37 (1965) 34.
8 K. I. Wood, Anal. Chem., 32 (1960) 537.
9 H. B. Mark, Jr., Talanta, 19 (1972) 717.
10 J. D. Ingle, Jr. and S. R. Crouch, Anal. Chem., 43 (1971) 697.
11 H. V. Malmstadt and H. L. Pardue, Anal. Chem., 33 (1961) 1040.
12 T. W. Hunter, J. T. Sinnamon and G. M. Hieftje, Anal. Chem., 47 (1975) 497.
13 J. K. Foreman and P. B. Stockwell, Automatic Chemical Analysis, Wiley, New York, 1975, pp. 45—54.

14 R. G. Bates, Chimia, 14 (1960) 111.
15 M. J. Rogers and K. G. Brandt, Biochemistry, 10 (1971) 4630.
16 M. J. Rogers and K. G. Brandt, Biochemistry, 10 (1971) 4636.
17 H. V. Malmstadt and H. L. Pardue, Clin. Chem., 8 (1962) 606.
18 K. B. Yatsimirskii, Kinetic Methods of Analysis, Pergamon, Oxford, 1966, pp. 50—51.
19 H. V. Malmstadt, C. J. Delaney and E. A. Cordos, Anal. Chem., 44 (1972) 79A.
20 R. E. Russo, R. Withnell and G. M. Hieftje, Appl. Spectrosc., 35 (1981) 531.

Analytica Chimica Acta, 141 (1982) 187—192
Elsevier Scientific Publishing Company, Amsterdam — Printed in The Netherlands

EFFECT OF SCALING ON CLASS MODELING WITH THE SIMCA METHOD

M. P. DERDE, D. COOMANS and D. L. MASSART*

Farmaceutisch Instituut, Vrije Universiteit Brussel, Laarbeeklaan 103, B-1090 Brussel (Belgium)

(Received 22nd April 1982)

SUMMARY

The first step in multivariate analysis is almost always the scaling of the variables. The pattern recognition technique SIMCA provides the possibility of scaling the variables over all the objects of the training set (classical scaling), or only over the objects belonging to the same group (separate scaling). The former method of scaling is the more used. The effect of separate scaling on the classification of objects with SIMCA is investigated for a data set consisting of the percentage distribution of fatty acids in olive oils originating from two neighbouring regions in Italy. It is shown that separate scaling has a beneficial effect on the classification.

Among the different pattern recognition techniques, a distinction can be made between discriminating techniques and class modeling techniques. The first describe decision rules based on the differences between the classes while the second compute separate mathematical descriptions for each class based on the similarities which exist between the objects of a class.

The first step in multivariate analysis is almost always the scaling of the variables to make the range between the different variables comparable. The transformation is applied over the variables of the objects of all the classes between which a separation is attempted. Usually, the z-transformation is used: each variable is given variance one and mean zero. However, the use of class modeling techniques provides the possibility of scaling only over the variables of objects belonging to the same class, i.e., each class is scaled separately. In this case, the mathematical descriptions obtained for each class are completely independent of each other. Although it is customary to use the classical way of scaling, Albano et al. [1] suggested that the class modeling technique SIMCA gives better results when each class is scaled separately. In this article, the effect of the separate scaling on the classification of objects with SIMCA is described and the method is applied to a set of analytical chemical data.

EXPERIMENTAL

Data and programs

The data set used in this investigation consists of the percentage distribution of seven fatty acids in 100 samples of virgin olive oil originating from two neighbouring regions of Italy: 50 samples from each of East and West Liguria [2, 3].

The analyses were done with the SIMCA-2T package which can be obtained from S. Wold (Institute of Chemistry, Umeå University, Sweden). A CDC CYBER 170/750 was used for calculations.

Methodology

When M variables are available for $N(Q)$ objects (samples) of class Q, the class modeling technique SIMCA describes the similarities between the objects of a class by a principal component model based on A components, given by the equation

$$x_{ik}^{(Q)} = \alpha_i^{(Q)} + \sum_{a=1}^{A_Q} \beta_{ia}^{(Q)} \theta_{ak}^{(Q)} + \epsilon_{ik}^{(Q)}$$

where $x_{ik}^{(Q)}$ is the original measurement of variable i for object k of class Q; $\alpha_i^{(Q)}$ is the mean of variable i in class Q; $\beta_{ia}^{(Q)}$ are the loadings giving the correlation of variable i with principal component a; $\theta_{ak}^{(Q)}$ are factors depending only on the object k; and $\epsilon_{ik}^{(Q)}$ are the residuals describing that part of the data which cannot be explained by the model. The residuals include errors of measurements, and fluctuations caused by biological variability, as well as imperfections in the approximation of class Q by the principal component model.

The number of components to be used in the principal component model is predicted by Wold's cross-validation criterion [4]. If the similarity between the objects of a class is high, the number of components A is much smaller than the number of variables M.

The class model for class Q can be evaluated by comparing the residual standard deviation of each object p of class Q, $S_p^{(Q)}$ with the residual standard deviation of class Q, $S_o^{(Q)}$

$$S_p^{(Q)} = \left[\sum_{i=1}^{M} \epsilon_{ip}^{(Q)2} / (M - A_Q) \right]^{1/2}$$

$$S_o^{(Q)} = \left[\sum_{i=1}^{M} \sum_{k=1}^{N_Q} \epsilon_{ik}^{(Q)2} / (M - A_Q)\,(N_Q - A_Q - 1) \right]^{1/2}$$

The comparison is made on the basis of an approximated F test with $(M - A_Q)$ and $(M - A_Q)(N_Q - A_Q - 1)$ degrees of freedom. In this way, a confidence interval at the α-level of significance is defined around the class model. In this investigation the 1% level of significance was used. According to

the principal component models developed by SIMCA for r different classes, three kinds of classification decisions are possible for objects of unknown origin: (1) object K is similar only to class Q and can therefore be unambiguously assigned to class Q; (2) object K is similar to more than one class (e.g., to class Q and class R) and so cannot be classified unambiguously in class Q and R; (3) object K is not similar to one of the r classes and must be considered as an outlier for the r classes.

In order to visualize the classification of objects according to the principal component model for each pair of classes Q and R, a standard decision diagram can be constructed with axes corresponding to the residual standard deviations, $S_p^{(Q)}$ and $S_p^{(R)}$, of objects to the class models. In fact, $S_p^{(Q)}$ and $S_p^{(R)}$ represent the distance of objects to the principal component model for class Q and class R, respectively. $S_o^{(Q)}$ represents the typical distance of objects to the principal component model for class Q, and is used to define a confidence interval around that model. An object is assigned to class Q if it falls inside the confidence interval or if it has a $S_p^{(Q)}$ value less than a critical value $s_{crit}^{(Q)}$, related to $S_o^{(Q)}$ and calculated on the basis of the approximated F test for a given level of significance. For this reason, two lines are drawn in the standard decision diagram according to the critical value for each of the principal component models. These divide the diagram into four parts, corresponding respectively to unique classification in each of the two classes, ambiguous classification, and to the outlier region (see Fig. 1). Extensive information on the methodology of SIMCA is given by Wold [1] and Wold and Sjöström [5].

RESULTS

Classical method of scaling

The final purpose of the application of SIMCA to multivariate data of groups of objects is the description of mathematical rules which enable one to classify objects of unknown origin. The objects used to construct the principal component models (training objects) must be representative of the class to which they belong, as the development of a class model with SIMCA is sensitive to a high degree of dissimilarity between the objects. Aberrant objects caused, for example, by a non-representative selection of the samples or by analytical errors, must be removed from the training set. Otherwise, unstable class models are obtained; i.e., principal component models which are heavily influenced by the deletion of one or more objects from the training set.

After the scaling of the variables in the classical way, a plot of the first and second principal component suggested that three objects of the East Liguria class (class 1) and one object of the West Liguria class (class 2) were dissimilar to the rest of the objects in their class. These objects were considered to be outliers and were removed from the training set. These outliers have a large influence on the principal components and have the effect of

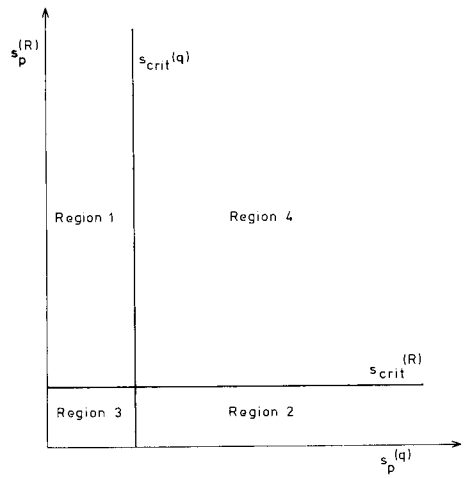

Fig. 1. Standard decision diagram for the classification of objects p into class Q or class R. Objects situated in region 1 and region 2 are unambiguously classified to class Q and class R, respectively. Objects situated in region 3, the overlap region, are classified to both classes Q and R. Objects situated in region 4 are considered to be outliers for both classes Q and R.

pressing together the other objects. When the outliers are deleted and the principal components are determined again then the remaining objects can be observed in greater detail and it is possible that outliers may be detected again. Therefore it is necessary to develop a stable model (also called class box) in a stepwise manner until all outliers have been eliminated. For each step, the number of patterns, the number of significant components and the objects which were indicated to be outliers, are given in Table 1. The number of outliers detected amounts to 15% for class 1 and 12% for class 2.

The decision rules obtained in this way were validated. This was done by deleting at random a third of the objects of the training set and placing them into the test set. These test objects were fitted to the principal component model constructed on the remaining two-thirds of the objects of the training set. This procedure was followed until all the training objects had been deleted once and only once. The validity of the principal component model is given by the prediction rate (rate of correctly classified test objects). The prediction rate amounted to 100% for both classes. The principal component models for the classes overlapped: two objects from East Liguria were assigned to the West Liguria class, i.e., two objects were not uniquely classified as they were situated in the overlap region of the standard decision diagram.

During the stepwise development of a principal component model for class 1, it seemed that a stable model was found after the second step (see Table 1) as no outliers were detected in the third step. The deletion of outliers of class 2 from the training set causes a change in the scaling of the

TABLE 1

Stepwise development of class models after scaling over all the objects of the training set[a]

Step	East Liguria class			West Liguria class		
	NPAT	NCOMP	NOUT	NPAT	NCOMP	NOUT
1	47	2	1	49	2	1
2	46	2	0	48	2	2
3	46	2	1	46	2	1
4	45	2	1	45	2	1
5	44	2	1	44	2	0
6	43	2	0	44	2	0

[a]NPAT: number of objects used to develop the decision model, NCOMP: number of principal components used in the principal component model, NOUT: number of outliers which were detected in the corresponding step.

remaining objects of the training set. This causes the principal component model for class 1 to change, so that again some objects are assigned as outliers. It can be observed that the classical way of scaling does not really provide completely disjoined class models. Therefore, separate scaling seemed to be indicated.

Separate scaling

The second stage of the investigation involved separate scaling. For class 1 the cross-validation criterion indicated that two principal components were sufficient to explain the similarities between the objects of this class. During the stepwise development of a representative class box, seven objects were assigned to be outliers. All but one of these were the same as those deleted in the classical procedure for scaling. Obviously the effect of separate scaling on the description of a principal component model is restricted for this class.

For class 2, the eigenvector projection achieved after separate scaling indicated a high degree of dissimilarity in class 2 (see Fig. 2). It was even possible to divide the objects into two subgroups. This inhomogeneity between the objects was not observed with the classical way of scaling. As the construction of a class model is sensitive to such a dissimilarity, each of the subgroups was approximated by a principal component model based on one component. The development of these two models leads to the detection of only two outliers in class 2 (Table 2).

The validation of the principal component models resulted in a prediction rate of 100% for classes 1 and 2. On the basis of the decision rules developed after separate scaling, all objects of the training set are unambiguously classified, i.e., it can be computed whether a virgin olive oil originating from Liguria comes from the western or eastern part of this region. This study shows clearly that separate scaling of classes has a beneficial effect on classification with SIMCA.

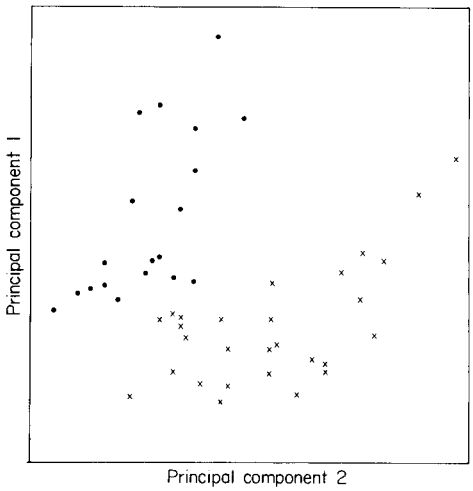

Fig. 2. Principal component projection of the objects of the West Liguria class (separate scaling). The objects were divided into subgroup A (×) and subgroup B (•).

TABLE 2

Stepwise development of a principal component model for each class after separate scaling[a]

Step	East Liguria class			West Liguria class					
	NPAT	NCOMP	NOUT	Subgroup A			Subgroup B		
				NPAT	NCOMP	NOUT	NPAT	NCOMP	NOUT
1	47	2	3	28	1	0	20	1	1
2	44	2	1				18	1	0
3	43	2	0						

[a]For abbreviations, see Table 1.

REFERENCES

1 C. Albano, G. Blomqvist, D. Coomans, W. J. Dunn, III, U. Edlund, B. Eliasson, S. Hellberg, E. Johansson, B. Norden, M. Sjöström, B. Söderström, H. Wold and S. Wold, Symposium i Anvendt Statistic, Denmarks tekniske Høgskole, 1981, p. 183.
2 M. Forina and C. Armanino, Ann. Chim. (Rome), in preparation.
3 M. Forina and E. Tiscornia, Ann. Chim. (Rome), in preparation.
4 S. Wold, Technometrics, 20 (1978) 397.
5 S. Wold and M. Sjöström, in B. R. Kowalski (Ed). Chemometrics: Theory and Application, American Chemical Society, Washington, 1977, p. 243.

Analytica Chimica Acta, 141 (1982) 193—205
Elsevier Scientific Publishing Company, Amsterdam — Printed in The Netherlands

REDUCTION OF SPECTRAL INTERFERENCES IN INDUCTIVELY-COUPLED PLASMA EMISSION SPECTROMETRY BY SELECTIVE SPECTRAL-LINE MODULATION

S. W. DOWNEY and G. M. HIEFTJE*
Department of Chemistry, Indiana University, Bloomington, IN 47405 (U.S.A.)
(Received 11th March 1982)

SUMMARY

Spectral interferences in inductively-coupled plasma (i.c.p.) emission spectrometry can be significantly reduced through the use of selective spectral-line modulation. In this method, a mirrored, rotating chopper directs the emission from an i.c.p. alternately through and past a flame; selective modulation is achieved when the flame contains absorbing atoms identical to emitting atoms in the i.c.p. The ability of selective spectral-line modulation to minimize broadband, narrow line, and scattered light spectral interferences is demonstrated. Signal-to-background ratios for detection with spectral-line modulation are shown to be higher than those obtained by conventional detection. The effect of modulating conditions on working curve slope and linearity is discussed and the limitations of the proposed method are critically evaluated.

The inductively coupled plasma (i.c.p.) has become a widely used source in atomic emission spectrometry (a.e.s.). However, the multi-wavelength advantage offered by a.e.s. is also responsible for one of its most problematic drawbacks — spectral interferences. Variable and sometimes subtle, these interferences often complicate elemental quantitation. Unresolvable spectral features from source background, spectral lines from matrix concomitants, and scattered light, all contribute to the spectral interference problem.

Most often, spectral dispersing devices that provide high resolution and low stray light are used to reduce spectral interferences. In conjunction with this costly approach, sophisticated software for correction of spectral background and interelement effects has been developed in an attempt to minimize interference from source background and matrix concomitants. Spectral interferences in i.c.p.e.s. have also led to the development of spectral-line selection algorithms for multi-element determinations. Unfortunately, unambiguous spectral line identification still can be very difficult when complex and/or unknown matrices are being examined. Equally troublesome when measuring an analytical spectral line are wavelength calibration and drift.

Selective modulation of spectral lines of interest offers the high resolution and freedom from spectral interferences afforded by costly spectrometers, yet is simple to employ and provides an automatic wavelength lock to the

elemental lines of interest. When desired elemental-line emission alone is modulated and synchronously detected, discrimination against other types of emission is possible.

Previously, selective spectral-line modulation has been used in this laboratory to improve continuum-source atomic absorption flame spectrometry [1, 2] and to minimize spectral interferences in flame emission spectrometry [3]. These systems were similar to that used earlier by Alkemade and Milatz [4].

In the present work, an a.e.s. system with spectral-line modulation similar to that reported earlier [3] was constructed and tested using an i.c.p. as the analytical emission source and with improved optical design. Here, emitted radiation from an i.c.p. is alternately directed through and around a modulating flame by a double-beam optical system. Selective absorption by atoms in the flame creates an element-specific net difference in intensities between the two beam paths, which can then be detected by a lock-in amplifier. All other spectral features not affected (absorbed) by the flame are at a d.c. level and remain undetected.

Because a flame is employed as an atom reservoir, very narrow spectral regions (lines) can be modulated. Consequently, all types of spectral interferences found in the i.c.p. can be reduced greatly by using spectral-line modulation: narrow-line, broadband, continuum and scattered light. Improved signal-to-background ratios (S/B) are therefore obtained with spectral-line modulation. Analytical working curves are linear, with their sensitivities (slopes) dependent upon modulating solution concentration.

EXPERIMENTAL

A schematic diagram of the spectral-line modulation detection system used with the i.c.p. is shown in Fig. 1. Details concerning individual components are summarized in Table 1. The system is comprised of three basic units: the emission source (i.c.p.), the double-beam optics, and the detector–demodulator.

A conventional-sized (20-mm o.d.) argon i.c.p. was used with a concentric pneumatic nebulizer–peristaltic pump system for sample introduction. The operating conditions of the torch were chosen for convenient examination of many elements and analytical wavelengths without realignment or recalibration of the optical train. Operating parameters were held constant unless otherwise stated.

The emitted radiation from the i.c.p. is transferred to the detector by a series of mirrors. M2 collimates the emitted radiation from the i.c.p. and M3 and M4 focus it onto the entrance slit of the monochromator. The rotating sector mirror, C, and the beam splitter, BS, chop and recombine the beams, producing the double-beam operation necessary for spectral-line modulation. M1 and M5 are flat, directional mirrors. The placement of the optics is such that a 1:1 image of the i.c.p. is formed at the entrance slit. The vertical slit selects a viewing region in the i.c.p. 15–30 mm above the load coils. The chopper constitutes the limiting aperture of the system,

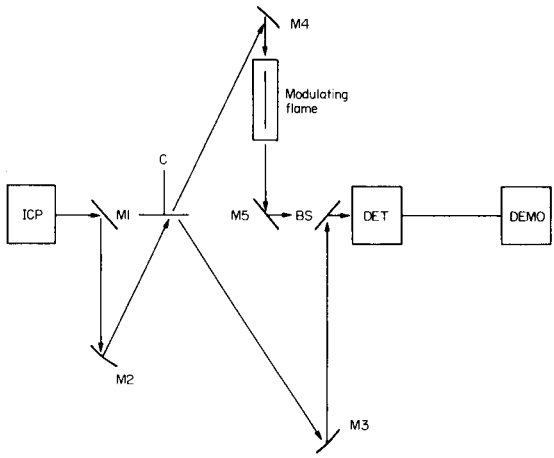

Fig. 1. Schematic diagram of double-beam spectral-line modulation system. M1, M5, flat mirrors; M2, M3, M4, spherically concave mirrors; C, rotating sector mirror; BS, beam-splitter used to combine beams; DET, monochromator and detector; DEMO, demodulating electronics and data storage. See Table 1 for details of components. The dimensions of the entire optical array are approximately 50 × 100 cm.

giving a numerical ratio of $f/10$. The flame is positioned after the chopper so that any flame-based emission will be at a constant level and suppressed by a.c. detection [3]. Air—acetylene and nitrous oxide—acetylene flames were used, depending on the atomization properties in the flame of the element being studied. The net throughput of both beam paths should be nearly identical in order to minimize beam imbalances in the spectral-line modulation system. When such imbalances exist, careful correction is necessary to isolate spectral-line modulation signals from intrinsic throughput difference effects [3]. Often, this is accomplished with a variable neutral-density filter placed in one beam.

The detector (DET in Fig. 1) consists of a medium-resolution monochromator, used to reduce detector noise, and a standard photomultiplier tube and amplifier. The demodulator (DEMO in Fig. 1) can be any frequency-selective and phase-sensitive device. Three such demodulator devices have been tried here: lock-in amplifier, differential-input boxcar integrator, and laboratory minicomputer (MINC). Any of these devices can be triggered by a reference signal taken from the chopper. Most wavelength scans reported here were obtained with the lock-in amplifier while most fixed wavelength data were obtained with the MINC minicomputer. The boxcar amplifier was used for initial characterization of the optical train.

The entire optical system is supported by a single, six-foot optical rail bed of the type described by Walters [5].

For comparison purposes, conventional emission data were obtained with the lock-in detection system by blocking entirely the beam path containing the modulating flame. This approach enables the same optical system to be

TABLE 1

System components and operating conditions

Inductively-coupled plasma	
Model HFP-2500F, 2.5 kW, 27.12 MHz with model AMN-PS-1 automatic impedance matcher (Plasma-Therm, Kresson, NJ)	
Input power	1 kW
Gas flow rates (Ar)	Coolant 16 l min^{-1}; plasma 0.5 l min^{-1}; nebulizer 0.9 l min^{-1}
Gas handling	Bulk liquid Ar, (Minewald Co., Indianapolis, IN) controlled by needle valves, monitored by calibrated rotameters (Matheson Co., Joliet, IL)
Sample solution uptake	1.0 ml min^{-1} delivered by peristaltic pump (Minipuls 2, Gilson Medical Electronics, Middleton, WI)
Nebulizer	Concentric glass type
Torch	20-mm o.d.
Flame	Supported on slot burner equipped with impinging bead nebulizer (Instrumentation Laboratory, Wilmington, MA): air/acetylene 10-cm slot; N_2O/acetylene 5-cm slot
Flame gas flow rates	Air 15 l min^{-1}, C_2H_2 3 l min^{-1}; N_2O 3 l min^{-1}, C_2H_2 2 l min^{-1}
Flame gas handling	Purified flame gases (Matheson, Joliet, IL) controlled by needle valves (Series M, Nupro, Cleveland, OH) monitored by calibrated rotameters (No. VFB, Dwyer Instruments, Michigan City, IN)
Flame solution uptake rate	4 ml min^{-1}
Optics	
Monochromator	EU 700 GCA/McPherson Instruments (Acton, MA), 0.35-m Czerny-Turner mount, slit width 50 μm, 1 Å spectral bandpass.
Chopper	Butterfly configuration, Model RC45 (Valtec, Costa Mesa, CA) 4.5-in. diameter front-surface aluminum with MgF_2 overcoat. Rotated at 38 Hz by synchronous motor.
Plane mirrors	M1, M5; 2-in. diameter front-surface aluminum with MgF_2 overcoat (Oriel Corp., Stamford, CN).
Concave mirrors	M2, M3, M4; 4-in. diameter front-surface aluminum with MgF_2 overcoat; focal length 50 cm (3B Optical, Gibsonia, PA).
Beam combiner	2 in. × 2 in. u.v. beam splitter, model SU51X (Optics for Research, Caldwell, NJ) 33% T, 33% R for 200—500 nm.
Optical mounts	Model 625A-2, 625A-4 mirror mounts (Newport Research Corp., Fountain Valley, CA).
Detection	
Photomultiplier	Hammamatsu R106, operated at 800—1000 V, supplied by Model 244 high-voltage power supply (Keithley Instruments, Cleveland, OH).
Amplifier	High-speed current amplifier, model 427 (Keithley Instruments, Cleveland, OH).
Reference detector	TIL 149 i.r. source and sensor assembly triggered by chopper.
Demodulation	
Lock-in amplifier	Model 220 lock-in amplifier (Princeton Applied Research Corp., Princeton, NJ).
Minicomputer	Digital Equipment Corp. MINC-11/03 laboratory minicomputer (Maynard, MA)
Boxcar amplifier	Model 162 boxcar averager with model 164 input gates (Princeton Applied Research Corp., Princeton, NJ).
Recorder	Model SR-204 strip-chart type, operated at 10 V full scale (Heath Co., Benton Harbor, MI).

used, providing an appropriate comparison between spectral-line modulation detection and conventional emission measurement.

All signal-to-noise ratio (S/N) and detection limit calculations were determined in the manner suggested by St. John et al. [6]. Stock solutions were prepared from reagent-grade metals, salts and acids [7].

RESULTS AND DISCUSSION

Reduction of spectral interference

Line interference. Spectral interference from poorly resolved elemental spectral lines can be extremely troublesome in conventional detection of i.c.p. emission. Routinely, correction factors for spectral line overlap and prudent wavelength selection must be employed even when high-resolution monochromators are used [8]. However, these problems are minimized by detection with spectral-line modulation.

Figure 2 illustrates the ability of the spectral-line modulation technique to reduce spectral-line interference. Conventional detection of the radiation from an i.c.p. containing a mixture of copper and palladium is illustrated in Spectrum 1. With a monochromator spectral bandpass of 0.1 nm, the Pd I 324.3-nm line is just barely resolved from the Cu I 324.7-nm line. Other spectral features present are the OH $A^2\Sigma^+$ (v = 0) → $X^2\Sigma^+$ (v = 0) band, several background spectral lines, and other Cu I and Pd I lines. Spectrum 2 of Fig. 2 shows the copper-selective spectrum with spectral-line modulated detection, in which both matrix-based and background spectral lines are suppressed. Graphically evident here is the modulation and detection of the OH band at 306 nm. This behavior is expected since water and its decomposition products are present in high concentration in the flame, both as a combustion product and from solvent aspiration. Trace 3 is the spectrum obtained when palladium is introduced into the modulating flame. Here copper and background spectral lines are suppressed. Again it is evident that all absorbers in the flame contribute to the spectral-line modulated spectrum; the OH band at 306 nm is prominent. Interestingly, the Pd I 342.1-nm line visible in Spectrum 1 of Fig. 2 is not present in Spectrum 3. The reason for this absence is that the air—acetylene flame used here cannot sufficiently populate the lower state of the 342.1-nm transition, 1191 cm^{-1} above the lower state involved in the Pd I 324.3- and 340.4-nm lines. Figure 2 also illustrates clearly the spectral simplification and unambiguous spectral line identification offered by detection with spectral-line modulation.

Band interference. Molecular emission from the i.c.p. consists of band spectra which can interfere with desired elemental spectral lines. Fortunately, the excellent atomization properties of the i.c.p. minimize band emission from sample species. However, band spectra are produced by solvent (H_2O) vapor and by entrained atmospheric gases and their reaction and fragmentation products. Figure 3 shows the interference of nitrogen on three Mo I spectral lines [9]. Spectrum 1 was obtained by conventional detection of

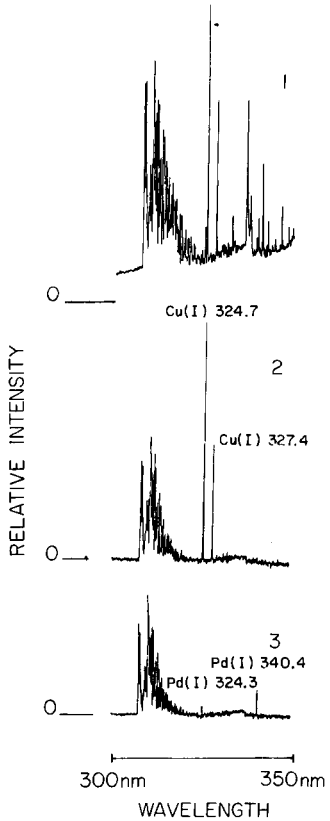

Fig. 2. (Left) Reduction of mutual copper and palladium line interferences with spectral line modulation. (1) Spectrum obtained using conventional detection of emission from 40 μg Cu ml^{-1} and 80 μg Pd ml^{-1} in i.c.p.; (2) Cu-selective spectral scan with spectral-line modulation using 1 mg Cu ml^{-1} in modulating flame; (3) Pd-selective spectral scan with spectral-line modulation using 1 mg Pd ml^{-1} in modulating flame.

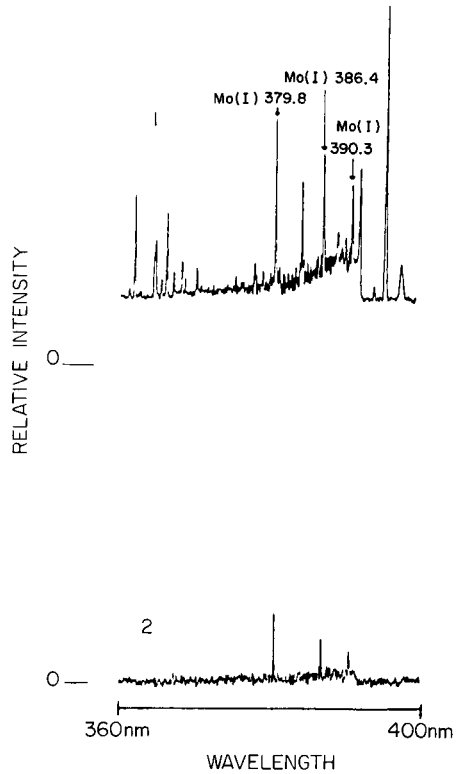

Fig. 3. (Right) Reduction of N_2^+ band interference on three molybdenum spectral lines with spectral line modulation. (1) Conventional emission spectrum of i.c.p. containing 40 μg Mo ml^{-1}; (2) spectrum obtained using spectral-line modulation detection with 10 mg Mo ml^{-1} in modulating flame.

the N_2^+ $B^2\Sigma_u^+$ (v = 0) → $X^2\Sigma_g^+$ (v = 0) bandhead with three Mo I resonance lines superimposed on it. Also present are spectral line features from the i.c.p. background, including, for example, the Ar I line at 383.5 nm. Spectrum 2 is the "Mo-selective spectrum", produced by spectral-line modulated detection with molybdenum in the modulating flame. The marked suppression of both band and line features from the i.c.p. background is obvious.

Another example of the ability of the proposed method to reject unwanted band interference is shown in Fig. 4. In this experiment, the monochromator was set on the Bi I 306.7-nm resonance line that falls on the R1 bandhead of the OH $A^2\Sigma^+$ (v = 0) → $X^2\Sigma^+$ (v = 0) transition [9]. As illustrated above

(cf. Fig. 2), this OH band is not entirely removed by detection with spectral-line modulation. However, the influence of the OH band can be reduced by employing high concentrations of bismuth in the modulating flame. Under these conditions, the absorption spectrum of the modulating flame, and therefore the effective spectral bandpass of the modulated network, is dominated by the bismuth line.

Curve 1 in Fig. 4 shows the increase in signal with slit width obtained during conventional detection of the OH background with a blank solution being aspirated into the i.c.p. Found here is a quadratic dependence of relative intensity upon monochromator slit width, indicative of continuum-like spectral behavior. When bismuth is added in relatively high concentration (2.5 mg ml^{-1}) to the modulating flame, the modulated detector rejects much of the background band emission and provides added selectivity for the detection of bismuth (cf. Curve 2, Fig. 4). The slope (1.3) of Curve 2 indicates good discrimination against large amounts of interfering radiation, even though OH in the flame modulates some of the background.

Scattered light. Elements such as calcium and magnesium, when present in high concentration in the i.c.p., generate strong ionic emission which is known to produce scattered-light-based spectral interferences [10, 11]. The spectral-line modulation approach can significantly reduce this interference, as shown in Fig. 5. Curve 1 shows the interference from the Ca II 393.3- and 396.8-nm radiation on the Al I 396.1-nm spectral line when conventional detection is used. In contrast, Curve 2 shows relative freedom from this interference during detection with spectral-line modulation. The slight upward trend apparent in Curve 2 is caused by the small but finite modulation of the line-broadened Ca II radiation that falls exactly at the aluminum wavelength [10].

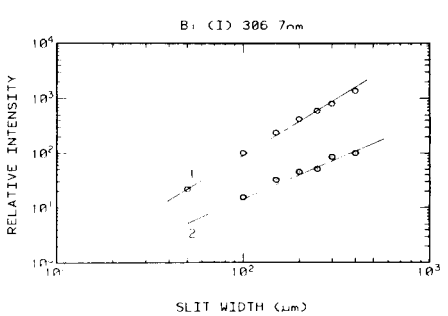

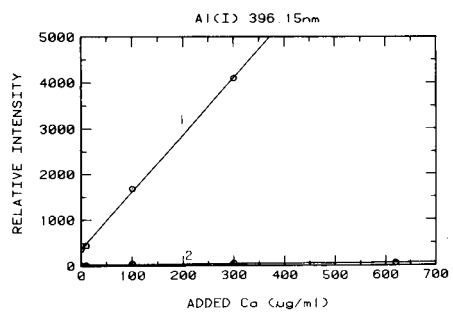

Fig. 4. Reduction of OH band interference on bismuth with spectral-line modulation. (1) Effect of slit width on conventionally detected signal from blank solution in i.c.p., showing increase caused by OH band; (2) spectral-line modulation detection of 250 μg Bi ml^{-1} in i.c.p. using 2.5 mg Bi ml^{-1} in modulating flame. See text for details.

Fig. 5. Reduction by spectral-line modulation of Ca II scattered light interference on aluminum. A solution of 100 μg Al ml^{-1} was nebulized into the i.c.p. Spectral slit width, 0.6 nm. (1) Conventional detection; (2) modulated detection using 10 mg Al ml^{-1} in a nitrous oxide—acetylene modulating flame.

Continuum background interference. The broad continuum spectral background from the i.c.p. can produce significant spectral interference if background drift occurs, especially if a spectrometer with poor spectral resolution is employed. One cause of drift in the continuum background is variation in r.f. power into the i.c.p. In Fig. 6, this situation is simulated by intentional power changes. Curves 1 and 2 of Fig. 6 show the effect of r.f. power on the conventionally detected signal from Cr I emission and background emission, respectively. Curve 2 is very similar to the background behavior at the Cr I 357.8-nm line reported by Berman and McLaren [12]. Curve 3 indicates the ability of the spectral-line modulation method to discriminate against background shifts (in obtaining Curve 3, no special background-correction procedures were employed). Significantly, the Cr signal detected with spectral-line modulation actually decreases slightly as r.f. power goes up, in marked contrast to the behavior of Curve 1. This decrease can be explained by the effect of r.f. power on the spatial emission profile of the chromium line. Edmonds and Horlick [13] reported that Cr I 425.4-nm emission shifts lower in the i.c.p. as the power is increased. In the present optical system, emission from lower regions of the i.c.p. would pass through higher spatial regions of the flame where the chromium atom concentration is lower. This change reduces the amount of chromium absorption that takes place, which subsequently decreases the modulated signal. Clearly, it is important to select a constant set of compromise conditions for measurements by the spectral-line modulation method.

Multi-element determinations

To employ spectral-line modulation for multi-element determinations, several elements can be introduced simultaneously into the modulating flame. Figure 7 illustrates this capability. Trace 1 of Fig. 7 is the conventionally

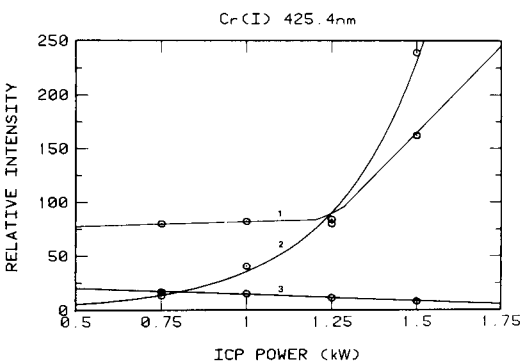

Fig. 6. Reduction of continuum background interference by the spectral-line modulation method. (1) Effect of r.f. power on the background-corrected signal from 100 μg Cr ml^{-1} (conventional detection); (2) effect of applied r.f. power on i.c.p. background (conventional detection); (3) effect of r.f. power on the signal from 100 μg Cr ml^{-1} in i.c.p. (with spectral-line modulation); 1 mg Cr ml^{-1} nebulized into modulating flame. See text for details.

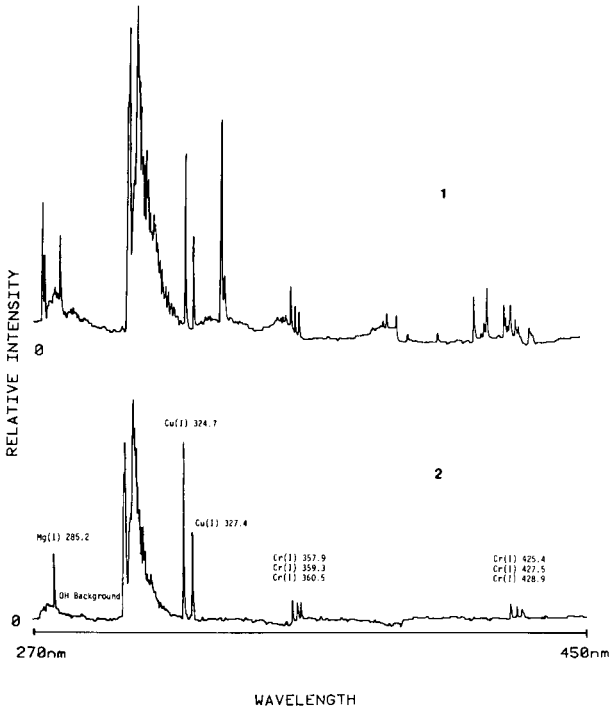

Fig. 7. Reduction of i.c.p. background in multi-element determinations with spectral-line modulation. (1) Conventionally detected spectrum of 40 μg ml^{-1} each of Cr, Cu and Mg in i.c.p.; (2) spectrum of same solution with spectral-line modulation; 1 mg ml^{-1} each Cr, Cu and Mg employed in modulating flame. See text for details.

detected spectrum of emission from the i.c.p., into which was introduced a solution containing 40 μg ml^{-1} each of Cr, Cu and Mg. Spectrum 2 was obtained from the same solution, but using spectral-line modulation, with Cr, Cu and Mg all present in the modulating flame. Importantly, the only features present in Spectrum 2 are the atomic resonance lines and the $A^2\Sigma^+$ ($v = 1$) $\rightarrow$ $X^2\Sigma^+$ ($v = 0$) and $A^2\Sigma^+$ ($v = 0$) $\rightarrow$ $X^2\Sigma^+$ ($v = 0$) bands of OH at 281 and 306 nm, respectively. Not surprisingly, the Mg II lines at 279.5 and 280.2 nm and the nine Cr II lines between 276 and 287 nm are not modulated, because the corresponding ions are not produced in high concentration in the modulating flame.

Analytical characteristics

Figure 8 shows the effect of modulating solution concentration on the working curves for copper obtained with spectral-line modulation. Understandably, higher modulating concentrations produce greater signal amplitudes and correspondingly larger working-curve slopes when spectral-line modulation is used. Of course, an increase in modulating solution concentration not only increases depth of modulation, but also the width of the modulating spectral interval. Moreover, high modulating solution concentrations would

limit the number of elements which could be simultaneously modulated, because of possible problems with sample introduction into the flame. Finally, many elements, unlike copper, emit strongly and would generate substantial detector shot noise if present in the modulating flame in high concentration. Consequently, the lower modulating solution concentrations employed in Fig. 8 (Curve 2 or 3) would be preferred in most analytical situations where extremely high sensitivity is not required.

A substantial advantage of spectral-line modulated detection over conventional detection is the improvement in signal-to-background ratio (S/B) revealed in Fig. 9. In Fig. 9, Curve 2, the background signal for spectral-line modulation was taken when a blank solution was sprayed into the i.c.p. and when a copper solution was introduced into the flame. Clearly, a much smaller portion of the spectral background is modulated, compared to the amount of background detected conventionally (Curve 1). As expected, the conventionally detected background increases as the square of the slit width, while the signal increases linearly with slit width. The net effect is the lowering of S/B (Curve 1). However, the decrease in S/B with slit width is small for the modulated method (Curve 2) because of the narrow absorbing-line profile in the flame.

Figure 10 explores this behavior in more detail. Curves 1 and 2 show the quadratic and linear dependence of intensity on slit width of the background and analyte signal, respectively. Unlike conventional detection, the background intensity detected in the modulated method, shown in Curve 4, has a slope less than 2 and, in fact, approaches unity. This behavior illustrates the line-like character of detection with spectral-line modulation. Because of this capability, large slit widths could be employed with spectral-line modulated instruments in light-limited situations, although S/N would not be expected to improve. As expected, the slope of Curve 3, the copper signal

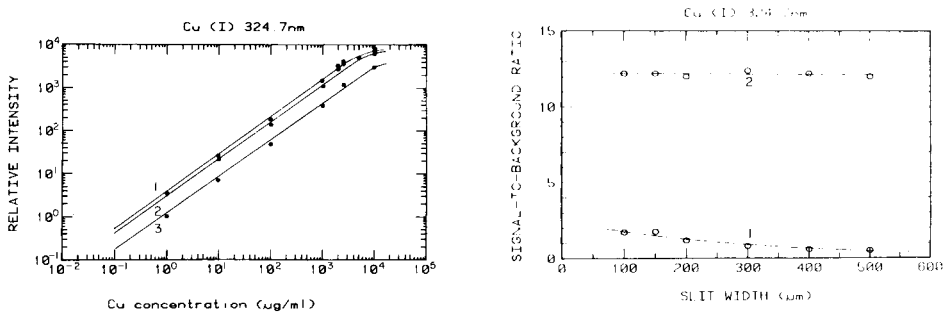

Fig. 8. Effect of modulating solution concentration on the working curves for copper with spectral-line modulation. Concentration of Cu in modulating flame (mg ml^{-1}): (1) 10; (2) 1; (3) 0.1.

Fig. 9. Influence of monochromator slit width on S/B for spectral-line modulation and conventional detection. (1) Conventional detection of 10 μg Cu ml^{-1} in i.c.p.; (2) the modulated detection using 10 mg Cu ml^{-1} in modulating flame.

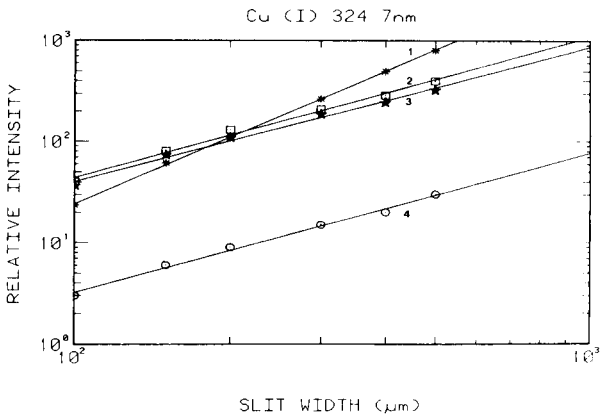

Fig. 10. Conventional detection of: (1) blank (background) in i.c.p.; (2) 10 μg Cu ml^{-1} in i.c.p. Spectral-line modulated detection using 10 mg Cu ml^{-1} in modulating flame for: (3) 10 μg Cu ml^{-1} in i.c.p.; (4) blank background in i.c.p.

with the modulated detection, is nearly unity. Curves 1 and 3 compare favorably to the bismuth data of Fig. 4.

Upon comparison, the slopes of Curves 2 and 3 of Fig. 10 are the same to within experimental error. This indicates that under these conditions, the absorption spectral line width in the flame is wider than the emission spectral line width of the i.c.p. Also, the absolute magnitude of Curve 3 is less than that of Curve 2 indicating the incomplete absorption intrinsic in any absorption experiment. As a result, the sensitivity of the spectral-line modulation method will be slightly lower than the sensitivity of conventional detection.

Table 2 compares several characteristics of spectral-line modulation and conventional detection of a number of elements at the μg ml^{-1} level. The conventional emission data were obtained on the same dual-beam system used for spectral-line modulation but with the flame-containing path blocked. Overall, signal-to-background ratios are ten times higher with spectral-line modulation, although signal-to-noise ratios (S/N) are slightly lower, except in two cases. As a result, detection limits were somewhat poorer with spectral-line modulation. A comparison of these detection limits with those in the literature [15] suggests that the dual-beam optical system used in this study is not particularly efficient and seems rather noisy. Of course, a portion of this increased noise originates in the modulating flame.

It is also evident in Table 2 that no correction is necessary for most interelement effects with spectral-line modulation. Sample-matrix-based interfering spectral lines have exceedingly small effects. Calibration for spectral interferences [11, 16] will therefore seldom be necessary with spectral-line modulation.

Attempts to modulate ion lines by using a nitrous oxide—acetylene flame were only marginally successful and would probably not be routinely useful. For example, the U II line at 409.0 nm was not detectable even at modulating

TABLE 2

Analytical characteristics of i.c.p.e.s. with spectral-line modulation

Element (line)	Ag(I)	Cr(I)	Cu(I)	Cu(I)	In(I)	Mg(I)
Wavelength (nm)	328.1	425.4	324.7	327.4	325.6	285.2
Signal/background for 1 μg ml⁻¹						
Emission	0.07	0.03	1.0	0.05	0.016	0.27
Modulated[a]	2.0	0.13	4.4	0.43	0.30	1.2
Signal/noise for 1 μg ml⁻¹						
Emission	6.0	6.0	17	9.0	2.0	30
Modulated[a]	2.0	2.0	35	3.0	3.7	25
Detection limit (μg ml⁻¹)						
Emission	0.1	0.35	0.08	0.2	1.0	0.07
Modulated[a]	1.0	1.0	0.04	0.7	0.6	0.12
Lit. [15]	0.0047	0.0093	0.0036	0.0065	0.08	0.0011
Interferences						
Interfering species	Zr II	Continuum	OH	Zr II	Cd I	OH
Wavelength (nm)	327.9	Broad	Broad	327.3	326.1	Broad
Type	Line	Background	Band	Line	Line	Band
Amount of interfering species equivalent to 1 μg ml⁻¹ analyte	150[b]	c	c	200[b]	470[b]	c
Interfering species contribution to modulated signal[a]	e	d	d	e	e	d

[a]10 000 μg ml⁻¹ analyte sprayed into air/acetylene modulating flame. [b]μg ml⁻¹. [c]Decreases S/B in conventional detection. [d]Reduced by spectral-line modulation. [e]None detected.

solution concentrations of 10 mg ml^{-1}. However, the Ca 393.3-nm line exhibited slight modulation, consistent with the work of Koirtyohann and Lichte [17]. In general, resonance atomic lines are best suited to detection by spectral-line modulation with a modulating flame.

Unfortunately, the use of high-temperature modulating ion reservoirs is unattractive. Such sources normally have small absorbing path lengths, broadened lines and greater background emission [3, 18]. For these reasons, the spectral-line modulation method seems at present unlikely to benefit from the frequently heralded "ion-line advantage" of the i.c.p.

Conclusion

From this work, it is apparent that the greatest advantages offered by the proposed method are element specificity and wavelength selectivity. For this reason, spectral-line modulation seems best suited for non-routine examination of unusually complex i.c.p. emission spectra and routine situations where high resolution instrumentation is impractical.

In the present system, the spectral-line modulation method is not suited for work where sub-trace detection limits are required or for quantifying elements that do not have atomic lines terminating in low-lying states in the i.c.p.

This work was supported in part by the Office of Naval Research and by the National Science Foundation through grant CHE 79-18073.

REFERENCES

1 R. L. Cochran and G. M. Hieftje, Anal. Chem., 49 (1977) 98.
2 R. L. Cochran and G. M. Hieftje, Anal. Chem., 50 (1978) 791.
3 S. W. Downey, J. G. Shabushnig and G. M. Hieftje, Anal. Chim. Acta, 121 (1980) 165.
4 C. T. J. Alkemade and J. M. W. Milatz, Appl. Sci. Res., 48 (1955) 289.
5 J. P. Walters, in D. M. Hercules, G. M. Hieftje, L. R. Snyder and M. A. Evenson (Eds.), Contemporary Topics in Analytical and Clinical Chemistry, Vol. 3, Plenum, New York, 1978, Ch. 3.
6 P. A. St. John, W. J. McCarthy and J. D. Winefordner, Anal. Chem., 39 (1969) 1495.
7 J. A. Dean and T. C. Rains, Flame Emission and Atomic Absorption Spectrometry, Vol. II, Dekker, New York, 1969, Ch. 13.
8 J. W. McLaren, S. S. Berman, U. J. Boyko and D. S. Russell, Anal. Chem., 52 (1981) 1802.
9 R. W. B. Pearse and A. G. Gaydon, The Identification of Molecular Spectra, Wiley, New York, 1941.
10 G. F. Larson, V. A. Fassel, R. K. Winge and R. N. Kniseley, Appl. Spectrosc., 30 (1976) 384.
11 C. E. Taylor and T. L. Floyd, Appl. Spectrosc., 34 (1980) 472.
12 S. S. Berman and J. W. McLaren, Appl. Spectrosc., 32 (1978) 372.
13 T. E. Edmonds and G. Horlick, Appl. Spectrosc., 31 (1977) 536.
14 N. Omenetto, S. Nikdel, J. D. Bradshaw, M. S. Epstein, R. D. Reeves and J. D. Winefordner, Anal. Chem., 51 (1979) 1521.
15 P. W. J. M. Boumans, Spectrochim. Acta, 36B (1981) 169.
16 G. W. Johnson, H. E. Taylor and R. K. Skogerboe, Appl. Spectrosc., 33 (1979) 451.
17 S. R. Koirtyohann and F. E. Lichte, Can. J. Spectrosc., 23 (1978) 98.
18 G. Horlick, personal communication, 1981.

Analytica Chimica Acta, 141 (1982) 207—212
Elsevier Scientific Publishing Company, Amsterdam — Printed in The Netherlands

THE DETERMINATION OF SULPHATE IN NATURAL WATERS BY INDUCTIVELY-COUPLED PLASMA EMISSION SPECTROMETRY

DOUGLAS L. MILES* and JENNIFER M. COOK

Hydrogeology Unit, Institute of Geological Sciences, Wallingford, Oxon OX10 8BB (Gt. Britain)

(Received 10th March 1982)

SUMMARY

Sulphate is determined simultaneously with other constituents by using inductively-coupled plasma emission spectrometry; the intensity of the 180.73-nm sulphur line is monitored. At a forward power of 1100 W, under compromise conditions, a 3 σ detection limit of 0.08 mg l^{-1} sulphate and a precision of 0.8% RSD at the 200 mg l^{-1} sulphate level were obtained. A small spectral interference from calcium is overcome by software corrections, and good agreement is demonstrated between the proposed method and spectrophotometric sulphate measurements for a variety of natural waters including seawater.

Since the pioneering work of Greenfield et al. [1] and Wendt and Fassel [2], development of the inductively-coupled plasma as a spectroscopic source has led in recent years to its application to the determination of a wide range of elements in a variety of matrices, including natural waters [3—7]. Such research has focussed primarily on the simultaneous measurements of alkali, alkaline earth and transition metal cations and the hydride-forming metalloid elements, to which this plasma is ideally suited. Partly because of instrumental restrictions, relatively little attention has been given to the determination of non-metals which exhibit their principal resonance lines in the vacuum ultraviolet, although Heine et al. [8] have drawn attention to the usefulness of this region. Investigations into the analytical application of vacuum ultraviolet lines, using a plasma source coupled to a modified atomic absorption spectrometer, have been reported very recently [9—11]. The advent of inductively-coupled plasma systems now employing vacuum spectrometers potentially extends the useful low wavelength range to include the u.v. lines of elements such as carbon, sulphur, phosphorus and iodine.

Under the pH and Eh conditions typical of most natural waters, sulphur occurs almost exclusively as the sulphate anion SO_4^{2-}; the hydrogensulphate ion, HSO_4^-, becomes significant in oxidising waters only below pH 4 [12]. Occasionally, under reducing conditions, small amounts of reduced forms of sulphur may be present, either as the HS^- ion or as dissolved H_2S, but their contribution to the overall sulphur budget is small. The determination of sulphate is an important measurement in the characterisation of the chemistry

0003-2670/82/0000-0000/$02.75

of natural water systems, but is not without its difficulties. The classical gravimetric technique, in which precipitation as barium sulphate is employed, is time-consuming and subject to errors caused by coprecipitation of other ions [13]. Titrimetric methods in ethanolic solution with thorin as indicator have been described [14--15], but the conditions necessary for satisfactory titrations are critical [16] and prior removal of cations from the sample by ion exchange is required. Automated spectrophotometric techniques [17—18] can provide fairly rapid sample throughput combined with reasonable precision, but removal of cations by ion exchange is again necessary. This paper describes a novel method for the measurement of sulphate in natural waters based on the determination of sulphur by inductively-coupled plasma emission spectrometry.

EXPERIMENTAL

Instrumentation and reagents

Plasma emission measurements were made using an Applied Research Laboratories 34000C system. Operating conditions are given in Table 1.

Spectrophotometric sulphate determinations were done with a Technicon AutoAnalyser II system employing the barium—thorin procedure of Henriksen and Bergmann-Paulsen [19].

A stock sulphate standard (10 000 mg l^{-1} sulphate) was prepared by dissolving 18.144 g of potassium sulphate, dried at 110°C, in deionised water and diluting to 1 l. Working standards for calibration were 1% (v/v) in hydrochloric acid (AristaR grade).

Sample collection and preservation

Groundwater samples were filtered on collection through 0.45-μm membrane filters and acidified to 1% (v/v) by the addition of AristaR-grade hydrochloric acid.

TABLE 1

Plasma system components and operating conditions

Spectrometer	ARL 34000 C Quantovac; 1-m Paschen-Runge mounting; grating ruled 1080 lines mm^{-1}, 0.309 nm mm^{-1} reciprocal linear dispersion (3rd order). Primary slit width 20 μm, secondary slit 50 μm. Hamamatsu R-306 photomultiplier tube
Wavelength	180.73 nm, 3rd order
Readout	Digital readout of mean signal from three 10-s integrations
Frequency	27.12 MHz
Forward power	1080 W
Reflected power	5 W
Observation height	17 mm above load coil
Argon flow rates	Coolant 11 l min^{-1}, plasma 1.2 l min^{-1}, carrier 1 l min^{-1}, light path purge 1.5 l min^{-1}
Nebuliser	Concentric glass, J. E. Meinhard model TR-30-A3

Standard seawater, batch P84, chlorinity 19.376‰ was obtained from the Institute of Oceanographic Sciences, Wormley, Gt. Britain.

RESULTS AND DISCUSSION

Sulphur emission intensities were monitored at the most sensitive 180.73-nm line [8]. At this wavelength, significant absorbance by molecular oxygen occurs and this effect was minimised by purging most of the light path between the plasma and the spectrometer with argon, via an open quartz tube extending from the primary optics to within 2 cm of the torch. Figure 1 shows the relationship between argon flow through the tube and sulphur emission intensity; high flow rates adversely affected the stability of the plasma and a flow rate of 1.5 l min^{-1} was used for all subsequent work.

Plasma operating conditions, in terms of gas flows and observation height, had been adjusted to the most suitable compromise settings for cation measurements, and these conditions were retained to preserve the advantages of simultaneous determinations. The sulphur emission signal varied with increasing forward power (Table 2), and on the basis of signal:background ratio a setting of 1080 W was selected. A typical calibration graph obtained under these conditions for sulphate in the range 0.5—10 000 mg l^{-1} is shown in Fig. 2. Short-term precision, calculated as a relative standard deviation for 20 successive 10-s integrations, was 0.81% at the 200 mg l^{-1} level and 1.2% at the 2800 mg l^{-1} level when seawater was aspirated. A 3 σ detection limit of 0.079 mg l^{-1} sulphate was calculated from measurements of the fluctuations of the background signal.

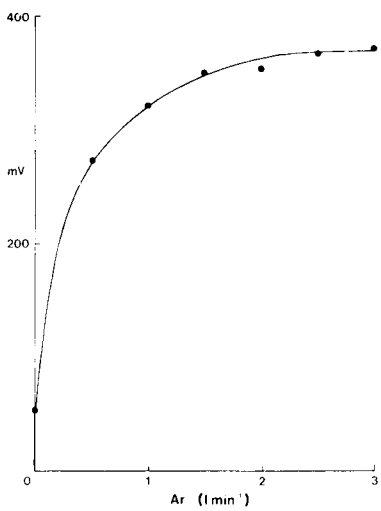

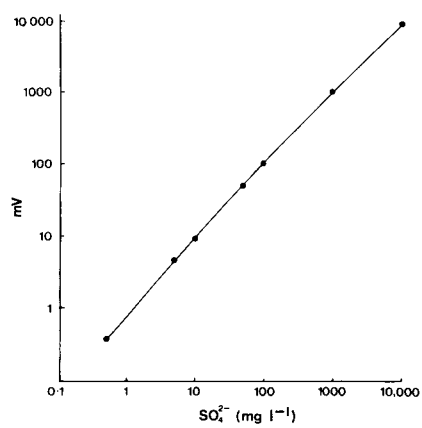

Fig. 1. The effect of argon purge flow rate on the sulphur emission intensity at 180.73 nm.

Fig. 2. Calibration graph for sulphate in the range 0.5—10 000 mg l^{-1}. Emission intensities in mV are background-corrected.

TABLE 2

Effect of plasma forward power on emission intensity at 180.73 nm

Power (W)	Signal (mV)		Signal:background
	Background	200 mg l^{-1} SO_4^{2-}	
920	4.1	325	79
1080	5.3	575	108
1350	9.0	950	106

Interferences

Spectral interferences from other elements were examined by mechanically displacing the spectrometer primary slit and scanning the 180.73-nm region while aspirating standard solutions prepared from Specpure reagents. Of the elements characteristically present as major components of natural waters, only calcium produced a slight interference. A weak calcium line at approximately 180.734 nm partially overlaps the sulphur line (Fig. 3), such that 1000 mg Ca l^{-1} produces an apparent sulphate signal of 25 mg l^{-1} sulphate. This corresponds to an enhancement of the sulphate signal in, say, seawater of 0.43%. Correction for this interference was easily achieved by establishing the relationship between calcium concentration and apparent sulphate signal and inserting this information in the controlling software. The effect of calcium was then automatically subtracted during the measurement of samples. In addition, Lee and Pritchard [20] have suggested that calcium interference may be further reduced by monitoring the sulphur emission at a lower observation height. No interference was detected from high concentrations of sodium and magnesium, and no shift in the nearby background signal was detected during the aspiration of seawater. Natural water samples

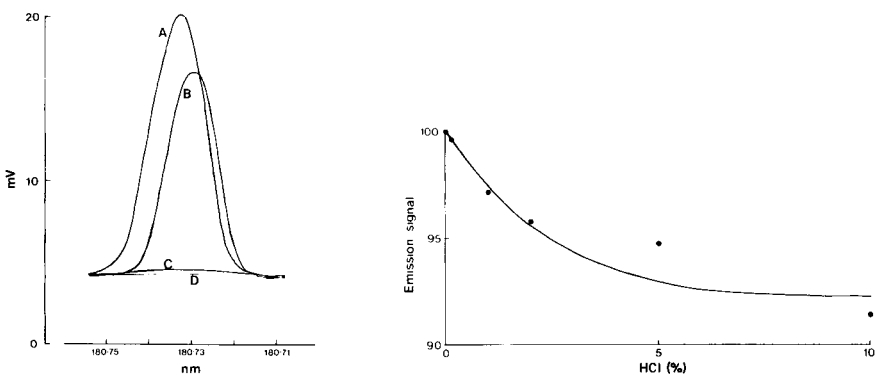

Fig. 3. Wavelength scans in the region of the sulphur 180.73-nm line while aspirating (A) 1000 mg Ca l^{-1}; (B) 25 mg SO_4^{2-} l^{-1}; (C) 1000 mg Mg l^{-1}; (D) 1% (v/v) HCl.

Fig. 4. The influence of HCl concentration on the sulphur emission signal at 180.73 nm.

TABLE 3

Comparison of results for sulphate by inductively-coupled plasma emission spectrometry with certified values for standard waters

Sample	Sulphate content (mg l^{-1})	
	I.c.p.e.s.	Certified value
EPA Quality Control Standard 2	7.3	7.2
IOS Standard Seawater	2800	2781

are normally acidified to stabilise them during storage, and the influence of hydrochloric acid concentration on the sulphur emission signal is indicated in Fig. 4. This effect is conveniently overcome by making the acid content of samples and standards identical at, for example, 1% (v/v).

The accuracy of the inductively-coupled plasma procedure was assessed by analysing waters of known sulphate composition, and by comparing measured sulphate values for a wide range of samples with those obtained for the same waters by an automated spectrophotometric procedure [21]. Table 3 shows good agreement between the sulphate measurements obtained and the nominal values for International Standard Sea Water and an EPA Quality Control Standard. Data on the comparison between the inductively-coupled plasma and the spectrophotometric procedures are given in Fig. 5. No systematic differences between the results from the two methods are indicated.

The authors thank Drs. W. M. Edmunds, M. Thompson and J. N. Walsh for their constructive comments on this paper, which is published with the approval of the Director, Institute of Geological Sciences (NERC).

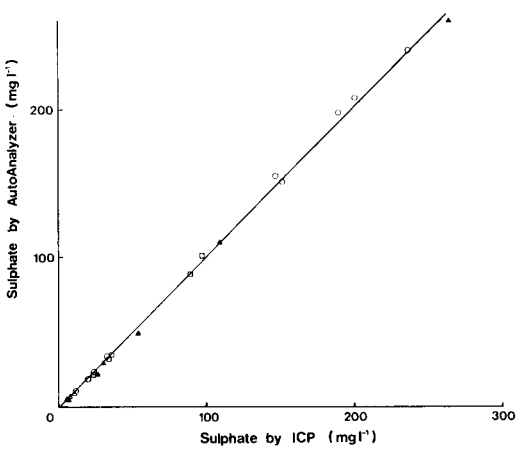

Fig. 5. Comparison of sulphate measurements by the inductively-coupled plasma and spectrophotometric methods for various natural waters. Groundwaters from: (▲) Recent sands, (○) Deccan Trap basalt, (□) Miocene limestone. (△) Rain water. Correlation coefficient $r = 0.99$.

REFERENCES

1 S. Greenfield, I. L. Jones and C. T. Berry, Analyst, 89 (1964) 713.
2 R. H. Wendt and V. A. Fassel, Anal. Chem., 37 (1965) 920.
3 R. K. Winge, V. A. Fassel, R. N. Kniseley, E. DeKalb and W. J. Hass, Spectrochim. Acta, 32B (1977) 327.
4 M. M. Moselhy, D. W. Boomer, J. N. Bishop, P. L. Diosady and A. D. Howlett, Can. J. Spectrosc., 23 (1978) 186.
5 J. R. Garbarino and H. E. Taylor, Appl. Spectrosc., 33 (1979) 220.
6 M. Hiraide, T. Ito, M. Baba, H. Kawaguchi and A. Mizuike, Anal. Chem., 52 (1980) 804.
7 M. Thompson, B. Pahlavanpour and L. T. Thorne, Water Res., 15 (1981) 407.
8 D. R. Heine, J. S. Babis and M. B. Denton, Appl. Spectrosc., 34 (1980) 595.
9 R. D. Ediger, At. Spectrosc., 1 (1980) 59.
10 D. W. Hoult, At. Spectrosc., 1 (1980) 82.
11 G. F. Wallace, At. Spectrosc., 1 (1980) 38.
12 J. D. Hem, US Geol. Surv. Water-Supply Pap. 1473.
13 Department of the Environment Standing Committee of Analysts, Sulphate in Waters, Effluents and Solids, HMSO, London, 1980, p. 5.
14 J. S. Fritz and S. S. Yamamura, Anal. Chem., 27 (1955) 1461.
15 G. R. Macchi, B. S. Cescon and D. Mameli-d'Errico, Arch. Oceanogr. Limnol., 16 (1969) 163.
16 J. C. Haartz, P. M. Eller and R. W. Hornung, Anal. Chem., 51 (1979) 2293.
17 J. M. Adamski and S. P. Villard, Anal. Chem., 47 (1975) 1191.
18 G. A. Persson, Air Water Pollut. Int. J., 10 (1966) 845.
19 A. Henriksen and I. M. Bergmann-Paulsen, Vatten, 30 (1974) 187.
20 J. Lee and M. W. Pritchard, Spectrochim. Acta, 36B (1981) 591.
21 J. M. Cook and D. L. Miles, Rep. Inst. Geol. Sci., No 80/5 (1980) 52.

Analytica Chimica Acta, 141 (1982) 213—224
Elsevier Scientific Publishing Company, Amsterdam — Printed in The Netherlands

THE DETERMINATION OF SELENIUM BY ATOM-TRAPPING ATOMIC ABSORPTION SPECTROMETRY

C. M. LAU, A. M. URE and T. S. WEST*

The Macaulay Institute for Soil Research, Craigiebuckler, Aberdeen, AB9 2QJ (Gt. Britain)

(Received 2nd March 1982)

SUMMARY

The application of atom-trapping atomic absorption spectrometry to the determination of selenium has been studied in detail. The optimum experimental parameters were established and the interference of major elements on the determination of selenium was studied using collection on a cold silica tube. The atom-trapping atomic absorption technique gives a detection limit of 0.03 ppm after 2-min collection on silica in an air—acetylene flame. This compares with ca. 1 ppm by the conventional absorption technique at the same 196.1-nm line. Methods to minimize interferences were examined, including the use of a double tube arrangement, an aluminium oxide-coated silica tube and ion-exchange separation. A combination of combustion in an oxygen flask and collection from an air—acetylene flame on the aluminium oxide-coated silica tube yielded satisfactory results in the analysis of four plant tissue samples.

The atom-trapping atomic absorption technique achieves greater sensitivity than conventional atomic absorption measurements by pre-concentrating the analyte atoms within the flame before measurement. When a water-cooled tube is located in the flame, the analyte atoms or their precursor species are trapped on the cold surface, and their subsequent release provides a much bigger (transient) signal than that obtained in the normal technique. This phenomenon of atom collection has been described [1] and further investigations have been made on the mechanism governing the trapping and release of analyte species [2]. The possibility of using metal instead of silica tubes [3] has also been examined and the technique has been applied to various elements such as arsenic, cadmium, lead, selenium and zinc [4].

The flame spectrometric determination of selenium is relatively more difficult than that of most elements because the principal resonance lines occur below 200 nm, causing unfavourable signal-to-noise ratios that are due to atmospheric and flame background absorption. A characteristic concentration (sensitivity) of 1.0 μg ml^{-1} selenium was reported by the conventional technique based on an air—acetylene flame and the 196.1-nm resonance line [5]. The alternatives of a separated air—acetylene flame [6, 7] and a premixed argon—hydrogen flame [8] enhanced the sensitivity only to a limited extent. A hydrogen selenide evolution technique has been developed

[9, 10] in order to provide higher sensitivity and overcome chemical interferences and electrothermal atomic absorption methods have been investigated [11—13]. Atomic fluorescence spectrometry has also been used for the determination of selenium in an air—acetylene flame; the detection limit is 0.25 ppm [14]. An atomic emission detection limit of 0.1 ppm has been recorded for the inductively-coupled radiofrequency plasma at 196.1 nm [15]. Other flame atomic spectrometric methods reported have attempted to increase sensitivity by pre-concentration in a modified hydrogen selenide trap [16], electrochemical pre-concentration [17] and chemical pre-concentration by either organic solvent extraction [18, 19] or ion exchange [20].

EXPERIMENTAL

Measurements were performed with the equipment described previously [1—4]. Silica or metal tubes (4-mm o.d.) were used as atom traps and were located 8 mm above the primary reaction zone of an air—acetylene flame burning on the suitably adapted burner head of a Varian-Techtron AA6 spectrometer.

A column (7 cm long, 1-cm diameter) of Amberlite IR-120 (analytical grade) cation exchanger was prepared in a 25-ml burette for ion-exchange experiments. The equipment used for the oxygen flask combustion technique for organic samples included two 5-l round-bottomed flasks provided with silica sample boats attached to the stoppers to seal the flasks during combustion and magnetic stirrers to mix the collecting solution after burning the samples in the flask [21].

The selenium stock solution was prepared by dissolving pure selenium metal in the minimum amount of concentrated nitric acid and making up to volume with distilled water. All other chemicals used were of analytical-reagent grade; the nitric acid and acetic acid used as collecting solutions in the oxygen flask were redistilled acids.

RESULTS AND DISCUSSION

Optimization of experimental parameters

The water-cooled silica tube was located initially 7 mm above the primary reaction zone of a fuel-rich air—acetylene flame. A single sharp peak, which appeared at 3 s and finished at 5 s from the start of heating up the tube, was obtained following collection during the aspiration of a selenium solution. The optimum position of the silica tube, found by moving it relative to the primary reaction zone of the flame and the optical path, corresponded to obscuration of one third of the light beam by the upper part of the tube at which position its base was 8 mm above the primary reaction zone.

The flame conditions were studied by varying the fuel flow rate. A marked increase in signal was obtained when the flame was altered to a more oxidizing

condition (Fig. 1). Collection of a 10-ppm selenium solution for 1 min provided six times greater sensitivity than the normal atomic absorption technique. This enhancement in sensitivity was higher with more dilute selenium solutions. Enhancements in sensitivities of ten, twenty and thirty times, compared to the normal technique, were obtained by collection for 30 s, 1 min and 2 min, respectively (Fig. 2). The precision of the method was checked by collecting from a 0.1-ppm selenium solution for 1 min; the experiment was repeated twelve times. The relative standard deviation was found to be 14%; the characteristic concentration (sensitivity) was 0.015 ppm and the detection limit was 0.034 ppm.

To gain some insight into the mechanism of trapping and release of selenium by the silica tube, both the position of the tube relative to the primary reaction zone and the flame conditions were varied during the process of collection and release. Only when the tube was maintained high up in an oxidizing flame did a large selenium signal result (Table 1). Collection of a concentrated selenium solution in both lean and rich flame conditions showed condensation of red clusters of selenium metal on the cold silica tube from a lean flame, and virtually none from a fuel-rich flame.

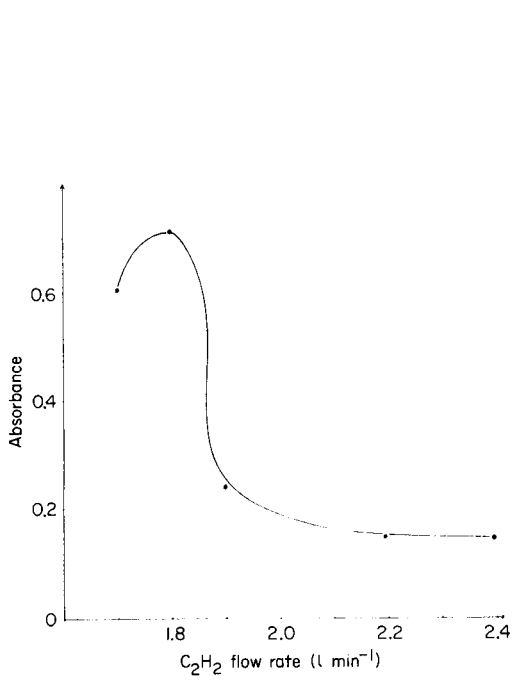

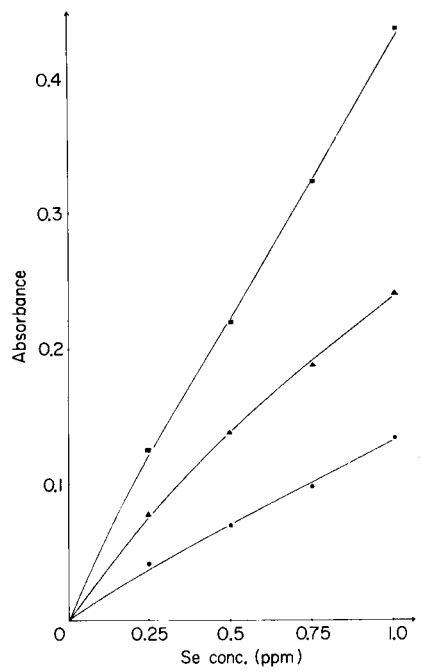

Fig. 1. Collection for 1 min of a 10 ppm selenium solution at various acetylene flow rates. The air flow rate was fixed at 10.7 l min^{-1}. The absorbance of the 10 ppm Se solution was 0.126 in the normal a.a.s. technique.

Fig. 2. Response of selenium as a function of collection time: (•) 30 s; (▲) 1 min; (■) 2 min.

TABLE 1

The effects of varying the distance between the tube and the primary reaction zone of the flame, and of varying the flame conditions by altering the fuel flow rate, during collection and on release

Variation of tube position[a]			Variation of flame conditions[b]		
During collection	On release	Absorbance	During collection	On release	Absorbance
High	High	0.080	Lean	Lean	0.376
High	Low	0.026	Lean	Rich	0.030
Low	High	0.023	Rich	Lean	0.014
Low	Low	0.024	Rich	Rich	0.027

[a]A 0.2 ppm selenium solution was collected for 1-min intervals, with a lean flame during collection and release.
[b]A 5 ppm selenium solution was collected for 30-s intervals, with the tube in the high position for collection and release.

Metal tubes as collectors for selenium

Copper, titanium, nickel and stainless steel tubes were studied as alternatives to silica for the collection of selenium. These tubes differ from silica in that their surface temperatures are lower both during collection and release. In addition, they may exhibit chemical interaction with the trapped analyte or concomitant species.

Copper tube. When a copper tube was located in the same position as the silica tube, a persistent high blank was found to occur at the selenium peak. Since it is known that selenium is frequently present as an impurity in copper, the blank is most probably due to this source. No further investigations were done with copper tubes.

Titanium tube. The use of a titanium tube had several disadvantages. An oxide layer formed on the surface of the tube upon repeated heating and cooling. This continuous change in the chemical and physical nature of the tube surface made reproducible measurements difficult. Furthermore, the tube became deformed after several cycles of heating and cooling and did not return to its original position. Otherwise, the behaviour of the titanium tube was similar to that of the silica tube, in that collection for 30 s of a 5 ppm selenium solution in a lean flame gave a sensitivity which was about four times better than conventional atomic absorption measurements in an air—acetylene flame at the 196.1-nm line.

Nickel tube. The nickel tube showed a better performance than either copper or titanium. Although it expanded on heating in the flame, it returned almost to the same position after cooling. A blank built up on repeated measurements of selenium, but this could be minimized by heating the tube for a longer time in the release cycle, 20 s compared to 15 s for silica. The major disadvantage of the nickel collector for selenium was that

its sensitivity was much lower than that of a silica tube. The same solution and collection time yielded only 30% of the sensitivity of the silica tube.

Stainless steel tube. Stainless steel was by far the best tube material amongst the metals studied as collectors for selenium. It was able to withstand the high temperature of the flame, bending only slightly in the heating cycle and quickly returning to the normal position on cooling. Experimental parameters were varied, but the behaviour was similar to that with the silica tube. The sensitivity of the selenium signal from this tube was, however, just about half that with a silica tube.

The applicability of the steel tube was further tested by collecting 2-ppm selenium solutions containing high concentrations of sodium or aluminium. They were found to interfere more severely with the selenium signal than when using a silica tube. Both cations when present at a concentration of 10 ppm showed little effect, but at 100 ppm the selenium signal was drastically reduced and became vanishingly small with 500 ppm of either cation. Probably the colder steel surface was susceptible to more deposition and this, combined with the film of water which condensed on the surface of the steel tube, lowered the collection efficiency for selenium.

Interference studies with the silica collector

The effects of up to five hundred-fold concentrations of potassium, sodium, calcium, magnesium, aluminium and iron on the determination of 1 ppm selenium were investigated by collection on a cold silica tube. The signals were measured at 196.1 nm following collection for 0.5, 1 and 2 min. Comparisons were made between a pure selenium solution and the one that contained 10 ppm of the foreign cation. The procedure was then repeated for solutions containing 100 ppm and 500 ppm of the cation.

Potassium and sodium salts

These alkali metals at 10 ppm concentrations did not affect the selenium signal, but there was visible attack on the surface of the silica. With the 100-ppm alkali metal solutions, depression or enhancement of the selenium signal was observed, depending on the anion. However, 500 ppm of an alkali metal caused a depression of the selenium signal in most cases. The alkali metals interfered because of their attack on the silica tube surface; in all cases, a white misty film was observed on the tube. This caused a change in the shape of the analytical peak. Initially, a single sharp peak was obtained but, as more alkali metal was collected, the signal peak became split and eventually became a single broad peak. This indicated that the trapped selenium was being released from a non-uniform surface as a result of chemical attack by the alkali metal on the silica. Broadening of the peak reduced the sensitivity of peak-height measurements. No attempt was made to integrate the signal over the peak width.

Calcium and magnesium salts. The selenium signal was altered greatly by the presence of $\geqslant$10 ppm of these ions. It changed progressively from a single

sharp peak to a double peak and then broadened with increasing concentration of calcium or magnesium. The mechanism of the alkaline earth metal interference differed from that of the alkali metals. The former tended to deposit on the tube surface as well as to attack the surface. A white layer of the metal oxide or carbonate was found on the surface after the experiments; and when it was brushed off, a white film remained. Under such conditions the response of the selenium signal was irregular, and depression or enhancement occurred even for the same salt at different concentrations.

Aluminium chloride. Aluminium chloride differed from the previous metals in not attacking the silica chemically. Instead, alumina deposited on the tube surface. The selenium peak underwent transition from a single to a double peak, then, as more alumina was deposited in subsequent experiments, it became a single peak again, but was slower to appear. The double peak signal was due to the release of selenium from alumina and silica surfaces, while the delayed single peak arose from an aluminium oxide surface alone. This delay was probably caused by the different thermal characteristics of the two surfaces. When 500 ppm aluminium was present, there was a depression of about 25% in the selenium signal compared to that from a pure selenium solution.

Iron chloride. The behaviour of iron was essentially similar to that of aluminium, in that it also deposited on the silica surface as an oxide, Fe_2O_3. The difference was that the presence of as little as 10 ppm of iron was enough to cause splitting and lowering of the selenium signals. No further experiments were done with iron salts.

Chloride mixture. The effect of a mixture of chlorides of all of the above cations on the determination of selenium was studied. The change in peak shape was essentially the same, i.e., from a single sharp peak to a double peak and subsequently a broad peak. Although the presence of 10 ppm of the cations did not cause much problem, 100 ppm and upwards severely depressed the selenium signal. The interference pattern produced by these ions together was complicated because the alkali and alkaline earth metals tended to attack the silica surface chemically, while aluminium and iron deposited on the tube surface as oxides.

Summary of interference studies. Table 2 summarizes the effects of the cations examined on the selenium signal. It is divided into two sections, the effect of the interferent depositing together with selenium, and its effect on the tube surface. The interferent could affect the selenium signal by co-depositing together with the free selenium atoms and hence trap some of them within the deposited layer, but it could also alter the silica surface by attacking it chemically or by forming an oxide layer.

Minimization of interference effects

The trapping technique was quite successful in measuring down to ppb ($\mu g\ l^{-1}$) levels of selenium. However, severe depression was encountered in the presence of several cations because of the deposition of the foreign ions

TABLE 2

Interference of cations on the selenium determination by collection on a cold silica tube[a]

Interferent	Conc. added (ppm)	Effect of interferent depositing with Se (% error)			Effect of interferent on tube surface (% error)
		30 s	1 min	2 min	
KNO_3	10	−14	0	0	−39
	100	+17	+54	+38	−49
	500	+20	0	+33	−77
K_2SO_4	10	0	0	0	+20
	100	−14	−37	−52	0
	500	−43	−48	−34	−47
NaCl	10	0	0	0	−37
	100	+18	+30	0	−33
	500	−19	0	+28	−73
$CaCl_2$	10	−14	−23	−38	−49
	100	0	+19	0	−56
	500	+37	+49	+46	−74
$Ca(NO_3)_2$	10	0	+20	0	0
	100	0	+25	0	0
	500	0	0	0	0
$Mg(NO_3)_2$	10	−33	−61	−43	−50
	100	+25	+39	+53	−31
	500	+28	+122	+23	−18
$MgCl_2$	10	0	+14	+26	0
	100	−22	0	+18	−41
	500	+113	+109	+76	−26
$AlCl_3$	10	−13	0	0	−33
	100	0	0	0	−38
	500	−16	−26	−24	−49
$FeCl_3$	10	0	0	+18	+16
	100	−40	−47	−52	0
	500	−43	−43	−21	−26
Chloride mixture	10	−29	+13	0	−16
	100	−17	0	0	−22
	500	−18	−47	−67	−29

[a]Enhancement is indicated by +, and depression by −. Errors within the ±10% range were discounted.

together with selenium on the tube surface. Therefore, some means of separating selenium from the other cations had to be found before this technique could be applied to plant analyses.

The double tube arrangement. A method for separating selenium from other cations after aspiration of the solution into the flame by means of a double tube arrangement was first investigated. The basis of this method is that most elements tend to deposit on a cold tube very close to the primary reaction zone whereas, exceptionally, selenium is trapped efficiently only

when the cold tube is higher up in the flame. An arrangement such as that shown in Fig. 3 should, therefore, allow the lower tube to trap most of the interferent species, leaving mainly selenium to be deposited on the upper tube. The upper tube was operated normally, i.e., with heating/cooling cycles for collection and subsequent measurements of selenium and the lower tube was maintained cold.

Both stainless steel and silica were tried in the lower tube position. The flame was split more than in a single tube arrangement, but was able to reunite underneath the upper tube. This arrangement yielded a sensitivity that was about 40% less than that of a single tube arrangement with a pure selenium solution.

The behaviour of the double tube system was tested for the elimination of interference effects by aspirating selenium solutions containing high concentrations of aluminium, sodium and potassium. The presence of 500 ppm aluminium slightly enhanced the determination of selenium. The same aluminium concentration in the single tube arrangement depressed the selenium signal by ca. 25%. Effects from the alkali metals were also minimized: 100 ppm of either potassium or sodium did not interfere, but with 500 ppm there was depression of the selenium signal.

Since the double tube arrangement allowed some of the interfering elements to deposit on the upper tube, especially when present in high concentrations, the same effects of deposition and chemical attack on the silica tube were still observed, although to a lesser extent.

Ion-exchange separation. The separation of selenium from interfering cations by means of ion-exchange offers another possibility because selenium normally exists in solution as SeO_3^{2-} or SeO_4^{2-}. A column (7 cm long, 1-cm diameter) of Amberlite IR-120H cation-exchanger was used for tests. The preliminary tests showed that the breakthrough for sodium occurred after 50 ml of 1000 ppm sodium had passed through the column. The recovery of selenium from pure solutions was more than 90%.

Because hydrogen ions are released from the cation-exchanger, to an extent depending on the concentration of the cations taken up, it was considered desirable to acidify the standards to match the sample. The acid strength, at least for hydrochloric acid, significantly affected the selenium

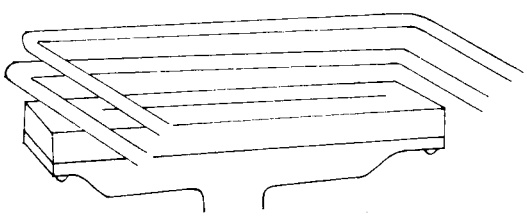

Fig. 3. Double tube arrangement; this diagram shows the two silica tubes mounted one above the other over the slot of the burner head. The lower tube is maintained cold throughout the operation, whilst the upper tube is operated in the usual collect/release cycle.

TABLE 3

Effect of inorganic acids on the absorbances obtained for 2 ppm selenium by collecting on a cold silica tube

HCl (M)				CH_3COOH (M)				HNO_3 (M)			
0	0.05	0.1	0.5	0	0.05	0.1	0.5	0	0.05	0.1	0.5
0.198	0.105	0.081	0.038	0.178	0.170	0.173	0.171	0.171	0.173	0.182	0.184

signal (Table 3). It was too inconvenient in practice to achieve this matching because the sample acidity varied from sample to sample according to its composition. An attempt to use an arbitrary, fixed hydrochloric acid strength, 0.1 M, for the standards was unsuccessful and apparent selenium recoveries of more than 100% were obtained because of a greater depression of the selenium signal in the standards than in the sample. As the effect of nitric acid on the selenium signal was not significant (<7%), similar tests were done with nitrate as the sample anion and 0.1 M nitric acid in the standard solutions; nearly complete recovery of selenium was obtained (Table 4).

The use of the ion-exchange method was restricted by the presence of hydrochloric acid in the final sample solution, by the limited capacity of the column to remove interfering cations, and by the dilution factor involved in preparing the final sample solution.

Oxygen flask combustion and an alumina-coated collection tube

There are two major procedures for sample decomposition used to release selenium from plant samples for measurement, namely acid digestion and the oxygen flask. A mixture of concentrated perchloric and nitric acid is commonly used for acid digestion, usually followed by treatment with concentrated hydrochloric acid to reduce all selenium species to Se(IV) for measurement by a technique such as fluorimetry [21]. With the oxygen flask technique [22], the solid sample is first compressed into pellets, then placed in a silica boat in an oxygen flask in which it is ignited. During the combustion, the selenium present in the sample vaporizes and dissolves in the absorption solution inside the flask. The latter procedure is more favourable here because most major elements such as potassium, sodium, calcium and magnesium remain in the ash.

The correct choice of absorbing solution has a profound effect on the

TABLE 4

Recovery of selenium from chloride- and nitrate-containing samples after the cation-exchange separation

Sample solution	1.0 ppm Se + 1000 ppm Na (Cl^-) + 1000 ppm Al (Cl^-)	1.0 ppm Se + 1000 ppm Na (NO_3^-)
Se recovered (ppm)	1.23, 1.26	0.96, 1.08

recovery of selenium. Absorption solutions prepared from concentrated hydrochloric, sulphuric acid and mixtures of acid solutions, bromine additions, etc., were examined but did not yield satisfactory recovery of selenium. A mixture of concentrated sulphuric acid and potassium persulphate provides satisfactory recoveries with fluorimetric methods of determination [23], but this mixture is not applicable to the atom-trapping technique for selenium because of the high cation concentration involved.

In more detailed tests with acidic absorbing solutions, 25 ml of 1 M and 5 M nitric acid were examined: the former gave 73% and the latter 81% recovery of selenium when artificial samples were spiked and burned in the oxygen flask. The same test was repeated with acetic acid and again the more concentrated acid solution gave better recovery (88% for 25 ml of 5 M acetic acid and 76% for 25 ml of 1 M acid). Smaller volumes of the acidic solutions were also used; 10 ml of various concentrations of the acid as the absorbing solution were compared with 25 ml of the same concentrations of acid. The former were made up to a final volume of 25 ml while the latter were made up to 50 ml. The recoveries of selenium in each case are shown in Table 5. Less selenium was recovered in the smaller volume of absorbing solution, but this is preferable because it gives a higher concentration of selenium in the final solution.

The solutions resulting from the combustion of plant samples by this oxygen flask were found to contain major elements, probably because ash fell from the silica boat during the combustion. Therefore, the solutions as prepared were unsatisfactory for measurements of selenium by the atom-trapping technique because of the interference problem mentioned earlier. Because the main trouble was chemical attack by the alkali and alkaline earth metals on the silica thus producing an irregular surface, the prevention of direct contact of these elements with the silica surface offered the possibility of a solution to the problem. Previously, aluminium was found to interfere only slightly by depositing as aluminium oxide on the tube surface; alumina was therefore used to prevent the alkali and alkaline earth metals attacking the tube.

A white coating of aluminium oxide was deposited on a silica tube by collecting aluminium from a 500 ppm aluminium solution for 10 min. Measurements of a 1.0 ppm selenium solution before and after the alumina-coating showed only a slight depression of the selenium signal. Various concentrations

TABLE 5

The effects of different acetic acid concentrations and volumes on the recovery of selenium by the oxygen flask method

Volume of acid (ml)	10	10	10	25	25	25
Molarity	2	2.5	4	2	2.5	4
Se recovery (%)	84	82	86	91	90	91
	87	78	86	94	90	—

of sodium were then added to the 1.0 ppm selenium solutions and the experiments were repeated. The results show no depression of the selenium signal, but rather a slight enhancement (Table 6). The surface of the coated tube was also examined, but no irregularity could be found.

Analysis of two mixed herbage plant samples and two clover plant samples. The plant samples were made into pellets of about 1 g. Four pellets of each plant sample were burnt, two at a time, in a 5-l oxygen flask; 10 ml of 2.5 M acetic acid were used as collecting solution and made up subsequently to 25 ml with distilled water. The standards were prepared by dilution from a 1000 ppm selenium stock solution, acetic acid and sodium acetate being added to each so that the final solution contained 1 M acetic acid and 50 ppm sodium. The atomic absorption was measured after collection for 2 min on an aluminium oxide-coated silica tube. The results are compared with those obtained by the standard fluorimetric method in Table 7. These results show that atom-trapping atomic absorption spectrometry can be applied to the determination of selenium in plant material.

Conclusions

The atom-trapping technique can be applied to the determination of selenium by collecting on a cold silica tube in an air—acetylene flame. Under optimum conditions of a very oxidizing flame and the tube located well above the primary reaction zone of the flame, sensitivity increases of ten-, twenty- and thirty-fold compared to the normal atomic absorption technique were obtained by collection for 30 s, 1 min and 2 min, respectively. The four metal tubes studied were of little practical use because of expansion on heating, low sensitivity or high interferences. Interference studies with the silica tube indicated that nearly all the cations examined interfered with the determination, either by chemical attack or by permanent deposition on the tube surface. Several techniques were examined to minimize interferences such as a double-tube arrangement, cation-exchange following an oxygen flask combustion and collection on an aluminium oxide-coated tube.

TABLE 6

The effect of sodium on selenium determination by collecting on an aluminium oxide coated tube for different lengths of time

	Absorbance	
	1 min collection	2 min collection
1.0 ppm Se	0.084	0.144
1.0 ppm Se + 10 ppm Na	0.086	0.140
1.0 ppm Se + 30 ppm Na	0.091	0.165
1.0 ppm Se + 70 ppm Na	0.090	0.162
1.0 ppm Se + 1000 ppm Na	0.083	0.142

TABLE 7

The selenium content of two mixed herbage and clover plant samples

Sample		Selenium found (ppm)	
		Atom-trapping atomic absorption	Fluorimetry
Mixed herbage	1	0.20	0.20
	2	0.63	1.0
Clover	1	0.59	0.43
		0.64	0.54
	2	0.57	0.74
		0.54	0.50

The latter in combination with the oxygen flask combustion was found to be entirely satisfactory in the analysis of plant samples. The results obtained were in broad agreement with those from fluorimetric analysis.

REFERENCES

1 J. Khalighie, A. M. Ure and T. S. West, Anal. Chim. Acta, 107 (1979) 191.
2 J. Khalighie, A. M. Ure and T. S. West, Anal. Chim. Acta, 117 (1980) 257.
3 J. Khalighie, A. M. Ure and T. S. West, Anal. Chim. Acta, 134 (1982) 271.
4 J. Khalighie, A. M. Ure and T. S. West, Anal. Chim. Acta, 131 (1981) 27.
5 C. S. Rann and A. W. Hambly, Anal. Chim. Acta, 32 (1965) 346.
6 D. N. Hingle, G. F. Kirkbright and T. S. West, Talanta, 15 (1968) 199.
7 G. F. Kirkbright, M. Sargent and T. S. West, At. Absorpt. Newsl., 8 (1969) 34.
8 H. L. Kahn and J. E. Schallis, At. Absorpt. Newsl., 7 (1968) 5.
9 O. E. Clinton, Analyst, 102 (1977) 187.
10 J. Azad, G. F. Kirkbright and R. D. Snook, Analyst, 104 (1979) 232.
11 G. T. C. Shum, H. C. Freeman and J. F. Uthe, J. Assoc. Off. Anal. Chem., 60 (1977) 1010.
12 V. B. Stein, E. Canelli and A. A. Richards, At. Spectrosc., 1 (1980) 61.
13 K. Safed and Y. Thomassen, Anal. Chim. Acta, 110 (1979) 285.
14 R. M. Dagnall, K. C. Thompson and T. S. West, Talanta, 14 (1967) 557.
15 G. F. Kirkbright, A. F. Ward and T. S. West, Anal. Chim. Acta, 64 (1973) 353.
16 R. J. Watling and H. R. Watling, Spectrochim. Acta, 35B (1980) 451.
17 W. Lund and R. Bye, Anal. Chim. Acta, 110 (1979) 279.
18 J. C. Chambers, Anal. Chem., 48 (1967) 2061.
19 T. Kamada, Talanta, 25 (1978) 15.
20 M. Ishizaki, Talanta, 25 (1978) 67.
21 J. H. Watkinson, Anal. Chem., 38 (1966) 92.
22 J. C. Lane, J. Agric. Res., 5 (1966) 177.
23 S. Forbes, G. P. Bound and T. S. West, Talanta, 26 (1979) 473.

Analytica Chimica Acta, 141 (1982) 225—232
Elsevier Scientific Publishing Company, Amsterdam — Printed in The Netherlands

SOLVENT EXTRACTION PROCEDURES FOR THE DIFFERENTIAL DETERMINATION OF ARSENIC(V) AND ARSENIC(III) SPECIES BY ELECTROTHERMAL ATOMIC ABSORPTION SPECTROMETRY

F. PUTTEMANS and D. L. MASSART*

Labo Analytische Scheikunde en Bromatologie, Farmaceutisch Instituut, Vrije Universiteit Brussel, Laarbeeklaan 103, 1090 Brussel (Belgium)

(Received 5th April 1982)

SUMMARY

Arsenic(III) can be extracted quantitatively from acidic media with ammonium pyrrolidinedithiocarbamate (APDC) and with diethyldithiophosphoric acid (HDEDTP). Arsenic(V) can only be extracted after preliminary reduction to the trivalent state. Potassium iodide or a mixture of hydrogensulphite/thiosulphate is recommended. When the extraction is done once with and once without addition of reducing agent, the arsenic(III) and the arsenic(V) contents can be differentiated. Some bottled mineral waters were analyzed. All the arsenic present appears to be in the pentavalent state.

The environmental chemistry of arsenic is complicated by the widely different properties of generally occurring arsenic compounds. Recent research has shown that both inorganic arsenite and arsenate as well as some organoarsenicals are the predominant species [1]. In general, it may be stated that organic arsenicals are more rapidly excreted than inorganic forms and that pentavalent arsenicals are cleared more quickly than trivalent ones [2]. Insofar as the degree of toxicity is approximately inversely proportional to the rate of excretion from the body, the general pattern of toxicity is as follows: $AsH_3 > As(III) > As(V) > R—As—X$. In view of this difference between arsenic(III) and arsenic(V), it can be important to differentiate between the two species in an analytical procedure.

Hydride generation methods are at present the most popular techniques for the separation of arsenic prior to its quantification by atomic absorption spectrometry (a.a.s.) in a wide range of materials [3, 4]. The arsine generated is swept into an argon—hydrogen flame or passed through a heated quartz cell in which the atomization takes place. The use of a liquid nitrogen trap has greatly improved the sensitivity and precision of the technique. Temperature-controlled selective volatilization from this trap makes it possible to differentiate between the different arsenic species.

Some of the arsenic species occur in very low concentrations so that reliable results are achieved only by means of the most sensitive methods of analysis. A useful method of separation and preconcentration is afforded by

0003-2670/82/0000-0000/$02.75

solvent extraction, prior to the quantification by electrothermal atomic absorption spectrometry, with a graphite furnace. Since arsenic(V) species cannot be extracted from acidic media, only arsenic(III) is selectively quantified. Prior to the extraction, however, arsenic(V) can be reduced with potassium iodide [5], with thiosulphate [6], or a mixture of hydrogensulphite and thiosulphate [7]. In this case, both oxidation states of arsenic are determined simultaneously and the arsenic(V) concentration is quantified by difference.

Among the other instrumental methods, differential pulse polarography seems to offer possibilities for quantifying arsenic in both oxidation states [8]. Separation and quantification of arsenic and organo-arsenic compounds have also been achieved by gas-chromatographic separation followed by flame ionization detection [9]. An excellent review of these chromatographic techniques, which have gained increasing popularity, was made by Uden and Henderson [10]. As the atomic absorption spectrometer is a much more familiar instrument to the specialist in inorganic trace analysis, it seemed of interest, however, to develop an a.a.s. procedure.

The present study makes use of two extraction systems similar to those described in the literature [6, 7]. Ammonium pyrrolidinedithiocarbamate (APDC) and *O,O*-diethyldithiophosphate (HDEDTP) are used as chelating agents for the quantitative extraction of arsenic(III) into chloroform, followed by back-extraction into an aqueous phase. Reduction of arsenic(V) to arsenic(III) allows the determination of total inorganic arsenic in environmental and mineral water samples. Optimum chelate concentration, the selection of optimum conditions for reduction and back-extraction, and the precision and accuracy of the combined extraction a.s.s procedures are discussed.

EXPERIMENTAL

Apparatus and reagents

A Perkin-Elmer 460 atomic absorption spectrometer, equipped with a PE HGA-76B graphite furnace atomizer and a deuterium background corrector was used with an arsenic electrodeless discharge lamp, operated at 8 W. For all determinations, the 193.7-nm arsenic resonance line was used with a slit width of 0.7 nm. Absorbances were read as the peak height (cm) of the signals recorded on a fast-response strip-chart recorder (PE 56). The furnace was flushed with argon (Air Liquide, N 46). The gas flow was stopped during the atomization period of the program to ensure maximum sensitivity. The temperature program consisted in drying at 150° C for 30 s, ashing at 750° C for 20 s (rate of temperature increase, 23° C s^{-1}) and atomization at 2500° C for 8 s (maximum power temperature increase and gas-stop mode). For the determination of arsenic, 50-μl fractions of the appropriate solutions were injected, followed by 50 μl of nickel nitrate solution as stabilizing agent. Aliquots are injected with Eppendorf micropipettes with disposable polypropylene tips.

Arsenic stock solution (1000 μg ml^{-1}). Dissolve 1.3203 g of As_2O_3 in 25 ml of 20% (w/v) potassium hydroxide solution. Neutralize with sulphuric acid and dilute to 1 l with 1% (v/v) sulphuric acid. Prepare daily working standards between 10 and 40 ng As ml^{-1}.

Nickel-containing stabilizing solution (2500 μg ml^{-1}). Dissolve 12.38 g of nickel nitrate in 1 l of 2% (w/v) nitric acid.

Back-extraction solutions. For use with the APDC/$CHCl_3$ system, dissolve 0.53 g of copper(II) chloride in 1 l of water. For the HDEDTP/$CHCl_3$ system, dissolve 2.68 g of copper(II) chloride per liter of water.

Reducing solutions. Prepare an aqueous 20% (w/v) solution of potassium iodide. For the hydrogensulphite/thiosulphate solution, add slowly to 40 ml of 1.48 M sodium metabisulphite solution a 20-ml portion of 4.5 M hydrochloric acid, followed by 40 ml of 0.056 M sodium thiosulphate.

Extracting solutions. Prepare an aqueous 0.1% (w/v) solution of ammonium pyrrolidinedithiocarbamate (Aldrich-Europe) freshly when required. Prepare a stock solution (0.5 M) of HDEDTP by diluting 8 ml of diethyldithiophosphate (Merck, zur synthese) with 42 ml of chloroform in a 50-ml flask. Store in a refrigerator. Prepare daily a working solution (5×10^{-3} M) in chloroform.

In order to avoid blank problems all acids (H_2SO_4, HNO_3 and $HClO_4$) were of the highest analytical purity. Except where mentioned, other chemicals used were of analytical grade (Merck). Freshly prepared twice distilled water was used for all experiments. All glassware was acid-washed before use. Cylindrical 50-ml separating funnels were used for all extractions.

Differential determination of the arsenic(III) and arsenic(V) content of bottled mineral water

Depending on the total concentration present, mix 5—50 ml of the sample with 2 ml of concentrated perchloric acid and 5 ml of the $HSO_3^-/S_2O_3^{2-}$ reducing mixture in a 100-ml flask. When only arsenic(III) is determined, omit the reducing solution. Dilute to the mark with water after a reaction time of 15 min. Mix 20 ml of the solution with 20 ml of chloroform containing 5×10^{-3} M HDEDTP. Shake vigorously for about 2 min. Back-extract a 10-ml portion of the chloroform layer with 5 ml of a 1000 ppm Cu(II) solution.

Interpolate the a.a.s. signals on a calibration graph obtained from the extraction of a blank and the appropriate standard solutions, which do or do not contain the reducing agent.

RESULTS AND DISCUSSION

Selection of the optimum concentration of APDC or HDEDTP

Figure 1A illustrates the a.a.s. signals obtained by injecting 100-μl fractions of the chloroform layer, obtained from the extraction of 20 ml of arsenic(III) standard solution (containing 10 ng As ml^{-1} or 20 ng As ml^{-1}) with 10 ml of chloroform in the presence of various amounts of APDC. The arsenic standard solutions were made 1.5% (v/v) in sulphuric acid, because quanti-

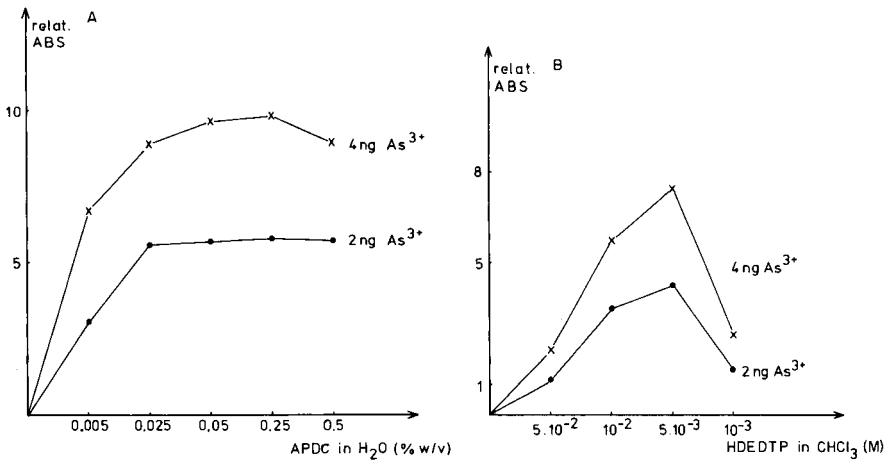

Fig. 1. Selection of the optimum concentration of extractant for As(III) from strong acidic media: (A) APDC into chloroform from 1.5% (v/v) H_2SO_4; (B) HDEDTP in chloroform from 1.0% (v/v) H_2SO_4.

tative extraction is only expected from strong acidic media [11]. Another advantage of using a sulphuric acid or perchloric acid medium is that extraction can be applied directly to the solution obtained from wet ashing with either a H_2SO_4/HNO_3 or $HClO_4/HNO_3$ mixture. It is seen that the recovery is maximal when 5 ml of 0.1% (w/v) APDC is added to 20 ml of the standard solution.

Diethyldithiophosphoric acid was selected from other dialkyldithiophosphates because of its greater selectivity [11]. Figure 1B gives the a.a.s. signals obtained by injecting 50-μl fractions of the chloroform layer obtained from the extraction of 20 ml of arsenic(III) standard solution (containing 20 ng ml^{-1} or and 40 ng ml^{-1}) with 10 ml of chloroform containing various concentrations of HDEDTP. The arsenic standard solutions contained 1.0% (v/v) H_2SO_4. An optimum is reached for a concentration of about 5×10^{-3} M HDEDTP. The optimum concentration seems to be more critical than it is for the APDC/$CHCl_3$ system.

Selection of the optimum conditions for quantitative back-extraction

Menis and Rains [12] described a procedure in which they use a solution of copper(II) chloride (1000 μg Cu ml^{-1}) in 2 M HCl for the back-extraction of arsenic from an organic layer. They exploited the fact that APDC has a greater binding affinity for copper than it has for arsenic. Arsenic is quantitatively released from its APDC complex when this is treated with a solution containing an excess of Cu(II) ions.

Figure 2A illustrates the a.a.s. signals recorded after injecting 50-μl fractions of the hydrochloric acid fraction obtained from the back-extraction of an arsenic-containing chloroform layer with a solution of 1000 ppm

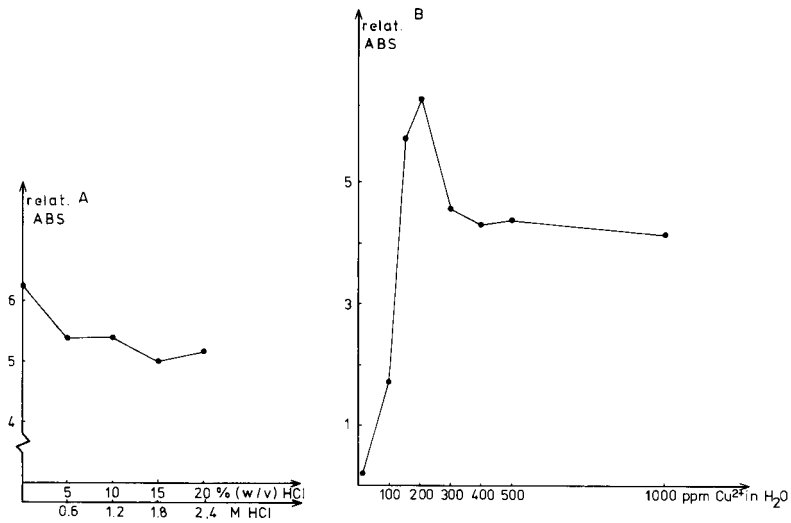

Fig. 2. Effect of reagent concentrations on the back-extraction efficiency of arsenic from the APDC—arsenic complex in chloroform: (A) effect of hydrochloric acid concentration with a 1000 ppm Cu(II) solution; (B) effect of Cu(II) concentration without hydrochloric acid.

copper(II), with various concentrations of hydrochloric acid. The best result is obtained when the copper solution does not contain any acid at all. It is known that hydrochloric acid exerts a negative influence on the absorbance signal of arsenic, so that the results of Fig. 2A are due more to the suppressing effect of hydrochloric acid on the absorbance signal of arsenic than to the back-extraction efficiency.

Figure 2B illustrates the signals recorded after injection of the aqueous layers obtained when the back-extraction is assisted by different concentrations of copper(II) in water. It is seen that the optimum copper(II) concentration is very critical and is about 200 ppm. The lower extraction recoveries for the higher concentrations of copper(II) are due to an effect of the copper concentration on back-extraction efficiency and not to a suppressing effect of the copper(II) on the absorbance signals for arsenic.

Similar experiments were conducted for the HDEDTP systems in chloroform and carbon tetrachloride. Figure 3 illustrates the back-extraction recoveries when the arsenic-containing organic layers are extracted with solutions of different copper(II) concentrations. Whereas 200 ppm Cu(II) is the optimum concentration for the APDC/$CHCl_3$ system, a concentration of 1000 ppm Cu(II) is necessary for the HDEDTP/$CHCl_3$ system.

The overall extraction recovery can be determined by comparing the calibration graph recorded after extraction and back-extraction of appropriate arsenic standard solutions with the calibration graph obtained by direct measurements of the same arsenic standard solutions. Extraction recoveries between 99.3 and 105.6% were calculated for both the APDC and HDEDTP

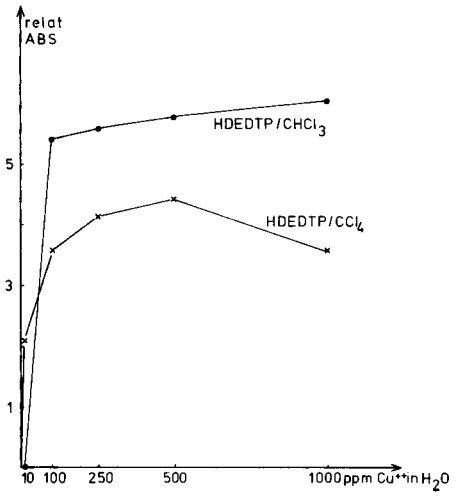

Fig. 3. Effect of the concentration of copper(II) solutions used for the back-extraction of arsenic from the HDEDTP—arsenic complex in chloroform and in carbon tetrachloride.

systems. Repeated extractions and measurements with both systems yielded coefficients of variation between 3.2 and 5.5%.

Selection of the optimum conditions for reduction and quantitative extraction of arsenic(V)

Under the same experimental conditions as those for trivalent arsenic, pentavalent arsenic is not extracted at all. In order to extract pentavalent arsenic, a reduction step must precede the extraction. Strong metallic reducing agents, such as Devarda's alloy, cannot be used because they generate hydrogen from strongly acidic media. Subsequently, the nascent hydrogen reduces arsenic(V) and arsenic(III) to volatile arsine, which must be avoided. Several other reducing agents were also tested. Attempts to use concentrated solutions of hydroxylammonium chloride or hydrazine sulphate failed. The most widely used reducing agent for arsenic(V) is potassium iodide, while Chakraborti et al. [7] suggested the use of a mixture of hydrogensulphite and thiosulphate.

When these two reducing agents were tested, the reduction and subsequent extraction was done from sulphuric acid medium and from perchloric acid medium with both APDC and HDEDTP as chelating agents. The overall extraction recoveries of these eight systems are represented in Table 1. From this table it is clear that the $HSO_3^-/S_2O_3^{2-}$ mixture can be used to reduce and extract pentavalent arsenic from either sulphuric acid or perchloric acid medium, regardless of which of the two chelating agents is used. When iodide is used as the reducing agent, quantitative extraction is observed only for the APDC system. The recoveries were calculated with regard to the absorbance signals obtained for an appropriate arsenic(III) standard solution treated in the same way as the arsenic(V) standard solutions. This is necessary because

TABLE 1

Survey of the extraction recoveries for arsenic(V) with different systems

System	Extraction recovery (%) after reduction with	
	20% KI	$HSO_3^-/S_2O_3^{2-}$
H_2SO_4/HDEDTP	79.5	99.1
H_2SO_4/APDC	96.0	95.6
$HClO_4$/HDEDTP	81.3	97.1
$HClO_4$/APDC	97.5	96.7

it was noticed that the addition of the reducing agent negatively influences the extraction of arsenic(III) itself. In practice, this means that appropriate standard solutions must be extracted under the same conditions as the sample solutions.

The accuracy of the procedure was further investigated by the analysis of the total arsenic content of NBS Reference Material 1571, Orchard Leaves. The organic matter was wet-ashed by a procedure that will be outlined in a later paper. The results were very satisfactory. Of course, this does not prove that the differentiation between As(III) and As(V) is accurate, because the destruction of the organic matter influences the oxidation state. However, it did show that the total amount of arsenic can be determined accurately.

In addition to the determination of the total arsenic content of biological materials, this extraction procedure offers the possibility of differentiating between As(III) and As(V) in samples which do not need a preliminary oxidative treatment, e.g., environmental and bottled mineral water samples. Indeed, only arsenic(III) is selectively measured when the acidified samples are extracted without the addition of reducing agents. In the presence of these agents, however, the sum of the two arsenic species is measured. The difference between the measurements gives the arsenic(V) content. This differentiation procedure (see Experimental) was first tried on synthetic mixtures of As(III) and As(V) in water. The results, summarized in Table 2,

TABLE 2

Results of the differentiation between As(III) and As(V) for standard mixtures of both species

Concentrations taken (ng ml^{-1})		Concentrations found (ng ml^{-1})		As(V) content calculated (ng ml^{-1})
As(III)	As(V)	As(III)	[As(III) + As(V)]	
10	30	9.3	38.7	28.4
20	20	19.5	39.7	20.2
30	10	28.5	39.6	11.2

TABLE 3

Arsenic content of some bottled mineral waters

Sample	Arsenic content found after extraction (ng ml^{-1})		Direct measurement of the total arsenic content by a.a.s. (ng ml^{-1})
	As(III)	[As(III) + As(V)]	
Vichy Celestine[a]	—	487.5	475.0
Vichy Saint-Yorre[a]	—	105.0	107.5
Apollinaris[a]	—	42.3	41.1

[a]Commercially available mineral waters.

are satisfactory. Some bottled mineral waters (n = 11) were analyzed for their arsenic content. Only in three of these was there sufficient arsenic to make the differentiation of interest (Table 3), but no arsenic(III) was found in any of these drinking waters. In order to exclude systematic errors in measuring the arsenic content of an unknown matrix relative to aqueous standards, the total arsenic content was measured by means of a standard addition procedure. It can be seen that there is good agreement between the total arsenic content found by direct measurements and the total concentration found after extraction.

The finding that no arsenic(III) is present in the mineral water samples examined agrees well with the statement of Braman and Foreback [13] that arsenate is probably the most common environmental form of inorganic arsenic. It is also an interesting result from a toxicological point of view in that it is generally accepted [2] that arsenic(V) species are less toxic than arsenic(III) species.

The authors thank F. G. W. O. for financial support and M. Devreese for technical assistance.

REFERENCES

1 L. Friberg, G. F. Nordberg and V. B. Vouck, Handbook on the Toxicology of Metals, Elsevier/North-Holland Biomedical Press, Amsterdam, 1979, p. 293.
2 B. A. Fowler, in R. A. Goyer and M. A. Mehlman, Advances in Modern Toxicology, Vol. 2, Wiley, New York, p. 79.
3 R. G. Godden and D. R. Thomerson, Analyst, 105 (1980) 1137.
4 R. R. Brooks, D. E. Ryan and H. Zhang, Anal. Chim. Acta, 131 (1980) 1.
5 A. Yasui, C. Tsutsume and S. Toda, Agric. Biol. Chem., 42 (1978) 2139.
6 K. S. Subramanian and J. C. Meranger, Anal. Chim. Acta, 124 (1981) 131.
7 D. Chakraborti, W. de Jonghe and F. Adams, Anal. Chim. Acta, 120 (1980) 121.
8 F. T. Henry, T. O. Kirch and T. M. Thorpe, Anal. Chem., 51 (1979) 215.
9 F. T. Henry and T. M. Thorpe, J. Chromatogr., 166 (1978) 577.
10 P. C. Uden and D. E. Henderson, Analyst, 102 (1977) 889.
11 J. Stary, The Solvent Extraction of Metal Chelates, McMillan Co., New York, 1964, p. 170.
12 O. Menis and T. C. Rains, Anal. Chem., 41 (1969) 952.
13 R. S. Braman and C. C. Foreback, Science, 182 (1973) 1247.

Analytica Chimica Acta, 141 (1982) 233—240
Elsevier Scientific Publishing Company, Amsterdam — Printed in The Netherlands

MECHANISM AND REMOVAL OF HALIDE INTERFERENCES IN THE DETERMINATION OF METALS BY ATOMIC ABSORPTION SPECTROMETRY WITH ELECTROTHERMAL ATOMIZATION

KOJI MATSUSAKI

Department of Industrial Chemistry, Technical College, Yamaguchi University, Tokiwadai, Ube 755 (Japan)

(Received 18th January 1982)

SUMMARY

The effects of halides on the graphite-furnace atomic absorption determination of Al, Be, Sr, Cr, Mn, Ni, Co, Cu, Zn, Pb, Cd and Ag have been studied from the view-point of chemical reactions in solution, particularly in terms of the hard and soft acid and base concept. The harder halides interfere strongly with the harder metals, and the softer halides with the softer metals. This indicates that the halide interferences arise initially from metal—halide complex formation in solution; this was confirmed by an examination of halide concentration effects on the atomic absorption signal. The ammonium salt of EDTA is a most suitable additive for removal of halide interferences, because it prevents metal—halide complexation, and readily volatile ammonium halide is produced.

Interference arising from a chloride matrix is frequently encountered in graphite-furnace atomic absorption spectrometry. Accordingly, elucidation of the interference mechanism and the establishment of a treatment to remove the interference are very important because some samples, such as seawater and blood, contain a large concentration of chloride and because hydrochloric acid is widely used for sample dissolution. Several mechanisms have been identified such as the formation of a volatile compound [1—3], a vapor-phase process [4—6] and occlusion of analyte in the matrix [7—10]. Also, in studies of aluminum [11], strontium [12], chromium [13] and beryllium [14], it was found that interference arises from reactions taking place in solution, by coordination of chloride not only to the analyte ion but also to co-existing cations. Similar interferences by fluoride, bromide and iodide are to be expected because they complex strongly with a number of metal ions.

In the present work, the effects of halides on the atomic absorption spectrometric signals of various metals were studied, by using a graphite atomizer. The interference mechanisms are interpreted in terms of the hard and soft acid and base concept [15], based on reactions in solution. A method for the removal of halide interferences is reported.

0003-2670/82/0000-0000/$02.75

EXPERIMENTAL

Apparatus and reagents

A Varian-Techtron model 63 carbon-rod atomizer was used in conjunction with a Varian-Techtron model 1200 atomic absorption spectrometer. A tube type of graphite cell was used and the absorption was measured under a nitrogen atmosphere. The signal was recorded with a Hitachi 056 recorder. Hitachi hollow-cathode lamps were used for each metal studied and a Varian-Techtron deuterium lamp was applied for background correction. Samples were added with a 5-μl Excalibur Autopet fitted with disposable tips.

All solutions were prepared from analytical reagent-grade chemicals and demineralized water, and stored in polyethylene bottles. The 1000-μg ml^{-1} stock metal solutions were prepared as follows: aluminum, manganese, cobalt, copper and zinc were prepared by dissolving the pure metals in nitric acid; nickel, lead, cadmium and silver from their nitrates; beryllium as its sulfate; and strontium as its carbonate. All solutions were finally made 0.1 M in nitric acid.

Procedure

A 5-μl sample was deposited in the center of the graphite tube and dried, ashed and atomized with nitrogen flowing over the furnace. The instrumental settings for each metal are summarized in Table 1 together with the concentrations used. The absorption signals during the atomization step were recorded and the peak height was taken as the analytical signal. A reagent

TABLE 1

Experimental conditions for the atomic absorption measurements

Analyte	Conc. (μg ml^{-1})	Wavelength (nm)	Slit width (nm)	N_2 flow rate (l min^{-1})	Atomization voltage[a] (V)
Al	2.5	309.3	0.5	5.5	7.0
Be	0.02	234.9	0.5	6.0	8.0
Sr	0.2	460.7	0.2	6.0	7.0
Cr	0.10	357.9	0.2	6.0	7.0
Mn	0.20	403.1	0.2	4.5	5.5
Ni	2.0	341.5	0.5	6.0	8.0
Co	10.0	346.5	0.2	6.0	7.0
Cu	0.13	324.7	0.5	4.0	5.4
Zn	50.0	307.6	0.2	4.0	4.5
Pb	0.25	283.3	0.5	4.0	4.2
Cd	4.0	326.1	0.2	4.0	5.0
Ag	0.10	338.3	0.2	5.0	5.0

[a]Drying for 30 s at 0.65 V (ca. 110° C); ashing for 30 s at 1.30 V (ca. 350° C); atomization time 4 s.

blank was run under the same conditions and a suitable correction applied. The applied voltage between the atomizer terminals was measured with a digital voltmeter connected in parallel and the temperature of the center of the graphite tube was measured with a platinum/platinum–rhodium thermocouple. The absorbances of metal solution containing the various sodium halides were measured and the ratios of their absorbances to the absorbance in the absence of halide (i.e., the relative absorbances) were calculated.

RESULTS AND DISCUSSION

Effect of halide on atomic absorption

The interferences of halides on the atomic absorption of a particular metal may result from the coordination of the halide ion to the metal ion in the sample solution. Therefore, the metal–halide affinities may reflect the magnitude of the interferences. These affinities are reasonably explained in terms of the hardness and softness of acids and bases [15]: the harder acids bind more strongly with the harder bases, and the softer acids with the softer bases. Of the metal ions investigated, aluminum, beryllium, strontium, chromium(III) and manganese(II) are "hard acids"; copper(II), zinc, lead, cadmium and silver(I) are "soft"; and cobalt(II) and nickel(II) are intermediate. The quantities E_n^* and E_m^* introduced by Klopman [16] are used as measures of hardness and softness of metal and halide ions, respectively, in aqueous solution. Metal ions with higher E_n^* values are harder acids, anions with lower E_m^* values are harder bases.

In order to determine the ashing conditions for suitable measurements of interferences, the effects of ashing temperature were examined, for an ashing time of 30 s. Some results for chloride are shown in Fig. 1. The behavior may be classified into three types. In the first, the absorbance

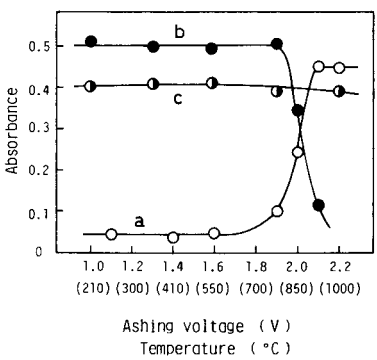

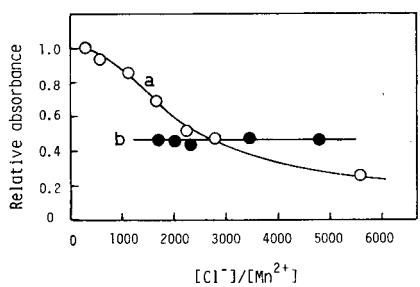

Fig. 1. Effect of ashing voltage (temperature) on the atomic absorption of (a) strontium, (b) zinc and (c) cobalt in the presence of 0.1 M NaCl.

Fig. 2. Effect of $[Cl^-]/[Mn^{2+}]$ molar ratio on the relative absorbance of manganese in the presence of NaCl. (a) $[Mn^{2+}] = 3.6 \times 10^{-6}$ M; (b) $[Cl^-] = 1.0 \times 10^{-2}$ M.

increases at higher temperatures, as seen for strontium. In the second, the absorbance decreases at higher temperatures, as seen for zinc. In the third, the absorbance is almost independent of temperature below 1100° C, as seen for cobalt. For the other halides, the extent of their interference varies but their general behavior is similar to that of chloride. It is interesting that the metals of the first type are hard acids, those of the second type are soft, and those of the third type are the intermediate species. Ashing was always carried out at a temperature which did not influence the atomic absorbance of the metal; this was 30 s at 350° C (1.3 V) unless otherwise specified.

The degree of halide interference for the various metals could be compared when the solutions contained the same molar concentration of the metal. However, it was difficult to use the same concentration for all metals because their atomic absorption sensitivities differ greatly. Thus, the molar ratio of halide to metal in the solution was used as a comparative parameter in the measurement of the degree of halide interference. The extent of the chloride interference on manganese is shown in Fig. 2. When the concentration of manganese is constant, the relative absorbance decreases with increasing chloride concentration. When the concentration of chloride is kept constant and that of manganese is varied, the absorbance relative to that of manganese without chloride is unchanged. The interferences for the other metals showed similar behavior to the chloride interference on manganese. These facts suggest that the halide interference does not depend on the molar ratio of halide to metal, but only on the concentration of halide in the solution. They also indicate that the standard addition method can be useful for the determination of metals in the presence of halides. Therefore, the concentrations of halide ions in the test solutions were maintained at 0.01 M, and that of the metal at about 10^{-6} M.

The relative absorbances of the metals in the presence of each halide are plotted against the E_n^* values of the metal ions in Fig. 3A–D. Fluoride, which is the hardest halide ($E_m^* = -12.8$ eV), shows the greater suppression of absorbance of the harder metal ions (Fig. 3A). It is interesting to note that the absorbance of silver, which is the "softest" metal ion studied, is enhanced. As seen in Fig. 3D, iodide, the softest halide ($E_m^* = -8.31$ eV), shows the greatest interference for the softer metal ions. Chloride ($E_m^* = -9.94$ eV) and bromide ($E_m^* = -9.22$ eV), which have intermediate values of E_m^*, show intermediate interference behavior (Fig. 3B, C). Although the solubility products for AgBr and AgI are greatly exceeded, absorption peaks are observed. This may be explained by the formation of $AgBr_2^-$ and AgI_2^- in the test solution [17, 18], because the amounts of bromide and iodide are greatly in excess of that of silver.

The relative absorbances of each metal in the presence of the halides were also plotted against the E_m^* value of the halide ion. The extent of suppression of the absorbance by the halide for the hard metals was in the order shown for strontium (Fig. 4, plot a), i.e., fluoride > chloride > bromide > iodide. For the soft metal ions, the order was reversed, as seen for cadmium (Fig. 4,

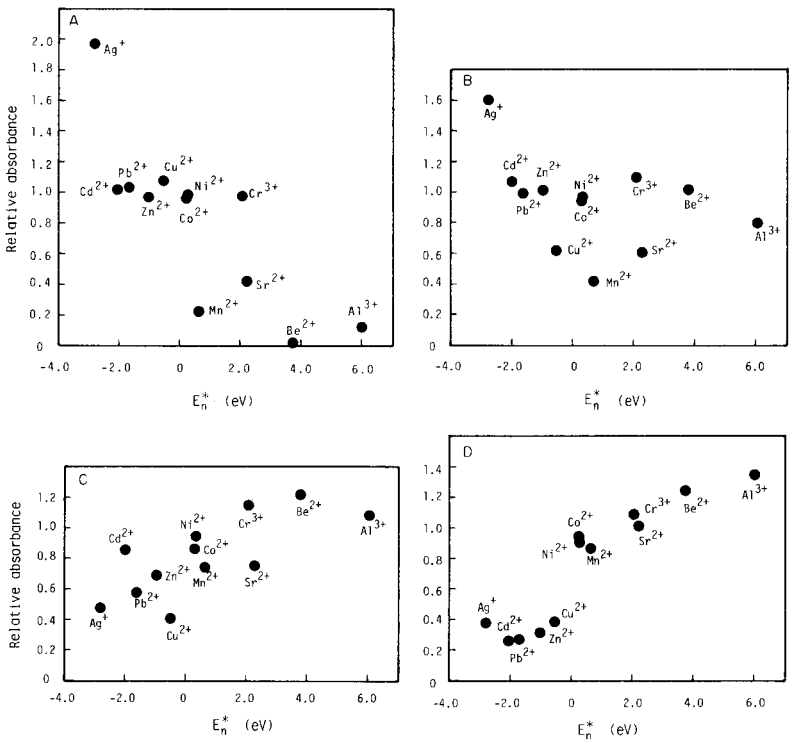

Fig. 3. Plot of E_n^* vs. relative absorbance of the metal ion in the presence of halides: (A) 0.01 M NaF; (B) 0.01 M NaCl; (C) 0.01 M NaBr; (D) 0.01 M NaI.

plot b). For the intermediate metals the extent of interference did not depend on the kind of halide. Thus the harder bases interfere strongly with the atomic absorption of the harder acids and the softer bases with that of the softer acids.

The halide interferences may arise from the formation of metal–halide complexes in solution, in the same manner as the chloride interference on aluminum [11], strontium [12], chromium [13] and beryllium [14]. In order to confirm this mechanism, the effect of halide ion (X^-) concentration on the atomic absorption signals was examined. Complex formation with metal ions M^{m+} may be described (ignoring coordinated water molecules) by $M^{m+} + nX^- \rightleftharpoons MX_n^{(m-n)+}$. The equilibrium constant is $K = [MX_n^{(m-n)+}]/[M^{m+}][X^-]^n$. The absorbance of each of the solutions is given by $A = a_1[M^{m+}] + a_2[MX_n^{(m-n)+}]$, where a_1 and a_2 are constants. Also $[M^{m+}]_t = [M^{m+}] + [MX_n^{(m-n)+}]$, where $[M^{m+}]_t$ is the total concentration of metal ion. For a solution containing no halide, $A_1 = a_1[M^{m+}]_t$, and for a solution in which the formation of halide complexes is complete, $A_2 = a_2[M^{m+}]_t$. Combination of these equations gives $(A_1 - A)/(A - A_2) = [MX_n^{(m-n)+}]/[M^{m+}]$. The total concentration of halide added, $[X^-]_t$, is approximately equal to $[X^-]$ under the present conditions, because the halide is in very large excess over the metal ion. Thus the equation becomes $\log[(A_1 - A)/(A - A_2)] = \log K + n \log[X^-]_t$.

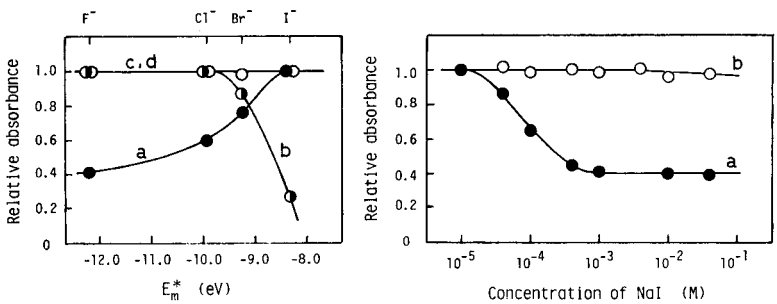

Fig. 4. Plot of E_m^* vs. relative absorbance of strontium and cadmium in the presence of 0.01 M sodium halide: (a) and (c) Sr; (b) and (d) Cd; (a) and (b) without EDTA; (c) and (d) 0.01 M Na_2EDTA added.

Fig. 5. Effect of NaI concentration on the relative absorbance of copper: (a) no addition; (b) 0.04 M $(NH_4)_2EDTA$ added.

Figure 5 shows the effect of iodide concentration on the relative absorbance of copper. The relative absorbance decreases with increasing concentration of iodide and becomes constant above 4×10^{-4} M, indicating that complex formation is complete above this concentration. Plots of log $[(A_1 - A)/(A - A_2)]$ vs. log $[X^-]_t$ for manganese with each halide result in straight lines with slope $n = 1$ (Fig. 6), while plots for cadmium, lead and copper with iodide are straight lines with slope $n = 2$ (Fig. 7). The other metals also gave linear plots with slope $n = 1$ or 2. These data suggest that halide interferences are attributable in these instances to the formation of mono- or

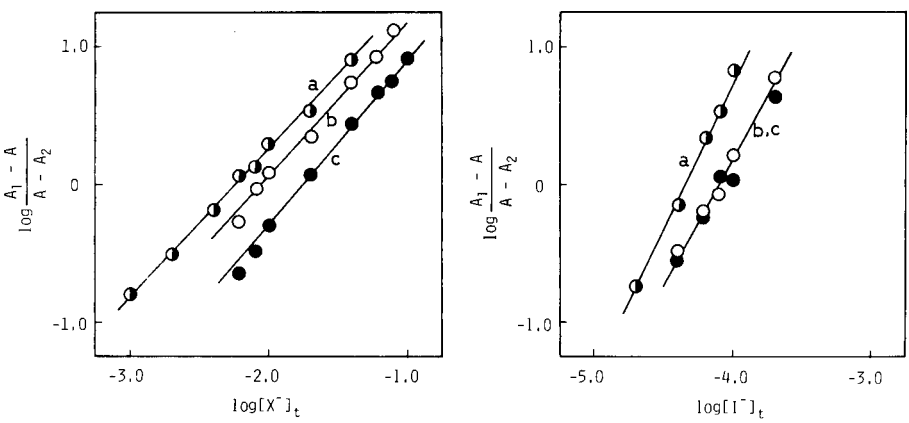

Fig. 6. Relationship between log $[(A_1 - A)/(A - A_2)]$ for manganese and log $[X^-]_t$. $[X^-]_t$ is the concentration of NaX added (mol l^{-1}): (a) NaF; (b) NaCl; (c) NaBr.

Fig. 7. Relationship between log $[(A_1 - A)/(A - A_2)]$ and log $[I^-]_t$ for (a) cadmium; (b) lead; (c) copper.

di-halo complexes of the analyte ion. Chloride interferences in strontium and chromium determinations have been interpreted in terms of monochloro complex formation [12, 13], and halide interferences in beryllium determinations, dihalo complex formation [14]. The halide interferences for the various metals were compared with the stability constants [19] of their mono- or di-halo complexes in aqueous solutions. Not surprisingly, the halide ions forming the strongest complexes show the greatest interferences.

Removal of the interferences

The halide interferences are shown above to be caused by metal–halide bonding in the sample solution. The addition of a masking agent to the sample solution to prevent this coordination would be expected to remove the halide interference as was achieved for the chloride interferences in aluminum [11], strontium [12], chromium [13] and beryllium [14]. The addition of EDTA to the standard and sample solutions should not only prevent halogen bonding but should also ensure that the analyte is present as the same chemical species in all solutions, thus ensuring uniform atomization. As can be seen in Fig. 4, the addition of EDTA removes the halide interferences for strontium and cadmium. This was also observed for the other metals. When EDTA was present, ashing was set for 30 s at 1.6 V (ca. 550° C) in order completely to ash the EDTA salt. Figure 8 shows the efficiency of EDTA in removing the interferences on aluminum, beryllium, strontium, chromium, manganese, nickel, cobalt and copper in the presence of various concentrations of chloride. Depressions of absorbance by chloride below 0.1 M are overcome by addition of 0.04 M Na_2EDTA. In all cases, the addition of an ammonium salt of EDTA is more effective.

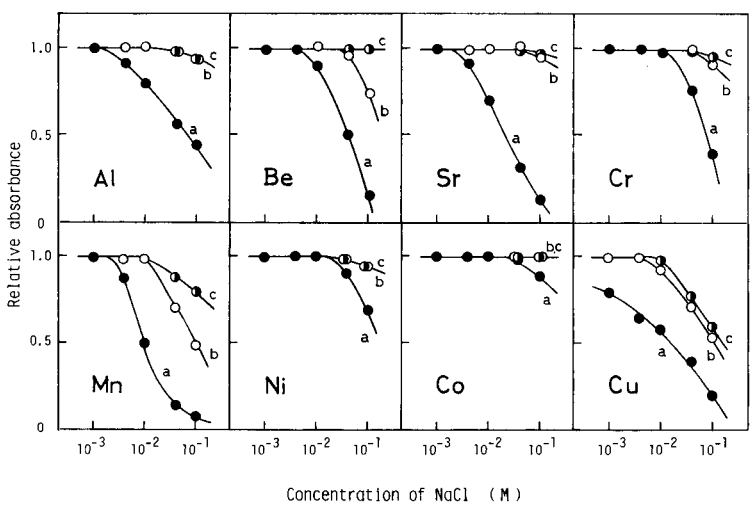

Fig. 8. Removal of NaCl interference on various metals by addition of 0.04 M Na_2EDTA or $(NH_4)_2EDTA$: (a) no addition; (b) Na_2EDTA added; (c) $(NH_4)_2EDTA$ added.

Chloride interferences have been removed by volatilizing out the coexisting chloride before the atomization step [11—14]. As the effects of ashing temperature on the atomic absorption of metals in the presence of other halides were similar to that for chloride, as described above, so the behavior of the other halides in the graphite furnace may be explained along the same lines as that of chloride. Accordingly, the ammonium salt of EDTA may be a more efficient additive than its sodium salt, because the ammonium halide formed is readily vaporized during the drying and ashing steps, and the background molecular absorption of the halide during atomization is also greatly decreased. This behavior should be more efficient for cations which bond strongly with EDTA. As can be seen in Fig. 5, the interference by iodide on copper is completely overcome by adding 0.04 M $(NH_4)_2$EDTA. In this case, the addition of Na_2EDTA caused problems with the measurement of copper absorbance, because the background caused by molecular absorption by sodium iodide was large.

The author expresses his gratitude to Professor Yuroku Yamamoto of Hiroshima University and Professor Takashi Yoshino of Yamaguchi University for suggesting this investigation and for valuable discussions.

REFERENCES

1 D. A. Segar and J. G. Gonzalez, Anal. Chim. Acta, 58 (1972) 7.
2 J. Aggett and A. J. Sprott, Anal. Chim. Acta, 72 (1974) 49.
3 C. W. Fuller, Anal. Chim. Acta, 81 (1976) 199.
4 J.-A. Persson, W. Frech and A. Cedergren, Anal. Chim. Acta, 92 (1977) 85, 95.
5 W. Frech and A. Cedergren, Anal. Chim. Acta, 82 (1976) 83.
6 E. J. Czobik and J. P. Matouseck, Anal. Chem., 50 (1978) 2.
7 R. B. Cruz and J. C. van Loon, Anal. Chim. Acta, 72 (1974) 231.
8 J. Smeyers-Verbeke, Y. Michotte, P. van den Winkel and D. L. Massart, Anal. Chem., 48 (1976) 125.
9 D. J. Churella and T. R. Copeland, Anal. Chem., 50 (1978) 309.
10 J. A. Krasowski and T. R. Copeland, Anal. Chem., 51 (1979) 1843.
11 K. Matsusaki, T. Yoshino and Y. Yamamoto, Talanta, 26 (1979) 377.
12 K. Matsusaki, S. Murakami and T. Yoshino, Nippon Kagaku Kaishi, (1980) 1126.
13 K. Matsusaki, T. Yoshino and Y. Yamamoto, Anal. Chim. Acta, 124 (1981) 163.
14 K. Matsusaki, N. Kameshima, S. Murakami and T. Yoshino, Nippon Kagaku Kaishi, (1981) 1715.
15 R. G. Pearson, J. Am. Chem. Soc., 85 (1963) 3533.
16 G. Klopman, J. Am. Chem. Soc., 90 (1968) 223.
17 E. Berne and I. Leden, Z. Naturforsch., Teil A, 8 (1953) 719.
18 I. Leden, Acta Chem. Scand., 10 (1956) 812.
19 L. G. Sillén and A. E. Martell, Stability Constants of Metal—Ion Complexes, The Chemical Society, London, 1964; Suppl. No. 1, 1971.

Analytica Chimica Acta, 141 (1982) 241—254
Elsevier Scientific Publishing Company, Amsterdam — Printed in The Netherlands

LOW-TEMPERATURE CONSTANT ENERGY SYNCHRONOUS LUMINESCENCE SPECTROSCOPY

EUGENE L. INMAN, JR. and JAMES D. WINEFORDNER*
Department of Chemistry, University of Florida, Gainesville, FL 32611 (U.S.A.)
(Received 11th March 1982)

SUMMARY

Constant energy synchronous luminescence spectroscopy is extended to low temperature conditions for the determination of polynuclear aromatic hydrocarbons. Low-temperature constant energy synchronous luminescence spectroscopy implements a constant energy difference between monochromators as each is scanned through the spectral region of interest. The major advantage of this development is the optimization of parameter selection used in each determination. While this investigation was performed at 77 K, theoretical considerations are extended to 4 K conditions. Application to multicomponent samples is also demonstrated.

In the determination of polynuclear aromatic hydrocarbons (PAHs), one often takes advantage of their intense luminescence, characteristic of this class of compounds. While offering excellent sensitivity, selectivity is limited by the extensive spectral overlap at room temperature. This is improved dramatically by reducing the sample temperature to liquid nitrogen (77 K) or liquid helium (4 K) temperatures. For PAH determination, this can be combined with the Shpol'skii effect by selecting an appropriate *n*-alkane solvent. This results in quasi-linear luminescence spectra where bands are reduced to 1—10 cm^{-1} bandwidths [1—4].

By combining the low-temperature spectral narrowing features with the unique characteristics of a laser excitation source, several techniques have been developed for the determination of PAHs in complex mixtures [5]. Laser-excited Shpol'skii spectroscopy (l.e.s.s.) has been successfully used in the direct determination of PAHs in liquid fuels [6—8]. Fluorescence line narrowing spectroscopy (f.l.n.s.) takes full advantage of the narrow line properties of laser excitation to yield spectra of reduced complexity [9—10]. Matrix isolation spectroscopy (m.i.s.) involves the dilution of the vaporized sample with an inert gas and its deposition on a cryogenic surface, where quasi-linear spectra are free from original matrix effects [11—13]. Each of these techniques makes use of selective excitation [14]. In selective excitation, the excitation source output, i.e., laser, is chosen to coincide exactly with the electronic absorption band of the molecule of interest, exciting that molecule but not exciting other molecules, the absorption bands of which fall outside

0003-2670/82/0000-0000/$02.75

this region. In this way, the conditions are optimized for the specific compound of interest.

In this work, an evaluation was made of combining the excellent band-narrowing features of low-temperature Shpol'skii matrices with synchronous luminescence spectroscopy. Synchronous luminescence spectroscopy requires the simultaneous scan of the excitation and emission monochromators, synchronized so that a well-defined relationship is maintained between the two wavelengths [15]. Conventionally, this relationship has been a constant wavelength difference, $\Delta\lambda$. In this manner, one takes full advantage of the use of two wavelength parameters to enhance selectivity. While synchronous luminescence spectroscopy has been described for determinations at room temperature [16], its application to low-temperature luminescence spectroscopy has been limited.

To provide a screening method for selective excitation techniques, synchronous luminescence spectroscopy using a broad-band excitation source has been used with a modified wavelength relationship to match the features present in low-temperature PAH spectra. Those provide a simple, relatively inexpensive technique that is complementary to the more expensive laser-excited techniques. Low-temperature constant energy synchronous luminescence spectroscopy (l.t.c.e.s.l.s.), in which a constant energy difference is maintained between the excitation and emission wavelengths, has been developed and is described.

EXPERIMENTAL

Reagents and instrumentation

A complete list of PAHs and solvents with their sources has been tabulated [17]. *n*-Heptane was selected as a compromise solvent because of its demonstrated Shpol'skii capabilities; it is not expected to be the optimum solvent for all the compounds studied.

A moderate-resolution laboratory-constructed fluorimeter was used to obtain conventional, as well as synchronous spectra, as shown in Fig. 1. A complete list of components and their manufacturers is given in Table 1. Monochromator control was achieved via a parallel interface with the microcomputer, with assembly language routines utilized for timing synchronization and data collection and storage. A constant energy difference is maintained between the monochromators by using a linear approximation. The emission monochromator is scanned at a constant rate while the excitation monochromator is variably scanned. To implement, the emission monochromator is incremented by a constant user-selected value, generally 0.1 nm. After each increment, the excitation monochromator is advanced the required number of steps to maintain the appropriate energy difference. The excitation steps are obtained from a "look-up" table, generated at the beginning of each scan. As the selected emission scan step is reduced, the scan appears continuous.

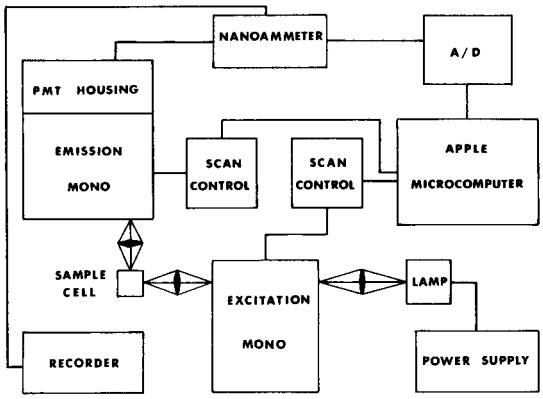

Fig. 1. Block diagram of instrumentation.

Methods

For all the spectra obtained, an excitation monochromator bandpass of 4 nm and an emission monochromator bandpass of 0.2 nm were used. A scan rate of 0.1 nm s^{-1} was used with a 0.5-s time constant. All spectra are uncorrected for instrumental response.

Samples are placed in a precision-bore Spectrosil quartz sample tube (Thermal American Fused Quartz Co., Montville, NJ 07045), 30 cm long, 5-mm o.d. and 3-mm i.d., that was sealed at one end. Each tube is rapidly cooled by placing it directly in a liquid nitrogen-filled dewar to prevent inhomogeneous freezing. Throughout this work, low-temperature experiments were done at 77 K using liquid nitrogen. To avoid frost from forming on the optical tip of the dewar, a gentle stream of nitrogen gas was flushed into the sample compartment.

BACKGROUND

Synchronous luminescence spectroscopy (s.l.s.) has been described as a method to enhance selectivity in PAH determination [18]. While improvements have been demonstrated over conventional luminescence spectroscopy, the broad-band nature of spectra obtained at room temperature restricts its use in multicomponent analysis. Low-temperature luminescence techniques yield quasi-linear, line-rich spectra, useful for fingerprint identification of PAHs. While narrowing the bands, a natural extension of s.l.s., Shpol'skii solvent spectral complexity makes low-temperature s.l.s. difficult to use routinely. Many of the concepts applicable to s.l.s. at room temperature become limited at reduced temperatures.

The development of conventional s.l.s. has been on a rather empirical basis, utilized in the screening of oil samples [19]. Vo-Dinh has discussed the fundamental principles of the technique from a more theoretical viewpoint [20]. A major consideration in optimizing conventional s.l.s. is the selection

TABLE 1

Experimental equipment used for l.t.c.e.s.l. spectrometer

Item	Model	Source
Eimac xenon arc lamp 300 W	R300-2	Eimac, Division of Varian, San Carlos, CA 94070
Eimac illuminator power supply operated at 15 A	PS 300-1	Eimac, Division of Varian
Excitation monochromator *f*/6.8, blaze λ = 250.0 nm 1180 lines/mm	EU-700	Heath Company, Benton Harbor, MI 49022
Monochromator scan controls	EU-700-51	Heath Company
Sample housing		American Instrument, Silver Spring, MD 20910
Emission monochromator *f*/6.8, blaze λ = 250.0 nm 1180 lines/mm	EU-700-77	GCA/McPherson Instrument, Acton, MA 01720
Programmable filter attachment	EU-700-56	GCA/McPherson Instrument
Photomultiplier module	EU-700-30	Heath Company
Photomultiplier tube	RCA-1-28	RCA, Lancaster, PA 17604
Nanoammeter		Laboratory constructed
Recorder	OmniScribe B5217-5I	Houston Instrument, Austin, TX 78753
A/D system	Laboratory constructed with a MDAS-8D 8-channel diff. 12-bit data acquisition system	Datel Systems, Mansfield, MA 02048
Microcomputer	Apple II with 48K RAM	Apple Computer, Cupertino, CA 95014

of the wavelength interval between the two monochromators, $\Delta\lambda$. A $\Delta\lambda$ suggested for routine PAH determination is 3 nm, approximately equivalent to the Stokes shift exhibited by PAHs in *n*-alkane solvents at room temperature. Recently, work has been described in an attempt to explain more fully the selection of $\Delta\lambda$ where small values are inappropriate [21]. Thus some PAHs do not exhibit strong 0—0 transitions and so $\Delta\lambda$ = 3 nm is not suitable; more spectral features result with a larger $\Delta\lambda$, and stray light is less of a problem at larger $\Delta\lambda$'s; $\Delta\lambda$ of 3 nm is also inappropriate at reduced temperatures. Therefore, many of the same concepts were extended to low-temperature determinations.

Mathematically, the data points defining an s.l.s. spectrum can be written as

$$M_{ij} = \sum_{k=1}^{r} \alpha_k x_{ik} y_{jk} \quad (1)$$

where M_{ij} is the measured relative luminescence intensity at excitation wavelength λ_i and emission wavelength λ_j, r is the number of luminescing com-

ponents present in the sample, α_k is the product of wavelength-independent terms for the k'th component and contains concentration information, x_{ik} is the product of excitation wavelength dependent terms at λ_i for the k'th component, and y_{jk} is the product of emission wavelength-dependent terms at λ_j for the k'th component [22]. In conventional s.l.s., a constant wavelength difference is maintained between the excitation and emission wavelengths. Thus, Eqn. (1) is restricted to

$$\lambda_j - \lambda_i = \Delta\lambda = \text{constant} \quad (2)$$

Luminescence spectra of PAHs exhibit regularly-spaced vibrational features at room temperature. This had led to the development of constant energy synchronous luminescence spectroscopy (c.e.s.l.s.), in which a constant energy difference is maintained between wavelengths. In this way, the restriction analogous to Eqn. (2) becomes

$$(1/\lambda_i - 1/\lambda_j) \times 10^7 = \Delta\bar{\nu} = \text{constant} \quad (3)$$

The spectral structure of PAHs is even more pronounced when Shpol'skii solvents are used at low temperature.

RESULTS AND DISCUSSION

A vibrational separation of about 1400 cm^{-1} is observed in PAH fluorescence spectra at room temperature. This separation is also observed in low temperature spectra. Table 2 lists several examples of this pattern in low-temperature fluorescence emission spectra. While the alkane solvent selected in use of the Shpol'skii effect may affect the narrowing properties of the luminescence spectra of analyte and solvent fields affect the electronic transition, the rela-

TABLE 2

Energy separation between spectral features in low-temperature fluorescence emission spectra

Compound	Peak wavelength (nm)	Difference (cm^{-1})	Compound	Peak wavelength (nm)	Difference (cm^{-1})
Pyrene	371.0—391.6	1420	Anthran-	429.5—456.6	1380
	371.6—392.4	1430	threne	432.2—459.7	1380
	376.7—398.0	1420		433.4—461.1	1390
	377.5—398.7	1410			
	382.4—404.4	1420	Chrysene	360.6—381.1	1420
	383.2—405.4	1430		364.8—384.4	1400
				368.5—388.6	1400
2,3-Benzo-	339.9—357.5	1450		372.9—393.2	1380
fluorene	348.9—367.4	1440			
	357.5—376.7	1430	9-Methyl-	388.7—411.1	1400
			anthracene	411.1—436.2	1400
Anthra-	375.4—396.0	1390			
cene	378.4—399.8	1420			
	380.5—402.1	1410			
	386.3—408.4	1400			

tive spacing of vibrational bands remains virtually unchanged [23] even though the exact positions of spectral features shift with solvent.

By lowering the sample temperature to 77 K, the Stokes shift between 0—0 excitation and emission peaks becomes small. At room temperature, PAHs in *n*-alkane solvents generally exhibit a 100—300-cm^{-1} Stokes shift. Because of this, a $\Delta\lambda$ of 3 nm is a good approximation in conventional s.l.s. This corresponds to about a 200-cm^{-1} value for $\Delta\bar{\nu}$ in c.e.s.l.s. At reduced temperatures, however, a $\Delta\bar{\nu}$ of 0 cm^{-1} would be necessary. This is impractical, owing to the intense Rayleigh scatter observed under these conditions. Integral multiples of 1400 cm^{-1} for $\Delta\bar{\nu}$ have been effectively used at room temperature, matching the vibrational distribution within luminescence spectra. A similar choice for $\Delta\bar{\nu}$ was used in low-temperature constant energy synchronous luminescence spectroscopy (l.t.c.e.s.l.s.).

As an approximation [24], the effective bandwidths of s.l.s. peaks are a function of both the excitation and emission bandwidths as

$$\delta\bar{\nu}_s = \delta\bar{\nu}_i\,\delta\bar{\nu}_j/(\delta\bar{\nu}_i^2 + \delta\bar{\nu}_j^2)^{1/2} \qquad (4)$$

where $\delta\bar{\nu}_s$ is the effective synchronous bandwidth (cm^{-1}), $\delta\bar{\nu}_i$ is the excitation bandwidth (cm^{-1}), and $\delta\bar{\nu}_j$ is the emission bandwidth (cm^{-1}). The main interest in this work was in the narrowing characteristic of the luminescence emission spectrum [24]. Therefore, conditions were selected with $\delta\bar{\nu}_i$ about twenty times larger than $\delta\bar{\nu}_j$. Under these conditions, $\delta\bar{\nu}_s$ is approximately equal to $\delta\bar{\nu}_j$. Selecting these values for $\delta\bar{\nu}_i$ and $\delta\bar{\nu}_j$ provides sufficient source intensity for adequate sensitivity, yet retaining relatively high emission monochromator resolution. Because excitation bands are often broader than emission bands, one gains little by reducing the excitation bandpass without going to a laser source.

L.t.c.e.s.l. spectra demonstrate several interesting features. Several examples illustrate these features. In using integral multiples of 1400 cm^{-1} for $\Delta\bar{\nu}$, the C—C stretch fundamental, the 1400-cm^{-1} interval is defined as a vibrational unit, with a $\Delta\bar{\nu}$ selected as a number of vibrational units from the resonant 0—0 transition. If a $\Delta\bar{\nu}$ of 0 cm^{-1} is used in l.t.c.e.s.l.s., a set of peaks is expected corresponding to a 0—0 excitation and a 0—0 emission transition. If a $\Delta\bar{\nu}$ of one vibrational unit is selected, i.e., $\Delta\bar{\nu}$ = 1400 cm^{-1}, two sets of peaks are expected. The set lowest in wavelength in the l.t.c.e.s.l. spectrum corresponds to a 0—1 excitation and a 0—0 emission transition. The second set corresponds to a 0—0 excitation and a 0—1 emission transition. The spectra in Fig. 2 were obtained from a solution of anthracene in *n*-heptane. Figure 2A is the conventional low-temperature fluorescence emission spectrum for this solution. The peaks from 375 to 390 nm, 390 to 415 nm, and 415 to 435 nm correspond to vibrational transitions 0—0, 0—1, and 0—2, respectively. Figure 2B is the l.t.c.e.s.l. spectrum of this solution using a $\Delta\bar{\nu}$ of 1400 cm^{-1}. If a $\Delta\bar{\nu}$ of 2800 cm^{-1} or two vibrational units, is selected, three sets of peaks are expected. They correspond to excitation/emission transitions of 0—2/0—0, 0—1/0—1, and 0—0/0—2. Figure 2C is the l.t.c.e.s.l.

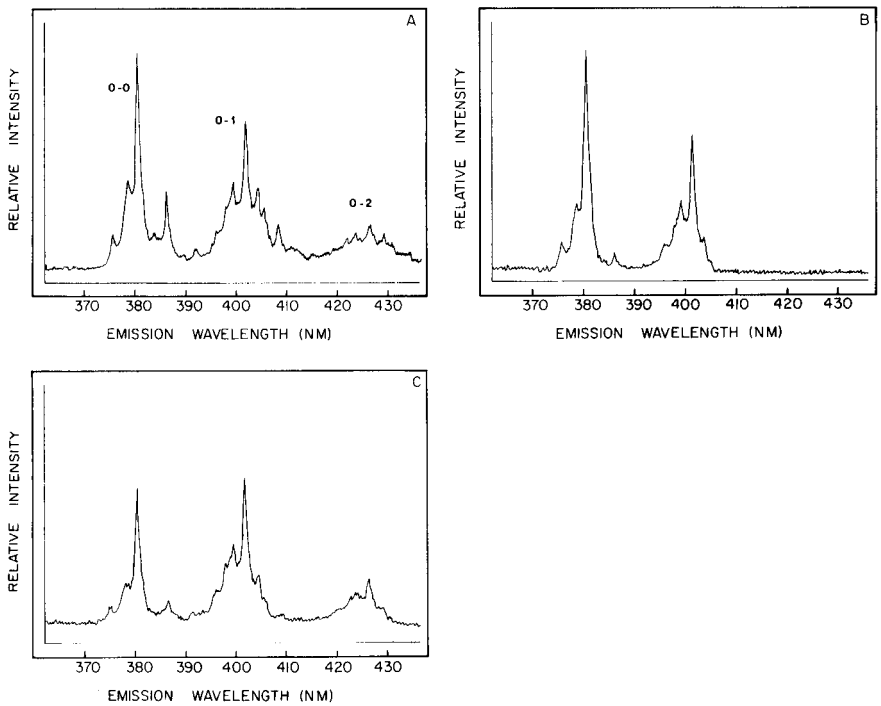

Fig. 2. A. Low-temperature fluorescence emission spectrum of anthracene in *n*-heptane; λ_{ex} = 248.0 nm. B. L.t.c.e.s.l. spectrum of anthracene in *n*-heptane; $\Delta\tilde{\nu}$ = 1400 cm^{-1}. C. L.t.c.e.s.l. spectrum of anthracene in *n*-heptane; $\Delta\tilde{\nu}$ = 2800 cm^{-1}.

spectrum of the anthracene solution with a $\Delta\tilde{\nu}$ of 2800 cm^{-1}. Note the remarkable similarity between Fig. 2A, B, and C. The peaks appear at the same positions, with differences only in relative intensity, as expected.

Figure 3 again demonstrates these relationships for a solution of 2,3-benzofluorene in *n*-heptane. Similar spectra can be obtained from two entirely different scan paths. Several advantages of this characteristic were studied to determine its analytical potential.

Pyrene was selected for investigation because of its lack of a strong S_1 0—0 or 0—1 excitation transition and its complex fluorescence emission spectrum, shown in Fig. 4A. An l.t.c.e.s.l. scan of a solution of pyrene in *n*-heptane with a $\Delta\tilde{\nu}$ of 1400 cm^{-1} yielded no peaks (no figure given) through its general emission range, as expected. A $\Delta\tilde{\nu}$ of 2800 cm^{-1} used in Fig. 4B exhibits one set of peaks corresponding to 0—2/0—0 excitation/emission transitions. Figure 4C is the spectrum obtained with a $\Delta\tilde{\nu}$ of 4200 cm^{-1}. Note that the positions of the peaks in l.t.c.e.s.l.s. are essentially the same as in conventional luminescence emission spectra. The relative intensities are different because the intensity is a function of the relative emission intensity, as well as the relative excitation intensity in l.t.c.e.s.l.s., whereas, in conven-

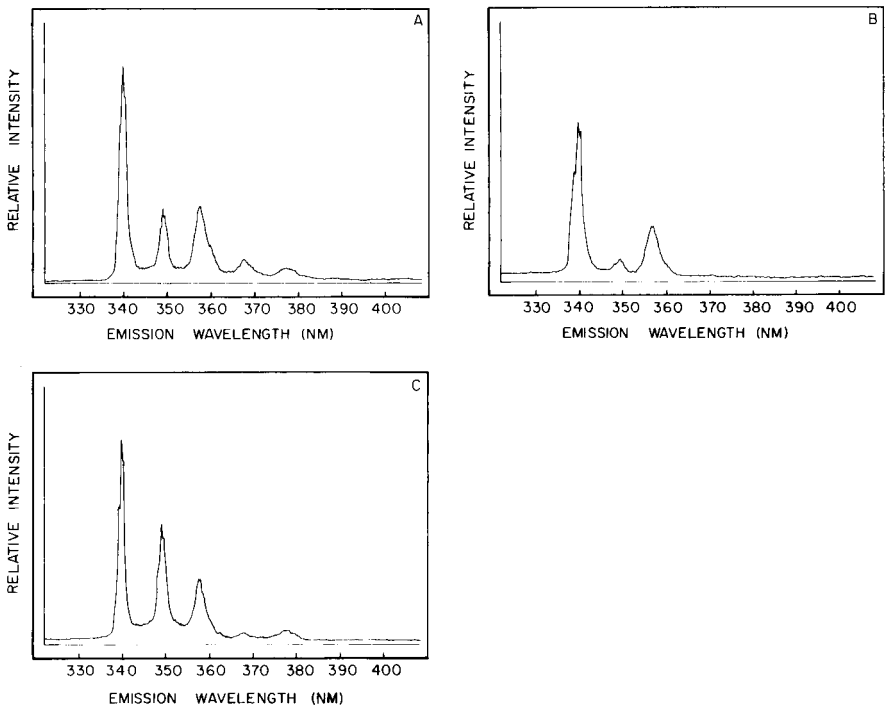

Fig. 3. A. Low-temperature fluorescence emission spectrum of 2,3-benzofluorene in *n*-heptane; λ_{ex} = 319.0 nm. B. L.t.c.e.s.l. spectrum of 2,3-benzofluorene in *n*-heptane; $\Delta\tilde{\nu}$ = 1400 cm^{-1}. C. L.t.c.e.s.l. spectrum of 2,3-benzofluorene in *n*-heptane; $\Delta\tilde{\nu}$ = 2800 cm^{-1}.

tional fluorescence emission spectra, relative spectral intensities are functions of only the emission intensities in that the excitation wavelength is held constant. The pyrene spectra illustrate the reduction in spectral complexity by this technique.

While a vast array of peaks is interesting for physical studies, the analytical chemist usually does not need and cannot use all the available information. The role that conventional s.l.s. plays in information utilization has been discussed by Vo-Dinh [20]. Selection of $\Delta\tilde{\nu}$ determines the complexity of the resultant spectra. For pyrene, this is clear. Also by using l.t.c.e.s.l., the spectral range for each compound is reduced, decreasing the probability of spectral overlap.

Many of the advantages of using energy relationships instead of wavelength relationships in s.l.s. as shown at room temperature are even more important at low temperatures. The $\Delta\tilde{\nu}$ selected is characteristic of a group of compounds and is not unique for a single component thought to be present in the sample of interest. Also the $\Delta\tilde{\nu}$ selected is independent of the spectral region, whether working from 300 to 400 nm or 500 to 600 nm, unlike $\Delta\lambda$ selection in conventional s.l.s. One of the major problems in $\Delta\lambda$ selection for conventional s.l.s. is that a $\Delta\lambda$ must be selected as a function of the spectral region of interest.

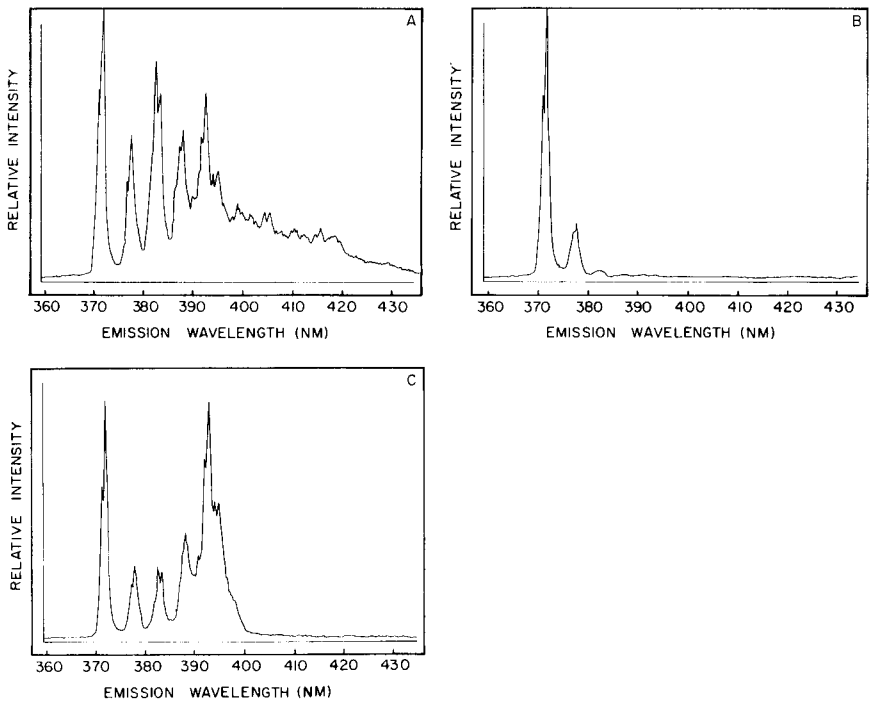

Fig. 4. A. Low-temperature fluorescence emission spectrum of pyrene in *n*-heptane; λ_{ex} = 337.0 nm. B. L.t.c.e.s.l. spectrum of pyrene in *n*-heptane; $\Delta\tilde{\nu}$ = 2800 cm^{-1}. C. L.t.c.e.s.l. spectrum of pyrene in *n*-heptane; $\Delta\tilde{\nu}$ = 4200 cm^{-1}.

To demonstrate the potential utility of this technique in multicomponent determinations, a seven-component PAH mixture was prepared in *n*-heptane. The compounds and their concentrations were: acenaphthene, 0.39 $\mu g\ ml^{-1}$; 2,3-benzofluorene, 0.20 $\mu g\ ml^{-1}$; pyrene, 0.40 $\mu g\ ml^{-1}$; 3,4-benzopyrene, 0.40 $\mu g\ ml^{-1}$; anthranthrene, 0.55 $\mu g\ ml^{-1}$; perylene, 0.90 $\mu g\ ml^{-1}$; and naphthacene, 0.90 $\mu g\ ml^{-1}$. These seven were selected to cover a large spectral range. If selective excitation were used, several spectra would be required if all components were known beforehand. With no prior knowledge of the compounds present, even more excitation wavelengths are needed. Figures 5—8 show the spectra for the mixture and standard solutions of each component by l.t.c.e.s.l.s. using a $\Delta\tilde{\nu}$ of 1400 cm^{-1} and 2800 cm^{-1}. Six of the seven compounds are identified from the 1400-cm^{-1} scan. Pyrene, as described earlier, required the 2800-cm^{-1} scan. Thus, only two scans are required to characterize all seven compounds.

For mixtures of unknown composition, the l.t.c.e.s.l. scan can be used as an aid to selective excitation techniques. This technique lacks some of the unique identification capabilities of the high-resolution laser-excited techniques. However, when used properly, its potential appears widespread. The

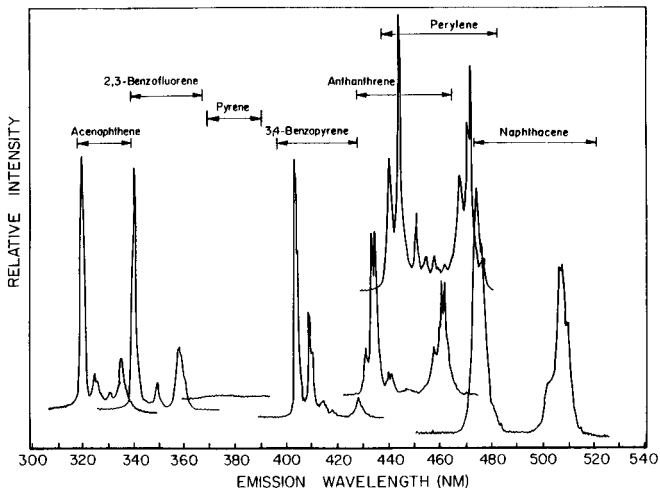

Fig. 5. L.t.c.e.s.l. spectrum of each component in the 7-component PAH mixture; $\Delta\bar{\nu}$ = 1400 cm^{-1}.

examples used here have been limited to liquid nitrogen conditions. If liquid helium (~4 K) or a He-refrigerator ($\lesssim$10 K) is used, additional narrowing is anticipated.

The effort toward continuously reducing the experimentally achievable temperature is widespread in analytical chemistry. However, below a temperature limit, l.t.c.e.s.l. may break down for several reasons. The $\Delta\bar{\nu}$ approximation of 1400 cm^{-1} for PAHs is just that, an approximation. Band broadening, to some extent, is a major reason for the success of c.e.s.l. Many of the vibrational energy spacings and the assumed independence from

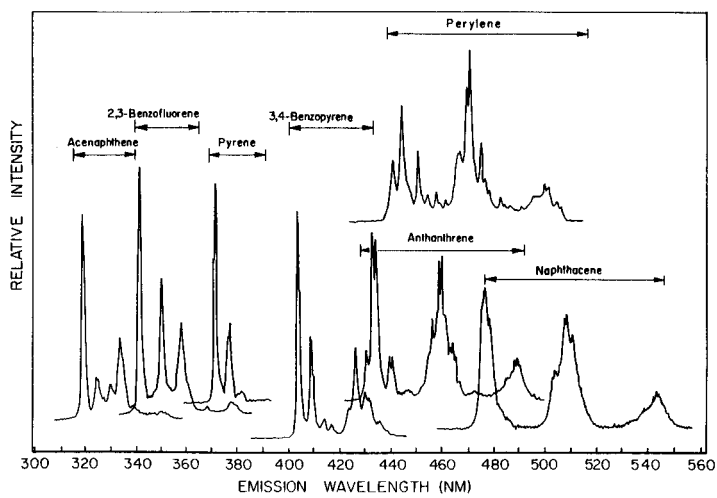

Fig. 6. L.t.c.e.s.l. spectrum of each component in the 7-component PAH mixture; $\Delta\bar{\nu}$ = 2800 cm^{-1}.

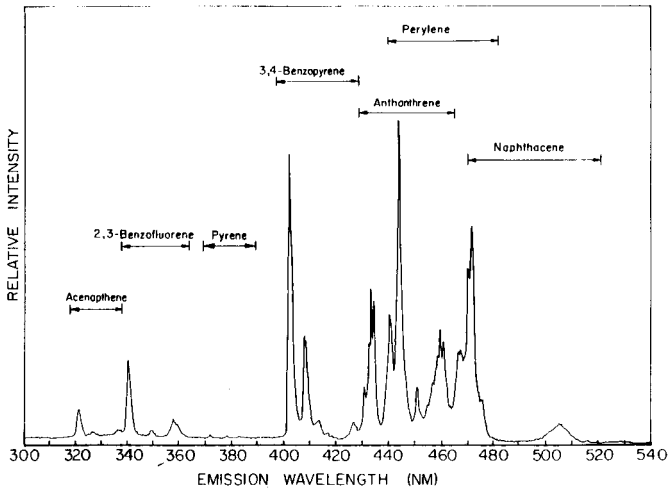

Fig. 7. L.t.c.e.s.l. spectrum of 7-component PAH mixture; $\Delta\tilde{\nu}$ = 1400 cm^{-1}.

solvent and temperature effects are also approximations. For infinitely narrow-line spectra, a $\Delta\tilde{\nu}$ must be selected for each compound of interest. While this suggests a powerful selectivity advantage, synchronous luminescence becomes more complicated and loses some of its appeal compared to the use of conventional luminescence spectra.

From the conclusions drawn from this work, one can speculate on the effect that the availability of an easily tunable laser excitation source, scannable over a wide range of wavelengths, would have on low-temperature s.l.s. techniques. One consideration is the site selection capabilities of a narrow-

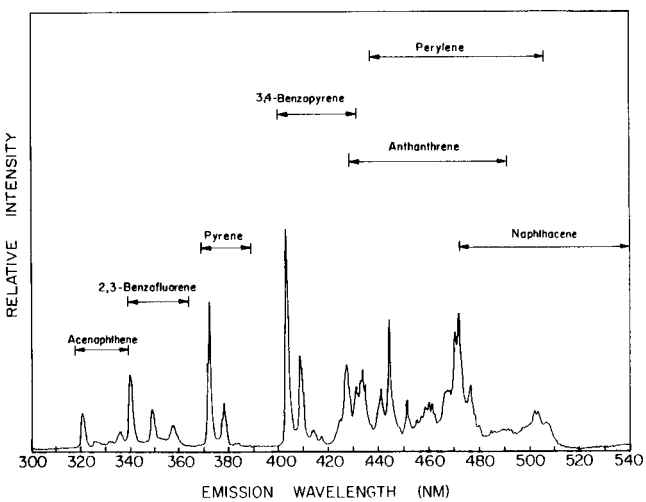

Fig. 8. L.t.c.e.s.l. spectrum of 7-component PAH mixture; $\Delta\tilde{\nu}$ = 2800 cm^{-1}.

band excitation source. The presence of multiple sites because of molecular orientation within the solvent matrix is distinguishable within low-temperature luminescence spectra. Essentially, the distribution of vibrational levels for each site is identical, with a difference in electronic transition energy only. Because of this, it is expected that if a narrow-line laser is used as the excitation source and is synchronously scanned, the multiplet of sites would appear in the l.t.c.e.s.l. spectrum (cf. Fig. 2). Thus, site selection is not possible with l.t.c.e.s.l.s.

While these results were obtained by fluorescence, low-temperature phosphorescence spectroscopy is also of analytical utility in PAH determinations. Many PAHs phosphoresce intensely, adding another selectivity capability. While the use of s.l.s. techniques in phosphorescence spectroscopy has been extensively discussed by Vo-Dinh for room-temperature conditions [25, 26], low-temperature phosphorescence has only recently been combined with s.l.s. [27]. From preliminary investigation, it appears that the principles of c.e.s.l. could be directly applied to low-temperature phosphorimetry.

Phosphorescence emission occurs at longer wavelengths than fluorescence emission because the lowest vibrational level of the first excited triplet state is lower in energy than the lowest vibrational level of the first excited singlet state. This difference is referred to as the singlet—triplet energy difference, Δ_{ST}. To apply c.e.s.l. to low-temperature phosphorimetry, the $\Delta\bar{\nu}$ must be selected to match the energy characteristics of the analyte. From this, $\Delta\bar{\nu}$ is selected as $\Delta\bar{\nu} = \Delta_{ST} + n\nu$, where ν is the vibrational energy spacing and n is an integer. The vibrational spectral distribution of the excited triplet manifold is similar to the spectral distribution of the excited singlet. The value of n is generally between 0 and 2, with increasing spectral complexity with increasing n. While a value of 0 for n is experimentally impractical for fluorescence, it can be used for phosphorescence because Rayleigh scatter is not a problem because of Δ_{ST}.

Vo-Dinh and Gammage [28] recognized the selectivity potential of Δ_{ST} in s.l.s. They described the use of the singlet—triplet energy difference to optimize $\Delta\lambda$ in s.l.s. for room-temperature phosphorescence. The value of Δ_{ST} is specific for each PAH in a mixture, with $\Delta\lambda$ calculated as an approximation to this energy difference. It was found that for multicomponent determinations, a series of $\Delta\lambda$'s can be selected, the series beginning with the smallest $\Delta\lambda$.

Another related physical process is the excitation of a molecule into a singlet electronic state other than the first excited singlet. Because emission occurs from the first excited singlet or triplet, this corresponds to an excess of energy in the excitation process over the emission process. Two additional equations can be written to include this situation. For fluorescence, this becomes $\Delta\bar{\nu} = \Delta_{S_n - S_1} + n\nu$; and for phosphorescence $\Delta\bar{\nu} = \Delta_{S_n - S_1} + \Delta_{ST} + n\nu$, where $\Delta_{S_n - S_1}$ is the energy difference between the lowest vibrational states of the nth excited singlet state and the first excited state.

A question of considerable importance is the extension of the concepts of l.t.c.e.s.l.s. to other groups of compounds. For example, polynuclear aromatic

compounds with a heteroatom of nitrogen or oxygen are present in oil samples, where they contribute to the luminescence of the sample. Carbonyl compounds often exhibit vibrational structure at the carbonyl frequency of 1750 cm^{-1}, while the Raman frequency of 1450 cm^{-1} can be seen in compounds with nitro groups. A complementary study to this work involves an analysis of low-temperature infrared and Raman spectra and the potential optimization of $\Delta\bar{\nu}$. This would be especially useful for quinolines, quinones, and *N*-heterocyclics.

CONCLUSIONS

Low-temperature spectroscopy demonstrates increasing selectivity advantages by the reduction of spectral bandwidths, offering fingerprint spectra with potential in analysis of complex mixtures. The use of synchronous techniques at low temperatures can provide an effective screening method for PAHs especially as a complement to laser-excited techniques. This work demonstrates the first use of synchronous luminescence techniques at low temperatures (i.e., below room temperature). By tracing parameter selection to low-temperature luminescence theory, the abundance of information available in low-temperature fluorescence and low-temperature phosphorescence spectra can be effectively used for analyte identification and quantitation. The important features of l.t.c.e.s.l.s. are therefore: (i) higher spectral information power at 77 K than at room temperature (other temperatures than 77 K may be better); (ii) narrower spectral bands with c.e.s.l.s. than with conventional luminescence spectrometry; by varying $\Delta\bar{\nu}$, it is possible to vary the complexity of the c.e.s.l. spectrum from a single peak to a multipeak spectrum similar to the conventional luminescence spectrum; (iii) a single $\Delta\bar{\nu}$ can be used throughout the entire c.e.s.l. spectral scan, whereas several $\Delta\lambda$'s must be used in constant wavelength synchronous luminescence (c.w.s.l.) if one is to obtain maximal spectral resolution and freedom from scatter interference; (iv) rather complex mixtures can be selectively measured with c.e.s.l. without the need for more complicated instrumentation, such as laser excitation and liquid helium cryogenic equipment; and (v) scatter (Rayleigh and Raman) can be minimized much more effectively by c.e.s.l. than by either c.w.s.l. (minimizes only Rayleigh scatter) and conventional luminescence (minimizes neither Rayleigh or Raman scatter).

This work was supported by NIH-GM-11373-18 and DOE-DE-AS05-780R06022.

REFERENCES

1 G. F. Kirkbright and C. G. deLima, Analyst, 99 (1974) 338.
2 R. Farooq and G. F. Kirkbright, Analyst, 101 (1976) 566.
3 A. Colmsjo and U. Stenberg, Anal. Chem., 51 (1979) 145.

4 A. Colmsjo and U. Stenberg, Chem. Scr., 9 (1976) 227.
5 E. L. Wehry, in E. L. Wehry (Ed.), Modern Fluorescence Spectroscopy, Plenum, New York, Vol. 4, 1981.
6 Y. Yang, A. P. D'Silva, V. A. Fassel and M. Iles, Anal. Chem., 52 (1980) 1350.
7 Y. Yang, A. P. D'Silva and V. A. Fassel, Anal. Chem., 53 (1981) 894.
8 Y. Yang, A. P. D'Silva and V. A. Fassel, Anal. Chem., 53 (1981) 2107.
9 J. C. Brown, J. A. Duncanson, Jr. and G. J. Small, Anal. Chem., 52 (1980) 1711.
10 J. C. Brown, M. C. Edelson and G. J. Small, Anal. Chem., 50 (1978) 1394.
11 E. L. Wehry and G. Mamantov, Anal. Chem., 51 (1979) 643A.
12 J. R. Maple and E. L. Wehry, Anal. Chem., 53 (1981) 1244.
13 J. R. Maple, E. L. Wehry and G. Mamantov, Anal. Chem., 52 (1980) 920.
14 L. A. Bykovskaya, R. I. Personov and Y. V. Romanovskii, Anal. Chim. Acta, 125 (1981) 1.
15 J. B. F. Lloyd, Nature (London), Phys. Sci., 231 (1971) 64.
16 T. Vo-Dinh and P. R. Martinez, Anal. Chim. Acta, 125 (1981) 13.
17 A. Jurgensen, E. L. Inman, Jr. and J. D. Winefordner, Anal. Chim. Acta, 131 (1981) 187.
18 T. Vo-Dinh, in E. L. Wehry (Ed.), Modern Fluorescence Spectroscopy, Plenum, New York, Vol. 4, 1981.
19 D. Eastwood, S. H. Fortier and M. S. Hendrick, Am. Lab., 10 (1978) 45.
20 T. Vo-Dinh, Anal. Chem., 50 (1978) 396.
21 E. L. Inman, Jr. and J. D. Winefordner, Anal. Chem., 138 (1982) 245.
22 I. M. Warner, G. D. Christian, E. R. Davidson and J. B. Callis, Anal. Chem., 49 (1977) 564.
23 B. E. Kohler, in C. B. Moore (Ed.), Chemical and Biochemical Applications of Laser, Academic Press, New York, Vol. 4, 1979.
24 E. L. Inman, Jr. and J. D. Winefordner, Analyst, submitted.
25 T. Vo-Dinh, R. B. Gammage and P. R. Martinez, Anal. Chem., 53 (1981) 253.
26 T. Vo-Dinh, R. B. Gammage, A. R. Hawthorne and J. H. Thorngate, Environ. Sci. Technol., 12 (1978) 1297.
27 M. M. Corfield, H. L. Hawkins, P. John and I. Soutar, Analyst, 106 (1981) 188.
28 T. Vo-Dinh and R. B. Gammage, Anal. Chem., 50 (1978) 2054.

Analytica Chimica Acta, 141 (1982) 255—262
Elsevier Scientific Publishing Company, Amsterdam — Printed in The Netherlands

CHEMILUMINESCENCE FOR THE DETERMINATION OF TRACES OF COBALT(II) BY CONTINUOUS FLOW AND FLOW INJECTION METHODS

SHINJIRO NAKAHARA, MASAAKI YAMADA* and SHIGETAKA SUZUKI
Department of Industrial Chemistry, Tokyo Metropolitan University, Setagaya-ku, Tokyo 158 (Japan)

(Received 15th February 1982)

SUMMARY

Flow injection analysis, with chemiluminescence detection, is used to determine traces of cobalt(II) by means of the gallic acid—hydrogen peroxide—sodium hydroxide system containing a small amount of methanol to increase the sensitivity. This permits the determination of cobalt(II) more selectively than any other chemiluminescent system with a detection limit of 0.04 $\mu g\ l^{-1}$ (continuous sample flow) or 0.04 ng (10-μl sample injection). The linear range is 3 orders of magnitude, the sampling rate is 20 h^{-1}, and the relative standard deviation is 5.9% for 0.06 ng Co(II) (n = 10). Silver(I), the strongest enhancer after cobalt(II), provides a signal 1.3% of that for Co(II). A few precipitants and complexing agents suppress the signal.

The use of solution chemiluminescence in analyses for inorganic and organic species at trace levels has received attention mainly because of the simplicity of the instrumentation, the low detection limits for some species, and the wide dynamic range, despite a lack of selectivity. Systems based on reagents such as luminol, lucigenin, lophine, and gallic acid have mainly been utilized for trace metals [1, 2]. In alkaline hydrogen peroxide solution, cobalt(II) is the most effective catalyst, the detection limits with the above reagents being 0.01, 0.02, 0.1, and 0.4 ppb, respectively [3].

Flow injection analysis (f.i.a.) is very suitable for the determination of various kinds of analytes based on chemiluminescence measurements [4]. Cobalt(II) in the picogram range has been detected by its catalytic effect on the oxidation of luminol [4], and cadmium(II) and zinc(II) in the subnanogram range by their inhibiting effects on the catalyzed oxidation [5]. The luminol system, however, suffers most from lack of selectivity; there are at least 30 different species that enhance light emission [6]. Consequently, the flow injection system for cobalt(II) based on luminol is subject to much interference.

This paper describes a f.i.a. chemiluminescence combination for sensitive, selective and rapid determination of cobalt(II) by employing gallic acid as a chemiluminescent reagent. This system appears to be the most selective

for cobalt; the chemiluminescence is enhanced by only a few other species [7]. As stated above, however, the system is the least sensitive for cobalt. The cobalt(II)-catalyzed oxidation of gallic acid by hydrogen peroxide in sodium hydroxide solution, to which a little methanol has been added to increase the sensitivity, has therefore been investigated for the determination of cobalt by continuous flow methods.

EXPERIMENTAL

Apparatus

A schematic diagram of the flow system is given in Fig. 1. An aqueous solution containing gallic acid, hydrogen peroxide, and methanol is supplied through R_1 and sodium hydroxide through R_2; R_3 represents a carrier stream for cobalt(II) and other species. This is an aqueous cobalt(II) solution for the continuous flow method, or pure water when cobalt(II) and other species are injected by means of a 10-μl rotary valve injector S (injection method). The streams are delivered by peristaltic pumps P and mixed at Y-joints J_1 and J_2. For adequate mixing of R_1 and R_2, a 2-m mixing coil M is placed between J_1 and J_2. Teflon tubing (1-mm i.d.) is used for flow lines except the pump tubes and detection flow cell D. This distance between J_2 and D is about 5 cm (the minimum distance achieved) and can be lengthened if necessary.

The detection flow cell consists of flexible, transparent polyvinyl chloride (PVC) tubing (0.8-mm i.d., 90 cm long) spiralled to a diameter of 42 mm on the adhesive surface of a piece of gummy tape (Fig. 2). The gummy tape is stuck on a photomultiplier tube (PMT) cooler, into which a PMT (Hamamatsu TV-R712) is installed and cooled at $-20°C$, so that the flow cell faces the PMT. The emission, which has an intense band at 643 nm and a weaker band at 478 nm, is observed directly by the PMT with no wavelength discrimination. The signal from the PMT is fed to an electrometer and then recorded via a laboratory-built low-pass active filter, whose frequency cut-off is ca. 0.1 Hz.

Reagents

Chemicals of analytical grade were used as received. The water used was prepared by distillation of Millipore (Milli-R) water in an all-pyrex glass

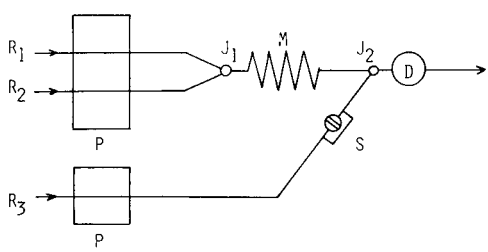

Fig. 1. Schematic diagram of the flow system (for key, see text).

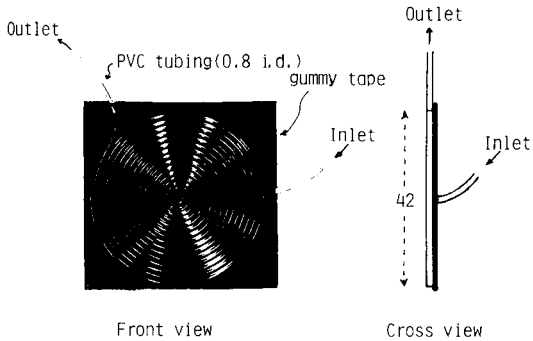

Fig. 2. Spiral flow cell for chemiluminescence detection (dimensions in mm).

apparatus, with a teflon membrane inserted to block mist evolved. Stock solutions (10^{-2} M) of various species were prepared by dissolving chlorides or nitrates, or sodium or potassium salts in water; some solutions were acidified with nitric acid. Gallic acid and hydrogen peroxide solutions were prepared daily.

RESULTS AND DISCUSSION

Reagent concentrations and the effect of methanol

Three reaction variables, the concentrations of gallic acid, hydrogen peroxide and sodium hydroxide were optimized at flow rates R_1, R_2 and R_3 of 1.2, 1.2 and 1.6 ml/min^{-1}, respectively, where R_3 was a 10^{-6} M cobalt(II) solution. The reagent concentrations giving the highest signal-to-noise ratio were found to be 0.02 M gallic acid (practically the maximum solubility at room temperature) with 0.3 M hydrogen peroxide, and 0.06 M sodium hydroxide. These concentrations are different from those used in a stopped-flow system by Stieg and Nieman [7, 8].

Small amounts of methanol were added to R_1 in an attempt to increase the sensitivity; this use of methanol was suggested by Slawinska and Slawinski [9]. The effect on the signal-to-noise ratio is shown in Fig. 3. Methanol concentrations above 1% (v/v) gave approximately constant signal enhancement, but the background signal also increased and there was a considerable increase in noise when the methanol concentration exceeded 4%. As a result, the best signal-to-noise ratio was obtained for 3% methanolic solution, for which the chemiluminescence signal was enhanced by a factor of 4. This methanol concentration had no undesirable effects on the PVC flow cell. Other water-soluble solvents such as ethanol, acetone and acetonitrile were also tested, but none surpassed methanol with regard to the enhancement effect.

For the gallic acid system, a chemiluminescence mechanism involving emission from singlet oxygen ($^1O_2$*) and intermolecular energy transfer has been proposed [9]. The luminescence enhancement by methanol may be explained in terms of the lifetime of $^1O_2$* and/or gallic acid oxidation pro-

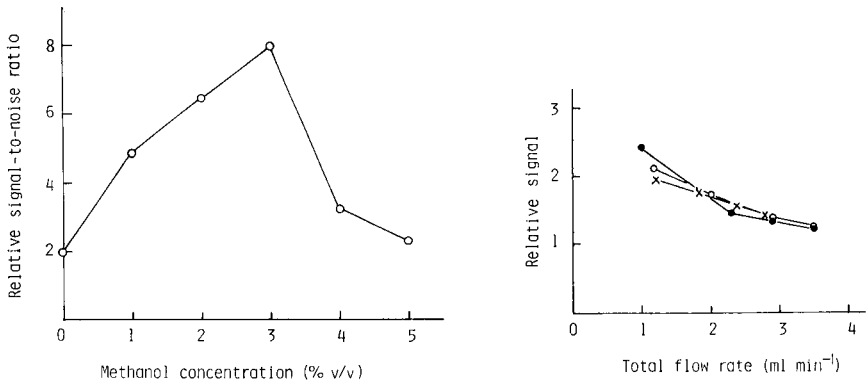

Fig. 3. Effect of methanol on luminescence signal-to-noise ratio: 0.02 M gallic acid, 0.3 M H_2O_2, 0.06 M NaOH, 10^{-7} M Co, continuous flow. $R_1 = R_2 = 0.3$ ml min^{-1}; $R_3 = 0.4$ ml min^{-1}.

Fig. 4. Effect of total flow rate on the relative signal (peak height). Concentrations as Fig. 3, except for 3% CH_3OH; 10-μl injections of 10^{-6} M cobalt solution; $(R_1 + R_2)/R_3$: (•) 1.5; (○) 0.5; (×) 1.0.

ducts; both intermediates and final products take part in the formation of $^1O_2^*$, and have longer lifetimes than in water alone (see the stopped-flow experiments below).

Total flow rate in the system

At too low or too high total flow rate, most of the chemiluminescent reaction proceeds outside the flow cell, which is 90 cm long, resulting in low signals. Thus the total flow rate dependence was explored at various flow rate ratios $(R_1 + R_2)$: R_3 for $R_1 = R_2$. The results shown in Fig. 4, indicate that the lower the total flow rate, the higher the chemiluminescence signal at each flow rate ratio, at least down to 1 ml min^{-1}, the minimum flow rate that could be achieved with the peristaltic pumps used. A total flow rate of 1 ml min^{-1} means that an injected cobalt solution travels through the spiral flow cell in 27 s. Considering that the luminescent reaction is slow [7], it seems likely that it is not complete within the 30-s traverse time, including the 3 s required to pass from J_2 to D (Fig. 1). The effect of lengthening the J_2—D distance at a total flow rate of 1 ml min^{-1} is presented in Fig. 5. The maximum signal is obtained with a J_2—D distance of ca. 70 cm.

Some signal profiles are shown in Fig. 6. The time from mixing until the maximum signal is recorded and until the signal disappears, increases as the J_2—D distance increases. This is attributable both to the dispersion of cobalt-(II) in the flowing solution, and to the slowness of the chemiluminescent reaction. The speed of the reaction depends on the cobalt(II) concentration as shown in Fig. 7, which gives signal profiles obtained in stopped-flow experiments under conditions where the cobalt solution flowed continuously at a

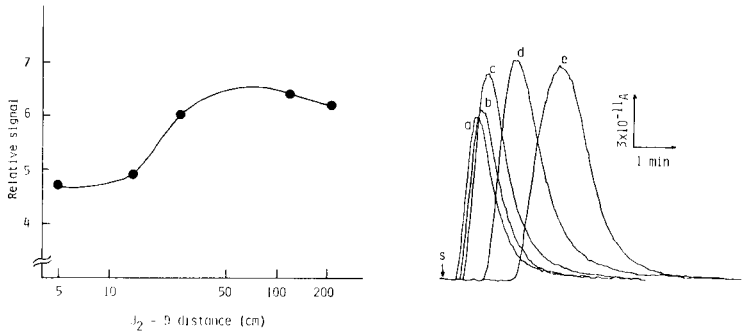

Fig. 5. J_2—D distance vs. chemiluminescence signal. Conditions as for Fig. 4, except R_1 = R_2 = 0.3 ml min^{-1}; R_3 = 0.4 ml min^{-1}.

Fig. 6. Signal profiles recorded in the experiments for Fig. 5. J_2—D distance: (a) 5 cm; (b) 14 cm; (c) 27 cm; (d) 119 cm; (e) 211 cm.

total flow rate of 13.5 ml min^{-1}, rapid enough that very little chemiluminescent reaction occurred during the time (<0.2 s) the solution flowed between J_2 and D (5 cm). Accordingly, the signal recorded should be very close to the undistorted emission profile. From Figs. 6 and 7 it can be said that 1×10^{-8} M cobalt gives such a slow reaction that integral detection of the emission by use of the present spiral flow cell is difficult. Figure 7 also shows that the profile is more drawn out in the presence of methanol.

The total flow rate chosen for further study was 1 ml min^{-1} (R_1 = R_2 = 0.3 ml min^{-1}, R_3 = 0.4 ml min^{-1}); a J_2—D distance of 5 cm was also chosen. This provides a sampling rate of 20 h^{-1}.

Calibration graphs and detection limits

Under the above determined conditions, calibration graphs were obtained for continuous sample flow (0.4 ml min^{-1}) and for injections (10 μl) of cobalt. Both graphs have linear ranges of about 3 orders of magnitude (Fig. 8); in the flow injection method, the slope is approximately unity. For larger

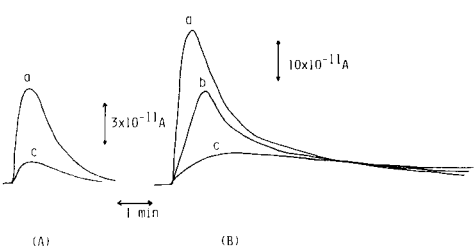

Fig. 7. Signal profiles recorded under stopped-flow conditions: 0.02 M gallic acid, 0.3 M H_2O_2, 0.06 M NaOH. A, without methanol, B, 3% methanol. Cobalt concentration in R_3: (a) 10^{-7} M; (b) 5×10^{-8} M; (c) 10^{-8} M.

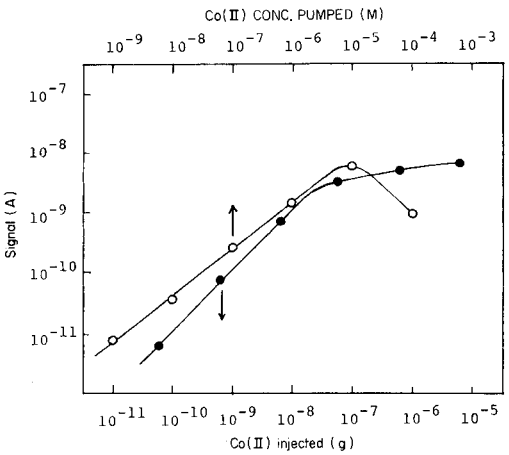

Fig. 8. Calibration graphs: (○) continuous flow; (●) 10-μl injection.

amounts of cobalt, the graph deviates from linearity, the deviation being larger for the continuous sample flow. This can be ascribed to the increasing absorption of emitted radiation by colored gallic acid oxidation products showing absorption maxima at 500—600 nm.

The detection limit for a signal-to-noise ratio of 3 is 7×10^{-10} M cobalt (ca. 0.04 ppb) for continuous sample flow and 0.04 ng for 10-μl sample injections. This is lower than the 7×10^{-9} M achieved in the stopped-flow system of Stieg and Nieman [7, 8] and comparable to the 0.05 ng obtained by the stopped-flow technique for f.i.a. based on catalytic spectrophotometry [10]. The relative standard deviation is 5.9% when 10 μl of the 1×10^{-7} M solution (ca. 0.06 ng) is successively injected ten times.

The detection limit is defined by the noise level, which depends on the background signal arising from impurities in the reagents and water used. Accordingly, an improvement of the detection limit would be expected with decreased background. Thus EDTA was added to the reagent stream R_1 in an attempt to mask chemiluminescence-enhancing metals. EDTA (10^{-6} M) slightly decreased the background (to 3×10^{-11} A) but the noise level remained unchanged at 2×10^{-12} A. The residual background seems to derive from impurities other than metals, presumably aldehydes (formaldehyde and acetaldehyde) in the methanol used. In the absence of methanol, the background almost disappeared on addition of EDTA. In the gallic acid system, formaldehyde produces relatively strong chemiluminescence in the range 560—580 nm, and it may be determined in water with a detection limit of 1 ppb [9]. Removal of aldehydes from methanol is therefore required for an improvement in the detection limit, so that picogram amounts of cobalt might be determined.

Interferences

Most solution chemiluminescence methods suffer from poor selectivity. The luminol, lucigenin, and lophine systems permit 30, 20 and 11 species, respectively, to enhance the luminescent reaction [6]. To avoid interferences, cobalt(II) has been separated from Ca, Mg, Fe(III), Mn(II) and Al by ion exchange before determination by the lophine method [11]. In contrast, the gallic acid system is fairly selective and only five other species (MnO_4^-, Mn(II), Ag, Cd and Pb) enhance the emission weakly [7]. For evaluation of this selectivity in the present system, various species were injected by means of the 10-μl valve. The results are given in Table 1 and compared to the values which Stieg and Nieman obtained [7]. They show that the selectivity is even greater in the flow system. Permanganate, cadmium and lead no longer give even slight emissions, and the effect of manganese(II) is decreased by an order of magnitude. In contrast, chromium(III) is found to show minor enhancement in the flow system. These changes probably arise from the differences in the experimental method and reagent concentrations, including the presence of methanol.

To check the effect of concomitant species on the signal for cobalt, 10 μl of a 10^{-4} M solution of each of the species listed in Table 1 was injected into stream R_3 of 10^{-7} M cobalt(II) solution. Only a few species influenced the cobalt signal; silver enhanced it by 18%, CN^-, S^{2-}, CrO_4^-, CO_3^{2-} and NH_3 suppressed it by 21, 20, 13, 6 and 5%, respectively, and EDTA suppressed it completely. When 10^{-5} M solutions of the above species were injected, no change in signal was observed except in the presence of EDTA, S^{2-} and CN^- which caused suppressions of 74, 9 and 3%, respectively. Injections of 10 μl of hydrochloric acid (pH 4.2) enhanced the signal by 3%. The suppressive interferences can be accounted for by precipitation or complexing of cobalt (II). The effect of acid may be to decrease precipitation of cobalt hydroxide. This study showed that the pH range of the solution injected should be 5—7. A wider range might be possible if stream R_3 were suitably buffered.

TABLE 1

Selectivity of the gallic acid chemiluminescence system

Species[a]	Relative signal		Species[a]	Relative signal	
	Present work	Ref. [7]		Present work	Ref. [7]
Co^{2+}	100	100	MnO_4^-	0	6.9
Ag^+	1.3	1.5	Cd^{2+}	0	1.4
Cr^{3+}	0.5	0	Pb^{2+}	0	1.2
Mn^{2+}	0.3	4.1	Zn^{2+}	0	0.1

[a] 10 μl of 10^{-4} M solution injected. Cu^{2+}, Fe^{3+}, Al^{3+}, Ni^{2+}, Ba^{2+}, Mg^{2+}, $Fe(CN)_6^{3-}$, CrO_4^{2-}, $Cr_2O_7^{2-}$, Ca^{2+}, F^-, Cl^-, Br^-, I^-, S^{2-}, CO_3^{2-}, NO_3^-, OCl^-, CN^-, SO_3^{2-}, SO_4^{2-}, NH_3, NH_4^+, EDTA gave rise to no emissions in either work.

At present, however, the pH of samples and reagents must be adjusted carefully because no suitable buffer has been found for the gallic acid system [12].

The interference effects can be used for determination of the interfering species. Sulphide at the ppm level, for example, can easily be determined, and complexing agents and complexing capacity could be determined in a similar manner. Complexing agents in natural waters are very important in solubilizing and transporting a number of trace metals, and their role in the toxicity and availability of trace metals to aquatic life is significant. In most investigations of complexing capacity, copper(II) has been chosen as the test ion because of its important role in biological activity, its strong and rapid complexation, and its relatively strong resistance to hydrolysis, and because it is determined easily. These properties are also possessed by cobalt(II).

Conclusions

The above results indicate that ultratrace amounts of cobalt(II) can be rapidly determined by f.i.a. based on the gallic acid chemiluminescence system. This provides a lower detection limit (0.04 ppb or 0.04 ng) for cobalt than that by most other instrumental techniques [12]. Although some other chemiluminescent systems provide lower detection limits, the gallic acid system has fewer interferences. There is room for much further development of the f.i.a.—chemiluminescence combination. In this particular example, better characteristics should be achieved by a faster reaction, which can be accomplished by placing a reaction coil between J_2 and D and putting it in a heating bath. This should provide increased sensitivity and perhaps higher sample throughput. Masking or removal of impurities responsible for the background signal will lower the detection limit. Consequently, the improved procedure should allow cobalt to be determined down to the picogram range. This work is in progress along with application to real samples.

REFERENCES

1 U. Isacsson and G. Wettermark, Anal. Chim. Acta, 68 (1974) 339.
2 D. B. Paul, Talanta, 25 (1978) 377.
3 M. Yamada and S. Suzuki, Bunseki Kagaku, (1980) 57.
4 J. L. Burguera, A. Townshend and S. Greenfield, Anal. Chim. Acta, 114 (1980) 209.
5 J. L. Burguera, M. Burguera and A. Townshend, Anal. Chim. Acta, 127 (1981) 199.
6 A. MacDonald, K. W. Chan and T. A. Nieman, Anal. Chem., 51 (1979) 2077.
7 S. Stieg and T. A. Nieman, Anal. Chem., 49 (1977) 1322.
8 S. Stieg and T. A. Nieman, Anal. Chem., 52 (1980) 800.
9 D. Slawinska and J. Slawinski, Anal. Chem., 47 (1975) 2101.
10 T. Yamane, Anal. Chim. Acta, 130 (1981) 65.
11 D. F. Marino and J. D. Ingle, Jr., Anal. Chem., 53 (1981) 292.
12 L. A. Montano and J. D. Ingle, Jr., Anal. Chem., 51 (1979) 926.

Analytica Chimica Acta, 141 (1982) 263—268
Elsevier Scientific Publishing Company, Amsterdam — Printed in The Netherlands

THE MECHANISM OF THE COBALT(II)-CATALYZED ELECTROGENERATED CHEMILUMINESCENCE OF LUMINOL IN AQUEOUS ALKALINE SOLUTION

KEIJO E. HAAPAKKA
Department of Chemistry, University of Turku, SF-20500 Turku 50 (Finland)
(Received 23rd December 1981)

SUMMARY

A rotating ring—disc electrode system is used where the disc electrode (carbon) is maintained at a negative potential to reduce oxygen to hydrogen peroxide, and a symmetric double-step potential is applied to the ring electrode (platinum). Cobalt(II) catalyzes the electrogenerated chemiluminescence of luminol at the ring electrode during the negative pulse of the double-step potential. A possible reaction scheme for this cobalt(II)-catalyzed emission process is outlined.

Metal ions generally catalyze luminol chemiluminescence in aqueous alkaline solutions when hydrogen peroxide is used as an oxidant. Much work has been done to elucidate the role of the metal ion [1—5]. It has been proposed that the metal ion—luminol complex is a necessary intermediate for light emission, or that the metal ion acts as a catalyst for hydrogen peroxide decomposition, generating a metal ion—hydrogen peroxide complex which reacts with luminol. According to Gillard and Spencer [6] superoxo—dicobalt(III) complexes react with luminol in aqueous alkaline solutions to generate light emission.

The mechanism of the electrogenerated chemiluminescence of luminol in aqueous alkaline solutions has been studied [7—9], and its feasibility for trace determinations of copper(II) has been indicated [10]. An apparatus which utilizes a rotating ring—disc electrode system has been constructed for mechanistic and analytical studies of luminol electrogenerated chemiluminescence [11]. A symmetric double-step potential is applied to the ring and the disc is maintained at a negative potential to reduce oxygen to hydrogen peroxide, which is transported to the ring electrode by the electrode rotation. Under these conditions, the luminol luminescence is generated at the ring electrode during the positive pulse of the double-step potential. This has been described in detail [12]. Cobalt(II) is also capable of catalyzing the luminol luminescence at the ring electrode during the negative pulse of the double-step potential; this has been utilized for the trace determination of cobalt(II) [13]. In the present paper, a possible reaction scheme for the cobalt(II)-catalyzed electrogenerated chemiluminescence of luminol in

0003-2670/82/0000-0000/$02.75

aqueous alkaline solution is proposed. The apparatus, reagents, procedures and method of measurement have already been described [11—13].

RESULTS AND DISCUSSION

The cobalt(II)-catalyzed luminescence, i.e., the cathodic chemiluminescence of luminol, has been illustrated (see fig. 5 [13]). An inhibiting effect of cobalt(II) on the luminescence was found during the positive pulse of the double-step potential, i.e., on the anodic luminescence. Also, in the presence of cobalt(II), the baseline (the intensity detected at zero potential) rose continuously during the luminescence measurement. The cathodic intensity was greatest at the platinum—glassy carbon (Pt—C) ring—disc electrode [13]. The mechanism of the cathodic luminescence at this electrode was therefore examined further. A pulsed potential with alternate zero and negative pulses was applied to the ring electrode instead of the symmetric double-step potential, but the cathodic luminescence was not observed. This indicates that some oxidation process at the ring electrode during the preceding positive pulse is necessary for the generation of the cathodic chemiluminescence.

The effect of disc potential on the cathodic intensity has been discussed [13]. Voltammetric measurements at the glassy carbon disc electrode indicated that oxygen reduction to hydrogen peroxide with a peak potential —0.70 V [12] was the only reduction process occurring under the conditions of the chemiluminescence measurements, and that luminol and cobalt(II) had no effect on this reduction. Consequently, the enhancing effect of disc electrode potential on the cathodic luminescence must be caused by the generation of hydrogen peroxide by oxygen reduction.

Role of cobalt(II)

Voltammetric measurements on 1.00×10^{-4} M cobalt(II) under the electrogenerated chemiluminescence conditions revealed no oxidation or reduction process of cobalt(II) at the platinum electrode over the range +1.0 to —0.8 V. Furthermore, cobalt(II) had no effect on the luminol electrooxidation [12]. On this basis, the cathodic luminescence of luminol does not originate from any electrochemical process of cobalt(II).

In the presence of ligands having nitrogen or nitrogen and oxygen donor atoms, cobalt(II) is capable of reacting with molecular oxygen to yield peroxo—dicobalt(III) complexes [14] which are oxidized by hydrogen peroxide to superoxo—dicobalt(III) complexes [15]. Superoxo—dicobalt(III) complexes react with luminol in aqueous alkaline solutions, emitting light [6]. As luminol has one amino and two carbonyl groups, it may induce the formation of a peroxo—dicobalt(III) complex which is oxidized by hydrogen peroxide in the solution flowing between the disc and ring electrodes to give a superoxo—dicobalt(III) complex. The other possible active form of cobalt is a cobalt(II)—hydrogen peroxide complex [5] also generated in the solution flowing between the two electrodes.

In order to shed light on these possible active forms of cobalt, the effects of different ligands on the intensity of the cathodic luminescence were determined. The results are presented in Figs. 1 and 2 (cf. fig. 11 [13]). Ammonia, tetraethylenepentamine and triethylenetetramine induce the formation of superoxo—dicobalt(III) complexes [14, 15] but, as shown in Figs. 1 and 2, these ligands strongly inhibit the cathodic luminescence of luminol. Hence the superoxo—dicobalt(III) complex is not the species of cobalt(II) capable of catalyzing the cathodic luminescence.

It is suggested, therefore, that the cobalt(II)—hydrogen peroxide complex is the active form of cobalt. As shown earlier [13], EDTA strongly inhibits the electrogenerated luminescence. EDTA forms a 1:1 cobalt(II) chelate where all the coordination sites of cobalt(II) are filled; this prevents the formation of the cobalt(II)—hydrogen peroxide complex, thus inhibiting the effect of cobalt on the luminescence. Because iminodiacetic acid and aminoacetic acid form 1:2 and 1:3 chelates to fill all the coordination sites of cobalt(II), the inhibiting effects of these ligands [13] can be explained similarly.

Effect of pulse amplitude

Figure 3 shows the effect of pulse amplitude on the intensity of the cathodic and anodic electrogenerated chemiluminescence of luminol. The cathodic and anodic light pulses at pulse amplitudes of 0.85 V and 1.40 V are shown in Fig. 4.

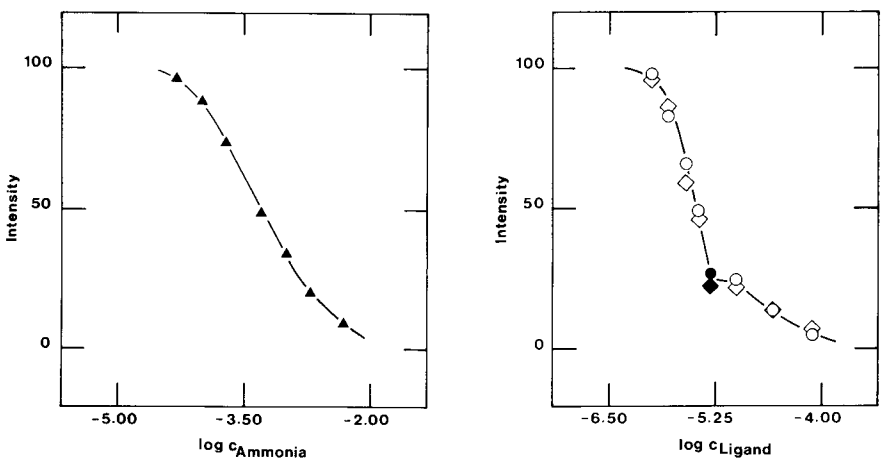

Fig. 1. Effect of ammonia on the cathodic luminescence of luminol at the Pt—C ring—disc electrode, intensity without ammonia = 100. Conditions: 0.100 M NaCl, disc potential −1.00 V, pulse amplitude 0.825 V, pH 10.0, H_3BO_3—NaOH buffer, 1.50×10^{-4} M luminol, rotation rate 350 rpm, pulse length 35.0 ms, 5.0×10^{-6} M cobalt(II), solutions saturated with oxygen.

Fig. 2. Effects of (○) tetraethylenepentamine and (◇) triethylenetetramine on the cathodic luminescence; (●) and (◆) indicate points where the concentrations of cobalt(II) and ligand are equal. Conditions as in Fig. 1.

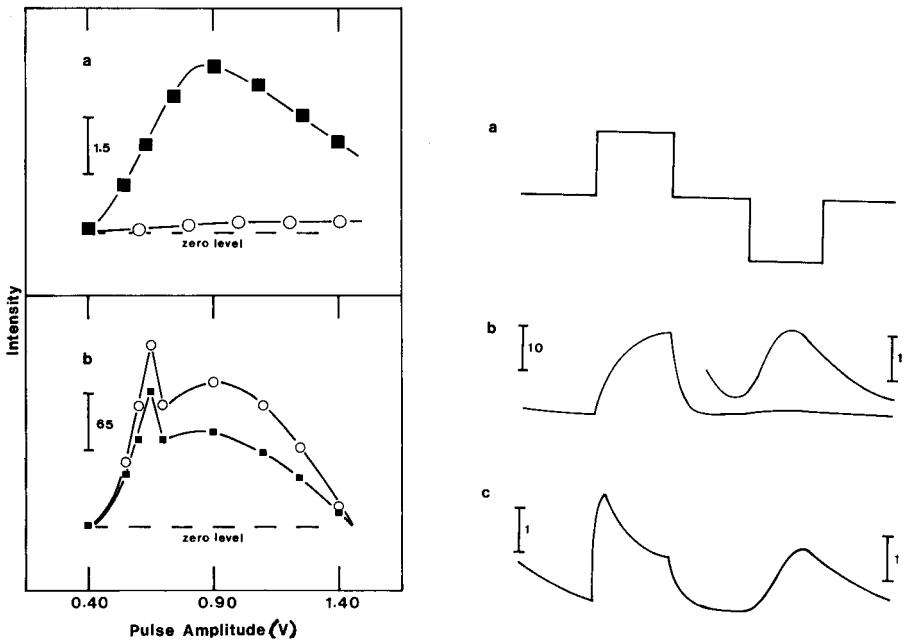

Fig. 3. Effect of pulse amplitude on (a) cathodic and (b) anodic luminescence (arbitrary units) of luminol at the Pt—C ring—disc electrode: (○) without cobalt(II); (■) with 5.0×10^{-6} M cobalt(II). Conditions: 1.00×10^{-4} M luminol, otherwise as for Fig. 1.

Fig. 4. The variation of luminol luminescence in the presence of cobalt(II) at the Pt—C ring—disc electrode, with different pulse amplitudes: (a) the symmetric double-step potential; (b) 0.85 V, (c) 1.40 V. Conditions as in Fig. 3.

The necessary electro-oxidation process for the generation of the cathodic luminescence can be either the formation of an oxide layer on the surface of the platinum ring electrode or luminol oxidation, with peak potentials of 0.50 V and 0.67 V, respectively [12]. Luminol and its oxidation product are not reduced at the platinum electrode. As concluded from Figs. 3 and 4, the anodic luminescence intensity is much suppressed by large pulse amplitudes, but this suppression has practically no effect on the cathodic intensity. This indicates that luminol oxidation is not needed for generation of the cathodic luminescence but the emission is generated only at the oxide-covered surface of the platinum ring electrode. Support for this view is obtained from the fact that the cathodic emission is not generated at a gold ring electrode [13], the surface of which is mainly free from an oxide layer under the electrogenerated chemiluminescence conditions [12].

The role of the oxide layer in the generation of the cathodic luminescence of luminol can be explained in the following way. During the positive pulse, the ring electrode surface is covered by the oxide layer. This lowers the luminol oxidation rate so that the luminol adsorbed onto the electrode is

not completely oxidized before the end of the pulse (see fig. 5 [11]). During the negative pulse, the oxide layer is reduced with the peak potential of −0.12 V [12]. This releases the "unoxidized luminol" and increases momentarily the luminol concentration in the vicinity of the ring electrode. The cobalt(II)—hydrogen peroxide complex reacts with this "unoxidized luminol" to generate the cathodic luminescence. The role of the oxide layer proposed is strongly supported by the fact that the end of the negative potential pulse has no effect on the cathodic emission pulse [13], which indicates that the light-emitting reaction does not take place at the ring electrode surface but in its vicinity.

Possible mechanism of the cobalt(II)-catalyzed cathodic luminescence

A mechanism for the uncatalyzed electrogenerated chemiluminescence of luminol has already been proposed [12]. The emitter is considered to be 3-aminophthalate [8, 16]. Under the present conditions, the prevailing species of luminol is its monoanion [17, 18] with which cobalt(II) probably forms a mixed complex that also involves hydroxide ions. The electrode

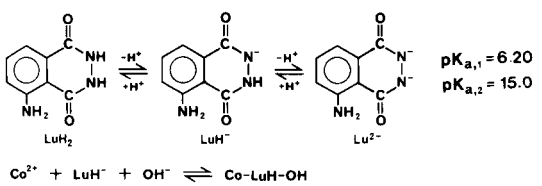

rotation gives a laminar flow of the solution from the disc to the ring electrode. Some of the oxygen thus transported to the disc electrode is reduced to hydrogen peroxide (pK_a = 11.65 [19]), which reacts with the mixed cobalt(II) complex to yield a cobalt(II)—hydrogen peroxide complex. During the positive pulse, the ring is covered by an oxide layer, which causes the production of "unoxidized luminol" at the beginning of the negative pulse, as described above; this reacts with the cobalt(II)—hydrogen peroxide complex and light is emitted.

The luminol anion reacts with the cobalt(II)—hydrogen peroxide complex yielding cobalt(III) ion and a luminol radical [5]. The luminol radical does not react with hydrogen peroxide or its anion to generate light [20], hence it is proposed that the luminol radical anion is oxidized by cobalt(III) ion to yield 3-aminoazaquinone, which is capable of reacting with the hydrogen peroxide anion with emission of light [21—23]. According to Eriksen et al. [22], this reaction directly generates a peroxide intermediate of luminol. On decomposition, the basic form of this intermediate generates excited 3-aminophthalate. The acidic peroxide intermediate decomposes via a non-luminescent reaction [12]. The reaction of the luminol radical with oxygen is the other possible light-emitting pathway, but this involves an additional intermediate, a luminol peroxide radical which is reduced to the peroxide intermediate of luminol.

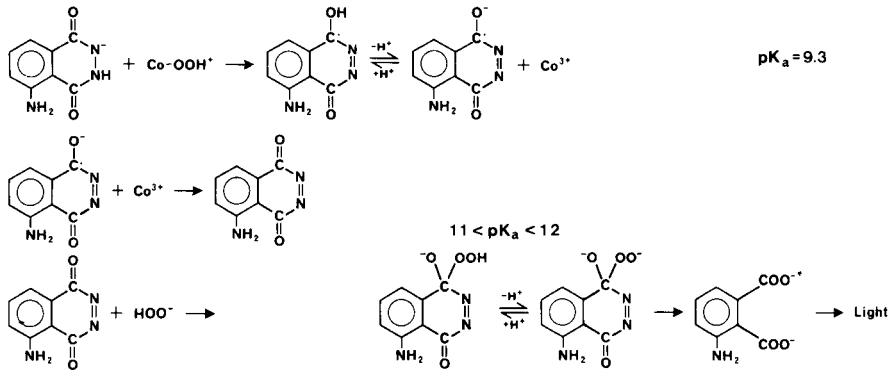

Unfortunately, the results of this study do not allow a definitive decision about the light-emitting pathways to be made. However, it is tempting to propose that the pathway based on the reaction of 3-aminoazaquinone with the hydrogen peroxide anion is mainly responsible for the cathodic luminescence of luminol because of the low intensity of the oxygen pathway [12].

Financial support of this study from the Finnish Cultural Foundation is gratefully acknowledged.

REFERENCES

1 L. Erdey, W. F. Pickering and C. L. Wilson, Talanta, 9 (1962) 653.
2 H. Ojima, Nippon Kagaku Zasshi, 84 (1963) 909; see Chem. Abstr., 61 (1964) 6439f.
3 A. K. Babko and L. I. Lukovskaya, Russ. J. Phys. Chem., 12 (1967) 87.
4 Y. N. Kozlov, Y. V. Koltypin, B. A. Rusin and Y. I. Skurlatov, Russ. J. Phys. Chem., 49 (1975) 1182.
5 T. G. Burdo and W. R. Seitz, Anal. Chem., 47 (1975) 1639.
6 R. D. Gillard and A. Spencer, J. Chem. Soc. A, (1970) 1761.
7 N. Harvey, J. Phys. Chem., 33 (1929) 1456.
8 B. Epstein and T. Kuwana, Photochem. Photobiol., 4 (1965) 1157.
9 B. Epstein and T. Kuwana, Photochem. Photobiol., 6 (1967) 605.
10 K. E. Haapakka and J. J. Kankare, Anal. Chim. Acta, 118 (1980) 333.
11 K. E. Haapakka and J. J. Kankare, Anal. Chim. Acta, 138 (1982) 253.
12 K. E. Haapakka and J. J. Kankare, Anal. Chim. Acta, 138 (1982) 263.
13 K. E. Haapakka, Anal. Chim. Acta, 139 (1982) 229.
14 R. D. Jones, D. A. Summerville and F. Basolo, Chem. Rev., 79 (1979) 139.
15 F. Basolo and R. G. Pearson, Mechanisms of Inorganic Reactions, Wiley, New York, 1967, p. 641.
16 D. F. Roswell and E. H. White, Methods Enzymol., 57 (1978) 409.
17 L. Erdey, I. Buzas and K. Vigh, Talanta, 13 (1966) 463.
18 K. E. Haapakka, J. J. Kankare and J. A. Linke, Anal. Chim. Acta, in press.
19 D. D. Perrin, Dissociation Constants of Inorganic Acids and Bases in Aqueous Solutions, Butterworths, London, 1969, p. 170.
20 G Merenyi and J. S. Lind, J. Am. Chem. Soc., 102 (1980) 5830.
21 E. H. White, E. G. Nash, D. R. Roberts and O. C. Zafiriou, J. Am. Chem. Soc., 90 (1968) 5932.
22 U. Isacsson, J. Kowalewska and G. Wettermark, J. Inorg. Nucl. Chem., 40 (1978) 1653.
23 T. E. Eriksen, J. S. Lind and G. Merenyi, J. Chem. Soc. Faraday Trans. 1, 77 (1981) 2137.

Analytica Chimica Acta, 141 (1982) 269—278
Elsevier Scientific Publishing Company, Amsterdam — Printed in The Netherlands

TRINITROBENZENESULFONIC ACID: A CHROMOPHORE, ELECTROPHORE AND PRE-COLUMN DERIVATIZING AGENT FOR HIGH-PERFORMANCE LIQUID CHROMATOGRAPHY OF ALKYLAMINES

W. LOWRY CAUDILL and R. MARK WIGHTMAN*

Department of Chemistry, Indiana University, Bloomington, IN 47405 (U.S.A.)

(Received 8th March 1982)

SUMMARY

Trinitrobenzenesulfonic acid is shown to be an ideal pre-column derivatizing agent for high-performance liquid chromatography of alkylamines. The reaction is quantitative and the trinitrophenyl derivatives are amenable to ultra-violet and electrochemical detection. Electrochemical detection with either a glassy carbon or pressure-annealed pyrolytic graphite working electrode provides lower detection limits than ultraviolet detection and thus is preferable for trace determinations.

Trinitrobenzenesulfonic acid (TNBS) was introduced as a derivatizing agent for amino acids in 1959 by Okuyama and Satake [1]. The trinitrophenyl (TNP) derivatives of aliphatic amines that can be formed in alkaline solutions have many properties that facilitate their use in quantitative work. Direct spectrophotometric determination is possible because TNP derivatives have an absorbance maximum at approximately 350 nm, a wavelength where TNBS is essentially transparent. The derivatives can be isolated in crystalline form in high yield so that authentic standards are easily obtained [2, 3]. In this report, it is shown that TNP derivatives are also advantageous for electrochemical detection because they are reduced at easily accessible potentials. There has been, however, little use of TNBS for trace determinations or as a pre-column reagent for the derivatization of compounds separated by liquid chromatography. It was recently shown that TNBS can be used quantitatively to derivatize γ-aminobutyric acid, a neurotransmitter, in whole rat brain homogenates using liquid chromatography with electrochemical detection (l.c.e.c.) [4].

Trinitrobenzenesulfonic acid is of interest as a derivatizing agent for use as an electrophore for l.c.e.c. to take advantage of the low detection limits of this method. The low detection limits of l.c.e.c. have been demonstrated for easily oxidized compounds where picogram measurements are routine [5, 6]. Carbon electrodes at fixed potential are used primarily in this application. Properly prepared electrodes are stable, and thus do not require electrode resurfacing or other forms of treatment for several months. However, carbon electrodes are not reliable when operated at very negative potentials.

Various interferences, either in the mobile phase or in the sample, cause the electrode response to deteriorate [7, 8]. Chief among these interferences is oxygen, the presence of which can lead to a large baseline offset and increased faradaic noise. To minimize these problems, detectors for reducible compounds have employed renewable mercury surfaces (dropping mercury electrodes or metal amalgams [9—15]). Another successful approach has been to use a dual-electrode system in which a generator electrode is used to form an oxidizable product [8]. However, electroreduction of trinitro compounds occurs at sufficiently low potentials that a single carbon electrode can be employed for trace level detection. For routine determinations, this approach offers many of the advantages demonstrated by l.c.e.c. in the oxidative mode.

EXPERIMENTAL

Reagents

All aqueous solutions were prepared in doubly-distilled water with reagent grade chemicals as described previously [4]. γ-Aminobutyric acid, β-alanine, L-alanine, glycine, α-aminobutyric acid, β-aminoisobutyric acid, δ-aminovaleric acid, 2,4-dinitrophenyl-γ-aminobutyric acid, and 2,4,6-trinitrobenzene-sulfonic acid (TNBS) were obtained from Sigma Chemical Company (St. Louis, MO). Crystalline forms of 2,4,6-trinitrophenyl-γ-aminobutyric acid, 2,4,6-trinitrophenyl-β-alanine, 2,4,6-trinitrophenyl-L-alanine, 2,4,6-trinitrophenyl-δ-aminovaleric acid, 2,4,6-trinitrophenylglycine, 2,4,6-trinitrophenyl-α-aminobutyric acid, and 2,4,6-trinitrophenyl-β-aminoisobutyric acid were prepared for use as standards with a procedure similar to that of Okuyama and Satake [1].

Microreaction

A sample (200 μl) containing the above-specified amino acids (except for δ-aminovaleric acid which served as internal standard) at pH 9.2 with 0.2 M potassium tetraborate is dispensed into an Eppendorf polypropylene test tube (1.5 ml, Brinkmann Instruments, Westbury, NY). The derivatizing agent, TNBS, (20 μl, 0.1 M) is added and the reaction is allowed to progress for 30 min. The reaction is terminated by the addition of perchloric acid (2.0 M, 180 μl) containing the internal standard, 2,4,6-trinitrophenyl-δ-aminovaleric acid (2.2×10^{-6} M). The final pH is 0.2. The sample is then extracted twice with 400-μl aliquots of toluene. A portion of the combined toluene fraction (500 μl) is back-extracted with pH 9.0 buffer (250 μl, Fisher, Cincinnati, OH). The aqueous phase, which contains the derivatized amino acids and the internal standard, is placed in a vial (V vial, 1.0 ml, Anspec Co., Ann Arbor, MI). The vial is sealed with a serum cap and the aqueous phase is deoxygenated by nitrogen bubbling for 2 min. The deoxygenated aqueous solution is then injected onto the column.

Apparatus

The liquid chromatographic apparatus was described previously [4]. A constant, reduced level of oxygen in the mobile phase was accomplished by deoxygenation of the mobile phase with nitrogen and the utilization of stainless steel tubing throughout the chromatograph. The columns were either 4.6-mm i.d. × 25 cm Biophase (5-μm particle size) reversed-phase columns (Bioanalytical Systems, West Lafayette, IN) or 2-mm i.d. × 50 cm Zipax (30-μm particle size) strong anion-exchange columns (SAX, DuPont, Wilmington, DE). The mobile phase for the reversed-phase separation contained citric acid (0.098 M), disodium hydrogenphosphate (0.016 M), acetic acid (0.43 M) (pH 2.5) and 38% methanol (HPLC Grade, Fisher, Cincinnati, OH). The SAX mobile phase consisted of potassium hydrogenphthalate (0.037 M), sodium acetate (0.039 M) and disodium ethylenedinitrilotetraacetate (0.001 M). The flow rate for the reversed-phase separation was 1.5 ml min^{-1} and for the SAX system was 0.8 ml min^{-1}.

For amperometric detection, the working electrode was made of glassy carbon (Tokai GC-20, Atomergic, New York, NY) or the oxidized basal plane of pressure-annealed pyrolytic graphite (Union Carbide Co., Parma, OH). The pyrolytic graphite electrode was pretreated with anodic oxidation as described elsewhere [16]. The glassy carbon was polished to a mirror finish with use of 600-grit sandpaper, followed by polishing on a felt cloth with 5-μm, 0.3-μm, and 0.05-μm alumina (Fisher, Cincinnati, OH), successively. The flow cell, identical for both electrode materials, was a modification of that previously described [16]. The auxiliary electrode was made of stainless steel which served as the upper block of the cell. A pre-cut spacer (51-μm thick; Tefzel, DuPont, Wilmington, DE) was laminated onto the auxiliary electrode. Lamination was achieved in 1 h at 260° C. The entire assembly was then clamped together with 4 bolts. The working electrode area was 0.33 cm^2 and the cell volume was 1.7 μl. The working electrode potentials were −0.6 V and −0.8 V vs. a saturated calomel electrode (SCE) for the reversed-phase and SAX systems, respectively. For ultraviolet (u.v.) detection, the optical unit of an Altex Model 300 isocratic liquid chromatograph (10-mm path length, 8-μl cell volume, Altex Scientific, Berkeley, CA) was used with single wavelength monitoring at 254 nm. Voltammetric studies employed a PARC Model 174A. Measurements were made with a disk-shaped glassy carbon electrode (0.058-cm^2 surface area).

RESULTS AND DISCUSSION

Properties of trinitrophenyl derivatives

Gram-scale quantities of the TNP derivatives of each of the amino acids were prepared and each possessed a sharp melting point (see Table 1). Ring substitution by the amino group is expected for these derivatives [17, 18] and was verified for the glycine derivative by mass spectrometry (parent ion m/z = 264). All of the TNP derivatives possess a high molar absorptivity at

TABLE 1

Recovery of the trinitrophenyl derivatives of the compounds cited after extraction and deoxygenation
(Melting points of the separately prepared derivatives are also given)

Compound	Recovery (%)[a]	M.p. (°C)	Compound	Recovery (%)[a]	M.p. (°C)
L-Alanine	100 ± 0.886	144—145	α-Aminobutyric acid	94.3 ± 2.26	119—120
γ-Aminobutyric acid	101 ± 0.643	149—151	β-Alanine	94.2 ± 2.44	189—189.5
β-Aminoisobutyric acid	101 ± 0.993	143—144	Glycine	91.2 ± 2.60	166—167
8-Aminovaleric acid	—	114—115			

[a]Mean recoveries determined with 1×10^{-6} M solutions of the amino acids. The 98% confidence limits ($n = 9$) were obtained from a 2-sided Student's t-test.

254 nm which makes them ideal for u.v. detection following liquid chromatographic separation (e.g., for the γ-aminobutyric acid derivative, $\epsilon = 2.2 \times 10^5$ l mol^{-1} cm^{-1}).

The electrochemistry of the γ-aminobutyric acid derivative was characterized at carbon electrodes to determine the parameters for amperometric detection. The response of the amperometric detector is directly proportional to the number of electrons per mole transferred in the electrolysis, which suggests that TNP derivatives are ideal because at very negative potentials they are reduced in an overall 18-electron process. This process is evidenced by polarography in aqueous solutions as three 4-electron, 2-proton, irreversible waves at moderate potentials and as a 6-electron wave at potentials that are near the negative limit for a mercury electrode. The 4-electron, 2-proton waves correspond to the reduction of each nitro group to the corresponding hydroxylamine [19—22]. At a carbon electrode in the buffer used for reversed-phase chromatography, only the first three reduction waves are apparent in the potential range available (Fig. 1). The peak potentials for these waves are shifted negatively with respect to those obtained at mercury electrodes. The peak potentials move in a negative direction with an increase in pH from 2 to 6 (43.7 mV/pH unit, 45.5 mV/pH unit, and 66.1 mV/pH unit for the first, second and third waves, respectively). The oxidation wave observed on the reverse scan suggests that the aromatic multi-hydroxylamine is the product of these reductions.

Figure 1 also shows a cyclic voltammogram for 2,4-dinitrophenyl-γ-aminobutyric acid. Dinitrophenyl derivatives can be easily formed from the more common derivatizing agent for amines, 2,4-dinitrofluorobenzene. The dinitrophenyl derivatives are reduced at more negative potentials than the corresponding TNP derivatives and only two voltammetric waves are observed. Therefore, the TNP derivatives are superior for amperometric detection with carbon electrodes, because they are easier to reduce and more electrons per mole of derivative are transferred at any given potential.

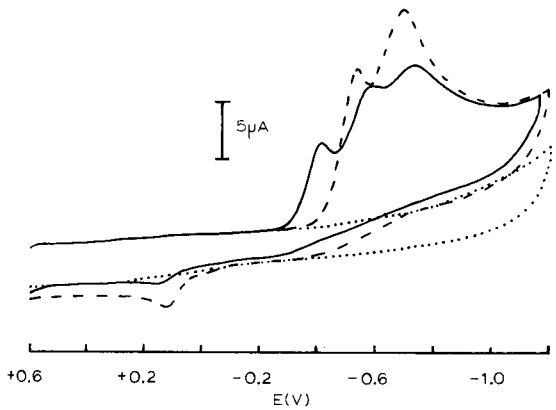

Fig. 1. Cyclic voltammograms at a glassy carbon electrode in the deoxygenated mobile phase used with reversed-phase columns. Scan rate, 200 mV s^{-1}. (—) 2,4,6-Trinitrophenyl-γ-aminobutyric acid, 1 × 10^{-4} M; (– – –) 2,4-dinitrophenyl-γ-aminobutyric acid, 1 × 10^{-4} M; (···) background.

L.c.e.c. of TNP derivatives

The TNP derivatives are readily separated by the reversed-phase column and are detected amperometrically with carbon electrodes (Fig. 2). An unexpected problem is that oxygen in solution is retained on reversed-phase columns. The retention time of the oxygen peak is virtually independent of the mobile phase composition, but is a function of flow rate. Because the concentration of oxygen in aqueous solutions is greater than 10^{-4} M at standard temperature and pressure, oxygen can be a significant interference for trace analysis. To remove oxygen, all samples were purged with nitrogen for 2 min in a sealed micro vial. As shown in Fig. 2, this procedure does not result in an alteration of the concentrations of trinitrophenyl derivatives even from volumes as small as 200 μl.

With amperometric detection, the noise depends on the magnitude of the residual current. For a faradaic species in the mobile phase, it has been shown that the value of the amperometric noise is dependent on the degree of fluctuations in the flow rate [13, 23, 24]. Thus, with amperometric detection at negative potentials, such as are required here, it is imperative to reduce the amount of oxygen in the mobile phase to trace levels unless totally pulse-free pumping systems are employed. For example, for a glassy carbon detector operated at —0.6 V in a deoxygenated mobile phase, a residual current of 53 nA was observed with a 0.6-nA peak-to-peak noise level. When the flow of nitrogen in the mobile phase was turned off, the residual current rapidly increased, and, at a residual current level of 380 nA, the peak-to-peak noise had increased 3-fold. Furthermore, oxygen in the buffer also leads to gradual fluctuations in the background signal as has been previously shown [8]. This may arise from outgassing of the solvent by the pump and it certainly precludes trace measurements.

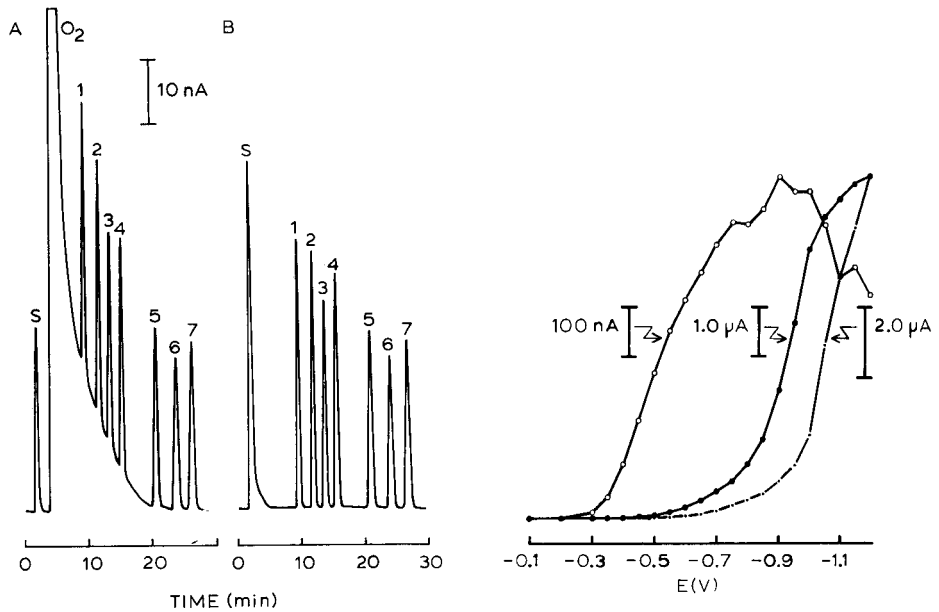

Fig. 2. Reversed-phase chromatograms with amperometric detection of a standard solution of TNP derivatives of amino acids (50 pmol of each derivative): (A) without sample deoxygenation; (B) with sample deoxygenation. Peak assignments: S, solvent front; O_2, oxygen; (1) glycine; (2) L-alanine; (3) β-alanine; (4) γ-aminobutyric acid; (5) β-aminoisobutyric acid; (6) α-aminobutyric acid; and (7) δ-aminovaleric acid.

Fig. 3. Hydrodynamic voltammograms at a glassy carbon electrode obtained following reversed-phase separation. Flow rate, 1.5 ml min^{-1}. (○) γ-Aminobutyric acid derivative (1×10^{-6} M); (●) O_2 in sample at room temperature and atmospheric pressure; (—·—) residual current.

The selection of the potential for detection of TNP derivatives involves a series of tradeoffs. This is illustrated in the hydrodynamic voltammograms for oxygen, the TNP derivatives, and the residual currents that were obtained by recording chromatograms at increasingly negative potentials (Fig. 3). The voltammograms of the other derivatives are very similar to that for the γ-aminobutyric acid derivative. The stepwise reduction that is apparent in Fig. 1 is hardly observed in the hydrodynamic voltammogram, possibly because the electrode surface had deteriorated after extended use. The composite waves are shifted to negative potentials as expected [25]. At potentials beyond —0.9 V, the current decreases suggesting either that electrogenerated products are reacting with the γ-aminobutyric acid derivative or that the electrode response is deteriorating. The dissimilarity in shape of the curve for injected oxygen to that for the background indicates that oxygen levels are effectively reduced. It can be seen that at —0.6 V, only partial electrolysis of oxygen occurs, and yet, as described above, this is of sufficient magnitude

to cause serious interferences unless removed. The magnitude of the residual current and the current for oxygen are considerably larger at the potential for the 12-electron reduction of the γ-aminobutyric acid derivative than at the potential for the 8-electron reduction (—0.6 V) and thus this potential was employed.

Micromanipulation of sample

The reaction of TNBS with primary amines has been shown to be a nucleophilic aromatic substitution with the rate-limiting step being the formation of a tetra-substituted ring carbon intermediate [17, 18]. The second-order rate constants for γ-aminobutyric acid, L-alanine, β-alanine and glycine have been shown to be 2—3 orders of magnitude greater than that of hydroxide ion [18]. The optimum pH for the reaction which will minimize side products, such as picric acid, and which will provide for 100% derivatization at room temperature, has been determined to be 9.0 [3].

Under the conditions described in the experimental section, the microreaction proceeds to 100% derivatization of the amine. The efficiency of the reaction was determined by comparing the amount of derivative formed under the conditions given in the experimental section with a known amount of authentic TNP derivative following separation on an anion-exchange column (Fig. 4A and B). Direct injection of the derivatized sample onto the reversed-phase column is not possible because TNBS remains in high concentration ($\sim 10^{-2}$ M) in the reaction mixtures. Trinitrobenzenesulfonic acid elutes very quickly on the reversed phase column and hinders trace determination of the TNP derivatives. High concentrations of TNBS also cause a considerable decrease in column lifetime. To alleviate these problems, an extraction procedure with toluene was employed. The recoveries obtained following the extraction procedure for deoxygenated samples are given in

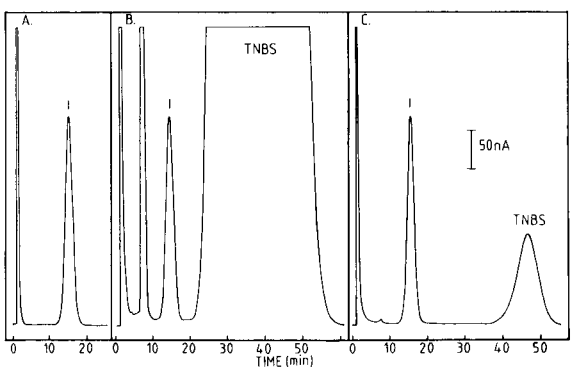

Fig. 4. Chromatograms obtained with the SAX column with amperometric detection. (A) Chromatogram of standard 2,4,6-trinitrophenyl-γ-aminobutyric acid (500 pmol, peak 1); (B) chromatogram of microderivatized γ-aminobutyric acid (500 pmol, peak 1); (C) chromatogram of microderivatized and extracted γ-aminobutyric acid (500 pmol, peak 1).

Table 1. The extraction procedure, which is based on the relative acidity of TNBS vs. the derivatives, is obviously very efficient for the compounds listed. Trinitrobenzenesulfonic acid is almost totally removed as are most other polar, unidentified reaction side products (Fig. 4C). However, this extraction procedure is not universal; more polar compounds such as TNP glutamate and TNP aspartate are only recovered at less than 50% yield. If larger sample volumes are available, pre-column cleanup with an anion-exchange resin would be preferable.

Because errors may arise during the manipulation of the small volumes as a result of dispensing errors or sample evaporation, the addition of an internal standard is essential [26]. For the compounds in this work, the TNP derivative of δ-aminovaleric acid is ideal for this role. Analysis of the working curves obtained from the l.c.e.c. chromatograms using the internal standard after microreaction and extraction shows that linear working curves for 1—500 pmol are found for all of the compounds employed. Unextracted, electroactive reaction side products co-elute with the β-alanine and glycine derivatives, but these are u.v.-transparent.

Comparison of detection methods

The u.v. detector and both types of electrochemical detectors are suitable for chromatographic detection of the TNP derivatives. Figure 5A shows a typical chromatogram of a micro-derivatized mixture of amino acids (corresponding to 25 pmol of each derivative) that was obtained with u.v. detection. All of the TNP derivatives are completely resolved. One undesirable feature is the appearance of a toluene peak at 42 min which increases the time of determination with respect to electrochemical detection.

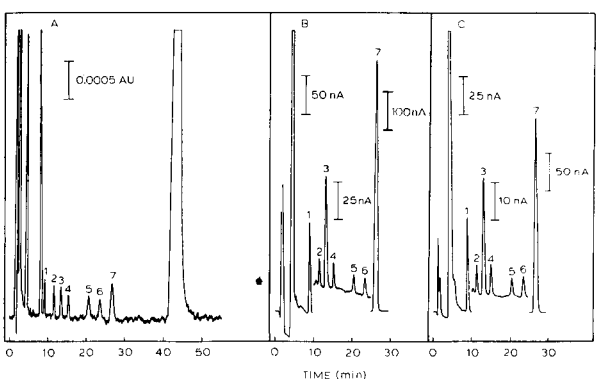

Fig. 5. Reversed-phase chromatograms of a microderivatized mixture of amino acids. (A) U.v. detection of 25 pmol of each derivative; (B) amperometric detection with glassy carbon (1 pmol of each derivative); (C) amperometric detection with the pyrolytic graphite (1 pmol of each derivative). Peak assignments: (1) glycine; (2) L-alanine; (3) β-alanine; (4) γ-aminobutyric acid; (5) β-aminoisobutyric acid; (6) α-aminobutyric acid; (7) the internal standard, δ-aminovaleric acid (50 pmol); (8) toluene.

Figures 5B and 5C show chromatograms of micro-derivatized mixtures of amino acids (corresponding to 1 pmol of each derivative) that were obtained with the glassy carbon and the pyrolytic graphite detectors, respectively. The signal-to-noise (peak-to-peak) ratios of the derivatized γ-aminobutyric acid peaks for the three modes of detection were found to be: u.v. detection (25 pmol of the derivative), S/N = 5.4; glassy carbon (1 pmol of the derivative), S/N = 8.0; and pyrolytic graphite (1 pmol of the derivative), S/N = 14. Comparison of these ratios for each of these detectors indicates that the pyrolytic graphite detector has detection limits ca. 2 × lower than the glassy carbon detector and ca. 66 × lower than the u.v. detector.

The difference in the signal-to-noise ratios of the two electrochemical detectors is consistently observed, and may arise because only a portion of the surface-oxidized basal plane of pyrolytic graphite is available for electrolysis, resulting in "islands" of carbon where electrolysis occurs. These isolated sites would be expected to be less dependent on flow rate fluctuations [23], and their presence is implied because the absolute amperometric current at these pyrolytic graphite electrodes is less than that of glassy carbon electrodes of identical geometric area. Freshly oxidized pressure-annealed pyrolytic graphite shows the theoretically expected dependence of current on geometric area [27, 28], but this response decays to a stable value after prolonged use [16], with the observed, improved signal-to-noise ratios. Although the differences in signal-to-noise ratios for the two electrochemical detectors are not significant for routine applications, these observations may be important for planning strategies to improve detection limits with electrochemical detectors. Despite the very high molar absorptivity of these compounds, the signal-to-noise ratios do demonstrate that the electrochemical detectors are preferable to u.v. detection for trace detection of TNP derivatives.

All of these data suggest that TNBS is an ideal derivatizing agent for the trace detection of alkylamines. The reaction is quantitative and the reagent can easily be removed before chromatographic separation of the derivatives because it is such a strong acid. The derivatives are well suited for both u.v. and electrochemical detection with the latter method preferred for trace determination.

The gifts of samples of pressure-annealed pyrolytic graphite from Union Carbide are gratefully acknowledged. This work was supported by NSF Research Grant BNS 81-00044. R.M.W. is an Alfred P. Sloan Fellow and the recipient of an NIH Research Career Development Award (K04 NS 00356-04).

REFERENCES

1 T. Okuyama and K. Satake, J. Biochem. (Tokyo), 47 (1960) 454.
2 K. Satake, T. Okuyama, M. Ohashi and T. Shinoda, J. Biochem. (Tokyo), 47 (1960) 654.
3 L. C. Mockrasch, Anal. Biochem., 18 (1967) 64.

4 W. L. Caudill, G. P. Houck and R. M. Wightman, J. Chromatogr., Biomed. Appl., 227 (1982) 331.
5 P. T. Kissinger, C. S. Bruntlett and R. E. Shoup, Life Sci., 28 (1981) 455.
6 I. N. Mefford, J. Neurosci. Meth., 3 (1981) 207.
7 P. T. Kissinger, Anal. Chem., 49 (1977) 447A.
8 W. A. MacCrehan and R. A. Durst, Anal. Chem., 53 (1981) 1700.
9 K. Bratin, P. T. Kissinger, R. C. Briner and C. S. Bruntlett, Anal. Chim. Acta, 130 (1981) 295.
10 R. Samuelson, J. O'Dea and J. Osteryoung, Anal. Chem., 52 (1980) 2215.
11 D. L. Rabenstein and R. Saetre, Anal. Chem., 49 (1977) 1036.
12 W. A. MacCrehan and R. A. Durst, Anal. Chem., 50 (1978) 2108.
13 W. A. MacCrehan, Anal. Chem., 53 (1981) 74.
14 R. C. Buchta and L. J. Papa, J. Chromatogr. Sci., 14 (1976) 213.
15 S. K. Vohra and G. W. Harrington, J. Chromatogr. Sci., 18 (1980) 379.
16 R. M. Wightman, E. C. Paik, S. Borman and M. A. Dayton, Anal. Chem., 50 (1980) 1410.
17 A. R. Goldfarb, Biochemistry, 5 (1966) 2570.
18 G. E. Means, W. I. Congdon and M. L. Bender, Biochemistry, 11 (1972) 3564.
19 U. B. Ehlers and J. W. Sease, Anal. Chem., 31 (1959) 16.
20 S. F. Dennis, A. S. Powell and M. J. Astel, J. Am. Chem. Soc., 71 (1949) 1484.
21 G. W. Jackson and J. S. Dereska, J. Electrochem. Soc., 112 (1965) 1218.
22 J. Pearson, Trans. Faraday Soc., 44 (1948) 683.
23 D. E. Weisshaar, D. E. Tallman and J. L. Anderson, Anal. Chem., 53 (1981) 1809.
24 D. G. Swartzfager, Anal. Chem., 48 (1976) 2189.
25 J. L. Anderson, D. E. Weisshaar and D. E. Tallman, Anal. Chem., 53 (1981) 906.
26 L. R. Snyder and Sj. van der Wal, Anal. Chem., 53 (1981) 877.
27 S. G. Weber and W. C. Purdy, Anal. Chim. Acta, 100 (1978) 531.
28 Y. Hirata, P. T. Lin, M. Novotny and R. M. Wightman, J. Chromatogr., Biomed. Appl., 181 (1980) 287.

Analytica Chimica Acta, 141 (1982) 279—286
Elsevier Scientific Publishing Company, Amsterdam — Printed in The Netherlands

CONDITIONS FOR SULFITE STABILIZATION AND DETERMINATION BY ION CHROMATOGRAPHY

MATS LINDGREN* and ANDERS CEDERGREN
Department of Analytical Chemistry, University of Umeå, S-901 87 Umeå (Sweden)
JAN LINDBERG
Analytical Research, Pharmacia Co., S-751 04 Uppsala (Sweden)
(Received 10th March 1982)

SUMMARY

The efficiencies of three groups of potential sulfite-stabilizing compounds were found to be in the order: carbonyls > alcohols = saccharides. A mole ratio of 1:1 between formaldehyde and sulfite was sufficient for stabilizing a sulfite solution for at least 72 h. The lower stabilizing efficiencies of the alcohols and saccharides examined could be compensated by using large excesses of these compounds. For example, if a 100-fold excess of glycerol over sulfite was used, the recovery of sulfite was 96% after 72 h compared with only 40% without addition of stabilizer. During separations by ion chromatography, almost no oxidation of the sample occurs provided the sample solution is directly injected into a deaerated eluent. For formaldehyde, the peak heights were found to depend on the molar ratio of the stabilizer to sulfite as well as on the concentration of sulfite. This effect was not found for the other stabilizers tested.

Addition of sulfite is widely used in the food and pharmaceutical industries to prevent oxidation and bacterial growth. One of the major problems concerned with the determination of sulfite originates from the instability of this ion in the presence of oxygen. This is the reason why various compounds have been proposed as stabilizers for sulfite throughout the years. One difficulty is to find a stabilizer which is compatible with the chosen analytical method.

Few methods based on ion chromatography [1] for the determination of sulfite have yet been published. Using this technique, Stevens and Turkelson [2] determined sulfite in boiler blow-down water. They recognized the problem of oxidation of the sulfite but did not try to overcome this by addition of any stabilizer. Hansen et al. [3] concluded that ion chromatography may be less suitable for the determination of sulfite because of oxidation during chromatography. They proposed the use of the sodium salt of hydroxymethylsulfonic acid in the preparation of standard solutions. Purging the solutions with argon was not found to be sufficient to prevent sulfite from being oxidized. Holcombe et al. [4] prepared their standard solutions of sulfite in either 60% isopropanol or in 10% formaldehyde, but did not

0003-2670/82/0000-0000/$02.75

elaborate on their stabilities. Dasgupta et al. [5] studied the stability of the formaldehyde—sulfite addition compound and found it to be excellent in a buffer of pH 4.

The purpose of the work described below was to study the efficiency of some selected potential sulfite-stabilizing compounds and their behavior in ion chromatographic analysis. Some stabilizers deliberately added or initially present in the sample may bind sulfite so strongly that erroneous sulfite levels are obtained. Depending on the stabilizer, different reaction products will be formed [6, 7].

EXPERIMENTAL

Equipment and chemicals

A Dionex model 12 ion chromatograph equipped with standard separator columns (glass or plastic), a standard suppressor column and a 0.1-ml sample loop was used for all experiments. The columns were supplied by the instrument manufacturer. Most experiments were run at a pump rate of 1.9 ml min^{-1}, with either 3.0 mM $NaHCO_3$/2.4 mM Na_2CO_3, or 3.5 mM Na_2CO_3/2.6 mM NaOH as the eluent. A Linear Instruments two-channel recorder was used. Concentrations were determined from peak heights.

All solutions were prepared in distilled water from reagent-grade chemicals unless otherwise stated. All standard solutions were prepared by weight. The system was calibrated for sulfite by using standard solutions prepared from sodium hydroxymethylsulfonate ($HOCH_2SO_3Na$; 98%; Aldrich). In the examination of sulfite stabilization, solutions were prepared from sodium sulfite and sodium hydrogensulfite. The stabilizers used were formaldehyde (solutions prepared from 37% w/v HCHO), acetone, glycerol, isopropanol, fructose, glucose and mannose. The ionic purities of the stabilizers were checked by ion chromatography and no impurities were found.

Procedures

Unless otherwise stated, the sulfite solutions were prepared with equal concentrations of sulfite and the possible stabilizer. The solutions were prepared by weight and the sodium sulfite or hydrogensulfite was dissolved in a solution of the stabilizer in order to prevent the oxidation of sulfite before the stabilizing tests were performed. The sulfite concentration was determined iodimetrically, with potassium iodate as primary standard.

RESULTS AND DISCUSSION

It has been stated [2, 3, 8] that sulfite can be oxidized during an ion-chromatographic run. In order to establish the extent of this oxidation within the chromatographic system, the sulfite concentration of a sample was determined both simultaneously with the injection into the ion chromatograph and after the sample had passed through the system. Table 1 shows that if a

TABLE 1

Recovery of sulfite for different ion-chromatographic conditions. The recoveries are based on iodimetric titration both simultaneously with the injection and after passing through the system

	Amount of sulfite (μmol)		Recovery (± s.d.) (%)[a]
	Injected	Found	
Eluent deaerated	0.449	0.446	99.4 (± 0.5)
Eluent not deaerated	0.478	0.454	94.8 (± 0.9)
Immediate injection	0.493	0.491	99.5 (± 0.5)
20 min in the loop	0.521	0.490	94.0 (± 1.5)

[a] $n = 5$.

deaerated eluent is used and the unstabilized sample is injected without delay, there is almost no oxidation of the sulfite in the system itself. This indicates that instability of the sulfite solution prior to the injection is the main problem. However, when the sample was kept in the teflon sample loop for 20 min, 94% recovery was obtained, compared with 99% for direct injections. This result is expected because oxygen permeates teflon tubing.

Stabilizers

Sulfite forms different stable compounds with aldehydes and ketones to form a hydroxysulfonic acid

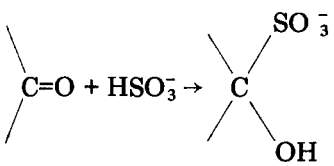

(1)

Alcohols and saccharides have also been proposed as stabilizers, although the stabilizing mechanism is more obscure in these cases. It may involve hydrogen bonding between e.g., saccharide and hydrogensulfite. The suitability of alcohols and saccharides as stabilizers for sulfite in ion chromatography was therefore also tested. The results of these experiments are given in Table 2. As can be seen, both formaldehyde and acetone give a very good stabilizing effect, formaldehyde being the most effective. For practical purposes, fructose and mannose may be used as stabilizers whereas glucose appears to have no stabilizing effect at all. Fructose is significantly better as a stabilizer than the other saccharides tested, which can be explained by the fact that aldohexoses exist mainly in their cyclic forms whereas ketohexoses (fructose) exist only partly in this form [9]. Isopropanol and glycerol are similar to the saccharides (except fructose) in their stabilizing ability. The last two columns in Table 2 show the stabilizing effects when the oxidizing conditions are increased by aeration or autoclaving. In the aeration experiment, all the

TABLE 2

The stability of sulfite in solution with different stabilizers at the same concentration as the sulfite
(All numbers are percentage recoveries)

	0 h[a]	4 h[a]	24 h[a]	72 h[a]	Aerated 15 min[b]	Autoclaved 101 kPa, 121°C[b]
Unstabilized	100	92	74	22	74	40
Formaldehyde	100	100	100	100	100	70
Acetone	100	100	100	98	98	70
Isopropanol	100	97	93	65	88	51
Glycerol	100	97	95	62	85	53
Fructose	100	100	96	78	95	47
Glucose	100	95	78	30	90	17
Mannose	100	98	95	68	92	43

[a]Room temperature, laboratory environment. [b]Freshly prepared solutions.

solutions of sulfite and stabilizer were freshly prepared and aerated for 15 min. Under these conditions, only formaldehyde and acetone work well as stabilizers. This means that with these stabilizers it is not necessary to deaerate the eluent before chromatography. As autoclaving is commonly used in the food and pharmaceutical industries, this treatment was also investigated. No stabilizer tested could prevent oxidation of sulfite during autoclaving (101 kPa, 121°C, 15 min). For each type of stabilizer, the actual figures obtained will vary with type of autoclave and initial concentration of oxygen.

Table 3 shows that not only the type of stabilizing compound but also the molar ratio of stabilizer to sulfite determines the stability of sulfite. This

TABLE 3

The recovery of sulfite using different molar ratios of stabilizer to sulfite, n_{stab}: $n_{SO_3^{2-}}$

Stabilizer	n_{stab}: $n_{SO_3^{2-}}$	Recovery (%)			
		0 h	4 h	24 h	72 h
Formaldehyde	1	100	100	100	100
Isopropanol	1	100	97	93	65
	10	100	98	97	94
	100	100	99	97	94
Glycerol	1	100	97	95	62
	10	100	98	95	84
	100	100	99	98	96
Fructose	1	100	100	96	78
	10	100	100	98	92
Glucose	1	100	95	78	30
	10	100	98	95	80

ratio has a profound effect on the sulfite stability if a less active stabilizer is used, e.g., glycerol. With this compound, acceptable stability (2% oxidation during 24 h) can be achieved by using a 100-fold excess of glycerol.

Ion chromatography

Koch [10] has shown that weak acids (e.g., nitrous acid) are not subject to Donnan exclusion in the suppressor column. He suggested that the same effect would be obtained with other weak acids such as acetic acid and sulfurous acid. No indication of such effects were found in the determination of sulfite. The simple reason for this is that sulfurous acid is completely in the HSO_3^- form (pK_1 = 1.89, 25° C) in the suppressor and will be excluded by the negatively charged resin in the suppressor column.

The ion-chromatographic conditions using the very efficient formaldehyde as stabilizer were first investigated. Figure 1A shows a chromatogram of a mixture of sulfite and sulfate both at a concentration of ~0.5 mM. Sulfite is separated from sulfate though not completely because of the state of the separator column. The peak in Fig. 1B is caused by the ionic compound formed between sulfite and formaldehyde. The retention time for sulfite is 15.9 min whereas the retention time for the peak in Fig. 1B is 17.2 min. The eluent used was 3.0 mM HCO_3^-/2.4 mM CO_3^{2-}, pH 10.4. The chromatograms of the same solutions using the eluent, 3.5 mM CO_3^{2-}/2.6 mM OH^-, which is recommended by Hansen et al. [3], are shown in Fig. 2. Using the same column set and the same flow rate, the resolution and the response are

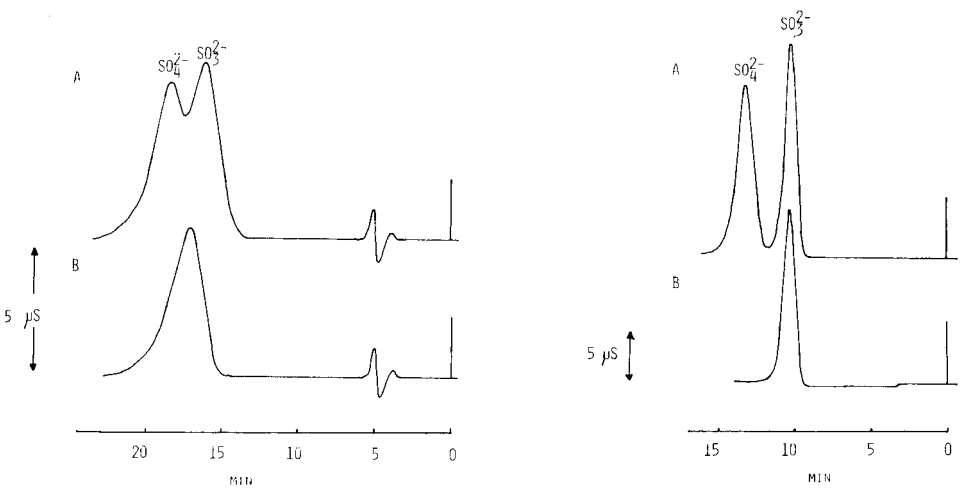

Fig. 1. Ion-chromatograms: (A) mixture of SO_3^{2-} and SO_4^{2-}, no stabilizer added; (B) mixture of SO_3^{2-} and formaldehyde in molar ratio 1:1. Concentrations ≈0.5 mM; eluent, 3.0 mM HCO_3^-/2.4 mM CO_3^{2-}; separator, 3 × 500-mm glass.

Fig. 2. Ion-chromatograms: (A) mixture of SO_3^{2-} and SO_4^{2-}, without stabilizer; (B) mixture of SO_3^{2-} and formaldehyde in molar ratio 1:1. Concentrations ≈0.5 mM; eluent, 3.5 mM CO_3^{2-}/2.6 mM OH^-; separator, 3 × 500-mm glass.

much better. When this eluent is used, the retention times for unstabilized sulfite and sulfite that is stabilized with formaldehyde are the same and shorter than the previous eluent: t_R (SO_3^{2-}) = t_R (SO_3^{2-}, CH_2O) = 10.3 min. The results shown in Figs. 1 and 2 can be explained by reaction (1). Thus formaldehyde will form hydroxymethylsulfonic acid (HMSA), which is a strong acid. In order to confirm this, a solution of HMSA (Aldrich, 98%) was prepared. Under identical conditions, the same retention time was obtained as for the peak in Fig. 1B, thus confirming reaction (1).

Figure 3 shows the difference in retention times between sulfite and HMSA as a function of the pH of the eluent, as determined by ion chromatography. The pH of the eluent was varied by changing the sodium hydroxide concentration whereas the concentration of sodium hydrogencarbonate was held constant at 3.5 mM. A (3 × 500-mm) separator glass column was used. When the difference between t_R (HMSA) and t_R (SO_3^{2-}) is zero, i.e., at pH 10.7, the HMSA is completely hydrolyzed under the conditions used. This means that SO_3^{2-} ions pass through the separator column whether aldehyde is added or not. However, at pH < 10.7, the ionic species is SO_3^{2-} if no aldehyde is added, and HMSA if aldehyde is added. This explains the different retention times.

The ion-chromatographic behavior of sulfite with different stabilizers present is summarized in Table 4. The effect of the molar ratio of stabilizer to sulfite on the peak height was measured for three concentration levels of sulfite. It is obvious that formaldehyde behaves quite differently from the other stabilizers. As the molar ratio of formaldehyde to sulfite is increased, the peak height decreases significantly and this effect is even more pronounced for higher concentrations of sulfite. The peak broadens as the molar ratio of formaldehyde to sulfite is increased, but this cannot be the full explanation, because the peak area also decreases. The other stabilizers will give constant peak heights irrespective of the molar ratios of stabilizer to sulfite for all sulfite levels.

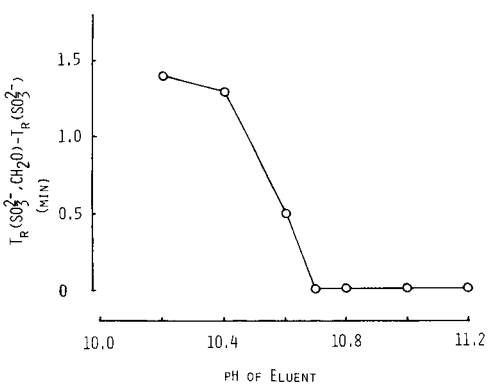

Fig. 3. The difference in retention times between HMSA and SO_3^{2-} as a function of the pH of the eluent. $n_{SO_3^{2-}}$: n_{CH_2O} = 1:1. Eluent, 3.5 mM HCO_3^{2-}.

TABLE 4

Peak heights as a function of different molar ratios of stabilizer to sulfite
(The peak heights for the ratio 1 are normalized to 100, for each individual stabilizer)

Stabilizer	$n_{stab}: n_{SO_3^{2-}}$	Molarity of sulfite (μM)		
		10	100	1000
Formaldehyde	1	100	100	100
	10	92	90	75
	100	41	35	23
Glycerol	1	100	100	100
	10	100	100	100
	100	100	100	100
Isopropanol	1	100	100	100
	10	100	100	100
	100	100	100	100
Fructose	1	100	100	100
	10	100	100	99
	100	98	97	93

Figure 4 shows calibration curves for sulfite with different concentrations of formaldehyde added. If the addition compound ($HOCH_2SO_3Na$) is used, a straight calibration curve is obtained. If an excess of formaldehyde is used, the calibration curves start to bend, and the more so, the larger the excess of formaldehyde.

The addition compound has been recommended as a standard substance for calibration curves. It is obvious from Fig. 4 that gross errors may be obtained if the molar ratio of formaldehyde to sulfite is not similar in the standards and samples. If a very large excess of formaldehyde is used, an

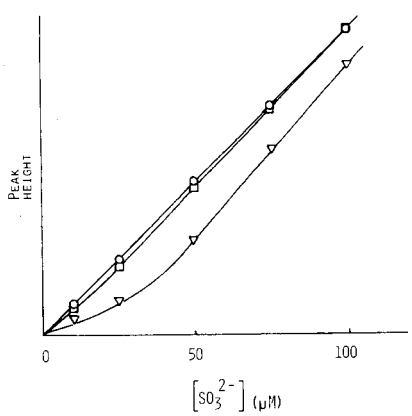

Fig. 4. Calibration graphs for sulfite with formaldehyde. (○) Addition compound ($HOCH_2SO_3Na$); (□) [CH_2O] = 0.1 mM; (▽) [CH_2O] = 1 mM.

additional drawback is that the slope of the calibration curve will decrease significantly which may be of importance if low concentrations of sulfite are to be determined. None of the other stabilizers tested gave a similar effect on the peak height when they were used in large excess.

Work is in progress to apply the results of this investigation to some pharmaceutical preparations.

Conclusion

Formaldehyde was found to be the most effective compound for preventing oxidation of sulfite. However, from an ion-chromatographic point of view, formaldehyde presents some drawbacks. The stability of the compound formed (HMSA) between sulfite and formaldehyde is pH-dependent. Alkaline eluents offer the best separations but cause hydrolysis of HMSA. The peak height is strongly dependent on the ratio of formaldehyde to sulfite. This is not the case for the other stabilizers. Any of them, e.g., glycerol, can be recommended if the molar ratio of stabilizer to sulfite exceeds 100.

REFERENCES

1 H. Small, T. S. Stevens and W. C. Bauman, Anal. Chem., 47 (1975) 1801.
2 T. S. Stevens, V. T. Turkelson and W. R. Albe, Anal. Chem., 49 (1977) 1176.
3 L. D. Hansen, B. E. Richter, D. K. Rollins, J. D. Lamb and D. J. Eatough, Anal. Chem., 51 (1979) 633.
4 L. J. Holcombe, B. F. Jones, E. E. Ellsworth and F. B. Meserole, in J. D. Mulik and E. Sawicki (Eds.), Ion Chromatographic Analysis of Environmental Pollutants, Ann Arbor Science, Ann Arbor, MI, 1979, p. 401.
5 P. K. Dasgupta, K. DeCesare and J. C. Ullrey, Anal. Chem., 52 (1980) 1912.
6 J. B. S. Bravermann, J. Sci. Food Agric., 4 (1953) 540.
7 D. L. Ingles, Chem. Ind., (1960) 1159; Aust. J. Chem., 13 (1960) 404; 15 (1962) 342.
8 N. P. Barkley, G. L. Contner and M. Malanchik, in J. D. Mulik and E. Sawicki (Eds.), Ion Chromatographic Analysis of Environmental Pollutants, Ann Arbor Science, Ann Arbor, MI, 1979, p. 115.
9 L. Eberson, Organisk Kemi, Almqvist och Wiksell, Stockholm, 1970, p. 427.
10 W. F. Koch, Anal. Chem., 51 (1979) 1571.

Analytica Chimica Acta, 141 (1982) 287—299
Elsevier Scientific Publishing Company, Amsterdam — Printed in The Netherlands

MICROSCALE FUNCTIONAL GROUP ANALYSIS OF MARINE AND SEDIMENTARY HUMIC SUBSTANCES

A. H. GILLAM[a] and J. P. RILEY*

Department of Oceanography, University of Liverpool, P.O. Box 147, Liverpool L69 3BX (Gt. Britain)

(Received 25 March, 1982)

SUMMARY

Methods are described for the microscale analysis of aquatic and sedimentary humic substances for several oxygen-containing functional groups including total acidity, carboxylic and phenolic hydroxyl groups, quinone groups and hydroxamate linkages. Coefficients of variation of the methods range from 4.9 to 12.9%.

The dissolved organic matter (DOM) in natural waters is a complex assemblage of decayed plant and soil materials and of the polymeric compounds produced by the random combination of these various biomonomers [1]. The dissolved polymeric compounds, or aquatic humic substances, can contribute up to 80% of the total dissolved organic carbon (DOC) in some waters [2—4]. The concentrations of aquatic humic substances are low, ranging from 10 mg l^{-1} in certain inland waters to <0.5 mg l^{-1} in oceanic waters, and studies of the chemical and physical characteristics of aquatic, especially marine, humic substances have therefore been hampered by difficulties in isolating sufficient quantities of organic material [5—9].

Although the classical methods for the determination of functional groups used by soil scientists [10, 11] have been used in several studies of humic substances in fresh water [12—14], it is necessary to scale them down before they can be employed with the limited amounts of humic materials available from waters with low organic loadings. A knowledge of the concentrations of the carboxylic and phenolic groups, as well as of the other oxygen-containing functional groups, is essential for an understanding of the interaction of, for example, trace metals with aquatic humic substances [15—18].

Humic substances are a major component of the organic fraction of recent marine sediments, comprising $\geqslant$ 40% of the total organic matter [19]. Measurements of the ^{13}C:^{12}C isotope ratios of sedimentary humic substances suggest that these compounds are not allochthonous detrital materials but autochthonous in nature [19]. Several studies [20—22] have indicated that

[a]Present address: Department of Oceanography, The University of British Columbia, 6270, University Boulevard, Vancouver, V6T 1W5, Canada.

0003-2670/82/0000-0000/$02.75

humic substances play an important role in the organometallic geochemistry of sediments. Microscale analysis of sedimentary humic substances is essential if studies are to be made of the changes in the nature of sedimentary organics with depth of burial.

Techniques have been available for many years for the elemental analysis of 1—5 mg samples of organic materials [23]. However, the classical functional group methods applied to soil and, more recently to aquatic humic substances require 50—100 mg of organic material [10]. Assuming that a typical sample size available for functional group analyses of aquatic humic materials would be 5—10 mg and that the concentrations of the various functional groups in humic substances are <10 meq g^{-1}, it would be necessary to determine <0.1 meq of the functional group. Such microscale samples require the use of specialised apparatus and techniques if suitable precision and accuracy are to be attained [24]. Techniques which have been developed for the microscale determination of total acidity (total exchangeable hydrogen ion), carboxylic and phenolic hydroxyl groups, ketonic carbonyls, quinone groups and hydroxamate groups in 5—10 mg samples of aquatic humic materials are described in the present paper; in general, they are based on classical procedures for soil analysis [10, 11].

EXPERIMENTAL

Reagents

All reagents were of the highest quality available and, unless specified, were used without further purification.

Total acidity determination. Barium hydroxide solution (ca. 0.01 M) was prepared by dilution of a 0.1 M $Ba(OH)_2$ solution [25] and was standardised against 0.05 M hydrochloric acid, using phenolphthalein as indicator. The standard solution was stored in a polyethylene bottle fitted with an ascarite trap. Hydrochloric acid (0.02 M) was prepared by dilution of the constant boiling acid. Distilled water was prepared free of CO_2 by nitrogen purging and was then stored in a polyethylene bottle fitted with an ascarite trap.

Carboxyl group determination. Calcium acetate solution was prepared by direct weighing of calcium acetate dihydrate. Sodium hydroxide (carbonate-free, ca. 0.05 M) was prepared by dilution of an 18 M NaOH solution which had been allowed to stand to remove sodium carbonate. The solution was then standardised with potassium hydrogenphthalate [26].

Carbonyl group determination. A standard dimethylaminoethanol solution (0.25 M) was prepared by diluting freshly distilled 2-dimethylaminoethanol (25 ml) to 1 l with 2-propanol. A 0.01 M solution was then prepared by dilution of the standard solution with 2-propanol. For the hydroxylammonium chloride solution (0.04 M), 2.78 g of the compound was dissolved in 300 ml of redistilled methanol and the solution was diluted to 1 l with 2-propanol.

A solution of perchloric acid (0.2 M), prepared by diluting 18 ml of 60% perchloric acid to 1 l with redistilled methyl cellosolve, was standardised as

recommended by Cheronis and Ma [24]. A 0.1 M solution of perchloric acid was prepared by suitable dilution with methyl cellosolve.

Quinone group determination. Tin(II) chloride solutions (0.05 and 0.01 N) were prepared by direct weighing of the dihydrate and dilution with de-aerated 0.5 M HCl; they were stored under nitrogen. Potassium dichromate solutions (0.05 and 0.01 N) were prepared by direct weighing and dilution with CO_2-free water. Carbonate-free sodium hydroxide solutions (0.25 and 0.1 M) were prepared as above and standardised against hydrochloric acid.

Hydroxamate group determination. The reagents and conditions described by Gillam et al. [27], were used in a modified Csaky test for the spectrophotometric determination of bound hydroxylamine.

Samples

Details of the techniques used for the isolation of aquatic and sedimentary humic substances used in this study have been described previously [28]. Briefly, aquatic humic substances were concentrated from water samples of large volume (100—200 l) from the Skaggerak, Irish Sea and various sites in N. Wales by adsorption on Amberlite XAD-2 resin. Sedimentary humic material was isolated from core samples taken in the Skaggerak and the Irish Sea, using the classical 0.5 M sodium hydroxide extraction method of soil science [10, 28].

Apparatus

A Radiometer PHM 64 pH meter was used with a Radiometer GK2301C combined glass—calomel electrode for the determination of total acidity, carboxyl and carbonyl groups. The instrument was standardised with NBS borate and equimolal phosphate buffers, having pH values at 20°C of 9.235 and 6.881, respectively [29]. For the determination of quinone groups, the same meter was used with a Radiometer P101 platinum electrode and a Radiometer K401 calomel electrode. A Radiometer ABU12 autoburette was used for titrations.

Procedures

Total acidity. Accurately weigh 5—10 mg of humic material into a 25-ml ground-glass stoppered conical flask. Add 10 ml of 0.01 M barium hydroxide solution and blanket with nitrogen. Stopper the flask and shake for 24 h at ambient temperature. Filter the suspension (GF/C) and rinse the flask and filter with three 10-ml aliquots of CO_2-free water. Combine the filtrate and washings and titrate potentiometrically with standard 0.02 M hydrochloric acid. Standardize the procedure by titrating 10 ml of 0.01 M barium hydroxide, determining the equivalence points by the Gran technique [30]. Plot $(V_o + V_i)10^{pH}$ against V_i to give $V_i = V_e$ (the equivalence volume) when $(V_o + V_i)10^{pH} = 0$; V_o is the original volume of the solution to be titrated and V_i is the titrant addition. Calculate the total acidity values in meq g^{-1}, using the method of Schnitzer and Khan [10].

Carboxyl groups. Weigh out accurately 5—10 mg of humic material into a 25-ml ground-glass stoppered conical flask. Add 10 ml of 0.01 M calcium acetate solution and blanket with nitrogen. Stopper the flask and shake for 24 h at ambient temperature. Filter and wash the precipitate, and titrate the combined filtrate and washings as described above. Determine the blank in the same manner, omitting the sample. Calculate the carboxyl content as described for the total acidity determination.

Carbonyl groups. Accurately weigh 5—10 mg of humic material into a 25-ml ground-glass stoppered conical flask. Add 5 ml of 0.01 M 2-dimethylaminoethanol solution and 5 ml of 0.04 M hydroxylammonium chloride solution. Stopper the flask tightly and immerse it in a water-bath at 70°C for 30 min. Cool to room temperature and titrate the excess of hydroxylamine potentiometrically with 0.1 M perchloric acid in methyl cellosolve. Determine the blank in the same fashion but omitting the sample. Plot $(V_o + V_i)10^{-E'/Q}$ against V_i as above; E' is the measured potential and Q = 59.16 mV at 25°C. Calculate the carbonyl content of the sample in terms of meq g^{-1} using the method of Schnitzer and Khan [10].

Quinone groups. Accurately weigh 5—10 mg of humic material into a 50-ml round-bottomed flask. Moisten the sample with 0.2 ml of ethanol and dissolve it in 5 ml of 0.1 M sodium hydroxide solution. Add 10 ml of 2.5 M sodium hydroxide solution, stopper the titration vessel and gently bubble the solution with nitrogen for 15 min. Add 5 ml of 0.01 N tin(II) chloride solution and continue bubbling for a further 60 min. Using a platinum and calomel electrode pair, titrate the excess of tin(II) potentiometrically with 0.01 N potassium dichromate solution. Run a blank in a similar fashion but omitting the sample. Plot $10^{E'/Q}$ against V_i to give $V_i = V_e$ when $10^{E'/Q} = 0$. Calculate the quinone content of the sample (meq g^{-1}) using the method of Schnitzer and Khan [10].

Hydroxamate groups. Dissolve the humic material (5—10 mg) in 4 ml of 2 M ammonia solution in a 10-ml pear-shaped flask. Add ~100 mg of activated charcoal and reflux the solution gently for 5 min. Filter the hot solution through a 3-mm layer of Celite 545 on a sintered glass filter of porosity 4. Reduce the filtered solution to dryness by rotary evaporation and redissolve in 5 ml of distilled water. Pipette 2-ml aliquots of the solution into two 15-ml screw-capped test tubes. Add 2 ml of 3 M sulphuric acid and hydrolyse the solution by autoclaving at 120°C for 4 h. Rinse the cooled solution into a 50-ml volumetric flask and add 7 ml of 2 M sodium acetate solution. Add 2 ml of sulphanilamide solution (1% w/v in 30% v/v acetic acid) and 2 ml of iodine solution (0.65% w/v in 1% w/v potassium iodide). Swirl the solution and allow to react for 5 min. Remove the excess of iodine by addition of 2 ml of sodium arsenite solution (1.5% w/v in distilled water) and add 2 ml *N*-(1-naphthyl)ethylenediamine solution (0.05% w/v in distilled water). Leave for 30 min for complete colour development. Dilute the solution to 50 ml and measure the absorbance in a 100-mm cell at 543 nm. Determine the blank by addition of the reagents (minus the iodine/arsenite reagents) to an aliquot (2 ml) of the acid-hydrolysed material in the same way.

RESULTS AND DISCUSSION

Total acidity

The chemical reactivity of humic substances is controlled largely by the variety of functional groups distributed within the macromolecular framework of these compounds. The most influential of these functional groups are the carboxylic and phenolic hydroxyl groups, which are responsible for the acidic nature of humic substances. The barium hydroxide method of Schnitzer and Khan [10] has been used in several studies of the total acidity of soil and sedimentary humic substances [10, 11, 31] and has been accepted as the most suitable method for aquatic humic substances [4, 12, 13]. Differential potentiometry [32] and titration calorimetry [33, 34] have also been used for total acidity determinations of humic substances. Although results from the differential method are usually in good agreement (± 0.2 meq g^{-1}) with those from the barium hydroxide method, Stuermer [35] and Gillam [28] have found that it is not suitable for aquatic humic substances.

Initial experiments with 50-mg portions of a peat humic acid sample showed that equilibrium with barium hydroxide was attained after 18 h. An equilibration time of 24 h was therefore adopted in the present study. Experiments using the end-point detection method recommended by Schnitzer and Khan [10] suggested that greater precision could be achieved by the use of a Gran plot to determine the equivalence points in the titration. The coefficients of variation for the determination of the end-points of the titration using a Gran plot, typified by Fig. 1, and that recommended by Schnitzer and Khan were 2.4% and 8.8%, respectively.

Replicate analyses (6) of 5—10-mg portions of a peat humic acid sample gave a mean value for the total acidity of 6.2 meq g^{-1} with a coefficient of variation of 4.9%. Table 1 shows data for the total acidity of aquatic fulvic acids of various origins; these range from 5.3 to 13.4 meq g^{-1} and are similar to those found earlier for both soil and water humic substances [4, 13]. Elemental analyses of the freshwater and sedimentary humic substances of this study indicate that between 34 and 88% of the oxygen in the aquatic humic substances studied is present in the carboxylic and phenolic hydroxyl groups. For the sedimentary humic substances the range was 18—42%. This clearly shows the dominance of the acidic oxygen-containing functional groups in aquatic humic compounds.

Carboxylic and phenolic hydroxyl groups

Aquatic humic substances are low-molecular-weight, polymeric, organic compounds highly substituted with carboxyl groups and in solution they behave as weak acid polyelectrolytes [36, 37]. Detailed information about the concentrations and dissociation constants of these weakly acidic functional groups is essential before an understanding of the complexing equilibria of metal ions with humic substances can be achieved. Several of the methods of calculating the number-average molecular weights (M_n) of aquatic humic

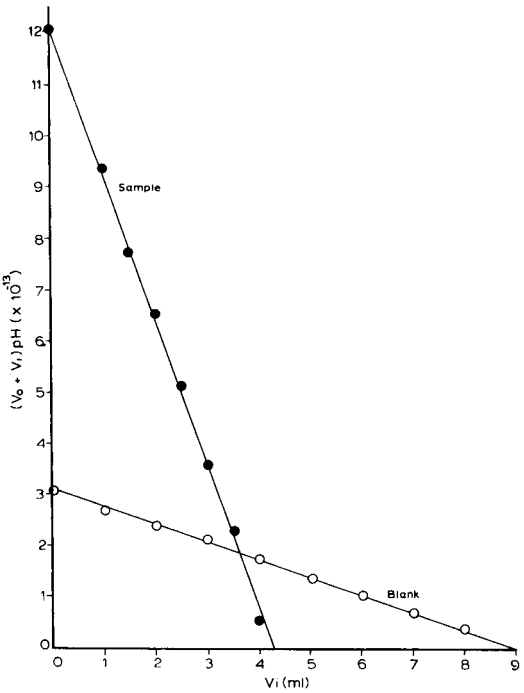

Fig. 1. Gran plots for the total acidity determination of humic substances. Sample is 10 mg of humic material with 10 ml of 0.01 M $Ba(OH)_2$. Blank is 10 ml of 0.01 M $Ba(OH)_2$. Titrant is 0.02 M HCl.

substances also require a knowledge of the concentrations and dissociation constants of these acidic functional groups [14]. An ion-exchange procedure involving the use of calcium acetate has been used by a number of workers [13, 38—40] for the determination of the carboxylic groups in various humic substances. Comparison of this method with a gravimetric technique [38] has shown it to be suitable for the determination of carboxyl groups in humic substances, despite some discrepancies with known organic acids. However, this technique has been criticised [34] on the grounds that humic substances are incompletely removed prior to the potentiometric titration and that, if the titration is continued to pH 9.8 as recommended by Schnitzer and Khan [10], acids other than acetic acid are titrated. This leads to an erroneously high value for the carboxyl content. To counter these objections, a filtration stage using a glass-fibre filter was introduced before the titration, for which a Gran technique was applied to determine the equivalence point. This permits carboxyl groups to be determined with accuracy and precision.

Initial experiments with 50-mg portions of a peat humic acid sample suggested that the reproducibility of the method of Schnitzer and Khan [10] was poor; six replicate analyses gave a mean value of 2.3 meq g^{-1} and a coefficient of variation of 15.9%. When the procedure described in this paper was

TABLE 1

Total acidity, carboxylic, phenolic hydroxyl and elements in aquatic and sedimentary humic substances

Sample	Functional groups (meq g^{-1})			Elements[d]			
	TA[a]	COOH[b]	P—OH[c]	C	H	N	O
Freshwater fulvic acids							
HM-1	12.2	10.1	2.1	44.2	3.5	3.2	49.1
CN-1	9.1	5.7	3.4	49.6	3.3	1.8	45.3
DE-1	5.5	4.6	0.9	52.9	3.6	3.4	40.1
Marine fulvic acids							
SK-1	10.7	7.1	3.6	45.4	5.9	7.8	40.9
SK-2	5.3	4.4	0.9	42.8	7.2	5.3	44.7
SK-3	9.2	7.6	1.6	43.9	6.1	6.4	43.6
SK-4	10.9	8.4	2.5	45.6	5.0	7.1	42.3
SK-5	13.4	8.9	4.5	45.7	7.3	6.6	40.4
SK-6	9.7	8.8	0.9	45.7	6.8	7.3	40.2
SK-7	5.8	4.4	1.4	45.8	6.0	6.4	41.8
SK-8	12.5	8.9	3.6	45.2	6.3	5.7	42.8
IS-1	8.2	6.7	1.5	46.7	7.1	5.6	40.6
Sedimentary humic acids							
SK-55-1	5.8	3.9	1.9	53.8	3.8	5.0	37.4
SK-86-1	4.1	2.4	1.7	50.3	4.5	4.8	40.4
SK-94-1	3.7	2.8	0.9	52.5	4.4	2.8	40.3
SK-96-1	2.8	1.9	0.9	52.0	4.5	3.5	40.0
SK-99-1	5.0	3.9	1.1	51.5	3.6	3.3	41.6
IS-37-1	4.6	3.2	1.4	54.9	4.3	2.9	37.9
IS-29	3.1	1.8	1.3	50.7	3.8	5.1	40.4
IS-37D	4.2	2.7	1.5	51.2	3.9	4.7	40.2
IS-38	3.8	2.2	1.6	53.5	4.3	3.4	38.8

[a]Total acidity. [b]Carboxylic groups. [c]Phenolic hydroxyl. [d]Determined with a Hewlett-Packard 185 CHN analyzer; oxygen calculated by difference.

applied with the same weight of sample, it proved possible to improve the precision considerably and the same peat humic acid gave a mean carboxyl content of 2.3 meq g^{-1} with a coefficient of variation of 6.5%. With 5—10-mg samples the coefficient of variation was 12.9%, which is still within the range (± 5—15%) generally agreed to be acceptable for the functional group analysis of humic compounds.

At present it is only possible to determine phenolic hydroxyl values as the difference between total acidity and carboxyl values [10]. Although a recent report has described a ^{13}C-enriched nuclear magnetic resonance method for the determination of hydroxyl functional groups in humic substances [41], in view of the inaccuracies of these procedures, there is obviously a need for the development of a direct method of determining the phenolic hydroxyl groups in humic substances.

The values for carboxylic and phenolic hydroxyl groups shown in Table 1 indicate that the marine fulvic acids have carboxyl group concentrations similar to those of freshwater fulvic acids. Sedimentary humic acids contain less carboxylic and phenolic hydroxyl groups than either the marine or the freshwater fulvic acids. No carboxyl or phenolic hydroxyl values were obtained for sedimentary fulvic acids, owing to their high ash contents ($\geqslant$15%). In contrast, the ash contents of the sedimentary humic acids were all $\leqslant$2%.

Carbonyl groups

Carbonyl groups are one of the major oxygen-containing functional groups present in humic and fulvic acids. They have been implicated in the chelation of the metals of waters and sediments [42, 43]. Methods for the determination of carbonyl groups in humic substances are based mostly on derivatisation techniques, such as oxime or phenylhydrazone formation. The increase in nitrogen content can be measured and related to the carbonyl concentration [44]. A method based on the polarographic determination of excess of 2,4-dinitrophenylhydrazine [45] has been shown to agree well with the more widely used oximation method [46].

The titrimetric oximation method for carbonyl determination [46] uses Martius yellow for detection of the end-point or a potentiometric method with a graphical determination of the end point [10]. The method described in this study is a modification of that of Schnitzer and Khan [10] and employs a Gran technique to determine the equivalence point of the titration.

Initial experiments using vanillin and benzil as model compounds suggested that if the oximation step was carried out by heating at 70°C for 30 min, the results were $\geqslant$97.5% of the theoretical values. The coefficient of variation for the vanillin determinations (6) was $\pm$0.2%. Replicate (6) determinations on 5—10-mg portions of peat humic and fulvic acid samples indicated that the coefficient of variation for this method was $\leqslant$5%. Typical Gran plots for the determination of the carbonyl groups of humic materials (10 mg) are shown in Fig. 2. The carbonyl values of the freshwater fulvic acids examined here ranged from 4.2 to 5.7 meq g^{-1} and were similar to those found by Weber and Wilson [13]. A somewhat greater range was found for marine fulvic acids, 1.3—6.5 meq g^{-1}. The carbonyl contents of the sedimentary humic acids studied were much lower than those of either the marine or freshwater humic substances, ranging from 1.2 to 3.0 meq g^{-1}, indicating that the humic material had been extensively altered following deposition.

Quinone groups

The presence of quinone groups in soil and sedimentary humic substances has been the subject of intensive debate for several years (see e.g. [47]); several authors [44, 48, 49] have claimed that such groups are not present in humic substances, whereas several others [50—55] have claimed to the contrary. Infrared spectroscopy has been used widely to determine the presence or absence of quinone groupings in humic substances [44, 48, 49, 54—57].

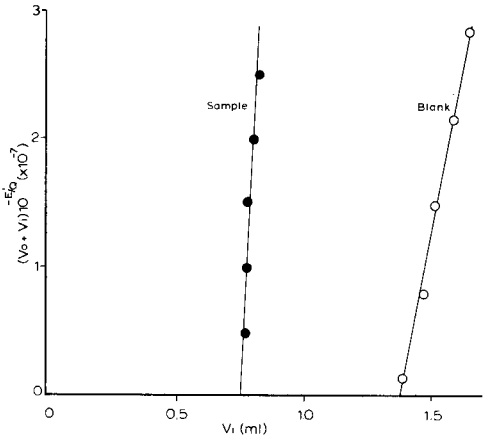

Fig. 2. Gran plots for the carbonyl group determination of humic substances. Sample is 10 mg of humic material with 5 ml of 0.01 M 2-dimethylaminoethanol and 5 ml of 0.04 M $NH_2OH \cdot HCl$. Blank is 5 ml of each oximation reagent. Titrant is 0.1 M $HClO_4$.

However, the 1770—1630 cm^{-1} region of the spectrum is extremely complex and few structural features can be confirmed by its use. Chemical methods for quinone determinations are based on reduction methods [47, 53—55, 58—60]. A comparison of the three most widely used methods [59] has shown that the alkaline tin(II) chloride and the alkaline triethanolamine—iron(III) techniques were both suitable for the determination of quinone groups in humic substances. The procedure described in this study is a modification of those of Vasilevskaya et al. [60] and Schnitzer and Riffaldi [59].

Examination of the titration data obtained for a peat humic acid sample indicated that the most precise Gran plot was one employing data from after the end-point has been reached. Although it is not entirely linear, a suitable extrapolation of the plot can be used to determine the end-point of the titration (see Fig. 3). The redox titration of tin(II) chloride with potassium dichromate.

$$3\,Sn^{2+} + Cr_2O_7^{2-} + 14\,H^+ \rightleftharpoons 3\,Sn^{4+} + 2\,Cr^{3+} + 7\,H_2O \qquad (1)$$

is such that the Gran function for an accurate determination of the end-point is extremely complex [61]; this is due to the dissimilar electron transfer in each half-cell reaction, the change in molecular nature of the chromium species (Cr_2 to 2 Cr) and the involvement of hydrogen ion. However, the function can provide a reproducible means of detecting the end-point of the $Sn^{2+}/Cr_2O_7^{2-}$ titration in the determination of quinone groups in humic substances. Several variations of the Gran function for oxidation—reduction reactions were tried [28], but curvature of the plots at certain values of V_i was found. The causes of this are either variations in the activity coefficient of the hydrogen ion or hydrolytic side reactions of the metal ions present.

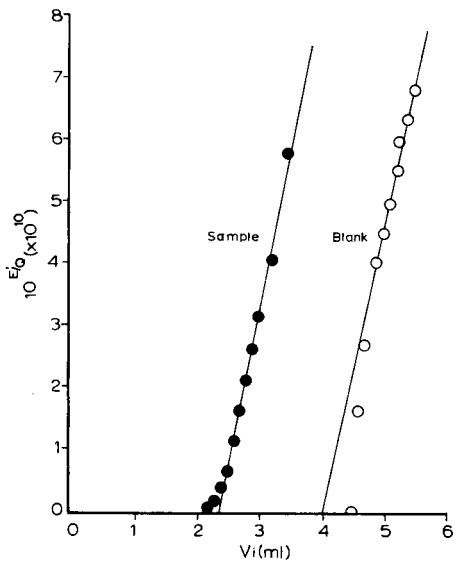

Fig. 3. Gran plots for the quinone group determination of humic substances. Sample is 10 mg of humic material with 5 ml of 0.005 M tin(II) chloride solution. Blank is 5 ml of the tin(II) solution. Titrant is 0.01 N $K_2Cr_2O_7$.

Scaling down of the method of Schnitzer and Riffaldi [59] to the analyses of 5—10 mg of peat humic substances gave a coefficient of variation of 9.8%, provided that the tin(II) chloride solution used for quinone reduction is freshly prepared every 3—4 titrations.

Vasilevskaya et al. [60] have shown that potassium dichromate does not react with the reduced humic substances, and previous studies [59, 60] have indicated that humic acids re-oxidised after the reduction, contain proportions of quinone groups were similar to those in the original samples, indicating that the reagent reacts virtually completely with polycyclic, molecularly complex quinones. Neither vanillin nor benzil reacted with the tin(II) reducing reagent.

No previous data have been reported for the quinone contents of aquatic humic substances. It was found that those examined in the present study (see Table 2) have a greater content of quinone groupings than do soil and sedimentary humic substances. Quinone values in the range 0.84—2.1 meq g^{-1} have been reported [59, 60] for soil humic substances, a range similar to that found for the sedimentary humic acids in this study.

The role of the quinone groups of humic substances in metal complexation, condensation/humification and growth stimulation reactions has been scarcely studied. Rashid [42] and Rashid and Leonard [43] have shown that humic substances and their constituents (amino acids and quinones) are effective solubilising agents for trace metals. The condensation reactions which are thought to be involved in the formation of humic substances

TABLE 2

Carbonyl, quinone and hydroxamate groups of aquatic and sedimentary humic substances

Sample	Functional groups (meq g^{-1})			Sample	Functional groups (meq g^{-1})		
	C=O[a]	Q=O[b]	HYX[c]		C=O[a]	Q=O[b]	HYX[c]
Freshwater fulvic acids				*Sedimentary humic acids*			
HM-1	4.2	1.81	0.0[d]	SK-55-1	1.2	0.73	0.0
CN-1	5.2	1.62	ND[e]	SK-86-1	1.8	0.69	ND
DE-1	5.7	1.48	0.0	SK-94-1	2.6	1.14	0.0
Marine fulvic acids				SK-96-1	1.8	1.17	ND
SK-1	4.2	3.31	0.05	SK-99-1	3.0	2.13	ND
SK-2	6.5	3.90	ND	IS-37-1	1.4	0.78	ND
SK-3	2.7	1.71	ND	IS-29	2.2	0.98	ND
SK-4	4.8	2.64	ND	IS-37D	1.9	1.03	ND
SK-5	3.4	2.13	0.08	IS-38	1.3	0.72	ND
SK-6	3.1	1.84	0.0				
SK-7	1.3	0.92	ND				
SK-8	3.4	1.98	ND				
IS-1	5.1	3.24	ND				

[a]Carbonyl groups. [b]Quinone groups. [c]Hydroxamate groups. [d]Below detection limit (0.04 meq g^{-1}). [e]Not determined.

[62–64] have been assumed to involve quinone formation with subsequent condensation with free hydroxyl or amino groups of other compounds.

The results of this study indicate that aquatic humic substances contain substantial amounts of quinone groups which, it has been suggested [65], play an important role in cell metabolism and growth. Enhancement of phytoplankton growth in the presence of humic substances has been observed by several authors [65–69].

Hydroxamate groups

The presence of the hydroxamate linkage —CO—N(OH)—, in aquatic humic substances has not previously been reported. Hydroxamic acids exhibit an extremely high affinity for iron(III) and their functions as microbial growth factors, antibiotics or iron chelating agents (siderophores) have been documented [70–72]. A study of four methods for the determination of hydroxamic acids has shown that the modified Csaky test for bound hydroxylamine is the most sensitive [27].

In comparison to other functional groups, hydroxamate groups are present only at low levels in aquatic humic substances. If these hydroxamates are considered to be part of a typical dihydroxamate siderophore with a relative molecular mass of 500, the siderophore content of aquatic humic substances is estimated to be ~1%, a concentration similar to that of the total amino acid concentration of freshwater humic substances [73]. Many hydroxamates

have been isolated from bacteria, fungi, yeasts (including the marine yeast *Rhodotorula rubra*) and unicellular algae [74—78]. However, this study presents the first indication that hydroxamates may be a significant component of the dissolved organic carbon in natural waters. Stability constant data [79] suggest that hydroxamate linkages may be partly responsible for the affinity of certain trace metals, notably copper and iron, for aquatic humic substances [16—18].

REFERENCES

1 R. G. Wetzel, Limnology, Saunders, Philadelphia, 1975, Ch. 17.
2 F. S. Wagner, Jr., Contrib. Mar. Sci., 14 (1969) 115.
3 D. H. Stuermer and G. R. Harvey, Deep-Sea Res., 24 (1977) 303.
4 J. H. Reuter and E. M. Perdue, Geochim. Cosmochim. Acta, 41 (1977) 325.
5 D. H. Stuermer and G. R. Harvey, Nature, 250 (1974) 480.
6 R. A. Kerr and J. G. Quinn, Deep-Sea Res., 22 (1975) 107.
7 R. F. C. Mantoura and J. P. Riley, Anal. Chim. Acta, 76 (1975) 97.
8 R. A. Kerr and J. G. Quinn, Mar. Chem., 8 (1980) 217.
9 G. L. Mills and J. G. Quinn, Mar. Chem., 10 (1981) 93.
10 M. Schnitzer and S. U. Khan, Humic Substances in the Environment, Dekker, New York, 1972.
11 M. Schnitzer, in M. Schnitzer and S. U. Khan (Eds.), Soil Organic Matter, Elsevier, New York, 1978, Ch. 1.
12 K. C. Beck, J. H. Reuter and E. M. Perdue, Geochim. Cosmochim. Acta, 38 (1974) 341.
13 J. H. Weber and S. A. Wilson, Water. Res., 9 (1975) 1079.
14 S. A. Wilson and J. H. Weber, Chem. Geol., 19 (1977) 285.
15 D. E. Wilson, Limnol. Oceanogr., 23 (1978) 499.
16 R. F. C. Mantoura, A. Dickson and J. P. Riley, Estuarine Coastal Mar. Sci., 6 (1978) 387.
17 Y. Sugimura, Y. Suzuki and Y. Miyake, J. Oceanogr. Soc. Jpn., 34 (1978) 93.
18 Y. Sugimura, Y. Suzuki and Y. Miyake, Deep-Sea Res., 25 (1978) 309.
19 A. Nissenbaum and I. R. Kaplan, Limnol. Oceanogr., 17 (1972) 570.
20 A. Nissenbaum and D. J. Swaine, Geochim. Cosmochim. Acta, 40 (1976) 809.
21 G. Sposito, K. M. Holtzclaw and J. Baham, Soil Sci. Soc. Am. J., 40 (1976) 691.
22 J. O. Nriagu and R. D. Coker, Environ. Sci. Technol., 14 (1980) 443.
23 M. R. Cottrell and F. H. Cottrell, in R. Belcher (Ed.), Instrumental Organic Elemental Analysis, Academic Press, London, 1977, p. 1.
24 N. D. Cheronis and T. S. Ma, Organic Functional Group Analysis by Micro and Semimicro Methods, Interscience, New York, 1964.
25 A. I. Vogel, Quantitative Inorganic Analysis, 2nd edn., Longmans, Green and Co., London, 1953.
26 J. Beukenkamp and W. Rieman, III, in I. M. Kolthoff and P. J. Elving (Eds.), Treatise on Analytical Chemistry, Part 1, Vol. 11, Wiley—Interscience, New York, 1975, p. 6975.
27 A. H. Gillam, A. G. Lewis and R. J. Andersen, Anal. Chem., 53 (1981) 841.
28 A. H. Gillam, Ph.D. Thesis, University of Liverpool, Liverpool, 1979.
29 CRC Handbook of Chemistry and Physics, R. C. Weast (Ed.), Chemical Rubber Co., Cleveland, 1969, p. D 102.
30 G. Gran, Acta Chem. Scand., 4 (1950) 559; Analyst, 77 (1952) 661.
31 M. A. Rashid and L. H. King, Geochim. Cosmochim. Acta, 33 (1969) 147; 34 (1970) 193.
32 O. K. Borggaard, Acta Chem. Scand., Ser. A, 28 (1974) 121.
33 E. M. Perdue, Geochim. Cosmochim. Acta, 42 (1978) 1351.

34 E. M. Perdue, J. H. Reuter and M. Ghosal, Geochim. Cosmochim. Acta, 44 (1980) 1841.
35 D. H. Stuermer, Ph.D. Thesis, Woods Hole Oceanography Institute, Massachusetts. Institute of Technology, Cambridge, MA, 1975.
36 D. S. Gamble, Can. J. Chem., 48 (1970) 2662; 50 (1972) 2680.
37 D. S. Gamble, A. W. Underdown and C. H. Langford, Anal. Chem., 52 (1980) 1901.
38 M. Schnitzer and U. C. Gupta, Soil Sci. Soc., Am. Proc., 29 (1965) 274.
39 W. Flaig, H. Beutelspacher and E. Rietz, in J. E. Gieseking (Ed.), Soil Components, Vol. 1, Springer-Verlag, Berlin, 1975, p. 1.
40 L. M. Whitby and M. Schnitzer, Can. J. Soil Sci., 58 (1978) 167.
41 M. A. Mikita, C. Steelink and R. L. Wershaw, Anal. Chem., 53 (1981) 1715.
42 M. A. Rashid, Chem. Geol., 9 (1972) 241.
43 M. A. Rashid and J. D. Leonard, Chem. Geol., 11 (1973) 89.
44 M. Schnitzer and S. I. M. Skinner, Soil Sci. Soc., Am. Proc., 36 (1965) 400.
45 M. Schnitzer and S. I. M. Skinner, Soil Sci., 101 (1966) 120.
46 J. S. Fritz, S. S. Yamamura and E. C. Bradford, Anal. Chem., 31 (1959) 260.
47 O. B. Maximov and L. I. Glebko, Geoderma, 11 (1974) 17.
48 G. H. Wagner and F. J. Stevenson, Soil Sci. Soc., Am. Proc., 29 (1965) 43.
49 B. K. G. Theng and A. M. Posner, Soil Sci., 104 (1967) 191.
50 C. Steelink and G. Tollin, Biochim. Biophys. Acta, 59 (1962) 25.
51 G. Tollin, T. Reid and C. Steelink, Biochim. Biophys. Acta, 66 (1963) 444.
52 C. Steelink, J. Chem. Educ., 40 (1963) 379.
53 T. A. Kukharenko and L. N. Yekaterinina, Sov. Soil Sci., (1967) 934.
54 S. P. Mathur, Soil Sci., 113 (1972) 136; Soil Sci. Soc., Am. Proc., 36 (1972) 611.
55 M. A. Rashid, Soil Sci., 113 (1972) 181.
56 M. Schnitzer, Soil Sci. Soc., Am. Proc., 37 (1973) 487.
57 St. Berger and A. Rieker, in S. Patai (Ed.), The Chemistry of Quinoid Compounds, Part 1, Wiley, London, 1974, p. 163.
58 L. I. Glebko, J. U. Ulkina and O. B. Maximov, Mikrochim. Acta, (1970) 1247.
59 M. Schnitzer and R. Riffaldi, Soil Sci. Soc., Am. Proc., 36 (1972) 772.
60 N. A. Vasilevskaya, L. I. Glebko and O. B. Maximov, Sov. Soil Sci., (1971) 224.
61 A. J. Bard and S. H. Simonsen, J. Chem. Educ., 37 (1960) 364.
62 J. McN. Sieburth and A. Jensen, J. Exp. Mar. Biol. Ecol., 2 (1968) 174; 3 (1969) 275.
63 D. K. Young, S. R. Sprang and T. F. Yen, in T. F. Yen (Ed.), Chemistry of Marine Sediments, Ann Arbor Science, MI, 1977, p. 101.
64 J. I. Hedges, Geochim. Cosmochim. Acta, 42 (1978) 69.
65 A. Prakash, in J. D. Costlow, Jr. (Ed.), Fertility of the Sea, Vol. 2, Gordon and Breach, New York, 1971, p. 351.
66 A. Prakash and M. A. Rashid, Limnol. Oceanogr., 13 (1968) 598.
67 W. Lange, Proc. 13th Conf. Great Lakes Res., 13 (1970) 58.
68 A. Prakash, M. A. Rashid, A. Jensen and D. V. Subbarao, Limnol. Oceanogr., 18 (1973) 516.
69 A. Prakash, A. Jensen and M. A. Rashid, in D. Povoledo and H. L. Golterman (Eds.), Humic Substances — Their Structure and Function in the Biosphere, Pudoc, Wageningen, 1975, p. 259.
70 J. B. Neilands, Struct. Bonding (Berlin), 1 (1966) 59.
71 C. E. Lankford, Crit. Rev. Microbiol., 2 (1973) 273.
72 J. B. Neilands, in G. Eichhorn (Ed.), Inorganic Biochemistry, Elsevier, Amsterdam, 1973, p. 167.
73 C. R. Lytle and E. M. Perdue, Environ. Sci. Technol., 15 (1981) 224.
74 L. J. Spencer, R. T. Barber and R. A. Palmer, in L. R. Worthen (Ed.), Food-Drugs from the Sea, Marine Technical Society, Washington, DC, 1972, p. 203.
75 T. P. Murphy, D. R. S. Lean and C. Nalewajko, Science, 192 (1976) 900.
76 F. B. Simpson and J. B. Neilands, J. Phycol., 12 (1976) 44.
77 K. M. Bailey, M.Sc. Dissertation, University of Washington, Seattle, 1977.
78 J. E. Armstrong, C. van Baalen, J. Gen. Microbiol., 111 (1979) 253.
79 G. Anderegg, F. L'Eplattenier and G. Schwarzenbach, Helv. Chim. Acta, 46 (1963) 1409.

Analytica Chimica Acta, 141 (1982) 301—309
Elsevier Scientific Publishing Company, Amsterdam — Printed in The Netherlands

THE DETERMINATION OF CHEMICAL OXYGEN DEMAND IN WASTEWATERS WITH DICHROMATE BY FLOW INJECTION ANALYSIS

TAKASHI KORENAGA* and HISAYOSHI IKATSU

School of Engineering, Okayama University, Tsushima-naka, Okayama-shi 700 (Japan)

(Received 19th January 1982)

SUMMARY

A simple method is described for the continuous determination of chemical oxygen demand (COD) in wastewater samples by flow injection analysis. Samples are injected into a water stream which merges with an acidic dichromate carrier solution. After reaction in a PTFE coil at 120°C, absorbances are measured at 445 nm. D-Glucose is satisfactory as a standard substance for COD in a variety of wastewaters. A sampling rate of 15 samples per hour can be achieved, and the detection limit and precision are 5 mg l^{-1} as COD and 0.4%, respectively. Chloride concentrations of $\geqslant$ 100 mg l^{-1} interfere slightly unless silver and/or mercury salts are added. COD values for various wastewater samples correlate well with those obtained by standard methods using dichromate or permanganate.

Continuous monitoring of chemical oxygen demand (COD) in wastewaters is important. Some attempts have been made [1—3] to use acidic permanganate as a carrier solution in a system based on flow injection analysis (f.i.a.), the useful methodology developed by Růžička and Hansen [4]. A fully automated f.i.a. system [3] has been developed for the continuous monitoring of COD(Mn) values in industrial wastewaters; the values found correlated well with those obtained by the Japanese official method of COD(Mn) optimized as a manual acidic permanganate value at 100°C [5]. In Western countries, however, the COD(Cr) value obtained by a dichromate reflux technique [6] is regarded as the standard method in preference to the time-consuming biochemical oxygen demand (BOD) test.

A recent f.i.a. system for continuous COD(Cr) measurements with acidic dichromate carrier [7] proved to be less sensitive than the earlier systems with acidic permanganate carrier solution [1—3] although it was reliable and trouble-free and had distinct advantages compared with the standard COD(Cr) method [6]. The present paper describes an improvement of the previous f.i.a. method with dichromate, to provide the sensitivity necessary for continuous measurements of COD(Cr) values in common wastewater samples. The system is evaluated for actual operation, and the results are compared with those obtained by standard methods using dichromate or permanganate [5, 6], and conventional and automatic methods for measurements of organic pollutants.

0003-2670/82/0000-0000/$02.75

EXPERIMENTAL

Reagents

Potassium dichromate in sulfuric acid (1+1). Potassium dichromate (0.60 g; previously dried at about 105°C for 2 h [6]) is dissolved in 500 ml of distilled water and the solution is diluted with 500 ml of concentrated sulfuric acid. This solution is ca. 0.002 M in dichromate and has an absorbance of about 0.45 at 445 nm.

Analytical reagent grade D-glucose [8, 9] is used as the standard substance for COD. Various concentrations of aqueous glucose solutions were checked by standard methods using dichromate or permanganate, and used for the f.i.a. system. All chemicals used were of analytical-reagent grade.

Instrument and procedure

A block diagram of the proposed system is shown in Fig. 1. The system is constructed of commercially available parts for high-performance liquid chromatography and poly(tetrafluoroethylene) (PTFE) tubings, selected to withstand continuous operation for long periods of time.

A Kyowa-seimitsu, Model KHU-W-52, double-reciprocating micro-pump is used to pump the 0.002 M potassium dichromate in sulfuric acid (1 + 1) and the distilled water separately at flow rates of 0.3 ml min^{-1}. Sample solution (100 μl) is injected through a Kyowa-seimitsu Model KMH-6V, hexagonal

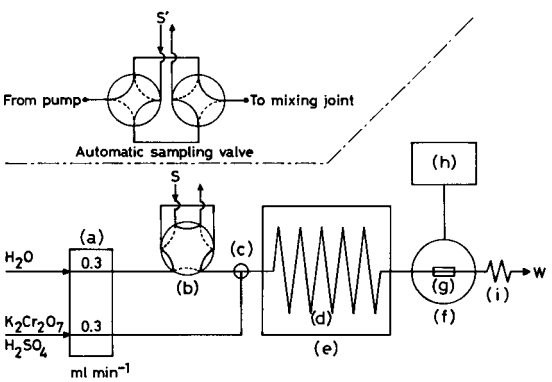

Fig. 1. Block diagram of the flow injection system. (a) Double reciprocating micro-pump; (b) hexagonal sample valve (sample volume, 100 μl); (c) PTFE Y-joint; (d) PTFE reaction tube (0.5-mm i.d., 50 m long); (e) thermostated bath (corn oil at 120 ± 0.5°C); (f) spectrophotometer (wavelength 445 nm); (g) quartz tubular flow-through cell (10-mm path length, 18-μl volume); (h) multi-range recorder; (i) PTFE back-pressure coil (0.25-mm i.d., 3 m long); (S) sample injection (manual sampling with glass syringe); (W) waste (waste volume, 0.6 ml min^{-1}). The automatic sampling valve is connected between the micro-pump (a) and the mixing joint (c) in place of the hexagonal rotary valve (b) for the continuous monitoring system; the sample solution (S') is continuously pumped and discretely injected into the water carrier stream at intervals of 4 min.

rotary valve into the stream of water. The streams merge at a Kyowa-seimitsu, Model KYU-1, PTFE Y-joint. Reaction proceeds in a 50-m coil made of PTFE tubing (0.5-mm i.d., 2-mm o.d.) which is heated at 120°C, in a Toyo-seisakusyo, Model VC-250, thermostated bath (accuracy ±0.5°C) containing corn oil. The reaction mixture then passes into a quartz tubular flow-through cell (10-mm path length, 18-μl volume) in a Shimadzu, Model UV-100-01 spectrophotometer, and the absorbance is measured at 445 nm. Absorbances are recorded continuously using a Nippon-denshi-kagaku, Model U-228, multirange recorder with 2 × expansion. A calibration graph of peak heights vs. the COD(Cr) or COD(Mn) values of aqueous glucose solutions in the range 0—340 mg l^{-1} is prepared.

RESULTS AND DISCUSSION

Standard substance for COD with acidic dichromate

Against the variety of COD substances in industrial wastewaters, the choice of standard is important if good correlation with standard methods [5, 6] is to be obtained. Compounds such as D-glucose, lactose, potassium hydrogenphthalate, and sodium oxalate, were tested as standard substances here. Glucose proved to be the best compromise in order to obtain good correlations, good recorder traces and linear responses, as has previously been reported [7—9].

Of course, chromium(VI) is quantitatively reduced to Cr(III) by such organic substances without formation of any precipitate, so that the proposed f.i.a. apparatus can be operated continuously for a longer time than those based on acidic permanganate [1—3]. In an actual COD(Cr) measurement, however, it should be noted that glucose is not always the best standard substance, because many organic substances are less readily oxidized by acidic dichromate solution than is glucose.

Instrumentation

For application in continuous monitoring of COD(Cr) in wastewater samples, the equipment must be durable and reliable. The choice of pumping system is vital. The peristaltic pumps widely used in f.i.a. are unsuitable because the present system is operated under at least 5 atm (measured by a Kyowa-seimitsu Model KPG-50N pressure gauge) by connecting a back-pressure PTFE coil (0.25-mm i.d., 3 m long) just after the flow cell. A double-reciprocating micro-pump for h.p.l.c. was therefore used to pump both the acidic dichromate solution and the water carrier stream. The water carrier stream for samples avoided the blank peak formed when samples were injected directly into the dichromate carrier solution [7].

For long reaction times, flow rates and tubing diameter and length are important parameters and must be chosen carefully to minimize peak broadening. In continuous monitoring, reagent consumption and the quantity of waste containing Cr(VI) are also important. The micro-pump could be used reproducibly at total flow rates of about 0.6 ml min^{-1} when the rather vis-

cous sulfuric acid (1+1) solution and water were pumped separately. Flow rates of 0.3 ml min^{-1} each were selected to maintain a constant 1:1 ratio. At these flow rates, a 50-m coil of seamless 0.5-mm i.d. PTFE tubing was optimal for the reaction, giving a residence time of about 20 min and a reasonable compromise between reaction time and peak broadening. The quantity of waste was below 1 l a day, causing few problems of waste treatment.

Effects of reaction temperature, acid concentration and sample volume

The effect of reaction temperature on the oxidation with potassium dichromate was first examined by using standard glucose solutions. Temperatures were maintained at 82, 91, 100, 111, 120, 130, 139, and 150°C in the thermostated bath. The results showed that a temperature of 120°C was most suitable; temperatures below 110°C lowered the sensitivity, and those between 120 and 140°C gave constant peak-height values, but above 150°C either bubbles were formed owing to vaporization of the solutions or the weakened PTFE tubing burst owing to the high back-pressure.

The ratio of the flow rates of the acidic dichromate solution and the water stream was fixed at 1:1 for studies of the effect of changing acidity at 120°C. When sulfuric acid was added to the water stream, the blank peaks obtained by injecting 100 μl of distilled water became large because of the increased absorptivity of dichromate at 445 nm. Thus sulfuric acid should be added only to the dichromate solution. When the final concentration of sulfuric acid was changed, in tests with aqueous glucose solutions, the peak heights remained constant when the final concentration exceeded 20% sulfuric acid, i.e., the initial concentrations exceeded 40% sulfuric acid. Accordingly, a 50% sulfuric acid solution of dichromate was used in all later work and the flow rates were maintained at 0.3 ml min^{-1}.

The absorbance of the potassium dichromate at 445 nm in the present system was about a sixth of the absorbance of potassium permanganate at 525 nm in the earlier system [3]. Attempts were made to improve the sensitivity by injecting 200-μl sample solutions but broad peaks were then obtained; 200 μl of sample occupied about 100 cm of the coil used, so that complete mixing and reaction might not occur even in the 50-m coil. The optimum sample volume was therefore 100 μl, introduced via the hexagonal valve having a 100-μl loop of PTFE tubing.

Calibration graph, reproducibility and precision

Figure 2 shows a typical output from the flow injection system when different concentrations of aqueous glucose solutions were injected. A plot of peak heights obtained under the recommended conditions for these glucose solutions vs. the COD(Cr) values determined by the standard method [6] was linear over the COD(Cr) range 0—160 mg l^{-1} but curved beyond 160 mg l^{-1} (Fig. 3). In contrast, with the previous method [7], a plot of peak areas vs. COD values was necessary to achieve a linear calibration graph.

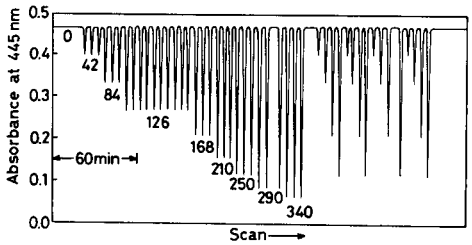

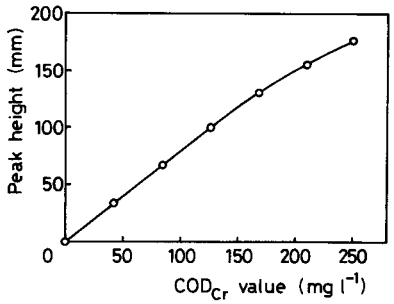

Fig. 2. Representative samples of COD(Cr) measurement by the proposed method for aqueous glucose solutions. The numbers on the peaks are the corresponding COD values expressed as mg l^{-1}.

Fig. 3. Calibration graph prepared with aqueous glucose solutions.

The detection limit of the method is 5 mg l^{-1} COD(Cr) (which gives a peak height of about 4 mm by the absorbance decrement at 445 nm against zero value); even lower values (2—3 mg l^{-1}) could be estimated if really necessary, because of the absence of blanks and base-line drift. This higher sensitivity compared to the earlier method [7] is achieved by using a separate sample carrier stream, and by increasing the sample volumes and the reaction temperature.

As also shown in Fig. 2, the reproducibility of this COD(Cr) measurement is good, reflecting the automatic character of the procedure. There is little opportunity for personal errors except in sample preparation. The precision of the method is good; the coefficient of variation was 0.4% in 10 determinations of 126 mg l^{-1} COD(Cr) with aqueous glucose solution. About 15 samples can be measured per hour. Samples can be injected at 4-min intervals, although the residence time necessary for the oxidation reaction is about 20 min at 120°C.

Effect of chloride, sample storage and sample filtration

In order to apply the present method to the measurement of COD(Cr) in actual industrial wastewaters, the effects of possible interfering ions must be known. Chloride ion, which is commonly present at levels of 10 mg l^{-1} in river water, was tested. Table 1 shows that more than 100 mg Cl^- l^{-1} interferes slightly with the COD measurement. However, the errors caused by 500 mg Cl^- l^{-1} would be tolerable in many situations. The positive errors are caused by oxidation of chloride to chlorine. No attention was given to spectral interferences from materials absorbing at 445 nm because the samples used were clear and colorless.

The samples in glass or polyethylene vessels were stored in a refrigerator (at about 4°C) as soon as they were sampled and could be stored for at least 2 weeks without any appreciable change in their COD values. If sulfuric acid

TABLE 1

Effect of chloride ion on the determination of D-glucose [126 mg l^{-1} COD(Cr)]

Cl^- (mg l^{-1})	0	10	30	50	100	300	500	1000
Peak ht. (mm)	99	100	98.5	99.5	103	105	108.5	114.5
Error (%)	—	—	—	—	+4	+6	+10	+16

(below pH 2) or mercury salt is added, the samples can be stored for more than 1 month. Filtration of the samples used here was unnecessary, as the samples were almost clear solutions. Turbid samples would require filtration and this would require great care to avoid altering the composition of the oxidizable organic substances present. Therefore, wastewater samples were injected directly into the flow injection system as soon as possible after collection.

Measurement of COD(Cr) in actual wastewaters

Various wastewater samples, obtained from chemical, food, engineering and textile industries, civic sewage, and the university, were analyzed successfully without any prior treatment by the proposed method. The results are presented in Table 2, which shows that the COD(Cr) values obtained in the flow injection system are within ±30% of the values from the standard COD(Cr) and COD(Mn) methods [5, 6]. The results were also checked by adding known amounts of glucose to the sample solutions and then determining the COD values. Good recoveries of the COD substance added were confirmed. With the continuous measurement, about 15 samples could be processed semiautomatically per hour.

Evaluation of the results and correlation to the standard methods

In Fig. 4A, the results for 40 wastewater samples from a food factory (D) in Okayama, which were obtained by the proposed method, are compared with those obtained with the standard COD(Cr) method [6] in order to evaluate their correlation. The f.i.a. values (y) shown are averages of three determinations and those shown for the standard method (x) are averages of two determinations. The correlation is fairly good ($y = 0.72x + 6.7$) with a correlation coefficient of 0.97. Figure 4B shows the correlation of the results from the f.i.a. method with those obtained with the standard COD(Mn) method used officially in Japan [5]. Again the correlation is fairly good ($y = 1.20x' + 12.5$, where x' is the COD(Mn) value), the correlation coefficient being 0.98. Accordingly, the proposed simple instrumental method based on f.i.a. seems adequately reliable for the determination of COD values in wastewaters.

Application to continuous monitoring

For continuous monitoring of COD substances, the system can be fully automated by replacing the manually operated hexagonal valve by an automatic sampling valve [3]. This automatic sampling valve (see Fig. 1) consists

TABLE 2

Measurement of COD(Cr) values in wastewaters by the proposed method and by standard methods
(The wastewaters were from the following sources: A—C, chemical industry; D, E, food industry; F—I, engineering factory; J—M, textile factory; N—Q, civic sewage; R, laboratory; S—W, river water)

Sample	Chemical oxygen demand ($mg\,l^{-1}$)			Sample	Chemical oxygen demand ($mg\,l^{-1}$)		
	Proposed method	Standard Cr method	Standard Mn method		Proposed method	Standard Cr method	Standard Mn method
A	69	90	74	R[a]	12	20	17
B	91	132	119		64	85	51
C	136	198	146		19	24	18
					20	25	20
D	210	250	158		9	13	10
	67	92	56		17[b]	18	15
	135	155	95		33[b]	48	36
	240	300	210		38[b]	47	38
	193	290	157		46[b]	52	44
E	196	300	260		41[b]	50	40
					67[b]	79	56
F	115	169	138		18	21	14
G	82	123	75		14	16	16
H	200	270	153		6	5	5.2
I	96	117	85		5	7	6.8
					<5 (3)	5	3.8
J	60	67	48				
K	133	149	139	S	12	20	20
L	85	120	111	T	7	12	9.4
M	105	171	123	U	<5 (4)	5	5.0
				V	<5 (3)	3	2.5
N	60	71	50	W	5	4	4.2
O	210	280	195				
P	1100	1450	1260				
Q	2300	2700	1870				

[a]Samples of laboratory wastewater taken on April 14, 1981 between 9:00 and 18:00.
[b]Samples taken and analyzed at 4-min intervals from 14:00 by continuous monitoring.

of a Kyowa-seimitsu Model KAM-4V-2 automatic double-quaternary exchanging valve and a Tateishi-denki Model H5B-4D digital timer. It allows direct introduction of 100-μl samples into the water carrier stream at intervals of 4 min.

Typical examples of results obtained in continuous monitoring of wastewater samples from the Center for Environmental Conservation Technology, Okayama University, are given in Table 2, along with the results from the standard titrimetric methods [5, 6]. The correlation coefficients between the f.i.a. and titrimetric methods were found to be significant, though the values by the f.i.a. method generally lie between the values obtained

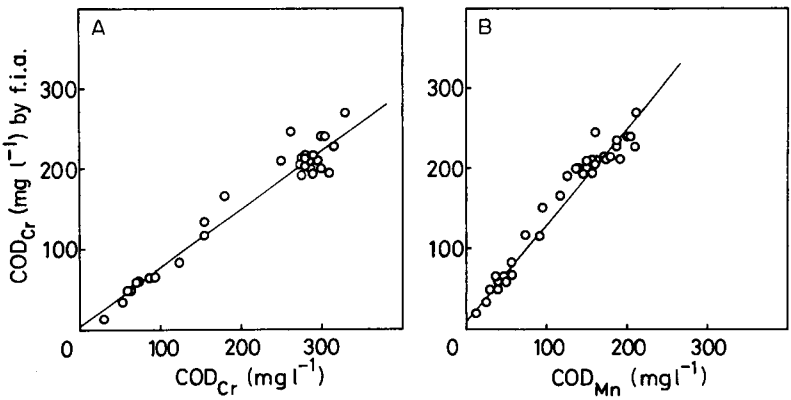

Fig. 4. Correlation of the results obtained by the proposed f.i.a. method with the results from (A) the standard COD(Cr) method, and (B) the standard COD(Mn) method. Sample was a wastewater from a food factory (D) in Okayama.

conventionally. It appears that COD substances in such wastewaters can be continuously monitored quite reliably without any prior treatment.

Conclusion

Use of the high-pressure micro-pump to force the rather viscous sulfuric acid (1+1) solution into thin PTFE tubing enables the system to maintain continuous operation for a long time. The method for COD measurement described above is simple, flexible, robust and inexpensive, and is suitable for continuous monitoring of wastewaters.

Commercial automatic water-quality analyzers for the determination of COD, TOD (total oxygen demand) or TOC (total organic carbon) have been reviewed [10, 11]. By comparison with other automatic methods, the proposed system has the advantages of simplicity and cheapness. It is faster than the other solution procedures though slower than the TOC and TOD determinations based on combustion in oxygen [12, 13]. The ranges of linear response are similar, as are the sample sizes required. The interference caused by chloride ion is small enough to be ignored in most cases, so that the addition of silver and/or mercury salts is not necessary. The precision of the analytical results appears to be better than that attainable by other methods despite the rapid sampling rate.

The authors are greatly indebted to Professors Kyoji Tôei, Teruo Takahashi and Tosio Moriwake of Okayama University for their helpful encouragement. The present work was partially supported by a Grant-in-Aid for Scientific Research from the Japanese Ministry of Education, Science and Culture, and also the Nissan Science Foundation.

REFERENCES

1 T. Korenaga, Bunseki Kagaku, 29 (1980) 222; Chem. Biomed. Environ. Instrum., 10 (1980) 273; Anal. Lett., 13A (1980) 1001.
2 T. Korenaga and H. Ikatsu, Bunseki Kagaku, 29 (1980) 497; Analyst, 106 (1981) 653; Nippon Kagaku Kaishi, (1981) 616.
3 T. Korenaga and H. Ikatsu, Bunseki Kagaku, 31 (1982) 135.
4 J. Růžička and E. H. Hansen, Flow Injection Analysis, Wiley, New York, 1981.
5 Japan Industrial Standard, JIS K 0102, 1974.
6 ASTM, D 1252, 1978.
7 T. Korenaga, Bull. Chem. Soc. Jpn., 55 (1982) 1033.
8 J. E. Shriver and J. C. Young, J. Water Pollut. Control Fed., 44 (1972) 2140.
9 A. Yamasaki, Y. Tanaka, Y. Kuge and S. Asada, Kogai To Taisaku, 14 (1978) 1133.
10 T. J. Kehoe, Environ. Sci. Technol., 11 (1977) 137.
11 N. Mizorogi, Kogai To Taisaku, 14 (1978) 714.
12 ASTM, D 3250, 1977.
13 ASTM, D 3560, 1977.

Analytica Chimica Acta, 141 (1982) 311—319
Elsevier Scientific Publishing Company, Amsterdam — Printed in The Netherlands

STUDIES WITH DITHIZONE
Part 35. A New Look at the Structure of Dithizone in Solution

H.M.N.H. IRVING* and A. T. HUTTON

Department of Analytical Science, University of Cape Town, Rondebosch 7700, C.P. (S. Africa)

(Received 10th March 1982)

SUMMARY

The traditional view that solutions of dithizone in organic solvents comprise equilibrium mixtures of thione- and thiol-forms which are individually responsible for the characteristic strong absorption bands around 620 and 440 nm is examined critically. It is shown that experimental values of $pH_{1/2}$, pK, and R (the peak ratio) can legitimately be used in calculations although they are compounded of parameters (partition coefficients, acid dissociation constants, etc.) relating to both of the alleged tautomeric forms and the equilibrium constant, K_T, governing the interconversion. Published attempts to calculate K_T from spectral data alone are shown to be unreliable.

Fourier-transform ^1H- and ^{13}C-n.m.r. spectroscopic measurements on dithizone, several of its alkyl homologues, and on ^{13}C- and ^{15}N-labelled analogues point to the existence of only a single molecular species in deuterochloroform, benzene or acetone. The marked solvatochromism has yet to be explained.

X-ray crystallographic studies of the analytical-reagent dithizone (3-mercapto-1,5-diphenylformazan; H_2Dz) leave no doubt that in the solid phase dithizone is composed of discrete, almost planar molecules (I) in which there is such extensive delocalisation of π-electrons along the chain N—N—C—N—N that individual single and double bonds cannot be distinguished. The C—S bond lies at the intersection of two mirror planes and the two symmetrically-placed imino hydrogen atoms are hydrogen-bonded to sulphur [1, 2].

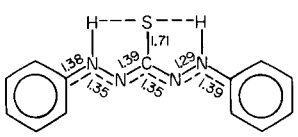

I

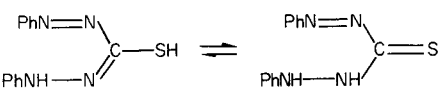

IIa IIb

Solutions of dithizone in organic solvents are strongly coloured and exhibit two well-defined absorption bands in the visible region (see Table 15 of [3]) which do not change their positions much with change of solvent although this does greatly, and apparently systematically, affect the values of the molar absorptivities $\epsilon_{max,1}$ and $\epsilon_{max,2}$. Thus, while the wavelength range is quite restricted ($\lambda_{max,1}$ 596—640 nm; $\lambda_{max,2}$ 440—462 nm), the intensity of absorption varies from $\epsilon_{max,2}$ = 1560 m^2 mol^{-1} in tetrachloromethane to 2760 and 2540 m^2 mol^{-1}, respectively, in *n*-hexane. Since impurities in dithizone, which are due mainly to oxidation or to photochemical reaction involving the solvent, tend to absorb below 550 nm, the "peak ratio", R = (absorbance at $\lambda_{max,1}$)/(absorbance at $\lambda_{max,2}$) increases to a maximum as such impurities are gradually eliminated and the peak ratio is often quoted as an index of purity [3—6]. It varies from 1.09 in *n*-hexane to 1.70 in tetrachloromethane and is as high as 2.60 in trichloromethane.

Metal complexes of dithizone, $M(HDz)_n$, are also strongly coloured with a single absorption band lying between those of the parent reagent: for example, $Zn(HDz)_2$ in tetrachloromethane has ϵ_{max} = 9600 m^2 mol^{-1} at 535 nm. These features led to the extensive use of dithizone for selective spectrophotometric determinations of microgram amounts of various metals and numerous monocolour, mixed colour, and reversion procedures have been developed [3, 5].

Preparations of dithizone by different synthetic routes (e.g., Fischer's [7] or Bamberger's [8] methods) do not distinguish between the alternative structures (IIa) and (IIb) and it has long been assumed that solutions of this reagent in organic solvents comprise an equilibrium mixture of the two tautomeric forms, each being responsible for one of the two pronounced bands in the visible spectrum [5]. It is implicit in all spectrophotometric procedures involving dithizone that its solutions obey Beer's law. As this has been verified experimentally [9], it follows that each of the postulated isomers must severally obey Beer's law and that their relative amount in any given solution remains unchanged, i.e., that tautomerization proceeds too rapidly to be detectable during the course of the experiments. Incidentally, this strict conformity with Beer's law enables us to reject Carlin's suggestion [10] that a dimeric form of dithizone (two intermolecularly hydrogen-bonded molecules in the thione form) is one of the species in equilibrium in solution.

Even when an aqueous alkaline solution containing sodium dithizonate, NaHDz, is acidified and shaken up with an immiscible organic solvent, the normal spectrum of dithizone is immediately established in the organic phase and there is no evidence for the conversion of the thiol (IIa) (which would be formed first) into the equilibrium amount of the thione form (IIb). The same is true when a solution of metal dithizonate is acidified or "reverted" by any other method which releases its equivalent of dithizone [9].

Proton n.m.r. spectrometry on solutions of dithizone presents difficulties owing to its very low solubility. Using the more soluble homologue 3-

mercapto-1,5-di-(2′-ethylphenyl)formazan, Coleman et al. [11] reported the following proton magnetic resonance spectrum in deuterochloroform; δ = 12.03(1.6 H, singlet, NH), 8.1 and 7.33(8 H, multiplet, aromatic), 3.0(4 H, quartet, CH_2), and 1.4(6 H, triplet, 2 × CH_3). They interpreted these results as indicating only a single species in solution and noted that the signal at δ 12.03 showed no evidence splitting over the range + 50°C to —45°C; cooling only sharpened the resonance line [11]. It is noteworthy that this broad peak only integrated for 1.6 protons (instead of 2) and the problem seemed to be resolved when Nabilsi [12], working with dithizone itself, reported an additional signal at δ 0.97 which with that at δ 12.61 integrated for exactly two protons. This was taken as demonstrating the presence of a second isomer, assumed to be the thiol form and comprising about 25% of the whole [12].

If solutions of dithizone really comprise equilibrium mixtures of thiol and thione tautomers, it must be realised that besides having different spectra (ultraviolet, visible, infrared and nuclear magnetic) each isomer would have its own characteristic solubility in a given organic solvent, different partition coefficients for distribution between aqueous and organic phases, and different acid dissociation constants. The experimentally measured values for dithizone will thus be a function of these characterizing parameters and of the relative amounts of the two tautomers in the equilibrium mixture. Specifically, the equilibrium shown schematically in Fig. 1 is considered here, and the following definitions are employed for the two acid dissociation constants, tautomeric equilibrium constants and partition coefficients: $K_{on} = [H^+][HDz^-]/[\text{thione}]$; $K_{ol} = [H^+][HDz^-]/[\text{thiol}]$; $K_T = [\text{thione}]/[\text{thiol}]$; $K_{T,o} = [\text{thione}]_o/[\text{thiol}]_o$; $p_{on} = [\text{thione}]_o/[\text{thione}]$; $p_{ol} = [\text{thiol}]_o/[\text{thiol}]$. The subscript o distinguishes species in the organic phase from those in the aqueous phase. Clearly $K_T = K_{ol}/K_{on}$ and $K_T/K_{T,o} = p_{ol}/p_{on}$.

If the hypothesis that solutions of dithizone contain two tautomeric forms in equilibrium is accepted, it follows that values for their absorptivities given in the literature must be underestimated because they have been obtained by dividing the absorbance at one of the wavelength maxima by the total concentration of dissolved dithizone (i.e., $[\text{thiol}]_o + [\text{thione}]_o$) rather than by the actual concentration of the relevant absorbing species. Thus

$$\epsilon_{ol}(\text{actual}) = \epsilon_{ol}(\text{reported}) \times ([\text{thiol}]_o + [\text{thione}]_o)/[\text{thiol}]_o = \epsilon_{ol}(\text{reported}) \times (1 + K_{T,o}) \quad (1)$$

$$\text{and } \epsilon_{on}(\text{actual}) = \epsilon_{on}(\text{reported}) \times (1 + K_{T,o})/K_{T,o} \quad (2)$$

$$\text{whence } R = \epsilon_{on}(\text{reported})/\epsilon_{ol}(\text{reported}) = [\epsilon_{on}(\text{actual})/\epsilon_{ol}(\text{actual})] \times K_{T,o} \quad (3)$$

In any given solvent, $K_{T,o}$ will be a constant and it follows that R will be a measure of the purity of the solute and will tend to a maximum as impurities absorbing at the shorter wavelength are progressively removed. The validity of this procedure is not affected by our not knowing the actual value of $K_{T,o}$.

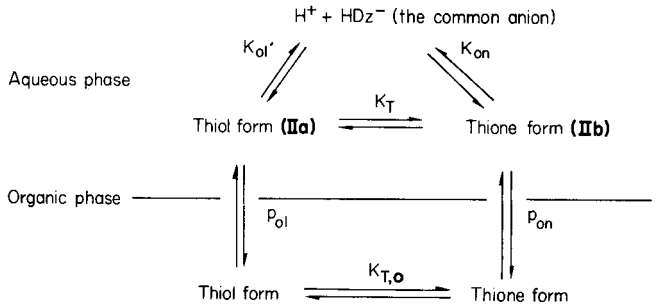

Fig. 1. Two-phase equilibria in the distribution of dithizone between aqueous and immiscible organic phases assuming that thiol—thione tautomerism is operative.

The acid dissociation constant of dithizone has frequently been used in theoretical discussions [3, 13] and it is now desirable to see whether any errors have been introduced by ignoring the fact that the value used, K(actual), is dependent on those of K_{on} and K_{ol}. Specifically the true value of the acid dissociation constant is given by

$$K(\text{actual}) = [H^+][HDz^-]/[\text{total undissociated dithizone}]$$
$$= [H^+][HDz^-]/([\text{thione}] + [\text{thiol}]) = 1/(1 + K_T)K_{on} \quad (4a)$$

or
$$= K_T/(1 + K_T)K_{ol} \quad (4b)$$

When the stability constants of a series of metal dithizonates are correlated with the proton affinity of the relevant ligand (i.e., with the reciprocal of the acid dissociation constant of the parent dithizone), it would seem appropriate to use values of K_{ol} rather than K(actual) (or indeed of K_{on}). The same choice of constant will apply in discussions of the rates and mechanism of metal-complex formation. This was clearly recognized by Math et al. [13] who correctly deduced Eqns. (4a) and (4b). However, they went on to assume that they could derive the value of K_T from the experimentally measurable value of the peak ratio, R, even to the extent of equating the two. This is fallacious. In the first place, Eqn. (3) is an oversimplification in that it assumes that the whole of the absorption at λ_1 (or λ_2) is due to the thione (or thiol) form alone. This assumes that the individual absorption bands do not overlap at all which is demonstrably false. Secondly, the identification of $K_{T,o}$ with R can be accepted only if the two linear absorptivities ϵ_{on} and ϵ_{ol} have identical magnitudes in each solvent used. Furthermore, the calculation of K_T, which is the actual constant actually needed in assessing the values of K_{ol} in an aqueous medium, can only be derived from $K_{T,o}$ if the ratio of the partition constants p_{on}/p_{ol}, is also known (see above).

Pel'kis and Dubenko [14] tried to resolve this difficulty by making the improbable assumption that the value of ϵ_{ol} was identical with that of ϵ_{max} for *S*-methyldithizone: this compound can readily be prepared by methylating the thiol form of dithizone (IIa) in alkaline solution [15]. From the measured absorbance of dithizone at $\lambda_{max,2}$, they calculated the value of

$[\text{thiol}]_o$ and, knowing the total concentration (a) of dithizone, they obtained $[\text{thiol}]_o$ by difference. From the observed absorbance A_1 of dithizone at $\lambda_{max,1}$, they then calculated ϵ_{on}, presumably ignoring the observable overlap of absorption bands. It is unfortunate that *S*-methyldithizone (and all its homologues) exist as *cis–trans* isomers which readily give equilibrium mixtures in solution with concomitant changes of spectra [16]. The Russian workers did not specify which isomer they were using for their basic measurements, and, as they did not report values of a, A_1 or A_2, it is impossible to check their calculations which appear to lead to the most remarkable conclusion that $\epsilon_{ol} = \epsilon_{on} = 5745$ m^2 mol^{-1} in tetra- or tri-chloromethane and 5768 m^2 mol^{-1} in benzene, i.e., virtually the same in all three solvents.

Taking the reported values $\epsilon_{ol} = 1590$ and $\epsilon_{on} = 4140$ m^2 mol^{-1} for trichloromethane (Table 1) and the figure 5745 reported by Pel'kis and Dubenko [14], introduction of Eqns. (1) and (2) leads to $K_{T,o} = 2.61$ and 2.58. As the experimental value for the peak ratio is $R = 2.59$, it must be concluded that the Russian authors were able to show not only that $K_{T,o} = R$ but that ϵ_{ol}(actual) = ϵ_{on}(actual) = 5745 m^2 mol^{-1}, unless they used a circular argument. In any case, it seems clear that some independent method must be used to obtain reliable values for the relative and absolute concentration terms [thione] and [thiol] in various solvents and to correlate these with the peak ratio R. In view of Nabilsi's results [12], the quantitative application of nuclear magnetic resonance spectroscopy offers the most attractive approach.

Before new results in this field are discussed, it is necessary to consider how values of $pH_{1/2}$ would be affected by the co-existence of two different solute species in equilibrium; for values of $pH_{1/2}$ have been widely used in theoretical discussions [3, 17].

The experimentally determined value for the partition coefficient (distribution ratio) of dithizone itself is given by

$$p(\text{exp}) = \text{total concentration in organic phase/total concentration in aqueous phase} = ([\text{thione}]_o + [\text{thiol}]_o)/([\text{thione}] + [\text{thiol}]) = p_{ol}(1 + K_{T,o})/(1 + K_T) \quad (5a)$$

$$\text{or} \quad = p_{on}K_T(1 + K_{T,o})/K_{T,o}(1 + K_T) \quad (5b)$$

Now the measured distribution ratio, D, at any pH value is given by

$$D = \frac{\text{total concentration of dithizone species in the organic phase}}{\text{total concentration of dithizone species in the aqueous phase}} = ([\text{thione}]_o + [\text{thiol}]_o)/[\text{thione}] + [\text{thiol}] + [HDz^-]) = p(\text{exp})/\{1 + (K(\text{actual})/[H^+])\} \quad (6)$$

and when pH $\gg$ pK(actual), log D = log p(exp) + pK (actual) — pH, so that when $D = 1$ (50% extraction), pH = $pH_{1/2}$

$pH_{1/2}(\text{exp}) = \log p(\text{exp}) + pK(\text{actual})$

precisely the result that is obtained if the partition of only a single solute is being considered [18].

TABLE 1

Proton nuclear magnetic resonance spectroscopic data for various 1,5-diarylthiocarbazones (as III) in $CDCl_3$, $(CD_3)_2CO$ and C_6D_6[a]

Ar	δ(NH)[b]			δ(CH, CH_2, or CH_3)			δ(ArH)		
Phenyl	12.60	12.63	12.84	—	—	—	7.56	7.65	6.93(m,10H)
o-Tolyl	12.80	12.86	13.13	2.63	2.58	2.01(s,6H)	7.62	7.62	7.24(m,8H)
m-Tolyl	12.54	12.63	12.85	2.43	2.42	1.86(s,6H)	7.34	7.43	6.76(m,8H)
p-Tolyl	12.65	12.63	12.87	2.42	2.39	1.86(s,6H)	7.27	7.37	6.60(d,*J*=8.0 Hz,
							7.58	7.75	7.05(d,*J*=8.0 Hz,
3,5-Dimethyl-phenyl	12.49	12.60	12.86	2.36	2.37	1.91(s,12H)	6.97	7.04	6.64(s,2H)
p-Ethylphenyl	12.50	12.60	12.91	1.24	1.24	0.90(t,*J*=7.6 Hz,6H)	7.27	7.38	6.66(d,*J*=8.2 Hz,
				2.68	2.70	2.20(q,*J*=7.6 Hz,4H)	7.59	7.77	[c] (d,*J*=8.2 Hz,
p-Isopropylphenyl	12.52	12.62	12.96	1.27	1.26	0.96(d,*J*=6.6 Hz,12H)	7.31	7.42	6.74(d,*J*=8.2 Hz,
				2.95	2.97	2.48(h,*J*=6.6 Hz,2H)	7.62	7.78	[c] (d,*J*=8.2 Hz,
p-*n*-Butylphenyl	12.52	12.50	12.90	0.93	0.93	0.81(t,*J*=6.6 Hz,12H)	7.27	7.36	
				1.47	1.47	1.23(m,8H)	7.59	7.75	
				2.65	2.66	2.23(t,*J*=7.2 Hz,4H)			

[a]Proton n.m.r. spectra recorded on a 90-MHz Varian XL-100CW spectrometer at room temperature. ^{13}C-n.m.r. spectra and ^{15}N-n.m.r. recorded on a Bruker WH-GODS pulse Fourier-transform spectrometer operating at 22.63 and 9.12 MHz, respectively. The chemical shifts are reported in the order $CDCl_3$, $(CD_3)_2CO$ and C_6D_6 as values of δ, ppm relative to TMS. The conventional designations are s, singlet; d, doublet; t, triplet; q, quartet; h, heptet; m, multiplet. [b] All these are singlet resonances integrating for 2H except in deuteroacetone solutions where the integrals vary from 0.7 to 1.5, owing to traces of D_2O in the solvent used. All these signals disappear completely on adding D_2O. [c]Signal obscured by solvent resonance.

Although the use of Fourier-transform n.m.r. spectroscopy has greatly facilitated measurements on sparingly soluble solutes, it must not be forgotten that enhanced signals may arise adventitiously from residual traces of protons in deuterated solvents. Contamination of $CDCl_3$ by traces of $CHCl_3$ will produce an adventitious line which enhances the integrated value for aromatic protons so that the intensity of other lines relative to this will be underestimated. For this reason a series of alkyl-substituted homologues of dithizone was synthesised, firstly to provide well-defined lines as references for integration purposes, and secondly to investigate the equivalence or other of the two aryl groups. Details of their preparation and those of compounds specifically labelled with ^{13}C and ^{15}N are fully reported elsewhere [19, 20].

The first disconcerting result was that Nabilsi's alleged peak at δ 9.7 in the ^1H-n.m.r. spectrum of dithizone and attributed by him to a thiol isomer could not be reproduced: it may have originated from some solvent impurity or even a spinning side-band of an intense TMS resonance.

The Fourier-transform ^1H-n.m.r. spectra of dithizone and several alkyl-substituted homologues (as III) were recorded in each of three solvents, i.e., $CDCl_3$, $(CD_3)_2CO$ and C_6D_6. In every case only one set of signals appeared for the substituent alkyl groups showing that these (and hence the two

aromatic rings) are exactly equivalent on the n.m.r. time scale (Table 1). Spectra at −50°C differed from those at +60°C only by the expected slight sharpening of the peaks. Moreover, the NH singlet at δ 12.6 always integrated for exactly two protons and disappeared immediately and completely on washing with D_2O. Owing to the possibility of tautomerism (e.g., **IIa** ⇌ **IIb**), *cis–trans* isomerism about the N:N- double bond and *syn–anti* isomerism about the :C=N· double bond, a very large number of conformations is possible though many of these are rendered less probable on steric grounds or by repulsion between unpaired electrons on tervalent nitrogen [3, 10, 20]. The new ^{1}H-n.m.r. results show that the two aryl groups are magnetically equivalent: this implies that discrete structures such as (**IIa**) or (**IIb**) (or analogous pairs with alkyl-substituted phenyl groups) cannot be present unless the rate of

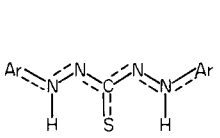

III

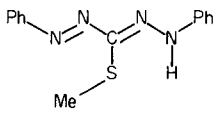

IV

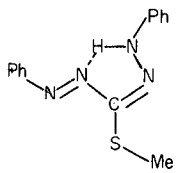

V

tautomerism is faster than the n.m.r. time scale. That the two non-aromatic protons must be bound to equivalent nitrogen atoms N(1) and N(5) (as in **III**) was established by labelling dithizone in both these positions with 96 atom-% ^{15}N. The proton-n.m.r. spectrum now showed the NH resonance as a doublet with $^1J(^{15}N—H)$ = 90.8 Hz which agrees very well with the value 92.2 Hz found for the yellow *anti*-s-*trans* isomer (**IV**) of *S*-methyldithizone where, of course, tautomerism is impossible [19, 20]. Had tautomerism occurred in the ^{15}N-labelled dithizone, the normal value of the ^{15}N—H coupling constant would have been roughly halved (to ≈ 45 Hz) as in the case of the pink *syn*-s-*cis* form of *S*-methyldithizone (V) where $^1J(N—H)$ = 47.6 Hz [19].

Further evidence was obtained by synthesising dithizone labelled with ^{13}C at C(3), starting from 91 atom-% $^{13}CS_2$ and using a modification of Fischer's synthesis [3]. The ^{13}C-n.m.r. spectrum in $CDCl_3$ showed only a single sharp line at δ 171.4 p.p.m. (downfield from TMS) in the broad-band ^{1}H-decoupled mode. However, in the proton-coupled spectrum this became a perfectly symmetrical 1:2:1 triplet with $^3J(^{13}C—N—N—H)$ = 6.0 Hz (unchanged at −50°C). This collapsed to a single resonance when the coupling to ^{1}H was removed by a D_2O wash. The same coupling constant, $^3J(H—N—N—^{13}C)$ = 6.0 Hz, was found in the doublet obtained in the ^{1}H-n.m.r. spectrum of ^{13}C-labelled dithizone. The conclusion seems inescapable that the two imino protons are magnetically equivalent as are the two aromatic residues, pointing to a highly symmetrical structure such as (**III**) already established to be the state in solid dithizone (I).

The view that only a single species is present in solution is consistent with

the fact that the spectrum of solutions of dithizone in chloroform does not vary over the range −50° to +60°: in particular, the peak ratio R does not change as it would if there were two species in equilibrium, unless the enthalpy change in their interconversion is negligible [21].

The conclusions drawn from the extensive new n.m.r. data which extend the early measurements of Coleman et al. [11] agree with those of Kemula, Gańko and Janowski on the infrared spectra of dithizones [22]. These show a broad absorption band in the region 3100—2800 cm^{-1} with several absorption maxima. On deuteration this band disappears and is replaced by one at ca. 2200 cm^{-1} assigned to the N—D stretching mode, and in the region 3100—3000 cm^{-1} only maxima corresponding to aromatic C—H stretches remain. There are no traces of S—H stretching bands (expected at about 2600 cm^{-1}). The close similarity between the i.r. spectrum of dithizone in solution and in the solid state appears to deny the possibility of tautomerism and it is perhaps significant that the diffuse reflectance spectrum of solid dithizone [20] shows a clearly defined band at 450 nm (similar situated to $\lambda_{max,2}$ in $CHCl_3$ or CCl_4) with a broad shoulder covering the region 580—610 nm which roughly corresponds with the location of $\lambda_{max,1}$ in organic solutions.

One last piece of evidence must be mentioned. Theoretical calculations of the energy and intensity of electronic transitions of various molecular species have recently been made by Spěváček and Spěváčeková [23] using LCAO, MO, SCF and LCI methods. Using a symmetrical model basically the same as (I) (save that one hydrogen atom is attached to sulphur as a thiol) they predicted a spectrum with two prominent bands in the visual region. Moreover, one is predicted at about 430 nm corresponding to the short-wave maximum found experimentally: the other is located at about 750 nm which is well away from the experimental value (ca. 640 nm): moreover the intensity of this longer wavelength band is predicted to be less than that at the shorter wavelength which is never the case (see table 15 [3]). Of course, such calculations do not take into account the effect of solvent on the spectra and the remarkable solvatochromism remains to be explained. It has not been possible to establish any regular relationship between ϵ_1 or ϵ_2 (or λ_1 or λ_2) or the peak ratio, R, with conventional scales of solvent parameters such as Kosower's Z values (and the linearly related E_T and Y scales [24]) or with Taft's π^* scale [25].

The smooth correlation for some dozen solvents between the value of R for dithizone and the equilibrium constant [keto]/[enol] for ethylacetoacetate was highly suggestive so long as it was thought that dithizone existed as mixture of tautomers in solution [3]. It must now be explained in different terms as must all aspects of its remarkable, and so far as we are aware, unique solvatochromism. What is certain, however, is that none of these solvent effects have any influence on the reliability of the many applications of dithizone in quantitative spectrophometric analysis [3].

REFERENCES

1 P. A. Alsop, Ph.D. Thesis, London University, 1971.
2 M. Laing, J. Chem. Soc., Perkin Trans., 11 (1977) 1248.
3 H. M. N. H. Irving, Dithizone, Analytical Sciences Monographs No. 5, The Chemical Society, 1977.
4 H. Fischer and W. Weys, Miss. Veroeff. Siemens-Werkung, 14 (1955) 41.
5 G. Iwantscheff, Das Dithizon und seine Anwendung in der Mikro- und Spurenanalyse, 2nd edn., Verlag Chemie, Weinheim, 1972.
6 H. Irving and D. C. Rupainwar, Anal. Chim. Acta, 48 (1969) 187.
7 E. Fischer and E. Besthorn, Annalen, 212 (1882) 316.
8 E. Bamberger, R. Padova and E. Ormerod, Annalen, 446 (1926) 260.
9 H. Irving et al., numerous unpublished observations.
10 C. H. Carlin, Ph.D. Dissertion, John Hopkins University, Baltimore, 1966.
11 R. A. Coleman, W. H. Foster, J. Kazan and M. Mason, J. Org. Chem., 35 (1970) 2039.
12 A. H. Nabilsi, Ph.D. Thesis, Leeds University, 1972.
13 K. S. Math, G. F. Fernando and H. Freiser, Anal. Chem., 36 (1964) 1762.
14 P. S. Pel'kis and R. G. Dubenko, Ukr. Khim. Zh., 24 (1957) 748, 754; cf. Dokl. Akad. Nauk SSSR, 110 (1956) 798.
15 H. Irving and C. F. Bell, J. Chem. Soc., (1954) 4253.
16 A. T. Hutton and H. M. N. H. Irving, J. Chem. Soc., Chem. Commun., (1981) 735. (Part 34 of series.)
17 H. M. N. H. Irving, N. F. Naqvi and C. G. Tilley, Anal. Chim. Acta, 100 (1978) 597.
18 H. Irving, S. J. H. Cooke, S. C. Woodger and R. J. P. Williams, J. Chem. Soc., (1949) 1847.
19 A. T. Hutton and H. M. N. H. Irving, J. Chem. Soc., Perkin Trans., in press.
20 A. T. Hutton, Ph.D. Thesis, Cape Town, 1980.
21 H. M. N. H. Irving and A. T. Hutton, Anal. Chim. Acta, 128 (1981) 261.
22 A. Janowski and T. Gańko, Bull. Acad. Pol. Sci., Ser. Sci. Chim., 16 (1968) 223; W. Kemula, T. Gańko and A. Janowski, Bull. Acad. Pol. Sci., Ser. Sci. Chim., 19 (1971) 325.
23 V. Spěváček and V. Spěváčeková, J. Inorg. Nucl. Chem., 38 (1976) 1299.
24 C. Reichardt, Angew. Chem., Int. Ed. Engl., 4 (1965) 29.
25 M. J. Kamlet, J. L. Abboud and R. W. Taft, J. Am. Chem. Soc., 99:18 (1977) 6027.

Analytica Chimica Acta, 141 (1982) 321—327
Elsevier Scientific Publishing Company, Amsterdam — Printed in The Netherlands

A SPECTROMETRIC, SEPARATION AND VOLTAMMETRIC STUDY OF THE COMPLEXATION REACTIONS OF BROMAZEPAM WITH IRON(II), COPPER(II) AND COBALT(II)

W. FRANKLIN SMYTH* and R. SCANNELL
Department of Chemistry, University College, Cork (Eire)
T. K. GOGGIN
Department of Neurology, Regional Hospital, Cork (Eire)
D. LUCAS-HERNÁNDEZ
Department of Chemistry, Euskal Herriko University, Bilbao (Spain)
(Received 21st April 1982)

SUMMARY

Bromazepam, in the form of a cationic iron(II) chelate, can be determined spectrophotometrically at 588 nm with a limit of detection of ca. 10^{-6} M. When this chelate is ion-paired with perchlorate, it can be extracted into organic solvents such as 1,2-dichloroethane and 4-methyl-2-pentanone, and determined by atomic absorption spectrometry with a limit of detection of 1.5×10^{-5} M bromazepam at the iron resonance 248.3-nm line. Ion-pairs involving the Fe(II), Cu(II) and Co(II) chelates and perchlorate can be separated by h.p.l.c. using a C_{18} reverse-phase column and a mobile phase of 4:1 water—methanol, with a u.v. detector at 242 nm. This approach allowed for the determination of iron(II) ions in aqueous solution with a limit of detection of 10^{-8} M. The h.p.l.c. method could also be used to quantify bromazepam spiked in plasma in the concentration range 1—10 μg ml^{-1}, following extraction of bromazepam from plasma and subsequent formation of the iron(II) ion-pair. Copper(II) forms a labile chelate with bromazepam in pH 4.8 acetate buffer which, when subjected to differential pulse voltammetry at the hanging mercury drop electrode, gives rise to a catalytic phenomenon which can be utilised for the determination of bromazepam in the concentration range 10^{-5}—10^{-9} M.

Bromazepam [I; 7-bromo-1,3-dihydro-5-(2-pyridyl)-2*H*-1,4-benzodiazepin-2-one] has aroused clinical interest as an anti-anxiety agent [1—3]. Its metabolic rate has been investigated [4—6] and it has been found that only the parent compound is present in blood after therapeutic administration. Both gas—liquid chromatographic methods with electron capture detection [6, 7] and differential cathode-ray polarographic methods [8] exist for the determination of bromazepam in plasma with detection limits of 5—10 ng ml^{-1} of plasma [6, 7] and 50 ng ml^{-1} [8]. Smyth et al. [9] have made a spectral, polarographic and voltammetric study of bromazepam and produced an indirect analytical method for the determination of 10^{-7} M concentrations of bromazepam, using differential pulse anodic stripping voltammetry of the free copper(II) ions remaining after complexation of an excess of this metal ion with bromazepam.

0003-2670/82/0000-0000/$02.75

The existence of the α,α'-dipyridyl moiety enables bromazepam to form complexes with divalent metal ions such as copper(II) and cobalt(II) [9]. This behaviour has been studied spectrophotometrically in relation to iron(II) ions [10] and applied to the determination of iron(II) [11] and haemoglobin [12] in serum.

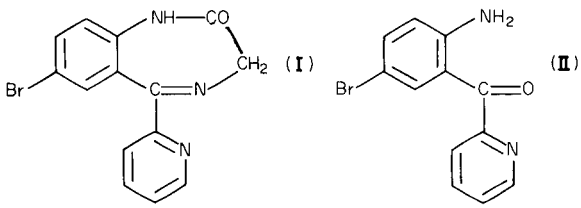

This paper is concerned with a study of the chelation of bromazepam (I) with Fe(II), Cu(II) and Co(II) using spectroscopic techniques such as u.v. and visible spectrophotometry and atomic absorption spectrometry, separation techniques such as solvent extraction and ion-pair high-performance liquid chromatography (h.p.l.c.) and differential pulse voltammetry, at the hanging mercury drop electrode with a view to enhancing the sensitivity and selectivity of analytical methods for the determination of trace concentration of bromazepam in the presence of non-chelating molecules such as benzophenone metabolites (II) and 1,4-benzodiazepines without pyridine groups, i.e., all other commercially available 1,4-benzodiazepines. The h.p.l.c. separation of bromazepam and its Cu(II), Fe(II) or Co(II) chelates, quite apart from its use in the determination of down to 10^{-8} M concentrations of iron(II) ions, could be of value in biochemical investigations on the binding of this benzodiazepine drug to trace concentrations of relevant metal ions contained in body fluids.

EXPERIMENTAL

Preparation of complexes

A stock solution (1×10^{-3} M) of the iron (bromazepam)$_3^{2+}$ chelate was prepared by dissolving 0.09 g of bromazepam (in 5 ml of methanol; Hoffmann-La Roche, Nutley, NJ) and 0.03 g of iron(II) sulphate in 100 ml of deionised water. This solution was subsequently diluted with deionised water to yield solutions covering the concentration range 1×10^{-6}—10^{-3} M in the iron chelate. The copper(II) and cobalt(II) complexes were prepared similarly. All were purple in colour.

Procedures

U.v.—visible spectrophotometry. The spectra of solutions in the above concentration range with respect to the iron(II) chelate were scanned in the region 200—700 nm using an SP5000 spectrophotometer, and a graph of absorbance vs. concentration was constructed for the 588-nm band. It should be noted that the absorbance of the ligand at 242 nm is considerably

enhanced by chelation, so that u.v.—visible detection following h.p.l.c. separation could be attempted at both wavelengths.

Solvent extraction of the iron(II) chelate and u.v.—visible spectrophotometry. Equal volumes (10 ml) of aqueous standard solutions of the iron chelate (10^{-3}—10^{-6}M) and 1,2-dichloroethane or 4-methyl-2-pentanone were equilibrated for 5 min, and the concentration of the complex remaining in the aqueous phase was estimated by scanning from 370 nm to 700 nm. This was repeated with other solutions saturated with potassium perchlorate.

Solvent extraction of the iron(II) chelate and atomic absorption spectrometry. A range of solutions containing various concentrations of bromazepam (0.1—1.0 × 10^{-4} M) in water/methanol was prepared from a 10^{-3} M stock solution. Solutions of 1 × 10^{-3} M iron(II) sulphate and saturated potassium perchlorate were also prepared in deionised water. Aliquots (10 ml) of the various bromazepam solutions were placed in separating funnels along with 10 ml of the iron(II) solution and either 10 ml of deionised water or 10 ml of the saturated perchlorate solution. These mixtures were equilibrated with 30 ml of the organic solvent for 5 min, and the organic layers were drawn off. Care was taken to ensure minimal loss of the solvent by evaporation and a non-bromazepam blank extraction was also done. The iron content of the organic layer was determined by using the resonance line at 248.3 nm and an oxygen—acetylene flame. Graphs of absorbance at 248.3 nm vs. the concentration of the complex were then constructed.

H.p.l.c. separation of the ion-pairs of the Cu(II), Co(II), and Fe(II) chelates with perchlorate. The complexes were prepared as indicated under Preparation of complexes. Potassium perchlorate (1 M) was added to the 10^{-3} M stock solutions of the complexes to form the appropriate ion-pairs prior to dilution of the solutions to yield 10^{-4}—10^{-6} M concentrations of the ion-pairs. For dilutions, the water/methanol (4:1) mobile phase was used, to avoid the interfering peaks from solvent front effects which occurred on injection of purely aqueous samples.

The reverse-phase C_{18} column LiChrosorb (25 cm × 4.6-mm i.d.; 10-μm particles) was chosen for the h.p.l.c. investigation of the Fe(II), Cu(II) and Co(II) ion-pairs. The flow rate was (1 ± 0.01) ml min^{-1} at a piston pressure of 40 Bar. A u.v.—visible detector was operated at 242 nm and 588 nm.

Differential pulse voltammetry of the copper(II) chelate at the hanging mercury drop electrode. A PAR Model 174A polarographic analyzer was used in conjunction with a Model 303 static mercury drop electrode. The drop time was set at 0.5 s in the differential pulse mode. The concentration of copper(II) ions was kept constant at 10^{-4} M while that of bromazepam was varied from 10^{-9} to 10^{-5} M. A pre-electrolysis time of 3 min at an initial potential of 0 V was used, together with a scan rate of 5 mV s^{-1} and a modulation amplitude of 25 mV.

RESULTS AND DISCUSSION

Solvent extraction of the iron(II) chelate and u.v.—visible spectrophotometry

Bromazepam (I), in the form of a cationic iron(II) chelate, gives a linear calibration curve of absorbance at 588 nm vs. concentration in the range 10^{-3}—10^{-6} M of the complex. This calibration curve was then used in order to monitor the transfer of this purple complex from the aqueous phase (pH 7.0) to 1,2-dichloroethane or 4-methyl-2-pentanone. Visual observation showed that transfer was only possible in the presence of perchlorate as an ion-pairing agent for the iron(II) chelate, $[Fe(bromazepam)_3]^{2+}$. When the visible spectrum of the aqueous phase was run after an extraction, it was found that its shape and the position of the absorption bands changed somewhat, invalidating the use of the calibration curve even when the organic solvents were used to presaturate the aqueous phases prior to preparation of the stock solutions and extraction. After extraction, with perchlorate present, the visible spectrum again changed.

Solvent extraction of the iron(II) chelate and atomic absorption spectrometry

To overcome the afore-mentioned effect, it was decided to monitor the transfer of the ion-pair to the organic solvent by measuring the atomic absorption of the iron(II) in the organic phase. It would also have been possible to monitor the decrease in the iron(II) concentration in the aqueous phase after extraction, but because iron(II) was added in excess over bromazepam for these extractions, the results would not have been accurate.

Linear calibration plots of the atomic absorption of the organic phase at the iron resonance 248.3-nm line vs. concentration of the complex in the aqueous phase were obtained for both 1,2-dichloroethane and 4-methyl-2-pentanone in the concentration range 0.05—1.00 $\times$ 10^{-4} M. This lower level (which corresponds to a limit of detection of 1.5 $\times$ 10^{-5} M in bromazepam) was established by the extraction of non-bromazepam-containing neutral compounds of the excess of ion(II) not involved in the chelating process (iron(II) perchlorate or sulphate).

H.p.l.c. separation of the ion-pairs of the Cu(II), Co(II) and Fe(II) chelates with perchlorate and application to the determination of iron(II) and bromazepam

Tests on the h.p.l.c. behaviour of these ion-pairs on a 10-μm LiChrosorb C_{18} reverse-phase column, with a 4:1 water/methanol mobile phase and u.v.—visible detection at 242 nm, showed that the retention times for bromazepam, $Fe(bromazepam)_3(ClO_4)_2$, $Cu(bromazepam)_3(ClO_4)_2$, and $Co(bromazepam)_3(ClO_4)_2$ were 296, 324, 365, and 339 s, respectively. The complexes were prepared with excess of bromazepam, which also appeared on the chromatograms at 296 s.

Of the three ion-pairs, only iron(II) yielded linear calibration plots of peak area vs. concentration of the ion-pair. Reproducibility of the absorbances of

the copper and cobalt ion-pairs was difficult to achieve, because of chelate lability and consequent partial breakdown of the chelates on the stainless steel column. This was illustrated when the Fe(II), Cu(II) and Co(II) ion-pairs were prepared in excess of metal ion and subjected to h.p.l.c. with u.v. detection at 242 nm. The iron(II) ion-pair gave a single peak at 324 s whereas the copper and cobalt ion-pairs both gave sizable peaks at 296 s corresponding to free bromazepam. To ensure that the iron(II) ion-pair was in fact that which was being observed, this ion-pair was injected onto the column with the detector set at 588 nm, a wavelength specific for the $Fe(bromazepam)_3$ species. A single peak was observed at 320 s which corresponds to $Fe(bromazepam)_3(ClO_4)_2$. No peak was observed for bromazepam because it does not absorb at this wavelength.

When 20-μl injections and a helium-degassed mobile phase were used, a linear calibration plot of peak area vs. concentration of the iron(II) ion-pair was obtained in the concentration range 10^{-3}—10^{-7} M. The relative standard deviations of the peak areas for repeated injections of this ion-pair at concentrations of 10^{-3} M and 10^{-7} M varied from 0.07% to 0.70%, respectively. The signal-to-noise ratio was found to be 2:1 on injection of a 10^{-8} M solution of the iron(II) ion-pair; this concentration was then designated as the limit of detection for this ion-pair under the h.p.l.c. conditions described above. The number of theoretical plates was 20 736, the height equivalent of the theoretical plate was 1.2×10^{-3} cm and the resolution factor R was 3.1 for the separation of the iron(II) ion-pair and the excess of bromazepam.

The h.p.l.c. procedure was briefly evaluated for the determination of bromazepam as the iron(II) ion-pair after extraction of bromazepam spiked in human plasma. Proteins were precipitated by the addition of 3:1 Na_2CO_3/$NaHCO_3$ to 1 ml of the spiked plasma sample followed by vortex mixing and separation of the supernatant liquid. Chloroform was used to extract bromazepam from the supernatant liquid, the chloroform was evaporated off at 50°C on a water bath, and the residue was reconstituted in the usual aqueous methanol mobile phase. Examination of this solution by h.p.l.c. showed that recoveries of the bromazepam were about 80% and that the bromazepam peak was well separated from other u.v.-absorbing substances co-extracted from the plasma. A ten-fold excess of iron(II) was then added to the above-mentioned residue after reconstitution in the aqueous methanol mobile phase; the ion-pair with perchlorate was then extracted and subjected to h.p.l.c. as previously described. The chromatograms showed a peak corresponding to free bromazepam as well as the iron(II) ion-pair, showing that not all the bromazepam was chelated under the conditions used. Even when a further excess of iron(II) was added to the above solution prior to injection, the height of the peak corresponding to the iron(II) ion-pair did not alter significantly. However, when the solution conditions following extraction and reconstitution were changed, i.e., when the pH of the reconstituted extract (9.2) was altered to the optimum pH of ca. 7.0 for chelation by the addition of anhydrous acetic acid, and the iron(II) chelate and perchlorate

ion-pair were then formed, no free bromazepam was observed in the chromatogram. A linear calibration graph of peak area corresponding to the iron(II) ion-pair versus the concentration of bromazepam spiked in the plasma was found in the concentration range 1—10 $\mu g\,ml^{-1}$. Detection of 0.1 $\mu g\,ml^{-1}$ concentrations of bromazepam spiked in plasma could also be accomplished by this method.

Differential pulse voltammetry of the copper(II) chelate at the hanging mercury drop electrode

In the presence of excess of copper(II) ions, it was found that the height of the bromazepam reduction wave corresponding to the >C=N— group at —0.57 V (vs. s.c.e.) in 0.1 M acetate buffer (pH 4.8) was enhanced after the hanging mercury drop electrode had been conditioned at 0 V for 3 min. This applied to solutions which were 10^{-9}—10^{-5} M in bromazepam and 10^{-4} M in copper(II) ions. Because bromazepam is not adsorbed at the h.m.d.e. under these conditions [the wave height from the >C=N— reduction of bromazepam does not increase with increasing conditioning/plating time at an applied potential of 0 V (vs. s.c.e.) in 0.1 M acetate buffer pH 4.8], a mechanism must operate whereby bromazepam is concentrated at the electrode surface by adsorption of the copper(II) chelate. The fact that the reduction potential corresponding to the enhanced peak is identical to the reduction potential of "free" bromazepam would suggest that at the time of charge transfer, the chelation of copper(II) to bromazepam is no longer effective at the electrode surface and that copper ions are involved in a catalytic mechanism. A further paper will be concerned with the mechanism of this phenomenon. A plot of peak height corresponding to the >C=N— reduction of bromazepam vs. the concentration of bromazepam was found to be linear in the concentration range 10^{-5}—10^{-9} M.

Conclusion

The copper(II) and iron(II) chelates with bromazepam could be used for selective determinations of trace concentrations of this 1,4-benzodiazepine by either differential pulse voltammetry at the h.m.d.e. or by spectrometric procedures after extraction or h.p.l.c. The h.p.l.c. method would be expected to be the most selective and sensitive for the determination of bromazepam in complex matrices such as plasma, especially when non-chelating degradation products/metabolites and other 1,4-benzodiazepines are present.

REFERENCES

1 E. Stovehill, H. Lee and T. A. Ban, Dis. Nerv. Syst., 27 (1966) 411.
2 R. J. Kerry, F. A. Jenner and I. B. Pearson, Psychosomatics, 13 (1972) 122.
3 K. Rickels, J. A. Pereira-Ogan, H. R. Chung, P. E. Gordon and W. Laudis, Curr. Ther. Res., 15 (1973) 679.
4 H. Sawada, Experientia, 28 (1972) 393.
5 H. Sawada, H. Yano and A. Kido, J. Pharm. Soc. Jpn., 92 (1972) 1237.

6 J. A. F. deSilva, I. Bekersky, M. A. Brooks, R. E. Weinfeld, W. Glover and C. V. Puglisi, J. Pharm. Sci., 63 (1974) 1440.
7 U. Klotz, J. Chromatogr., 222 (1981) 501.
8 F. E. Senguen and H. Oeschlager, Arch. Pharm. (Weinheim), 308 (1975) 720.
9 M. R. Smyth, T. S. Beng and W. Franklin Smyth, Anal. Chim. Acta, 92 (1977) 129.
10 J. D. Sabatino, O. W. Weber, G. R. Padmanabhan and B. Z. Senkowski, Anal. Chem., 41 (1969) 905.
11 B. Klein, L. B. Lucas and R. L. Searcy, Clin. Chim. Acta, 26 (1969) 517.
12 B. Klein, B. K. Weber, L. Lucas, J. K. Foreman and R. L. Searcy, Clin. Chim. Acta, 26 (1969) 77.

Analytica Chimica Acta, 141 (1982) 329—335
Elsevier Scientific Publishing Company, Amsterdam — Printed in The Netherlands

SPECTROPHOTOMETRIC DETERMINATION OF THIOCYANATE VIA COPRECIPITATION AND THERMAL DECOMPOSITION OF COPPER(I) THIOCYANATE

T. MAJEWSKI and A. CYGANSKI*

Institute of General Chemistry, Technical University, Żwirki 36, 90-924 Łódź (Poland)

(Received 3rd August 1981)

SUMMARY

A method for determination of thiocyanate (6—100 μg) is described. It is based on the coprecipitation of copper(I) thiocyanate with copper(I) iodide, followed by decomposition of copper(I) thiocyanate in air at 450° C. The decomposition products are CuS, CuO, SO_2, CO_2 and N_2. Released sulphur dioxide is absorbed in sodium tetrachloromercurate(II) solution, and determined spectrophotometrically with bleached *p*-rosaniline. The method is unaffected by the presence of halides, sulphide, sulphite and thiosulphate.

A method for determination of thiocyanate by thermal decomposition of silver thiocyanate at 600° C was described earlier [1]. A similar determination can be made based on the thermal decomposition of copper(I) thiocyanate at 450° C. The advantages of the latter method are a considerably lower decomposition temperature and twice the amount of sulphur dioxide evolved; sulphur dioxide is the species which is finally determined spectrophotometrically. As the investigation proved, the determination is applicable in the presence of large amounts of halides, sulphide, sulphite and thiosulphate.

EXPERIMENTAL

Apparatus and reagents

The thermal decomposition studies were done with a derivatograph (MON OD 102/1500° C) with α-alumina as the inert substance. Other operating conditions were: maximum temperature 1000° C, heating rate 5° C min^{-1}, differential thermal analysis sensitivity 1/20, thermogravimetric sensitivity 200 mg, differential thermogravimetric sensitivity 1/15, mass of sample 250 mg. For x-ray diffraction analysis of the sinters produced by heating copper thiocyanate, a DRON-1 x-ray analyser was used with copper radiation and a nickel filter. The intensities of the reflections were measured with a scintillation counter. Diffractograms were recorded with an automatic recorder for 20 angles from 2 to 70°.

A solution for reduction of copper(II) was prepared, containing 53.5 g of

ammonium chloride and 3 g of hydrazine sulphate in 1 l of water [2]. A 0.1 M sodium tetrachloromercurate(II) solution was prepared by dissolving 27.2 g of mercury(II) chloride and 11.7 g of sodium chloride in water and diluting to 1 l. To prepare a bleached *p*-rosaniline solution, 4 ml of an aqueous solution 1% (w/v) of *p*-rosaniline hydrochloride and 6 ml of concentrated hydrochloric acid were mixed and diluted to 100 ml [3]. Formaldehyde (0.2%) was prepared directly before use by diluting 5 ml of 40% formaldehyde to 1 l with distilled water.

Preliminary studies

Study of sinters from copper(I) thiocyanate. In order to examine the course of the reactions, decomposition products from copper(I) thiocyanate were prepared under conditions similar to those of the derivatographic determination. Weighed 250-mg samples of the salt were heated at 5° C min^{-1} to the critical temperatures determined from the differential thermal analysis curve, i.e., 450, 560 and 850° C. The loss in mass of each product was verified by comparison with the values from the thermogravimetric curve.

Chemical analysis. The amount of sulphur in the sinters was determined by fusion with sodium peroxide and sodium carbonate [4]. Sulphate was determined after dissolving the product in hot (1 + 5) hydrochloric acid [4]. Copper was determined by dissolving the sinters in hot (1 + 1) nitric acid, evaporating the solution to dryness, dissolving the residue in water and determining copper electrogravimetrically [5].

The composition of the gaseous products obtained at 450° C was also determined. Sulphur dioxide was absorbed in 0.1 M tetrachloromercurate(II) solution and titrated with 0.1 M NaOH [1]. Carbon dioxide was determined gravimetrically by absorption on Ascarite [6]. Nitrogen was determined by the Dumas method, Körbl's reagent being used as an auxiliary oxidant [7].

As release of sulphur dioxide at a given temperature is of utmost importance for this analytical method, the sulphur dioxide released from copper(I) thiocyanate at different temperatures was determined under conditions similar to those used later to determine thiocyanates. A sample of copper(I) thiocyanate (250 mg) was heated in a furnace at 5° min^{-1} up to the desired temperature and then kept at that temperature for 15 min. Air was passed through at 5 l h^{-1}. Released sulphur dioxide was absorbed in sodium tetrachloromercurate(II) solution, and then titrated [1].

Determination of thiocyanate (6—100 μg)

A 60-ml portion of the reducing solution for copper(II) was added to 20 ml of 0.1 M copper sulphate solution, which was diluted with water to 200 ml and heated to boiling. The solution should be completely decolorized on heating. A thiocyanate solution (20 ml), to which 1 ml of 0.1 M potassium iodide had been added, was added with stirring. Potassium iodide is used to precipitate copper(I) iodide, which acts as a carrier for small amounts of

thiocyanate. The solution was heated briefly and subsequently cooled in water. The precipitate was filtered through a porosity 4 sintered-glass crucible, washed with water and ethanol. The crucible, with the precipitate, was put in a silica vessel and placed in a furnace. The vessel was connected with a bubbler, containing 25 ml of 0.1 M sodium tetrachloromercurate(II) and air was passed through at 5 l h^{-1}. Heating to 450° C was conducted at 15° min^{-1}. After reaching 450° C, the vessel was maintained at this temperature for 15 min. The solution was poured from the bubbler into a 50-ml volumetric flask and 5 ml of the bleached *p*-rosaniline solution and 5 ml of 0.2% formaldehyde were added. The solution was diluted to 50 ml with sodium tetrachloromercurate(II) solution and allowed to stand for 30 min, and the absorbance was measured at 560 nm in a 1-cm cell, against a blank taken through the whole procedure. A calibration graph was prepared by taking known amounts of thiocyanate through the whole procedure.

RESULTS AND DISCUSSION

Thermal analysis curves for copper(I) thiocyanate are shown in Fig. 1. They show that a fast exothermic transformation, involving rapid mass loss, occurs at 450° C. Between 450° and 470° C, the mass increases, but it then remains constant up to 700° C; above 700° C the mass decreases. A curve showing the relationship between the amount of evolved sulphur dioxide and the temperature up to which it was heated, is given in Fig. 2. It shows that the amount of the sulphur dioxide increases rapidly as the temperature is raised to 450° C, but then attains a constant level.

X-ray diffraction patterns of copper(I) thiocyanate and its decomposition

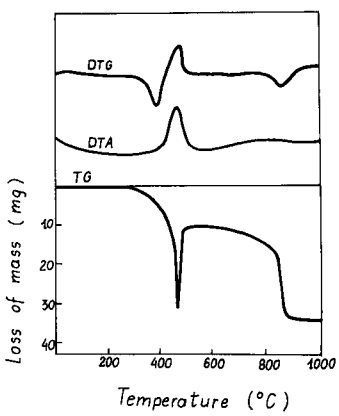

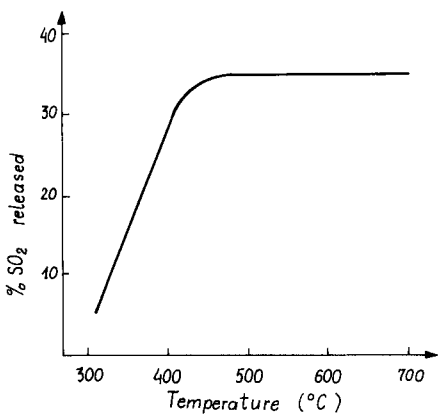

Fig. 1. Thermal analysis curves for copper(I) thiocyanate. TG, thermogravimetry; DTG, differential thermogravimetry; DTA, differential thermal analysis.

Fig. 2. Temperature-dependence of the proportion of sulphur dioxide evolved during thermal decomposition of copper(I) thiocyanate.

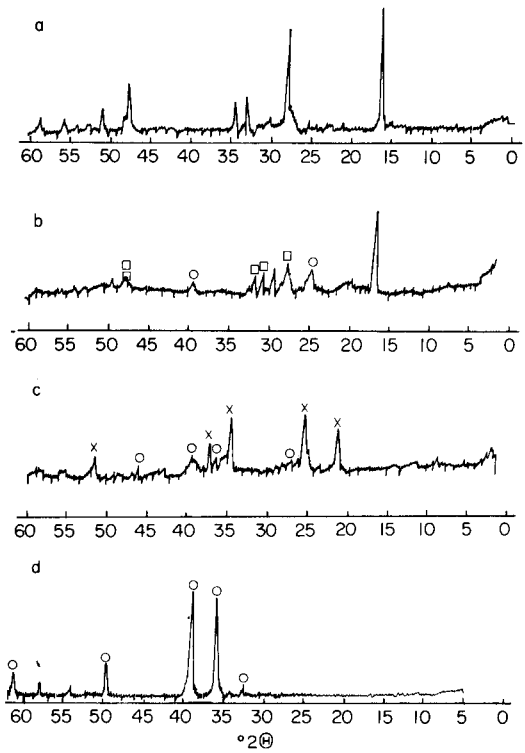

Fig. 3. X-ray diffraction patterns of (a) copper(I) thiocyanate, and its decomposition products prepared at (b) 450°, (c) 650° and (d) 850° C. (X) $CuSO_4$, (○) CuO and (□) CuS.

products prepared at various temperatures are shown in Fig. 3. Analytical results for the decomposition product obtained at 450, 560 and 850° C are given in Table 1, as well as the results for the mass loss of the decomposition product and the composition of the gaseous products obtained at 450° C. The percentage of gaseous products is calculated in relation to the mass of CuSCN. These results, and the x-ray diffraction pattern investigations, indicate the following decomposition reaction of copper(I) thiocyanate at 450° C

$$3CuSCN + 6O_2 \rightarrow CuS + 2CuO + 2SO_2 + 3CO_2 + \tfrac{3}{2}N_2 \quad (1)$$

Copper(II) oxide and copper(II) sulphide are shown to be present in the sinters by x-ray diffraction (Fig. 3). It should be noted that, according to Duval [8], the minimum mass at 450° C occurring on the thermogravimetric curve corresponds to the formation of copper(I) sulphide and thus to the reaction

$$6CuSCN + 3O_2 \rightarrow 3Cu_2S + 3SO_2 + 6CO_2 + 3N_2 \quad (2)$$

The composition of the product, content of evolved sulphur dioxide and

TABLE 1

Composition of the products formed during decomposition of copper(I) thiocyanate

Temp. of sinter preparation (°C)		Sinter (%)		Gaseous products (%)			Mass loss (%)
		Cu	S	SO_2	CO_2	N_2	
450	Found	73.95	12.45	34.9	51.8	16.2	31.20
	Calc. from Eqn. (1)	74.84	12.58	35.1	51.2	16.5	30.19
	Calc. from Eqn. (2)	79.85	20.14	26.3	18.1	17.5	34.63
560	Found	60.25	10.30	34.9	—	—	11.60
	Calc. from Eqn. (3)	59.81	10.06	35.1	—	—	12.65
850	Found	78.15	—	—	—	—	35.00
	Calc. from Eqn. (4)	79.88	—	—	—	—	34.62

mass loss calculated in accordance with this reaction are given in Table 1. The results obtained (Table 1) indicate that decomposition is according to Eqn. (1), and not Eqn. (2). Duval did not investigate the decomposition products; he based his argument on mass loss only.

The mass increase occurring above 450° C involves the reaction

$$CuS + 2CuO + 2O_2 \rightarrow CuSO_4 + 2CuO \qquad (3)$$

This reaction is suggested both by the results in Table 1, and by the x-ray diffraction studies (Fig. 3). The conclusion from this reaction is that the ratio between CuO and $CuSO_4$ is 2:1. Bacanov and Zalivina [9] found the ratio to be 3:1, and Margulic and Ponomarev [10] stated 1:1. The second mass loss, at 600° C, is caused by copper(II) sulphate decomposition. Copper oxide is the decomposition product (Table 1). It must be stressed that copper(I) thiocyanate decomposes in nitrogen in quite a different way. The decomposition results in the formation of copper(I) sulphide [9, 11].

The results for some pure thiocyanate determinations are given in Table 2. They show that 6—100 μg of thiocyanate can be determined accurately. Satisfactory precision is confirmed by relative standard deviations of 2.7%, 1.5% and 2.4% for mean thiocyanate values of 19.85, 59.85 and 100.2 μg ($n = 5$), respectively.

The possibility of determination of thiocyanate in the presence of chloride, bromide and iodide, which also form sparingly soluble precipitates with copper(I), and in the presence of reducing sulphur anions (S^{2-}, $S_2O_3^{2-}$, SO_3^{2-}), was investigated. After precipitation in the presence of thiosulphate or sulphite, the precipitate and mother liquor were boiled for 45 min to decompose copper(I) thiosulphate. The results for microgram amounts of thiocyanate in the presence of milligram amounts of anions are given in Table 3.

TABLE 2

Results for determination of thiocyanate in pure solution

Amount of thiocyanate (μg)		Error (%)	Amount of thiocyanate (μg)		Error (%)
Taken	Found		Taken	Found	
102.4	100.2	−2.1	47.45	48.5	2.2
88.35	87.0	−1.5	33.85	34.5	1.9
74.05	75.5	2.0	20.35	19.9	−2.5
61.05	59.9	−2.0	6.75	7.0	3.7

TABLE 3

Determination of thiocyanate (10.9 μg) in the presence of other anions

Anion	Amount (mg)	SCN^- found (μg)	Error (%)
Cl^-	17.73	10.7	−2.0
Br^-	19.96	10.6	−2.8
I^-	11.69	11.2	3.2
S^{2-}	24.32	11.2	3.1
$S_2O_3^{2-}$	26.18	10.6	−2.8
SO_3^{2-}	15.30	10.8	−0.9

They show the absence of interferences from the anions studied. Copper(I) iodide, of course, is used as a carrier.

Heavy metal cations that form sparingly soluble compounds with thiocyanate or iodide (i.e., silver, mercury(I), lead and bismuth) or oxidize iodide (iron(III)) must not be present. Thiocyanate can be determined in the presence of bismuth or iron(III) if an excess of iodide is used. Cadmium, mercury(II), cobalt, nickel, manganese, zinc, iron(II), aluminium, chromium and alkali and alkaline earth metals do not interfere. The interferences were investigated by determination of 28 μg of thiocyanate in the presence of the various cations in amounts 100—200 times in excess. The errors were less than 4%.

If a sample contains thiocyanate and iodide, addition of potassium iodide to form a carrier is unnecessary and the method can be used to determine thiocyanate and iodide simultaneously. First, the total mass of CuSCN + CuI is determined followed by measurement of the amount of sulphur dioxide evolved during thermal decomposition. For the determination of 37.9 μg of thiocyanate and 12.6 mg of iodide, the results were 39.0 μg and 12.4 mg, respectively.

Conclusions

The results given in Table 2 show that the thermal decomposition spectrophotometric method of thiocyanate determination is accurate. The method

also shows good precision. A great advantage of the method is its applicability in the presence of a considerable amount of chloride, bromide, iodide, sulphide, thiosulphate and sulphite ions (Table 3). Thus the method can be applied in the presence not only of those ions that, like thiocyanate, form sparingly soluble compounds with copper(I), but also of other reducing sulphur anions.

REFERENCES

1 A. Cygański and T. Majewski, Analyst, 104 (1979) 167.
2 J. Krauss, Angew. Chem., 40 (1927) 354.
3 P. W. West and G. C. Gaecke, Anal. Chem., 28 (1956) 1816.
4 M. Struszyński, Analiza ilościowa i techniczna, Vol. 3, PWN, Warsaw, Poland, 1954, p. 231.
5 G. O. Müller, Quantitativ-Anorganisches Praktikum, S. Hirzel Verlag, Leipzig, 1971, p. 274.
6 J. P. Dixon, Modern Methods in Organic Microanalysis, D. Van Nostrand, London, 1968, p. 40.
7 J. Körbl, Mikrochim. Acta, (1956) 1705.
8 C. Duval, Inorganic Thermogravimetric Analysis, Elsevier, Amsterdam, 1953, p. 251.
9 C. C. Bacanov and E. N. Zalivina, Zh. Neorg. Khim., 17 (1972) 306.
10 E. V. Margulic and V. D. Ponomarev, Izvest. Akad. Nauk Kaz. SSR, Ser. Metall. Obogashch. Ogneuporov., 3 (1958) 9; Chem. Abstr., 55 (1961) 3361a.
11 M. Kabesowa, T. Sramko, J. Gazo, E. K. Zumadilov and V. I. Nefedov, Therm. Anal., 13 (1978) 55.

Analytica Chimica Acta, 141 (1982) 337—344
Elsevier Scientific Publishing Company, Amsterdam — Printed in The Netherlands

EBULLIOMETRIC DETERMINATION OF SOLUBILITY PRODUCTS

WALACE A. DE OLIVEIRA
Instituto de Química, Universidade Estadual de Campinas C.P. 6154, Campinas — SP (Brazil)
(Received 3rd April 1982)

SUMMARY

A method for the determination of solubility products at boiling temperatures is described. It is based on the changes of temperature which occur during the ebulliometric titration involving the precipitation reaction of interest. Thermodynamic solubility products are obtained by extrapolation of results to infinite dilution or through ebulliometric determination of activity coefficients. Solubility products of barium fluoride, strontium sulfate and thallium(I) chloride, at the boiling temperature, were determined and show good agreement with literature values.

Quantitative information about precipitation equilibria can be obtained through a knowledge of solubility product constants. The determination of these constants is important and several methods [1] have been used for this purpose. Precipitation reactions occur with a net change in the total number of particles in solution and can be followed by means of ebulliometric measurements, enabling the precipitation equilibrium to be studied. The development of methods for the determination of solubility products in boiling solutions is desirable because the experimental conditions are not favorable for other methods.

In this work, the application of ebulliometric titrations [2] for the determination of solubility products, at boiling temperatures, was investigated. In order to test the method, the solubility products of barium fluoride, strontium sulfate and thallium(I) chloride were determined. These compounds were chosen because they represent different types of precipitate, have different solubilities and do not significantly involve other equilibria in solution.

EXPERIMENTAL

An apparatus similar to that previously described [3] was used. It consists of a pair of identical ebulliometers where the solution being titrated is brought to boiling and the titrations are then done. Boiling-temperature changes are measured with a pair of matched thermistors, connected to a Wheatstone bridge, the imbalance voltage of which is presented to a strip-chart recorder. Temperature uncertainty was about 6×10^{-5} °C.

Ebulliometric titrations were done by first charging the ebulliometers with the solution to be titrated. After boiling-temperature equilibrium was attained, pellets of the titrant were added through the condensers while the temperature changes were recorded. The following titrations were done: solutions of sodium fluoride of various concentrations titrated with barium chloride; solutions of strontium chloride of several ionic strengths, adjusted with sodium chloride, titrated with sodium sulfate; solutions of sodium chloride in the range of concentration 0.106—0.194 mol kg^{-1} titrated with thallium(I) nitrate.

Measurements were also conducted by charging the ebulliometers only with distilled water and adding pellets of thallium(I) chloride, after boiling-temperature equilibrium had been reached. Reagent-grade chemicals were used in all experiments.

RESULTS AND DISCUSSION

Titration curves

Typical titration curves are shown in Figs. 1 and 2. The curve for the precipitation reaction of barium fluoride (Fig. 1A) shows a clear end-point, at the intersection of the two straight-line segments. The slope of the line before the end-point is positive, indicating that the reaction is not complete at the boiling temperature. In this case a slope equal to zero would be expected [2] if the reaction were complete. Figure 1B shows a poor end-point but the titration curve presents the general shape predicted by theory [2]. Titration of sodium chloride with thallium(I) nitrate (Fig. 2) gave curves which indicate a quite soluble precipitate. At the beginning of the

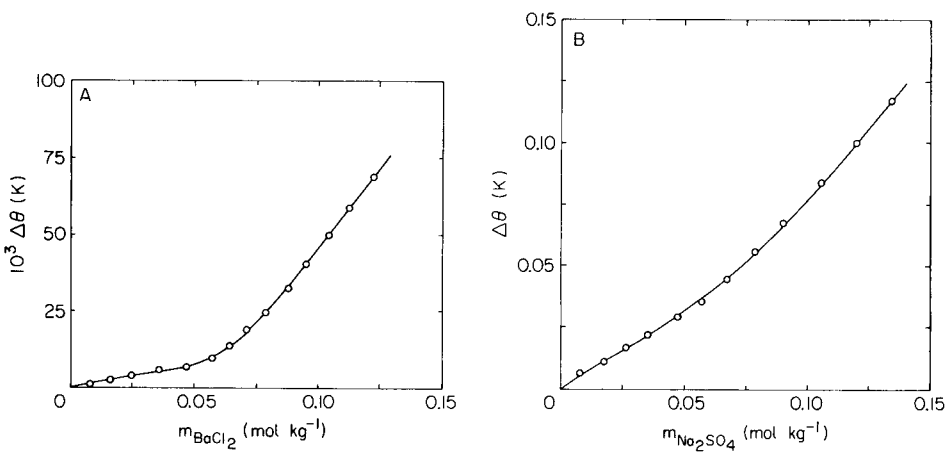

Fig. 1. Ebulliometric titrations. A. Titration of a 0.142 mol kg^{-1} solution of sodium fluoride with barium chloride dihydrate. B. Titration of a 0.0655 mol kg^{-1} solution of Sr^{2+}, of ionic strength 0.655 mol kg^{-1}, with sodium sulfate.

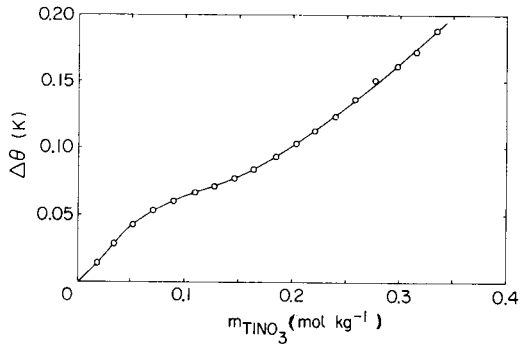

Fig. 2. Ebulliometric titration of a 0.194 mol kg^{-1} solution of sodium chloride with thallium(I) nitrate.

titration (up to 0.05 *m* $TlNO_3$), the amount of titrant added probably was not sufficient to cause precipitation. As titration proceeds, the slope of the curve decreases, indicating that precipitation is occurring. The end-point is, however, not well defined.

Calculation of solubility products

It is necessary to derive equations for the calculation of the solubility products from the data obtained in an ebulliometric titration. Because these equations vary with the type of precipitate and with the order of addition of reagents, it is advisable to treat one precipitate at a time.

Titration of a solution of sodium fluoride with barium chloride. Following the general procedure given previously [4], it is possible to write

$$d\theta/K_b = dm_{Na^+} + dm_{F^-} + dm_{Ba^{2+}} + dm_{Cl^-} \quad (1)$$

where $d\theta$ is the boiling-temperature change caused by addition of titrant, K_b is the ideal ebullioscopic constant, and m represents the molality of the various species. It was assumed in the derivation of Eqn. (1) that the activity coefficients do not change during the titration. This is a valid assumption because only the data up to the equivalence point are used for calculations, and in this titration region, addition of titrant causes the substitution of fluoride by chloride in solution. Introduction into Eqn. (1) of the analytical molality of the titrant m_{BaCl_2} gives

$$d\theta/K_b = dm_{F^-} + dm_{Ba^{2+}} + 2m_{BaCl_2} \quad (2)$$

(m_{Na^+} does not vary during the titration). Integration of Eqn. (2) within the limits of the titration yields

$$\Delta\theta/K_b = m_{F^-} - mi_{NaF} + m_{Ba^{2+}} + 2m_{BaCl_2} \quad (3)$$

where mi_{NaF} is the initial molality of the titrand. Conservation of mass gives

$$mi_{NaF} = m_{F^-} + 2P \quad \text{and} \quad m_{BaCl_2} = m_{Ba^{2+}} + P$$

where P indicates the number of moles of precipitate formed per kilogram of solvent. Solving these equations simultaneously with Eqn. (3) gives expressions for $m_{Ba^{2+}}$ and m_{F^-} which are substituted in the equation of the molal solubility product constant, $K'_{so}(BaF_2) = m_{Ba^{2+}} m^2_{F^-}$, yielding

$$K'_{so}(BaF_2) = [\Delta\theta/3K_b]\,[(2\Delta\theta/3K_b) + mi_{NaF} - 2m_{BaCl_2}]^2 \quad (4)$$

Titration of sodium chloride with thallium(I) nitrate. The above arguments give, for the molal solubility product constant, $K'_{so}(TlCl) = m_{Tl^+}m_{Cl^-}$, the following equation

$$K'_{so}(TlCl) = [\Delta\theta/2K_b]\,[(\Delta\theta/2K_b) + mi_{NaCl} - m_{TlNO_3}] \quad (5)$$

where mi_{NaCl} is the initial molality of titrand and m_{TlNO_3} is the analytical molality of titrant.

Titration of strontium chloride with sodium sulfate. The only difference here from the above cases is the change in ionic strength with addition of titrant, because of replacement of Sr^{2+} by $2Na^+$ in the solution. For this reason, the titrations were done in the presence of a supporting electrolyte, ten times more concentrated than the titrand, in order to avoid appreciable changes in the activity coefficients. For the molal solubility product constant, $K'_{so}(SrSO_4) = m_{Sr^{2+}} m_{SO_4^{2-}}$, the above arguments yield the equation

$$K'_{so}(SrSO_4) = [(\Delta\theta/2K_b) - 0.5\,m_{Na_2SO_4}]\,[(\Delta\theta/2K_b) + mi_{SrCl_2} - 1.5m_{Na_2SO_4}] \quad (6)$$

where $m_{Na_2SO_4}$ is the analytical molality of titrant and mi_{SrCl_2} is the initial molality of the solution being titrated.

Equations (4–6) were used for the calculations of the molal solubility products. In each titration, 4–6 portions of titrant were added, up to the equivalence point, and the K'_{so} value was calculated for each titration point. In the case of barium fluoride and strontium sulfate, the average values of each titration were tabulated as a function of the ionic strength of the solution being titrated. These results are given in Table 1. The standard deviations of the average value in each titration was between 5 and 20%, with more uncertainty being found for the more diluted solutions.

Values of $K'_{so}(TlCl)$ as a function of ionic strength were not obtained because the large solubility of thallium(I) chloride at the boiling temperature did not allow acquisition of data sufficient for extrapolation to infinite dilution. The average result of titrations done at an ionic strength of 0.130 mol kg^{-1} was 8.6 ($\pm$0.8) $\times$ 10^{-3} mol^2 kg^{-2}.

Extrapolation to infinite dilution

The relationship between the thermodynamic solubility product K^o_{so}, defined in terms of the activity of the ions and the molal solubility products is given by $K^o_{so} = K'_{so}\gamma^2_\pm$ for strontium sulfate and $K^o_{so} = K'_{so}\gamma^3_\pm$ for barium

TABLE 1

Molal solubility products for barium fluoride and strontium sulfate

Barium fluoride		Strontium sulfate	
I (10^{-3} mol kg^{-1})	$10^6\ K'_{so}$	I (mol kg^{-1})	$10^5\ K'_{so}$
32.1	2.1	0.078	0.50
44.5	3.4	0.100	0.50
53.5	4.5	0.132	0.79
63.0	2.9	0.166	1.6
81.6	4.0	0.201	2.0
102	5.0	0.263	3.2
142	7.9	0.395	4.0
180	5.0	0.655	2.5

fluoride; $\gamma_\pm$ is the mean activity coefficient for the respective compound. If the Debye-Hückel equation is used to represent the activity coefficients, then for strontium sulfate

$$\log K'_{so} = \log K^\circ_{so} + (4.723 I^{1/2})/(1 + \mathring{a}\ 0.3406\ I^{1/2}) \quad (7)$$

and for barium fluoride

$$\log K'_{so} = \log K^\circ_{so} + (3.542 I^{1/2})/(1 + \mathring{a}\ 0.3406 I^{1/2}) \quad (8)$$

where $\mathring{a}$ is the distance of closest approach, I is the ionic strength and the numerical constants [5] are for the temperature of 98.3°C and the molal scale. Equations (7) and (8) indicate that a plot of log K'_{so} against $I^{1/2}/(1 + \mathring{a}\ 0.3406\ I^{1/2})$ gives the thermodynamic solubility product. However, the difficulty is that the value of $\mathring{a}$, at the boiling temperature, is not available. For this reason, the data of Table 1 were fitted to Eqns. (7) and (8) with the help of a general multiparametric curve-fitting program [6]. The following values were obtained

$K^\circ_{so}(BaF_2) = 8\ (\pm 2) \times 10^{-7}$ mol^3 kg^{-3}; $\mathring{a} = 4.4$ Å

and $K^\circ_{so}(SrSO_4) = 7\ (\pm 3) \times 10^{-7}$ mol^2 kg^{-2}; $\mathring{a} = 4.0$ Å

The value of $K^\circ_{so}(SrSO_4)$ obtained in the present work is in agreement with literature data [7] about the solubility of strontium sulfate, at the same temperature (98.3°C). Direct comparison of the present result for $K^\circ_{so}(BaF_2)$ is not possible because of the lack of literature data. Nevertheless, the solubility product found at the boiling temperature is very close to that (1.0×10^{-6} mol^3 kg^{-3}) for 25°C and is consistent with the observation [7] that the solubility of barium fluoride does not change much with temperature.

The present results for the distance of closest approach are very similar to the values calculated by Kielland [8] for the single ions at 25°C: 5, 3.5, 5 and 4 Å, respectively, for Ba^{2+}, F^-, Sr^{2+} and SO_4^{2-}. This similarity is in

agreement with much earlier findings [9], which indicate that the parameter $\mathring{a}$ does not vary substantially with temperature.

Measurements with thallium(I) chloride

The solubility of thallium(I) chloride makes it possible to measure the boiling-temperature elevations of its solutions, up to saturation. These measurements were undertaken to provide additional ebulliometric data and also to allow the determination of activity coefficients, for the calculation of the thermodynamic solubility product.

Table 2 gives the boiling-temperature elevations (θ) as a function of the molalities m of thallium(I) chloride. As can be seen, the temperature remains constant when the solution becomes saturated. The solubility was determined graphically, from these data, by plotting θ against m and finding the intersection of the two straight-line segments, before and after saturation. The value so found was 9.8×10^{-2} mol kg^{-1}. Literature data [7] about the solubility of thallium(I) chloride in water at the same temperature, gives 9.9×10^{-2} mol dm^{-3}, in good agreement with the value determined by means of ebulliometric measurements.

The osmotic coefficients ϕ of thallium(I) chloride solutions given in Table 2 were calculated from the equation

$$\phi = 0.9854\theta/m - 3.159 \times 10^{-3}\theta^2/m + 8.96 \times 10^{-6}\theta^3/m \qquad (9)$$

which was obtained by procedures outlined previously [10]. The activity coefficients were obtained from the osmotic coefficients, by first fitting the data to the equation [3]

$$\phi = 1 - [1.359/(V_1^3 m)]\,[1 + V_1 m^{1/2} - 2\ln(1 + V_1 m^{1/2}) - 1/(1 + V_1 m^{1/2})] \qquad (10)$$

TABLE 2

Boiling-temperature elevations (θ), osmotic coefficients (ϕ), and mean activity coefficients ($\gamma_\pm$), as functions of the molality of TlCl

Molality (10^{-3} mol kg^{-1})	θ (10^{-3} °C)	ϕ	$\gamma_\pm$	Molality (10^{-3} mol kg^{-1})	θ (10^{-3}°C)	ϕ	$\gamma_\pm$
5.7	5.7	0.985	0.912	69.4	64.4	0.914	0.775
11.2	11.0	0.968	0.884	79.2	74.7	0.929	0.766
18.5	17.8	0.948	0.858	92.1	86.0	—	—
25.5	24.3	0.939	0.840	104.1	90.0	—	—
31.6	30.6	0.954	0.827	115.1	91.4	—	—
37.2	35.4	0.938	0.817	125.5	91.4	—	—
45.3	43.2	0.940	0.804	135.1	91.4	—	—
48.3	46.1	0.941	0.780	146.0	91.4	—	—
54.8	51.7	0.930	0.791	159.8	91.4	—	—
62.5	59.6	0.940	0.782	173.0	91.4	—	—

where the parameter V_1 comes from the Debye-Hückel equation and is equal to 0.3406 $\mathring{a}$. The fit yielded a value of $V_1 = 1.535$ kg$^{1/2}$ mol$^{-1/2}$. Thus, the mean activity coefficients $\gamma_\pm$ of thallium(I) chloride were given by

$$\ln \gamma_\pm = -1.359\, m^{1/2}/(1 + 1.535\, m^{1/2}) \qquad (11)$$

which was used to obtain the results given in Table 2.

The present values for the distance of closest approach and for the mean activity coefficients of thallium(I) chloride are a little higher than would be expected on the basis of previous studies [11] on diluted solutions and at lower temperatures. This fact and also the behavior of the slopes of the titration curves suggest the possibility of ion-pair formation in boiling solutions of thallium(I) chloride. In order to verify this suggestion, ion-pair formation constants K'_f were calculated by using the data for θ and m of Table 2, with the expression [10] $K'_f = (2m - \theta/K_b)/(\theta/K_b - m)^2$. The results for K'_f were plotted against $m^{1/2}/(1 + 1.19\, m^{1/2})$ and yielded a value of 15 ± 5 kg mol^{-1} for the thermodynamic ion-pair formation constant. At ionic strength 0.130 mol kg^{-1}, the value of K'_f was around 1.7 kg mol^{-1}, which indicates that the ion-pair Tl^+Cl^- represents less than 10% of the total species in the boiling solution. Since this was considered to be within the experimental error, the procedure used to calculate K'_{so}(TlCl) (Eqn. 5) was not modified to account for ion-pair formation.

For a solution of thallium(I) chloride of ionic strength 0.130 mol kg^{-1}, Eqn. (11) gives a mean activity coefficient of 0.729. Following Robinson and Stokes [5], this value of $\gamma_\pm$ is divided by the degree of dissociation (= 0.87), to take into account the ion-pair formation, and substituted in the expression $K^\circ_{so} = K'_{so}\, \gamma^2_\pm$. This procedure gives a value of 6.0 (±0.6) × 10^{-3} mol^2 kg^{-2} for the thermodynamic solubility product of thallium(I) chloride.

Evaluation of the technique

Solubility can be determined by ebulliometry by means of direct measurements [3] or by using a titrimetric procedure, with comparable precision. Direct measurements are usually slower and applicable only to more soluble compounds (with $K'_{so} \geqslant 1 \times 10^{-3}$), whereas ebulliometric titrations make it possible to work with less soluble compounds. The lowest solubility product that can be determined depends on the precision of the boiling-temperature measurements. For example, the best precision reported for ebulliometry [12] would enable a K'_{so} value as low as 10^{-16} mol^3 kg^{-3} to be determined for a compound of the type of barium fluoride. However, the dependability of the results decreases when very small temperature changes are to be measured.

The method described above is quite simple, uses inexpensive instrumentation and permits the determination of solubility products over a range of temperature. The basic requirements are that all solutes must be stable and non-volatile at the temperature of measurements. It seems possible to conclude that ebulliometric measurements can be useful for the study of

solubility equilibria at boiling temperatures, in systems where other methods cannot be applied efficiently.

The author is grateful to CNPq-Brazil for a research fellowship received during the course of this work.

REFERENCES

1 G. J. Papariello and W. J. Mader, in J. M. Kolthoff and P. J. Elving (Ed.), Treatise on Analytical Chemistry, Part 1, Vol. 7, Ch. 84, Interscience, New York, 1967.
2 W. A. de Oliveira, Anal. Lett., 14 (1981) 1391.
3 W. A. de Oliveira and L. Meites, Anal. Chim. Acta, 93 (1977) 3.
4 W. A. de Oliveira, J. Coord. Chem., 9 (1979) 7.
5 R. A. Robinson and R. H. Stokes, Electrolyte Solutions, Butterworths, London, 1955, pp. 491, 397.
6 L. Meites, The General Multiparametric Curve-Fitting Program CFT4, Computing Laboratory, Department of Chemistry, Clarkson College of Technology, Potsdam, New York, 1976.
7 W. F. Linke, Solubilities of Inorganic and Metal Organic Compounds, American Chemical Society, Washington, DC, 1958, pp. 1519, 359, 1566.
8 J. Kielland, J. Am. Chem. Soc., 59 (1937) 1675.
9 R. A. Robinson and H. S. Harned, Chem. Rev., 28 (1941) 419.
10 W. A. de Oliveira and J. M. B. Lima, J. Chem. Thermodyn., 12 (1980) 1065.
11 I. A. Cowperthwaite, V. K. La Mer and J. Barksdale, J. Am. Chem. Soc., 56 (1934) 544.
12 E. L. Zichy, Soc. Chem. Ind. (London), 17 (1963) 122.

Analytica Chimica Acta, 141 (1982) 345—351
Elsevier Scientific Publishing Company, Amsterdam — Printed in The Netherlands

RADIOCARBON EVALUATION OF NATURAL/SYNTHETIC RATIO IN CITRIC ACID SAMPLES

ENNIO CAMPI and EDOARDO MENTASTI
Istituto di Chimica Analitica, Università di Torino (Italy)
PAOLO VOLPE*
Istituto di Chimica Generale ed Inorganica, Università di Torino, 10100 Torino (Italy)
(Received 4th December 1981)

SUMMARY

A method is described for the evaluation of the natural/synthetic ratio in citric acid samples. The method is based on measurements of the activity of carbon-14 present in citric acid of natural origin. The parameters that affect the radiocarbon counting (background emission, scintillation quenching and relative efficiency) are discussed. Two different procedures are described which can also be applied to the evaluation of the natural/synthetic origin of other carbon-containing compounds.

Measurements of the relative abundance of the isotopes of some elements have been used in several cases in order to distinguish between natural and synthetic products [1]. As an example, carbon-14 counting has been suggested in order to assess the purity of natural products such as cinnamic-aldehyde from cinnamon and caffeine from coffee and tea [2]. Comparison of the ^{14}C,$^{13}C/^{12}C$ ratios and $^{2}H/^{1}H$ ratio have been taken into account for distinguishing between natural and artificial food flavors [3—5]. Ageing of a brandy has also been evaluated by means of natural carbon-14 radioactivity measurements [6], as has the origin of products from alcohol and vinegar [7, 8].

The ^{14}C isotope, which is present in the atmosphere mainly as $^{14}CO_2$, is produced naturally by the neutrons from cosmic radiation through the reaction: $^{14}_{7}N + ^{1}_{0}n \rightarrow ^{14}_{6}C + H^{1}_{1}p$ [9]. The relative natural abundance of ^{14}C with respect to stable carbon in the atmosphere is $\sim 10^{-12}$. After the nuclear explosions which took place very heavily in the fifties, the number of the neutrons available for the reaction with ^{14}N increased remarkably, and the specific radioactivity, in terms of disintegrations per minute (dpm) in one gram of natural carbon in the atmosphere, was doubled around 1963; later it decreased almost exponentially as a consequence of the slow uptake by living organisms, and nowadays one gram of natural carbon shows a characteristic activity of ~18 dpm. Living organisms, which exchange carbon from the environment, contain a carbon-14 percentage corresponding to that in

the atmosphere during their lifetime [10]. Dead materials contain carbon-14 in a proportion corresponding to that present in the atmosphere in their lifetime, and the subsequent period of radioactive decay: $^{14}C \rightarrow {}^{14}N + \beta^-$ with $t_{1/2}$ = 5670 years [10]. For example, fossil hydrocarbons, which are millions of years old, have now a carbon-14 content of virtually zero, as have all the synthetic products derived from them. Therefore these products can be distinguished from analogous products extracted from living organisms or from materials derived from recently dead organisms.

The present paper describes a method which enables samples of natural/synthetic citric acid to be differentiated and the ratio to be quantified.

EXPERIMENTAL

Chemicals and instrumentation

The natural citric acid used throughout this work was a natural product from 1978 (Liquichimica, Robassomero, Torino). Synthetic citric acid was a commercial analytical-grade sample (Merck).

The instrument used for the radioactivity measurements of the samples was a Packard TRI-CARB Model 2002 (2-channel) liquid scintillation counter. Insta-Gel (Packard) scintillator was used with each sample.

Densities of aqueous solutions of citric acid

Portions (15.0, 20.0, 25.0 and 30.0 g) of anhydrous citric acid were dissolved in water and the solutions were diluted to 50 ml in volumetric flasks. From the weight of the solutions, the densities as a function of the relative percent (w/w) of citric acid were found at 25.0°C (see Table 1). A plot can be drawn from the data reported in Table 1 in order to interpolate the densities of solutions prepared with a given weight percent. The point which represents the saturated solution [11] (see last line of Table 1) is easily extrapolated from this plot.

Procedures

Two different procedures were examined; they are described below. The first general method (A) was used in the developmental work and takes into account the efficiency, internal quenching and activity yield for the primary β-emission and secondary scintillation. The second procedure (B) is a rapid comparison method which can be adopted for systems whose behaviour has already been checked by procedure (A).

Measurements of radioactivity. Different portions of citric acid solutions were mixed in 20-ml vials with Insta-Gel scintillator so that the total volume of the solution was 15.0 ml; the radioactivity was then measured. Each vial was previously filled with a mixture of Insta-Gel and distilled water in order to measure the background counts to be subtracted from each measurement done with the sample contained in that vial, with the same quantity of scintillator and the same total volume of solution. Five independent

TABLE 1

Densities of aqueous solutions of citric acid at 25.0°C

Anhydrous citric acid (g)	Weight of resulting 50-ml soln.	Density ($g\ ml^{-1}$)	Citric acid content (% w/w)
15.00	56.07	1.12	26.8
20.00	57.77	1.155	34.6
25.00	59.63	1.19	41.0
30.00	61.73	1.235	48.6
		1.315[a]	61.7[a]

[a]Obtained from Ref. [11]: 100 g of saturated citric acid solution contains 67.5 g of monohydrated citric acid at 25°C; 100 ml of saturated solution contains 42.7 ml of water.

measurements, with different vials, were done for every sample; counting was done ca. 24 h after the vials had been inserted in the instrument, in order to ensure complete quenching of the luminescence from the gel formed; three independent countings from each vial were done over a period of 50 min each.

For preliminary measurements, 100% natural citric acid stock solutions were used in order to estimate the characteristic radioactivity as a function of citric acid concentration, of relative quantity of scintillator and of internal quenching effect.

Procedure A. The counts per minute which can be obtained for a sample of 100% natural citric acid can be computed from

$$\text{cpm (nat.)} = 18VdXE6\ (\text{atomic wt. C})/(\text{m.w. citric acid}) = 18Y \qquad (1)$$

where 18 represents the disintegrations per minute for each gram of natural carbon, E is the efficiency (for the definition and evaluation, see below), d is the density of the citric acid solution of known weight percent (X) and volume (V ml), and Y is the activity yield (see below). The experimental cpm value for the sample under test is then measured as indicated above. The percentage of natural citric acid in the natural/synthetic sample is therefore given by the ratio between the experimental cpm counts for the mixture and the cpm (nat.) obtained from Eqn. (1): 100 (cpm (expl.)/ cpm (nat.).).

Procedure B. A more straightforward procedure can be adopted with the aid of a calibration plot. If the ratio between natural and synthetic citric acid of a mixture must be evaluated, one portion of citric acid is dissolved with distilled water in a 20-ml vial (with a final density between 1.20 and 1.30, i.e., 30—60% w/w) with sufficient Insta-Gel scintillator to give a final volume of 15 ml. Its radioactivity is then measured. An identical portion of 100% natural citric acid is used to prepare a similar mixture in another 20-ml vial. The radioactivity of the second vial permits the construction of a linear calibration plot of cpm's as a function of percentage (w/w) of natural citric acid in the mixture. From this plot, the composition of the sample can be obtained.

RESULTS AND DISCUSSION

Three stock solutions (20, 50 and 60%, w/w) were prepared from 100% natural citric acid, and three analogous solutions from 100% synthetic citric acid. The densities of these sets of solutions were 1.09, 1.245 and 1.305 g ml^{-1}, respectively. Portions (p) of 2.0, 4.0, 6.0 and 8.0 ml of each solution were mixed with $(15-p)$ ml of Insta-Gel scintillator in the vials, and ^{14}C activities were measured as described above. The background count for each vial was found to lie around 30 cpm. The mean difference between background and synthetic citric acid counts was ±0.5 cpm. These observations were obtained with each of the portions (2, 4, 6, 8 ml) of the 20, 50 and 60% (w/w) solutions, indicating that the presence of synthetic citric acid, even in large quantity, does not modify appreciably the background radiation.

The corrected counts obtained from natural citric acid, mixed with the same quantity of scintillator as used for the background emission radiation, are reported in Table 2. The masses of carbon present in the vials are also listed, as well as the number of disintegrations per minute (dpm) from these

TABLE 2

Experimental activities (cpm) for natural citric acid samples and related quantities as a function of percent citric acid and volumes of the solutions mixed with the scintillator

		Volume of citric acid solution in vial (ml)			
		2.0	4.0	6.0	8.0
Citric acid	cpm[a]	2.02 ± 0.34	4.24 ± 0.41	5.82 ± 0.18	
20% (w/w)	g C[b]	0.164	0.327	0.491	
d = 1.09	dpm[c]	2.95	5.89	8.85	
	eff. E %	68.5	71.9	65.8	
	Y[d]	0.112	0.235	0.323	
Citric acid	cpm[a]	5.73 ± 0.16	11.2 ± 0.5	14.3 ± 0.9	
50% (w/w)	g C[b]	0.467	0.934	1.401	
d = 1.245	dpm[c]	8.41	16.8	25.2	
	eff. E %	68.1	66.7	56.8	
	Y[d]	0.318	0.623	0.796	
Citric acid	cpm[a]	7.27 ± 0.76	14.0 ± 1.4	21.2 ± 0.9	22.8 ± 0.7
60% (w/w)	g C[b]	0.587	1.175	1.762	2.350
d = 1.305	dpm[c]	10.55	21.2	31.7	42.2
	eff. E %	68.9	66.1	66.8	54.0
	Y[d]	0.404	0.777	1.177	1.269

[a]Each cpm value is obtained by subtracting the background reading from the sample reading; the error is the standard deviation estimate over 15 cpm measurements (5 independent triplicate measurements, see Procedure).
[b]Computed from the volume and percentage (w/w) of the citric acid solution.
[c]Computed by assuming, for a natural product of 1978, 1 g C = 18 dpm.
[d]Activity yield computed from the efficiency E and the mass of carbon in the citric acid.

quantities, obtained by assuming that each gram of natural carbon element contains carbon-14 in a proportion able to undergo 18 dpm. The cpm/dpm ratios give the efficiency ratio E, which is about 70% in the case of the less concentrated solutions and becomes smaller at increased concentrations of citric acid (Table 2). This observation shows that citric acid has some scintillation quenching properties under these conditions. Therefore, in order to measure the relative proportion of natural to synthetic citric acid in a sample, experimental evaluation of the dpm and of the efficiency with 100% natural citric acid at a particular concentration is necessary for proper comparison with the values obtained from the citric acid sample under test at the same concentration and with the same scintillator proportion.

The activity yield Y provides useful information on the sensitivity and application of the method; the yield is given by the product between efficiency E and grams of carbon in the analyte in the vial. The latter quantity is obviously limited by the concentration of the citric acid solution and its solubility in the scintillator solution; citric acid solution can be mixed with the Insta-Gel solution in a proportion up to about 55% but at these values the efficiency generally decreases. Figure 1 reports the Y values as functions of the volumes of citric acid and the percentage of citric acid in each vial; the plots show that the more concentrated citric acid solutions provide the best sensitivity despite the lower relative efficiency (see Table 2).

In order to evaluate the possibility of analytical resolution in samples of mixed composition, mixed solutions of natural and synthetic citric acid were then prepared from the 60% (w/w) citric acid stock solutions ($d = 1.305$).

The ratios of natural citric acid to synthetic citric acid in the solutions

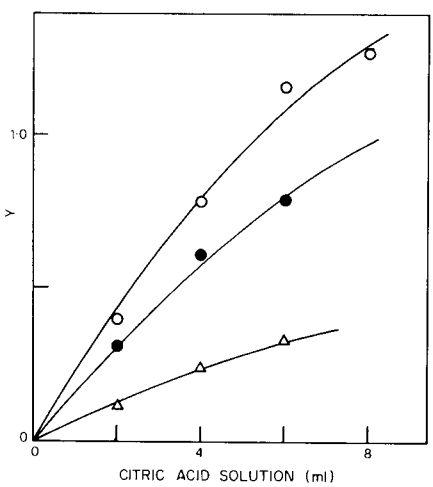

Fig. 1. Variation of the activity yield Y as a function of the volume of citric acid solution mixed with the scintillator in the vials, for different natural citric acid concentrations: (△) 20; (•) 50; (○) 60% (w/w).

were 1:3, 1:1 and 3:1, the total citric acid concentration being kept constant at 60% (w/w) in distilled water. For each mixture (5 independent measurements for both background and sample), 8 ml was mixed with 7 ml of scintillator (see Table 3) and measured as described above. Table 3 shows the results, together with the expected values obtained from the stoichiometric carbon-14 content, the counting efficiency (54%) previously obtained at this concentration, and the dpm typical for 1 g of carbon (18 dpm) for a 1978 100% natural compound. The data collected in Table 3 are very satisfactory.

A more straightforward method (procedure B) can be adopted with the aid of a calibration plot. Figure 2 shows the calibration plot for the mixtures A, B and C reported in Table 3; the calibration line was drawn according to the value cpm = 22.8 reported in Table 2 for the conditions of Table 3. The arrows indicate the results for the citric acid samples reported in Table 3.

Conclusion

The present method seems to be unique, as no alternative techniques are available. It enables the origin of a product which contains citric acid to be established. The determination requires some grams of product for reliable evaluation. The uncertainty in the determination arises mainly from errors associated with the radioactivity measurements. The mean uncertainty of each activity measurement is about ±0.50 cpm, so that the absolute error in the natural citric acid evaluation is about ±0.050 g of carbon, which corresponds for the most concentrated solutions (8 ml of 60% (w/w) citric acid solution) to about ±2.0% citric acid.

Other mixtures such as those containing ethanol or acetic acid, for which the present method has been previously used, allow higher counting

TABLE 3

Evaluation of natural/synthetic ratio in citric acid mixtures with counts per min., related quantities and relative abundance found for each component

Solution	A	B	C
Natural acid added (%)	25.0	50.0	75.0
Synthetic acid added (%)	75.0	50.0	25.0
cpm (exptl.)	5.33 ± 0.87	11.2 ± 0.5	16.1 ± 1.1
Natural carbon (g)	0.587	1.175	1.762
dpm[a]	10.6	21.2	31.7
cpm (calc.)[a]	5.70	11.8	17.1
Natural acid found (%)	23.4	49.1	70.6
Synthetic acid found (%)	76.6	50.9	29.4

[a]For the computation, see Experimental.

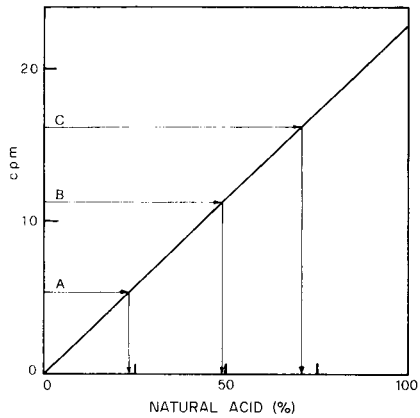

Fig. 2. Calibration plot for the evaluation of the relative percentage of natural citric acid in mixtures A, B and C.

efficiencies and therefore lower absolute quantities to be used. However, the sensitivity of the method can be increased by modifying the counter to accommodate larger vials with sample solutions of lower concentration.

REFERENCES

1 See, e.g., K. G. Sloman, A. K. Foltz and J. A. Yeransian, Anal. Chem., 53 (1981) 242R; and earlier biennial reviews.
2 J. E. Noakes and P. G. Hoffman, Liq. Scintill. Counting: Recent Appl. Dev., (Proc. Int. Conf.), 2 (1979) 457; Chem. Abstr., 93 (1980) 112430s.
3 J. Bricout and J. Koziet, Flavor, Foods and Beverages: Chem. Technol. (Proc. Conf.), (1978) 199.
4 L. W. Donor, D. Chia and J. W. White, Jr., J. Assoc. Off. Anal. Chem., 62 (1979) 928.
5 O. Carro, C. Hillaire-Marcel and M. Gagnon, J. Assoc. Off. Anal. Chem., 63 (1980) 840.
6 F. Mecca, Boll. Lab. Chim. Prov. (Italy), 27 (1976) 326.
7 V. Faltings, Angew. Chem., 64 (1952) 605.
8 F. Mecca, A. Sapegno and P. G. Spaggiari, Chim. Ind., 52 (1970) 880.
9 G. Friedlander and J. W. Kennedy, Nuclear and Radiochemistry, Wiley, New York, 1962.
10 R. C. Weast (Ed.), Handbook of Chemistry and Physics, 61st edn., CRC Press, Boca Raton, FL, 1980.
11 The Merck Index, 9th edn., Merck, Rahway, NJ, 1976.

Analytica Chimica Acta, 141 (1982) 353—358
Elsevier Scientific Publishing Company, Amsterdam — Printed in The Netherlands

Short Communication

CATALYTIC—KINETIC DETERMINATION OF SOME IODINE-CONTAINING ORGANIC COMPOUNDS WITH DIFFERENT CATALYTIC ACTIVITIES BY A BIAMPEROSTATIC METHOD

SIEGBERT PANTEL

Institut für Analytische Chemie, Chemisches Laboratorium der Universität, D-7800 Freiburg i.Br. (W. Germany)

(Received 30th March 1982)

Summary. Iodine-containing organic compounds of the general formula X—C_6H_4—I catalyze the Sandell—Kolthoff reaction to different extents; the catalytic activities depend on the other substituent and on the relative positions of the X and iodine substituents. 4-Iodophenol, 2-iodophenol and 4-iodo-*N*,*N*-dimethylaniline can be determined in the microgram range.

The oxidation of arsenic(III) with cerium(IV) is catalyzed not only by inorganic iodide [1] but also by iodine-containing organic compounds such as thyroxine [2—4], proteins [2, 5, 6], hormones and drugs [7]. The Sandell—Kolthoff reaction is therefore often used to determine micro amounts of these species by kinetic methods. It has been shown that the catalytic activity of iodine in organic compounds is inferior to that of inorganic iodide [8] and differs with the kind of organic radical [9]. It will be shown below that the catalytic activity of iodine in substituted iodobenzenes of the general formula X—C_6H_4—I is strongly dependent on the nature of X and on the relative positions of the substituents in the benzene ring.

As the catalytic activity of these iodo compounds is sometimes rather small, a very sensitive measuring method is needed for the indicator reaction. A stat-method seemed suitable [10]. In the indicator reaction, $A + B \overset{K}{\rightleftharpoons} X + Y$, the concentration of one reactant (A or B) can be kept very low and constant during measurements. As some of the iodine compounds are easily oxidized [11, 12], the concentration of cerium(IV) was kept low in this work. Another problem was that some of the iodo compounds are not soluble enough in water to provide measurable catalytic activity. Ethanol was therefore added to the indicator reaction mixture, and could be used up to a 20% ethanolic solution. More ethanol caused precipitation of the reactants and had a disadvantageous effect on the reaction rate.

As some of the iodo compounds give strong yellow complexes with cerium(IV), photometric regulation of the stat-apparatus was not possible; the potentiometric method [13—15] keeps the ratio of Ce(IV) to Ce(III) constant rather than a preset concentration of cerium(IV). Therefore, the

0003-2670/82/0000-0000/$02.75

biamperometric method [8, 16] was used here. The reaction conditions are chosen so that the uncatalyzed reaction proceeds with measurable speed (Fig. 1, line A—B); after the addition of the catalyst, the reaction rate increases (line B—C), and the difference $\Delta \tan \alpha = \tan \alpha_K - \tan \alpha_O$ is a measure of the catalytic activity. This procedure has the advantage that the effect of interfering trace impurities can be compensated because their contribution is included in α_O.

As a measure of the catalytic activity of the iodo compounds in comparison to that of inorganic iodide, a "relative molar coefficient of catalytic activity" F is introduced. Coefficient F is defined as the quotient of the molar concentrations of iodide and the respective iodo compound, which have exactly the same catalytic activity, thus $F = C_{I^-}/C_{RI}$. For example, $F = 0.025$ means that 1 nmol of iodide has the same catalytic activity as 40 nmol of the iodo compound if the reaction volume is the same. Calibration graphs are drawn for $\Delta \tan \alpha$ vs. iodide concentration and the iodo compound concentration; from these plots, a $\Delta \tan \alpha$ value is chosen, the relevant concentrations of iodide and iodo compound are read, and F is calculated. If the graphs are linear (as in the examples given below), any $\Delta \tan \alpha$ may be chosen. If the graphs are not linear, the $\Delta \tan \alpha$ value selected must obviously be reached by all the compounds of interest [9], and this value must be indicated, e.g., $F(\Delta \tan \alpha = 0.2) = 0.025$. The F values found for nine 4-substituted iodobenzenes are listed in Table 1. There are also remarkable differences between the catalytic activities of isomeric iodophenols and iodoanilines (Table 2).

Experimental

Reagents. All the iodo compounds, whether purchased (EGA, Steinheim, W. Germany) or prepared by standard methods, were purified by dissolving in benzene, and extracting three times with 1 M thiosulphate solution and five times with water. After evaporation of the benzene, the crude products

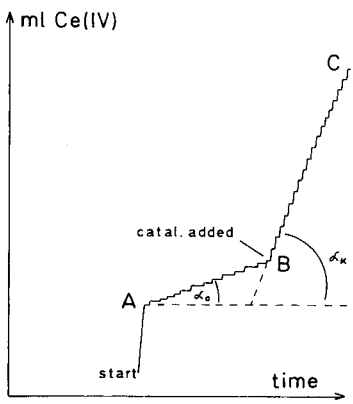

Fig. 1. Recorder trace for the biamperometrically controlled addition of 0.06 M Ce(IV) in the catalyzed oxidation of arsenic(III).

TABLE 1

Catalytic activities of 4-substituted iodobenzene, X—C_6H_4—I, in comparison to iodide ($F = 1$)

Radical —X	F value	Radical —X	F value	Radical —X	F value
—H	0.00006	—OC_6H_5	0.003	—OH	0.42
—COOH	0.0003	—CH_3	0.003	—NH_2	0.48
—OCH_3	0.0003	—$C(CH_3)_3$	0.007	—$N(CH_3)_2$	0.53

TABLE 2

Catalytic activities of isomeric monosubstituted iodobenzene

Compound	F value	Compound	F value
2-Iodophenol	0.09	2-Iodoaniline	0.005
3-Iodophenol	0.0015	3-Iodoaniline	0.012
4-Iodophenol	0.42	4-Iodoaniline	0.48

were purified by distillation, sublimation or recrystallization until the catalytic activity remained constant after two successive purification steps. All substances were characterized through boiling point, melting point, refractive index or i.r. spectroscopy.

Equipment. The apparatus used has been described [16]. It consists of a Combi-Titrator 3 D (Metrohm, Herisau, Switzerland) with a current-to-voltage transducer and two mV sources (Fig. 2). A 50-ml test tube (30-mm o.d.) serves as reaction vessel, and is mounted in a thermostated aluminium block (25.0 ± 0.2°C). A double platinum electrode and the capillary end of the burette (Mikrodosimat, 1-ml) are fitted through a plastic lid on the test tube. The tip of a 500-μl Eppendorf pipette is inserted through a 5-mm hole in the lid. The reaction mixture is stirred magnetically. The recorder speed was 1 cm min^{-1}.

Procedure for 4-iodophenol. To the measuring vessel are added 2 ml of 0.2 M arsenic(III) solution (prepared from As_2O_3 by dissolution in sodium hydroxide solution and adjustment to pH 8.4 with 1 M H_2SO_4), 5 ml of 2 M sulphuric acid, 5 ml of ethanol (extra pure) and twice-distilled water up to 24.5 ml. After thermostating for 3 min, the measuring device is compensated to zero (U_2, Fig. 2) and 200 μl of 0.06 M cerium(IV) sulphate solution (in 0.4 M H_2SO_4) is added. Then the feed-back resistor (R_f, Fig. 2) is immediately balanced so that the mV-meter shows exactly 600 mV (preset working potential) and automatic addition of 0.06 M cerium(IV) solution from the Mikrodosimat is started. After 6 min, 0.5 ml of an ethanolic solution of iodophenol is added from the Eppendorf pipette. The recorder traces are similar to that shown in Fig. 1. A calibration graph is drawn by plotting $\Delta \tan \alpha$ vs. catalyst concentration. It was linear over the range 4—40 nmol of 4-iodophenol.

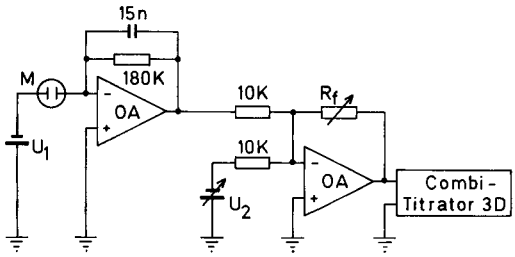

Fig. 2. Circuit diagram: M, measuring vessel with double platinum electrode; OA, operational amplifiers (McKee-Pedersen MP-1006); U_1, 100-mV stabilized (MP-1008); U_2, ±2-V stabilized (MP-1008).

When not in use, the indicator electrode is stored in ca. 1 M ascorbic acid solution and pre-conditioned daily by a test run with 1 μg of iodide. The electrodes must be properly conditioned otherwise the reproducibility of the recorder traces is poor.

Determination of F values for unstable or weakly active compounds. In such cases, only two runs are made with different catalyst concentrations within the solubility range and the Δ tan α values are extrapolated from the initial rates of the addition plots. From these data, a calibration graph is drawn and used to calculate the *F* values, as described above. These values are not as exact as those obtained for stable, highly active compounds, but they give a reasonable idea of the order of magnitude of *F*.

Results

Iodophenols. The most active of the isomeric iodophenols, 4-iodophenol (Table 2), could be determined sensitively in the lower microgram range. Some results are given in Table 3. 2-Iodophenol can be determined similarly in the range 20—200 nmol in 25 ml (Table 3). 3-Iodophenol is not stable under the conditions used; it forms a precipitate with cerium(IV). Its *F* value was extrapolated from the initial rate of the catalyzed reaction as described above.

Iodoanilines. Under the conditions recommended above, 2- and 3-iodoaniline are relatively unstable. The recorder plots for these isomers become flat after a short time, indicating deactivation of the catalyst, and the solution becomes coloured. The recorder plot for the 4-isomer curves upwards and becomes linear after some minutes; this means that the catalytic activity increases during the initial reaction. From the linear parts of the addition plots, the tan α_K values can be read, and a linear calibration graph is obtained over the range 3—30 nmol/25 ml.

The stability of iodoanilines is somewhat increased by methylation of the amino group. Thus 4-iodo-*N*,*N*-dimethylaniline can be determined in the range 2—20 nmol/25 ml by the method described above for 4-iodophenol. Some results are given in Table 3. Ethanolic solutions of 4-iodo-*N*,*N*-dimethylaniline decompose on standing and become red-violet [11, 12].

TABLE 3

Determination of monosubstituted iodobenzenes as catalysts in the Sandell—Kolthoff reaction

4-Iodophenol (μg/25 ml)		2-Iodophenol (μg/25 ml)		4-Iodo-*N*,*N*-dimethylaniline (μg/25 ml)	
Given	Found	Given	Found	Given	Found
1.41	1.43	4.40	4.60	0.80	0.80
1.50	1.45	7.62	7.70	0.88	0.91
2.20	2.42	8.80	7.92	1.76	1.82
3.17	2.94	11.43	11.66	1.80	1.76
3.48	3.63	15.24	14.96	2.55	2.65
3.65	3.52	18.05	17.60	2.65	2.58
4.40	4.40	22.86	23.10	3.35	3.38
5.68	5.80	26.67	27.72	3.40	3.40
6.58	5.80	30.48	30.36	4.05	3.99
8.91	8.62	38.10	38.06	4.55	4.55

Discussion

The organic compounds tested catalyze the Sandell—Kolthoff reaction to different degrees. The catalytic activity is strongly dependent on the second substituent in the benzene molecule. Only radicals that can donate electrons to the ring system seem to provide appreciable catalytic activity (Table 1). Iodobenzene itself and 4-iodobenzoic acid have only a very small effect while 4-nitroiodobenzene shows no measurable activity under the conditions used. Yet it does not seem to be possible to coordinate the catalytic activities of the various compounds with the substituent constant σ for the radicals in the Hammett equation [17, 18]. However, the catalytic—kinetic method may be used to distinguish between isomers of some iodine-containing compounds by utilizing the F coefficient, and it provides a sensitive determination of certain compounds.

The author is greatly indebted to Professor Dr. Herbert Weisz for his encouragement and helpful discussions.

REFERENCES

1 E. B. Sandell and I. M. Kolthoff, J. Am. Chem. Soc., 56 (1934) 1426.
2 W. Heerspink and G. J. Op de Weegh, Clin. Chim. Acta, 39 (1972) 327.
3 J. C. Arcq and A. Arcq, Clin. Chim. Acta, 48 (1973) 287.
4 H. P. de Vries, Z. Klin. Chem. Klin. Biochem., 13 (1975) 97.
5 H. V. Malmstadt and T. P. Hadjiioannou, Anal. Chem., 35 (1963) 2157.
6 P. J. Ke, R. J. Thibert, R. J. Walton and D. K. Soules, Mikrochim. Acta, (1973) 569.
7 E. Mutschler, Arzneimittelwirkungen, Wissenschaftl. Verlagsgesellschaft, Stuttgart, 1970.
8 S. Pantel and H. Weisz, Anal. Chim. Acta, 89 (1977) 47.

9 H. Lepper, Diploma Thesis, Freiburg, W. Germany, 1978.
10 S. Pantel, Anal. Chim. Acta, 104 (1979) 205.
11 S. Ghosal and S. K. Dutta, Indian J. Chem., 6 (1968) 301.
12 R. Hand, M. Melicharek, D. J. Scoggin, R. Stotz, A. K. Carpenter and R. F. Nelson, Collect. Czech. Chem. Commun., 36 (1971) 842.
13 H. Weisz, D. Klockow and H. Ludwig, Talanta, 16 (1969) 921.
14 D. Klockow, H. Ludwig and M. A. Giraudo, Anal. Chem., 42 (1970) 1682.
15 H. Weisz, K. Rothmaier and H. Ludwig, Anal. Chim. Acta, 73 (1974) 224.
16 S. Pantel and H. Weisz, Anal. Chim. Acta, 70 (1974) 391.
17 L. P. Hammett, J. Am. Chem. Soc., 59 (1937) 96.
18 H. H. Jaffé, Chem. Rev., 53 (1953) 191.

Analytica Chimica Acta, 141 (1982) 359—364
Elsevier Scientific Publishing Company, Amsterdam — Printed in The Netherlands

Short Communication

PULSE POLAROGRAPHIC STUDY OF THE ELECTROCHEMICAL REDUCTION OF LUCIGENIN IN AQUEOUS MEDIUM

R. J. MURPHY and G. SVEHLA*

Department of Analytical Chemistry, The Queen's University of Belfast, Belfast BT9 5AG, Northern Ireland (Gt. Britain)

(Received 6th April 1982)

Summary. The electrochemical reduction of lucigenin (bis-*N*-methylacridinium nitrate) in aqueous solution was studied by normal pulse polarography, normal pulse polarography with differential detection of the current, and differential pulse polarography with cathodic and anodic pulses at several pulse amplitudes. The effects of pH and lucigenin concentration were studied. In confirmation of an earlier d.c. polarographic study, lucigenin is shown to be reduced in two separate one-electron steps. An adsorption peak accompanies the first step, while the second, below pH 3.5, is catalytic owing to chemical regeneration of the intermediate reduction product at the electrode surface.

In a previous publication [1] the electrochemical reduction of lucigenin in aqueous solution was studied by d.c. Tast polarography at a dropping mercury electrode, by cyclic voltammetry at an amalgamated gold pin electrode and at a hanging mercury drop electrode, and by microcoulometry. The effects of pH, lucigenin concentration and temperature were studied and special methods were applied to study the suspected adsorption and catalytic (regeneration) currents. A spectrophotometric study was also reported. It was found that lucigenin is reduced in two separate one-electron steps. An adsorption prewave accompanies the first step while the second, below pH 3.5, is catalytic, owing to the chemical regeneration of the intermediate reduction product at the electrode surface. Voltammetric studies by other workers [2, 3] had suggested a two-electron irreversible reduction to dimethylbiacridone.

It was decided to follow the d.c. work with a pulse polarographic study; and in particular to examine the catalytic character of the second reduction step observed below pH 3.5, using the greater resolution and sensitivity offered by the pulse technique. Pulse polarography was developed originally by Barker and Gardiner [4] and its sensitivity and resolution as well as its use in the study of reduction processes [5—7] are well known.

Experimental

Reagents. A commercial preparation of lucigenin (bis-*N*-methylacridinium nitrate; > 97% pure, Aldrich Chemical) was used; aqueous 2×10^{-3} mol l^{-1} solutions were prepared daily and the appropriate dilutions were made for

0003-2670/82/0000-0000/$02.75

each experiment, incorporating the required concentration of supporting electrolyte. All supporting electrolytes, buffer solutions and maximum suppressors were prepared from analytical-grade reagents. Oxygen-free nitrogen was used for deaeration.

Apparatus. A Tacussel PRG5 pulse polarograph equipped with a Tacussel CPRA DME cell and coupled to a Hewlett-Packard HP 7035B x—y recorder was used to record all the polarograms. The polarograms were recorded at a scan rate of 4 mV s^{-1} with the low-pass filter in the "Max" position and minimum damping. Polarograms were recorded using the four pulse polarographic modes available on the instrument: differential pulse polarography (d.p.p.) with cathodic and anodic superimposed pulses, normal pulse polarography (n.p.p.) and normal pulse polarography with differential detection of the current (d.n.p.p.). For differential pulse polarography with cathodic and anodic superimposed pulses, the pulse amplitudes (ΔE) were 1, 2, 5, 10, 20, 50 and 100 mV. The capillary used throughout the study had the following characteristics: outflow velocity m = 0.612 mg s^{-1}; drop lifetime t = 1.0 s; height of mercury column h = 60 cm. A saturated calomel electrode was used as the reference electrode with a platinum pin auxiliary electrode. A Philips PW 9414 pH meter with a combined glass/reference electrode was used for pH measurements.

Procedure. An appropriate volume of lucigenin solution (2×10^{-3} mol l^{-1}) was mixed with the supporting electrolyte and four drops of 0.4% Triton X-100 solution, and diluted to 50 ml with distilled water; 20-ml aliquots of the solutions were deaerated with a stream of nitrogen for 10 min. The pH of the solutions was measured before and after the polarograms were recorded.

Results

The d.p.p. behaviour of lucigenin was investigated within the widest possible pH and concentration ranges for each peak. Two well-defined peaks and a double peak were obtained. Peak I formed at E_p = —0.190 V, and at lucigenin concentrations above 10^{-4} mol l^{-1} a second peak appeared at E_p = —0.380 V (Fig. 1). This peak was enumerated peak II as only under certain conditions of concentration and pulse amplitude did the peak separate into two measurable individual peaks. Peak III formed at E_p = —1.530 V. These potentials were obtained with a 50-mV cathodic pulse. A typical polarogram obtained with 50-mV cathodic and anodic pulses is shown in Fig. 2.

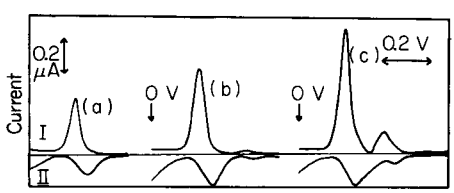

Fig. 1. D.p.p. current—potential curves of (a) 5×10^{-5}, (b) 10^{-4}, (c) 1.6×10^{-4} mol l^{-1} lucigenin in 0.1 mol l^{-1} KCl/0.05 mol l^{-1} boric acid; pH 5.0, ΔE = 50 mV. (I) Cathodic pulse; (II) anodic pulse.

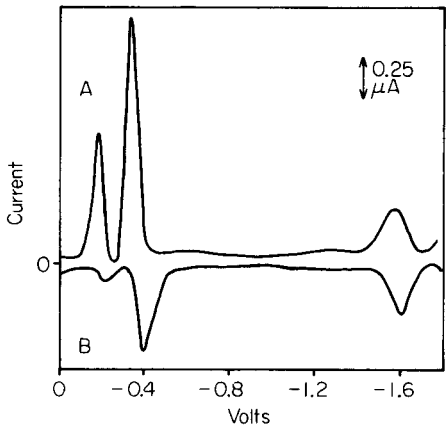

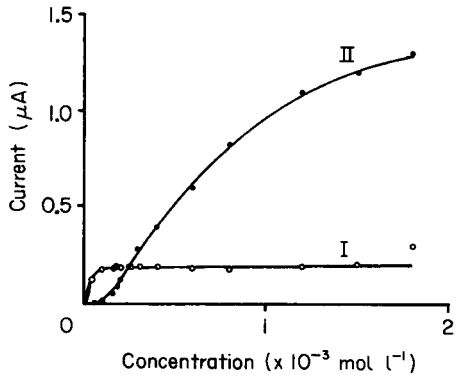

Fig. 2. D.p.p. current—potential curves of 8×10^{-4} mol l^{-1} lucigenin in 0.1 mol l^{-1} KCl/ 0.05 mol l^{-1} boric acid; pH 5.0; ΔE = 50 mV. (A) Cathodic pulse; (B) anodic pulse.

Fig. 3. D.p.p. current—concentration plots for peaks I and II of lucigenin.

Polarograms were obtained at different lucigenin concentrations and the peak heights were plotted against concentration. The measurements for wave I gave a typical adsorption plot (Fig. 3). The current measurements for peak II were for the combined peak. Up to a concentration of 10^{-3} mol l^{-1} peak II increases virtually linearly with concentration (Fig. 3). Its intercept with the concentration axis coincides with that concentration at which peak I becomes fully developed. The current—concentration plot for peak III is curved. The effect of concentration on the peak potentials was also studied. The peak potential of peak I moves gradually from —0.190 V to less negative potentials with increasing lucigenin concentration, reaching —0.17 V at 1.8×10^{-3} mol l^{-1}. The peak potential of peak II shifts from —0.38 V at 10^{-4} mol l^{-1} to —0.33 V at 3×10^{-4} mol l^{-1} and then remains constant at higher concentrations. Peak III moves to more negative potentials with increasing concentration reaching —1.60 V at 1.5×10^{-3} mol l^{-1}. As before, these potentials were obtained with a 50-mV cathodic pulse.

The effect of pH on the peak potentials of the three peaks was investigated in detail, as this can provide valuable information on the acid—base equilibria in which the oxidised and reduced species are involved. The peak potentials of peaks I and II were unchanged throughout the pH range. The peak potential of peak III shifted to more negative potentials below pH 3.5 (Fig. 4A). The effect of pH on the height of the three peaks was also examined; peaks I and II were unaffected by change in pH. The height of peak III was independent of pH in the range pH 3.5—11.0. Between pH 3.5 and 3.0 there was a slight decrease in peak height but below pH 3.0 the peak height started to increase rapidly reaching about 3 times the original height at pH 2.0 with a 100-mV cathodic pulse. The rate of increase of peak height was greater at

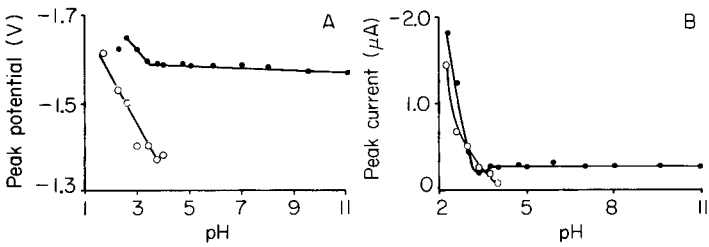

Fig. 4. Effect of pH on (A) the peak potential and (B) the peak current of (•) lucigenin, (○) supporting electrolyte for 8×10^{-4} mol l^{-1} lucigenin in 0.1 mol l^{-1} KCl/0.05 mol l^{-1} boric acid/HCl; 20-mV cathodic pulse.

smaller pulse amplitudes (Fig. 4B). However, below pH 3.0 the decomposition of the supporting electrolyte affected the resolution of the lucigenin peak. When the d.n.p.p. mode was used, the individual peaks could be measured down to pH 1.7. The reason for the difficulty in resolving the two peaks below pH 2.0 can be seen from Fig. 4A. The peak caused by decomposition of the supporting electrolyte moves rapidly to more negative potentials with decreasing pH until eventually the peaks merge. The peak from the supporting electrolyte forms at −1.40 V in the presence of lucigenin whereas a blank run shows a peak potential of −1.60 V.

The values of the peak potentials for the cathodic and anodic pulses should fit the equation $E_p = E_{1/2} - \Delta E/2$ for a reversible electrode process, and the value calculated for $E_{1/2}$ should be the same for all cathodic and

TABLE 1

Polarographic data obtained by d.p.p. for 4×10^{-4} mol l^{-1} lucigenin at pH 5.0

ΔE (mV)	E_{pc} (V)	Calc. $E_{1/2}$ (V)	i_{pc} (μA)	$W_{1/2}$ (mV)	E_{pa} (V)	Calc. $E_{1/2}$ (V)	i_{pa} (μA)	$W_{1/2}$ (mV)	$E_{pc} - E_{pa}$ (mV)	i_{pc}/i_{pa}
Peak I										
10	−0.200	−0.205	0.133	35	−0.210	−0.215	0.095	55	10	1.395
20	−0.195	−0.205	0.345	40	−0.207	−0.197	0.140	62	12	2.464
50	−0.179	−0.204	1.130	42	−0.208	−0.183	0.190	85	29	5.947
100	−0.134	−0.184	1.440	60	−0.205	−0.155	0.230	120	71	6.261
Peak II										
10	−0.360	−0.365	0.185	58	−0.374	−0.369	0.130	65	14	1.423
20	−0.354	−0.364	0.445	60	−0.375	−0.365	0.225	70	21	1.978
50	−0.334	−0.359	1.190	68	−0.390	−0.365	0.400	90	56	2.975
100	−0.306	−0.356	1.400	108	−0.410	−0.360	0.470	120	104	2.979
Peak III										
10	−1.562	−1.567	0.050	90	−1.558	−1.553	0.050	100	4	1.000
20	−1.555	−1.565	0.110	105	−1.570	−1.560	0.095	94	15	1.158
50	−1.547	−1.572	0.240	105	−1.585	−1.560	0.245	100	38	0.980
100	−1.530	−1.580	0.380	124	−1.610	−1.560	0.42	115	80	0.927

anodic pulse amplitudes. Calculated values of $E_{1/2}$ at different cathodic and anodic pulse amplitudes are shown in Table 1. Peak I shows the greatest variation between $E_{1/2}$ values for cathodic and anodic pulses and this variation increases with pulse magnitude. The calculated $E_{1/2}$ values for peaks II and III are consistent, indicating a reversible process. The reversibility of peak II indicated by the $E_{1/2}$ values is not supported by the ratio of the cathodic peak current (i_{pc}) to the anodic peak current (i_{pa}) shown in Table 1. The current ratios for peak III are close to unity, suggesting a reversible process. For a reversible process, $(E_{pc} - E_{pa})$ should equal ΔE. From Table 1 it can be seen that $(E_{pc} - E_{pa})$ is almost equal to ΔE for peak II whereas the results for peak III are too low for a reversible process. A differential pulse peak at small amplitude has a half-width, $W_{1/2}$, of $3.52\,RT/nF$, which gives a value of $(90.4/n)$ mV for a reversible process. For larger values of $-\Delta E$, $W_{1/2} \rightarrow \Delta E$. The $W_{1/2}$ values obtained are included in Table 1.

Discussion

Previous work [1] involving cyclic voltammetry, d.c. polarography and microcoulometry had shown that wave II underwent a one-electron irreversible reduction and wave I was an adsorption prewave to wave II. Above pH 3.5, wave III was shown to be a reversible diffusion wave corresponding to a one-electron reduction. The d.p.p. results confirm these findings although peak II would appear to have some reversible character from the $E_{1/2}$ (calc.) and $(E_{pc} - E_{pa})$ results. The d.p.p. results also confirm the catalytic character of peak III below pH 3.5. When d.c. polarography was used, separate measurements of the lucigenin wave III and the wave from the decomposition of the supporting electrolyte became increasingly difficult as the pH approached 2.0 but accurate measurements were possible with d.p.p. With the d.n.p.p. mode, it was possible to measure the two peaks down to pH 1.7.

Above pH 3.5 the d.p.p. results are consistent with the reduction mechanism already described from the d.c. polarographic results:

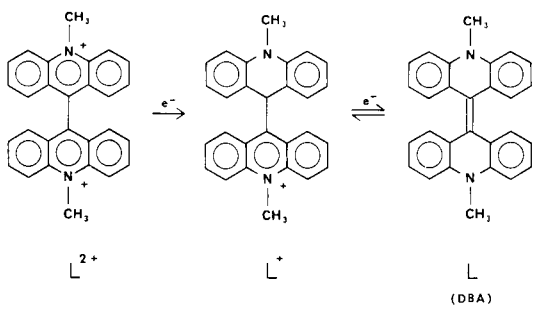

First the lucigenin cation L^{2+} takes up a single electron to form an intermediate monocation L^{+}, and then the uptake of a second electron produces dimethylbiacridone, L; the second reaction is reversible. These d.p.p. results support the view that the increase in current of peak III at low pH values is most probably due to a catalytic regeneration peak. The reduction product

dimethylbiacridone is capable of taking up a proton in an equilibrium reaction, $L + H^+ \rightleftharpoons LH^+$, followed by regeneration of L^+ and the evolution of hydrogen, $LH^+ \rightarrow L^+ + \frac{1}{2}H_2$. Thus, further molecules of L^+, not supplied by diffusion, become available for reduction at the electrode surface, allowing an increased current to flow. A study of the electrochemical oxidation of lucigenin is under way.

R. J. M. acknowledges financial assistance from the Department of Agriculture for Northern Ireland.

REFERENCES

1 R. J. Murphy and G. Svehla, Anal. Chim. Acta, 125 (1981) 73.
2 K. D. Legg, D. W. Shive and D. M. Hercules, Anal. Chem., 41 (1969) 1560.
3 S. Wada, K. Maeda and K. Nakada, Nippon Kagaku Kaishi, 5 (1977) 639.
4 G. C. Barker and A. W. Gardiner, AERE Harwell C/R 2297, 1958; Fresenius Z. Anal. Chem., 173 (1960) 79.
5 E. P. Parry and R. A. Osteryoung, Anal. Chem., 37 (1965) 1634.
6 J. M. Christie, J. Osteryoung and R. A. Osteryoung, Anal. Chem., 45 (1973) 210.
7 O. Vittori and M. Porthault, Analusis, 4 (1976) 152.

Analytica Chimica Acta, 141 (1982) 365—369
Elsevier Scientific Publishing Company, Amsterdam — Printed in The Netherlands

Short Communication

VOLTAMMETRIC DETERMINATION OF MORPHINE IN POPPY STRAW CONCENTRATE AT A GLASSY CARBON ELECTRODE

R. S. SCHWARTZ* and C. R. BENJAMIN
Technical Services Division, U.S. Customs Service, Washington, DC 20229 (U.S.A.)
(Received 1st March 1982)

Summary. Morphine is determined by oxidation at a glassy carbon electrode in methanolic carbonate buffer. Samples are taken up in dilute hydrochloric acid, and aliquots are transferred to the supporting electrolyte for differential pulse voltammetry. Precision averaged 1—2% and linear calibration graphs were obtained over the range 10—40 ppm. Results compared favorably with those obtained by other methods.

Opium alkaloid drugs, those narcotic alkaloids derived from the opium poppy (*Papaver somniferum*), have important legal uses, especially in medicine and medical research. The most abundant and the most economically important opium alkaloid is morphine. Because of legal restrictions on both the domestic growing of opium poppy and the importation of finished alkaloid drugs, the domestic requirements for these drugs are met by licensed domestic production from imported raw materials derived from the opium poppy, namely opium and poppy straw concentrate. Opium is the dried gum obtained by slitting the immature seed pod of the opium poppy, collecting the juice, and allowing it to dry. It contains about 10% anhydrous morphine. Poppy straw concentrate is a light brown to dark brown powder obtained by extracting the whole, dried poppy plant, filtering extraneous vegetable matter, and removing the solvent. It contains 50% or more anhydrous morphine.

The Customs Service is interested in these materials because they are imported. While opium has been imported for many years, it is only since 1975 that poppy straw concentrate has been allowed to enter the U.S. While at one time the tariff on opium was based on its morphine content, presently both raw materials are permitted in this country free of duty. However, the determination of the morphine content is still important both for statistical and law enforcement purposes.

Morphine has been determined by gas chromatography using a derivatization step [1—3], by radioimmunoassay [4], by high-performance liquid chromatography [5], and recently, by liquid chromatography with electrochemical detection (l.c.e.c.) [6—7]. The l.c.e.c. approach is based on the ease with which morphine can be oxidized. Many of these methods are highly sensitive and selective, and are generally considered to be rapid. Nevertheless,

as has been pointed out by Chan and Fogg [8], at higher concentrations a voltammetric method can be simpler and less time-consuming, and may be the method of choice if sufficient selectivity can be achieved.

The voltammetric determination of morphine and other opium alkaloids at graphite, platinum, and glassy carbon electrodes has been investigated [9, 10]. It was shown that alkaline supporting electrolytes are most suitable. However, detailed results on actual samples giving linearity, reproducibility, and comparison of results with those obtained by other established methods were not presented. In this communication, a voltammetric method is presented for the determination of morphine in poppy straw concentrate which is rapid, accurate, sensitive, and involves minimal sample preparation. The method is based on anodic differential pulse voltammetry in alkaline supporting electrolyte at a glassy carbon electrode. Results are compared with those obtained by established methods.

Differential pulse voltammetry in the anodic mode was chosen because of its low detection limits and easily interpreted peak responses. Fairly low concentrations of analyte could be employed which reduced the amount of electrode fouling encountered. Use of a methanolic supporting electrolyte further reduced electrode fouling. It was also found that peak heights were more reproducible using a constructed baseline rather than by subtracting a blank. This was done automatically by the instrumentation employed in this study when operated in the "tangent fit" mode. As has been pointed out by Coetzee et al. [11], cathodic pretreatment of the glassy carbon electrode considerably improved reproducibility, probably because of the removal of an adsorbed surface film. Phosphate, borate, and carbonate buffers over the pH range 9—11 were investigated as supporting electrolytes and 0.1 M pH 10 carbonate buffer was found to be most suitable. When this supporting electrolyte was used, a reproducibility of 0.4% r.s.d. was attained for repeated scans on a standard 20 ppm morphine solution. Linearity was excellent over the range 0—40 ppm anhydrous morphine; correlation coefficients (r^2) of better than 0.999 were routinely obtained.

Experimental

Reagents. The supporting electrolyte was composed of analytical-reagent grade chemicals and water obtained from a Millipore system consisting of a reverse osmosis unit in series with a Milli-Q polishing unit which produced water of 18 Mohm purity. An aqueous 0.1 M, pH 10 carbonate buffer was prepared by dissolving 8.4 g of sodium hydrogencarbonate in 900 ml of water, adjusting to pH 10 with 50% (w/v) sodium hydroxide solution, followed by dilution to 1 l with water. The supporting electrolyte consisted of a mixture of methanol and this carbonate buffer (4 + 1). The solvent used for both samples and standards was 0.01 M HCl. Morphine hydrochloride (Merck) was used as a working standard; purity was checked by using freshly opened U.S.P. reference standard morphine sulfate.

Stock solutions of samples and standards having anhydrous morphine concentrations in the 1000 ppm range were prepared by dissolving between

60 and 80 mg of either sample or standard in 0.01 M HCl followed by dilution to 50 ml with 0.01 M HCl. Poppy straw concentrate sample solutions were sonicated for several minutes to insure complete dissolution of the morphine.

Instrumentation. An EG&G Princeton Applied Research Model 384/4 polarographic analyzer system was used. This incorporated the following units: the Model 303 SMDE electrode assembly with built-in Ag/AgCl reference electrode element and Pt wire counter electrode; Model G159 reference electrode jacket with Vycor tip for electrical contact filled with saturated KCl/AgCl; Model G173 glassy carbon working electrode consisting of a glassy carbon disc of 7 mm^2 surface area epoxy-sealed in a 9-cm length of 5-mm o.d. glass tubing; and a Model G57 cell bottom of borosilicate glass having a working volume of 3—15 ml.

Electrode pre-treatment. Treatment of the glassy carbon electrode was important in obtaining reproducible results. The electrode was polished prior to each series of measurements using an aqueous suspension of 0.5-μm alumina on a felt pad. Prior to each measurement, the electrode was conditioned as follows. While the solution was stirred, magnetically controlled by the M384 system (M305 magnetic stirrer), the electrode was cycled 5—6 times between +0.5 and —1.0 V at 100 mV s^{-1}; the potential was then held at —1.0 V for 60 s in order to effect a "cathodic cleansing" [11]; the initial potential of 0 V was then applied for 20 s; the stirring was then stopped while the initial potential of 0 V was maintained for an additional 15 s. At this point the electrode was ready for measurements.

Procedure. Differential pulse voltammetry was employed with a pulse height of 50 mV a pulse repetition time of 1 s, and a scan rate of 10 mV s^{-1}. Deaeration was found to be unnecessary.

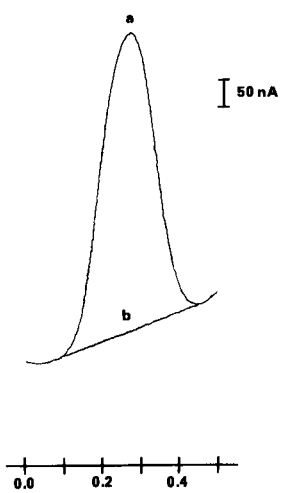

Fig. 1. Typical voltammogram showing constructed baseline: (a) 10 ppm anhydrous morphine; (b) baseline constructed using tangent-fit mode.

TABLE 1

Experimental precision

Sample[a]	D1	F1	P	Y	F2
Replicates	4	6	3	4	3
R.s.d. (%)	1.9	1.4	1.4	1.9	1.3
				Average r.s.d. =	1.6%

[a]D = Dutch, F = French, P = Polish, Y = Yugoslavian.

For measurements, 10 ml of supporting electrolyte was transferred by pipet into a clean, dry cell; a spike containing a small measured volume of stock solution of sample or standard (100 μl for sample and 100—400 μl for standard) was then added; the electrode was then conditioned and a scan was recorded from 0.00 V to +0.50 V (vs. Ag/AgCl). Peak heights were automatically determined by the M384 system using the tangent-fit mode. Concentrations were determined by comparison with a calibration graph. Figure 1 shows a typical voltammogram with the constructed baseline which was automatically determined by the M384 system in the tangent-fit mode.

Results and discussion

In order to test the proposed method, samples of poppy straw concentrate previously analyzed by gas and liquid [12] chromatographic methods developed in the Customs Service, were tested. The g.c. method was a modification of the procedure of Furmanec [13]. The first five samples were subjected to replicate determinations to establish experimental precision. Results are listed in Table 1.

In Table 2 are listed the results for the proposed method and comparative results obtained by the gas and liquid chromatographic methods. It is seen that the proposed method gives results which are similar to those obtained by either of the other two methods. In addition, the proposed method is rapid, requiring less than 5 min to run a sample and involves no sample preparation other than dissolution and transfer of an aliquot to the supporting electrolyte. In contrast, the g.c. method involves extraction and derivatization steps with attendant increase in working time and possibility for sample loss. The l.c. method, while having the advantages of requiring minimal sample preparation and of profiling all the major alkaloids in a single run, is, however, slower than the proposed method, requiring about 25 min per sample.

As has been pointed out [9, 10], it is the phenolic portion of the morphine molecule which is responsible for its electroactivity. Other major opium alkaloids such as codeine, thebaine, papaverine and narcotine are phenol ethers rather than phenols and so are not electrochemically active at low potentials as is morphine. Thus, the other major opium alkaloids do not interfere in the voltammetric determination of morphine which eliminates any need for prior separation, greatly simplifying sample preparation.

TABLE 2

Determination of morphine in poppy straw concentrate samples by the voltammetric and chromatographic methods

Sample	Anhydrous morphine found (%)			Sample	Anhydrous morphine found (%)		
	D.p.v.	L.c. [12]	G.c. [13]		D.p.v.	L.c. [12]	G.c. [13]
Dutch 1	72.9	74.6	79.7	Dutch 2	70.8	71.0	71.4
French 1	66.9	63.4	65.9	French 3	60.9	59.2	60.5
Polish	65.5	65.1	69.1	Dutch 3a	73.4	70.7	70.8
Yugoslavian	77.6	78.1	80.8	Dutch 3b	79.0	76.6	76.7
French 2	60.5	58.0	60.5	Dutch 3c	75.0	74.4	74.5

The authors wish to acknowledge the assistance of the Chicago U.S. Customs Laboratory in providing the poppy straw samples and the g.c. data used. This paper was presented at the Federation of Analytical Chemistry and Spectroscopy Societies, Philadelphia, PA, September 1981.

REFERENCES

1 J. E. Wallace, H. E. Hamilton, K. Blum and C. Petty, Anal. Chem., 46 (1974) 2107.
2 S. H. Weinstein, M. Alteras and J. Gaylord, J. Pharm. Sci., 67 (1978) 547.
3 G. E. Martin and J. S. Swinehart, Anal. Chem., 38 (1966) 1789.
4 S. Spector and C. W. Parker, Science, 168 (1970) 1347.
5 K. Aramaki, T. Hanai and H. F. Walton, Anal. Chem., 52 (1980) 1963.
6 R. G. Peterson, B. H. Rumack, J. B. Sullivan, Jr. and A. Makowski, J. Chromatogr., 188 (1980) 420.
7 J. E. Wallace, S. C. Harris and M. W. Peek, Anal. Chem., 52 (1980) 1328.
8 H. K. Chan and A. G. Fogg, Anal. Chim. Acta, 105 (1979) 423.
9 B. Proska and L. Molnar, Anal. Chim. Acta, 97 (1978) 149.
10 P. Surmann, Arch. Pharm. (Weinheim), 312 (1979) 734.
11 J. F. Coetzee, G. H. Kazi and J. C. Spurgeon, Anal. Chem., 48 (1976) 2170.
12 B. C. Pettitt and C. E. Damon, J. Chromatogr., 242 (1982) 189.
13 D. Furmanec, J. Chromatogr., 89 (1974) 76.

Analytica Chimica Acta, 141 (1982) 371—376
Elsevier Scientific Publishing Company, Amsterdam — Printed in The Netherlands

Short Communication

ELECTROCHEMICAL OXIDATION AND DETERMINATION OF HIGH-MOLECULAR-WEIGHT STERICALLY HINDERED PHENOLS

C. McCRORY-JOY* and J. M. ROSAMILIA

Analytical Chemistry Research Department, Bell Telephone Laboratories, Murray Hill, NJ 07974 (U.S.A.)

(Received 9th December 1981)

Summary. The use of differential pulse voltammetry for the determination of Irganox 1010, a sterically hindered phenol used as an antioxidant, prompted an investigation of the electrochemical behavior of several other commercially available high-molecular-weight hindered phenols used as antioxidants and stabilizers. Although these compounds generally have at least two phenol groups per molecule, their electrochemical behavior is similar to that of simpler hindered phenols such as 2,4,6-tri-*t*-butylphenol. Detection limits ranging from 1.3 to 8.2 ppm were obtained in a methanol—0.07 M sulfuric acid medium. The oxidation of alkylphenols in neutral or acidic media is accompanied by follow-up chemical reactions, leading to formation of passivating films on the surface of the glassy carbon electrode. In alkaline media, the corresponding phenoxide is oxidized electrochemically to the corresponding stable phenoxy radical and filming can be avoided.

The mechanism of electrochemical oxidation of simple phenols has received considerable attention in recent years [1—3], and several reports concerning electroanalytical applications of the results are available [4—8]. Sterically hindered phenols substituted at the 2, 4, and 6-positions with bulky groups are used as antioxidants in materials such as low-density polyethylene and polyfunctional methacrylate monomers. The use of differential pulse voltammetry (d.p.v.) at a glassy carbon electrode (GCE) for the determination of Irganox 1010 [9, 10] or tetrakis[methylene-3-(3′,5′-di-*t*-butyl-4′-hydroxyphenyl) propionate] methane has led to further electrochemical investigation of certain commercially available high-molecular-weight hindered phenols, using cyclic voltammetry at a GCE and controlled-potential coulometry (c.p.c.) as well as d.p.v., in methanol and acetonitrile solutions. Comparisons have been made to simpler substituted phenols such as 2,4,6-tri-*t*-butylphenol and di-*t*-butyl-4-methylphenol (BHT). The study was intended to establish the usefulness of d.p.v. for quantifying these substances. Cyclic voltammetry and c.p.c. were used in attempts to determine the nature of the electrochemical oxidation processes involved.

Experimental

Apparatus. Differential pulse voltammograms were obtained by using a Princeton Applied Research (PAR) 174A polarographic analyzer and a

0003-2670/82/0000-0000/$02.75

Hewlett-Packard 7046A X-Y recorder. A glassy carbon working electrode (0.35 cm^2), and a saturated calomel reference electrode were used. All d.p.v. scans were recorded at a scan rate of 10 mV s^{-1} and a modulation amplitude of 5 mV. A PAR 173 potentiostat/galvanostat with a PAR 176 current-to-voltage converter module was used in conjunction with a PAR 175 universal programmer for cyclic voltammetry studies. Controlled-potential coulometry experiments were performed in attempts to determine n, the number of electrons transferred in a given electrochemical oxidation, using electrodes made of Union Carbide WCA graphite cloth [1, 2] and a PAR 179 digital coulometer module. Contact to the graphite cloth was made with a platinum wire. Sample sizes ranging from 1.1 to 2.3 mg were used. Counter electrodes made of platinum wire were used for all experiments.

Reagents. Electronic-grade methanol (J. T. Baker) and acetonitrile (Omnisolv; Matheson, Coleman, and Bell) were used. Sulfuric acid was obtained from J. T. Baker Chemical Company. Other materials were tetrabutylammonium perchlorate (TBAP) suitable for polarographic use (Eastman Chemical Company), a 20% (w/w) solution of tetramethylammonium hydroxide (TMAH) in methanol, di-*t*-butyl-4-methylphenol and 2, 4, 6-tri-*t*-butylphenol (all Aldrich Chemical Company). The Irganox compounds were obtained from the Ciba-Geigy Corporation; a minimum assay of 98% by ultraviolet spectroscopy was specified for all the compounds. The assay for Irganox 1010 was 99%. Solutions were purged with prepurified nitrogen to remove any oxygen present.

Procedure. The dependence of peak current on phenol concentration was investigated for each compound in methanol containing 0.07 M H_2SO_4 and in some cases in methanol containing 0.1 M TBAP. The calibration plots obtained were based upon the observation of a single well-defined oxidation peak in every case. Detection limits (d.l.) were calculated using the relationship $d.l. = st/k$ where s is the standard deviation in μA for the current residuals from the least squares straight line, t is the appropriate constant at the 95% confidence level for $n - 2$ degrees of freedom where n is the number of data points and k is the slope in μA/ppm of the least-squares straight line [11]. Nine data points over the range 0—400 ppm were used in the calculations except for I-1035, I-1098 and I-1024 for which the points were taken over the range 0—800 ppm.

The effect of adding sulfuric acid to solutions of the phenols in methanol—0.07 M sulfuric acid and methanol—0.1 M TBAP was investigated by cyclic voltammetry in order to ascertain that the undissociated phenol is the only form present in the methanol—0.07 M sulfuric acid medium. Methanol containing 0.1 M TMAH was used to investigate the electrochemical behavior of the corresponding phenoxide ions. Investigations in acetonitrile containing 0.1 M TBAP or 0.1 M TMAH were made for purposes of comparison. For experiments involving TMAH, the phenol solution was purged with nitrogen prior to the addition of base because the resulting phenoxide species are sensitive to air oxidation, just as observed for simpler hindered phenols [1, 2].

Samples of a polyfunctional methacrylate monomer containing I-1010, hydroquinone, and methylhydroquinone were examined in the methanol—0.07 M sulfuric acid medium. The detection of 1-1010 in this monomer in a methanol—0.10 M TMAH medium was attempted while considering the possibility of measurements in basic media, which has been reported for the liquid chromatographic–electrochemical determination of BHT in lubricating oils at a glassy carbon electrode [12].

Results and discussion

Calibration plots for Irganox compounds were linear over the range 0—400 ppm in the methanol—0.07 M sulfuric acid medium and in some cases a larger range of linearity was observed. All the compounds were stable in this medium and all yielded a well-defined oxidation peak. Solutions were used within a few hours of preparation. No evidence of decomposition was observed during this time period, but if the solutions were allowed to stand overnight d.p.v. results showed that the peak currents were substantially lower and additional peaks were observed. In some cases the solution turned dark on standing. The peak potentials, regression parameters, and detection limits are summarized in Table 1. Increasing the sulfuric acid concentration of methanol or addition of sulfuric acid to methanol—0.1 M TBAP solutions of phenols produced no change in the electrochemical behavior of the phenols. The electrochemical oxidation of these compounds is accompanied by the formation of passivating films on the surface of the electrode. These films may be removed by wiping the surface with a cloth wetted with methanol. Film formation of this type is commonly observed for simpler phenols [1—3] and is attributed to the products of follow-up reactions of the radicals produced by oxidation. No advantage is gained by using an acetonitrile—sulfuric acid medium as solvent. Cyclic voltammetry and d.p.v. showed that the oxidation of a given phenol is accompanied by film formation in this medium as well.

TABLE 1

Peak potentials, n-values, detection limits and regression parameters for hindered phenol calibration data in methanol—0.07 M H_2SO_4

E_p[a] Compound	(V vs. SCE)	n/OH groups[b]	Detection limit (ppm)	Slope ± s.d. (μA/ppm)	Intercept ± s.d. (μA)	Standard error (μA)
I-1076	+0.86	1.6	6.7	0.04 ± 0.00	1.84 ± 0.03	0.12
I-1098	+0.79	1.6	11.1	0.07 ± 0.00	1.10 ± 0.03	0.34
I-259	+0.90	1.3	8.2	0.07 ± 0.00	0.44 ± 0.00	0.26
I-1035	+0.89	1.7	9.3	0.08 ± 0.00	1.43 ± 0.01	0.31
I-1024	+0.90	3.3	3.4	0.26 ± 0.00	1.35 ± 0.01	0.38
I-1010	+0.98	1.9	6.8	0.08 ± 0.00	0.48 ± 0.00	0.24
I-1093	+0.88	1.7	6.6	0.12 ± 0.01	0.56 ± 0.01	0.32

[a]Obtained by d.p.v. [b]Ratio of n to number of OH groups, obtained by c.p.c.

Film formation makes the use of d.p.v. more time-consuming because the electrode must be cleaned between scans, and would cause a serious problem in the use of the GCE as an on-line detector. Because previous work [1, 2] showed that certain hindered phenols do not exhibit film formation in basic media and that the GCE was suitable as a detector for BHT [11], solutions of Irganox compounds containing TMAH were studied.

The results obtained for the analysis of liquid monomer samples in methanol—0.07 M H_2SO_4 showed that the glassy carbon electrode is useful in this medium for the determination of high-molecular-weight hindered phenols. Samples having designated concentrations of 4000 ppm and 1500 ppm I-1010 were found to contain 3864 ppm with a relative standard deviation (r.s.d.) of 1.3% and 1424 ppm with a r.s.d. of 1.8%. Previous determinations of I-1010 in aged monomer formulations using acidic media have always yielded results lower than the nominal concentration, owing to decomposition of the phenolic additives.

Tentative calibration plots prepared for the Irganox compounds in methanol—0.10 M TMAH showed that the detection limits for the high-molecular-weight phenols are considerably higher in this medium, with values ranging from 28 to 50 ppm for the compounds studied. Initial attempts to analyze liquid monomer samples containing Irganox 1010 did not produce results which compared favorably in reproducibility with those obtained in the methanol—0.07 M H_2SO_4 medium. The corresponding results in the methanol—0.10 M TMAH medium were 3983 ppm with 4.6% r.s.d. and 1549 ppm with 9.2% r.s.d.

Cyclic voltammetric investigations in basic media indicated electrochemical behavior similar to that observed for simpler hindered phenols [1, 2]. The addition of TMAH to solutions of the phenols in either methanol—0.1 M TBAP or acetonitrile—0.1 M $NaClO_4$ produced a new peak at a considerably less positive potential than that of the undissociated phenol oxidation shown in Fig. 1 for Irganox 1010, as recorded in Table 2. The new peak is due to the oxidation of phenoxide ion present in the basic solution and corresponds to the d.p.v. peak used to prepare the calibration plots. Potential cycling reveals that electrode filming is avoided in basic media if the switching potential is made less positive than that of the phenol oxidation peak.

Previous investigators proposed [1, 2] on the basis of three successive oxidation peaks observed in basic media for 2,4,6-tri-*t*-butylphenol and 2,6-di-*t*-butyl-4-isopropylphenol, that the oxidation of phenoxide ion is followed by further oxidation of the phenoxy radical resulting in the formation of the corresponding cyclohexadienone, and finally that protons produced by the second reaction reacted with phenoxide ion to produce phenol for which a third oxidation peak was recorded. At high concentrations of TMAH in the case of high-molecular-weight hindered phenols, two peaks were observed in every case. The variation of the phenoxide ion and phenol peak currents as a function of the concentration of TMAH indicated that at the highest practical concentrations of TMAH, all the phenol originally

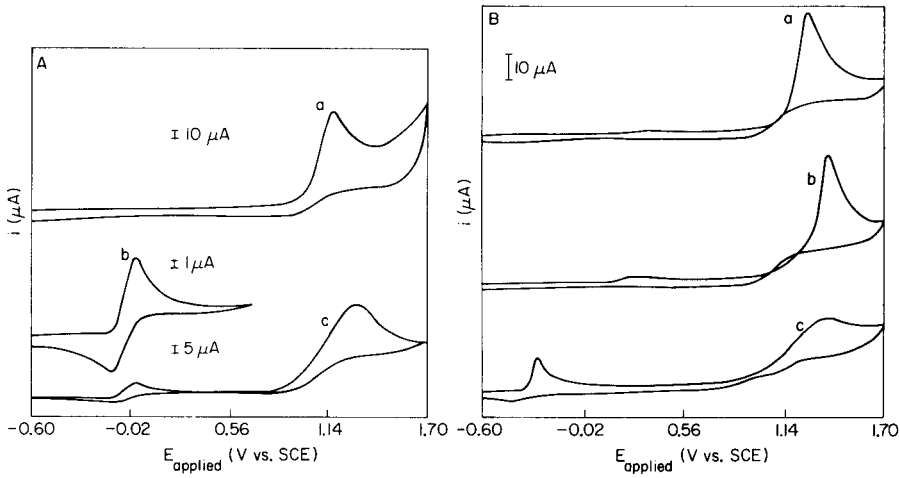

Fig. 1. Effect of addition of TMAH to solutions containing Irganox 1010. (A) 1000 ppm Irganox 1010 in methanol—0.1 M TBAP: (a) no TMAH added; (b) 0.05 M TMAH; (c) 0.10 M TMAH. (B) 2000 ppm Irganox 1010 in acetonitrile—0.1 M TBAP: (a) no TMAH added; (b) 0.01 M TMAH; (c) 0.05 M TMAH.

TABLE 2

Oxidation peak potentials for the phenoxide form of several hindered phenols in methanol and acetonitrile solutions from cyclic voltammetry

Compound	Methanol—0.10 M TBAP, 0.10 M TMAH	Acetonitrile—0.10 M $NaClO_4$, 0.1 M TMAH
I-1098	−0.03	−0.23
I-259	+0.01	−0.24
I-1035	−0.01	−0.26
2,4,6-Tri-*t*-butylphenol	+0.01	−0.19

present is not converted to the phenoxide form. The electrochemical oxidation of the high-molecular-weight hindered phenols studied does not necessarily proceed in exactly the same manner as that for simpler phenols under these conditions.

The use of the basic medium described for d.p.v. or amperometric detection in a flowing stream would be useful except for the lack of complete conversion to the phenoxide form at the highest attainable TMAH concentration. Detection limits would be lower even under conditions exhibiting better reproducibility because the d.p.v. peak current due to a one-electron transfer is measured.

Controlled-potential coulometry experiments (Table 1) in acidic media do not necessarily reflect the electrode reactions observed in the cyclic voltammetric experiment for several possible reasons, the most important

being inaccuracies introduced by filming of the carbon cloth electrode, follow-up chemical reactions occurring during the course of the experiment, and differences in the time scale of the experiments [13]. All the n values obtained are low compared to the value which would be obtained, for example, for a two-electron oxidation for each phenolic group, except for a higher value obtained for I-1024.

The comparative cyclic voltammetric behavior of Irganox compounds and simpler hindered phenols in acidic and basic media suggests that similar electrochemical reaction mechanisms are involved. The phenols are oxidized in acidic solution to produce phenoxonium ions followed by reaction with traces of water or other nucleophiles present to produce the corresponding cyclohexadienone [1—3]. In basic solution the reversible oxidation of phenoxide ions to the corresponding phenoxy radicals demonstrates that the high-molecular-weight hindered phenoxy radicals are stable, and as expected, the extent of any coupling reactions is limited.

In addition to the mechanistic and analytical information derived from this investigation, the oxidation potentials give some indication of the relative ease of oxidation of the members of the Irganox series. Previous studies have reported attempts to correlate oxidation potentials with the effectiveness of phenols as antioxidants [14—16].

REFERENCES

1 J. A. Richards, P. E. Whitson and D. H. Evans, J. Electroanal. Chem., 63 (1975) 311.
2 J. A. Richards and D. H. Evans, J. Electroanal. Chem., 81 (1977) 171.
3 A. Ronlan, in A. J. Bard and H. Lund (Ed.), Encyclopedia of Electrochemistry of the Elements, Dekker, New York, 1978, Vol. XI, Ch. 2.
4 J. C. Suatoni, Anal. Chem., 38 (1966) 1271.
5 J. Furukawa, S. Yamashita and T. Katani, Adv. Chem. Ser., 85 (1968) 110.
6 H. E. McBride and D. H. Evans, Anal. Chem., 45 (1973) 446.
7 S. C. Rifkin and D. H. Evans, Anal. Chem., 48 (1976) 2174.
8 L. Foley and L. M. Kimmerle, Anal. Chem., 51 (1979) 818.
9 Princeton Applied Research Corporation Application Brief A-S "Antioxidants", 1976.
10 C. McCrory-Joy and J. M. Rosamilia, presented in part at the Pittsburgh Conference, Atlantic City, NJ, March 1981.
11 R. K. Skogerboe and C. L. Grant, Spectrosc. Lett., 3 (1970) 215.
12 L. Foley and F. M. Kimmerle, Anal. Chem., 51 (1979) 818.
13 A. J. Bard and K. S. V. Santhanam, in A. J. Bard (Ed.), Electroanalytical Chemistry, Dekker, New York, 1970, Vol. 4, pp. 225—252.
14 J. L. Ballard and P. ten Have, Discuss. Faraday Soc., 2 (1947) 252.
15 G. E. Panketh, J. Appl. Chem. (London), 7 (1957) 512.
16 K. U. Ingold, Chem. Rev., 61 (1961) 563.

Analytica Chimica Acta, 141 (1982) 377—382
Elsevier Scientific Publishing Company, Amsterdam — Printed in The Netherlands

Short Communication

COATED-WIRE ORGANIC ION-SELECTIVE ELECTRODES IN TITRATIONS BASED ON ION-PAIR FORMATION
Part 3. Determination of Cationic Triarylmethane Dyestuffs[a]

K. VYTŘAS* and M. DAJKOVÁ[b]

Department of Analytical Chemistry, College of Chemical Technology, 532 10 Pardubice (Czechoslovakia)

(Received 2nd November 1981)

Summary. Aqueous solutions of seven cationic triarylmethane dyestuffs can be titrated with sodium tetraphenylborate using as indicator electrode an aluminium wire coated with a PVC membrane plasticized with 2-nitrophenyl 2-ethylhexyl ether or tricresylphosphate. Titrations are possible in unbuffered and buffered media within the pH range 4—10. Characteristic titration data are given for determinations of malachite green B, setoglaucin 0, brilliant green, fuchsine, methyl violet, crystal violet, and Victoria blue B.

The cationic triarylmethane dyestuffs can be precipitated from aqueous solutions with an anionic reagent such as sodium tetraphenylborate. Although such ion-pairs are often employed as electroactive components in liquid membranes of various ion-selective electrodes (especially for anions such as nitrate, perchlorate, alkylsulphates and arenesulfonates), few papers have dealt with the determination of these dyes by potentiometric titration. Simple titrations based on ion-pair formation with visual end-points are difficult or impossible because the dye solutions are usually deeply coloured.

The titration of crystal violet with sodium tetraphenylborate can be followed [2] by using a liquid-state electrode with a natural rubber membrane saturated with solutions of crystal violet- 12-tungosilicate or tetraphenylborate in 1,2-dichlorobenzene. This titration can also be followed with the commercial Crytur 19-15 potassium ion-selective electrode based on a PVC membrane containing valinomycin and dipentylphthalate [3], with the Orion tetrafluoroborate or cyanide electrode [4], or even with simple coated-wire electrodes [5]. Acidic dyestuffs can be titrated with crystal violet solutions [6]. A picrate-selective, liquid-membrane electrode based on crystal violet picrate in nitrobenzene is suitable for following two-phase titrations of crystal violet and other basic dyes with picric or 3,5-dinitrosalicylic acid [7, 8].

[a]For Part 2, see [1].
[b]Present address: Regional Agricultural Laboratory, Agrochemical Corporation, 738 01 Frýdek-Místek, Czechoslovakia.

It has been shown [1, 5, 9] that, for potentiometric titration purposes, the electrodes can be covered with blank membranes containing only a plastic matrix and a plasticizer. In such titrations, as is well known, the potential change at the end-point must be well defined, but the slope of the electrode response need be neither reproducible nor Nernstian and the actual potential at the end-point is of secondary interest. In the present communication, results are reported for a wide selection of the triarylmethane dyestuffs (Table 1), to assess further the possibilities of such electrodes.

Experimental

Solutions. Sodium tetraphenylborate stock solution (2.5%) was prepared, stored and standardized as described previously [1, 9]. Titrant solutions were prepared by suitable dilution.

Stock solutions of the triarylmethane dyestuffs (Table 1) were prepared from commercial specimens at the approximate concentrations given in parentheses: crystal violet (0.02 M), fuchsine (0.01 M), malachite green B (0.02 M), methyl violet (0.02 M), brilliant green (0.02 M) [all from Lachema,

TABLE 1

List of titrated dyestuffs

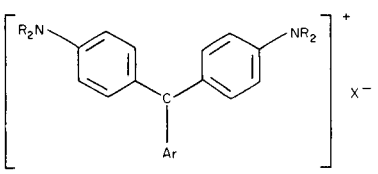

Common name	Colour Index No. and C.I. Name [10]	Substituents [10] R	Ar	X^-	Molecular mass [10]
Malachite green B	42000 Basic Green 4	CH_3	phenyl	$ZnCl_3^-$	1403.35[b]
Setoglaucin 0	42025 Basic Blue 1	CH_3	2-chlorophenyl	Cl^-	399.37
Brilliant green	42040 Basic Green 1	C_2H_5	phenyl	$ZnCl_3^-$	593.34[c]
Fuchsine	42510 Basic Violet 14	H	3-methyl-4-aminophenyl	Cl^-	409.92[d]
Methyl violet[a]	42535 Basic Violet 1	CH_3	4-(*N*-methyl)-aminophenyl	Cl^-	393.96
Crystal violet	42555 Basic Violet 3	CH_3	4-(*N*,*N*-dimethyl)-aminophenyl	Cl^-	407.99
Victoria blue B	44045 Basic Blue 26	CH_3	4-(*N*-phenyl)-amino-1-naphthyl	Cl^-	506.09

[a]A mixture of the hydrochlorides of the more highly methylated pararosanilines, mainly the *N*-tetra-, penta-, and hexamethyl derivatives. The manufacturer's data are for the pentamethyl derivative. [b]For $3C_{23}H_{25}ClN_2 + 2ZnCl_2 + 2H_2O$, similarly for [c]dihydrate and [d]tetrahydrate.

Czechoslovakia], Victoria blue B (0.01 M), and setoglaucin 0 (0.02 M) [both from Geigy, Switzerland].

Equipment. A universal pH meter OP-204/1 (Radelkis, Budapest) was used. The potential changes were monitored by an appropriate ion-selective electrode and a double-junction saturated calomel reference electrode (0.01 M $NaNO_3$ salt bridge). Coated-wire ion-selective electrodes were prepared by using an aluminium conductor [5, 9] from tetrahydrofuran solutions of PVC and plasticizer (diamylphthalate, dioctylphthalate, didecylphthalate, dioctylsebacate, tricresylphosphate, or 2-nitrophenyl 2-ethylhexyl ether). A poly(vinylbutyral) (PVB) membrane plasticized with 2-nitrophenyl 2-ethylhexyl ether was also tested. Ion-exchangers were not added; the electrodes were pre-conditioned by the appropriate ion-pair titration.

Procedure. Titrations were made at room temperature. About 50 ml of the solution was titrated in a 100-ml beaker; the titrant was added from a 10-ml automatic burette and stirring was done magnetically. If necessary, the pH value of the solution titrated was adjusted by addition of Britton-Robinson buffer and checked with glass and saturated calomel electrodes. When strongly acidic media were needed, hydrochloric acid was added.

Results and discussion

Titrations of unbuffered solutions. As was shown for titrations of organic cations with tetraphenylborate [3], the shape of the titration curve is governed primarily by the solubility product of the precipitate formed. With increasing mass of the cation, the solubility of the corresponding tetraphenylborate usually decreases, thus both the steepness and the overall potential break increase. As the triarylmethane dyestuffs tested are ionic compounds of high molecular mass and almost symmetrical charge distribution, most of the dyes were titrated without difficulties. In titrations of crystal violet, methyl violet, fuchsine, and setoglaucin 0, the equilibrium potential of the pre-conditioned electrodes was established very quickly after each addition of titrant (this contrasts with the titrations when the Crytur 19—15 electrode was used, which took up to 45 min [3]). Figure 1 shows that the electrode membranes plasticized with 2-nitrophenyl 2-ethylhexyl ether or tricresylphosphate gave the most useful titration curves. These electrodes (working code numbers 878C and 878M) were therefore preferred in further studies.

Titrations of malachite green B and Victoria blue B were somewhat slower but the titration curves could be reproducibly recorded after small delays in the vicinity of the end-point. Such delays are usually observed when cationic impurities are present in the sample, but no other coloured species were observed when the purity of these samples was tested chromatographically. In contrast, methyl violet, which is a mixture of methylated pararosaniline derivatives, gave a clean potential break without delays, all the species being titrated together. In titrations of brilliant green, the electrode potential was established slowly, which made the titrations longer and the curves less reproducible. The titration curves of these dyestuffs are shown in Fig. 2.

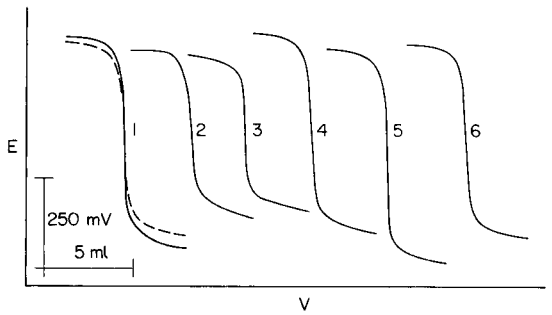

Fig. 1. Influence of plasticizer on the shape of titration curves of crystal violet (ca. 5 × 10^{-3} M, 50 ml) with sodium tetraphenylborate (ca. 7 × 10^{-2} M) for coated-wire electrodes plasticized with (1) 2-nitrophenyl 2-ethylhexyl ether; (2) diamylphthalate; (3) dioctylphthalate; (4) didecylphthalate; (5) tricresylphosphate; and (6) dioctylsebacate. Full lines are for PVC membranes, and the dashed line for a PVB membrane.

Titrations in buffered media. All the dyes were also tested in titrations over the pH range 3—10. The presence of the buffers did not significantly influence the shape of the particular titration curve. The potentials were usually established more slowly, but the curves were reproducible and the end-point readings remained the same.

Another situation can occur if the medium is such that the dye can be involved in protolytic equilibria. For example, crystal violet can form yellowish green or orange cations with different positive charges [11]. This protonation also influenced the shapes of the titration curves of crystal violet in such media; for 5 × 10^{-3} M crystal violet, the potential jump was sharp in 0.01 M HCl, but showed two inflections in 0.1 M and 1 M HCl; the latter curve was particularly diffuse.

Influence of dilution. The possibilities of determining triarylmethane dyestuffs in more dilute solutions were tested for crystal violet. Stock solutions of the dye and tetraphenylborate were diluted 10-, 100-, and 1000-fold compared to their initial concentrations, and the titration curves were

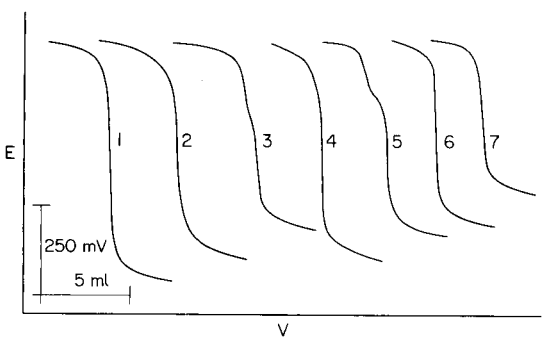

Fig. 2. Titration curves of ca. 5 × 10^{-3} M solutions of (1) crystal violet; (2) methyl violet; (3) malachite green B; (4) brilliant green; (5) Victoria blue B; (6) setoglaucin 0; and (7) fuchsine with ca. 6 × 10^{-2} M sodium tetraphenylborate using an 878C electrode.

TABLE 2

Analytical data for titrations of triarylmethane dyestuffs

Sample	Given (mg)	Assay[a] (%)	Buffer (pH)	Electrode used	Titration curve	
					Overall potential break (mV)	Steepness near end-point (mV/0.1 ml)
Crystal violet	122.4	86.6 ± 1.2	—	878C	600—700	90—120
	111.0	87.2 ± 1.3	—			
	111.0	86.6 ± 1.9	4.0		540—560	75—80
	111.0	86.5 ± 1.9	5.5		510—530	75—80
	111.0	85.4 ± 1.3	7.2		420—460	70—80
Fuchsine	83.6	87.0 ± 2.1	—	878C	430—460	80—100
	56.3	87.4 ± 1.3	—	878M	420—460	90—100
	56.3	86.3 ± 0.9	5.6		420—440	90—100
	44.9	86.9 ± 1.5	—		420—460	80—100
	44.9	89.6 ± 2.3	9.5		420—460	90—100
Malachite green B	150.3	75.1 ± 3.8	—	878C	500—520	50—80
Methyl violet	118.2	85.2 ± 1.0	—	878C	560—620	75—90
Setoglaucin 0	119.8	27.4 ± 2.2	—	878C	550—560	80—90
Brilliant green	167.1	33.6 ± 7.8	—	878C	330—340	80—100
Victoria blue B	151.8	46.1 ± 1.3	—	878C	540—560	60—80

[a]Mean of 3—4 titrations with relative standard deviation.

recorded. The dilution caused both the steepness and the overall potential jump of the titration curves to decrease, of course, but the potential jumps were surprisingly well pronounced for titrations of 10 mg and 1 mg of crystal violet and were usable even for 0.1 mg. Unfortunately, the end-points did not remain constant, being shifted to higher values by the dilution. Yet the titration curves were well reproducible so that the problem can be solved by standardization against a verified dye sample at about the same concentration.

Precision and accuracy. Finding standard samples is probably the most difficult problem because commercial specimens of triarylmethane dyestuffs usually contain many impurities. As a sufficiently reliable and independent reference method, e.g. photometry, is always influenced by the choice of standard substance, it is practically impossible to assess the accuracy of the proposed titrations. As indicated by the assay values given in Table 2, not a dyestuff tested was of 100% purity. The only comparable values available are for crystal violet: assays of other commercial samples of it have given results of 89.3% [3] and 87.6% [4]. Selig [4] also showed, by elemental analysis, that the precipitate formed with crystal violet has a 1:1 stoichiometric ratio of cation to anion; this is expected also for other samples. This kind of ion-pair was observed also in other studies of triphenylmethane dyes [12]. Despite these problems, the titrations of triarylmethane dyestuffs with tetra-

phenylborate are reproducible as far as relative deviations are concerned, and can be recommended for analytical production control.

REFERENCES

1 K. Vytřas, M. Dajková and V. Mach, Anal. Chim. Acta, 127 (1981) 165.
2 A. G. Fogg and K. S. Yoo, in E. Pungor and I. Buzás (Eds.), Ion Selective Electrodes (Conf., Budapest, September 1977), Elsevier, Amsterdam (and Akadémiai Kiadó, Budapest), 1978, p. 369.
3 K. Vytřas, Collect. Czech. Chem. Commun., 42 (1977) 3168.
4 W. Selig, Mikrochim. Acta, (1980/II) 133.
5 K. Vytřas, M. Dajková and M. Remeš, Cesk. Farm., 30 (1981) 61.
6 A. G. Fogg, A. A. Al-Sibaai and K. S. Yoo, Anal. Lett., 10 (1977) 173.
7 I. A. Gurev and T. S. Vyatchanina, Zh. Anal. Khim., 34 (1979) 976.
8 A. A. Kalugin and I. A. Gurev, Zh. Anal. Khim., 35 (1980) 2424.
9 K. Vytřas, M. Remeš and H. Kubešová-Svobodová, Anal. Chim. Acta, 124 (1981) 91.
10 Colour Index, Vol. 4, 3rd edn., The Society of Dyers and Colourists, Bradford, 1971.
11 E. Bányai, in E. Bishop (Ed.), Indicators, Pergamon, Oxford, 1972.
12 S. Motomizu, S. Fujiwara and K. Tôei, Anal. Chim. Acta, 128 (1981) 185.

Analytica Chimica Acta, 141 (1982) 383—386
Elsevier Scientific Publishing Company, Amsterdam — Printed in The Netherlands

Short Communication

A COMPUTER-BASED PROGRAMMABLE WAVEFORM GENERATOR

J. MOZOTA*

Departamento de Química, Universidad Simón Bolívar, Apartado 80659, Caracas 1080 (Venezuela)

B. E. CONWAY and D. F. TESSIER

Chemistry Department, University of Ottawa, Ottawa (Canada)

(Received 25th January 1982)

Summary. The programmable waveform generator, which is capable of producing complex voltage—time programs, is based on a PDP-11/34 minicomputer with associated DIGITAL hardware. The desired waveform is obtained by clock-controlled output of a symmetrical triangular voltage sweep. The software can be readily adapted to any computer system. Ramp sections of 1 mV s^{-1}—50 V s^{-1} and potential pulses of 50 μs—500 s can be obtained.

One of the problems in electrochemical research is an occasional need for complex electronic instrumentation which is not available commercially. In a study of surface processes by cyclic voltammetry, it has been shown [1, 2] that elaborate voltage—time programs are sometimes needed to elucidate the behaviour of certain systems, in particular the role of adsorbed ions in the electrochemistry of metals [2]. Although some programmable function generators are commercially available, their cost is high and their performance is not always ideal. Analog instruments have limitations on the complexity of the waveform that they can generate, whereas digital instruments suffer from poor voltage resolution.

As minicomputers have become increasingly used in research laboratories for a multitude of tasks [3, 4], a computer-based programmable waveform generator such as is described below, should be useful, if only for those occasions when a complex waveform is needed. A somewhat similar generator, but constructed with hard-wire logic, has been described by Sherwood et al. [5].

Experimental

A PDP-11/34 minicomputer with 32K words of RAM, two RX-01 floppy-disk units and a RL-01 hard-disk was utilized, together with the following interfaces: a KW11-K programmable clock and an AA11-K, 12-bit, D/A converter. Programs were written in FORTRAN IV and MACRO-11 (DIGITAL's assembly language). The FORTRAN section handled the input

0003-2670/82/0000-0000/$02.75

of the parameters needed to specify the desired waveform, and the MACRO-11 routine was responsible for controlling the output of the waveform. The MACRO subroutine JFG1M.MAC is shown in Fig. 1. There are five arrays (NP, NS, NC, MS and I) built in the FORTRAN section of the program (listings are available on request); NP contains the number of programs per sweep; NS contains the clock codes for every program; NC contains the counter values for the buffer of the clock; MS contains the number of points per program; and I contains the symmetrical triangular waveform.

The approach used is based on building a symmetrical triangular waveform between the required potential limits, in voltage steps of height determined by the resolution of the D/A converter (here, this was 2.5 mV), i.e., a staircase type of waveform. This triangular waveform could be offset by an external supply to locate the waveform at the required d.c. level, because the waveform was built in the positive direction for programming convenience.

Through software, the user indicates at which points in the waveform a change of program is required (NP), whether the new program is to be a voltage ramp or a constant potential section, and the time parameters for either of the latter regimes (NS, NC), i.e., sweep rate for the voltage ramp or duration of the constant potential. The program then calculates the clock status (NS) and buffer register codes (NC) for the KW11-K, and how many points correspond to each program (MS). The waveform is then available on a real-time basis at one channel of the D/A converter, being output point-by-point at the time intervals required to reproduce the desired sweep. The D/A converter had a rise and settling time to 0.1% of the final value of 4 μs.

The resulting voltage–time programs were recorded on a Tektronix-5115 storage oscilloscope or on a Nicolet-Explorer II digital oscilloscope with X—Y output capability.

```
.MAIN.  MACRO V03.02B 01:05:14 PAGE 1

     1          170404                          CLSTAT=170404           ;DEF OF STATUS AND BUFFER ADDRESSES
     2          170406                          CLKBUF=170406           ;FOR KW11-K AND AA11-K INTERFACES
     3          170430                          CLKCOU=170430
     4          170416                          DISTAT=170416
     5          170426                          DA3OUT=170426
     6 000000   005067  170416          GEN::   CLR DISTAT              ;CLEAR DISPLAY STATUS
     7 000004   016704  000000'         MLOOP:  MOV NP,R4               ;SET UP COUNTER FOR NUMBER OF
     8                                                                  ;PROGRAMS ON A SWEEP
     9 000010   012700  000002'                 MOV #NS,R0              ;R0 POINTS TO CLOCK CODES
    10 000014   012701  000146'                 MOV #NC,R1              ;R1 POINTS TO CLOCK COUNTERS
    11 000020   012702  000312'                 MOV #MS,R2              ;R2 POINTS TO # OF POINTS/PROGRAM
    12 000024   012703  000456'                 MOV #I,R3               ;R3 POINTS TO VOLTAGE RAMP
    13 000030   012167  170406          XLOOP:  MOV (R1)+,CLKBUF        ;LOAD CLOCK BUFFER
    14 000034   012067  170404                  MOV (R0)+,CLSTAT        ;LOAD CLOCK STATUS WITH APPROPRIATE RATE
    15 000040   012205                          MOV (R2)+,R5            ;SET UP COUNTER FOR # OF POINTS
    16 000042   012367  170426          ALOOP:  MOV (R3)+,DA3OUT        ;LOAD Y CHANNEL(D/A)
    17 000046   042767  000200  170404          BIC #200,CLSTAT         ;CLEAR DONE FLAG IN CLOCK STATUS(PRECAUTION)
    18 000054   105767  170404          BLOOP:  TSTB CLSTAT             ;CHECK IF COUNTING FINISHED
    19 000060   100375                          BPL BLOOP               ;LOOP IF NOT
    20 000062   005305                          DEC R5                  ;DEC COUNTER
    21 000064   001366                          BNE ALOOP               ;LOOP IF NOT DONE
    22 000066   042767  000001  170404          BIC #1,CLSTAT           ;****IMPORTANT****
    23                                                                  ;STOP CLOCK BEFORE CHANGING ITS PARAMETERS
    24 000074   005304                          DEC R4                  ;DEC # OF PROGRAMS COUNTER
    25 000076   002354                          BGE XLOOP               ;LOOP IF NOT DONE
    26 000100   000741                          BR MLOOP                ;LOOP ALWAYS FOR CONTINUOUS DISPLAY
    27 000102   000207                          RTS PC
    28 000000                                   .PSECT DATA,GBL,OVR     ;SECTION FOR PARAMETER PASSING FROM FORTRAN
    29 000000                           NP::    .BLKW 1                 ;NUMBER OF PROGRAMS IN A SWEEP
    30 000002                           NS::    .BLKW 50.               ;CLOCK CODES ARRAY
    31 000146                           NC::    .BLKW 50.               ;CLOCK COUNTERS ARRAY
    32 000312                           MS::    .BLKW 50.               ;NUMBER OF POINTS/PROGRAM ARRAY
    33 000456                           I::     .BLKW 1601.             ;POTENTIAL RAMP ARRAY
    34          000001                          .END
```

Fig. 1. Program listings for the subroutine JFG1M.MAC.

Results and discussion

Examples of generated waveforms. Figures 2 and 3 show some examples of complex voltage—time waveforms generated by means of the program outlined above. Four waveforms are displayed in Fig. 2; waveform (a) is a regular triangular sweep, whereas (b)—(d) show sweeps with up to four changes of sweep rate. Figure 3 illustrates waveforms that include changes of sweep rate and sections of constant potential.

Applications of the generator. The programmable waveform generator was tested in routine work, to compare its performance with that of standard function generators. Under the same conditions, the results obtained were

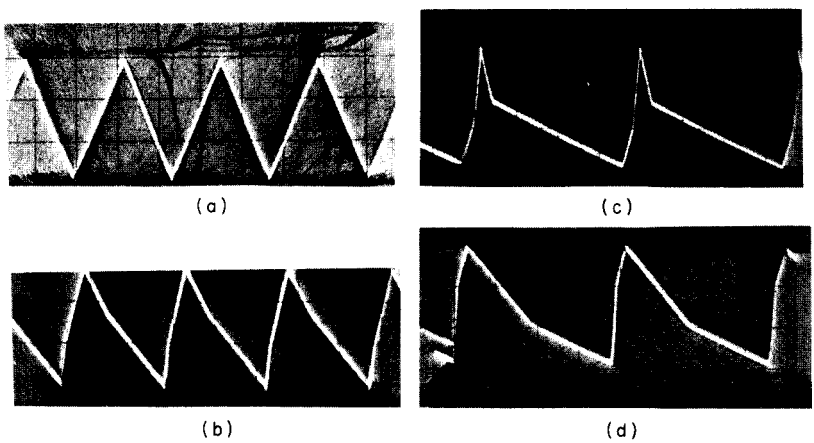

Fig. 2. Set of four different waveforms from the programmable generator, as recorded on a storage oscilloscope.

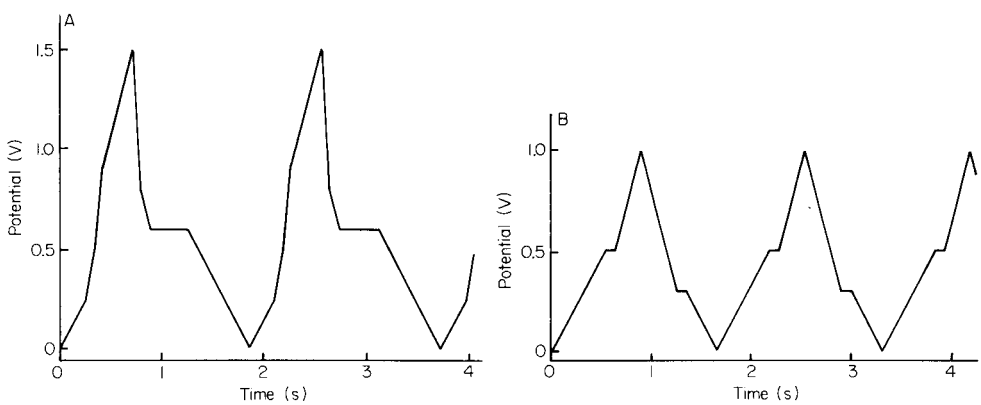

Fig. 3. Complex voltage—time waveforms from the programmable generator. (A and B) Output to an X—Y recorder through a digital oscilloscope.

absolutely identical. With a slight software modification, which altered the height of the potential steps, it was also used in steady-state polarization measurements as described by Mozota and Conway [6].

The main drawback of the computer-based generator is the need to terminate the sweep program in order to change the value of one of its parameters. However, the generator has been applied to the study of ion-adsorption effects, where complex waveforms were used to isolate and identify certain variables of the process [2].

One of us (J. M.) acknowledges the award of a CONICIT (Venezuela) scholarship. Grateful acknowledgement is made to the National Research Council of Canada for funding the PDP-11/34 minicomputer and a post-graduate scholarship to D. F. T.

REFERENCES

1 M. E. Folquer, J. O. Zerbino, N. R. de Tacconi and A. J. Arvía, J. Electrochem. Soc., 126 (1979) 592.
2 B. E. Conway and J. Mozota, J. Chem. Soc., Faraday Trans. 1, in press.
3 S. P. Perone and D. O. Jones, Digital Computers in Scientific Instrumentation. Applications to Chemistry, McGraw-Hill, New York, 1973.
4 K. F. Drake, R. P. van Duyne and A. M. Bond, J. Electroanal Chem., 89 (1978) 231.
5 W. G. Sherwood, D. F. Untereker and S. Bruckenstein, Anal. Chem., 47 (1975) 84.
6 J. Mozota and B. E. Conway, J. Electrochem. Soc., 128 (1981) 2142.

Analytica Chimica Acta, 141 (1982) 387—392
Elsevier Scientific Publishing Company, Amsterdam — Printed in The Netherlands

Short Communication

AMPEROMETRIC TITRATION OF CALCIUM, STRONTIUM AND BARIUM AND THEIR MIXTURES IN PRESENCE OF LARGE AMOUNTS OF ALKALI METAL SALTS

M. WOJCIECHOWSKI, S. RUBEL* and W. FALKOWSKA
Department of Chemistry, University of Warsaw, Warsaw (Poland)
(Received 16 November 1981)

Summary. Trace amounts of alkaline earth metals are titrated with triethylenetetraaminehexaacetic acid; lead(II) is added as indicator and the current is measured by square-wave polarography. At pH 13.3, calcium, strontium and barium give a common end-point corresponding to the total content of alkaline earth ions. Copper and cadmium interfere but small concentrations of Ni, Al, Mg, Zn, Mn(II) and Fe(III) are tolerated. The alkaline earth metals can be determined in the presence of 1000-fold amounts of lithium and 10^5-fold amounts of sodium or potassium ions.

The production and application of different high-purity materials require rapid and accurate procedures for the determination of impurities. Besides calcium, the main impurities in alkali metal salts are strontium and barium. In many cases, it is enough to know the total content of some groups of compounds, and this is generally true for alkaline earth metals in salts. Complexiметric titrations with amperometric end-point detection are simple and appropriate for many trace metals. In the case of alkaline earth metals, the oxidation current of EDTA at a platinum [1] or graphite electrode [2], the oxidation current of the mercury—titrant complex [3—5] and the reduction current of an added ion [6—9] have served to indicate end-points.

Trace amounts of calcium are readily titrated with triethylenetetraaminehexaacetic acid (TTHA) when amperometric detection with lead(II) as indicator ion is used [9]. Such procedures were therefore examined for strontium and barium determinations as well as for the sum of alkaline earth metals. In these titrations, the relationships between the conditional stability constants of the complexes of the ion determined and the indicating ion with the titrant must be suitable. To choose the best titrant and optimal conditions, calculations were done with the stability constants of the Ca(II), Sr(II), Ba(II) and Pb(II) complexes of EDTA, DCTA, DTPA, TTHA, EGTA, EEDTA and HEDTA in the pH range 10—14 [10]. The calculated data for four complexes are shown in Fig. 1. It appears that titration of the total content of calcium, strontium and barium, using lead(II) as indicator ion is possible with TTHA at pH 13.3, DTPA at pH 13.3 and EGTA at pH 12.3.

Experimental

Apparatus. A square-wave polarograph (Model OH104, Radelkis) was used

0003-2670/82/0000-0000/$02.75

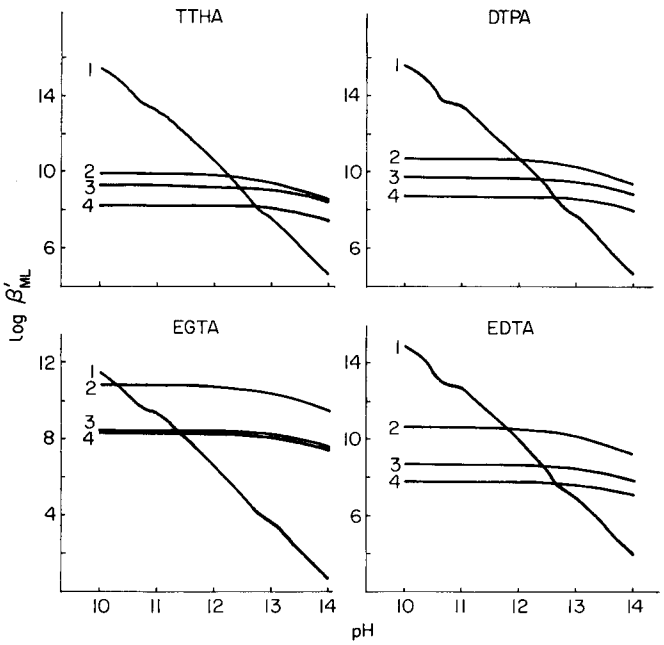

Fig. 1. The dependence on pH of the conditional stability constants of the TTHA, DTPA, EGTA and EDTA complexes with: (1) Pb(II); (2) Ca(II); (3) Sr(II); (4) Ba(II).

with a dropping mercury electrode (DME) which had the following characteristics: m = 3.76 mg Hg s^{-1}, t = 2.7 s in 0.1 mol l^{-1} KCl at 0 V for h = 50 cm. A tungston reference electrode and a platinum auxiliary electrode were used. The titrant was added from 0.250-ml autoburette (Model ABU13, Radiometer) through a polypropylene capillary dipped in the solution in a 20-ml polypropylene beaker.

Reagents. Purified TTHA [9] was used as a 1.0×10^{-2} mol l^{-1} solution, which was standardized by visual titration of zinc(II) solution [11]. Calcium and barium strontium nitrate solutions (1.0×10^{-2} mol l^{-1}) were standardized by conventional EDTA titrations. Working solutions were prepared by appropriate dilutions.

Preparation of hydroxide and chloride solutions of alkali metals free from alkaline earth metals. Alkali metal salts of analytical-grade purity were found to contain, depending on the producer, 10^{-4}—10^{-3}% of alkaline earth metals. To purify the solutions, calcium, strontium and barium were separated on Dowex A1 ion-exchanger [12]. To avoid contamination from glass, tygon tubing (1-cm i.d.) was used to hold the 20-cm resin bed. Before use, the ion-exchanger was converted to the appropriate form (lithium, sodium or potassium), and washed with 400 ml of hydrochloric acid (1 + 1) and 200 ml of triply-distilled water. The alkali metal hydroxide solution (1 mol l^{-1}) was added to the column and, after rejection of the first 150 ml, the eluate was collected in a polyethylene bottle. For the purification of chloride solutions, columns were washed with hydrochloric acid and water as above,

treated with 120 ml of 2 mol l^{-1} LiOH (NaOH or KOH) and washed with 300 ml of water, before the alkali metal salt solution was made alkaline and added. The first 150 ml was rejected and the eluent collected as above. This procedure was used to purify 2-mol l^{-1} solutions of LiCl, NaCl and KCl made 0.01 mol l^{-1} in LiOH, NaOH and KOH, respectively.

Procedure for amperometric titration of the total alkaline earth metal content. The alkali metal salt (4 g) containing 0.5—2.5 × 10^{-3}% of alkaline earth metals was dissolved in a little water in a 50-ml quartz volumetric flask. The solution was diluted to the mark after addition of 10 ml of 1 mol l^{-1} NaOH and 0.5 ml of 1 × 10^{-3} mol l^{-1} lead nitrate. An aliquot (5 ml) was transferred to the amperometric cell and titrated without deaeration by 1 × 10^{-3} mol l^{-1} TTHA solution, 0.020-ml portions being added. After each addition, the solution was stirred magnetically for 1 min, and the square-wave polarographic peak of lead ions (E_p = 0.155 V vs. W electrode) was recorded. After the end-point, indicated by decreased peak height, another four portions of titrant were added. Peak heights were then measured and the end-point was calculated from the titration curve or by the least-squares method. The content of alkaline earth metals was calculated as the calcium equivalent.

Results and discussion

Preliminary tests. Because barium(II) is the most difficult alkaline earth metal to titrate, forming the least stable complexes, the best complexing agent was selected on the basis of barium(II) titrations at the calculated pH values. When a mixture of barium and lead ions was titrated with DTPA in 0.2 mol l^{-1} NaOH at pH 13.3, both metals were titrated simultaneously; there was no end-point for barium, probably because the difference between the conditional stability constants (K') of the BaDTPA and PbDTPA complexes was actually smaller than the calculated differences or because of slow reactions. EGTA could be used at pH 12.3, but TTHA proved to be the best titrant. The effect of pH on the titration curves for barium with TTHA was tested in the range pH 13.18—13.48. Even within this range, the end-point sharpness increased with increase in pH because the difference between K' (BaTTHA) and K' (PbTTHA) increased. As a compromise between different effects, pH 13.3 was selected for further work, in agreement with calculations.

After this choice of medium, titrations of Ca(II), Sr(II) and Ba(II) solutions with TTHA were tested, as well as the possibility of titrating Ca + Sr, Ca + Ba, Sr + Ba, and Ca + Sr + Ba mixtures. The titration curves obtained are shown in Figs. 2 and 3. As can be seen, the end-point is less well defined for barium than for calcium and strontium (Fig. 2); calcium and strontium are titrated together when there is a break in the curve corresponding to barium (Fig. 3). These curves correspond to the fact that the calcium and strontium complexes with TTHA are more stable than the barium complex. For mixtures of calcium, strontium and barium, the second break in the titration plot corresponds to the sum of the metals (Fig. 3).

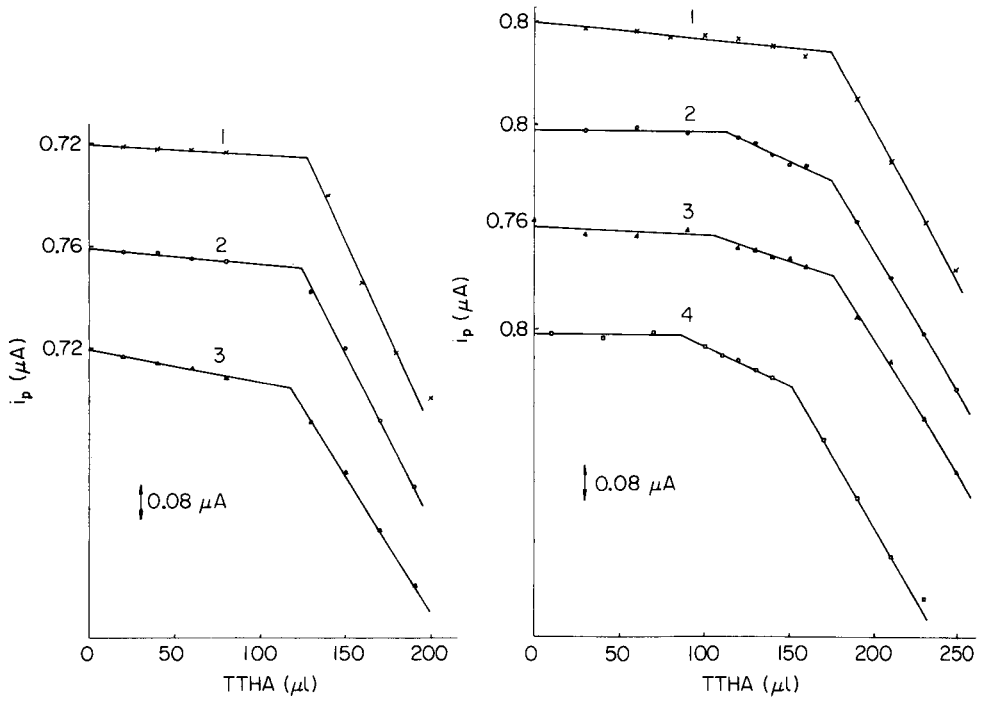

Fig. 2. Titrations in 0.2 mol l^{-1} NaOH solution (pH 13.30) with 10^{-3} mol l^{-1} TTHA: (1) Ca(II); (2) Sr(II); (3) Ba(II). About 200 nmol of each metal was titrated.

Fig. 3. Titrations of mixtures of alkaline earth metals in 0.2 mol l^{-1} NaOH (pH 13.30) with 10^{-3} mol l^{-1} TTHA. (1) Ca(II) + Sr(II) in molar ratio 2:5; (2) Ca(II) + Ba(II) in molar ratio 5:2; (3) Sr(II) + Ba(II) in molar ratio 5:2; (4) Ca(II) + Sr(II) + Ba(II) in molar ratio 1:1:1.

Some titrations of barium done at 20, 30, 40 and 50° C showed that the higher temperatures improved the end-points, indicating a faster complexation reaction; however, positive errors in the barium results suggested some leaching of calcium from the glass capillary at the higher temperatures so that ambient temperatures are recommended.

Titration of model solutions of calcium, strontium and barium salts. The optimal conditions described above were used in titrations of the three metals separately and in mixtures; the concentration of alkaline earth metals was of the order 10^{-5} mol l^{-1}. Titrations of the separate metals (50—175 nmol) gave results within 4% of the true values with relative standard deviations of 1.5—5% (n = 6). Results obtained for mixtures are presented in Table 1; the precision and accuracy of these titrations are very good.

Effect of other metals. Because the aim of this work was to examine alkali metal salts, the effects of large amounts of lithium, sodium and potassium chlorides on the titration curves for calcium, strontium and barium were investigated. With increasing concentrations of lithium ions, the shape of the

TABLE 1

Results of amperometric titration of the mixtures of alkaline earth metals (Conditions: 0.2 mol l^{-1} NaOH, pH 13.3, 10^{-5} mol l^{-1} Pb^{2+}, 10^{-3} mol l^{-1} TTHA)

Metals (molar ratio)	Taken (nmol)	Found[a] (nmol)	Error (%)	R.s.d. (%)
Ca + Sr				
1:1	100.2	99.1	−1.1	2.3
5:2	175.7	178.3	+1.5	1.4
2:5	175.0	173.7	−0.7	0.9
Ca + Ba				
1:1	99.6	98.9	−0.7	2.5
5:2	175.1	172.6	−1.4	1.7
2:5	173.4	171.1	−1.3	2.4
Sr + Ba				
1:1	99.0	100.1	+1.1	1.0
5:2	173.8	174.0	+0.1	1.6
2:5	172.9	171.1	−1.1	2.2
Ca + Sr + Ba				
1:1:1	149.3	149.8	+0.3	1.2

[a]The results given are the mean of 6 titrations (3 titrations of each of two separately prepared solutions).

titration curves for barium became worse (Fig. 4A) causing decreased precision and negative errors. The large amounts of lithium compared to lead and barium ions significantly decreased the conditional stability constants of the TTHA complexes. However, less than 0.01 mol l^{-1} lithium (1000-fold excess) did not interfere, nor did 1 mol l^{-1} sodium or potassium ions (10^5-fold excess). Some examples are given in Fig. 4B.

The influence of other metals which may contaminate alkali metal salts was also tested. The barium titration was unaffected by 10-fold amounts of nickel ions or 100-fold amounts of aluminum, with respect to lead ions, or by Mn(II), Mg, Zn and Fe(III) ions at the same concentration as lead. Copper and cadmium ions at the same concentration as lead made the titration impossible.

Determination of total content of alkaline earth metals in analytical-grade sodium chloride. It was checked initially that the analyzed salt did not contain metal ions that could interfere with the determination. Four samples of the same batch of salt were analyzed by the recommended procedure. Each sample was divided into two lots and 2 or 3 titrations were done on portions of each lot. From these 17 titrations the mean content of alkaline earth metals given as calcium content was found to be 7.2×10^{-4}% (range 7.0—7.5 $\times$ 10^{-4}%; r.s.d. 1.8%). These results indicate that even trace amounts of alka-

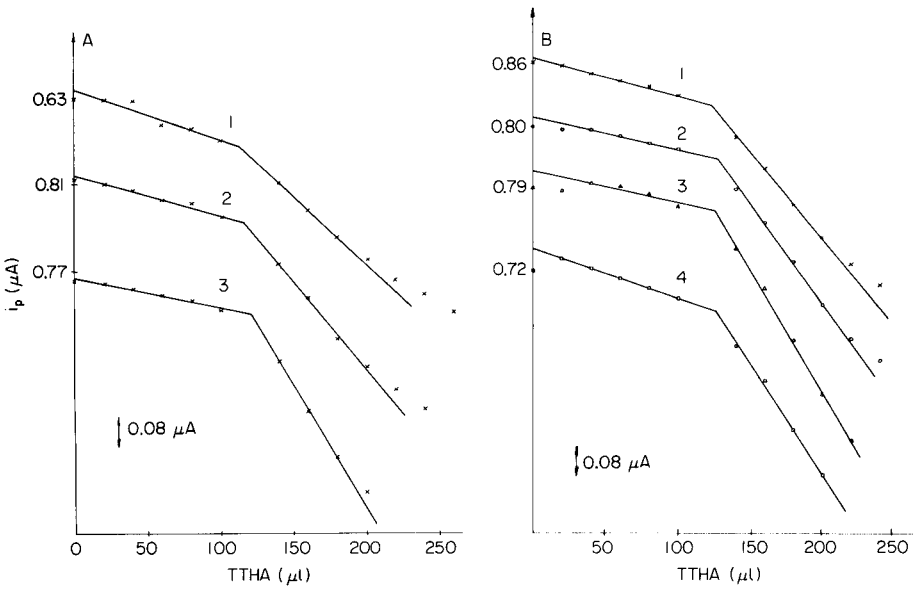

Fig. 4. Titration curves for barium. (A) Effect of lithium with 0.2 mol l^{-1} NaOH (pH 13.3) at lithium concentrations of (1) 0.10 mol l^{-1}, (2) 0.05 mol l^{-1}, (3) 0.01 mol l^{-1}. (B) Effect of sodium with 0.2 mol l^{-1} KOH (pH 13.3) at sodium concentrations of (1) 1.0 mol l^{-1}, (2) 0.5 mol l^{-1}, (3) 0.1 mol l^{-1}; (4) without sodium.

line earth metals can be determined in sodium chloride. As large amounts of potassium do not interfere with the titrations, the same method should be applicable to potassium chloride. Other potassium and sodium salts can be analyzed provided that the anion has no complexing properties towards lead and alkaline earth metals.

REFERENCES

1 S. H. Prased, J. Indian Chem. Soc., 53 (1976) 206.
2 J. Vorlicek and F. Vydra, Collect. Czech. Chem. Commun., 31 (1966) 2510.
3 G. Boef, F. Freese, M. M. P. F. Kramer and H. Poppa, Talanta, 17 (1970) 1006.
4 M. Kodama and M. Murata, Bull. Chem. Soc. Jpn., 41 (1968) 2405.
5 S. Rubel and M. Wojciechowski, Anal. Chim. Acta, 115 (1980) 69.
6 R. Pribil and E. Vicenova, Chem. Listy, 46 (1952) 535.
7 H. A. Laitinen and R. F. Sympson, Anal. Chem., 26 (1954) 556.
8 M. L. Richardson, Talanta, 10 (1963) 103.
9 S. Rubel and M. Wojciechowski, Anal. Chim. Acta, 109 (1979) 67.
10 W. Falkowska, Thesis, Warsaw University, 1980.
11 R. Pribil and V. Vesely, Talanta, 9 (1962) 939.
12 L. O. Rodney, D. Harvey, P. F. Collins and R. B. Ellestad, Talanta, 7 (1961) 187.

Analytica Chimica Acta, 141 (1982) 393—397
Elsevier Scientific Publishing Company, Amsterdam — Printed in The Netherlands

Short Communication

DETERMINATION OF PHOSPHORUS AT THE ng g^{-1} LEVEL IN NIOBIUM BY A RADIOCHEMICAL NEUTRON ACTIVATION METHOD

R. CALETKA*, C. VORWALTER and V. KRIVAN

Sektion Analytik und Höchstreinigung der Universität Ulm, N 26, D-7900 Ulm-Donau (W. Germany)

(Received 26th February 1982)

Summary. Radiochemical neutron activation enables phosphorus to be determined at extremely low levels in niobium. The post-irradiation processing involves decomposition of the sample in hydrofluoric acid with a minimum of nitric acid, separation of most of the radionuclides on coupled anion-exchange (Dowex-1) and cation-exchange (Dowex-50) columns, and the substoichiometric extraction of molybdophosphate with tetraphenylarsomium chloride in dichloroethane. For a 100-mg sample, an irradiation time of 12 h, and a thermal neutron flux of 8×10^{13} n cm^{-2} s^{-1}, the limit of detection is 2 ng g^{-1}.

Although phosphorus can be expected to be a relevant impurity in niobium, there are few references in the literature to its determination and significance, especially in niobium of good and high purity. This situation arises because the determination of phosphorus in niobium is difficult. To solve this analytical problem, use has been made mostly of spectrophotometry after adequate separation. Fedorov [1] separated phosphorus from the niobium matrix by co-precipitation on the collector $(MnO_2)_x(Fe_2O_3)_y(H_2O)_z$ from fluoride solutions in the presence of boric acid, and determined it by spectrophotometry or visual colorimetry as molybdophosphoric acid. The high limit of detection (20 ppm) restricts the applicability of this technique. A similar detection limit was reported by Chernikhov and Dobkina [2] after separation as molybdophosphate. Notkina et al. [3] reported separation of the niobium matrix by extraction from 11 M HCl into amyl acetate while phosphorus and some other impurities remained in the aqueous phase. However, no data were given on the actual procedure and the limit of detection.

Recently, Yang et al. [4] described a technique which can be judged as considerable progress in this field. It is based on the separation of phosphorus as phosphate by adsorption on a thin layer of cadmium carbonate followed by its determination either directly by spectrophotometry as molybdenum blue or indirectly via molybdenum by flameless atomic absorption spectrometry or i.c.p. emission spectrometry. Detection limits at the picogram level can be achieved in principle. However, owing to the high overall occurrence of phosphorus, the limit of detection as well as the accuracy depend mainly on the size of the blank and on how reproducible it is.

Among the different methods applicable to the determination of phosphorus, only activation analysis can be done without introduction of any blank. This advantage makes activation analysis the technique of choice if low contents of phosphorus have to be determined in niobium. The purpose of the present work was therefore to develop an analytical technique based on activation with reactor neutrons. The developed technique allows the blank-free determination of phosphorus at the ppb level and was applied in the analyses of niobium samples of different grades of purity including the highest purity grade presently available.

Experimental

Chemicals and apparatus. All reagents used were of "pro analysi" grade. Dowex-1 X8 and Dowex-50 WX8 (both 100—200 mesh; Fluka) were washed with water to remove fine particles, purified with 3 M $HClO_4$ (Dowex-1) or 3 M HCl (Dowex-50) and finally washed again with water.

Plastic disposable pipettes of 7-mm diameter, closed with the Luer caps, were used for the preparation of ion-exchange columns. The resin beds had heights of 5 and 10 cm for Dowex-50 and Dowex-1, respectively. After packing, the columns were preconditioned with 20 ml of 2 M HF shortly before use. The separations were done at a flow rate of 0.5—0.7 ml min^{-1}.

For the determination of distribution coefficients under batch conditions, 2 ml of aqueous phase was shaken with an equal volume of organic phase (extraction experiments) or with 50 mg of vacuum-dried ion-exchanger (ion-exchange experiments).

A high-resolution γ-ray spectrometer and a GM-counter (for β-rays) were used for the measurement of radioactivity.

Samples and standards. A sample portion of about 100 mg was cut with a diamond saw from each niobium material, etched for about 20 s in a mixture of hydrofluoric and nitric acids (9:1), washed with twice-distilled water and wrapped in an aluminium foil for irradiation. Standards containing 10 μg of phosphorus were prepared by pipetting a corresponding amount of a stock phosphoric acid solution into cleaned high-purity Suprasil ampoules.

Irradiation and chemical procedure. With each sample series, two standards were irradiated together in the Karlsruhe FR-2 reactor at a thermal neutron flux of 8×10^{13} cm^{-2} s^{-1} for 12 h.

After the irradiation, the samples were etched once more and weighed. Then, each was placed in a 10-ml disposable syringe and decomposed with 0.5 ml of concentrated hydrofluoric acid and a minimum of concentrated nitric acid (about 0.3 ml used in small portions) [5]. When dissolution was complete, 100 μg of inactive phosphorus (as phosphate) was added and the solution was diluted with water to about 8 ml. The solution was then applied to coupled columns of Dowex-1 and Dowex-50, and elution was done with 20 ml of 2 M HF. The eluate was measured for its γ-radioactivity (if the determination of other radionuclides was also required) and then evaporated

nearly to dryness under an i.r. lamp. The residue was dissolved in 2 ml of 0.15 M H_2SO_4 and 0.2 ml of 0.2 M ammonium molybdate was added. Finally, phosphorus was extracted substoichiometrically with 1.0 ml of 4×10^{-3} M tetraphenylarsonium chloride in 1,2-dichlorethane [6] in a plastic syringe for 3 min. Aliquots of the organic phases were measured for their β-activity.

After irradiation, the quartz ampoules containing the phosphorus standards were etched and opened. The contents were redissolved in 0.15 M H_2SO_4 and diluted with water to 10 ml. Aliquots (1 ml) of this solution were treated in exactly the same way as samples.

Results and discussion

In activation with neutrons, only ^{32}P can be used as the indicator radionuclide being a pure β-emitter ($t_{1/2}$ = 14.3 days). For this reason, ^{32}P has to be separated in a radiochemically pure form before the β-activity is counted, as simultaneously counting the activity of other radionuclides leads to systematic errors. For a selective separation of phosphorus, it is sensible to remove first the niobium matrix and the highly active radionuclides. Several methods have been suggested for the separation of niobium from other elements. Extraction with tri-*n*-butylphosphate [7, 8] is unsuitable for the present purpose because a high concentration of sulphuric acid is required. Extraction with amyl acetate from hydrofluoric acid [3] was unattractive. In previous work [5], extraction with diantipyrylmethane in dichloroethane from 15 ± 5 M HF was used to remove niobium. Phosphorus (as phosphate) was not extracted with 0.2 diantipyrylmethane in dichloroethane in the 3—30 M range of hydrofluoric acid concentrations; the estimated distribution ratio for phosphorus was less than 10^{-3} over the whole acid concentration interval. Consequently, this technique could form the first stage of a separation procedure.

From the practical point of view, however, the most suitable method for the quantitative separation of niobium and other refractory metals from many other elements is based on ion-exchange from hydrofluoric acid media [9—11]. A systematic study was conducted on the adsorbability of phosphate ions on Dowex-1 and Dowex-50 from hydrofluoric and hydrochloric acid solutions under batch conditions. These experiments confirmed that phosphate was adsorbed only to a negligible extent ($D \leqslant 1$) over a wide range of acid concentrations (1—24 M HF and 1—8 M HCl), which agrees well with earlier data [12, 13]. Under dynamic column conditions, the possibility of phosphate separation was tested for the following systems: 2 M HF/Dowex-1; 2 M HF/Dowex-50; 10 M HF/Dowex-1 and 8 M HCl/Dowex-1. Some typical elution curves are given in Fig. 1.

These results indicate that several separation techniques based on extraction or ion-exchange should be feasible for the separation of phosphorus from niobium and many other elements. The ion-exchange method was selected for its convenience and for the high decontamination factors attainable for the phosphorus fraction with regard to the radionuclides constituting

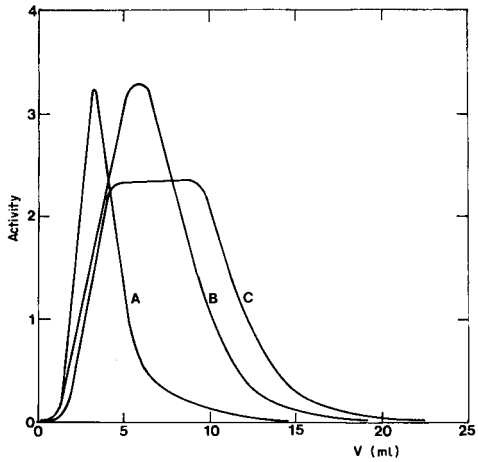

Fig. 1. The elution of phosphate ion from Dowex-1 X8 and Dowex-50 WX8 exchange columns: (A) 100 μg P in 1 ml of 10 M HF, Dowex-1; (B) 100 μg P in 1 ml of 8 M HCl, Dowex-1; (C) 100 μg P and 100 mg Nb in 5 ml of 2 M HF, Dowex-1 plus Dowex-50. The radioactivity of the eluate is given in arbitrary units; V is the volume of the eluate (ml). Dowex-1 column, 8 × 0.7 cm; Dowex-50 column, 4 × 0.7 cm (both 100—200 mesh); flow rate, 0.5 ml min^{-1}.

the main activities. A system of two columns coupled together was applied, first a column of Dowex-1 anion-exchanger and then a column of Dowex-50 cation-exchanger; elution was done with 2 M HF. Under these conditions, the niobium matrix as well as other impurities such as Hf, Mo, Ta, W, and Zr are retained quantitatively on Dowex-1, while the alkali metals, alkaline earth metals, rare earths, Co, Cu, Mn, Ni, Y, Zn, and others are retained on Dowex-50 [14]. In the eluate, beside phosphorus, radioisotopes of chromium, iron and neptunium (from uranium) were detected. After measurement with a high-resolution γ-ray spectrometer, the eluate was evaporated to remove fluoride ions and phosphorus was estimated via substoichiometric extraction of molybdophosphoric acid with tetraphenylarsonium chloride in dichloroethane [6]. Measurements by γ-spectrometry and checking the half-life of the extracted portion proved that the organic phase after the substoichiometric extraction was free from any detectable activity of accompanying radionuclides in all the niobium samples investigated.

The advantages of this technique are its high sensitivity and the freedom from blank; these features allow a high degree of accuracy. In addition to phosphorus, some other impurities might be determined simultaneously. Under the experimental conditions used, the limit of detection was found to be 0.2 ng of phosphorus or 2 ng g^{-1} for a 100-mg sample of niobium. This is adequate even for analysis of niobium of the highest purity. However, if necessary, the limit of detection could be further improved by processing larger samples, by applying longer irradiation times and by using a low-

TABLE 1

Contents of phosphorus determined in niobium samples of different grades of purity

Sample	Phosphorus content[a] ($\mu g\ g^{-1}$)	Sample	Phosphorus content[a] ($ng\ g^{-1}$)
Nb-P[b]	46.6 ± 5.8	Nb-WCT[b,c]	60.8 ± 7.5
Nb-ES[b]	1.8 ± 0.2	Nb-R 1[d]	23.8 ± 15.2
		Nb-R 2[e]	8.2 ± 2.6

[a]Averages from 4 determinations with average deviations. [b]Commercially available. [c]Purified by remelting under vacuum in an electron beam furnace, and further purified at the Laboratorium für Reinstoffe, MPI, Stuttgart [15]. [d]Obtained by refining electrolysis of Nb-WCT in an alkali metal fluoride melt. [e]Obtained from Nb-R1 by zone-refining in ultra-vacuum, decarburization and annealing.

background 2π or 4π beta counter. An improvement of the detection limit by a factor of 100 should be possible.

The recommended technique was applied to niobium samples of different purities. The results are given in Table 1. It can be seen that, nowadays, niobium of extremely high purity with regard to phosphorus can be produced.

Financial assistance was provided by Bundesministerium für Forschung und Technologie, Bonn. Grateful acknowledgement is made to the Institut für Radiochemie, Kernforschungszentrum Karlsruhe, for irradiation facilities. The authors thank Professor G. Tölg and Dr. K. Schulze, MPI für Metallforschung, Stuttgart, for discussions and for supplying the high-purity niobium samples.

REFERENCES

1 A. A. Fedorov, New Methods for Determining Phosphorus, Metallurgiya, Moscow, 1965, p. 128.
2 Yu. A. Chernikhov and B. M. Dobkina, Collected Papers of Giredment, Metallurgizdat, Moscow, 1961, p. 79; see I. M. Gibalo, Zh. Anal. Khim., 21 (1966) 718.
3 M. A. Notkina, E. I. Petrova, T. V. Cherkashina and Yu. A. Chernikhov, Tr. Kom. Anal. Khim., 15 (1965) 81.
4 M.-H. Yang, G. Kaiser and G. Tölg, International Symposium on Microchemical Technique, Davos, 1977, see G. Tölg, Fresenius Z. Anal. Chem., 294 (1979) 1.
5 R. Caletka and V. Krivan, Fresenius Z. Anal. Chem., in press.
6 G. A. Perezhogin and L. P. Sidorova, Zh. Anal. Khim., 24 (1969) 570.
7 G. I. Shamanenkova, V. I. Firsov, V. P. Shelkova and M. N. Shulepnikov, Zh. Anal. Khim., 28 (1973) 323.
8 R. Caletka, W. Fabian and V. Krivan, Fresenius Z. Anal. Chem., 310 (1982) 39.
9 D. H. Wilkins, Talanta, 2 (1959) 355.
10 G. Auboin, F. Dugain and I. Laverlochere, Bull. Soc. Chim. Fr., (1965) 547.
11 W. G. Faix and V. Krivan, Fresenius Z. Anal. Chem., 302 (1980) 269.
12 J. P. Faris, Anal. Chem., 32 (1960) 520.
13 F. Nelson, T. Murase and K. A. Kraus, J. Chromatogr., 13 (1964) 503.
14 R. Caletka and V. Krivan, Anal. Chem., in press.
15 K. K. Schulze, J. Met., 33 (1981) 33.

Analytica Chimica Acta, 141 (1982) 399—403
Elsevier Scientific Publishing Company, Amsterdam — Printed in The Netherlands

Short Communication

DETERMINATION OF ARSENIC IN REFRACTORY METALS BY RADIOCHEMICAL CHARGED-PARTICLE ACTIVATION ANALYSIS

CHATURVEDULA S. SASTRI and VILIAM KRIVAN*
Sektion Analytik und Höchstreinigung, Universität Ulm, 7900 Ulm (W. Germany)
(Received 22nd April 1982)

Summary. Arsenic is determined in tantalum and tungsten matrices via $^{75}As(p, n)^{75}Se$ and $^{75}As(d, 2n)^{75}Se$ reactions. Two ion-exchange procedures, with Dowex-1 columns, are described for the separation of the indicator radionuclides. Data on thick target yields for the $^{75}As(p, n)^{75}Se$ reaction are given. With 13-MeV proton or 15-MeV deuteron irradiation for 2 h at a current of 5 μA, the detection limit for arsenic is at the 10 $\mu g\ kg^{-1}$ level.

Relatively little information is available on the content and the role of arsenic in refractory metals, mainly because of the lack of powerful and reliable techniques for the determination of arsenic in such matrices [1, 2]. Recently, a radiochemical neutron activation technique based on a multistage separation procedure has been developed in this laboratory, which permits the determination of arsenic in niobium at $\mu g\ kg^{-1}$ levels. However, the application of neutron activation in the analysis of other refractory metals, especially tantalum and tungsten, is connected with serious difficulties because of high thermal neutron cross-sections and resonance integrals for the reactions $^{181}Ta(n, \gamma)^{182g}Ta$ (half-life = 115 d) and $^{186}W(n, \gamma)^{187}W$ (half-life = 23.8 h), which result in the production of extremely high matrix activities. For this reason, extraordinarily high decontamination factors are required in the separations. In addition, the high matrix activity makes it necessary to take special precautions regarding radiation protection of the personnel.

In this communication, a method is presented for the determination of arsenic, based on proton and deuteron activation, which does not produce high matrix activities of tantalum and tungsten. In this method, use is made of the reactions $^{75}As(p, n)^{75}Se$ and $^{75}As(d, 2n)^{75}Se$ and a group and/or a specific separation of the ^{75}Se indicator radionuclide.

Experimental

Sample preparation. The samples were prepared as thick targets cut from a sheet (tungsten) or from a rod (tantalum) and were etched for 10 s in 40% hydrofluoric acid—65% nitric acid (9 + 1) prior to irradiation. The standards were prepared by mixing arsenic as arsenic trioxide with high-purity graphite

and pressing into pellets. To study the role of interference, selenium was obtained in the elemental form as powder and pressed into thick pellets. The samples and standards were wrapped in 20-μm thick aluminum foils.

Irradiations. Irradiations were done in the internal beam of the isochronous cyclotron at Kernforschungszentrum, Karlsruhe, with 15-MeV deuterons and 13- and 22-MeV protons. Samples were irradiated at currents ranging from 5 to 10 μA for 10—180 min and standards at a current of 100 nA for 5—10 min. In order to obtain thick target yield curves, additional irradiation of standards were made with 10-, 17- and 20-MeV protons. The target holder was water-cooled and the current was measured with a Faraday cup.

Chemical separations. After irradiation, the samples were etched for a second time in 40% hydrofluoric acid—65% nitric acid (9 + 1) to remove possible surface contamination. The etching time varied from 50 s for procedure I to 10 s for procedure II (see below). They were dissolved in 5 ml of 40% hydrofluoric acid by dropwise addition of concentrated nitric acid. After the addition of selenium carrier, the chemical separation was achieved by ion-exchange on a Dowex-1 column (ca. 25 cm high, 0.6-cm diameter). Two slightly different chemical separation procedures were used.

Procedure I. The Dowex-1 column (100—200 mesh) was pre-washed with 15 ml of 40% hydrofluoric acid—methanol (1 + 2). The matrix dissolved in hydrofluoric acid/nitric acid was applied to the column, and the fraction containing selenium was obtained by eluting with 15 ml of 40% hydrofluoric acid—methanol (1 + 2). This procedure was used for tantalum and tungsten samples which were irradiated with 15-MeV deuterons, and for tungsten samples irradiated with 22-MeV protons.

Procedure II. After dissolution of the sample, nitric acid was eliminated by evaporation of the solution under an infrared lamp almost to dryness. The residue was dissolved in 5 ml of 10 M hydrofluoric acid. The Dowex-1 column (as above) was pre-washed with 15 ml of 10 M hydrofluoric acid. After the sample solution had been applied, the column was washed with 15 ml of 10 M hydrofluoric acid. The collected fraction contained nuclides of selenium, cobalt, chromium, etc. From this fraction, ^{75}Se was separated by extracting three times with 5 ml of 0.005 M dithizone in chloroform, and the combined organic phases were washed with 10 M hydrofluoric acid and measured. This procedure was used for tungsten samples irradiated with 13-MeV protons.

Measurements. The separated fractions were counted with a Ge(Li) detector which had a relative efficiency of 20.9% with respect to a 3 × 3 in. NaI(Tl) detector and a resolution of 1.9 keV for the 1332-keV γ-ray of ^{60}Co. Depending on the activity level, the counting times varied from 10 to 22 h. The method of Ricci and Hahn [3] was used to quantify the results.

Results and discussion

Sensitivities and interferences. Table 1 lists the nuclear reactions leading to the production of ^{75}Se. The sensitivities and detection limits obtainable for different irradiation energies with protons and deuterons are given in Table 2.

TABLE 1

Nuclear reactions for the production of ^{75}Se

Principal nuclear reaction	Q value (MeV)	Interfering element	Interfering reaction	Q value (MeV)
$^{75}As(p, n)\,^{75}Se$	−1.6	Br	$^{79}Br(p, \alpha n)\,^{75}Se$	−7.1
		Kr	$^{80}Kr(p, \alpha pn)\,^{75}Se$	−16.2
$^{75}As(d, 2n)\,^{75}Se$	−3.9	Se	$^{74}Se(d, p)\,^{75}Se$	+5.8

TABLE 2

Sensitivities and detection limits for arsenic in tantalum and tungsten

Activation	Irradiation energy (MeV)	Sensitivity at 5 μA for 2 h (dpm/ppm)	Interference-free detection limit in Ta and W[a] (ppb)
Proton	13	640	8
	22	880	6
Deuteron	15	530	7

[a]Irradiation and counting conditions: current 5 μA; irradiation time 2 h; measured for 10 h with the specified Ge(Li) detector.

The limits of detection are estimated for tantalum (or tungsten) matrix. For any other matrix, they differ slightly, depending on the particle range in that matrix. To obtain detailed information about the variation of sensitivity with irradiation energy, thick target yields were determined for incident proton energies varying from 10 MeV to 22 MeV and the results are shown in Fig. 1. It can be seen that irradiations with protons of higher energy increase the sensitivity only slightly, but lead to a large increase of the matrix

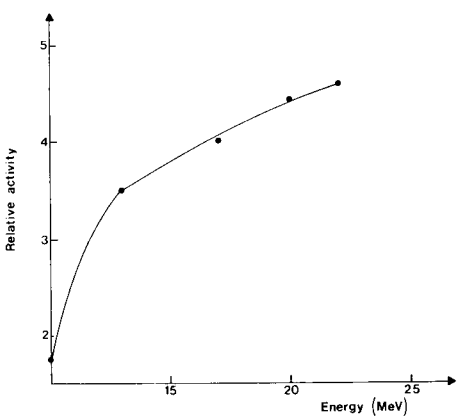

Fig. 1. Thick target yield curve for the reaction $^{75}As(p, n)\,^{75}Se$.

activity. For irradiations with 15-MeV deuterons or 13-MeV protons, the sensitivity is of the same order. However, with 15-MeV deuterons, interference from selenium via the reaction $^{74}Se(d,p)^{75}Se$ can be expected. For equal concentrations of selenium and arsenic, the experimentally determined interference amounts to less than 2%.

Separation of selenium from the irradiated matrix. For the separation of selenium, the two procedures outlined above were tested with ^{75}Se as tracer. When 40% hydrofluoric acid—methanol (1 + 2) was used as eluent (procedure I), lithium, boron and nitrogen could be determined via ^{7}Be [4, 5] in the same batch of samples as arsenic. Hence, ^{75}Se was separated from tantalum or tungsten by the procedure described for the separation of ^{7}Be from such a matrix [6]; the presence of methanol is helpful in retaining ^{7}Be totally on the column even in the presence of large quantities of nitric acid. The first fraction containing ^{75}Se was obtained by eluting with a mixture of hydrofluoric acid and methanol and the second fraction containing ^{7}Be was obtained by eluting with pure hydrofluoric acid. The separation yields were studied using the Dowex-1 column as described above. Selenium always passed through the column with a recovery of 97.3 ± 1.0% for the tungsten matrix and of 98.7 ± 0.5% for the tantalum matrix.

In procedure II, hydrofluoric acid was used as eluent with the same sort of Dowex-1 columns. The ion-exchange separation was necessary to remove the matrix activity occurring in the form of ^{181}Re, ^{182}Re, ^{183}Re, etc. After dissolution of the sample in HF/HNO_3 medium, rhenium is only partly retained if the sample solution is applied directly to the column [7]. Retention is improved after oxidation to perrhenate by evaporating the sample solution to near dryness. Removal of nitric acid is also necessary to prevent its interference with the extraction of selenium with dithizone. During the evaporation under an infrared lamp, there was no detectable loss of selenium in any of the eight experiments done under the described conditions. After evaporation, the residue was treated as described in the Experimental section, the selenium being extracted with dithizone in chloroform [8]. The yield of selenium was 97.5 ± 1.0% for the tantalum matrix and 98.0 ± 1.0% for the tungsten matrix. The same procedure can be followed for the analysis of niobium.

Application. The results obtained for arsenic in tungsten and tantalum matrices are given in Table 3. The accuracy of the method is indicated by the results obtained after proton and deuteron activation, which are in satisfactory agreement. As an example, the γ-ray spectrum of the selenium fraction of a tungsten sample, after extraction with dithizone in chloroform, is shown in Fig. 2.

This work was financially supported by the Bundesministerium für Forschung und Technologie, Bonn. The authors thank the Kernforschungszentrum, Karlsruhe, for providing irradiation facilities. Special thanks are due to Dr. R. Caletka for useful discussions.

TABLE 3

Arsenic content of tungsten and tantalum samples found by irradiation under different conditions

Metal	As content (mg kg^{-1})[a]		
	15-MeV deuterons	13-MeV protons	22-MeV protons
Tungsten (Plansee)	1.8 ± 0.8 (3)	2.1 ± 0.2 (3)	—
Tantalum (Plansee)	1.3 (2)	—	1.6 ± 0.2 (4)

[a]Number of samples irradiated in each case is given in parentheses.

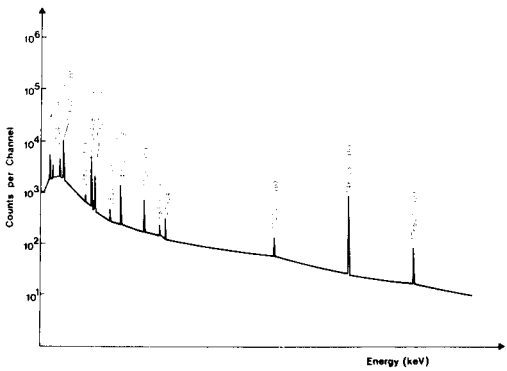

Fig. 2. γ-Ray spectrum of selenium fraction of a tungsten sample irradiated with 13-MeV protons at 10-μA current for 10 min. Measuring time 80 000 s; decay time 25 d. 'B' denotes background.

REFERENCES

1 V. Krivan, Pure Appl. Chem., 54 (1982) 787.
2 H. Mai, in Spurenanalyse in hochschmelzenden Metallen, VEB Deutscher Verlag für Grundstoffindustrie, Leipzig, 1970.
3 E. Ricci and R. L. Hahn, Anal. Chem., 37 (1965) 742.
4 C. S. Sastri, R. Caletka and V. Krivan, Anal. Chem., 53 (1981) 765.
5 C. S. Sastri and V. Krivan, Anal. Chem., 53 (1981) 2242.
6 C. S. Sastri, R. Caletka and V. Krivan, J. Radioanal. Chem., 70 (1982) 273.
7 W. G. Faix, R. Caletka and V. Krivan, Anal. Chem., 53 (1981) 1719.
8 R. Caletka and V. Krivan, Fresenius Z. Anal. Chem., 311 (1982) 177.

Analytica Chimica Acta, 141 (1982) 405—410
Elsevier Scientific Publishing Company, Amsterdam — Printed in The Netherlands

Short Communication

THE HIGH-PERFORMANCE LIQUID CHROMATOGRAPHY AND DETECTION OF PHOSPHOLIPIDS AND TRIGLYCERIDES
Part 1. Nonpolar Stationary Phase Chromatographic Behavior in Ultraviolet Transparent Mobile Phases

BRUCE JON COMPTON[a] and WILLIAM C. PURDY*

Department of Chemistry, McGill University, 801 Sherbrooke St. W., Montreal, Quebec H3A 2K6 (Canada)

(Received 4th February 1982)

Summary. The liquid chromatographic retention behavior of triglyceride and phospholipid molecular species in the nonpolar stationary (reverse) phase mode is presented for mobile phases compatible with ultraviolet detection. Interpretation of the results by means of the Kovats retention index suggests that correlation of retention to structure requires information on the number of acyl double bonds contained within the lipid molecular species in question. This, in turn, indicates that detection plays a major role in elucidating lipid structure because insufficient information is contained in the chromatographic retention data.

The nonpolar stationary (reverse) phase mode of high-performance liquid chromatography (h.p.l.c.) has gained wide acceptance as a versatile tool for the separation of many different classes of compounds. When the technique is applied to the separation and quantitation of triglyceride or phospholipid molecular species, several problems are encountered. These two lipid classes have limited solubility in the mobile phases normally used with nonpolar stationary phases, and exhibit extremely long retention times with C_{18}-type stationary bonded phases. This necessitates the use of mobile phases containing isopropanol or chloroform to increase solute solubility [1—3] and to reduce retention to an acceptable level. Consequently, detection becomes difficult because if the lipids possess chromophores, these exhibit only end-absorption below the u.v. cut-off of the mobile phases normally employed. For this reason, triglycerides and phospholipids have been quantified by using detectors based either on differential refractometry, infrared absorption, or the transport-type moving-wire flame ionization detectors [4—6]. All of these detectors are, to varying degrees, represented by commercial models, though none is particularly sensitive nor well characterized for triglycerides and phospholipids. Also, because of the

[a]Present address: Merck Sharp and Dohme Research Laboratories, P.O. Box 2000, Rahway, NJ 07065, U.S.A.

0003-2670/82/0000-0000/$02.75

large number of naturally occurring triglycerides and phospholipids, identification of any particular chromatographic band can be a major undertaking.

Data correlation methods

The approach used to correlate retention data for triglycerides and phospholipids to structure, involves a method analogous to the Kovats retention index system used for gas—liquid chromatography [1, 3, 7, 8]. The relationship between retention, one measure being the chromatographic capacity factor k', and the structure of triglycerides and phospholipids can be described with the Kovats index, I, by

$$\log k' = BI_s + A \tag{1}$$

where k' has its usual meaning [9] of $(V_R - V_o)/V_o$, V_R and V_o being retention and column void volumes, respectively; B is the Kovats retention index parameter, a general measure of the selectivity of the system; I_s is 100 n where n is the number of methylene groups in the standard alkyl series (n-alkanes, alcohols, esters, etc.) used to establish the index; and A is the system characteristic related to the capacity of the system for a standard series.

When applied to liquid chromatography in the past, I_s has provided useful correlation of structure to retention [10], development of an eluotropic series [11], and investigation of the role of argentation [5] and mixed retention modes (adsorption and partitioning) of amines and alcohols in the reverse-phase system [12].

Two attempts [1, 3] at correlating phospholipid structure to retention showed double-bond effects to be of particular interest in molecular species identification. These effects can be described by

$$I_u = I_s - CD_b \tag{2}$$

where I_u is the index observed for unsaturated triglyceride and phospholipid species, D_b is the total unsaturation of the compound, and C is a correlation factor for unsaturation effects on I_s. By employing saturated standards and Eqn. (1) to calibrate a column for a particular mobile phase and temperature, Eqn. (2) can be used to investigate unsaturation effects on retention.

Experimental

The chromatographic unit consisted of a Waters 6000A pump, U6K injector, Model R401 differential refractive index detector (Waters Scientific, Mississauga, Ontario), Schoeffel SF770 variable wavelength detector (Schoeffel Instrument Corp., Westwood, NJ), and a laboratory-designed column, column thermostat unit, and post-column reactor detector. Ancillary equipment included a Honeywell Electronik 196 recorder and a solvent degassing system based on the helium displacement method [13].

The laboratory-designed column made of stainless steel tubing (0.2-cm i.d., 30 cm long) was packed with a hexyl-bonded stationary phase on a

silica support (C_6, 5 μm; Phase Separation, Hanappage, NY) by using the equal-density method [14].

The following solvent, mineral acid, and lipid standards were used: acetonitrile (British Drug Houses); orthophosphoric acid (American Chemicals); acyl glycerides, fatty acids or their esters (Sigma Chemical); and synthetic 1,2-diacyl-3-phosphatidylcholines (Serdary Research Laboratories, London, Ontario). All lipids were dissolved in chloroform—methanol to give standards listed in Table 1.

Mobile phases were degassed with helium and pumped through the injector and column into the SF770 and then the R401 detector or the post-column reactor. Each standard was investigated at least three times (n = 3) and retention was measured at peak mode. Void-volume measurements were taken from strip-chart recordings.

Mobile-phase compositions varied for triglycerides from 80 to 100% CH_3CN/H_2O, as indicated in the text. For phospholipids, 90/10/0.1 CH_3CN/H_2O/concentrated H_3PO_4 was used. The column was maintained at 60 ± 1°C.

Results

Triglycerides and phospholipids were investigated simultaneously for systematic comparison of their retention behavior. One interesting aspect of phospholipid retention not generally exhibited by acylglycerides is the mixed-mode retention (adsorption and partitioning) observable in the chromatographic system [4]. This is seen in Fig. 1 when the retention of phosphatidylcholine-dilinolenoyl (N = 10) on the C_6-bonded column is compared to that of dioleoylglyceride under varying mobile-phase phosphoric acid concentrations.

The retention of triglyceride and phospholipid standards for various mobile phases is summarized in Table 1. When I_u values for unsaturated triglycerides and phospholipids are corrected by using Eqn. (2) and C = 200, the resulting I-corrected values (I_c) are similar to the I_s for the corresponding saturated standards. These results are comparable to previously reported work [3] with a C_{18}-bonded phase with non-u.v. transparent mobile phases. The C_6-bonded column used in this work allowed u.v. transparent mobile phases to be used without inconveniently long retention times.

Linear-regression analysis of all data is presented in Table 2.

Discussion

The most immediate use of the separation and detection method described above is for determining molecular species profiles. This can be accomplished only if chromatographic bands can be assigned to a particular molecular species, a task requiring well-characterized retention behavior of triglycerides and phospholipids.

A previous study [4] showed that adsorption played a major role in retention of phospholipid molecular species but reasonable chromatographic efficiency and u.v. detection was possible by the method described. The

TABLE 1

Retention, I_u and C values for triglycerides and phospholipids

N[a] Acyl[b]	$I(D_b)$[c]	k' values for various % CH_3CN[d]				
		80	85	90	95	100
Triglycerides						
1 *n*-Hexanoic	1800	0	0	0	0	0
2 *n*-Octanoic	2400	1.05	0	0	0	0
3 *n*-Decanoic	3000	3.11	1.74	0	0	0
4 *n*-Dodecanoic	3600	11.20	6.51	2.63	0	0
5 *n*-Tetradecanoic	4200	ND[e]	17.87	7.44	1.97	0
6 *n*-Hexadecanoic	4800	ND	ND	20.60	4.71	0
7 *n*-Octadecanoic	5400	ND	ND	ND	20.45	0
8 *n*-Eicosanoic	6000	ND	ND	ND	ND	P[f]
9 *n*-Docosanoic	6600	ND	ND	ND	ND	P
10 Cis-*n*-Hexadecenoic	4800(3)	ND	17.28 (4158,214)	6.69 (4131,223)	1.78 (4193,202)	0
11 Cis,cis-9,12-octadecadienoic	5400(6)	ND	22.54	7.63 (4209,199)	1.94 (4239,194)	0
12 Trans-9-octadecenoic	5400(3)	ND	ND	—	4.32 (4647,251)	0
13 Cis-9-octadecenoic	5400(3)	ND	ND	18.75 (4731,223)	3.59 (4626,258)	0.94
14 Cis-6-octadecenoic	5400(3)	ND	ND	—	4.03 (4614,262)	0
15 Cis-13-docosenoic	6600(3)	ND	ND	—	—	2.79
Phospholipids		k' value for $CH_3CN/H_2O/H_3PO_4$ (90:10:0.1)				
1 *n*-Hexanoic PC	1200	5.5				
2 *n*-Octanoic PC	1600	7.6				
3 *n*-Decanoic PC	2000	9.7				
4 *n*-Dodecanoic PC	2400	13.9				
5 *n*-Tetradecanoic PC	2800	17.5				
6 *n*-Hexadecanoic PC	3200	27.0				
7 *n*-Octadecanoic PC	3600	38.0				
8 Cis-9-Octadecenoic PC	3600(2)	28.4 (3299,150)				
9 Cis,cis-9,12-octadecadienoic PC	3600(4)	20.9 (2914,171)				
10 Cis,cis,cis,-9,12,15-octadecatrienoic PC	3600(6)	15.7 (2555,174)				

[a] N = standard number. Sample volumes injected were 1—5 µl. [b] Acyl refers to the systematic name in 1,2,3-triacylglycerol or 1,2-diacylphosphatidylcholine. [c] I = Kovats index for triglycerides 1—9 and phospholipids 1—7. For triglycerides 10—15 and phospholipids 8—10 the values are uncorrected for D_b. Values in parentheses are total degree of lipid unsaturation, D_b. [d] I_u and C values are in parentheses as (I_u,C). [e] ND, not detected. [f] P, precipitation in mobile phase.

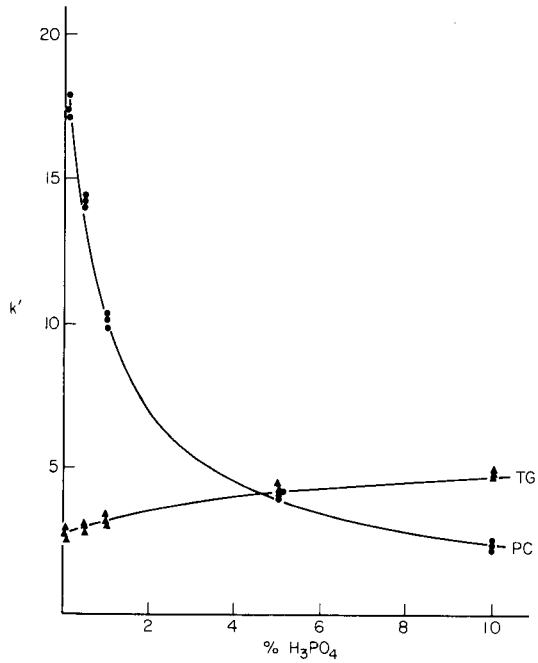

Fig. 1. Retention of phospholipid standard 10 (PC) and 1,2-dioleoylglycerol (TG) at various mobile phase (90% CH_3CN/H_2O)—concentrated H_3PO_4 contents.

TABLE 2

Linear regression parameters for saturated lipid data in Table 1

%CH_3CN	B[a]	A[a]
Triglyceride		
80	$8.57 (\pm 0.12) \times 10^{-4}$	$-2.05 (\pm 0.12)$
85	$8.43 (\pm 0.20) \times 10^{-4}$	$-2.27 (\pm 0.24)$
90	$7.47 (\pm 0.02) \times 10^{-4}$	$-2.26 (\pm 0.00)$
95	$8.47 (\pm 0.37) \times 10^{-4}$	$-3.30 (\pm 0.60)$
Phospholipid		
90	$3.46 (\pm 0.11) \times 10^{-4}$	$3.12 (\pm 0.29) \times 10^{-1}$

[a] A and B are coefficients in Eqn. (1).

mechanism of adsorption is not known and, as shown in Fig. 1, is related to the strong donor—acceptor properties of the phosphocholine moiety. The phosphatidylcholine (PC) class was chosen as a model because of its wide applicability. The results indicate that class separation of triglycerides from phospholipids could be accomplished with changes in phosphoric acid content of the mobile phase and that the adsorptive role is important in a variety of alkyl-bonded silica based stationary phases.

The structure–retention relationship of triglyceride or phospholipid molecular species for the C_6 column used here indicates that structural assignment cannot be based solely on retention data. The results presented in Tables 1 and 2 were employed to calculate C values for unsaturation effects. There are no apparent trends seen in C for either lipid class, shown in parentheses in Table 1, and the only observation is that the effect of unsaturation is greater on triglycerides than on phospholipid retention. Placement and orientation of double bonds (triglyceride standards, $N = 12–14$) showed no significant difference in C but these effects were not systematically studied as elsewhere [15]. Also, the physicochemical mechanism responsible for double-bond effects on I was not treated in this empirical approach.

This work was initiated primarily for use in developing a system for quantitation of lipid molecular species. It is a prerequisite for the evaluation of the u.v. detector and post-column reactors to be presented later. It is apparent that chromatography on bonded nonpolar stationary phases can be used to fractionate triglyceride and phospholipid molecular species. However, because retention is dependent on total lipid hydrophobicity, structural assignments require more information than can be gleaned from retention data alone.

The authors acknowledge the assistance of J. R. Weber and S. N. Young and the financial support of the Natural Sciences and Engineering Research Council of Canada.

REFERENCES

1 R. D. Plattner, G. F. Spencer and R. Kleiman, J. Am. Oil Chem. Soc., 54 (1977) 511.
2 P. T.-S. Pei, R. S. Henly and S. Ramachandran, Lipids, 10 (1975) 152.
3 N. A. Porter, R. A. Wolf and J. R. Nixon, Lipids, 14 (1979) 20.
4 B. J. Compton and W. C. Purdy, J. Chromatogr., 169 (1979) 39.
5 B. Vonach and G. Schomburg, J. Chromatogr., 149 (1978) 417.
6 W. L. Erdahl and O. S. Privett, Lipids, 12 (1977) 797.
7 E. Kováts, Helv. Chim. Acta, 41 (1958) 1915.
8 E. Kováts, Adv. Chromatogr., 1 (1965) 229.
9 L. R. Snyder and J. J. Kirkland, Introduction to Modern Liquid Chromatography, Wiley, New York, 1973, p. 27.
10 J. K. Baker and C.-Y. Ma, J. Chromatogr., 169 (1979) 107.
11 K. Karch, I. Sebastian, I. Halasz and H. Engelhardt, J. Chromatogr., 122 (1976) 171.
12 N. E. Hoffman and J. C. Liao, Anal. Lett., A11 (1978) 287.
13 S. R. Bakalyar, M. P. T. Bradley and R. Honganen, J. Chromatogr., 158 (1978) 277.
14 I. S. Krull, M. H. Wolf and R. B. Ashworthy, Am. Lab., May (1978) 45.
15 J. P. Roggero and S. V. Coen, J. Liquid Chromatogr., 4 (1981) 1817.

Analytica Chimica Acta, 141 (1982) 411—417
Elsevier Scientific Publishing Company, Amsterdam — Printed in The Netherlands

Short Communication

CHARACTERIZATION OF POLYCYCLIC AROMATIC HYDROCARBONS AND HYDROAROMATICS IN A DISTILLABLE COAL-DERIVED SOLVENT BY CHROMATOGRAPHIC AND CORRECTED FLUORESCENCE METHODS

T. W. ALLEN and R. J. HURTUBISE*
Department of Chemistry, University of Wyoming, Laramie, WY 82071 (U.S.A.)
H. F. SILVER
Chemical Engineering Department, University of Wyoming, Laramie, WY 82071 (U.S.A.)
(Received 8th March 1982)

Summary. Polycyclic aromatic hydrocarbons and hydroaromatics were separated from a coal-derived distillate by dry-column chromatography and high-performance liquid chromatography. Individual components in the isolated fractions were characterized by corrected excitation fluorescence spectrometry. With the chromatographic data and the fluorescence data, compound identification was possible in some cases.

The separation and identification of polycyclic aromatic hydrocarbons (PAHs) is an important consideration in many fields, and many analytical methods have been developed for PAHs [1]. Polycyclic aromatic hydrocarbons and hydroaromatics are of particular interest in coal liquefaction research because of their ability to improve the yield of solvent-refined coal [2]. Separation of PAHs by nonpolar stationary (reverse) phase high-performance liquid chromatography (h.p.l.c.) has been the subject of many publications [3—12].

Fluorescence spectroscopy is widely used for the characterization and identification of PAHs. Kershaw [13] used uncorrected fluorescence excitation and emission spectra to characterize PAHs in coal-derived liquids. Although such uncorrected spectra are useful in characterizing various PAHs at low concentration levels, the spectra are dependent on instrument characteristics such as source output and detector response. Synchronous fluorescence techniques, in which the excitation and emission wavelengths are scanned simultaneously at a set $\Delta\lambda$, have been useful for characterization of PAHs in certain multicomponent mixtures [9, 14], but limitations revealed by Latz et al. [15] show that the technique should be used with some caution.

Corrected excitation fluorescence spectroscopy has been available for some time but has received relatively little attention in the characterization of complex samples. Porro et al. [16] discussed many advantages of corrected fluorescence spectra and specifically showed their potential use with PAHs.

0003-2670/82/0000-0000/$02.75

For example, the corrected excitation spectrum for a compound is, for practical purposes, identical to its absorption spectrum, but because of the low detection limits of fluorescence spectroscopy, can often be obtained at a much lower concentration than the corresponding absorption spectrum. This is particularly advantageous for situations in which a standard compound is not available, but its absorption spectrum or corrected excitation spectrum is available in the literature for comparison. Also, corrected excitation spectra are not as dependent on instrumental factors as uncorrected spectra.

In this work, dry-column chromatography, h.p.l.c., and corrected fluorescence excitation spectra were combined for the isolation and characterization of PAHs and hydroaromatics in a coal-derived distillate sample.

Experimental

Instrumentation. The liquid chromatograph used was a Waters model ALC/GPC 244 equipped with a model 6000A pump, a model U6K injector, a model 440 absorbance detector set at 254 nm and 280 nm, and a strip-chart recorder. A μ-Bondapak C_{18} column (10-μm particle size; 3.9-mm i.d. × 30 cm) from Waters was used with methanol:water (65:35 v/v) at 1.0 ml min^{-1} and ambient temperature. The spectrofluorimeter used was a Farrand MK2 with a corrected excitation module and a Farrand Autoprocessor-1 microprocessor unit.

Reagents. Baker h.p.l.c. grade methanol was filtered through a Millipore type F-H 0.45-μm filter. Distilled water was treated with a Milli-Q filtering system (Millipore) with a final 0.22-μm filter. Cyclohexane (99+%; Aldrich Chemical Co., Milwaukee, WI) or *n*-hexane (>99%; Phillips Chemical, Borger, TX) was used to dissolve standard compounds and samples. 1,2-Dihydropyrene was obtained from Laramie Energy Technology Center and 1,2,6,7-tetrahydropyrene from Pittsburgh Energy Technology Center. All other compounds were obtained commercially and were used as received.

Sample. The coal-derived distillate sample (177—425°C) was obtained from the liquefaction of Wyodak coal in Wilsonville, AL.

Procedure for reference spectra. Cyclohexane or *n*-hexane solutions of standards were injected onto the h.p.l.c. system. If the injection volume was kept small, no adverse effects other than slight band broadening were seen from using the cyclohexane or *n*-hexane. The major eluting peak was collected in a clean vial from a short piece of tubing (0.009-in. i.d.) at the exit port of the detector. The corrected excitation spectrum was recorded at a fixed emission wavelength corresponding to a maximum in the emission spectrum.

Procedure for sample spectra. Polycyclic aromatic hydrocarbon fractions were isolated from 50 mg of the coal-derived sample by dry-column chromatography as described previously [17, 18]. Acid treatment [17] was used to remove basic nitrogen compounds. The isolated fractions were dissolved in *n*-hexane or cyclohexane and injected onto the h.p.l.c. system. The eluting peaks were collected in clean vials at 2-ml to 4-ml intervals, and corrected excitation spectra were obtained for each subfraction. The void volume of the column was found to be 2.75 ml by eluting methanol.

Results and discussion

Retention data on the h.p.l.c. system and corrected excitation fluorescence spectra were obtained for the thirty-one PAH and hydroaromatic compounds listed in Table 1. In some cases, the uncorrected emission spectrum was also recorded. No two corrected excitation spectra were found to be identical. In ambiguous cases, such as 1,2-benzofluorene and 2,3-benzofluorene, the emission spectra should also be obtained. The excitation and emission spectra clearly differentiated the two benzofluorenes (Fig. 1).

The coal-derived distillate sample was initially separated into four fractions that were concentrates of PAHs containing 6,5,4, and 3 aromatic rings. This step involved an acidified silica column and an aluminum oxide dry column [17, 18]. The procedure allowed *a priori* prediction of the location of PAHs and hydroaromatics on the dry column [18]. The 3-ring fraction contained the most material and was initially chosen for investigation on the h.p.l.c. system; however, the general approach is applicable to the other ring fractions.

Most PAHs and hydroaromatic compounds behave predictably on the reversed-phase h.p.l.c. system used and migrate according to a chromatographic correlation factor, F, developed earlier [10, 19]. The factor F correlates various structural features of the compounds with log k'. The h.p.l.c. chromatogram resulting from separation of the 3-ring fraction is given in Fig. 2, with fractions collected as shown. Approximately 30 μg of the 3-ring fraction was injected, and spectra of the h.p.l.c. fractions could be obtained directly without concentration of the fractions. Based on the chromatographic correlation factor, F, tentative assignments were made for some of the peaks in the h.p.l.c. fractions. Corrected excitation spectra were then obtained for all the fractions at the appropriate emission wavelengths to

TABLE 1

Standard compounds investigated

1. Acenaphthene	17. Fluorene
2. Acenaphthylene	18. 1,2-Benzofluorene
3. Anthracene	19. 2,3-Benzofluorene
4. Bibenzyl	20. Naphthalene
5. Biphenyl	21. 2,3-Dimethylnaphthalene
6. 2,3-Benzanthracene	22. Perylene
7. 9,10-Dihydroanthracene	23. Phenanthrene
8. 9,10-Dimethylanthracene	24. 9,10-Dihydrophenanthrene
9. 7,12-Dimethylbenz(a)anthracene	25. Pyrene
10. 2-Methylanthracene	26. 1,2-Dihydropyrene
11. 9-Methylanthracene	27. 1,2,6,7-Tetrahydropyrene
12. 1,2,3,4,5,6,7,8-Octahydroanthracene	28. 1,2,3,6,7,8-Hexahydropyrene
13. Chrysene	29. *p*-Terphenyl
14. Fluoranthene	30. 5,12-Dihydrotetracene
15. 3,4-Benzofluoranthene	31. Triphenylene
16. 1,2,3,4-Tetrahydrofluoranthene	

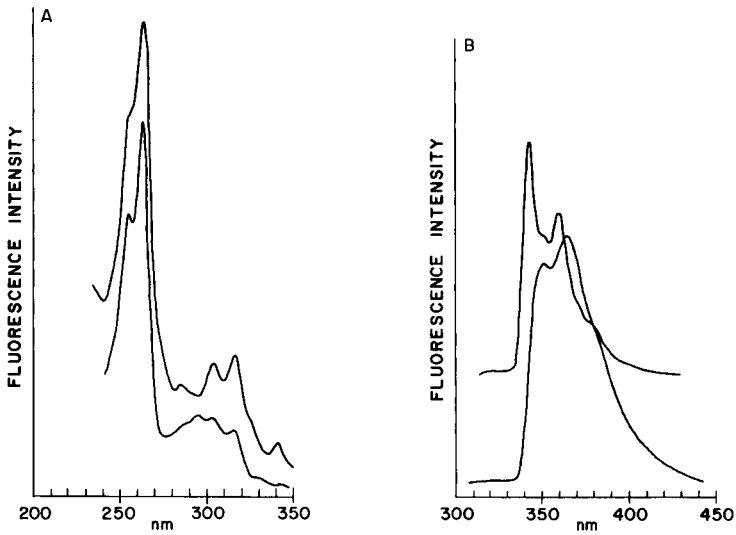

Fig. 1. A. Corrected excitation spectra of 2,3-benzofluorene, λ_{em} 360 nm (upper curve) and 1,2-benzofluorene, λ_{em} 370 nm (lower curve). B. Uncorrected emission spectra of 2,3-benzofluorene, λ_{ex} 255 nm (upper curve) and 1,2-benzofluorene, λ_{ex} 255 nm (lower curve).

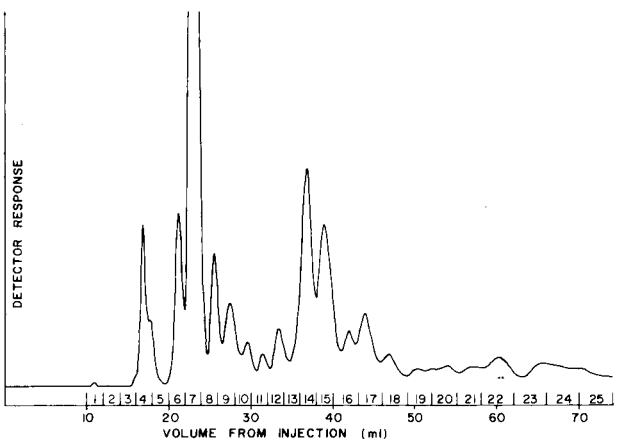

Fig. 2. Reversed-phase h.p.l.c. chromatogram of the three-ring PAH fraction from dry column separation of the distillable coal-derived solvent. Ultraviolet detector set at 254 nm.

determine if any of the suspected compounds were present in the fraction. Comparison with reference spectra allowed characterization of several compounds in the sample. For this particular fraction, the seven compounds identified were naphthalene, fluorene, phenanthrene, anthracene, 9,10-

dihydrophenanthrene, fluoranthene, and pyrene. These compounds corresponded to fraction numbers 1,6,7,8,9,12, and 13 (Fig. 2), respectively. The major limitation in characterizing additional compounds was the lack of reference compounds. An extensive literature search was not undertaken to find appropriate absorption spectra. 2,3-Benzofluorene was, however, identified in an h.p.l.c. separation of the 4-ring fraction from the coal-derived distillate sample. Figures 3 and 4 show typical examples of reference spectra compared to spectra obtained from h.p.l.c. fractions which were isolated from the 3-ring fraction. In Fig. 3B, the inset spectrum, taken from Porro et al. [16], corresponds very well to the lower spectrum which was obtained from an h.p.l.c. fraction. Figure 3B indicates one of the advantages of the use of corrected excitation spectra.

Speculation can be made on alkyl-substituted components isolated in the h.p.l.c. fractions by noting the shift of the excitation spectrum compared to the spectrum of the parent compound. Figure 5 shows the corrected excitation spectrum of a fraction which would correspond to the elution of a methylpyrene, based on the chromatographic F factor. This spectrum appears almost identical to the reference spectrum for pyrene, but is shifted toward slightly longer wavelengths. The shift to longer wavelengths suggests that the compound is a monosubstituted methylpyrene [20]. The fact that a methylpyrene appeared in the 3-ring PAH fraction indicates the initial dry-column step does not cleanly separate 3- and 4-ring PAH compounds. However, the respective 3-, 4-, 5-, and 6-ring fractions are rich in the given PAH ring type [17, 18].

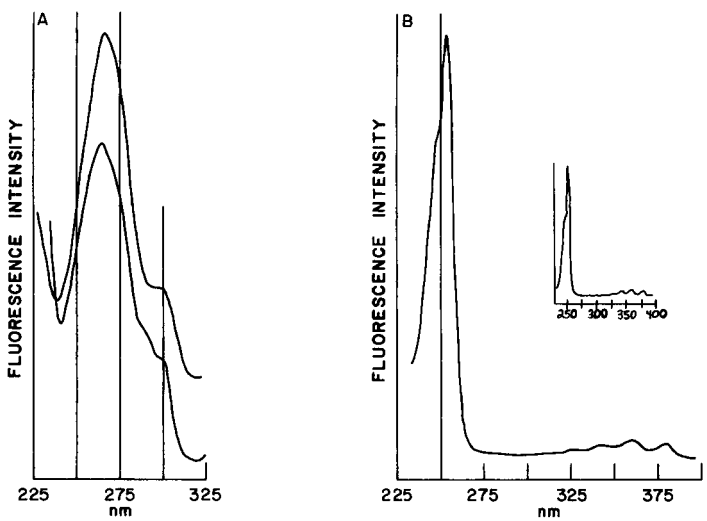

Fig. 3. A. Corrected excitation spectra of 9,10-dihydrophenanthrene (upper curve) and fraction 9 (lower curve), λ_{em} 330 nm. B. Corrected excitation spectra of anthracene (inset, ref. 18) and fraction 8 (lower curve), λ_{em} 400 nm.

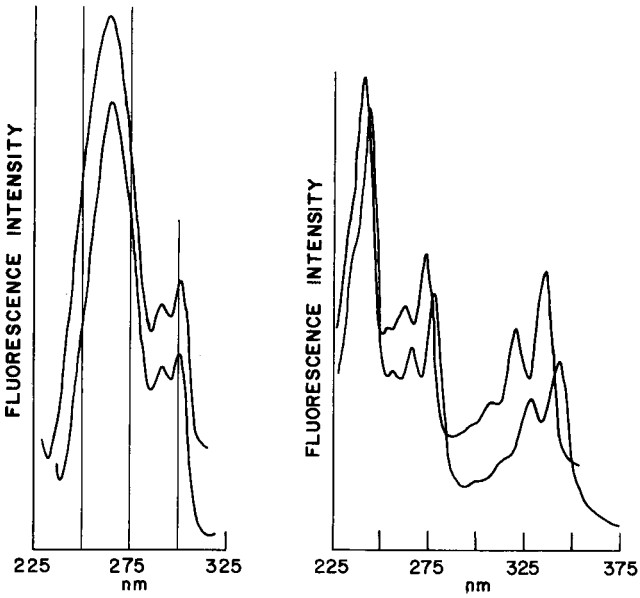

Fig. 4. Corrected excitation spectra of fluorene (upper curve) and fraction 6 (lower curve), λ_{em} 310, 320 nm.

Fig. 5. Corrected excitation spectrum of pyrene (upper curve) and fraction 22 (lower curve), λ_{em} 400 nm.

The particular combination of dry column chromatography, reverse-phase h.p.l.c., and corrected excitation fluorescence spectroscopy should find use in the isolation and characterization of PAH and hydroaromatics not only in coal-derived liquids, but also in other complex mixtures. The present work centered on PAHs and hydroaromatics containing fewer than five aromatic rings, because of their abundance in the coal-derived distillate samples. However, variation of the mobile phase composition in the reverse-phase h.p.l.c. system would allow a similar investigation of PAHs and hydroaromatics with five or more aromatic rings [6, 12]. Alteration of the dry column procedure would be necessary for compounds with six or more aromatic rings.

Financial support was provided by the Department of Energy, Washington, DC, Contract DE-AC22-79ET14874.

REFERENCES

1 M. L. Lee, M. V. Novotny and K. D. Bartle, Analytical Chemistry of Polycyclic Aromatic Compounds, Academic Press, New York, 1981.
2 D. D. Whitehurst, T. O. Mitchell and M. Farcasiu, Coal Liquefaction, Academic Press, New York, 1980.
3 R. Amos, J. Chromatogr., 204 (1981) 469.
4 A. L. Colmsjo and J. C. MacDonald, Chromatographia, 13 (1980) 350.

5 E. Katz and K. Ogan, J. Liq. Chromatogr., 3 (1980) 1151; Chromatogr. Newsl., 8 (1980) 20; J. Chromatogr., 188 (1980) 115.
6 K. Ogan, E. Katz and W. Slavin, Anal. Chem., 51 (1979) 1315.
7 M. A. Fox and S. W. Staley, Anal. Chem., 48 (1976) 992.
8 M. Dong, D. C. Locke and E. Ferrand, Anal. Chem., 48 (1976) 368.
9 T. Katoh, S. Yokoyama and Y. Sanada, Fuel, 59 (1980) 845.
10 J. F. Schabron, R. J. Hurtubise and H. F. Silver, Anal. Chem., 49 (1977) 2253.
11 P. Roumeliotis, K. K. Unger, G. Tesarek and E. Mühlberg, Fresenius Z. Anal. Chem., 298 (1979) 241.
12 P. A. Peaden, M. L. Lee, Y. Hirata and M. Novotny, Anal. Chem., 52 (1980) 2268.
13 J. R. Kershaw, Fuel, 57 (1978) 299.
14 T. Vo-Dinh, R. B. Gammage, A. R. Hawthorne and J. H. Thorngate, Environ. Sci. Technol., 12 (1978) 1279.
15 H. W. Latz, A. H. Ullman and J. D. Winefordner, Anal. Chem., 50 (1978) 2148.
16 T. J. Porro, R. E. Anacreon, P. S. Flandreau and I. S. Fagerson, J. Assoc. Off. Anal. Chem., 56 (1973) 607.
17 R. J. Hurtubise and J. D. Phillip, Anal. Chim. Acta, 110 (1979) 245.
18 R. J. Hurtubise, T. W. Allen and H. F. Silver, Anal. Chim. Acta, 126 (1981) 225; 140 (1982) 153.
19 R. J. Hurtubise, T. W. Allen and H. F. Silver, J. Chromatogr., 235 (1982) 517.
20 G. G. Guilbault, Practical Fluorescence: Theory, Methods, and Techniques; Dekker, New York, 1973, p. 614.

Analytica Chimica Acta, 141 (1982) 419—425
Elsevier Scientific Publishing Company, Amsterdam — Printed in The Netherlands

Short Communication

SPECTROPHOTOMETRIC DETERMINATION OF ANIONIC SURFACTANTS BY CONVERSION OF THE LEUCO-BASES OF TRIPHENYLMETHANE DYES

HARVEY POBINER* and HENRY T. HOFFMAN, Jr.

American Can Company, Princeton Research Center, P.O. Box 50, Princeton, NJ 08540 (U.S.A.)

(Received 11th January 1982)

Summary. A one-phase, one-reagent, spectrophotometric technique is reported for the detection and determination of anionic surfactants of the sulfonate and sulfate types. Both applications are based on conversion of the colorless leuco-bases of triphenylmethane dyes (Brilliant Green and methyl violet) to colored (quinoid) forms by the anionic surfactants. The quantitative method, in the absorption and reflectance modes, is applicable to anionic surfactants in the 0—1500 ppm range; the spectrophotometric procedure can be automated. Residual surfactant can be detected at the 0.01% level on the surface of cellulosic products.

A simple spectrophotometric method for detection and determination of anionic surfactants is described. The chemistry is based on the conversion by anionic surfactants of the colorless leuco-base of a triphenylmethane dye to the colored (quinoid) form. The method was developed initially for detecting residual surfactant on a paper substrate in a manufacturing process. It was then developed further for the determination of surfactant in aqueous samples and subsequently for use in an on-line process analyzer. This work is an extension of the Abramovich method [1] which is described in Longman's text [2] as having possibilities for wide application. The method has a significant advantage compared with the methylene blue procedure of ion pairing with an anionic surfactant [3, 4], in that no extraction of the dyestuff or the complex into a hydrocarbon phase is necessary. This obviates phase separation and is of particular value for on-line determinations.

The quantitative procedure described below is based on the use of Brilliant Green (Basic Green 1), which was selected from a study of similar dyes for its facility in being converted into a stable, colorless leuco-base that responds instantly to color restoration. Both sulfate ($R—OSO_3Na$) and sulfonate ($R—SO_3Na$) anionic surfactants respond to the method. Absorption spectrophotometric and reflectance methods are described below. The reactions of the leuco-base conversion for Brilliant Green are probably as follows.

0003-2670/82/0000-0000/$02.75

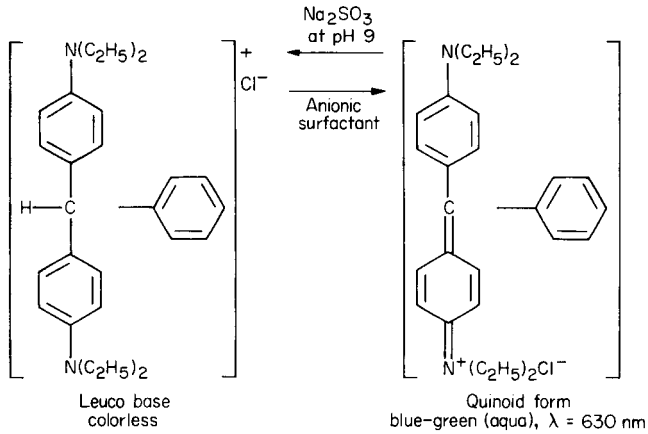

Longman [2] suggests that the reaction requires the presence of micelles provided by the dyestuff and the surfactant. Further, the critical micelle concentration of the surfactant is reduced by high concentrations of inorganic salts. The micelles probably exclude sulfite ions and a colored ion-pair forms between the dyestuff and the surfactant.

The method was principally used here for two sulfonate types, Arco A-OK (a mixture of a hydroxyalkane sulfonate, $RCH(OH)SO_3Na$ and an alkene sulfonate, $RCH{=}CH{-}CH_2SO_3Na$, in the C_{16}—C_{18} range) and Aerosol-OT (a sodium dioctyl sulfosuccinate), and for sodium dodecyl (lauryl) sulfate.

Extraction–spectrophotometric methods for anionic surfactants that have been described have been based on azo pyridinium iodide salts [5], copper(II)/1,10-phenanthroline [6], iron(II) chelates similar to ferroin [7], dyestuffs such as Azure A [8], Remacryl Blue B, Red 2BL [9] and Acridine Orange [10], and a diethyldithiocarbamate derivative [11]. Longman [2] indicated that Rose Bengal, acriflavine and dichlorofluorescein could be used as single-phase titrants for anionic surfactants.

Experimental

Instrumentation. A Beckman model 5240 double-beam recording spectro-reflectometer was used for method development. In actual practice, a simple colorimeter can be used. For continuous monitoring, the method was successfully tested on an on-line modular process colorimeter (Technicon Industrial Systems, Auto Analyzer II System).

Chemicals. The eleven triphenylmethane dyes screened (Aldrich Chemical; Matheson, Coleman and Bell; Fisher Scientific) were used as received. Brilliant Green was Aldrich reagent no. 86,087-5. All solutions were prepared from analytical reagent-grade chemicals.

The α-olefin sulfonate tested is available from Chevron Chemicals and can also be obtained as Ultrawet A-OK surfactant from Arco Chemical. The sodium dioctyl sulfosuccinate is available as a 75% solution from American Cyanamid. Sodium dodecyl sulfate (SDS) tested was from Gallard-Schlesinger

Chemical. The solid surfactants were dried at 105°C for 2 h before use; the liquid surfactant was used as received.

Buffer, pH 9.0. Dissolve 2.384 g of sodium tetraborate hexahydrate in ca. 400 ml of deionized water, pipet in 23.0 ml of 0.1 M HCl and dilute to 500 ml with deionized water.

Leuco-bases of Brilliant Green and methyl violet. Dissolve 0.05 g (±0.2 mg) of Brilliant Green in 75 ml of methanol. Add 370 ml of deionized water followed by 6.0 g (±1 mg) of sodium sulfite; the blue–green solution will become essentially colorless. Use 0.05 M H_2SO_4 to adjust the solution to pH 9.0. Add 25.0 ml of the pH 9.0 buffer and dilute to exactly 500 ml with deionized water. Store in a low actinic glass-stoppered vessel. The shelf life of this solution exceeds 4 months. Dissolve ca. 0.02 g of methyl violet in 10 ml of methanol and add the solution to ca. 300 ml of deionized water. Add 7 g of sodium sulfite, adjust to pH 9 with ca. 8 ml of 0.05 M H_2SO_4 and stir in 1 g of activated charcoal (20–40 mesh). Form a charcoal bed on a sintered-glass funnel (no. 40 medium) by adding a suspension of $\leqslant$0.05 g of finely ground activated charcoal in deionized water, allowing the charcoal to settle, and then applying suction. Filter the methyl violet leuco-base solution through this charcoal bed. The filtrate should be colorless; if it is not, repeat the charcoal treatment. Store in a spray bottle for the qualitative use; shelf life is about one month.

Calibration procedure with Brilliant Green. Prepare a 2.00 g l^{-1} solution of the anionic surfactant in deionized water. Pipet the desired amounts (0–20 ml) of this solution into 100-ml volumetric flasks and add 10.0 ml of the Brilliant Green leuco-base solution; swirl the flasks, and dilute to the mark with deionized water. After about 1 min, measure the absorbance at 630 nm, and set up a calibration graph of the least-squares equation for the linear range.

Quantitative procedure for samples. Deliver 20–50 g of filtered aqueous sample into a 100-ml volumetric flask; pipet in 10 ml of the leuco-base of Brilliant Green and swirl the flask gently. Prepare a control by pipetting 10 ml of the leuco-base into another flask. Dilute both solutions to 100 ml with deionized water and measure the absorbance at 630 nm. Correct for the control, and calculate the concentration of anionic surfactant in the sample from the calibration. If the absorbance is less than 0.1, repeat the procedure on a larger sample or with longer optical paths.

Spectroreflectance for opaque samples. A spectroreflectance method is necessary to determine the anionic surfactants added to certain opaque commercial latex formulations. Prepare blends of sodium dioctyl sulfosuccinate at concentrations of 0–0.15% (w/w) in latex. Pipet a series of 10-ml aliquots into 100-ml volumetric flasks so that the solutions contain 0.00–0.010 g of surfactant. Pipet in 10 ml of the Brilliant Green leuco-base, and proceed as before. Run the absorbance curves in the total spectral reflectance mode. On the Beckman model 5240 spectroreflectometer, the I_o is obtained with the control emulsion in a pair of 1-in. light scattering cells in position on the barium sulfate-coated integrating sphere.

Qualitative test procedures. The colorless leuco-base solution is most conveniently applied to a paper substrate from a conventional spray bottle. If no characteristic color develops within 1 min, then no significant anionic surfactant residue is present on the paper. The time restriction is necessary because the leuco-base gradually acquires color on exposure to air. Obviously, it is necessary to take precautions to avoid contamination from the surfactants which are frequently present in laboratory glassware or on bench tops.

Results and discussion

Procedures involving electrical conductivity, surface tension, titrimetry, foaming potential, and zeta potential were investigated, but did not offer the advantages of speed, limit of detection, and ease of on-line control available with the spectrophotometric method. A series of triphenylmethane dyes was evaluated for completeness of conversion to a colorless or lightly colored leuco-base, and for response of the leuco-bases to anionic surfactants. The results of this screening study, expressed as absorptivity relative to surfactant concentration, are listed in Table 1. Brilliant Green met the quantitative selection criteria better than any other dye tested: it provided a colorless and stable leuco-base; it did not form a sediment on standing (a problem with some triphenylmethane dyes); and it did not require filtration on preparation.

The Brilliant Green leuco-base solution can replace the methyl violet leuco-base solution for qualitative use. The former solution has the advantages that no charcoal treatment is needed for complete decolorization of the leuco-base and that shelf life is longer. Because of the lower absorptivity of Brilliant Green, per weight of anionic surfactant, it is potentially less sensitive than methyl violet as a qualitative test solution.

TABLE 1

Triphenylmethane dyes screened for leuco-base conversion and response to anionic surfactant

Dye	Leuco-base solution	Response to anionic surfactant	Wavelength (nm)	Absorptivity ($l\ g^{-1}\ cm^{-1}$)
Aniline blue	Colorless	None	595	0.00
Basic fuchsine	Colorless	Weak	550	0.55
Brilliant Green	Colorless	Strong	630	3.36
Crystal violet	Light violet	Strong	592	6.73
Ethyl violet	Light violet	Weak	595	1.02
Malachite green oxalate	Colorless	Weak	630	0.16
Methylthymol blue	Dark green	None	600	0.00
Methyl violet	Light violet	Strong	585	5.80
New fuchsin (Basic Violet 2)	Light yellow	Weak	555	0.61
Patent blue	Intense blue	None	628	0.00
Rosolic acid	Light red	Very weak	527	0.05

In order to assess the effect of decolorization of the dye and the extent of restoration of color by surfactant, the sodium sulfite concentration was varied from 0.4% to 7.5% in leuco-base reagent. At the 0.4% concentration, only 91.6% of the color of methyl violet was removed and 97.5% of the color was restored by 0.01% anionic surfactant; at a 1.2% concentration, 95.5% of the color of methyl violet was reduced and 100% of the color was restored by the surfactant. At the highest concentration of sodium sulfite used here (7.5%), the molecular absorption spectra showed a wavelength shift and band broadening, coupled with a decrease in absorbance; this effect was not examined further. At the 1.2% concentration of sodium sulfite, Brilliant Green became colorless in solution and 100% of the expected absorbance was realized on reaction; this concentration was therefore chosen for the recommended method.

The color developed from the leuco-base reagent tends to change with time. When methyl violet was used, the absorbance decreased by 2% 5 min after mixing, by 8% after 30 min, and by 24% after 25 h. In a study of the restored Brilliant Green color, the absorbance increased by 1% after the first 10 min, and then decreased by 14% after 18 h. It is recommended that the absorbance be measured immediately following color development and dilution.

A representative calibration curve for an alkyl/alkene sulfonate is shown in Fig. 1.

Reflectance curves. Spectral reflectance (Fig. 2) proved to be quite useful for determining the anionic surfactant, sodium dioctyl sulfosuccinate, added to certain latex formulations that are white, opaque suspensions. The blue—green color of Brilliant Green was discernible in the emulsion containing a polymeric binder and an acidic cross-linking agent. The surfactant was readily quantified by the difference technique, where the reference is the color-developed emulsion control. Zero suppression and ordinate expansion enhanced the appearance of the reflectance spectra.

Repeatability, accuracy and working range. The standard deviation in measuring 0.01 g of hydroxyalkane/alkene surfactant with four separately prepared solutions of Brilliant Green was ±0.005 absorbance and the standard deviation for a single solution measured eight times was ±0.019 absorbance.

The accuracy of the method based on the quantitation of known concentrations of hydroxyalkane/alkene sulfonate in the 200—1000 ppm range in aqueous solution was found to average 99.8%. Two of the blends were checked by the two-phase titration technique [3] and the differences between the colorimetric and titrimetric methods averaged 5%. The general working ranges of the methods are 0—500 ppm of the hydroxyalkane/alkene sulfonate and 0—200 ppm of the sodium dodecyl sulfate in 50-g aqueous samples by the absorption spectrophotometric method, and 0—1500 ppm of the sodium dioctyl sulfosuccinate in 50-g latex emulsions by the spectro-reflectometric method. The detection limit in a 1-cm cell is about 1 mg of the sodium dodecyl sulfate and about 3 mg of the hydroxyalkane/alkene

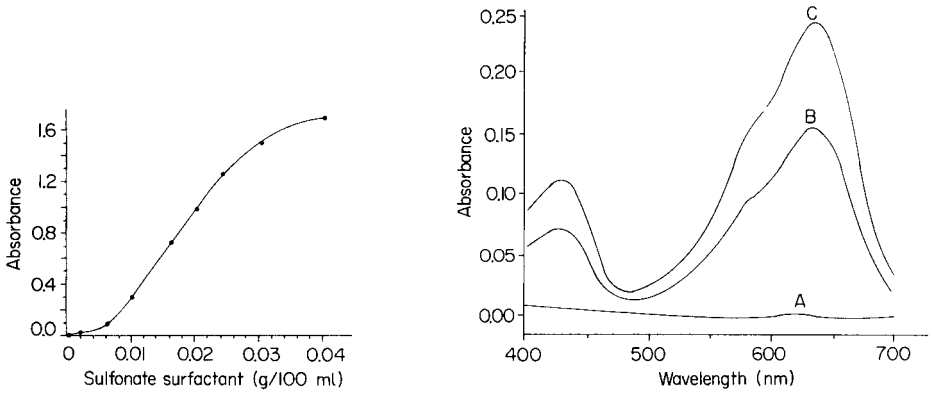

Fig. 1. Calibration curve obtained for hydroxyalkane/alkene sulfonate surfactant (Ultrawet A-OK) as a function of restoration of color to a leuco-base Brilliant Green solution. Surfactant concentration refers to the final solution measured. Absorbance refers to 630 nm in 1-cm cells.

Fig. 2. Spectroreflectance curves of sodium dioctyl sulfosuccinate in opaque polymer emulsions as a function of color restoration to leuco-base Brilliant Green. A, Control emulsion without surfactant; B, 0.0067 g of surfactant/100 ml of final solution; C, 0.0131 g of surfactant/100 ml of final solution.

surfactant per 100 ml of the final solution. Lower levels of 20—60 ppm can then be determined in 50-g samples. In the reflectance mode, about 3 mg of the sodium dioctyl sulfosuccinate per 100 ml can be determined as a lower limit.

Interferences. The interferences of some oxidizing and reducing agents were investigated. Blends were prepared containing surfactant and impurity in weight ratios ranging from 1/0.56 to 1/2.22. Among the potential impurities studied were KIO_3, $FeCl_3$, HNO_3, H_2SO_4, $HClO_4$, HCl, $Na_2S_2O_3$, $NH_2OH \cdot HCl$, and $H_2C_2O_4 \cdot 2H_2O$. At the concentration level of 0.016 g hydroxyalkane/alkene surfactant per 100 ml, the recoveries ranged from 98.1 to 103.9%. Following the addition of sulfuric acid at the higher end of the weight ratios investigated, it was necessary to readjust the pH to 9.0 for quantitative conversion to the quinoid color.

Most anionic surfactants respond to this method much like they would respond to the methylene blue ion-pairing method.

Automated procedure. The method for anionic surfactant was demonstrated on a modular Technicon Autoanalyzer Model II. Flow-rates were 1 ml min^{-1} for the leuco-base, 0.14 ml min^{-1} for the sample line, 2 ml min^{-1} for an aqueous diluent, and 0.32 ml min^{-1} for the air line. A linear calibration was obtained for the 60—400 ppm range. The cycle time between successive runs was 3.5 min.

The technical assistance of Arthur L. Allen and Ronald K. Chen, and the cooperation of Adolph Strzepek, are respectfully acknowledged.

REFERENCES

1 E. S. Abramovich, U.S.S.R. Patent No. 122,336, Tekst. Promst., 20 (1960) 41.
2 G. F. Longman, The Analysis of Detergents and Detergent Products, Wiley, New York, 1975, Ch. 9, 10 and 18.
3 M. J. Rosen and H. A. Goldsmith, Systematic Analysis of Surface-Active Agents, 2nd edn., Wiley, New York, 1972, Ch. 5.
4 J. Kawase, A. Nakae and M. Yamanaka, Anal. Chem., 51 (1979) 1640.
5 K. Higuchi, S. Monya, Y. Shimoishi, H. Miyatta and K. Tôei, Bunseki Kagaku, 29 (1980) 180.
6 A. Le Bihan and J. Courtot-Coupez, Analusis, 6 (1978) 346.
7 C. G. Taylor and J. Waters, Anal. Chim. Acta, 69 (1974) 363.
8 L. K. Wang, S. F. Kao, M. H. Wang, J. F. Kao and A. L. Loshin, Ind. Eng. Chem., Prod. Res. Dev., 17 (1978) 186.
9 S. Ianeva and R. Borisova-Pangarova, Talanta, 25 (1978) 279.
10 Z. I. Chalaya and O. M. Voznaya, Zh. Anal. Khim., 27 (1972) 204.
11 G. R. E. C. Gregory, Analyst, 91 (1966) 251.

Analytica Chimica Acta, 141 (1982) 427—430
Elsevier Scientific Publishing Company, Amsterdam — Printed in The Netherlands

Short Communication

CONTINUOUS FLOTATION OF TRACE AMOUNTS OF NITRITE ION IN WATER

MAMORU AOYAMA*, TOSHIYUKI HOBO and SHIGETAKA SUZUKI

Department of Industrial Chemistry, Faculty of Technology, Tokyo Metropolitan University, Fukasawa, Setagaya-ku, Tokyo (Japan)

(Received 19th January 1982)

Summary. A flotation method in which sample is continuously fed at flow rates of 2—3 l h^{-1} into a separation tube is described. The nitrite (3—40 $\mu g\ l^{-1}$) is continuously converted to an azo dye for spectrophotometric measurement at 15-min intervals.

Foam separation methods (flotation) have received much attention for the concentration of trace species in water [1—6]. Depending on the processes involved, flotation methods can be generally divided into coprecipitation flotation [1], adsorption colloid flotation [2] and ion flotation [3]. Of these, ion flotation has the advantage that it can be used for the continuous concentration of trace species [7], and so appears most promising for water quality monitoring systems. Various procedures have been worked out in this laboratory for the selective ion flotation of trace species in waters, including methylmercury(II) chloride [8], copper(II) [7, 9], chromium(VI) [10, 11], sulfide [12] and nitrite [13].

In this communication, a flotation—spectrophotometric method is proposed for the determination of nitrite ion. All the solutions involved, including the sample, are pumped continuously, and the procedure is suitable for the determination of nitrite ion at the $\mu g\ l^{-1}$ level in water.

Experimental

Apparatus. A schematic diagram of the continuous flotation system is shown in Fig. 1. The 570-mm long separation tube (A) has been described [11]. The mixing chambers shown in Fig. 2 were devised and used for G_1 and G_2 in Fig. 1. The absorbance of the subsided foam solution was measured by using a Yanagimoto model UO-101 derivative spectrophotometer with 1-cm cells.

Chemicals. Stock solutions (1 mg ml^{-1}) of nitrite were prepared by dissolving sodium nitrite which had been dried for 4 h at 110°C. *p*-Aminobenzenesulfonamide (ABSA; analytical grade) was used as a 2% (w/v) solution in 100 ml of (1 + 9) hydrochloric acid prepared just before use. Aqueous *N*-1-naphthylethylenediamine (1% w/v NEDA) solutions were also prepared

0003-2670/82/0000-0000/$02.75

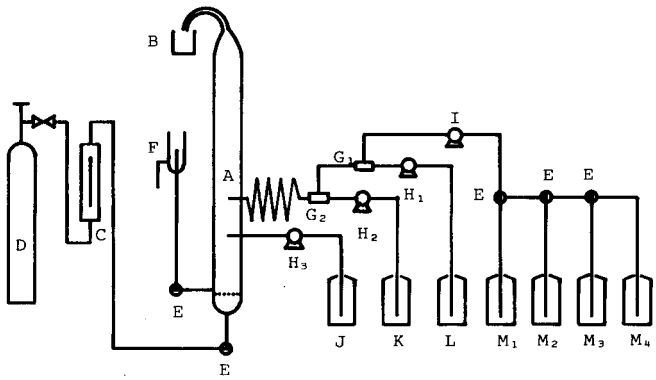

Fig. 1. Schematic diagram of continuous foam separation system. (A) Separation tube; (B) foam collector (containing 5 ml of 1-propanol); (C) flow meter; (D) nitrogen cylinder; (E) three-way cock; (F) effluent drain; (G_1, G_2) mixing chambers; (H_1, H_2, H_3) plunger pumps; (I) diaphragm pump; (J) surfactant solution (1% SLS) reservoir; (K) 1% NEDA solution reservoir; (L) 2% ABSA solution reservoir; (M_1, M_2, M_3, M_4) sample reservoirs. The coil between G_2 and A is 8 m long.

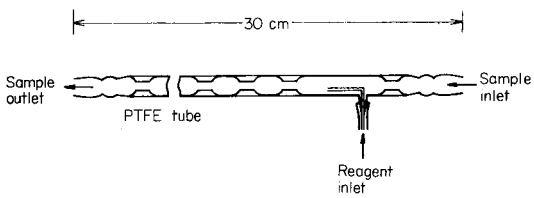

Fig. 2. Mixing chambers G. The glass tube (8-mm o.d.) has numerous constrictions, each about 3-mm i.d. and 5 mm long. Near the sample inlet, a PTFE tube (2-mm o.d., 1-mm i.d.) is used to introduce NEDA or ABSA reagent; it is connected to the glass tube by a flexible plastic sleeve.

freshly. An aqueous 1% solution of sodium lauryl sulfate (SLS) was used. All other chemicals used were of analytical grade. Water was purified by distillation and ion exchange.

Procedure. Pure water (1 l) was poured into the separation tube, nitrogen was passed into the tube at about 147 ml min^{-1}, and the 1% SLS solution was pumped at a flow rate of 0.115 ml min^{-1}. Then the sample, 2% ABSA and 1% NEDA solutions were pumped at flow rates of 2 l h^{-1}, 0.350 ml min^{-1} and 0.170 ml min^{-1}, respectively. In order to achieve complete mixing, the sample was first mixed with ABSA solution in chamber G_1, and then mixed with NEDA solution in chamber G_2 before entering the separation tube. The foam came out of the separation tube and subsided in the collector vessel containing 5 ml of 1-propanol. This solution was intermittently transferred to a 50-ml volumetric flask and 2 ml of concentrated hydrochloric acid was added to make the acidity about 0.48 M. The solution was diluted to the mark with water, and the absorbance at 545 nm was measured against a water reference.

Results and discussion

Initially, the continuous flotation method was tested at sample solution feed rates of 2 l h^{-1}. The nitrite ion should be converted to an azo dye before entering the separation tube, to obtain high recoveries of nitrite ion, thus a sufficiently long mixing tube must be used for sample introduction to allow formation of the azo dye. In this work, 8 m of polytetrafluoroethylene (PTFE) tubing (7.5-mm o.d., 6.0-mm i.d.) was found suitable.

In order to establish the optimum conditions for steady-state flotation of nitrite ion, various factors, such as supply rates of SLS, ABSA and NEDA, flow rate of nitrogen and so on, were studied. As the ion flotation depends on the static attractive forces between the required species and the surfactant as well as on the area of the liquid—gas interface, the effect of the SLS supply rate on the nitrite recovery was investigated. Quantitative recoveries were achieved above 0.115 ml min^{-1} of 1% SLS solution; this flow rate was therefore used, because the concentration ratio decreased at higher SLS supply rates. Tests with different supply rates of 2% ABSA and 1% NEDA solutions showed that nitrite recoveries were quantitative with supply rates of more than 0.300 l min^{-1} and 0.150 ml min^{-1} for the 2% ABSA and the 1% NEDA solutions, respectively. The interface area between gas and liquid depends on the size of bubbles, which is affected by the gas flow rate. A study of the effect of the nitrogen flow rate in the range of 60—190 ml min^{-1} showed that recoveries were satisfactory over the range 140—190 ml min^{-1}. The optimum flotation conditions derived based on the above results were as follows: 0.115 ml min^{-1} of the 1% SLS solution, 0.350 ml min^{-1} of the 2% ABSA solution, 0.170 ml min^{-1} of the 1% NEDA solution, and 147 ml N_2 min^{-1}.

The collectors were replaced every 15 min, and the recoveries were measured by spectrophotometry. As shown in Fig. 3, steady-state flotation was achieved about 1 h after the initiation of sample introduction. In this case, recovery was about 96%. The response for sudden changes in the concentration of nitrite ion was also investigated. As can be seen from Fig. 4, whether the nitrite concentration decreased or increased, constant recovery was obtained about 1 h after the sample change. This method allows the concentration of nitrite ion in the range 3—40 $\mu g\ l^{-1}$ of sample to be measured quantitatively.

Continuous flotation at sample solution feed rates of 3 l h^{-1} was also tested. The optimum conditions were the same as those described above, except for the 1% SLS solution supply rate, which was optimally 0.195 ml min^{-1}. Further, the PTFE coil was lengthened to 10 m, to make mixing complete. Similar satisfactory results were obtained from this system.

It was concluded from all these results that effective concentration of nitrite ion at low $\mu g\ l^{-1}$ levels can be achieved through this continuous system, though there is a delay in obtaining results after concentration changes. Connection of an appropriate continuous photometric detector to this system will facilitate a continuous nitrite monitoring system.

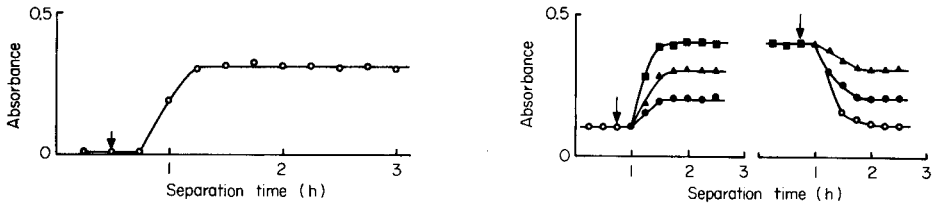

Fig. 3. Variation of absorbance with time for a nitrite solution (30 $\mu g\ l^{-1}$) at a feed rate of 2 l h^{-1}. Conditions as recommended under Experimental. The arrow indicates where pumping started.

Fig. 4. Response to sudden concentration change in the continuous foam separation of nitrite solution. Nitrite concentration: (○) 10 $\mu g\ l^{-1}$; (●) 20 $\mu g\ l^{-1}$; (▲) 30 $\mu g\ l^{-1}$; (■) 40 $\mu g\ l^{-1}$. Conditions as recommended under Experimental. The arrows indicate where samples were changed.

This work was supported in part by a research grant from the Ministry of Education, Japan.

REFERENCES

1 M. Hiraide, Y. Yoshida and A. Mizuike, Anal. Chim. Acta, 81 (1976) 185.
2 J. H. Tzeng and H. Zeitlin, Anal. Chim. Acta, 101 (1978) 71.
3 K. Sekine and H. Onishi, Anal. Chim. Acta, 62 (1972) 468.
4 S. Nakashima, Anal. Chem., 51 (1979) 654.
5 M. Hiraide, T. Ito, M. Baba, H. Kawaguchi and A. Mizuike, Anal. Chem., 52 (1980) 804.
6 J. Elhanan and B. L. Karger, Anal. Chem., 41 (1969) 671.
7 S. Suzuki, T. Hobo and Y. Asaumi, Bunseki Kagaku, 31 (1982) 13.
8 T. Hobo, T. Ogura, S. Suzuki and S. Araki, Bunseki Kagaku, 24 (1975) 288.
9 T. Hobo, Y. Sudo, S. Suzuki and S. Araki, Bunseki Kagaku, 27 (1978) 104.
10 M. Aoyama, T. Hobo and S. Suzuki, Bunseki Kagaku, 30 (1981) 224.
11 M. Aoyama, T. Hobo and S. Suzuki, Anal. Chim. Acta, 129 (1981) 237.
12 M. Aoyama, T. Hobo and S. Suzuki, Bunseki Kagaku, 31 (1982) E7.
13 M. Aoyama, T. Hobo and S. Suzuki, Bunseki Kagaku, 31 (1982) E99.

Analytica Chimica Acta, 141 (1982) 431
Elsevier Scientific Publishing Company, Amsterdam — Printed in The Netherlands

Corrigendum

G. S. Caravajal, K. I. Mahan and D. E. Leyden, The determination of uranium by thin-film x-ray fluorescence spectrometry after coprecipitation with an iron dibenzyldithiocarbamate carrier complex.

Anal. Chim. Acta, 135 (1982) 205—214.

p. 214, references 12 and 13 should read:

12 A. Hubaux and B. Vos, Anal. Chem., 42 (1970) 849.
13 L. A. Currie, Anal. Chem., 40 (1968) 586.

ANALYTICA CHIMICA ACTA, Vol. 141

AUTHOR INDEX

(continued from inside of cover)

Printed in The Netherlands.

ontinued from outside of cover)

(continued on page 438)

CONTENTS

(Abstracts/contents lists in: Anal. Abstr.; Biol. Abstr.; Chem. Abstr.; Curr. Contents Phys. Chem. Earth Sci., Life Sc. Index Med.; Mass Spectrom. Bull.; Sci. Citation Index; Excerpta Med.)

(continued on inside page of cover)